Edith Cowan University

Research Online

Theses : Honours

Theses

2003

Device structure effects on electrical crosstalk in Backwall Illuminated CMOS compatible photodiode arrays

Paul Vernon Jansz
Edith Cowan University

Follow this and additional works at: https://ro.ecu.edu.au/theses_hons

 Part of the Signal Processing Commons

Recommended Citation

Jansz, P. V. (2003). *Device structure effects on electrical crosstalk in Backwall Illuminated CMOS compatible photodiode arrays*. https://ro.ecu.edu.au/theses_hons/355

This Thesis is posted at Research Online.
https://ro.ecu.edu.au/theses_hons/355

Edith Cowan University

Copyright Warning

You may print or download ONE copy of this document for the purpose of your own research or study.

The University does not authorize you to copy, communicate or otherwise make available electronically to any other person any copyright material contained on this site.

You are reminded of the following:

- Copyright owners are entitled to take legal action against persons who infringe their copyright.

- A reproduction of material that is protected by copyright may be a copyright infringement. Where the reproduction of such material is done without attribution of authorship, with false attribution of authorship or the authorship is treated in a derogatory manner, this may be a breach of the author's moral rights contained in Part IX of the Copyright Act 1968 (Cth).

- Courts have the power to impose a wide range of civil and criminal sanctions for infringement of copyright, infringement of moral rights and other offences under the Copyright Act 1968 (Cth). Higher penalties may apply, and higher damages may be awarded, for offences and infringements involving the conversion of material into digital or electronic form.

DEVICE STRUCTURE EFFECTS ON ELECTRICAL CROSSTALK IN BACKWALL ILLUMINATED CMOS COMPATIBLE PHOTODIODE ARRAYS.

Paul Vernon Jansz

Student # 0885203

Honours Thesis

Faculty of Computing, Health and Science

Edith Cowan University

Perth, Western Australia

Bachelor of science Honours (Physical Science)

June 2003

Principal Superviser – Dr Steven Hinckley

USE OF THESIS

The Use of Thesis statement is not included in this version of the thesis.

ABSTRACT

Contemporary research into Cameras-on-a-CMOS chip technology has been focused on frontside illuminated configurations, in which the photo sensing element or picture element (pixel) and the signal processing circuitry are integrated in the same plane making up the photo sensing unit (PSU). Frontside illuminated configurations are disadvantaged in a number of ways, including the incompatibility of different CCD and CMOS processing technologies that are currently used and low areal fill factors.

Current investigations have demonstrated that a number of these disadvantages can be overcome by adopting a backside illuminated architecture, where an upper seeing pixel thin film crystalline-Silicon integrated circuit is mounted above a lower signal processing Application Specific IC (ASIC). As well as allowing the combination of different processing technologies for the pixel and ASIC, there is a marked increase in the areal fill factor as the processing circuitry is no longer in the same plane as the photodiode.

Though there is much crosstalk minimization investigation for various frontside illuminated pixel configurations, some progress with crosstalk minimization in backside illuminated vertical single junction photodiode pixels has been made. More extensive selection of configuration parameters needs to be investigated for backside illuminated pixel response resolution optimization and hence crosstalk suppression optimization, compared to the same pixel configurations front illuminated.

This research has made a comparative investigated of crosstalk in backside illuminated and frontside illuminated single junction photodiode and vertical double junction photodiode CMOS compatible pixels, using a commercial 2D device simulation package, SEMICAD DEVICE (1994). Comparison of pixel total, electron and hole quantum efficiency response and Absorption Volume data is undertaken. This is so that the underlying carrier drift-diffusion dynamics responsible for optimal pixel response resolution may be qualitatively understood, allowing prediction of even more optimal photodiode pixel configurations.

The effect of varying the double junction and single junction photodiode pixel's geometry on response resolution is considered. Only for the former is the effect of doping, biasing and introducing highly doped pixel boundary trenches on response resolution undertaken. Additionally, for the former pixel, the effect of introducing a guard-ring electrode on its electrical response resolution is investigated.

For single junction photodiode pixels, the boundary trench isolation, a highly doped recombination boundary trench placed either side of each pixel's well, showed considerably less pixel response resolution and hence more crosstalk than using the guard-ring electrode configuration. However the boundary-trench-isolation-pixel's response was an improvement on the unguarded single junction photodiode pixel's response.

The outer junction of the double junction photodiode pixel acts in the same way as the guard-ring electrode for the single junction photodiode pixel, by suppressing the pixel response away from the pixel centre. However for pixels with similar geometry of outer well and substrate to the single junction photodiode guarded pixel, the outer junction "guard" improves the pixel response resolution more than the electrode guard does. However for shallow pixels their response resolutions are not significantly different, in that response outside the "well" (outer well in double junction photodiode pixels) is insignificant. The response resolution is more flexibly varied inside this "well" for the double junction than for the guarded single junction photodiode pixel.

Generally the frontside illuminated photodiode pixels have better response resolution and hence crosstalk suppression than the same pixel backside illuminated. This is due primarily to their greater depletion region absorption volume proportion. This results from the closer proximity of their photogenerated carrier-envelope to their pixel's depletion region. However as frontside and backside illuminated pixel absorption volume proportions converge, their response resolution becomes less distinguishable.

The predictive advantage of pixel absorption volume data for optimal pixel response resolution is evident. Such data can help to narrow the selection of possible optimal pixel configurations. However simulation is still the necessary final arbiter without the more costly fabricated-device testing option available.

DECLARATION

I certify that this thesis does not, to the best of my knowledge and belief:

(a) Incorporate without acknowledgement any material previously submitted for a degree or diploma in any institution;

(b) Contain any material previously published or written by another person except where due reference is made in the text;

(c) Contain any defamatory material.

Signature.....

Name Paul V. Jansz-Dawetzky

Date 18th Dec 2003

ACKNOWLEDGEMENT

I acknowledge the valuable help of the following people and organisations.

To Dr Steven Hinckley who, as my honours supervisor, always provided timely and accurate support in providing suggestion on research directions, data analysis and presentation, as well as correcting many thesis revisions and final thesis presentation.

To my dear wife, Janis ("deputy supervisor") and the honours coordinator, Dr Glenn Hyndes, who patiently maintained confidence that the thesis would be completed.

To the three Davids, Dr Macdougall, Dr Wilson and Dr Lucas in assisting me regarding mathematical considerations related to simulation statistics and AVP integral evaluations. All very approachable and wanting to be of assistance.

To the Edith Cowan University School of Engineering and Mathematics, for providing the use of their facilities and simulation software, SEMICAD DEVICE™.

To dearest Jana Melicevic, a promising literary composer, who taught me the essence of imagination, exploration, creativity, intuitiveness, thoroughness, and a healthy disdain for narrow minded reductionism.

To my Christian family and friends who cared enough to pray amongst other things that I would know wisdom, insight and direction for this project from God's omniscient resources.

To my highly esteemed classical and folk music colleagues who have been waiting patiently for the return of their violinist and Hungarian gypsy fiddler, respectively, to come down from the roof of his academic excellence !!

"Nagyon Szépen Köszönöm !!"

"Stored in what you pieced together;

Coming to explore to full adventure;

Time and pieces, puzzle now nothing;

Find will you home at last."

Jana Jansz (1997) Chapter 11, p 4.

INDEX

1. INTRODUCTION

1.1 Purposes and Methods.

The primary purpose of this project is to optimize the photo-electrical response resolution, including central sensitivity and electrical crosstalk suppression for the backwall illuminated (BW) (Fig 1.1) complimentary metal oxide semiconductor (CMOS) compatible photodiode pixel. This is compared and contrasted with the frontwall illuminated (FW) pixel of the same configuration. Improved pixel response resolution ultimately can be translated into improved pixel fabrication resolution. The secondary purpose is to understand how the optimal configuration improves the response resolution, while other configurations reduce it.

The primary purpose is achieved by simulating the photocurrent response of various single junction photodiode (SJPD) and double junction photodiode (DJPD) pixel configurations and comparing these electrical responses between each illumination mode, pixel configuration and pixel absorption volume proportions (AVP). The AVP is a calculated statistic that represents the proportion of the total incident light energy that is absorbed in a given substructure of the illuminated pixel cross-section.

The secondary purpose will be achieved by using both the AVP and electrical response data to probe the device operation. This comparison between the simulated electrical response parameters and the AVP Statistics will result in the development of an understanding of the reason for the optimality of certain pixel configurations over others. Furthermore, that the macroscopic pixel configuration characteristics that optimize the BW pixel response, being then understood at a qualitative level of device photo-generation and carrier dynamics, will enable the predicting of further optimization and the demonstration of the extent the AVP statistic can be useful in that process.

1.2 Background.

Contemporary research into Cameras-on-a-CMOS chip technology has been focused on FW architectures, in which the active pixel sensor (APS) and the signal processing circuitry are integrated in the same plane. This architecture is disadvantaged in a number of ways, including low areal fill factors and the incompatibility of different charge coupled device (CCD) and CMOS processing technologies that are currently used. Current investigations have demonstrated that a number of these disadvantages can be overcome by adopting a BW approach [Hinckley, Gluszak, & Eshraghian, 2002], where an upper seeing photodiode pixel array IC is mounted above a signal processing, application specific integrated circuit (ASIC). As well as increasing the areal fill factor, and thus increasing its resolving power, this concept also allows the combination of different processing technologies and semiconductor materials for the two integrated circuits.

Although crosstalk minimisation has been investigated for various FW photodiode configurations [Brouk, et al. 2002; Kang, 2002; Furumiya, et al. 2001], crosstalk minimisation in BW pixels needs more investigation. This is so that the advantages of enhanced BW pixel response resolution, if any, over FW pixels can be determined. For example, in one investigation on FW photodiode pixels, it was found that, to reduce crosstalk, the gap between junctions needs to be optically shielded and the adjacent junctions needs to be reverse-biased [Brouk, et al. 2002].

This is the first ever investigation of the performance of BW CMOS compatible photodetectors. The investigation will make use of a commercial two-dimensional (2D) device simulation package, SEMICAD DEVICE™ to model the permutations of the photodiode pixel configurations. This is to approach, if not to arrive at, the photodiode pixel configuration that optimizes the electrical response resolution. This involves maximizing the electrical response at each pixel centre (sensitivity), while totally suppressing pixel response for illuminations outside the pixel boundary if not the pixel's well. BW and FW pixel responses are compared, to understand why their responses differ, if they do, and then apply that knowledge to further optimization of

primarily BW pixel configuration, though this may also benefit FW pixel optimization.

1.3 Pixel Configuration and The AVP.

Configuration parameters that could effect the SJPD pixel response resolution, including crosstalk suppression, are level of junctioning, p-n junction depth, well width, substrate thickness, pixel pitch, dopant concentrations, well and substrate doping type reversal, electrode widths, positions, number and their degree of voltage biasing. Also included is the geometry, doping and biasing of boundary isolation structures. The setting of each of these geometric, doping and electrical parameters constitutes a pixel's ***configuration.*** Configuration parameters that could effect the DJPD pixel response resolution / crosstalk are those for the SJPD but are doubled as this pixel has an extra well so that the number of geometric, doping, biasing and electrode parameters are increased.

The development of the ***Absorption Volume Proportion*** (AVP) statistic has been undertaken to understand how the pixel's response profile depends on where in the device cross-section the incident light is absorbed. It determines in what way the incident light is distributed in regions of the pixel that have significant effect on the pixel's electrical response. Noting how the AVP profile varies with the pixel's photocurrent response profile may prove fruitful in understanding how the macroscopic changes to the pixels configuration parameters enhance or suppress optimal pixel response resolution.

Figure 1.1 shows the array of three SJPD pixels, as simulated in this project. It shows the well and substrate that surrounds each well. Also the illumination orientation for BW and FW pixels is shown.

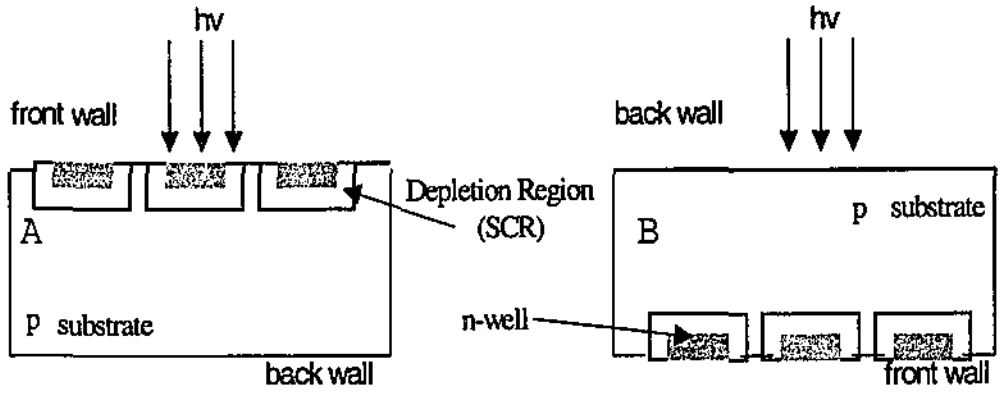

Figure 1.1 The basic p-substrate / n-well Photodiode pixel (A) FW, (B) BW.

1.4 The Investigated Pixel Configuration Parameter Changes.

The effect of changing the following pixel configuration parameters on pixel electrical response resolution will be investigated in this project.

1.4.1 Unguarded SJPD Pixels.

1. Pixel well depth.
2. Pixel substrate thickness.
3. Pixel Boundary Trench Isolation.

1.4.2 Guarded SJPD Pixels.

1. Pixel well depth.
2. Pixel substrate thickness.
3. Guard-ring electrode placement.
4. Guard-ring electrode size.
5. Image electrode size.
6. Well doping concentrations.
7. Substrate doping concentrations.
8. Doping type of well and substrate reversal.
9. Junction reverse bias.

1.4.3 **Unguarded DJPD Pixels.**

1. Pixel image (inner) well depth.
2. Pixel image well width.

1.5 **Research Questions.**

The primary interest here is to see what effect the above changes to the pixel configuration have on the simulated pixel photocurrent data and the AVP data and then explain these effects. Thus the following questions need to be answered.

(a). What effect do these pixel configuration changes have on simulated pixel response resolution and crosstalk ?

(b). What effect do these pixel configuration changes have on calculated AVP profile ? This is for the pixel configuration parameter for which changes effect the AVP statistics.

(c). What understanding of the processes responsible for improvements in response resolution and crosstalk reduction can be gained by observing the relationship between the calculated AVP and simulated electrical response ?

(d). The three types of crosstalk suppressing pixel configurations investigated are boundary trench isolation, guard electrode and guard depletion region. Can these three pixel configurations be placed in some meaningful order of response resolution and crosstalk suppression ?

(e). Having gained an understanding of how response resolution can be improved, is it possible to predict more optimally resolved pixel configurations ?

1.6 Research Objectives.

The objectives basically revolve around tasks that need to be achieved to fulfill the primary purpose of this project. They are itemized below.

1. Formulate the relationship between the device structure and the software parameters.

2. Develop SEMICAD DEVICE simulation device and run files.

3. Develop AVP Excel spreadsheet.

4. Run the simulations that generate the pixel electrical response for each parameter variation investigate for Sections 1.4.1 to 1.4.3.

5. Calculate and tabular pixel AVP data relevant to Section 1.4.1 to 1.4.3.

6. Develop results tables of pixel electron and hole and total QE and NQE for the illumination positions included in each simulation scan of the pixel array.

7. Graph pixel response statistics against associated illumination position as well as against the varied configuration parameter associated with the response statistic. When appropriate include AVP profiles.

8. Determine the device dynamics that explains the pixel response resolution enhancement qualitatively.

9. Predict further improved pixel configurations from an understanding of the previous point (8).

10. Access the value of the AVP statistic in predicting better pixel configuration.

2. LITERATURE REVIEW

In an array of light detecting devices (pixels), electrical crosstalk occurs when photocarriers, generated within the volume of one pixel, diffuse into and are captured by an adjacent pixel, contributing to its photocurrent. Investigating the effect of changes to various pixel configuration parameters on crosstalk reduction is undertaken in this project. The more resolved a pixel's response, the more enhanced is its response towards the pixel centre, and the more suppressed its response is elsewhere in the pixel and so crosstalk is also suppressed. Because enhancements in response resolution impacts directly on crosstalk reduction, research that aims to enhance the former, tackles reducing crosstalk simultaneously.

The pixel is the photoactive volume of the photo sensing unit (PSU), the later including the pixel and the infrastructure that reads, amplifies and resets the pixel, that makes the PSU an active pixel sensor (APS). This infrastructure may be laterally (FW PSU) or vertically (FW TFA PSU and BW PSU) placed with reference to the pixel.

As used in the first paragraph, "pixel configuration" refers to the physical attributes associated with each pixel. The pixel configuration parameters include; the type of intrinsic material used, the position of doped, intrinsic or insulated structures in the pixel cross section, junction widths and depths, the number of junctions, doping levels associated with each structure, biasing, and the size and placement of electrodes.

Pixel arrays are usually illuminated on the front surface on which the electrodes are exposed or unconventionally on the back surface, which is usually the electrode free substrate. Though there has been some research focused on reducing crosstalk or noise in BW pixels (Hinckley 2002), (Holland nd) owing to the BW pixel benefits of increased resolution and spectral sensitivity, the investigation of crosstalk

mechanisms has mainly concerned itself with FW pixels (Brouk et al., 2000) (Furumiya et al., 2001) (Briaire & Krisch, 2000) (Kang, 2002) (Mutoh, 2003).

2.1 Backwall Illuminated Pixel Crosstalk

Hinckley, Jansz, Gluszak & Eshragian (2002) concluded that in backwall illuminated (BW) arrays, structures need to be developed that either reduce optical generation or increase minority carrier recombination in the region between pixels, in order to reduce crosstalk effects, while at the same time maintaining the advantages of BW pixel spectral responsivity compared to FW pixels.

While deep highly doped structures running horizontally through the epi-layer / substrate region of the pixel array (deep epi-well) may increase recombination of "free" diffusing substrate, crosstalk photocarriers in FW pixels, they suppress the BW pixel response. This is due to all the photogenerated carriers in BW pixels diffusing into the deep epi-well from below, and so reducing image electrode capture. The latter BW SJPD would benefit more from STI type recombination-increasing structures for reducing crosstalk (Kang, 2002) as these restrict side-way photocarrier diffusion into adjacent photodiodes.

Hinckley, Jansz, Gluszak & Eshragian (2002) also showed that the reduction in substrate thickness appeared to increase BW and FW pixel response resolution with the direct consequence of reduced crosstalk. This was due in part to the attenuation of the substrate region under the pixels' wells, running the length of the array, which provided a passageway for "free" diffusion across the backside of the array. Attenuation reduced the volume of this crosstalk super highway so contributing to the increase in response resolution. Furthermore, the shallower substrate allowed closer proximity of the photogenerated carrier envelope to the BW pixel's Space Charge Region (SCR = depletion region), with resulting enhanced capture-volume, also contributing to increased response resolution.

2.2 Frontwall Illuminated Pixel Crosstalk.

Brouk et al., (2002) demonstrates that crosstalk in frontwall illuminated (FW) pixels may be reduced by optically shielding the gap between junctions and reverse biasing the adjacent junctions. This included single junction photodiode (SJPD) and double junction photodiode (DJPD) pixel configurations. In the case of SJPD, crosstalk is quite similar for n^+/p compared to n/p configurations (Brouk et al., p. 18). Recombination-increasing p^+ structures on either side of the n^+ wells (Brouk et al., p. 17) may be the reason for the slightly better reduction in crosstalk, a reduction that is counteracted by the presence of the n^+ well; a reduction possibly more noticeable if it had been used with an n- well instead of an n^+ well. However Brouk et al (2002) does not consider highly doped p-wells, as deep trench isolation, that could contribute to crosstalk reduction.

Brouk et al., (2002) demonstrates that crosstalk is more reduced in double junction structures compared to single junction devices. In the $p^+/n/p$ DJPD, the added electric field of the inner shallow p^+/n junction, drives minority carriers away from the outer, deeper n/p photocarrier collection junction, to be recombined in the silicon substrate bulk region. Noted also is the fact that as the photodiode pitch increases the crosstalk reduces.

The pixel response parameter, quantum efficiency (QE), is a measure of the number of captured photocarriers per photon of incident light. To compare the pixel QE for illumination at the boundary of the pixel (a nominal measure of crosstalk) the QEs are normalized (NQE). The crosstalk NQE is the quotient of the QE response for illumination at the pixel boundary and the Maximum QE for a particular pixel. This is a relative measure of crosstalk. Device structures or configuration parameter changes in the pixel that reduce crosstalk will reduce the crosstalk NQE.

Increasing the pixel's sensitivity without increasing the boundary QE response can lower the relative crosstalk NQE. Increasing the sensitivity can be achieved by increasing the pixel maximum QE. Furumiya et al., (2001, p 2221) uses a deep p-well in a FW DJPD configuration, with p on p^+ substrate and anti-reflective film /

double photo shield, to increase the maximum QE. This increases the sensitivity by 110% for 550 nm light and gives a conversion gain of 30 $\mu V/e^-$ and 1 % crosstalk.

Though it may be possible to use photo shielding in BW configurations, it is not the priority of this present research to investigate crosstalk-reducing ***surface*** structures, which has been studied for FW configurations. Rather, at this time, the priority is to study different ***sub-surface*** configurations that have benefits to response resolution and crosstalk reduction.

Some studies have demonstrated crosstalk-reducing benefits for FW pixel configurations that may also be beneficial for BW configurations. Kang (2002) investigates a 2D device simulation of a pinned (i.e. DJPD) photodiode array (Figure 2.1). Pinning is simply applying a reverse bias across the two junctions of a DJPD such that both depletion regions (SCR) extend into the outer well volume to the point where they meet, thus pinning the voltage and making the intervening layer completely depleted. Thus the entire outer well is depleted (n-well in PNP or p-well in NPN DJPD) and is available for carrier separation and capture, increasing sensitivity and maximum QE. This contributes to other mechanisms that add to give a substantial reduction in crosstalk over the conventional photodiode.

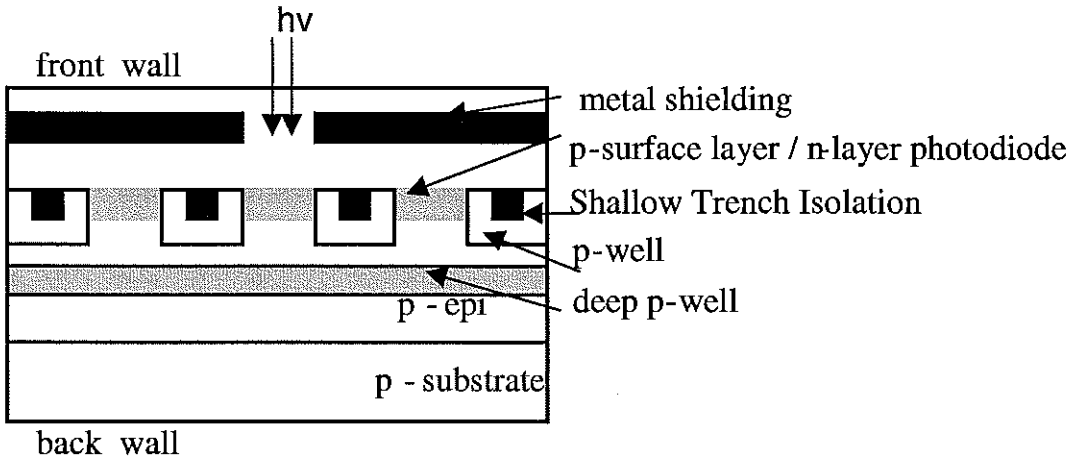

Figure 2.1 FW pinned PD with p-well shroud and deep p-well. (Kang, 2002 p2)

In this Pinned photodiode (PPD), Shallow Trench Isolation (STI) is required to reduce the device area. It is shrouded in p-well to decrease the dark current, not primarily to decrease the pixel crosstalk (Kang, 2002 p2). This brings up an

important point that crosstalk is not the only noise source for PSU arrays. Though a particular BW configuration may reduce crosstalk, sources of other noise need to be investigated such as dark or reverse saturation current. However this project only investigates crosstalk.

Light towards the near ***ultraviolet*** penetrated insufficiently, with the resulting absence of minority carriers to cause crosstalk. This will also happen in BW configurations resulting in reduced sensitivity for shallow junction depth pixels, where the SCR is beyond the penetration depth of the incident wavelength (Hinckley et al, 2002). For FW and BW pixels, light towards the near ***infrared*** penetrated deeper into silicon, producing minority carriers in the p-substrate and p-epi-layer. The minority carriers originating in the p-epi-layer caused the crosstalk problem. For the FW pixel in Figure 2.1, recombination in the deep p-well, situated in the p-substrate prevented minority carriers, produced in the p-substrate, contributing to crosstalk (Kang, 2002 p2). Furthermore, the thicker the deep p-well, the less the crosstalk, especially for light towards the near Infrared. However this is not a structure that can be used to improve BW pixel response resolution due to it acting to also reduce sensitivity.

The p-well that shrouds the STI reduces minority carrier diffusion also, as carrier recombination is increased in the p-well. Thus carriers generated in the region between the STI and n-well in the photodiode mostly recombined in the p-well shroud, reducing crosstalk. However the effect on crosstalk of the p-well shroud was subtler than for the deep p-well. If the p-well shroud extended more deeply into the substrate maybe crosstalk reduction would be less subtle. This is a point of investigation in our present research. Finally, crosstalk variation for different distances between pixels was not significantly different, with the maximum variation of half a percent in crosstalk, for FW light towards the near infrared (Kang, 2002).

Lulé et al., (2000) demonstrates the merits of the FW ***Thin-film-on-ASIC (TFA)*** with respect to sensitivity and limits of scaling exceeds all other competing devices including both FW SJPD, FW Photo gate, FW pinned DJPD and charge-coupled device (CCD). This is encouraging for the present investigation as BW pixels, with

their electrodes on the opposite side of the illuminated face, lends itself to the 3D configuration of TFA.

Furthermore the present investigation focuses on SJPD and DJPD architectures of which the Pinned PD (PPD), the next best image sensor (Lulé et al., 2000) is a member. One extrapolation that one might suggest from Lulé et al. findings is that any investigation into elucidating the optimum image sensor architecture should explore a configuration that possesses the advantages of both the PPD and TFA. In this case the thin film is the PPD or a more optimum double junction structure backwall illuminated in a TFA configuration. However the recombination and generation models that have been defined for the simulations in this project do not include Auger recombination, which may arise for such fully depleted pixel configurations. Future investigations will address the benefits of fully depleted pixel configurations for enhancing response resolution and eliminating crosstalk.

Noting the exhaustive research by Lulé et al., the sensitivity, scaling limitations and other advantages or disadvantages of each FW pixel configuration is stated below as a necessary comparison to the present investigations associated with BW PSU configurations.

2.3 Pixel Sensitivity Characteristics and FW Pixels Compared.

In an investigation of crosstalk it is important not to forget the effect that a crosstalk-beneficial change in the PSU's configuration may have on sensitivity and visa versa. It is therefore important to be aware of how present PSU configurations compare to each other's sensitivity. A pixel response of zero crosstalk but a 100-fold reduction in sensitivity is a pixel with great crosstalk reduction but poor response resolution.

Sensitivity is used to characterise image sensors. It is a measure of the efficiency of the conversion of Electro-magnetic Radiation (EMR) into electrical information. The quantum efficiency (QE) is used as the primary photodetector transfer characteristic. It is obtained from the spectral response SR(λ) which is the ratio of the photo current

recorded at the photo sensor unit's (PSU) electrode and the power of the incident wavelength. The QE is then the product of SR(λ) and a ratio of the present energy of one incident photon and the present value of the electronic charge i.e. the energy of the incident light expressed in eV. (Lulé et al., 2000,p2111)

The collected photocharge Q, given that the photo sensing unit is irradiated with a spectral power density Φ(λ) (W/cm^{2}nm), (Lulé et al., 2000 p 2111) is expressed as

$$Q = A_{eff} * T_{int} * \int SR(\lambda) * \Phi(\lambda) * d\lambda \qquad [2\text{-}1]$$

Where t_{int} is the integration time and A_{eff} is the effective photoactive area of the photo-sensing unit (PSU) and illumination is constant. Here $A_{eff} = FF * A_{pix}$, where FF is the fill factor, which is the portion of the PSU which contributes to photosensitivity, and A_{pix} is the PSU surface area.

The Voltage change, V, that results from the collected photo-generated charge is inversely proportional to the integration capacitance (C_{int}) such that

$$V = \frac{Q}{C_{int}} = \frac{FF * A_{pix} * T_{int}}{C_{int}} * \int SR(\lambda) * \Phi(\lambda) * d\lambda \qquad [2\text{-}2]$$

Sensitivity refers to the input and output response of the pixel not to amplification by associated devices incorporated in the PSU. Any monolithic PSU integrated circuitry producing gain, reduces FF unlike TFA type PSU (Lulé et al., p2111).

The pixel sensitivity is obtained by dividing the optical energy incident on the pixel during the integration time into the integrated photo-voltage as follows,

$$S_w = \frac{FF * A_{pix} * \int SR(\lambda) * \Phi(\lambda) * d\lambda}{C_{int} * \int \Phi(\lambda) * d\lambda} \qquad [2\text{-}3]$$

This is the radiometric sensitivity (V/(μ J/cm^2)). Integration occurs over the wavelengths where SR(λ) is not zero. It does not overestimate the sensitivity as does the photometric sensitivity for CMOS sensors with significant infrared QE. (Lulé et al., p2112)

Lulé et al.(2000, p2112) calculate the spectrally resolved sensitivity for the RGB colour channels of a PPD imager with 7.8 μ m pitch and that of a colour filter array TFA with 7.0 μ m pitch. These results show that TFA, which uses amorphous -Si:H based detector, is more sensitive below 700 nm while the PPD using crystalline Silicon is more sensitive above 700 nm.

2.3.1 **Standard Photodiode Imagers.**

In the Standard Photodiode (PD) pixel (vertical SJPD), all carriers photogenerated in the space charge region (SCR) are collected. Deep substrate minority carriers can diffuse, due to the concentration gradient, to the SCR and also be accumulated. For PD imagers with bulk PD, the use of vertical overflow drains, like for current CCD sensors, though reducing crosstalk, do not allow the diffusion of carriers from the bulk to the SCR of the PD, thus reducing the red and IR sensitivity. Though crosstalk is reduced the sensitivity is also reduced. Comparisons that investigate crosstalk and sensitivity need to make use of the Normalized QE which is the ratio of the QE associated with the PSU crosstalk response to the PSU maximum QE. Loss of sensitivity is not necessarily a problem if suitably configured, noise reduced, amplification circuitry is utilized. (E.g. TFA configuration). (Lulé et al,. p2113).

Typically, for a 14 μ m pitch FW pixel in a 0.8 μ process with 60 % fill factor (FF), the PD contributes 93 fF to the total integration capacitance of 102 fF, equivalent to only 1.6 μ V/e$^-$ conversion gain. Its sensitivity is only 1. 8 V/(μ J/cm^2). The use of micro lenses on pixels with small PSE may lead to acceptable sensitivities (Lulé et al., p2113).

2.3.2 **Photogate Imagers.**

The Photogate imager removes the problem of large capacitance. CCDs operate in the same way concerning integration, transport and readout inside each pixel. During integration, the photo charge is accumulated in the potential well under the Photogate. The rest of the photosensitive area, a small portion of the total area, including the transmission gate and the floating diffusion, contributes to the charge-to-voltage conversion capacitance, which is why it is small (3.6 fF) equivalent to a large $44\,\mu V/e^-$ conversion gain, allowing for a high sensitivity. Additionally correlated double sampling (CDS), including subtraction of kTC (thermal) noise (large for small capacitance : 1 mV for 3.6 fF) is permitted by this reset-transfer-readout operation of the Photogate imager (Lulé et al., 2000 p2114).

One draw is the low transparency of polysilicon, which is 22% at 500 nm, decreasing further for shorter wavelengths. This results in the large conversion gain being largely lost, due to the intensity lost in the overlying polysilicon gate material. Increasing the photogate size, increases sensitivity but reduces resolution. Standard size pixels of $16\,\mu$m pitch in 0.8 μ CMOS process achieve 10.32 $V/(\mu J/cm^2)$ or 4 V/lxs (Lulé et al., p2114).

2.3.3 **Pinned Photodiode Imagers.**

Replacing the MOS varactor in CCDs, the pinned photodiode (PPD) was developed as a reduced dark-current (I_D) detector and has been used successfully in CMOS pixels also. Its operation is as follows,

> "The PPD basically consists of a p^+np^-structure where both p layers are on substrate potential (GND). As the voltage applied to the n-layer is increased, the depletion regions of both pn-junctions grow towards each other. At...the pinned voltage V_p, the depletion regions meet and no more majority carriers can be extracted from the device. The device is fully depleted...the potential can not be increased any further. The voltage is pinned".
>
> (Lulé et al., p2114).

The PPD is fully depleted initially for light sensing. The PPD potential reduces below V_p during the integration phase, when photogenerated majority carriers are stored in the SCR. First the floating diffusion (FD) is reset to a given potential, which may be read out for true correlated double sampling. Next the transfer gate is opened and the photo charge is completely transferred to FD, whose voltage needs to be above V_p to effect total transfer, while the PPD operates below V_p (Lulé et al., 2000 p2115).

The complete transfer of charge from a large capacitance diode into the small floating diode capacitance results in a large charge-to-voltage conversion gain which translates into sensitivity enhancement. Microlensing enhances this further to give a sensitivity yield of 5.5 V/(μ J/cm^2) (Lulé et al., p2115).

Another advantage is that the charge collection region is separated from the surface into the depths of the pixel through the p^+ region, like a CCD buried channel. A reduction in I_D and white point defects results from the pinning of the surface that has a high density of recombination centres. (Lulé et al., p2115).

The depth and doping of the three regions can vary for a given target V_p, which becomes strongly dependent (V_p) on the n-depth for higher doping, especially the doping of the n well. To ensure satisfactory operation above and below V_p, the depth and doping needs to be tightly controlled. Also complexity and cost is added to the CMOS process because large scale or twin well processes are needed to establish the needed moderately doped p-layer so that the other higher doped levels can be superimposed. However if the market demand is such that the cost for the extra mask steps is insignificant, this fact of added cost and complexity is no road block, as Motorola has shown (Lulé et al., p2115).

PPD is advantaged over the Photogate as it has a higher QE, requires less control signal wiring and, due to surface pinning, has reduced I_D and white point defects, all of which translates into higher sensitivity. It however has to be adapted to each new

process generation. (Lulé et al., p2115). Unpinned DJPD may still exhibit comparable sensitivity to the PPD.

2.3.4 **Thin Film on Application Specific Integrated Circuit (TFA).**

The PD pixel is deposited on the ASIC to give a FF of 100%. The PD consists of a rear electrode on an a-Si:H diode and a transparent conductive oxide (TCO) front electrode. There are no layers on top of the PD to reduce light penetration. The TCO thickness is optimized to minimize reflection losses. QE is 60% for most of the visible range; equivalent to 1 fA / μ m ^{2} diode area at 1 lx daylight illumination (1 lx = 1.46 fW/ μ m ^{2} or 0.146 μ W/cm^2 at 555 nm) (Lulé et al., 2000 p2115).

Lulé et al., (p2115) relates an example of a colour sensor that has been engineered in TFA technology where the PSU consists of three colour specific PDs, each detecting one of each of the three primary colours. This is not unique as studies on BW SJPD pixels have also demonstrated spectral range specificity, using crystalline Silicon, not amorphous-Si:H. Hinckley, Gluszak & Eshraghian (2000) show that for a BW vertical SJPD pixel, wavelength sensitivity is dependent on junction depth and substrate thickness. FW pixels of similar configuration showed only marginal dependence of wavelength sensitivity on thickness and junction depth. In the BW case, as the junction depth increased from 1 to 10μm, for a 12 μm substrate thickness, the wavelength sensitivity peak blue shifted (0.7 to 0.4μm). As the pixel thickness increased from 3 to 13μm, the wavelength sensitivity peak red shifted (0.4 to 0.8μm). The conclusion being that by adjusting the thickness and junction depth of the BW vertical SJPD, the pixels may be tailored to a specific spectral range. However the crosstalk is a problem for this BW pixel configuration, hence this project.

A typical TFA sensor in 0.8 μ m CMOS technology, with pixel pitch 10 μ m has a sensitivity of 8 V/(μ J/cm^2) or 3.1 V/lxs which, though lower than the Photogate, has a resolution 2.5 times that of the Photogate pixel (Lulé et al., p2115).

For the TFA, lowering the capacitance can increase the sensitivity. This can be achieved by increasing the thickness of the intrinsic layer or by reducing the area of the rear electrode. However I_D will increase with thickness of the intrinsic layer, so the electrode area reduction is the best option as long as the electric field exceeds around 5 kV/cm. The use of ring shaped rear electrodes, providing good collection and capacitance reduction, has been suggested (Lulé et al., 2000 p2115).

2.4 The Effect of Scaling On Pixel Sensitivity.

It is important to consider the background literature in this area as the project at hand is seeking to eliminate the problem of electrical crosstalk, which increases with pixel down sizing. This increase is due to the pixels in the array being closer together and thus minority carriers, generated in the bulk, have shorter distances to diffuse to adjacent pixels and so contribute to crosstalk. This has been shown to be more the case for SJPD configurations. (Briaire & Krisch, 2000)

Decrease in pixel pitch below $5\,\mu$m is not warranted as this represents the limit of camera lens diffraction or resolution limit. However with the advent of colour specific pixels one APS will include more than one pixel: the Bayer patterned RGB colour sensor has $2\,\mu$m pixel pitch (Lulé et al., p2116). Thus this is the limit of pixel pitch for which crosstalk reduction should be focused.

Table 2.1 shows the technological parameters for different process generation. As the doping increases, the mobility, lifetime and diffusion length of carriers will decrease. This is necessary for pixels to decrease in size without a corresponding substrate originated minority carrier crosstalk. However this increase in physical resolution will introduce other types of noise: I_D generating shot noise, hot-carrier effects, transistor off current, gate oxide leakage, PN junction tunneling leakage (SCR widths are narrower), kTC noise caused by the decrease in integration capacitance (Lulé et al., p2116). A number of these problems would be eliminated with BW imaging chip as the image signal processing circuitry is removed to another chip environment.

For FW pixels, to eliminate kTC and 1/f noise, real correlated double sampling (CDS) will become necessary. In other PSU, such as TFA, where CDS is not available, weak reset or active reset circuitry per PSU, can be used with certain limitations. (Lulé et al., p2116).

Table 2.1 Process Generation Technology parameters.

Process (μm)	0.8	0.5	0.35	0.25	0.18	0.1
Supply Voltage (V)	5 – 3.3	5 – 3.3	5 – 3.3	2.5 – 1.8	1.8 – 1.5	1.2 – 0.9
Interconnect levels	2	2 - 3	4 - 5	5 - 6	6 - 7	8 - 9
Substrate Doping (cm^{-3})	$8x10^{16}$	$1.2x10^{17}$	$2.5x10^{17}$	$3.4x10^{17}$	$5x10^{17}$	$1x10^{18}$
Junction depth - D/S (nm)	350 - 450	300 - 400	200 - 300	50 - 100	36 - 72	20 - 40
Depletion Region (μm)	0.71	0.57	0.39	0.24	0.19	0.1
Mobility (cm^2/Vs)	825	715	550	485	425	345
Carrier life time (μs)	3.6	2.3	1.1	0.8	0.6	0.3
Diffusion Length (μm)	88	68	41	33	25	15

Thus there are other sources of noise other than electrical crosstalk that need to be addressed when down sizing both photo sensing unit (PSU) and pixel.

The scaling trend of doping-increase, decreasing mobility, lifetime and diffusion length of carriers, has a beneficial effect on the diffusion collection efficiency, improving performance for visible light applications (Lulé et al., p2117).

Table 2.2 shows the effect on sensitivity and other important CMOS pixel parameters, of reducing pixel pitch, for Standard PD (std), PPD (ppd), TFA (tfa) and a TFA sensor with minimum rear electrode (min) (Lulé et al., p2118).

Table 2.2 Scaling trends of CMOS pixel parameters.

Techno – logy	0.8 μm			0.35 μm			0.25 μm			0.18 μm					
Sensor type	std	ppd	tfa	std	ppd	tfa	std	ppd	tfa	std	ppd	tfa	min	ppd	tfa
Area of pixel (μm^2)	14 x 14	14 x 14	14 x 14	7 x 7	7 x 7	7 x 7	5 x 5	5 x 5	5 x 5	5 x 5	5 x 5	5 x 5	5 x 5	3 x 3	3 x 3
FF (%)	60	60	100	60	60	100	60	60	100	80	80	100	100	44	100
Area of PSE (μm^2)	118	118	196	29	29	49	15	15	25	20	20	25	25	4	9
$C_{diffusion}$ (fF)	5.75	7.19	5.75	2.7	3.4	2.7	1.87	2.14	1.87	0.65	0.83	0.65	0.65	0.83	0.65
C_{gate} (fF)	2.06	2.06	2.06	1.1	1.1	1.1	0.67	0.67	0.67	0.45	0.48	0.48	0.48	0.48	0.48
$C_{parasitic}$ (fF)	1.0	1.0	NA	0.6	0.6	NA	0.6	0.6	NA	0.5	0.5	NA	NA	0.5	NA
C_{diode} (fF)	93.4	NA	12	37.2	NA	4.3	37.7	NA	2.5	23.7	NA	2.5	1.0	NA	~1.6
$C_{integration}$ i.e. C_{DF} (fF)	102	10.3	19.8	41.6	5.1	8.1	40.8	3.41	5.0	25.3	1.81	3.6	2.13	1.81	2.73
q/C (μV/e)	1.5	15.5	8.1	3.8	31.4	19.8	3.9	46.9	32.0	6.4	89.0	45.0	75.0	89.0	59.0
S : V/ ($\mu J/cm^2$)	1.8	17.7	23.2	1.1	8.9	14.2	1.57	6.8	11.9	1.2	17.1	16.3	27.3	3.4	7.7

For these imagers, as the technology reduces, the integration capacitance and the sensitivity decrease as the above table demonstrates. This is another reason why investigating pixel configurations that reduce electrical crosstalk become even more critical as the pixel architecture shrinks. So the later is increasing while the sensitivity (i.e. maximum QE) is decreasing which leads to an even more inflated Normalized crosstalk QE.

Lulé et al., (2000, p2119) clearly highlights the advantages of the TFA configuration over the other FW CMOS pixels,

> "While scaling effects that increase leakage current or reduce dynamic range affect c-Si and a-Si:H equally, only TFA imagers are immune against negative scaling impacts on sensitivity such as salicidation or SOI. Special process enhancements are necessary to keep sensitivity of c-Si detectors acceptable under scaling. For PPD image modules, salicidation blocking, implantation and microlenses are necessary. These process modules need to be adapted to every new process generation while the TFA backend process is ... adaptable to any new chip generation with ... fine tuning. In the future, the sensitivity of all investigated imager types will diminish with scaling since the photoactive region shrinks very quickly. If pixel size is always shrunk with the feature sizes, then TFA will remain to be the best option of the technologies known in literature today with regard to sensitivity.".

This is encouraging to note because this investigation is aimed at exploring various BW pixel, which is a configuration ably suited for TFA orientation. The difference is that doped crystalline Silicon rather than amorphous Si:H is used as the device material under simulated investigation.

Considering that the bulk of current research is focused on FW pixel sensitivity improvements with very little dedicated research on crosstalk suppression and response resolution optimization for BW SJPD and DJPD pixels it is clear that an investigation of the kind that is now being undertaken is way overdue.

3. THEORY

This section introduces in the first part, the general theory of semiconductor physics that relates to the operation of the Photodiode and the development of the equations used in simulating the device response to incident light. In the second part of this section, the theory and equations associated with absorption volume proportion (AVP) is considered and developed. This is an important statistic, as it is used in the results to understand the simulated electrical response of the device under investigation.

3.1 The Physics of Semiconductor Devices

To understand the electrical dynamics of the photodiode, the device under investigation, and the equations used in simulating the device response to incident light, it is important to appreciate some basic concepts in solid state physics and then develop the equations associate with the carrier dynamics.

3.1.1 The Band Structure of Solids.

There are three types of electronically defined solids that are considered at present in the study of solid state physics: conductors, insulators and semiconductors. Their electrical behavior is determined by the degrees their valance and conduction bands are separated energetically. This band of multiple energy level splitting occurs in atomic lattices because when atoms are brought close together, their electronic energy wave functions overlap, splitting the possible energy levels that are available. In a many atom crystal lattice this splitting is so extensive the valence and conduction energy shells appear as ***bands***. The energy gap between the top of the valence band and the bottom of the conduction band is called the band gap, E_g (Figure 3.1).

For insulators this band gap is relatively large and the bands are "far apart". Therefore, the chance of valance band electrons being promoted to the energetically distant conduction band is very low and so their conductivity is relatively insignificant. For conductors the bands overlap so their conductivity is relatively large. Semiconductors have their band gap relatively close so that changes in temperature, optical excitation and impurity content can cause their conductivity to vary by many orders of magnitude. Figure 3.1 shows the typical band structure of different solids above zero K. Figure 3.1a occurs in one-valence electron atoms such as Cu, Au and Ag. Conducting materials also have the bands overlapping as in Figure 3.1b, especially for metals with two valence electrons. There is no conduction in Figure 3.1d, which is typical of insulators. For Figure 3.1c, at a given temperature or steady state energy supply an equilibrium concentration of electrons exist in the conduction band. This is characteristic of semiconductors.

Semiconductors can be either elemental or compound. Elemental semiconductors consist of a single species of atom and are found in column IV of the periodic table: silicon or germanium. Compound semiconductors consist of more than one atomic species from columns in the periodic table symmetrically either side of group IV elemental column. The device that this investigation simulates uses the elemental semiconductor, silicon.

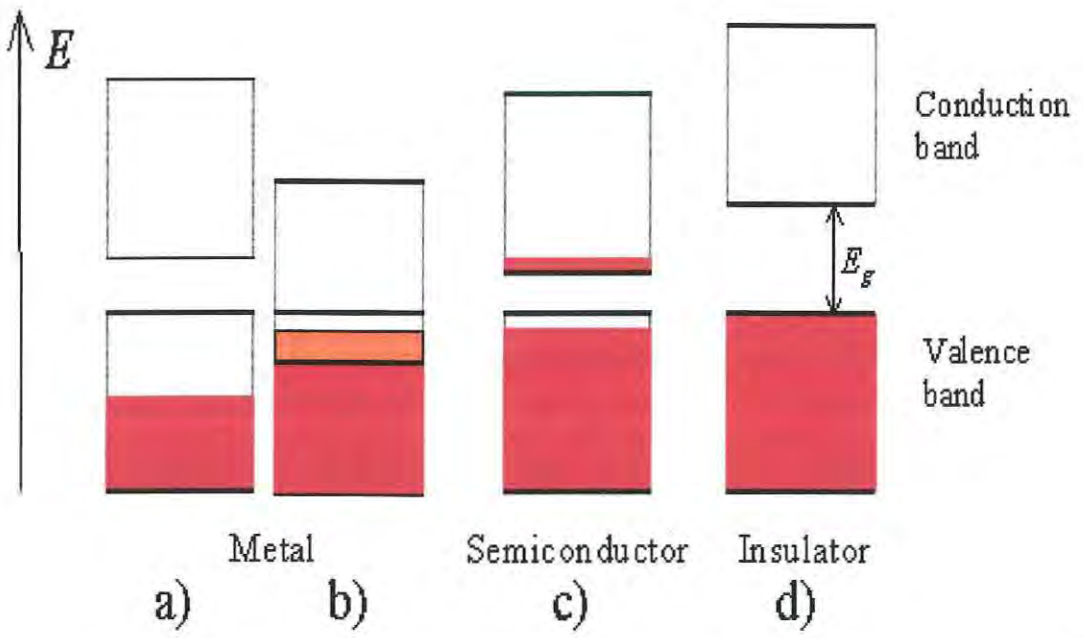

Figure 3.1 Energy band diagrams of different solids. (Van Zeghbroek 2002).

3.1.2 **Intrinsic Semiconductors.**

The present solid state knowledge of semiconductors can demonstrate two types of semiconductor: intrinsic and extrinsic.

All semiconductors at absolute zero generally do not conduct as all valance electrons occupy the highest most quantum energy state associated with each atom in the crystal lattice, the valence band. As energy is imparted to the crystal lattice (as light) of energy greater than the energy gap between the valence and conduction bands (E_g) some valence electrons absorb the energy and are promoted to the conduction band. This leaves a vacancy, a positive "***hole***", in the valence shell associated with the host atom. Thus this absorption process generates "***electron-hole pairs***" (EHP). Hole energies increase downward through the conduction and valance bands while the reverse is the case for the electron energies.

For a particular steady supplied energy state the rate of EHP generation and the rate of recombination are a constant such that an equilibrium population of electrons (n_0) and holes (p_0) are continuously available, zero at zero K. For example, in an intrinsic semiconductor, n_0 and p_0 are 1.5×10^{10} cm^{-3} at 300 K (room temperature), also known as the intrinsic carrier concentration, n_i. This is much less than the silicon atom density of 5×10^{22} cm^{-3}. Thus the few electrons in the conduction band are free to move about via the many available empty states.

3.1.3 **Extrinsic Semiconductors.**

Extrinsic semiconductors are intrinsic semiconductors that have had other atomic species introduced to their crystal lattice causing additional levels being created in the intrinsic species' energy band structure, usually within the band gap (the gap between the semiconductor bands in Figure 3.1). The choice of doping species result in the production of either n-type or p-type doped extrinsic semiconductor.

In the ***n-type*** semiconductor, there is a surplus of electrons as the doping atoms have more valence electrons than the host atoms. Hence they are donor species, donating electrons to the lattice structure. Their donor doping concentration is N_D and their introduced energy levels are in the band gap, closer to the conduction band than the valance band. In the ***p-type*** there is a surplus of holes as the dopant has less valence electrons than the host atoms. Hence they are acceptor species accepting electrons. Their acceptor doping concentration is N_A and their introduced energy levels are in the band gap, closer to the valence band. The donor and acceptor species used in the simulations are Arsenic (As) and Boron (B) respectively.

The equilibrium electron (n_0) and hole (p_0) concentrations are now raised above the intrinsic equilibrium carrier concentrations (n_i). They are related to N_D and N_A by the law of mass action in the following way if N_D or N_A are $>> n_i$.

$$(n_0) \cdot (p_0) = (n_i)^2 \qquad [3\text{-}1]$$

If $p_0 >> n_i$ then $p_0 = N_A$, and if $n_0 >> n_i$ then $n_0 = N_D$.

In the simulations n-type and p-type material of 10^{17} and 10^{15} cm^{-3} doping, respectively, are used. In the n-type semiconductor, the electron is the ***majority*** carrier with an equilibrium concentration equivalent to the Arsenic doping concentration of 10^{17} cm^{-3}. From Equation [3-1], the equilibrium ***minority*** hole concentration will be only 2,250 cm^{-3}. Similarly for the p-type semiconductor, the minority electron concentration is calculated still very low at 225,000 cm^{-3}. Hence the terms minority and majority carriers are used. Thus for any EHP generating process, which produces equal carrier concentrations, the excess minority carrier concentration will be noticed far more compared to its thermal equilibrium concentration than the excess in the majority carrier population. The latter is usually still less than its thermal equilibrium carrier population.

3.1.4 **Carrier Generation Processes.**

As this investigation is concerned with light detecting semiconductor devices, one generation process that is particularly applicable is ***light absorption carrier generation*** (Figure 3.2). If the incident light is of energy greater than the band gap an EHP is produced, the electron and hole absorbing the photon energy as kinetic energy. For ionization caused by high energy beams, multiple EHP are produced whose number is proportional to the energy of the particle (Figure 3.2)

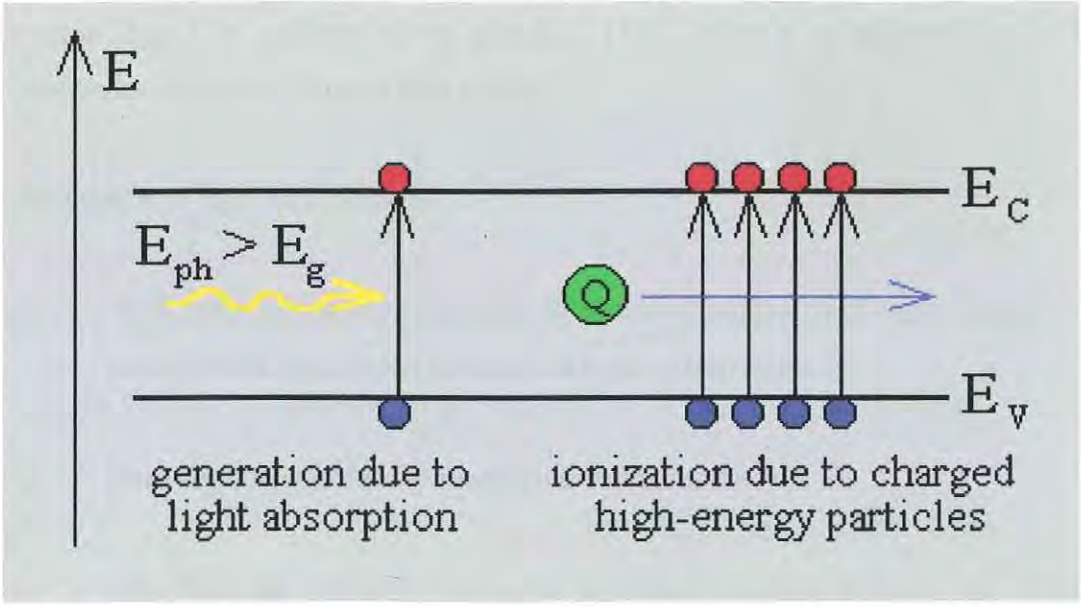

Figure 3.2 Carrier generation due to photogeneration and ionization by high-energy particle beams (Van Zeghbroek 2002).

For light travelling through a medium, such as a semiconductor, the photon attenuation through the medium decays exponentially. The rate of decay of intensity at a particular depth in the medium, is proportional to the intensity of the EMR at that depth. The proportionality constant for this function is called the ***absorption coefficient (α)*** and its relationship to the absorbed light intensity (I(x)) at a particular penetration depth (x) is given by

$$I(x) = I_0 \exp\{-\alpha x\} \qquad [3\text{-}2]$$

Electromagnetic radiation (EMR) travelling through a medium, such as a semiconductor, can be described more generally by Maxwell's equations which show

that the waves have a form given by the electric field vector dependence (Singh 1994, p 158),

$$F = F_0 \exp\{i\omega [(n_r/c) - t] \} \exp(-\alpha z/2) \qquad [3\text{-}3]$$

Here, z is the propagation direction, ω is the light frequency, n_r is the refractive index, and, α is the absorption coefficient of the medium. If α is zero, the wave propagates without attenuation with a velocity c/n_r However for non-zero α, the photon flux I is represented by Equation [3-2] where z is replaced by x, the penetration distance. (Singh 1994, p 158)

Absorption of light may occur as :

a) Intra-band absorption by valence electrons promoting them to the higher energy band, usually the conduction band or trap states.

b) Intra-band absorption by conduction band electrons.

c) Inter-band absorption by carriers in trap states occurring between the valence and conduction bands. This occurs with extrinsic materials.

In Silicon the absorption coefficient, governing the way light is absorbed for different wavelength of light (λ), has been shown (Melchior 1972) to be

$$\text{Log } \alpha = 13.2131 - 36.7985(\lambda) + 48.1893\ (\lambda)^2 - 22.7562\ (\lambda)^3 \qquad [3\text{-}4]$$

Equation [3-4] is used to generate the absorption coefficient for light at 633 nm, which is used in the simulations in this project. Equation [3-4] gives an absorption coefficient of 0.2323 μm^{-1} for a wavelength of 633 nm.

Figure 3.3 shows the variation in penetration depth with variation in incident light wavelength for silicon, generated from Equation [3-4].

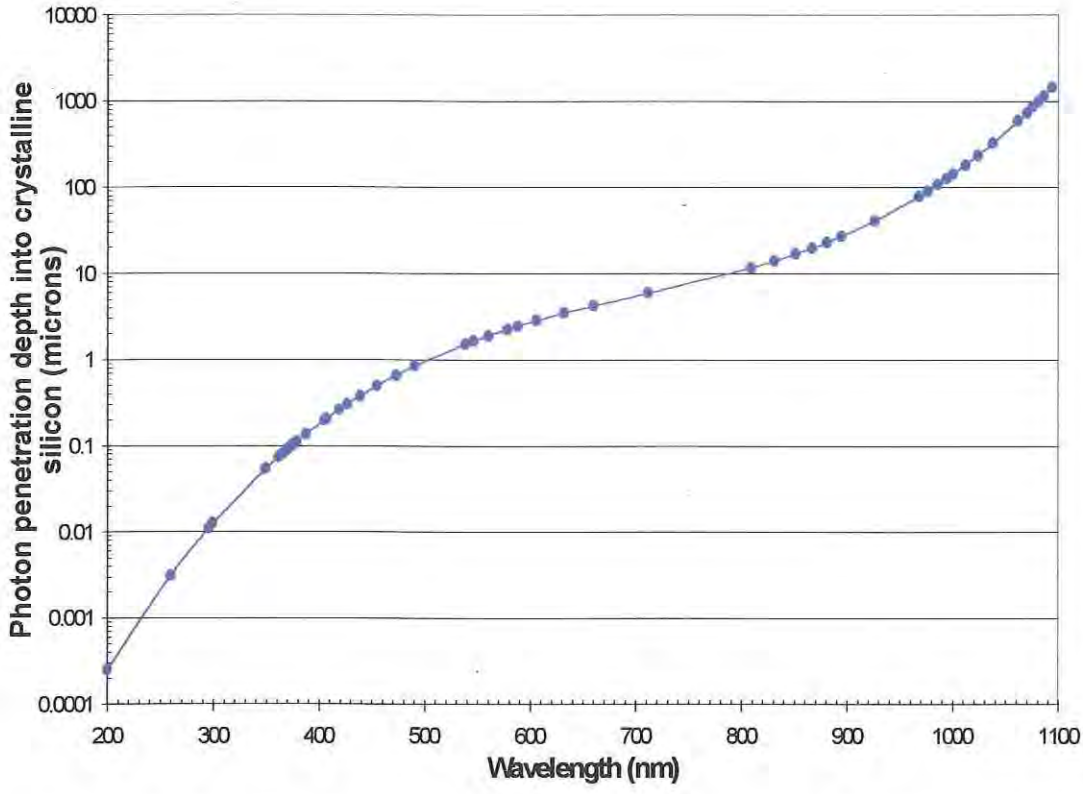

Figure 3.3 Photon penetration depth into c-Si vs wavelength (Melchior 1972).

The Absorption Volume is the "volume" of light energy absorbed in a given volume (3D), cross section (2D) or linear distance (1D) of an absorbing medium, such as a semiconductor. The Absorption Volume Proportion (AVP) is that proportion of the incident light that is absorbed in a given geometric region of the semiconductor. It may be expressed as a percentage. The AVP formulae to calculate the AVP for particular regions in the simulated device, based on Equation [3-2], are given in section 3.2. The development of these formulae are presented in Appendix XX.

In photogeneration, assuming that each absorbed photon creates one electron-hole pair, the electron and hole generation rates are given by Equation [3-5], where α is the absorption coefficient of the material for the given photon energy of in the incoming photon and P(x) is the illumination intensity, q is the electronic charge, λ is the wavelength, h is planck's constant, c is the current determined speed of light in a vacuum, and A is the area of illumination

$$G_p,\text{light} = G_n,\text{light} = \alpha.\frac{q\lambda P(x)}{hcA} \qquad [3\text{-}5]$$

Impact ionization , another generation process, can be caused by an electron or hole, with energy much larger or much smaller than the conduction or valance band edge, respectively (Figure 3.4). This is the counterpart of Auger recombination described below. The excess energy is given off to generate an EHP through a band-to-band transition. Both electrons and holes can cause avalanche multiplication in semiconductor diodes under high reverse bias in this way. Though the simulated photodiode in this investigation is necessarily reverse biased, the levels are not significant enough for impact ionization to be factored into the simulation's generation-recombination model parameters.

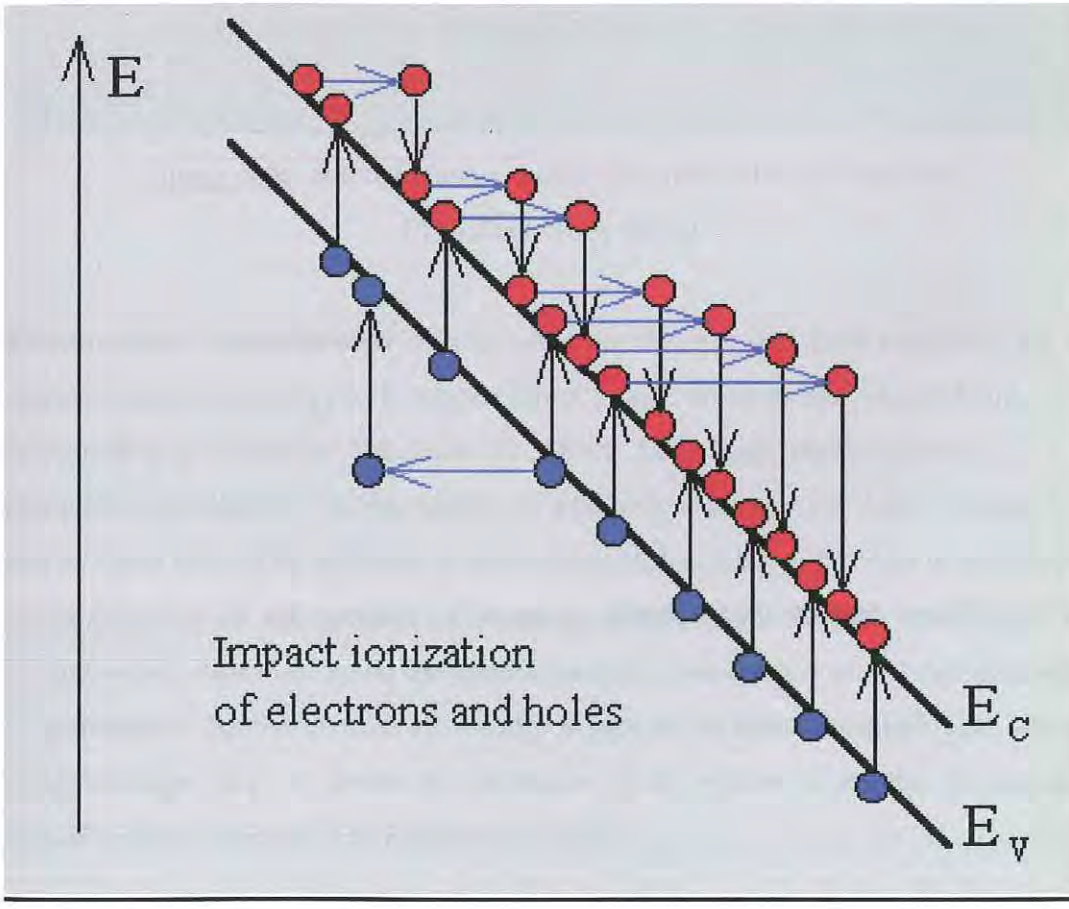

Figure 3.4 Impact ionization and avalanche multiplication of carriers influenced by a large EMF (Van Zeghbroek 2002).

3.1.5 **Carrier Recombination Processes.**

After generation, carriers last for a certain time called their carrier lifetime, and then recombine. Figure 3.5 shows a number of possible modes of recombination.

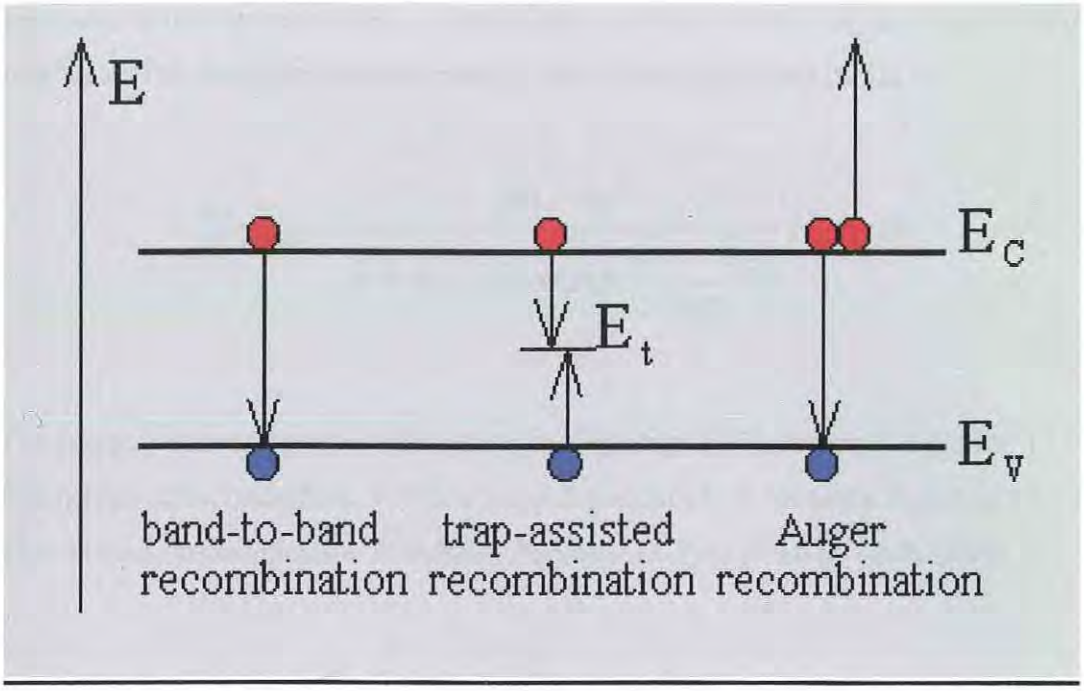

Figure 3.5: Semiconductor, carrier recombination mechanisms. (Van Zeghbroek 2002).

Band-to-band recombination occurs when an electron and hole annihilate by the electron giving up energy as it relaxes directly back down to the valence band. This is typically a radiative transition in direct band gap semiconductors. This recombination depends on the density of available electrons and holes. Since both carrier types need to be available in the recombination process, the rate is expected to be proportional to the product of n and p. However in thermal equilibrium the recombination rate must equal the generation rate since there is no net recombination or generation. As the product of n and p equals n_i^2 in thermal equilibrium, the net recombination rate is given by Equation [3-6] where b is the bimolecular recombination constant (Van Zeghbroek 2002).

$$U_{b-b} = b(np - n_i^2) \qquad [3\text{-}6]$$

Trap-assisted recombination or Shockley-Read-Hall (SRH) recombination occurs when the transition from the conduction to the valance band occurs via a "trap state" in the band gap. The presence of a doping species in extrinsic semiconductors or a

structural defect can cause this. Annihilation can occur in the valance band or in the trap-state. The net recombination rate for SRH (Van Zeghbroek 2002) is

$$U_{SHR} = \frac{pn - n_i^2}{p + n + 2n_i \cosh(\frac{E_i - E_t}{kT})} N_t v_{th} \sigma \qquad [3\text{-}7]$$

For p-type semiconductors, where p >> n, Equation [3-7] becomes Equation [3-9]. For n-type semiconductors, where n >> p Equation [3-7] becomes Equation [3-10]. The minority recombination lifetime in Equation [3-7] is given by (ibid. 2002)

$$\tau = \frac{1}{N_t v_{th} \sigma} \qquad [3\text{-}8]$$

SRH recombination is included in the simulation model used in this project.

Auger recombination is a non-radiative band-to-band transition, where the energy loss is given away to generate another EHP. It is the main recombination process for devices with extremely high carrier concentrations due to high carrier injection due to high excitation levels and high doping levels. The process involves three particles and thus scales with the third power of the carrier densities (Nextnano3 2003). This mode of recombination at high excitation energies can be radiative or non-radiative (IOFFE 2003). This recombination is a possible simulation configuration parameter that could have been included in this investigation. However for the doping, biasing and photon-excitation regimes used in the simulations this recombination process did not need to be factored into the simulation model environment.

The ***recombination rate*** is proportional to the excess carrier concentration. No recombination takes place if the carrier concentration, more noticeably the minority carrier concentration, equals its thermal equilibrium value as in Equation [3-1]. The recombination rate equations for p-type (U_n) and n-type (U_p) semiconductors are given by

$$U_n = G_n - R_n = (n_p - n_{p0}) / \tau_n \quad [3\text{-}9]$$

and

$$U_p = G_p - R_p = (p_n - p_{n0}) / \tau_p \quad [3\text{-}10]$$

where n_p, p_n, G_n, n and R_n are the minority electron and hole concentrations, and the generation and recombination rate for electrons, respectively. The denominator is the average minority carrier lifetime. For ***direct recombination*** the minority carrier lifetime is

$$\tau_i = \{\alpha_r(n_0 + p_0)\}^{-1} \quad [3\text{-}11]$$

where "i" represents "n" or "p" for direct recombination lifetime of minority electrons and holes in p-type and n-type extrinsic semiconductors. "α_r" is the constant of proportionality for recombination (cm^3/s) that defines the excess minority electron (δn) and hole (δp) concentrations at time t in Equations [3-12] and [3-13] in p-type and n-type material, respectively.

$$\delta n_p(t) = \delta n_0 \exp\{-\alpha_r(n_{p0} + p_{p0})t\} \quad [3\text{-}12]$$

and,

$$\delta p_n(t) = \delta p_0 \exp\{-\alpha_r(p_{n0} + n_{n0})t\} \quad [3\text{-}13]$$

Indirect recombination involves a series of smaller energy losses to the lattice as heat, via introduced doping impurity levels or traps in the band gap as discussed above. Here the minority carrier lifetime is complicated by each carrier in a generated EHP to be capture separately. The one that recombines may be re-excited before the other recombines.

3.1.6 Carrier Transport Processes: Drift and Diffusion.

Electrons and holes in a crystal lattice can not be considered to be completely free as they interact with the periodic potential of the lattice. Thus their wave-particle motion is not the same as electrons in free space. Thus an effective mass (m*) is

used in the equations of electrodynamics that are applied to charge carriers in a solid and is given by (Reynolds 2002)

$$m_n^* = \left(\frac{h}{2\pi}\right)^2 \left(\frac{d^2E}{dk^2}\right)^{-1} \qquad [3\text{-}14]$$

Where m_n^* is the effective mass of an electron (Kg), h is plancks constant (J-s), E is the energy and k is the wave vector (cm^{-1}). The effective mass takes into account the shape of the energy bands in 3D k-space, taking averages over the various energy bands.

Both conduction-electrons and valance-holes move in the lattice until they recombine. Without the presence of an electric field the electron then ***diffuses*** in the direction of lowest conduction-electron concentration in the crystal lattice due to the concentration gradient. In the presence of an electric field the conduction electron drifts through the crystal lattice in the opposite direction to the electric field towards the cathode.

For holes, drift and diffusion operate similarly, except these transport modes result from a series of electron hole pair production and recombination. The initial hole recombines or is quenched with an electron from an adjacent atom in the crystal lattice. This then creates another hole in the adjacent atom, which itself is quenched. Thus the original "hole" appears to "move" in the lattice associated with each atoms valance band. Without an applied voltage holes diffuse, otherwise they appear to drift towards the anode in the direction of the applied voltage.

Figure 3.6 shows that, in an applied voltage, holes drift less and have lower mobility (μ). This is due in part to their movement process as well as the holes having a greater effective mass as shown by,

$$\mu = qt/m^* \qquad [3\text{-}15]$$

Where μ is the *mobility*, q is the *electronic charge* and t is the *mean free time*, representing the mean time between scattering events of the carriers in the crystal lattice.

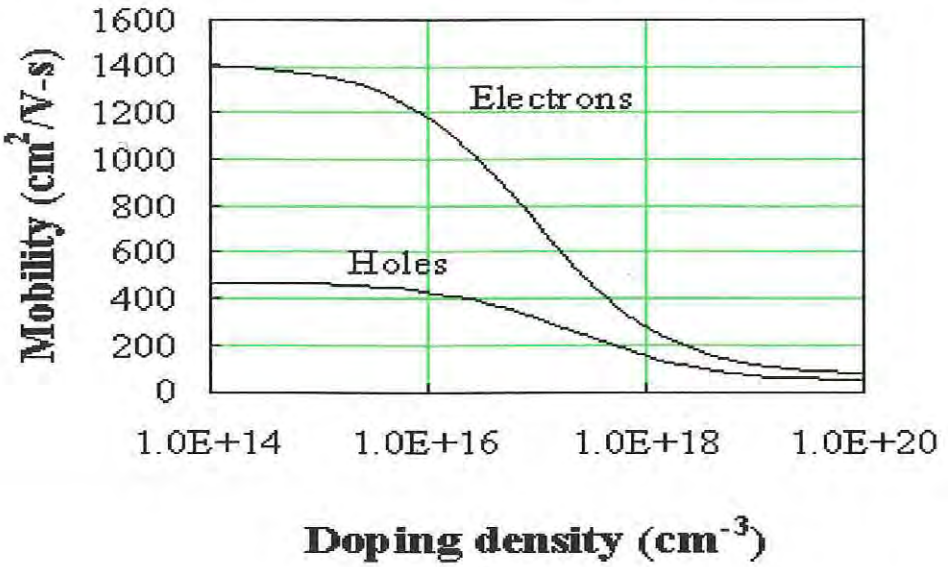

Figure 3.6 Carrier mobility against doping concentration (Van Zeghbroek 2002).

For low doping, the mobility of both carriers is constantly limited by phonon scattering. At higher doping, the mobility decreases due to ionized impurity scattering, depending on the type of dopant. Figure 3.6 shows the mobility of electrons and holes in phosphorous and boron doped silicon, respectively. The mobility is linked to the total concentration of ionized dopants.

The minority carrier mobility, the main charge carrier in low injection photogeneration processes, depends on the total impurity density. The empirical Equation [3-16] gives the minority carrier mobility at particular doping concentrations and is (Van Zeghbroek 2002).

$$\mu = \mu_{min} + \frac{\mu_{max} - \mu_{min}}{1 + \left(\frac{N}{N_r}\right)^{\alpha}} \qquad [3\text{-}16]$$

The parameters for Equation [3-16] are recorded in Table 3-1.

Table 3-1: Parameters for [3-16]. (Van Zeghbroek 2002)

	Arsenic	Phosphorous	Boron
μ_{min} ($cm^2/V\text{-}s$)	52.2	68.5	44.9
μ_{max} ($cm^2/V\text{-}s$)	1417	1414	470.5
N_r (cm^{-3})	9.68×10^{16}	9.20×10^{16}	2.23×10^{17}
α	0.68	0.711	0.719

The minority carrier mobility is approximated by the majority carrier mobility in a semiconductor with the same number of impurities, as shown in Equation [3-16]. The resulting carrier mobility is summarised in Table 3-2. This is over the doping ranges used in the simulated pixel configurations in this project.

Table 3-2: Mobility in silicon for different doping levels, (ibid. 2002)

N	Arsenic	Phosphorous	Boron
10^{15} cm^{-3}	1359	1362	462
10^{16} cm^{-3}	1177	1184	429
10^{17} cm^{-3}	727	721	317
10^{18} cm^{-3}	284	277	153
10^{19} cm^{-3}	108	115	71

As Figure 3.6 shows, holes have the lower mobility. This means that hole drift contributes less to the conductivity (σ) of the semiconductor demonstrated by

$$\sigma_p = qp\mu_p \qquad [3\text{-}17]$$

For the electron conductivity (σ_n) the hole carrier concentration (p) is replaced by n. This can be seen in Figure 3.7 that compares carrier Resistivity (Conductivity^{-1}).

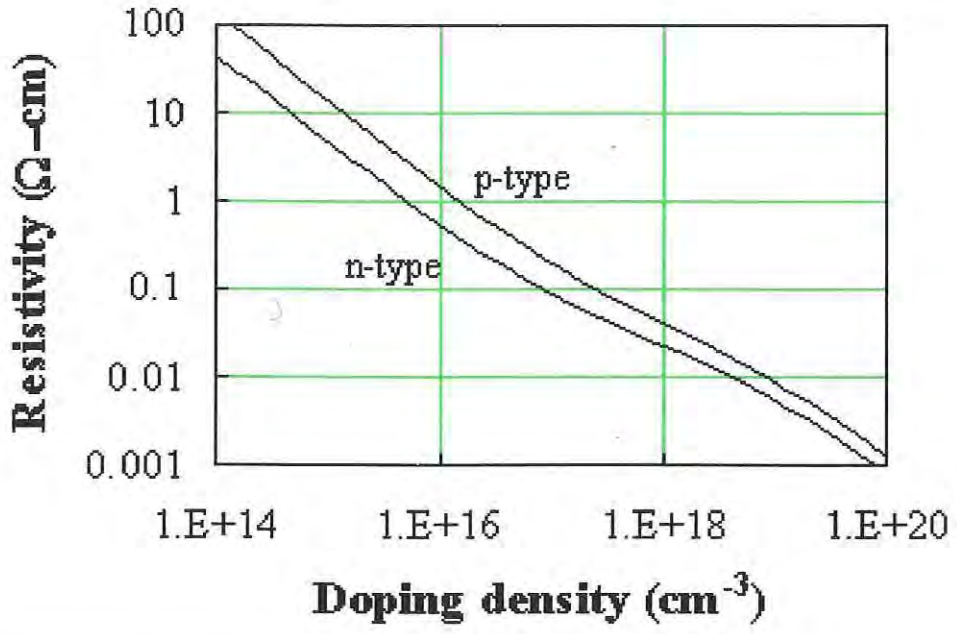

Figure 3.7 Resistivity of semiconductors against doping. (Van Zeghbroek 2002)

Therefore for devices such as semiconductor light detectors where sensitivity of the capturing electrode is an issue, it is better to use an image-cathode as electrons have a higher mobility, resulting in a better conductivity and a higher electrode current. This is related to the carrier mobility in the device.

Considering the diffusion process further, this process is due to random thermal motion that in itself does not give a current or net movement of charge. With a concentration gradient, photogenerated for example, the generated envelope spreads outwards towards the regions with less minority carrier concentration. Given that the product of the carriers thermal velocity and mean path length is defined as the diffusion coefficient (D_n or D_p) an expression for the resulting electron and hole current density (J) due to diffusion can be shown to be Equations [3-18] and [3-19], respectively

$$J_n = qD_n \frac{dn}{dx} \qquad [3\text{-}18]$$

$$J_p = -qD_p \frac{dp}{dx} \qquad [3\text{-}19]$$

The Einstein relation Equation [3-20] shows how the electron and hole diffusion lengths, in Equation [3-21], are proportional to their mobilities.

$$D = \mu . \frac{kT}{q} \qquad [3\text{-}20]$$

$$L = \sqrt{D.\tau} \qquad [3\text{-}21]$$

where D is the diffusion coefficient, k is Boltzmann's constant, T is the temperature, q is the electronic charge, μ is the mobility, L is the diffusion length and τ is the recombination lifetime. From Equations [3-20] and [3-21], in intrinsic silicon, electrons diffuse farther than holes by up to 1.7 times ($\sqrt{1350/480}$) at 300 K.

The product of the conductance, Equation [3-17], and the electric field (ε) gives the drift current. Combining these expressions for drift and diffusion currents, Equations [3-17], [3-18] and [3-19], expressions for the total electron and hole current densities becomes Equations [3-22] and [3-23], respectively.

$$J_n = qn\mu_n\varepsilon + qD_n\frac{dn}{dx} \qquad [3\text{-}22]$$

$$J_p = qn\mu_p\varepsilon - qD_p\frac{dp}{dx} \qquad [3\text{-}23]$$

By summing Equations [3-22] and [3-23], the total current density is obtained, which, when multiplied by the area normal to the currents direction, gives the total current.

In modeling devices with uniform as well as non-uniform material compositions, the simulation package use for this project, SEMICAD DEVICE (1994), uses Equations [3-24] and [3-25], as quasi-electric field vectors in Equations [3-22] and [3-23], respectively.

$$\varepsilon_n = -\nabla\{\psi + \frac{1}{q}(k.T.\ln(N_C) + k.T.\ln(\gamma_n) + \chi + \Delta E_C)\} \quad [3\text{-}24]$$

and

$$\varepsilon_p = -\nabla\{\psi + \frac{1}{q}(k.T.\ln(N_V) + k.T.\ln(\gamma_p) + \chi + E_G - \Delta E_V)\} \quad [3\text{-}25]$$

This accounts for any spatial variation in the material composition and the band parameters. N_v and N_c are the effective density of states for the valance and conduction bands. χ is the electron affinity, E_G is the band gap energy and ΔE_c, ΔE_v are offsets in each band due to bandgap narrowing. Included is the temperature profile kT, so the simulation package, will properly simulate thermal gradients in the device, if present, except for the temperature gradient term of current density. (SEMICAD DEVICE Manual 1994 p. 286)

3.1.7 **Continuity Equations.**

The change in carrier concentration over time at a specific point in a semiconductor is due to the difference in the carrier current density arriving and leaving that point. Additionally it is due to the difference in generation and recombination rate at that point. This is what the continuity equations describe. Using a Taylor series expansion of the difference between the current densities rates of change, the continuity equations for electrons and holes are Equations [3-26] and [3-27], respectively (Van Zeghbroek 2002).

$$\frac{\partial n(x,t)}{\partial t} = \frac{1}{q}\frac{\partial J_n(x,t)}{\partial x} + G_n(x,t) - R_n(x,t) \quad [3\text{-}26]$$

and

$$\frac{\partial p(x,t)}{\partial t} = -\frac{1}{q}\frac{\partial J_p(x,t)}{\partial x} + G_p(x,t) - R_p(x,t) \quad [3\text{-}27]$$

Substituting Equations [3-22] and [3-23] into Equations [3-26] and [3-27], respectively, produces two partial differential equations as a function of the electric field (from Gauss' law), and the hole and electron concentrations, the latter being demonstrated (ibid. 2002) as

$$\frac{\partial n(x,t)}{\partial t} = \mu_n n \frac{\partial \mathcal{E}(x,t)}{\partial x} + \mu_n \mathcal{E} \frac{\partial n(x,t)}{\partial x} + D_n \frac{\partial^2 n(x,t)}{\partial x^2} + G_n(x,t) - R_n(x,t) \qquad [3\text{-}28]$$

For the equivalent hole continuity equation, the first two terms in Equation [3-28] are negated and all the "n" letters are replaced by "p". The SEMICAD DEVICE simulation solves this equation with the Poisson Equations ([3-31a]) for each node of the finite element mesh into which the simulated device structure is grided.

The diffusion equations arise from Equation [3-28] in regions where the electric field is small. And so the current is only due to diffusion. Also the simple model for the net recombination rate is applicable (Equations [3-9] and [3-10]). Thus the time dependent diffusion equations (Van Zeghbroek 2002) are obtained. For minority electrons this equation is

$$\frac{\partial n(x,t)}{\partial t} = D_n \frac{\partial^2 n_p(x,t)}{\partial x^2} - \frac{n_p(x,t) - n_{p0}}{\tau_n} \qquad [3\text{-}29]$$

By replacing the "n" and "p" by "p" and "n" in Equation [3-29], the time dependent diffusion equations for minority holes is obtained.

In the case where material is being illuminated with a constant excitation source, of photons for example, a steady state is arrived at for Equation [3-29] equating it to

zero. The general solution for minority hole concentration, p_n as a function of position is

$$p_n(x \geq x_n) = p_{n0} + Ae^{-(x-x_n)/L_p} + Be^{(x-x_n)/L_p} \quad [3\text{-}30]$$

where p_{n0} is the equilibrium minority hole concentration, x_n is the position of the depletion region edge in the n-type material, L_p is the hole diffusion length and A and B are constants. By reversing "p" and "n" an expression for the steady state solution for the minority electron concentration as a function of position is obtained. Here L is the diffusion length as in Equation [3-21]. The diffusion coefficients are calculated using the Einstein relation, Equation [3-20]. (Zeghbroeck Van B. 2000)

3.1.8 **The Drift – Diffusion Model.**

This model contains all the equations previously described. These equations are summarised below. The assumptions are that the dopants are fully ionized, in steady state (variable independent of time), at constant temperature, and the doping regimes are such that the device is non-degenerate – i.e. the Fermi energy level is 3kT above the valance band edge or below the conduction band edge for holes and electrons respectively. The ten equations are italixed numerically below :

1. ***The charge density (ρ) equation*** : $\rho = q(p - n + N_d^+ - N_a^-)$ [3-31]

This is used in the Poisson's Equation [3-32], and solves for the electrostatic potential the former being given in Equation [3-32] below.

$$\frac{d^2\psi}{dx^2} = -\frac{\rho}{\varepsilon_s} = -\frac{q}{\varepsilon_s}(p - n + N_d^+ - N_a^-) \quad [3\text{-}32]$$

Here the charge density, ρ, is written as a function of electron, hole, ionized donor and acceptor concentrations. In the simulation model Equation [3-32] becomes

$$\nabla(\varepsilon.\nabla\psi) = q\{n - p + \sum_{allspecies}([N_a-]-[N_d+]+[N_{aa}-]-[N_{dd}+])\} \qquad [3\text{-}33]$$

where ε is the permittivity, q is the electronic charge, N_a and N_d are the concentrations of ionized acceptors and donors and N_{aa} and N_{dd} are the concentrations of ionized acceptor and donor-traps. N_a and N_d calculations assume local charge neutrality; these values are not changed throughout a simulation. N_{aa} and N_{dd} are calculated accurately at each bias point and time instance. (SEMICAD DEVICE™ Manual 1994 p. 285).

2. ***Electric fields and potential equations*** :

$d\varepsilon/dx = \rho / \varepsilon$ (Electric field equation) [3-34]

$d\phi/dx = -\varepsilon$ (Potential equation) [3-35]

$dE_i/dx = q\varepsilon$ (Intrinsic energy level equation) [3-36]

3. ***Carrier concentration equations*** :

$n = (n_i)\exp(F_n - E_i) / kT$ (electron concentration) [3-37]

$p = (n_i)\exp(E_i - F_p) / kT$ (hole concentration) [3-38]

Fn and Fp are the electron and hole quasi-Fermi energy levels, respectively.

4. ***Drift and diffusion current density equations*** : Equations [3-22] and [3-23].

5. ***Continuity equations*** in steady state with SRH recombination as used in SEMICAD DEVICE simulations for electrons and holes being Equations [3-39] and [3-40], respectively.

$$0 = \frac{1}{q}\frac{\partial J_n}{\partial x} - \frac{np - n_i^2}{n + p + 2n_i \cosh(\frac{E_t - E_i}{kT})}\frac{1}{\tau} \qquad [3\text{-}39]$$

and

$$0 = -\frac{1}{q}\frac{\partial J_p}{\partial x} - \frac{np - n_i^2}{n + p + 2n_i \cosh(\frac{E_t - E_i}{kT})}\frac{1}{\tau} \qquad [3\text{-}40]$$

3.1.9 **The p-n Junction.**

When n-type and p-type semiconductors are brought together, a region depleted of carriers results. This region extending from the junction into each n-type and p-type region results is called the "depletion region" or the "Space Charge Region" (SCR). To reach thermal equilibrium, electrons close to the junction diffuse across the junction into the p-type region, where hardly any electrons are present. This also happens for holes on the p-side diffusing into the n-side. This leaves a region of ionized donors and acceptors depleted of mobile carriers. This SCR or depletion region extends from $x = -x_p$ to $x = x_n$ in Figure 3.8.

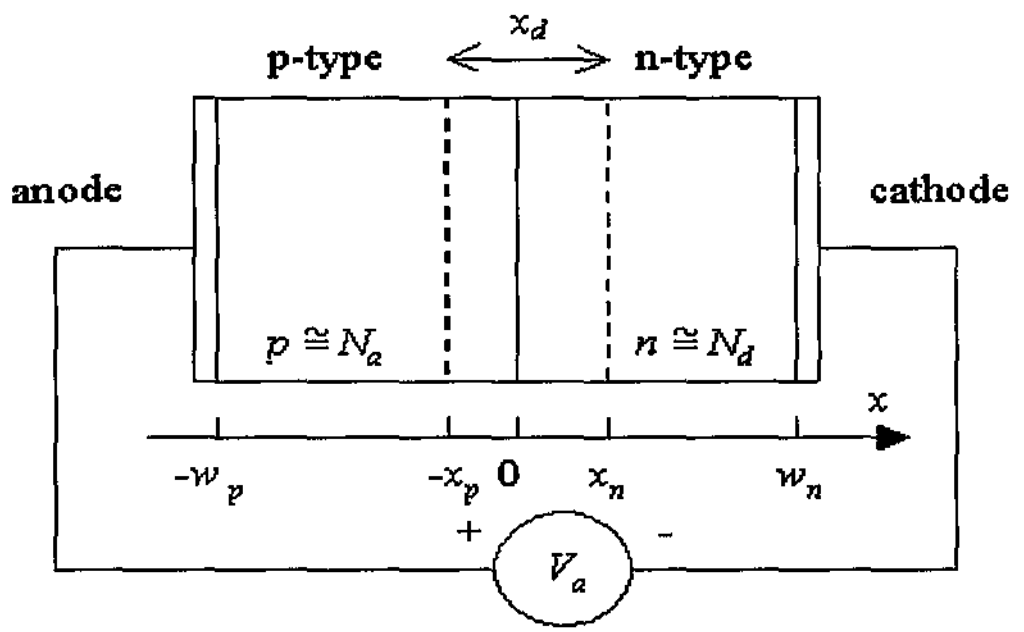

Figure 3.8 Idealized diode cross section and SCR with width X_d.(Van Zegh' 2002)

The ionized donors' and acceptors' charges, cause an electric field, which results in a drift of carriers in the opposite direction to their diffusion. When both currents are balanced thermal equilibrium is reached as indicated by a constant Fermi energy level (E_F) across the junction as depicted in Figure 3.9.

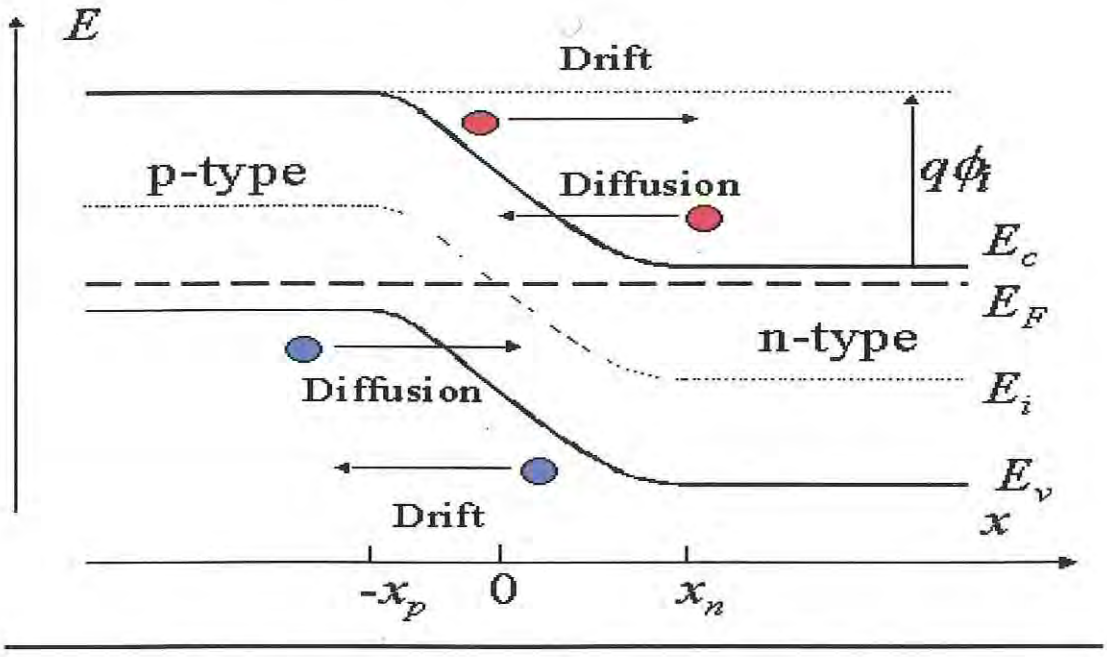

Figure 3.9 Energy Band diagram of p-n junction in thermal equilibrium (Van Zeghbroek 2002).

Note that ϕ_I is the in built or thermal equilibrium potential of the p-n junction. This is caused by the work function difference between the two semiconductor types and is related to the doping concentrations on either side of the junction as

$$\phi_i = V_t \cdot \left(\ln \left(\frac{n_n \cdot p_p}{n_i^2} \right) \right) \qquad [3\text{-}41]$$

where V_t is kT/q = 25.9 mV at 300 K. ϕ_I is sometimes called the barrier height or diffusion potential and is sometimes represented by V_B. The terms n_n and p_p are approximately N_d and N_a, respectively, far from the junction.

Under forward bias, there is an increased minority carrier concentration at the edges of the SCR ($-X_p$ and X_n in Figure 3.8) than in equilibrium with no applied voltage.

This exponential increase is called minority carrier injection. The applied bias is pushing carriers into the semiconductor region from across the junction. Figure 3.10 shows the effect on the energy band diagram for forward biasing a p-n junction. Note that the barrier height decreases allowing current to pass.

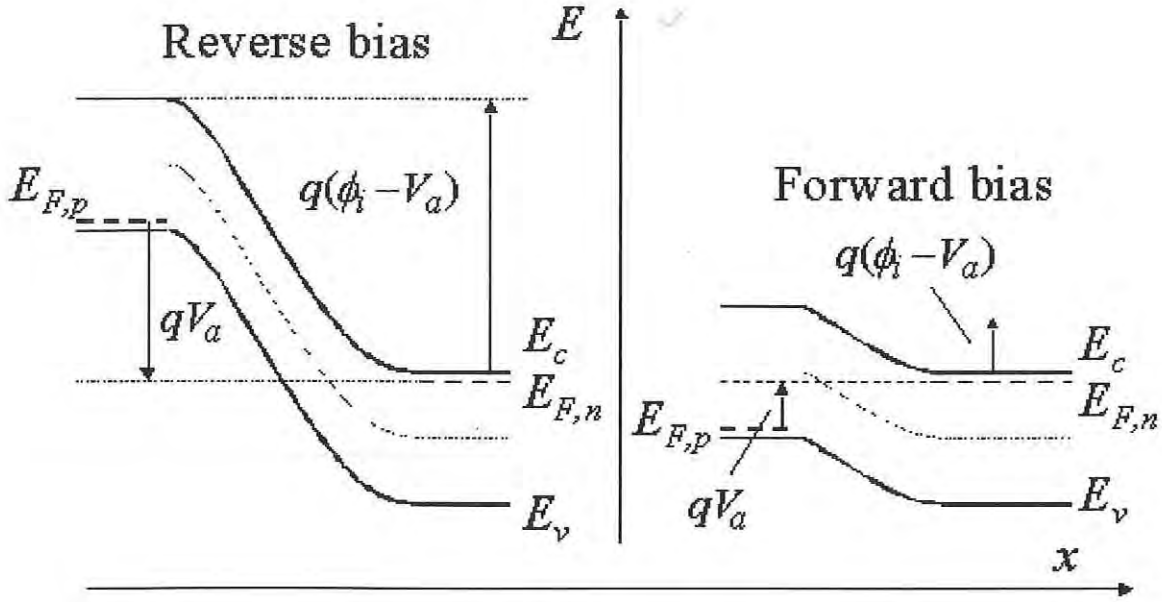

Figure 3.10 Energy Band diagram of p-n junction under different bias (ibid 2002).

Under forward bias the SCR width (X_d in Figure 3.8) is seen to decrease and the current through the diode changes with the applied forward bias as Figure 3.11 shows.

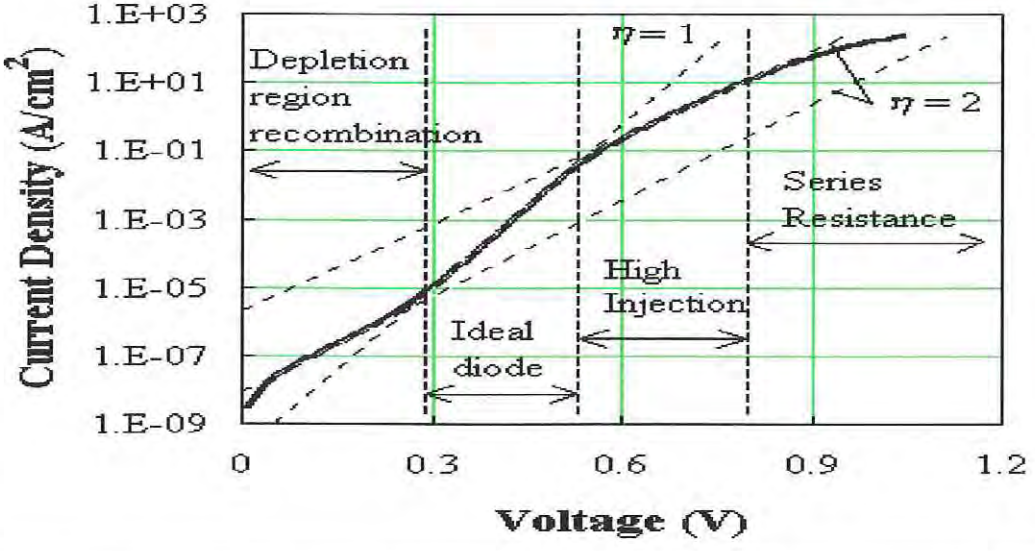

Figure 3.11 Current voltage characteristic under forward bias (ibid Figure 4.4.5).

These four regions can be observed, although the high injection region rarely occurs, as the series resistance limits the current first.

Under reverse bias, there is a reduced minority carrier concentration at the edges of the SCR than in equilibrium. This exponential decrease is called minority carrier extraction and results in an increase in barrier height (Figure 3.10) and an increase in the SCR width. Figure 3.12 shows the current through the diode is now very slight, reversed in direction to forward bias, but is constant and insensitive to voltage change.

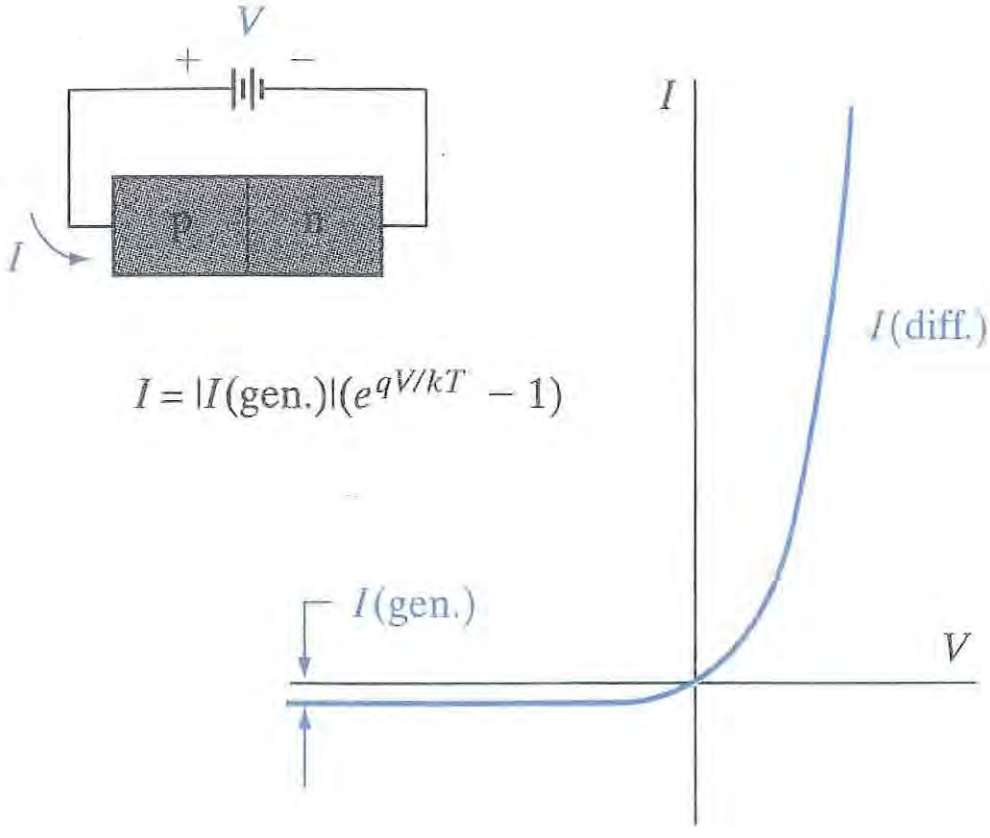

Figure 3.12 Current voltage characteristics under forward and reverse bias.

It is called the dark, generation (I(gen.)) or saturation current (I_S), and its value is changed by temperature or carrier injection, e.g. photogeneration. The reverse current is proportional to the light intensity and not the applied voltage, which is ideal for the photodiode light detecting ability. This is the reason the simulated photodiode devices are reverse biased.

The total potential across the semiconductor must equal the difference between the applied voltage and the built in potential (Van Zeghbroek 2002) giving

$$\phi_i - V_a = \frac{qN_d x_n^2}{2\varepsilon_s} + \frac{qN_a x_p^2}{2\varepsilon_s} \qquad [3\text{-}42]$$

where X_n and X_p are the distance the SCR penetrates into the n-type and p-type regions of the diode, respectively.

It can be shown (Van Zeghbroek 2002) that the Total SCR width is

$$x_d = \sqrt{\frac{2\varepsilon_s}{q}\left(\frac{1}{N_a} + \frac{1}{N_d}\right)(\phi_i - V_a)} \qquad [3\text{-}43]$$

Hence the SCR width is dependent on bias and doping concentrations of the diode. As the reverse bias is increased the SCR width increases. A similar increase occurs if the doping decreases. Here the SCR width is more dependent on the region on that side of the metallurgical junction that is least doped.

The junction capacitance density (F/cm^2) dominates a reverse biased diode over the charge storage capacitance. It is also related to doping and biasing levels, shown by

$$C_j = \sqrt{\frac{q\varepsilon_s}{2(\phi_i - V_a)}\frac{N_a N_d}{N_a + N_d}} \qquad [3\text{-}44]$$

An increase in reverse bias decreases the capacitance, while increase in doping increases the capacitance.

The general expression for the ideal diode current is found by applying some boundary conditions of an operating diode, to the general solution of the diffusion equation [3-27], for each of the quasi-neutral regions. Assuming that the quasi-Fermi energies are constant throughout the SCR, then the minority carrier hole and

electron concentration at the SCR edges are given by Equations [3-45] and [3-46], respectively, with reference to Figure 3.8 (Van Zeghbroek 2002).

$$p_n(x = x_n) = p_{n0} e^{V_a / V_t} \quad [3\text{-}45]$$

$$n_p(x = -x_p) = n_{p0} e^{V_a / V_t} \quad [3\text{-}46]$$

The carrier density at the metal contacts is assumed to equal the thermal equilibrium carrier concentrations, which implies that excess carriers immediately recombine at the metal contacts. Thus further boundary conditions represented by the following Equations [3-47] and [3-49] arise, with reference to Figure 3-8 again.

$$p_n(x = W_n) = p_{n0} \quad [3\text{-}47]$$

and

$$n_p(x = -W_p) = n_{p0} \quad [3\text{-}48]$$

Assuming steady state, an expression for the total current through the photodiode (Van Zeghbroek 2002) becomes

$$I = A[J_n(x = -x_p) + J_p(x = x_n) + J_r] \cong I_s(e^{V_a / V_t} - 1) \quad [3\text{-}49]$$

$$I_s = qA[\frac{D_n n_{p0}}{L_n} \coth(\frac{w'_p}{L_n}) + \frac{D_p p_{n0}}{L_p} \coth(\frac{w'_n}{L_p})] \quad [3\text{-}50]$$

The expression for the reverse saturation current is given as Equation [3-50].

The SRH Recombination-generation photocurrent, can be obtained by integrating the trap-assisted (SRH) recombination rate (Equation [3-5]) over the width of the SCR.

This results in an expression for the effective width, X' and is define (Van Zeghbroek 2002) as

$$x' = \frac{\int_{-x_p}^{x_n} \frac{1}{\tau} \frac{n_i^2 (e^{V_a/V_t} - 1)}{n + p + 2n_i \cosh(\frac{E_t - E_i}{kT})} dx}{U_{SHR,\max}} \qquad [3\text{-}51]$$

Then the expression for the SRH current, due to trap-assisted recombination in the SCR, (Van Zeghbroek 2002) is given by

$$J_{SHR} = \frac{q n_i x'}{2\tau} (e^{V_a/2V_t} - 1) \qquad [3\text{-}52]$$

The X' still needs to be determined by performing a numerical integration. However, an upper estimate of the current can be obtained by substituting X' with the SCR width as it is larger than the effective width (X').

3.1.10 **The Photodiode.**

A conventional photodiode is a p-n diode that is operated in reverse bias so that the current response of the diode is proportional to the applied incident light and not the applied voltage (Figure 3.12). Though the applied voltage widens the SCR and can effect the capture efficiency of the electrode measuring the photocurrent, the electrical response is dependent on the location and intensity of the photogenerated carrier concentration. Figure 3.13 shows a p^+n single junction photodiode (SJPD).

The photodiodes used in imaging applications is included in an array of similar photodiodes that detect the incident light. Each photodiode in these imaging arrays

is called a picture element (pixel) and is identical in dimension to the other pixels, with a characteristic surface width (Pitch) and substrate thickness (thickness).

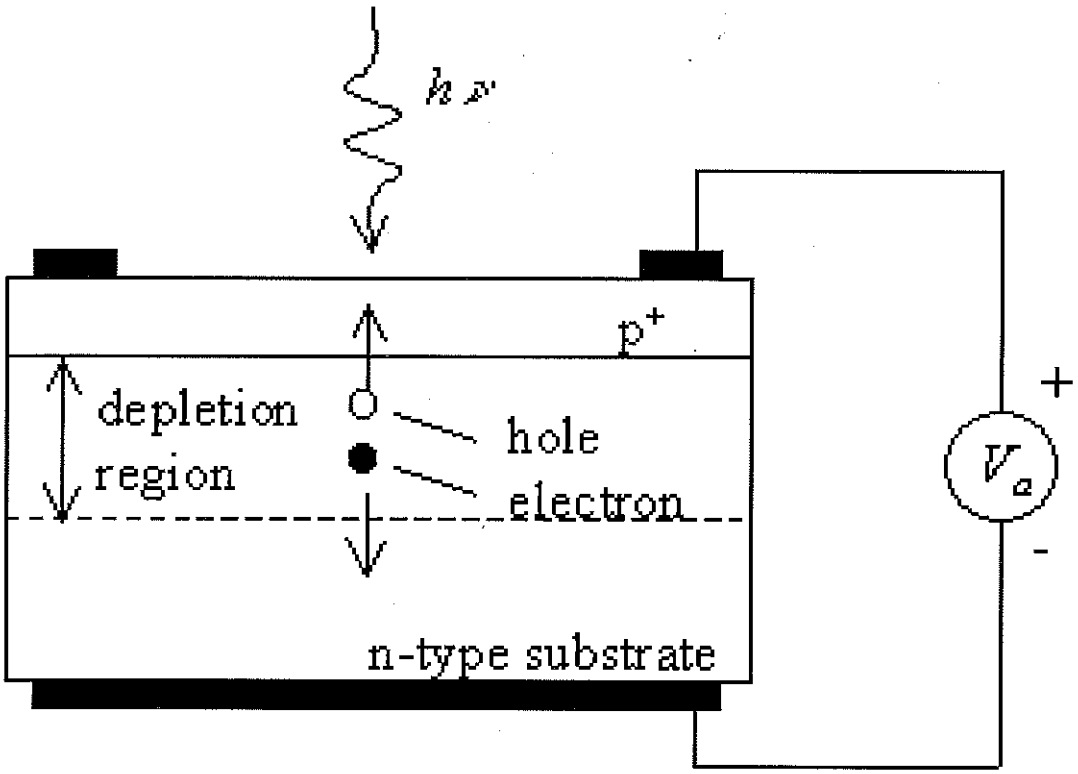

Figure 3.13 An idealized photodiode and carrier motion (Van Zeghbroek 2002)

For the conventional photodiode, each pixel volume of substrate is implanted with a well of semiconductor that is of opposite doping type to the substrate. In Figure 3.13 this photodiode, if it existed in an array, would have a p^+ well, surrounded by n-substrate semiconductor material. The anode on the p^+ well would be the electrode that would be used to measure the photocurrent. Thus the well would be the "image-well" and the anode the "image-anode".

The conventional SJPD appears in two dimensions as a rectangular well embedded into the top of a less doped, much larger square substrate. From above it looks like a square annulus, with the well in the centre, surrounded by substrate. This well can be called the image-well as the carriers that are collected at the electrode on the well's surface contribute to the image-current attributed to that photodiode pixel. This is illustrated as a row of three SJPDs in Figure 3.16. Note that the substrate is contiguous along the back of the array of photodiodes.

The image-well's doping type is usually of higher doping than the substrate. This doping regime is chosen so that the SCR penetrates into the substrate more than into the image-well. This benefits drifting-carrier capture in the substrate. Thus in this project the standard SJPD pixel, the well and substrate unit uses a 10^{17} and 10^{15} cm^{-3} doped n-well and p-substrate, respectively. By default it is also reverse biased by 2 volts making the SCR width 1.88 μm (from Equation [3-43]). A capacitance of 5.544 nF/cm2 can also be calculated from Equation [3-44].

The double junction photodiode (DJPD) is simply a SJPD with an extra well implanted into the inner volume of the exposed original well, now the outer well, as shown in Figure 3.14. Again the inner-well (image-well) doping is of opposite type to the outer well, making it the same doping type as the substrate. The DJPD pixel is like two PDs in one. Usually the image-well is of higher doping than the outer well, which in turn is of higher doping than the surrounding substrate. All image carriers photogenerated in the substrate are captured by the outer SCR. Only image carriers photogenerated inside the outer well are captured by the image electrode. This introduces noise-reducing benefits.

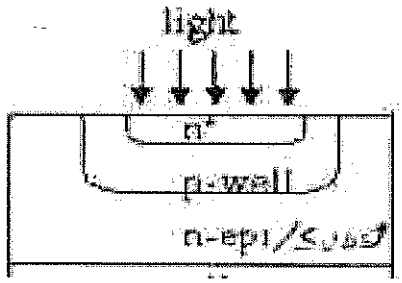

Figure 3.14 Vertical NPN Double Junction Photodiode.

A NPN DJPD pixel (Figure 3.14) has an n-image-well and is associated with an image cathode, with electrons as the image-minority carrier. Likewise the PNP DJPD has a p-image-well associated with an image-anode and the image carriers are holes.

The photo-generated carriers cause a photocurrent, which opposes the forward biased diode current. Hence it can be a photo detector under reverse bias or no bias, as the

I_{ph} is proportional to the incident light intensity. Under forward bias the photodiode acts as a solar cell, that generates electrical power.

Equation [3-53] demonstrates the expression for the photocurrent in a reverse biased SJPD under steady state conditions of light illumination.

$$I_{op} = qAG_{op} (L_p + L_n + W) \qquad [3\text{-}53]$$

This expression is understood diagrammatically from Figure 3.15, in that an additional generation rate, G_{op} (EHP/cm^3-s) participates in the normal reverse bias saturation current. The minority carriers photogenerated in the SCR, and a diffusion length (L) either side of the SCR, participate in this photogenerated current. This leads to the expression for the photocurrent (I_{op}) above. This current adds to the reverse saturation current given by Equation [3-50].

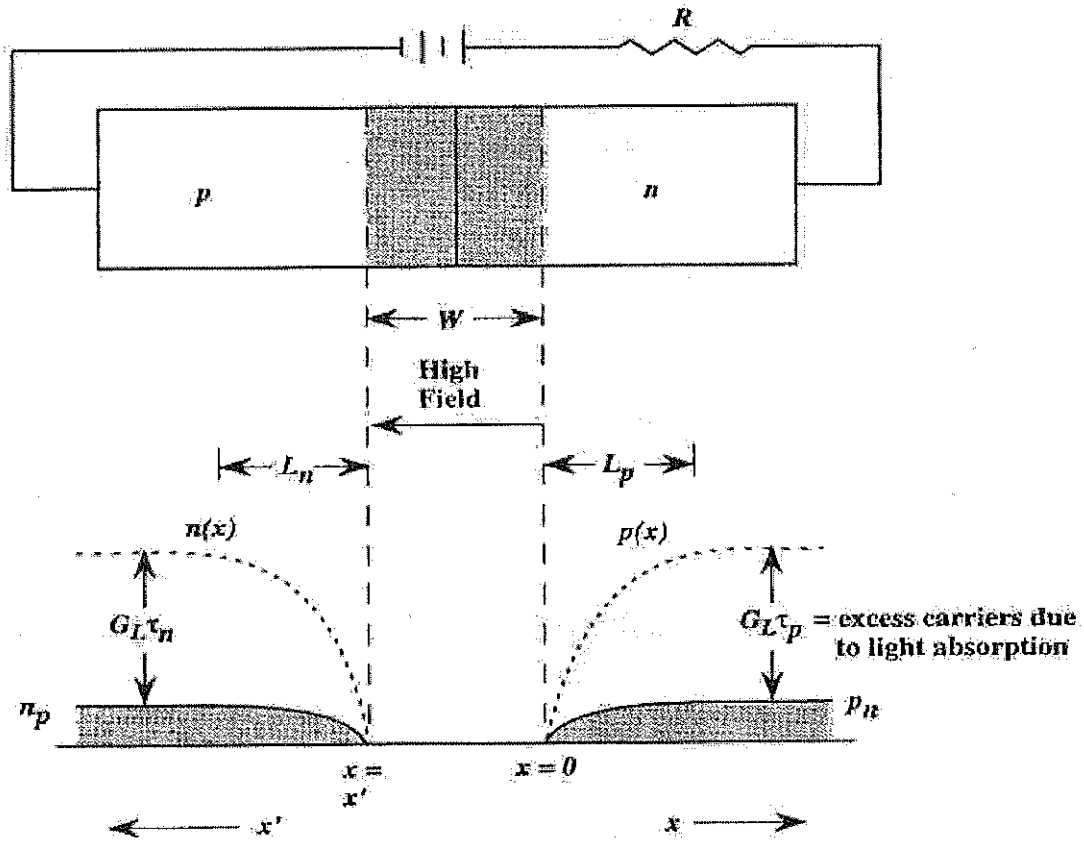

Figure 3.15 A schematic of a p-n diode and the minority carrier concentration in the absence and presence of light. At the SCR edge the high electric field sweeps the minority charge away to zero. (Singh 1994 p. 473)

Responsivity (R), Quantum efficiency ($\eta(\lambda)$), dark current (I_S) and bandwidth are the primary characteristics of a PD. The Responsivity is the quotient of the photocurrent and the incident optical power (A/W). The quantum efficiency (QE) being,

$$\eta(\lambda) = \frac{hcI_{\lambda}}{\lambda q P_{opt}} \qquad [3.54]$$

where I_λ is the photocurrent at incident wavelength λ, h is Planck's constant, c is the speed of light, q is the electronic charge, and P_{opt} is the incident spectral power. This gives the number of carriers that are actually captured at an electrode for every photon incident on the device surface, whether or not reflectance effects exist for the device's total configuration.

The simulations associated with this honours project, involve shining a laser of 633 nm across an array, 160 μm long, consisting of three PD pixels each with a pixel pitch of 50 μm and a well pitch of 20 μm (Figure 4.1). Understanding the QE response of the central pixel for different pixel well depths, doping and biasing regimes for SJPD and DJPD arrays is the main focus of this honours project.

To compare between the electrical response of arrays with different pixel configurations, the QE is normalized (NQE). The NQE for illuminations at position "x" along the array is compared to the maximum QE response at position "Max". This is represented by Equation [3.55] below.

$$NQE(x) = \frac{QE(x)}{QE(Max)} \qquad [3\text{-}55]$$

Since Auger recombination is not included in the simulation model it is important that the PD configurations simulated have SCR widths that are less than the distance between the underside of the well and the back wall of the substrate. This is so that each PD pixel's substrate is not fully depleted to the back wall. If this occurred in reality, generation and recombination processes other than the SRH process may

dominate the devices photocurrent generation processes. This means that for the PD pixels simulated, the distance must be less than the SCR substrate penetration distance, which is 99% of the SCR width, hence 1.86 um, for the doping regimes of the default SJPD pixel mentioned above.

3.1.11 Electrical Crosstalk

The *total absolute* electrical crosstalk can be defined as the image electrode QE value for a given pixel when all pixels surrounding the given pixel are being illuminated while the given pixel is not illuminated. The *total relative* electrical crosstalk can be defined as the NQE value of a given pixel when all pixels surrounding the given pixel are being illuminated while the given pixel is not illuminated. In this project's 2D simulation, the crosstalk determined is the pixel image QE or NQE response for illumination by the 5 um wide simulated laser at the *boundary* of the central pixel of the three pixel array. These 2D values are called the absolute and relative 2D crosstalk, respectively. They vary proportionately with the 3D crosstalk values.

There are two crosstalk mechanisms [Kang, 2002]:

1) **Electrical crosstalk** : As a consequence of photon generated carriers (electrons or holes) within the nominal collection / absorption region of the photon incident pixel, crosstalk results, because associated minority carriers undergo diffusion to be collected by surrounding pixels.

2) **Optical crosstalk:** This is crosstalk that is produced by the multiple reflection, refraction, and scattering of radiation between different surfaces within the chip. These include interfaces between insulators, silicon, epi-layer, and exterior surfaces of the chip and its packaging.

This honours project investigates electrical crosstalk in PD arrays that are illuminated from the front, directly onto the PDs' exposed electrodes, well and substrate, frontwall illuminated (FW) and illuminated from underneath the PD, backwall illuminated (BW), on the substrate surface (Figure 3-16).

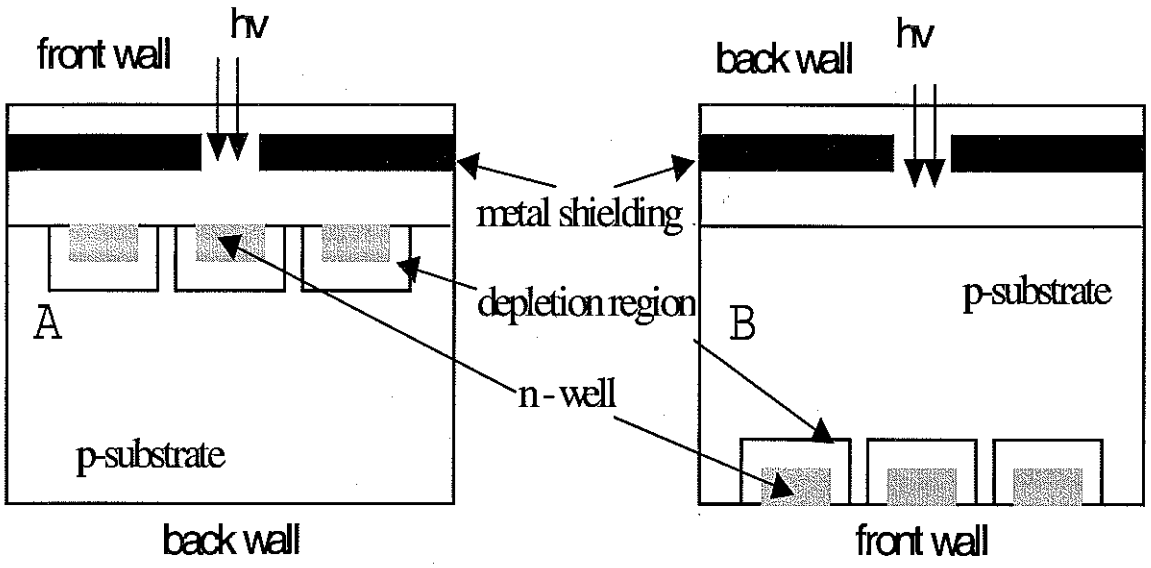

Figure 3.16 The basic 3 pixel p-n PD array (A) FW, (B) BW.

The electrical crosstalk mechanism in all photodiode picture elements (pixels) is a by-product of normal photogenerated minority carrier drift and diffusion. Here a minority photocarrier, generated in the volume of a particular pixel, diffuses out from the photogeneration region, as a result of the concentration gradient set up by the generation process. It then comes under the influence of an adjacent pixel's image capture field, and is then captured.

The result of this pixel carrier-sharing process is a false inflation of the collection photocurrent (I_{ph}) of the neighbouring collecting pixel, while a false deflation of the collection I_{ph} of the pixel in which the collected carriers were originally photogenerated. Thus any signal at a given pixel's image electrode from illumination outside the boundary of that pixel is electrical crosstalk.

Figure 3.17 demonstrates more graphically that electrical crosstalk occurs when some of the charge carriers generated between the depletion region and the p-substrate diffuse to adjacent pixels instead of back to the exposed pixel. Most of the charge carriers generated in the depletion region, driven by the electric field, are collected by the exposed photodiode, and hence do not contribute to electrical crosstalk. Likewise, the carriers generated in the p-substrate are efficiently recombined due to the short minority carrier lifetime. (Kang 2002).

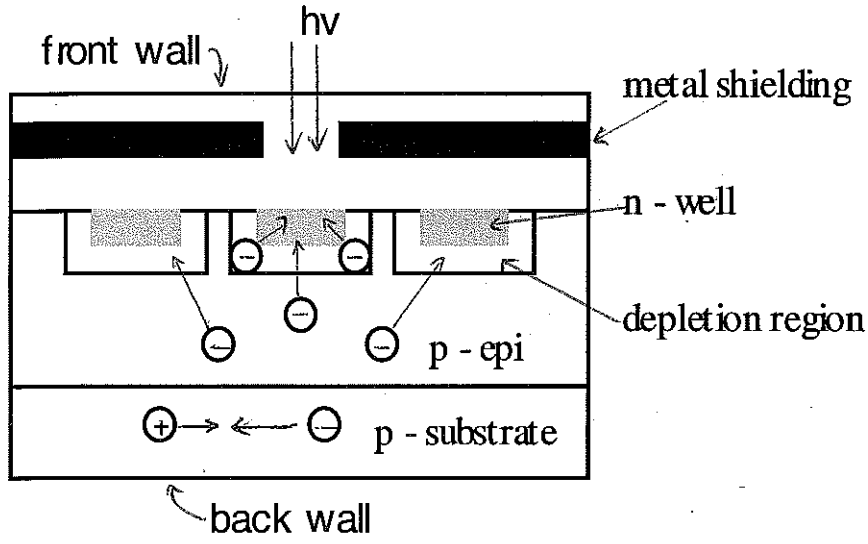

Figure 3.17 The electrical crosstalk mechanism in a conventional FW SJPD array of three pixels. (Kang 2002).

Ideally the condition of negligible crosstalk is reached when the electrical response for illuminations outside the pixel's boundary are the same constant minimum QE and NQE response. This means that for ideal negligible crosstalk the pixel's image photocurrent profile will represent a "flat-line" for illuminations outside the pixel. This is demonstrated for some pixel configurations investigated in this project. This does not mean that the response must be of maximum intensity inside the pixel. A pixel configuration that gives a QE response that is enhanced at the centre while "flat-lining" elsewhere between the pixel's boundaries (good response resolution), indicates that the pixel's boundaries can be brought closer to the pixel's well walls without increasing crosstalk. This translates to further reduction in pixel pitch and hence increased picture resolution.

3.1.12 Modes of Illumination and the Photodiode Pixel Sensor.

Frontwall illuminated (FW) pixels can be active (Figure 3.18) or passive (Figure 3.19). Figure 3.18 shows an Active pixel sensor.

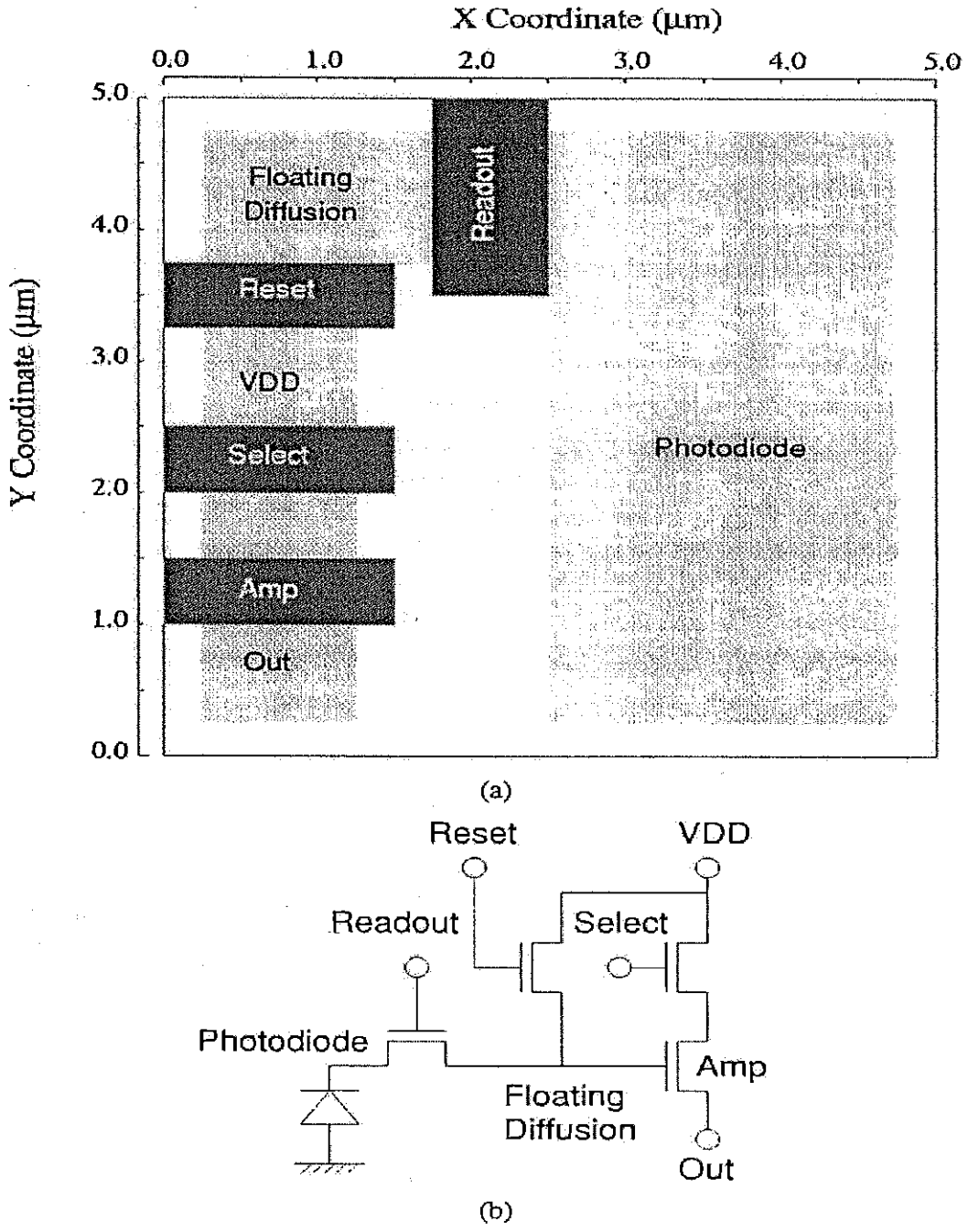

Fig. 1. Cell structure of analyzed device. (a) Gate and diffusion layout. (b) Equivalent circuit.

Figure 3.18 Active Pixel Sensor. (Mutoh 2003 p. 19)

Conventional Pixel sensors are FW pixels and have their signal processing transistor infrastructure on the same plane as the photodiode or other photosensing element. They can be active (Figure 3.18) or passive (Figure 3.19) depending on where the signal processing circuitry is included: inside each pixel (active) or outside the sensing array (passive).

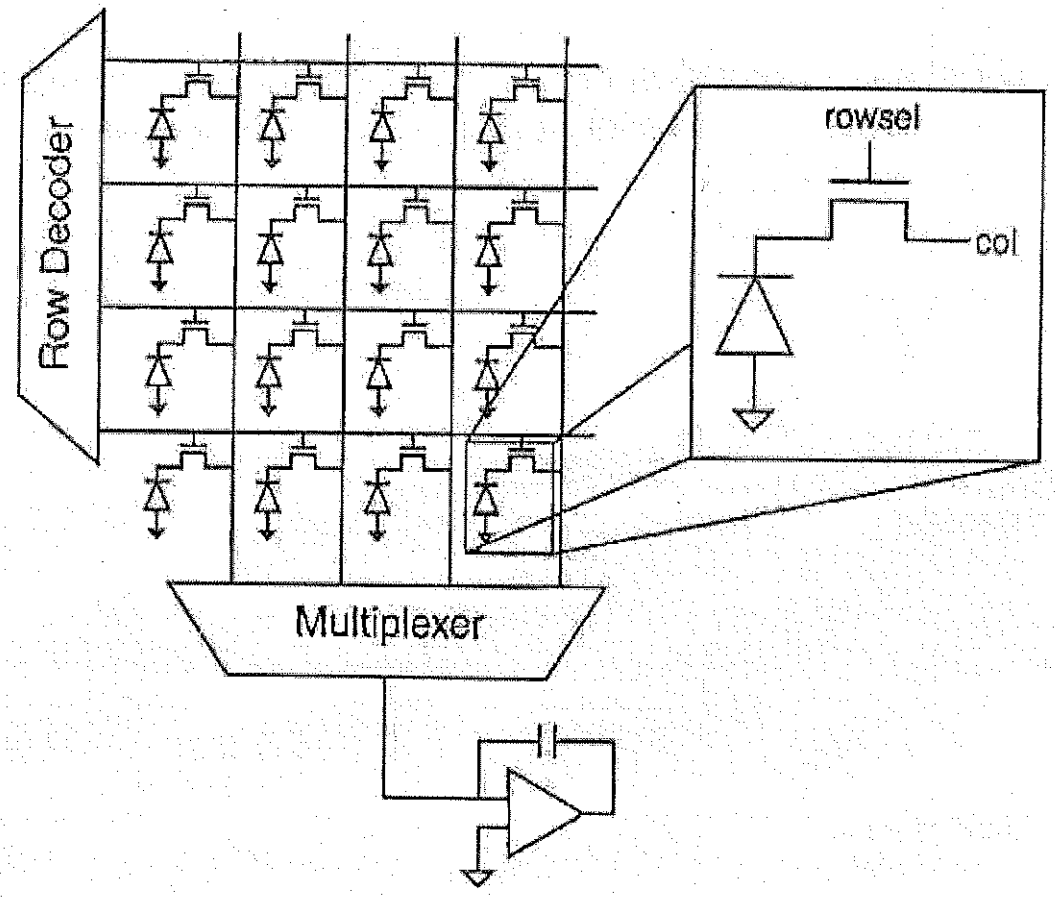

Figure 3.19 Passive Pixel Sensor. (Fujimori, Wang & Sodini 2000, p. 2031).

FW pixel sensors are disadvantaged in a number of ways including:

1. Incompatibility of different imaging or processing technologies for the chips.
2. Low fill factors (FF) in the active pixel sensor (Figure 3.18) as processing circuitry uses up pixel space.
3. Passive pixel sensors (PPS) (Figure 3.19) experience charge-signal disturbances on column-lines, as charge-to-voltage conversion is not achieved in PPS volume.
4. Signal-disturbance-correcting implants and fabrication steps are costly and complex for PPS.
5. Not able to tailor to specific wavelength range.

FW pixel sensors are advantaged by broad spectral sensitivity due to similar close proximity of incident illumination to pixel depletion or space charge region (SCR)

and as such their quantum efficiency is generally higher than backwall illuminated (BW) pixel sensors. However, due to the region of absorbing substrate between the illuminated backwall and the SCR of the BI pixel, this illumination mode is advantaged by being able to be made broadly wavelength specific (Hinckley et al 2000). Figure 3.20 shows a BW SJPD array flip-chip Indium bump bonded to an application specific IC (ASIC) that contains the signal processing circuitry.

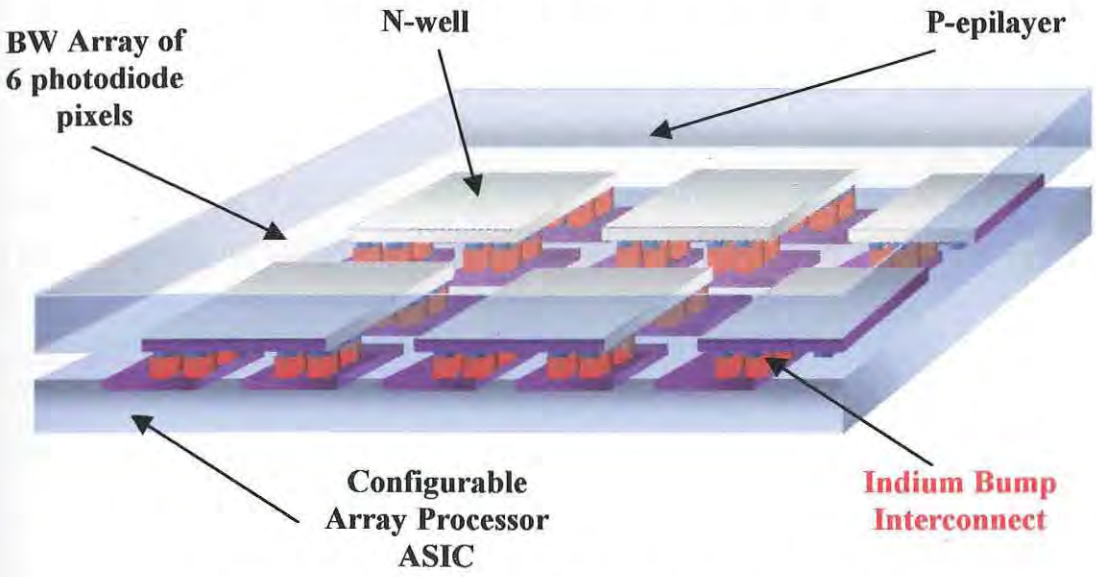

Figure 3.20 3D Reconfigurable BI Photodiode Array.

Advantages of BW over FW imager arrays include:

1. Near 100 % fill factor.
2. Combination of different processing technologies for the chips.
3. Flexibility tailoring the colour response of each pixel (wavelength selective).

Disadvantage of BW compared to FW imager arrays warranting this investigation:

1. lower response resolution resulting in higher electrical crosstalk.

This disadvantage is due primarily to the carrier envelope being photogenerated in the substrate that is contiguous across the backside of the imager array that acts as an electrical crosstalk "super highway". This free diffusion of image carriers across multiple pixels results in significantly more crosstalk in this mode of illumination compared to the imager array frontwall illuminated.

3.1.13 **Introducing The Crosstalk Reduction Methods.**

Knowing that crosstalk is one symptom of poor pixel QE response resolution the technique employed to improve this resolution is to increase the image-electrode's capture field efficiency close to the pixel centre while attenuating the pixel response away from the centre. By far the most important process to suppress is "free" substrate diffusion as the diffusion length of carriers is longer than the pixel pitch in most conventional image arrays, indicating a possible solution. If the problem is substrate in origin, then reduce the substrate thickness. Attenuating this "free" diffusion passage will centre the pixel's QE response profile much more, giving better response resolution and crosstalk suppression.

The next step is to increase the pixel sensitivity or image-electrode capture efficiency by bringing the SCR closer to the photogenerated carrier envelope, so that the minority carriers have a shorter distance to reach the SCR and be swept into the image-electrodes capture field. This increases the probability of a larger capture volume. Though this increases the capture efficiency across the whole pixel, the attenuated "free" diffusion passage will tend to limit the crosstalk carrier capture for illuminations away from the centre. Thus increasing the central response of the pixel while suppressing the response away from the centre.

Though crosstalk reduction is achievable for the conventional SJPD pixels, the results are not significant, especially for the BW pixel as the location of the photocarrier envelope in the pixel volume will also effect the pixel QE response. If the carrier envelope is closer to the SCR then diffusion to it is more probable. Thus as FW is directed immediately onto the SCR and well its response for the conventional SJPD pixel is better, more response resolved than the BW pixel. In the BW pixel the carrier envelope is photogenerated nearer the back wall, encouraging more "free" substrate diffusion. This is another reason why limiting the thickness is especially helpful for better QE response resolution in the BW conventional SJPD pixels.

Better reduction of crosstalk, compared to the conventional SJPD pixel, may be achieved by adding highly doped trenches to the substrate on either side of each pixel's well in the imaging array. This has been called ***Boundary Trench Isolation (BTI)*** and is illustrated in Figure 3.21 as the p^+ diffusion trenches either side of the pixel's central n well. BTI is not to be confused with buried trench isolation, which is a term that is more commonly used, and refers to a pixel structure of similar purpose.

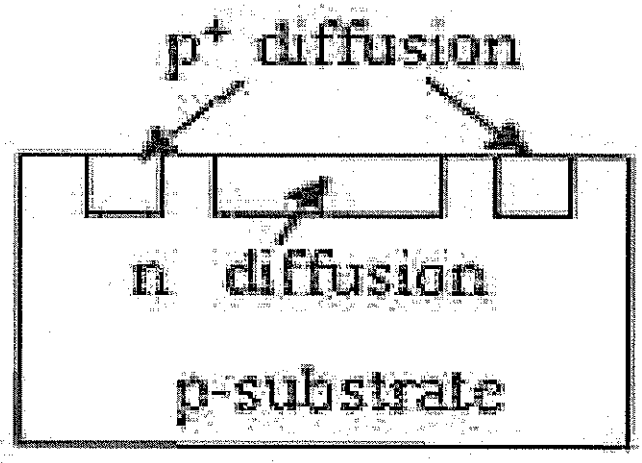

Figure 3.21 Boundary Trench Isolation (BTI).

The introduction of the BTI will increase recombination of the minority carriers in the substrate on and outside of the BTI boundary while enhancing the pixel response towards the pixel's centre. There are more recombination sites in the more highly doped BTI regions so that the mobility and diffusion length of the photocarriers is reduced (Figure 3.6 and Equations [3-20] to [3-23] inclusive) at the pixel's boundary. This results in better response resolution: more central response and less eccentric response. These structures are so named because they are associated with the boundary of the pixel. Similarly the BTI structures can consist of insulating SiO_2, which may limit crosstalk further. However this alternative is not investigated in this present project but will be considered in future research.

Another method is to introduce "***guard-ring***" electrodes surrounding the pixel's image-electrode, the original well electrode at which the photocurrent is being

measured. The competing capture field of the surrounding guard-ring will attenuate the image-electrodes response away from the centre while leaving the image-electrode's central response only partially affected. This results in an increased pixel image response resolution and crosstalk suppression.

Theoretically the use of a ***double junction Photodiode (DJPD)*** should have the same resolution improvement effect on the image electrode as the guarded pixel. Here the outer junction acts in the same way as the guard-ring capture field, though this time the outer junction completely encapsulates the inner image well. This means that all carriers photogenerated outside the outer well are captured by the outer junction while most carriers generated in the outer well are captured by the inner junction of the image-well. Therefore in theory the inner ***image-pixel*** associated with the inner SCR should respond electrically as if it were totally isolated from the electrical environment outside the outer well.

The inner image response should behave as a normal FW or BW SJPD unguarded (naked) pixel, but only inside the outer well environment. In theory the results of this investigation may show excellent pixel QE response resolution that can be adapted to the response shape desired by the CMOS fabrication engineer, by varying doping, biasing and geometric regimes associated with the image pixel.

3.2 Absorption Volume Proportion (AVP)

3.2.1 Micro Versus Macro.

Section 3.1 explained the theory for the simulated pixel QE response to illuminated light at the microscopic level of the simulated finite element grid; at the node level of the pixel. Though this response reflects the sum of all the individual carrier concentrations at the node level, the actual image-electrode response is a macroscopic one. Furthermore the microscopic node responses reflect to some degree the macroscopic configuration parameters that define the pixel's electrical

behaviour. The doping, bias and pixel geometry regimes all impact on the behaviour of the pixel at the quantum level, the later determined by the drift-diffusion model as applied by the simulation using the Poisson and continuity equations to numerically calculate the pixels photoelectric behaviour.

This section seeks to view and explain the pixel's photoelectric behaviour by exploring a macroscopic tool called the absorption volume proportion (AVP) that shows how the absorbed light is distributed in the pixel, particularly in the regions of the pixel that affect the pixel's photoelectric behaviour.

In this project only two nominal regions are used. They are the SCR (space charge region or depletion region associated with the photodiode's junction) and non-SCR. The latter constitutes all of the pixel volume excluding the volume occupied by the SCR. This analysis approach centres on the SCR as it is this region that is most influential in the pixel's photoelectric behaviour, as Section 3.1 has demonstrated. The SCR is especially associated with the drift transport process, as carriers, on arriving at its outer envelope, are quickly swept across it into the image-electrodes capture field. Thus the AVP calculated for this region is sometimes denoted the drift component of the total pixel AVP.

The non-SCR, including the well region and the substrate region, is especially associated with the diffusion transport process for carriers photogenerated in this region. Thus the AVP calculated for this region is sometimes denote as the diffusion component of the total pixel AVP. This is not exactly true as the electrode capture fields may extend beyond the SCR at levels that initiate photocarrier drift before the carrier reaches the SCR purely by diffusion alone. However it is certainly a region in which photogenerated carriers are less dominated by drift than by diffusion.

The AVP is determined by applying Equation [3-2] to the region of interest and calculating the proportion of the incident light intensity (given the value 1) that is actually absorbed in the region of interest. Remembering that the direction of illumination of the pixel is important as BW pixels light attenuates initially from the back wall of the pixel, while FW pixels from the front wall. Thus a FW and BW AVP statistic is calculated for each region.

The quantum budget is a qualitative term used to denote the amount of photon energy that is available to be absorbed in the pixel, which may not all be absorbed ("spent") in the pixel as the beam may exit the pixel and be transmitted. The AVP statistics in this project is a tool that shows how the quantum budget is spent in the pixel as it enters and leaves; i.e. how much photon energy is absorbed in the SCR (SCR AVP) and how much is spent in the non-SCR AVP. Simply by replacing the incident light intensity by 100, the AV percentage can be computed.

A 1.4 Mb discette is provided with the solutions applied in an Excel spreadsheet. This is to provide the opportunity to explore what effects changes to the pixel's doping, biasing and architectural geometry have on the various AVP data calculated.

Furthermore, only the 2D AVP equations are presented, although 3D AVP results are available in the spreadsheet. The Excel spreadsheet will be elaborated on after the AVP equations have been presented. The author's experimental manual contains a full set of worked solutions the main portion of which is presented in Appendix XX (Appendix 20).

3.2.2 **SJPD Pixel AVP Equations.** (Don't worry! This will not hurt a bit !!)

The calculation depends on defining pixel lengths that will be needed for the absorption equation to act upon.

$$I(x) = I_0 \exp\{-\alpha x\} \qquad [3\text{-}2]$$

In the Excel spreadsheet, the SCR width is calculated from Equation [3-43] as indicated in the bracketed expressions beside "W_{out}" and "W_{in}" below. The Excel spreadsheet allows comparison between different pixel configurations of biasing, doping and pixel geometry. The AVP data can be compared graphically with the QE and NQE responses of the pixels, which may demonstrate significant power to predict pixel response. Though only 2D AVP equations are given, because they apply to the 2D simulated pixels, 3D total pixel AVP may be determined.

3.2.2.1 ***Variable definition:***

α = absorption coefficient: from Equation [3-4];

I_0 = incident intensity;

P = pixel pitch (50 um);

W_{well} = well width (20 um);

D_j = Depth of the junction (well depth);

L_w = laser width (5 um);

W_{scr} = SCR width = Equation [3-43];

W_{out} = SCR width in the substrate ([1-(substrate doping/well doping)]*[3-43]);

W_{in} = SCR width in the well ($W_{scr} - W_{out}$);

T = thickness of the substrate.

3.2.2.2 ***BW SJPD total 2D pixel SCR AVP*** [3-56]

$$= (I_0 / P) \{ ([\exp(-\alpha.(T - d_j + W_{in})) - \exp(-\alpha.T)].[2.W_{scr}]) +$$

$$([\exp(-\alpha.(T - d_j)) - \exp(-\alpha.(T - d_j + W_{in}))].[W_{well} + (2.W_{out})]) +$$

$$([\exp(-\alpha.(T - d_j - W_{out})) - \exp(-\alpha.(T - d_j))] . [W_{well}]) +$$

$$(\frac{2.W_{out}}{n} * \sum_{i=1}^{n} [\exp(-\alpha.(T - d_j - \frac{W_{out}}{n} * \sqrt{n^2 - i^2})) - \exp(-\alpha.(T - d_j))]) \}.$$

The four lines associate with four SCR regions, which are backwall illuminated !!

Line 1 = from the level of the SCR edge in the well to front wall;

Line 2 = from the level of the junction to the level of the SCR edge in the well;

Line 3 = from the level of the SCR edge in the substrate to the level of the junction;

Line 4 = the quarter-circular regions of the SCR associated with the well corners.

3.2.2.3 ***FW SJPD total 2D pixel SCR AVP*** [3-57]

$$= (I_0 / P) \{ ([1 - \exp(-\alpha.(d_j - W_{in}))].[2.W_{scr}]) +$$

$$([\exp(-\alpha.(d_j - W_{in})) - \exp(-\alpha.d_j)].[W_{well} + (2.W_{out})]) +$$

$$([\exp(-\alpha.d_j) - \exp(-\alpha.(d_j + W_{out}))].[W_{well}]) +$$

$$(\frac{2.W_{out}}{n} * \sum_{i=1}^{n} [\exp(-\alpha.d_j) - \exp(-\alpha.(d_j + \frac{W_{out}}{n} * \sqrt{n^2 - i^2}))]) \}$$

The four lines associate with four SCR regions, which are Frontwall illuminated !! They are the same four regions as in the BW pixel's SCR AVP for Equation [3-56].

3.2.2.4 ***BW SJPD 2D pixel SCR AVP for 5 um wide beam on pixel well wall.*** [3-58]

$$= (I_0 / L_w) \{ ([\exp(-\alpha.(T - d_j + W_{in})) - \exp(-\alpha.T)].[W_{scr}]) +$$

$$([\exp(-\alpha.(T - d_j)) - \exp(-\alpha.(T - d_j + W_{in}))].[(L_w/2) + W_{out}]) +$$

$$([\exp(-\alpha.(T - d_j - W_{out})) - \exp(-\alpha.(T - d_j))] . [L_w/2]) +$$

$$(\frac{W_{out}}{n} * \sum_{i=1}^{n} [\exp(-\alpha.(T - d_j - \frac{W_{out}}{n} * \sqrt{n^2 - i^2})) - \exp(-\alpha.(T - d_j))]) \}.$$

The four lines associate with the same four SCR regions as for the BW pixel in Equation [3-56]. The difference is in the 5 μm wide region of the SCR that is intersected by the illumination over the pixels well wall. Notice the exponential part of each line is identical to Equation [3-56] while pixel pitch (P) is replaced by laser width (L_w).

3.2.2.5 ***FW SJPD 2D pixel SCR AVP for 5 um wide beam on pixel well wall.***

[3-59]

$$= (I_0 / L_w) \{ ([1 - \exp(-\alpha.(d_j - W_{in}))].[W_{scr}]) +$$

$$([\exp(-\alpha.(d_j - W_{in})) - \exp(-\alpha.d_j)].[(L_w/2) + W_{out})]) +$$

$$([\exp(-\alpha.d_j) - \exp(-\alpha.(d_j + W_{out}))].[L_w/2]) +$$

$$(\frac{W_{out}}{n} * \sum_{i=1}^{n} [\exp(-\alpha.d_j) - \exp(-\alpha.(d_j + \frac{W_{out}}{n} * \sqrt{n^2 - i^2}))]) \}$$

As in equation [3-58], the same applies for this equation in relation to the other FW pixel AVP equation [3-57].

3.2.2.6 ***BW SJPD 2D pixel SCR AVP for 5 um wide beam on pixel centre.***

$$= I_0 \ [\exp(-\alpha.(T - d_j - W_{out})) - \exp(-\alpha.(T - d_j + W_{in}))]. \qquad [3\text{-}60]$$

This is simply a 5 μm slice of the SCR normal to the well's bottom edge, that is astride the pixel centre. It is the 5 μm wide region of the SCR from the level of the SCR edge in the substrate, to the level of the SCR edge in the well. Distances are reference to the back wall of the pixel.

3.2.2.7 ***FW SJPD 2D pixel SCR AVP for 5 um wide beam on pixel centre.***

$$= I_0 \ [\exp(-\alpha.(d_j - W_{in})) - \exp(-\alpha.(d_j + W_{out}))]. \qquad [3\text{-}61]$$

This is simply a 5 um slice of the SCR normal to the well's bottom edge, that is astride the pixel centre. It is the 5 um wide region of the SCR from the level of the SCR edge in the well to the level of the SCR edge in the substrate. Distances reference to the front wall.

3.2.2.8 *Total pixel AVP.* [3-62]

$$= I_0.[1 - \exp(-\alpha.T)].$$

When $I_0 = 1$, Equation [3-62] gives the proportion of the total quantum budget spent in the whole pixel.

3.2.2.9 *Non-SCR AVP.*

All the SCR AVP above have non-SCR AVP associated with them. They are calculated as the difference in the Total pixel AVP (Equation [3-62]) and each associated SCR AVP. Additionally this AVP can be divided into two parts: inside and outside the pixel's well. This can give additional information that can explain the pixel's electrical response for illuminations inside and outside the well. However this project considers the more general non-SCR AVP statistics only.

3.2.2 **DJPD pixel AVP Equations.**

For the FW pixel AVP statistics the AVPs associated with the image-pixel are calculated with the pixel's lengths of the inner junction applied to the SJPD pixel AVP equations. The incident intensity is the same for the SJPD pixel.

For the BW pixel AVP statistics the same applies, except this time the incident intensity is reduced to a proportion of the original intensity that remains after the light has been absorbed in the substrate and SCR of the outer junction which the incident light encounters first.

Because the image-well width was not fixed in the DJPD simulations only the total 2D and central (5 μm wide) illumination AVP data were determined for the range of pixel configurations investigated. For the worked solutions see the original experimental notes photocopied for your convenience in Appendix XX (i.e. Appendix 20).

4. METHOD

The method used to investigate which pixel configuration has optimal response resolution and how it has optimum crosstalk suppression and central sensitivity, involves a research cycle. This cycle consists of collecting simulation results for a given range of pixels with a particular configuration parameter being varied. Then these results are compared graphically with the pixels' AVP data. Following this an attempt is made to explain the pixel response qualitatively taking into consideration the AVP, electron and hole and total QE response profiles. Also a comparison is made between BW and FW pixel response to again explain the advantages and disadvantages between them. Then the pixel relative crosstalk suppression is considered comparing BW and FW pixel NQE responses. The cycle then returns, investigating the variation of another pixel configuration parameter and includes an addition step that compares the new profiles with the previous responses for optimization considerations once again.

The order of pixel configuration parameter variation testing is,

1. Naked pixel response profile – effect of thickness and well depth.
2. Naked pixel response profile – effect of boundary trench isolation (BTI).
3. Guarded pixel response profile – effect of thickness and well depth.
4. Guarded pixel response profile – effect of well electrode width and placement.
5. Guarded pixel response profile – effect of well and substrate doping.
6. Guarded pixel response profile – effect of junction reverse biasing.
7. DJPD pixel response profile – effect of inner well width and depth.

Result statistics of total, electron and hole QEs, NQE and AVP data are used to compare the three main pixel types. As mentioned in the theory section, the naked pixel is a SJPD pixel with only a central image-electrode on the pixel's well. The guarded pixel is a naked pixel with an additional well electrode completely

surrounding the central image-electrode. The last type is the double junction photodiode (DJPD).

As data continues to be gathered a wider comparison between pixels can be made so that further understanding can be gained regarding optimizing pixel configurations. Furthermore, extrapolating this understanding with the application of AVP data as an operational probe tool, to predict more optimal pixel configurations, will also be explored.

This chapter considers the device structure and configuration parameters for the simulated pixels. The simulation file tools used to create the simulations are also defined. Finally a summary of the investigation protocol is given with an explanation of the simulation tool, SEMICAD DEVICE.

4.1 **Simulation Parameters.**

The Device simulation package used is commercial 2D finite-element package, called SEMICAD DEVICE.

The device structure, as shown in Figure 4.1, is compatible with 0.5 μm CMOS technology with a 2 metal n-well process.

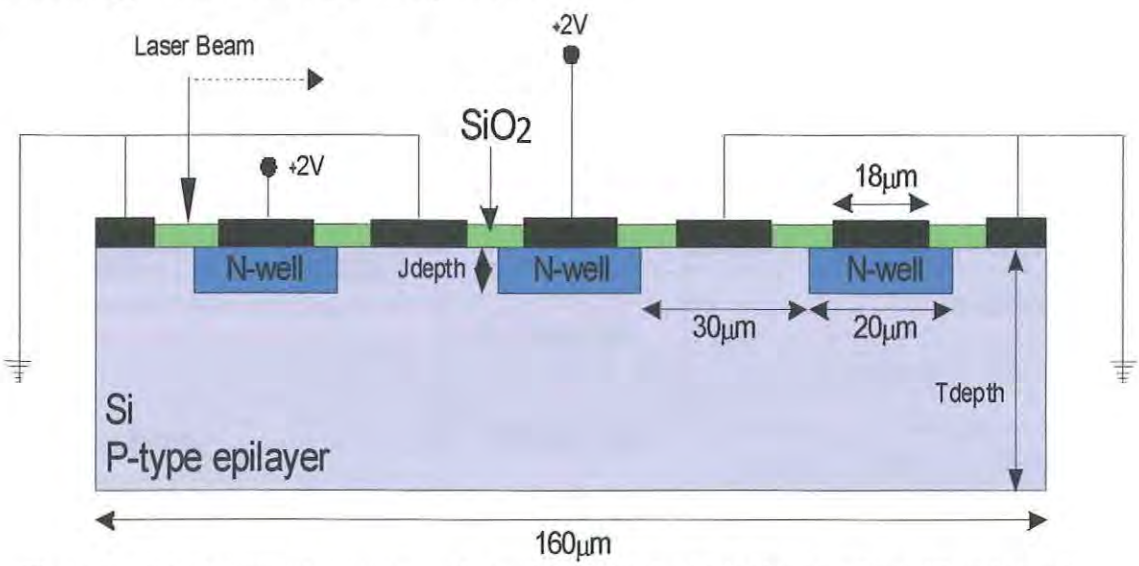

Figure. 4.1 Schematic cross-section of SJPD naked pixel array front illuminated.

This configuration allows the photodiode to accommodate flip-chip indium bump bonding to the processing chip in the back illuminated configuration. The device structure modeled is based on a previously fabricated photodiode array (Brouk I., Nemirovsky Y., Lachowicz S., Gluszak E.A., Hinckley S., Eshraghian K. 2002).

Figure 4.1 shows the basic configuration for the N well / P substrate naked SJPD pixel. The reverse doping type, but the same doping concentrations apply to the P well / N substrate SJPD. The BW mode is identical in structure, but with the laser illuminating from the bottom of the diagram, onto the backwall of the pixel.

The standard dimensions include an array width of 160 μm, an n-well width of 20 μm, a substrate thickness of 12 μm, and an emitter thickness (junction depth) of 2 μm. Ohmic contacts were contacted to the pixels' front surface (Figure 4.1). Contacts to the n-well emitters were grounded, and the ohmic p-substrate contacts were held at -2 volts, so that each pixel is 2 volts reverse biased.

Figure 4.2 shows the conventional vertical DJPD. It has an inner image-well inside an outer guard-well. The inner well and substrate are of opposite doping type to the outer well so that inner and outer PN junction are gererated. The doping concentrations conventionally increase from substrate through to inner well so that the SCRs penetrate outwards from each well into the outer well and substrate for the inner and outer SCRs respectively.

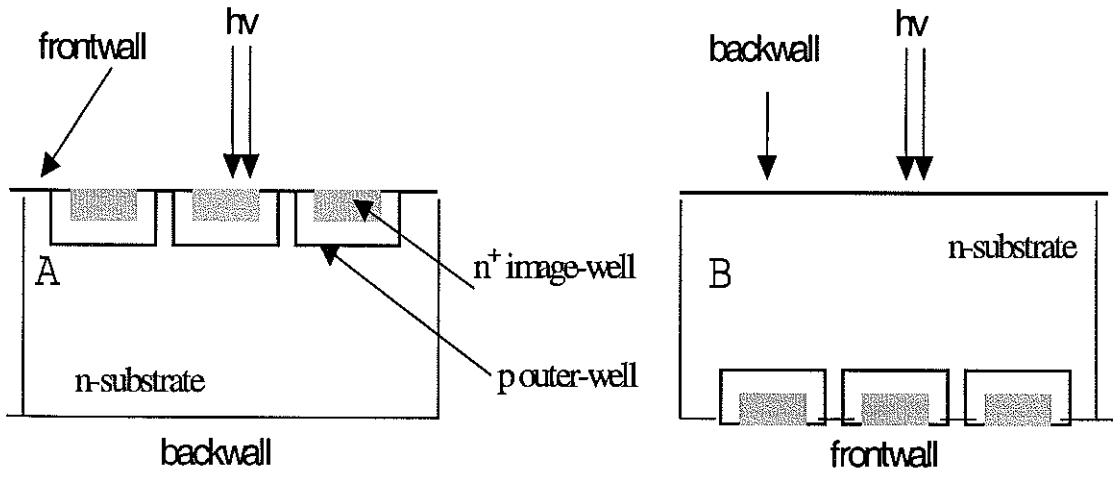

Figure 4.2 Array of three vertical NPN DJPD FW and BW reference pixels

For the reference vertical PNP DJPD pixel, the doping types are reversed from that of the default NPN DJPD pixel (Figure 4.2), whiie the doping concentrations remain the same. In 2D, the image electrode is now at the centre of the inner well with the outer well electrodes appearing either side of the image electrode on the outer well's exposed surface. The dimensions of the outer well and array substrate are equivalent to those for the reference vertical SJPD array pixels (Figure 4.1).

4.1.1 **The Pixel Configuration Parameters.**

"Configuration" refers to the following parameters being set at particular values for the tri-pixel array in one simulation. Each pixel is identical.

(A) Pixel topography – using square pixels, pitch (width) is a parameter.

(B) Pixel volume shape – pixel depth (substrate depth) is a parameter.

(C) Well topography – using square wells, for SJPD, well width is a parameter. For DJPD the parameters are 3a) inner well width and 3b) outer well width.

(D) Well volume shape – for this research using square wells, for SJPD, well depth is a parameter. For DJPD the parameters are, 4a) outer well depth and, 4b) inner well depth .

(E) Isolation trench and layer topography and volume shape – these are structures in the Pixel cross section that may add to the capture of unwanted photocarriers, such as crosstalk carriers. Only boundary trench isolation (BTI) structures are investigated, and that only for SJPD. Their parameters consist of,

5a) 2D surface width,
5b) 2D sub-surface depth and
5c) location either side of the pixel's well.

(F) Doping – the setting of a particular type of doping for structures in the 2D cross section – "p" type or "n" type – and their concentration values are parameters. In SJPD pixels the parameters are

6a) Substrate doping type and concentration and
6b) well doping type and concentration.

In DJPD pixels the parameters include

6a) substrate doping type and concentration,
6b) outer well doping type and concentration and
6c) inner well doping type and concentration.

For other regions or structures, of which there is only one other for this research, namely the BTI wells, the parameter is

6d) BTI well doping type and concentration.

(G) Reverse Biasing – the applying of a particular voltage to an electrode at the surface or the photodiode pixel that makes the intervening diode junction not forward biased. The bias determines the electric flux density in the capture volume associated with the biased electrode. Thus the voltage applied to electrodes on the frontwall of the simulated array are parameters.

(H) Electrode number per structure – Generally a single electrode is applied per structure i.e. per well and substrate.

(I) Electrode placement – This parameter effects the electrode's electric field capture volume location. The position of the image-electrode is always at the centre of each pixel.

(J) Electrode size – this last parameter effects the extent (width and depth) of the electric field at a particular location. Hence this parameter determines the pixel's capture volume.

4.1.2 The Default or Reference Configuration Parameter Values :

TABLE 4.1 The default SJPD pixel Configuration Parameter values.

Pixel Configuration Parameters	Value
A. Pixel topography : Pitch.	50 μm.
B. Pixel volume shape : Substrate depth.	3 μm
C. Well topography : width.	20 μm.
D. Well volume shape : well depth.	2 μm
E(a). BTI width.	2 μm
E(b). BTI depth.	0 μm
E(c). BTI centre of location in pixel.	10 μm either side of the pixel well walls
F(a). Doping : Substrate.	P or N-type : 10^{15} cm^{-3}
F(b). Doping : Well.	N or P-type : 10^{17} cm^{-3} (opposite type to Substrate)
G. Reverse biasing.	2 volts : (applies to all PN junctions) Cathodes are biased and anodes earthed .
H(a). Electrode number : Both Substrate and well	1
I(a). Electrode placement : Substrate	Centred on the pixel boundaries at positions 5, 55, 105 and 155 μm.
I(b). Electrode placement : Inner well (only well in SJPD)	Centred on each well at position 30, 80 and 130 μm. (for guarded SJPD, both outer electrodes end 1 μm from well's edges).
J(a). Electrode width : Substrate	10 μm (2 μm in some studies)
J(b). Electrode width : Inner well (only well in SJPD)	18 μm (single electrode SJPD); 4 μm (triple electrode SJPD); 1.6 μm (DJPD).

TABLE 4.2 The Default DJPD Pixel Configuration Parameter Values.

Pixel Configuration Parameters	Value
A. Pixel topography : Pitch.	= SJPD
B. Pixel volume shape : Substrate depth.	= SJPD
C. Well topography : width.	= SJPD
D. Well volume shape : well depth.	= SJPD
F(a). Doping : Substrate.	= SJPD
F(b). Doping : outer Well.	= SJPD
F(c). Doping : inner well.	P or N-type : 10^{18} cm^{-3} (opposite type to outer well)
G. Reverse biasing.	= SJPD
H(a). Electrode number : Substrate Inner	= SJPD
H(b). Electrode number : Inner Well	1
H(c). Electrode number : Outer well	2
I(a). Electrode placement : Substrate	= SJPD
I(b). Electrode placement : Inner well	= SJPD
I(c). Electrode placement : Outer well	Ending 1 μm from outer well's edges.
J(a). Electrode width : Substrate	= SJPD
J(b). Electrode width : Inner well	1.6 μm (DJPD).
J(c). Electrode width : Outer well	6.4 μm.

All Laser Illumination: λ = 0.633 μm; Laser width = 5 μm; Laser power = 0.1 μW.

4.2 The SCAN and Calculated Electrode Data.

One simulation scan ("SCAN") consists of simulating the scanning of a 5 μm wide 0.1 μW laser of 633 nm, at ***5 μm intervals***, across the 160 um surface of the array detailed in Figure 4.1, with the starting illumination position at the left side of the

array, the "zero μm position". In the array cross section (Figure. 4.1), the central pixel appears between the 55 μm and 105 μm positions, i.e. the central pixel boundaries fall at these two locations.

Of interest is the image-electrode response of the central pixel for each illumination position of the scan. This response is a current profile generated at the central electrode (image electrode) on the central well of the central pixel.

A *frontwall illuminated* (FW) scan is one where the beam passed over the front surface of the array. This is the surface that features the electrode contacts.

A *backwall illuminated* (BW) scan is one where the beam passes across the back wall of the array which is the substrate surface.

Each finite element simulation in each SCAN relies on only Shockley-Read-Hall (SRH) recombination (Auger recombination has been excluded at this time) so that results for fully depleted array pixels can not be fully relied upon and require further verification by simulations using an Auger recombination definition in the device file (Section 4.6). Of particular interest are the total, electron and hole currents captured by the central electrode, the image electrode of the central pixel, for each of the illumination positions of the laser.

4.3 The Absorption Volume Proportion (AVP).

The AVP is a calculated device probe statistic that represents the proportion of incident light absorbed by the SCR and the non-SCR associated with a pixel of given configuration and illumination mode, wavelength, power and illumination width (Section 3.2). AVP data when compared with QE data, from the simulations, helps to associate trends between each data set. This lends benefits to an understanding of the carrier dynamics associated with a particular configuration. This consequently may benefit understanding crosstalk suppression and sensitivity enhancement that result in optimal pixel response resolution.

Tabulated Absorption volumes are recorded as percentages of the total incident illumination intensity. Graphed Absorption volumes are the AVP proportionate data, representing values from zero to one. The pixel configuration parameters that directly effect this statistic are the width and depth of wells, the doping levels on either side of junctions, the bias across junctions, the mode of illumination (BW or FW) and the width, position, power and wavelength of the illuminating beam.

4.4 About The Result Statistics.

The result statistics that are obtained from each individual simulation, include the quantum efficiency (QE) and the normalized QE (NQE) of the total, electron and hole currents.

4.4.1 The Result Statistics defined.

The QE is a ratio of the number of captured carriers per incident photon. Knowing the charge on one carrier (C), the electronic charge, and the "captured" carrier current (C/sec), the number of captured carriers/sec is obtained. Then knowing the energy of one photon and the total incident power (J/s), the number of photon/ sec is obtained. The QE is then the quotient of the former to the later.

The NQE for a particular illumination position is the quotient of the QE at the central pixel's image-electrode for that position and the maximum QE at the central pixel's image-electrode. Usually the maximum QE is captured when the illumination position is over that central pixel's image-electrode; i.e. at the 80 μm illumination position. However this may not be the case if the capture efficiency is greater at another illumination position for a given pixel configuration and illumination width.

The relative crosstalk, experienced by the central pixel's image-electrode, is defined as the NQE of the total current captured by that image-electrode when the laser is illuminating over the 55 μm position or the 105 μm position; the boundaries of the central Pixel. This is not the total crosstalk, which is more precisely obtained with a

3D simulation. However, with this "relative" value, the boundary NQE, it is possible to compare between relative crosstalk (pixel boundary NQE) and well-edge NQE response for different pixel configurations, so that limits to resolution and fill factor increase may be ascertained.

For comparison with the collected QEs and NQEs, per SCAN, for a give subset of pixel configuration parameter permutations, included are the calculated AVP for the space charge region (SCR) or depletion layer and the non-SCR or the region of the pixel not bounded by the pixel's SCR. For the DJPD configurations, the inner SCR's and inner non-SCR's absorption volumes have been calculated as changes in these volumes ultimately effect the DJPD pixel image-electrode response. This is because photo carriers generated in the pixel volume outside the inner edge of the outer well's SCR, are captured by the outer junction of the pixel or by the outer junction of a neighbouring pixel and are therefore excluded from image-electrode capture.

4.4.2 **The Result Statistics.**

The results section reports on the effects of the pixel configuration parameter variation, in BW and FW pixel, on the following result statistics and absorption volume proportions (AVP).

1. *The QE responses of the image-electrode for illumination over various positions within the central pixel, including the boundaries.*

   This is to gain an understanding of the extent of image-carrier capture suppression inside the pixel for future investigations involving resolution increase and down scaling for particular pixel configurations. This examination of the QE response is also to allow comparison between the different modes of illumination. The mechanisms underlying the IE's total current QE response may be elucidated by comparison with calculated AVP data for both illumination modes. Also, reference may be made, in some configuration parameter studies, to the electron and hole QE response.

2. *The Maximum QE (measure of sensitivity) and central QE (expected maximum) responses are compared for different BW and FW pixel configurations.*

   Though a particular pixel configuration may have excellent boundary normalized QE (NQE), i.e. minimal relative crosstalk, its maximum QE and hence its sensitivity may be reduced. The mechanism underlying each and any deviation between the two QE values, may be elucidated again, by comparison with calculated AVP data and the minority photocarrier QE data. Understanding the response of these two result statistics, impacts on understanding crosstalk reducing measures, as the relative crosstalk is inversely related to one of these values and possibly both.

3. *Pixel boundary normalized QE (NQE) response of the image-electrode i.e. at the 55 μm and 105 μm illumination positions (Figure 4.1).*

   This is acquired to discover which configuration, in the group of SCANs, has the least boundary NQE and hence the least relative crosstalk. Again the mechanisms underlying the IE's NQE response, may be elucidated by comparison with calculated AVP data as well as trends already observed for the boundary QE and maximum QE.

4. *NQE response at the image-electrode for illumination over the central pixel's well wall i.e. at the 70 μm and 90 μm positions.*

   Especially in the case of DJPD configurations, this result statistic is obtained to discover which configuration in the group of SCANs has the least outer-well-edge NQE and hence possibly the best configuration for fill factor increase. Again the mechanisms underlying the image-electrode's NQE response, may be elucidated by comparison with calculated AVP data.

4.5 The Investigation Senario.

The effects on the above result statistics, of varying the following photodiode pixel configuration parameters are reported on.

For **SJPD** pixels:

The effect of varying –

- Substrate and well depth in naked pixel;
- Boundary trench isolation (BTI) well depth and width in naked pixel;
- Substrate and well depth in guarded pixel;
- The size and position of well electrodes in guarded pixel;
- Doping of wells and substrate in n-well and p-well guarded pixel;
- Pixel electrode biasing;

For **DJPD** : For both PNP and NPN pixels:

The effect of varying –

- Inner well depth;
- Inner well width;

The above result statistics are reported and compared for each pixel configuration. Trends in these statistics are compared qualitatively with device photocarrier mechanics, resulting from the photon absorption characteristics, the number and localizations of SCRs, photocarrier drift, diffusion and mobility. These characteristics are determined by the biasing and doping regimes and the geometry of structures (wells, BTI, etc) associated with the pixel array cross section.

4.6 The Simulation tool: SEMICAD DEVICE™.

To run a simulation, two files need to be defined: the *device file* and the *run file*.

In the ***Device file***, the basic array parameters and operating conditions are defined. These include material type, optics, recombination type, array pixel infrastructure geometry, doping species, doping concentrations, ohmic contact (electrode) size, placement and biasing as well as illumination beam number, their intensity, wavelength and width. For a basic example, the original template from which all the device files originate can be viewed in Appendix XVIII.

The ***Run file*** contains the program that does the simulation. It defines the parameter value loops which constitute the SCAN and contains the following elements:

1. Inputs the device file.
2. Redefines configuration parameters predefined in the device file.
3. Simulates the interaction of the beam with the 2D array cross section
4. Outputs a requested selection of calculated current and / or QE values to a defined output file for each scan position.

The run file calls to the input file (device file) and then runs the SCAN, outputing defined pixel response characteristics for each position of the scan to an output file ("<name>.dat"). Conveniently for the run file's pixel geometry variation loops, the array is defined inverted to Figure 4.1 so that backwall illumination is from above.

For a basic example of a run file, the original template from which all the run files originated can be viewed in Appendix XIX.

The numerical simulation divides the array cross section into a mesh, consisting of square, triangular and rectangular structures. On average SEMICAD DEVICE™ mesh nodes are about 0.5 μm apart. The grid is finer nearer electrodes and contacts between structures of different doping type and / or concentration, such as BTI wells, epilayer and junction structures.

The Poisson and electron and hole current continuity equations are solved using increasing degrees of Newton-Raphson Method computations, until the numerical solutions converge to give the hole and electron concentrations for each node in the mesh. From these concentrations the current density captured by each electrode is calculated. Under certain conditions these computations do not converge and the result is recorded as undefined. This can occur for silicon devices with illumination wavelengths near the violet end of the spectrum because the light is completely absorbed at the device's surface, with negligible sub surface absorption and subsurface photocarrier generation.

This iterative, finite element method calculates the electron and hole currents across the array that are captured by the electrodes for each illumination position. Therefore one scan of an array of pixels of a particular pixel configuration, involves making this total array current calculation 32 times as there are 32 individual illumination positions across the array, scanning from the 0 μm position to the 160 μm position. To save time some SCANs are attenuated to extending from the 30 μm to the 130 μm illumination position.

5. RESULTS

This chapter presents the resulting graphical profiles for the effect of various configuration parameters on the total, electron and hole quantum efficiencies (QE), the normalized QE (NQE) and in some cases the absorption volume proportion (AVP). This is for both the naked and guarded vertical single junction photodiode (SJPD) pixels, as well as the vertical double junction photodiode (DJPD) pixel. The variation of some parameters does not change the AVP. For the DJPD the inner SCR AVP and the AVP of the remaining region inside the DJPD pixel's outer well, not including the inner SCR, is also considered.

NB: Only in the Appendix is "BI" and "FI" used for the acronym of "Backwall illuminated" pixel and "frontwall illuminated" pixel, respectively.

5.1 The Vertical SJPD Pixel.

The full set of result statistics generated from the simulation data for each parameter studied is tabulated in the results Appendices I and II. Results demonstrating the underlying trends in the total result set are presented graphically.

5.1.1 Effect of Substrate Thickness and Well Depth on Naked Pixels.

The two variables are studied together because they are related in terms of pixel response (Hinckley, Jansz, Gluszak, Eshraghian 2002) (Hinckley, Gluszak, Eshraghian 2000). The scan provides QE data for illumination positions across the 160 μm length of the array. Since it is the central pixel's image-cathode response that is of interest, and the response is symmetical about the centre of the pixel, (i.e. symmetrical about the 80 μm position), the graph of these results only shows illumination positions 40 to 80 μm.

Figure 5.1 shows the BW pixel QE against illumination position, for pixels thicknesses of 3, 6 and 12 μm and well depth of 0.5. 1, 2, 4 and 8 μm, where possible. The boundary occurs at position 55 μm. The data are grouped by substrate thickness (SD) in that the 3, 6 and 12 μm thicknesses have points represented by squares, triangles and circles, respectively. Within each substrate group is the minimum and maximum well depth i.e. junction depth (JD) response. For pixels having other well depths, their responses fall inside these "boundaries". "SD/JD = 12/4" refers to a pixel with a substrate and well depth of 12 μm and 4 μm, respectively.

As the substrate thickness reduces, the QE profile reduces. As the well depth reduces the profile again reduces. The boundary QE is a minimum for the shallowest substrate, though it has the least sensitivity, indicated by having the lowest maximum QE response. However the suppression at the boundary is proportionately more than at the centre of the pixel, implying that the boundary normalized QE (NQE) will also be a minimum for the shallowest pixels. All of this confirms previous findings that the shallowest BW pixel has the best response resolution (Hinckley, et al 2002) (Hinckley, et al 2000). This implies that it has the minimum crosstalk and maximum central QE, the latter being a measure of the pixel's sensitivity.

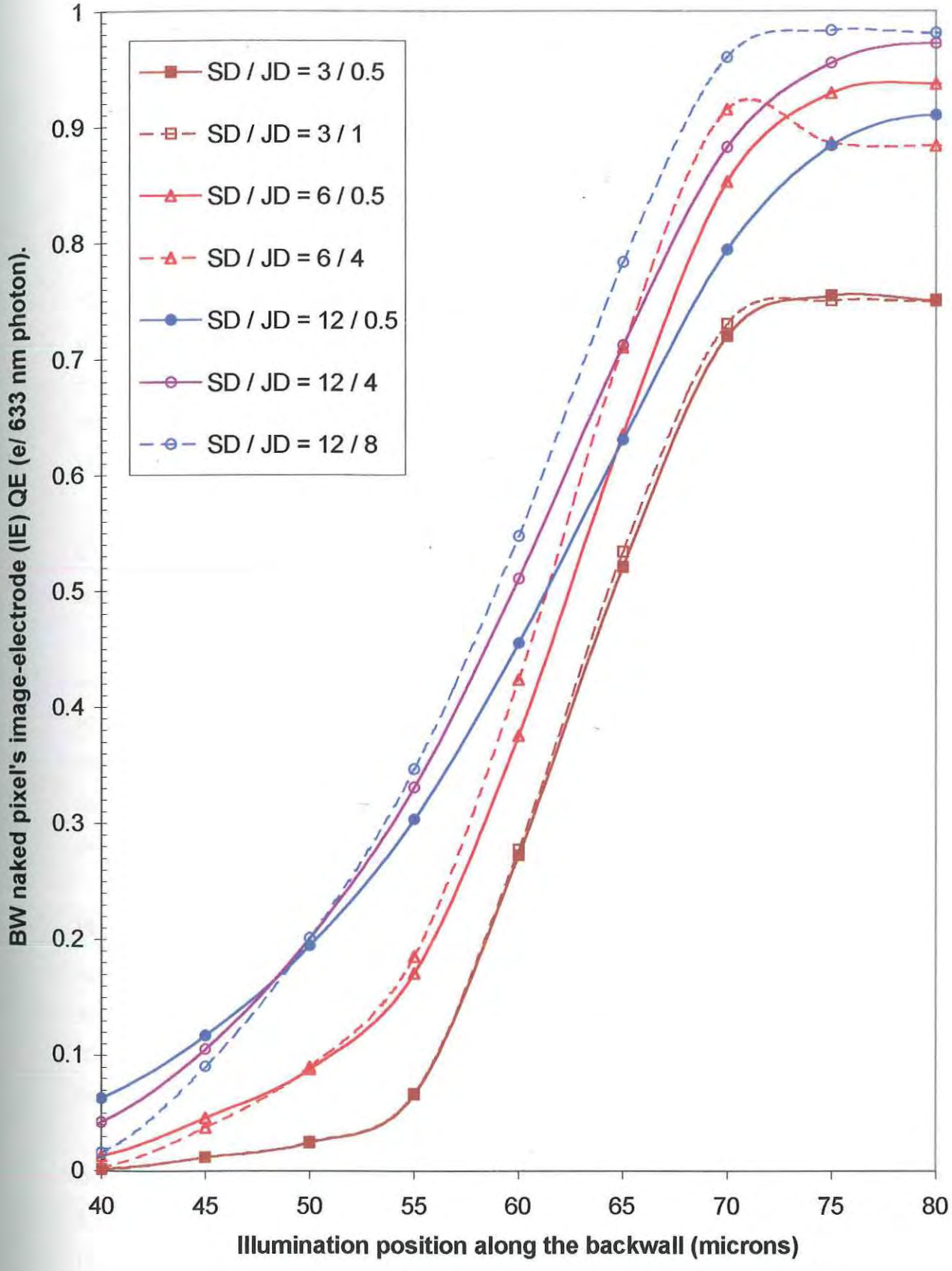

Figure 5.1: BW naked SJPD : single electode on well (18um): The IE QE dependence on well and substrate depth for illuminations from the centre of the adjacent well to the centre of the central well.

Figure 5.2 shows the FW pixel QE against illumination position, for pixels thicknesses and well depth similar to Figure 5.1. The boundary occurs at illumination position 55 μm. The data is grouped by substrate thickness (SD) and then by well depth in the same way as for Figure 5.1. "SD/JD = 12/4" refers to a pixel with a substrate and well depth of 12 μm and 4 μm respectively.

Note the suppression for illuminations over the well region increases with increasing well depth (JD), clearly more pronounced for this mode of illumination. Also the more proximate the illumination to the well centre, the worse is the problem. Without the benefit of Absorption volume proportion (AVP) data, the physical reason is not immediately clear.

Common to both modes of illumination is that the shallowest substrate pixel (3 μm) is insensitive to well depth. Contrasting both modes of illumination, outside the well, the BW pixel QE response is less steep than the FW response, implying a less suppressed QE response. This degree of enhancement of the BW pixel response lessens, as substrate thickness decreases, until the responses for both is indistinguishable. It is unclear from the total QE data, without reference to the individual carrier response and AVP data, the reason for the suppressed profile inside the well for the thicker substrate, deeper well pixels.

Figures 5.1 – 5.2 represent the QE against illumination position, demonstrating the spread of the response. Also useful for analysis purposes is graphing against the varying parameter. In this way each line on this transformed graph represents the QE response at one illumination position. Also AVP data can be included for comparison with the QE response across the pixel.

Initially the relationship between QE response and the ***well's depth*** is considered. Using the deepest substrate pixel (12 μm) with varying depth of well, a survey of illumination positions from 45 to 80 μm is undertaken, i.e. illumination positions from the pixel centre outwards. The relationship of the electron QE (hence the hole QE) and the AVP profile for illumination over the well wall (70 μm position) and at the centre (80 μm position) are compared to the simulated QE position profiles.

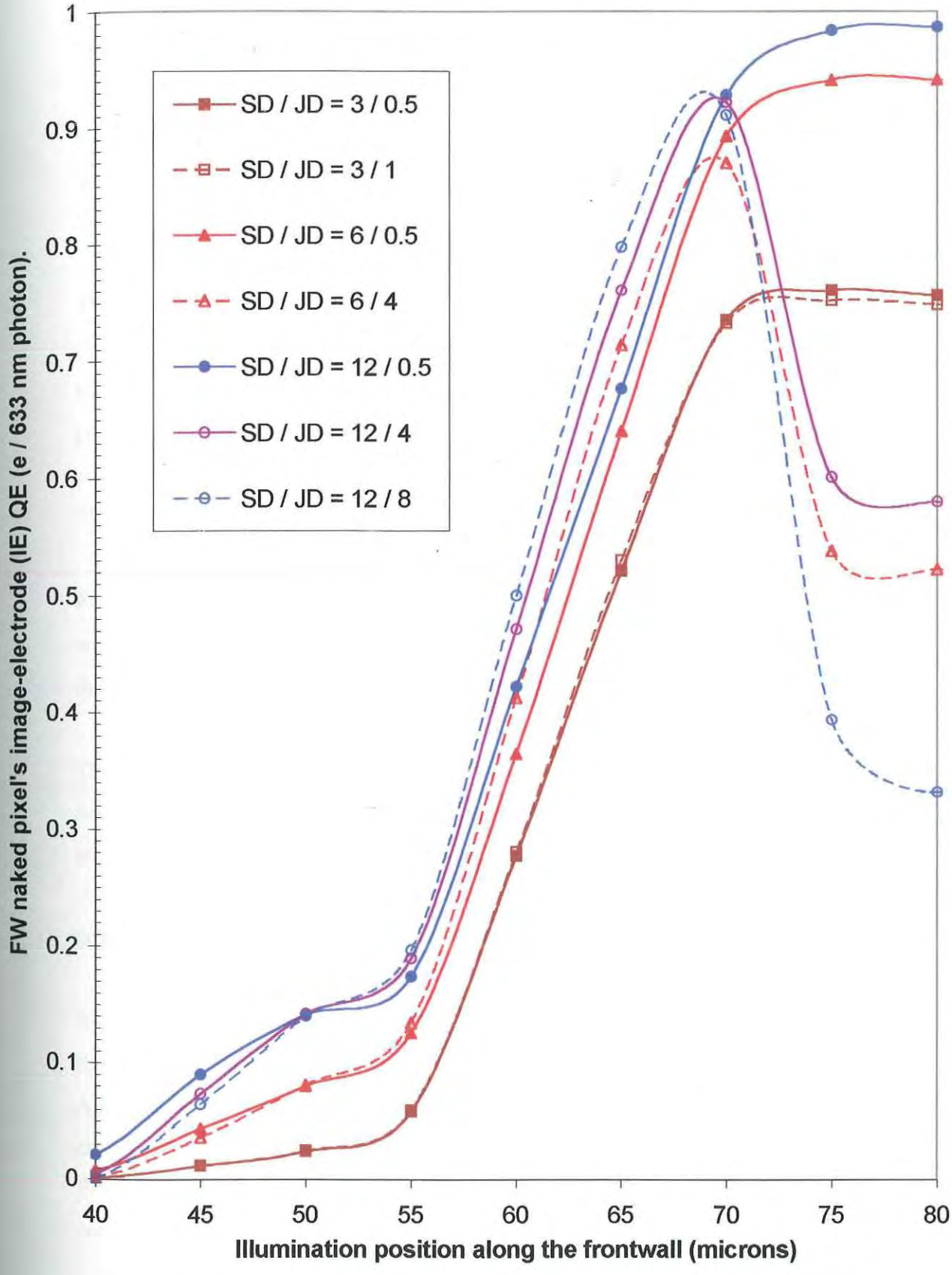

Figure 5.2 : FW naked SJPD : single electode (18 um) on well: The IE QE dependence on well and substrate depth for illuminations from the centre of the adjacent well to the centre of the central well.

The relationship between QE response and ***well depth*** is now investigated.

Figure 5.3 shows the BW pixel QE response for the 12 μm thickness substrate and well depth from 0.5 to 8 μm for illuminations *outside the central well* compared to the AVP data. For full QE and AVP results see Appendices I and II, respectively.

The slope increases positively as illumination moves closer to the well wall (70 μm position), the space charge region (SCR) envelope. The SCR AVP also increases indicating increasing capture efficiency as well depth increases and proximity to SCR increases. The diffusion component, which is proportional to the non-SCR AVP response, has more influence on the QE response further from the SCR, countering the drift component increasing with junction depth.

Figure 5.4 shows the FW pixel QE response for the 12 μm thickness substrate and well depth from 0.5 to 8 μm for illuminations *outside the central well* compared to the AVP data. . For full QE and AVP results see Appendices I and II, respectively.

The response parallels the SCR AVP data more than the BW response, as the illumination approaches the well wall. This is related to the higher SCR AVP profile and the better resultant capture efficiency, making the drift component dominate more than for the BW pixel. The BW pixel is dominated more by the diffusion component owing to more absorption away from the SCR.

It is noticeable that the FW pixel QE (55 μm profile) is more suppressed away from the well, while more enhanced next to the well, compared to the BW response. Again the increased capture efficiency by all pixels encourages less "free" crosstalk carrier diffusion from outside the pixel boundaries, while enhancing capture closer to the well wall. Also the FW and BW pixel's negative hole QE profile is minimal outside the well, owing to the minority carrier generated in this p-substrate region being the electron.

(cf/ Results naked SJPD: Appendix I & II.)

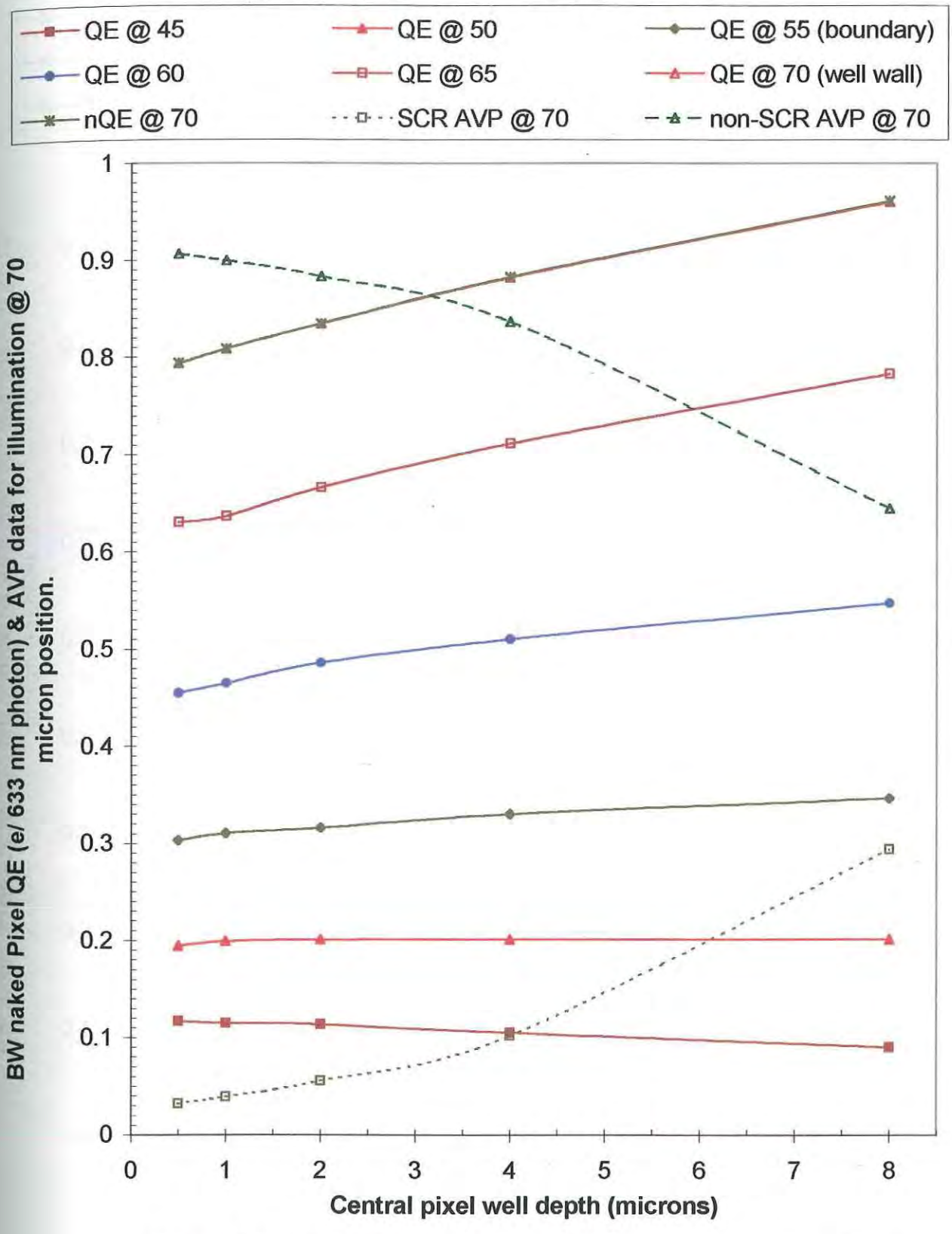

Figure 5.3 : BW SJPD : single well electode (18 um): The IE QE dependence on well and substrate (12 um) depth for illuminations outside central well compared to AVPs for illumniation over the central well's wall.

(cf/ Results naked SJPD: Appendix I & II.)

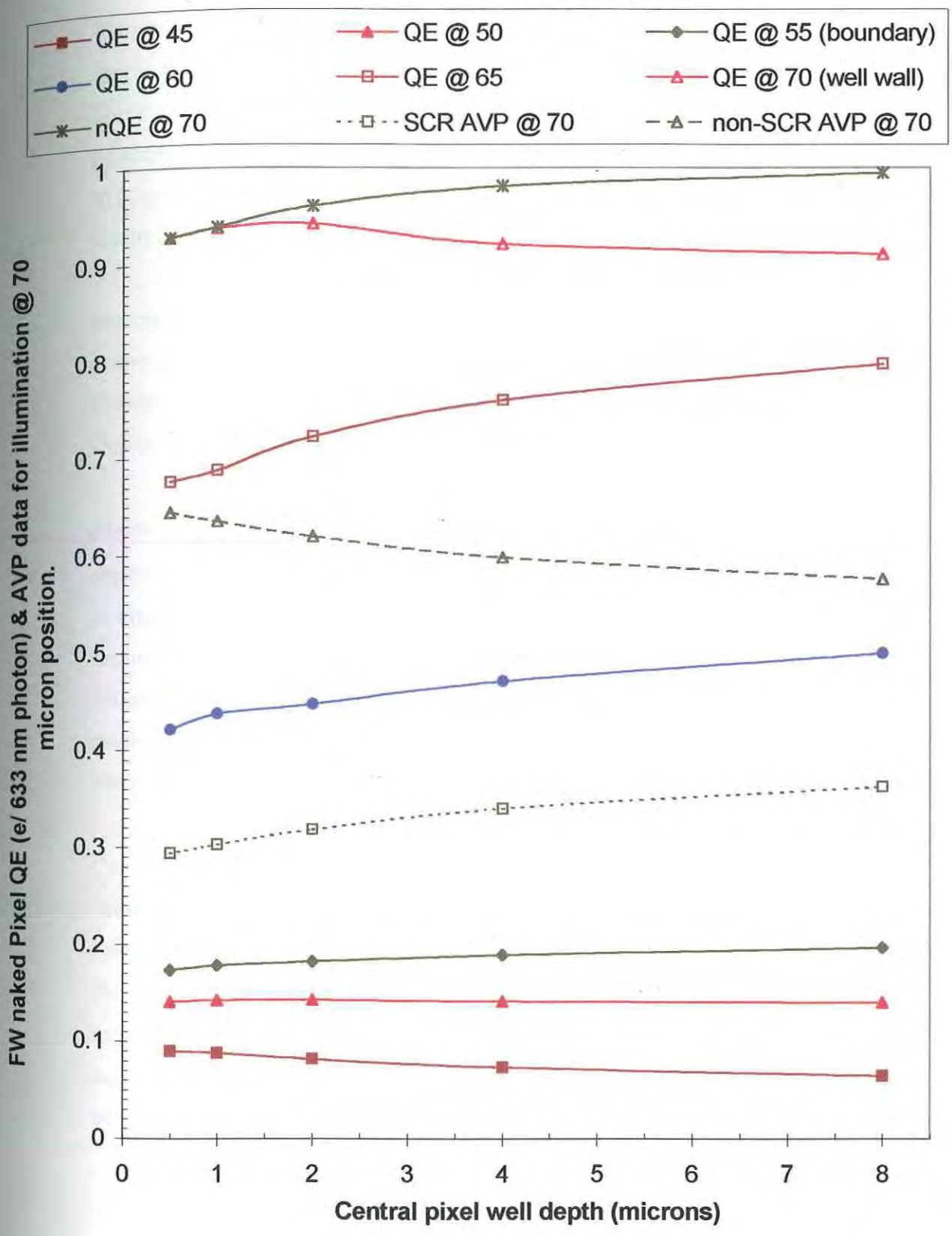

Figure 5.4: FW naked SJPD : single well electode (18 um): The IE QE dependence on well and substrate (12 um) depth for illuminations outside central well compared to AVP for illumination over the central well's wall.

Figure 5.5 shows the BW pixel QE response for the 12 μm thick substrate and well depths from 0.5 to 8 μm for illuminations *over the central well wall and centre.* These are contrasted with the BW pixel AVP profiles for similar illumination positions. If the electron QE is above the total QE, the gap represents the hole QE, indicative of negative hole current generated in the n-well. For full QE and AVP results see Appendices I and II, respectively.

For the BW pixel, the QE suppressing hole current is only noticeable at the well centre and only for the deepest well, where a larger portion of the non-SCR AVP is absorbed. This advantage for the deeper BW SJPD pixels is not significant as the shallower pixels present better reduced boundary QE (crosstalk) advantages.

Figure 5.6 shows the FW pixel QE response for the 12 μm thick substrate and well depths from 0.5 to 8 μm for illuminations *over the central well wall and centre.* As in Figure 5.5, these are contrasted with the AVP profiles. For the FW pixel, the QE suppressing hole current is very noticeable, increasing towards the pixel centre, where, due to the immediate proximity of the illumination to the well, a greater portion of the non-SCR AVP is absorbed, compared to the BW pixel. For full QE and AVP results see Appendices I and II, respectively.

Comparing the two AVP profiles between the 70 and 80 μm illumination positions, between BW and FW pixels, it is noted that the FW pixel response changes considerably, reversing the direction of response for increasing well depth. Due to the continuous illumination of an increasing SCR volume over the well wall and a increasingly distant SCR volume at the well's centre, the maximum QE, the most sensitive illumination position, shifts from the centre to the well wall. This advantages the BW pixel as has been already noted.

(cf/ Results naked SJPD: Appendix I & II.)

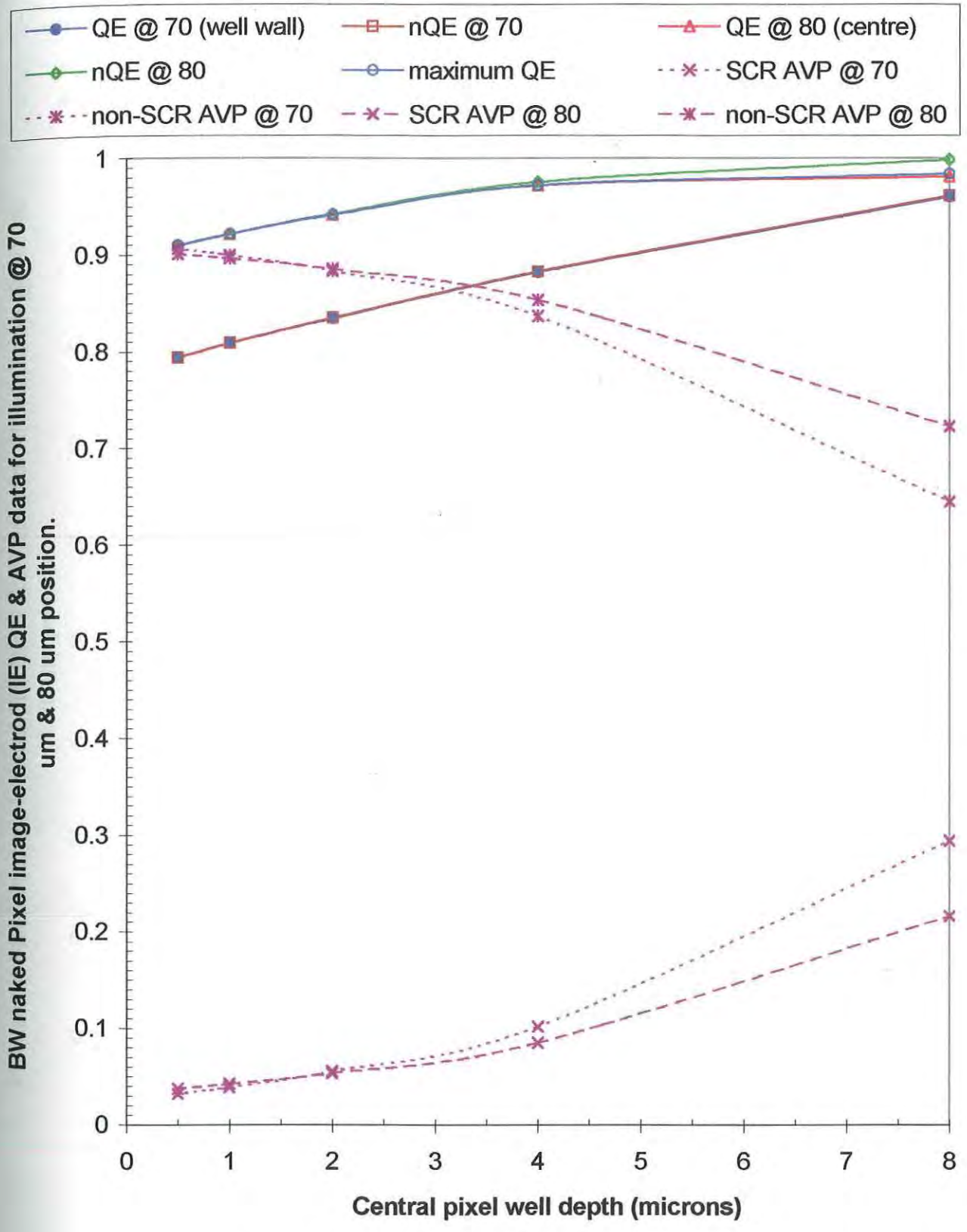

Figure 5.5: BW naked SJPD: single well electode (18 um): The IE QE dependence on well and substrate (12 um) depth for illuminations over the central well, compared to well wall and central illumination AVP data.

(cf/ Results naked SJPD: Appendix I & II.)

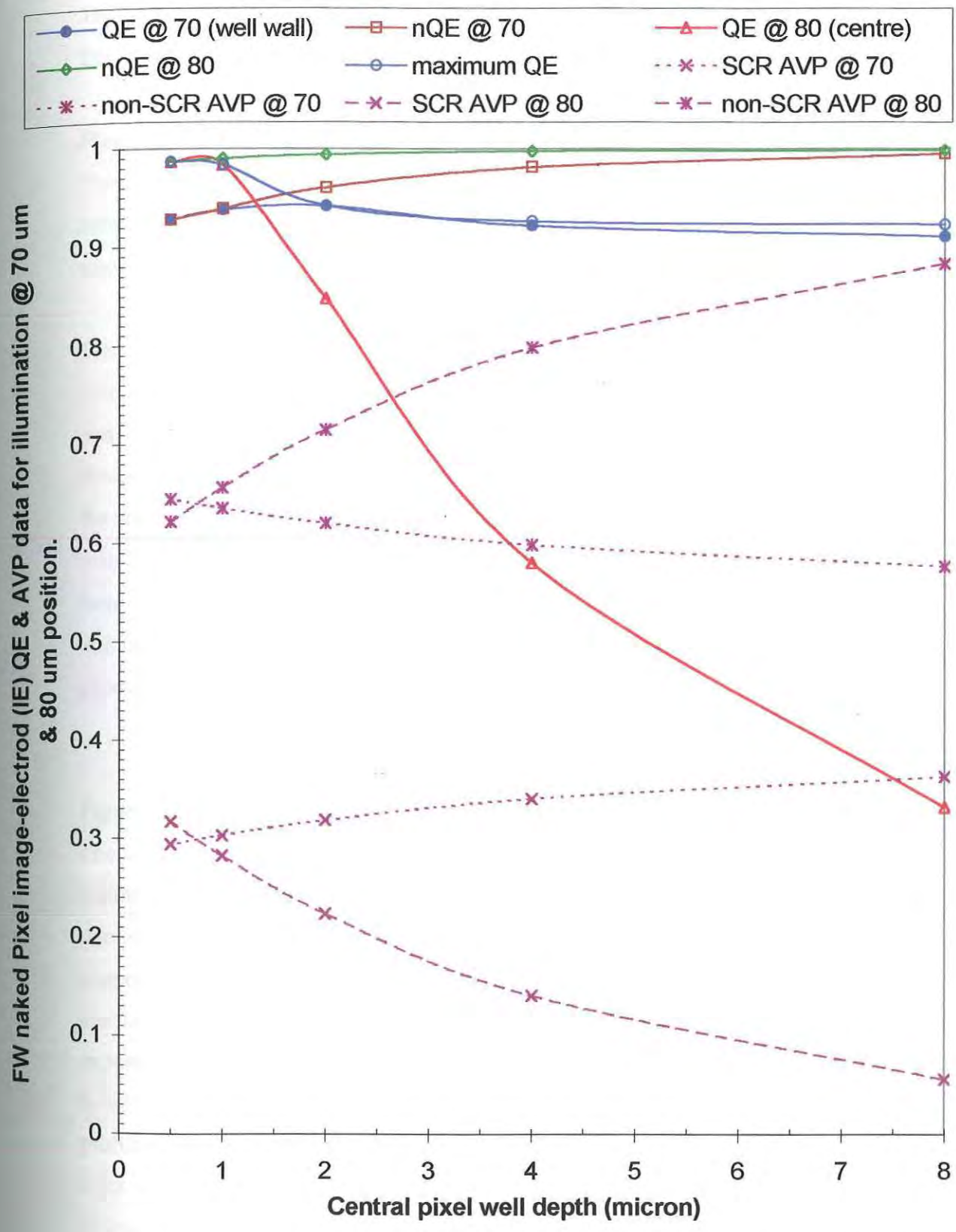

Fig 5.6: FW naked SJPD: single well electode (18 um): The IE QE dependence on well and substrate (12 um) depth for illuminations over the central well, compared to well wall and central illumination AVP data.

The relationship between QE response and ***substrate thickness*** is now investigated. This is important for comparison with the above response for well depth variation.

Figure 5.7 shows the BW pixel QE response against varying substrate thickness. Here the 3/1, 6/1 and 12/1 guarded pixels will be considered where 3/1 means substrate and well depth of 3 μm and 1 μm, respectively. For full QE and AVP results see Appendices I and II, respectively.

The response is linear from the pixel boundary outwards. The rising QE profile, compared to the exponentially decreasing SCR AVP profile and the increasing non-SCR AVP profile indicates that the increasing pixel capture efficiency is dominated by more diffusion component of the photocarrier transport. Furthermore, the coincidence of the electron QE (nQE) and total QE (QE) profiles for illumination over the pixel well (70 and 80 μm positions) indicates insignificant hole QE (pQE) from inside the well. This indicates that the increasing pixel capture efficiency is dominated by diffusion in the increasing p-substrate of minority electron photocarriers.

Figure. 5.8 shows the FW pixel QE response against varying substrate thickness. The same pixel geometries for Figure 5.7 are considered here. For full QE and AVP results see Appendices I and II, respectively. The BW response is similar, though this response is more enhanced next to the well and inside the well, while more suppressed away from the well, towards the pixel boundary. This is due to the constant SCR AVP profile, which is decreasing in the BW pixel, that enhances capture efficiency close to the well while limiting the diffusion component in the substrate that reduces crosstalk capture, owing to a less enhanced non-SCR AVP profile compared to the BW pixel. Similar to the BW pixel, the nQE and QE profiles coincide, indicating that photogeneration in the p-substrate dominates as the source of image carriers. Note the 3/1 BW pixel and 3/1 FW pixel QE response are similar owing to their similar AVP profiles, again reiterating the importance of the AVP statistic in predicting whether a particular pixel configuration has optimal crosstalk, sensitivity and trans-pixel QE characteristics that includes suppressed QE profile outside the well and an enhanced QE profile inside the well.

(cf/ Full Results naked SJPD : Appendix I & II)

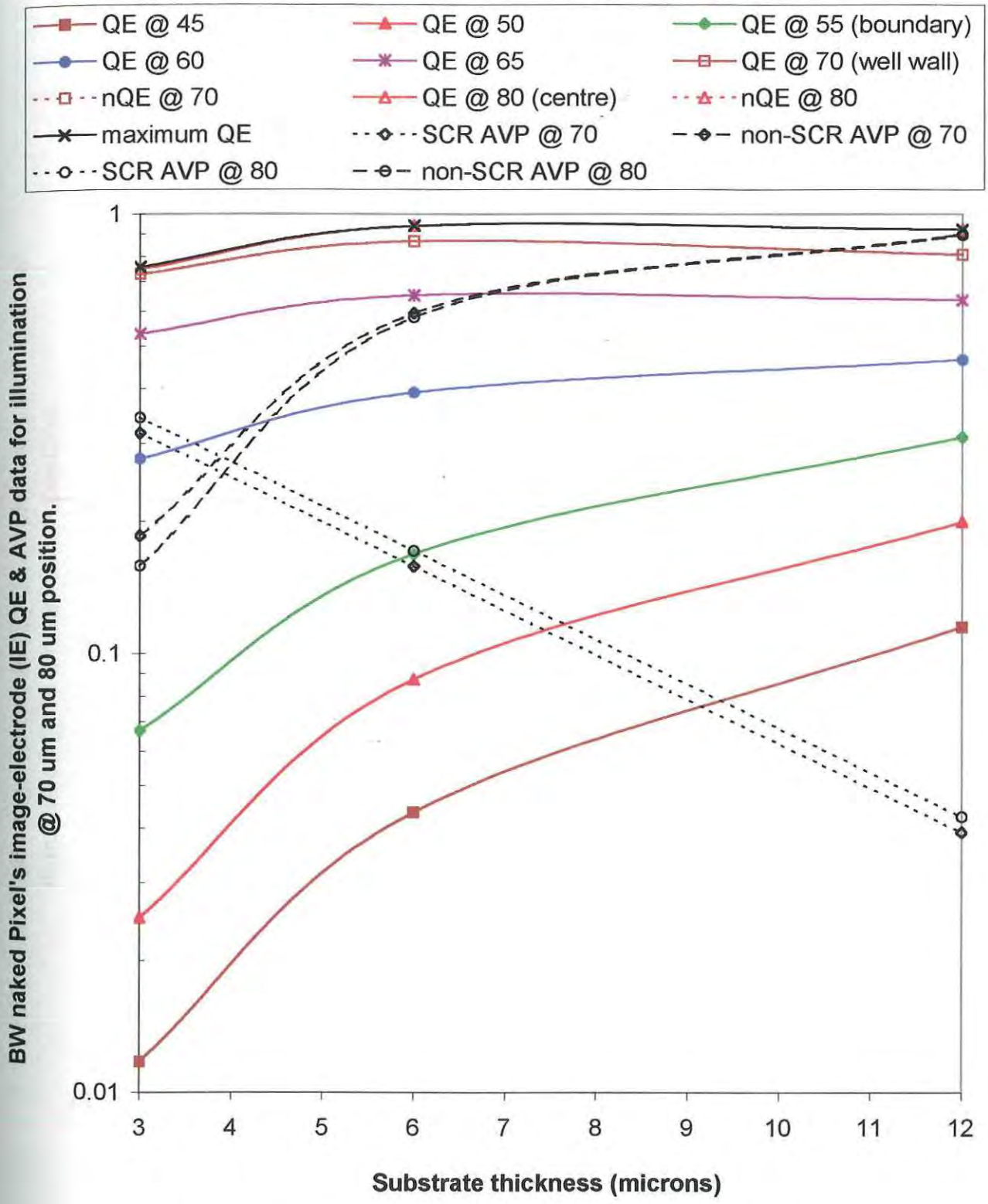

Figure 5.7: **BW naked SJPD: 1-electrode on well (18 um): The IE QE dependence on substrate thickness and well depth 1 um for illuminations from the pixel centre outwards, compared to well wall & central AVP data.**

(cf/ Results naked SJPD: Appendix I & II.)

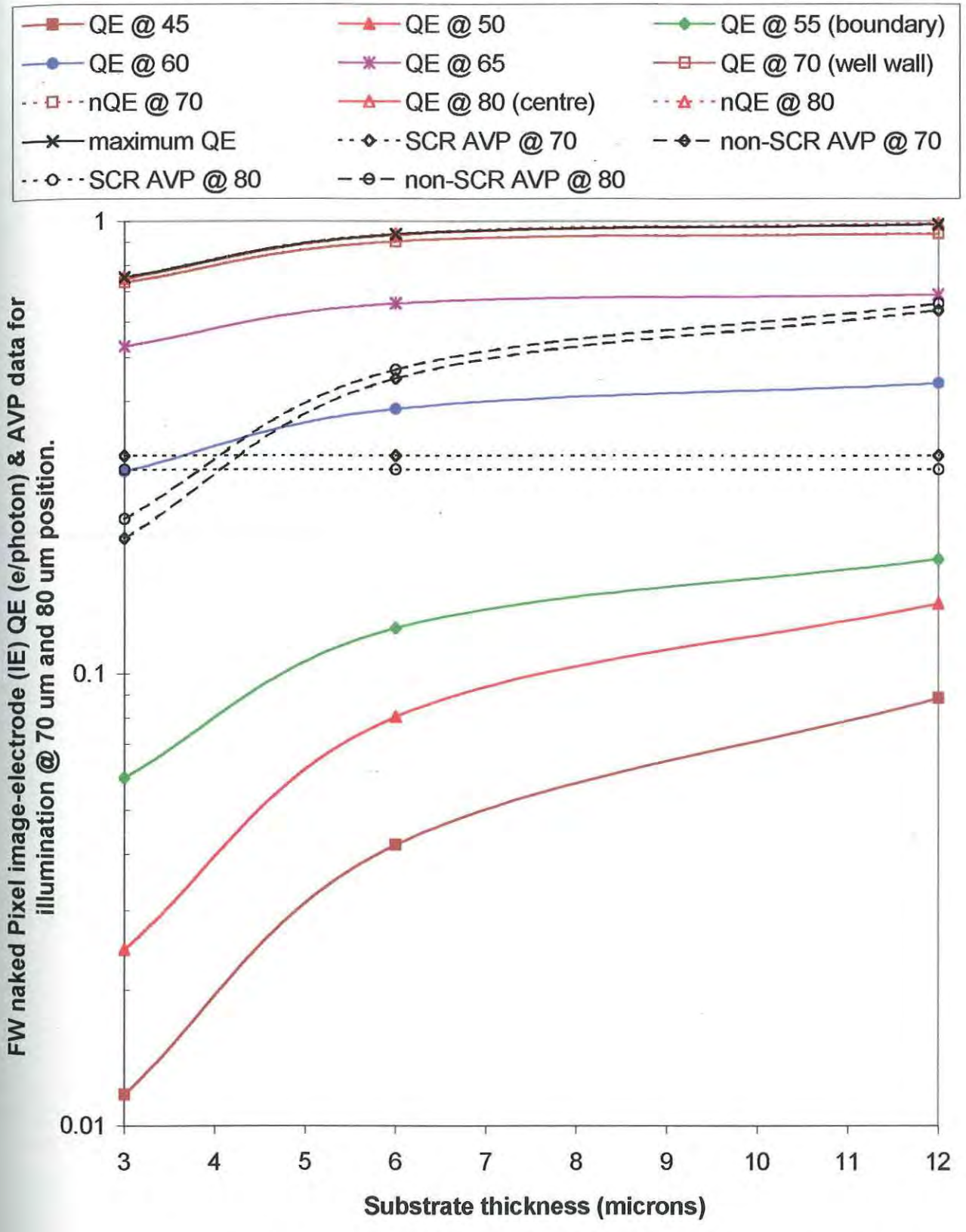

Figure 5.8: **FW naked SJPD: 1-electrode on well (18 um): The IE QE dependence on substrate thickness and well depth 1 um for illuminations from the pixel centre outwards, compared to well wall & central AVP data.**

Figure 5.9 shows the comparison of the NQE profiles for the BW pixel and FW pixel with the shallowest thickness, having the best NQE profiles. The lower FW pixel boundary NQE is not significant enough to make any distinction between the two modes of illumination. The profile indicates that the NQE responses for these pixels are insensitive to well depth. For full NQE and AVP results see Appendices I and II, respectively.

The minimum boundary NQE response is relatively insensitive to changes in well depth, within the limited range that could be tested owing to the shallowness of the substrate and the 1.86 μm wide portion of the SCR that penetrates the substrate below the well junction. The minimum NQE value is 0.077, recorded for the shallowest well and substrate FW pixel. The same pixel BW has an NQE value of 0.087, 13% more, and is also the minimum value for all the BW pixels considered.

The lowest relative crosstalk occurs where the 2D total pixel SCR AVP is greater than the minimal non-SCR AVP (Appendix II). This has a dual effect. Firstly, the minimization of the diffusion in the substrate surrounding the well reduces the Pixel's boundary QE (Figures 5.1 & 5.2). Secondly, a suppression of the QE-reducing hole current, generated less in the shallower wells, tends to maximize the QE and hence maximizing the maximum QE (Figures 5.1 & 5.2). These two effects, due to the shallower well and substrate geometry, serve to minimize the boundary NQE, thus minimizing the pixel's relative crosstalk.

(cf/ Full Results naked SJPD : Appendix I & II)

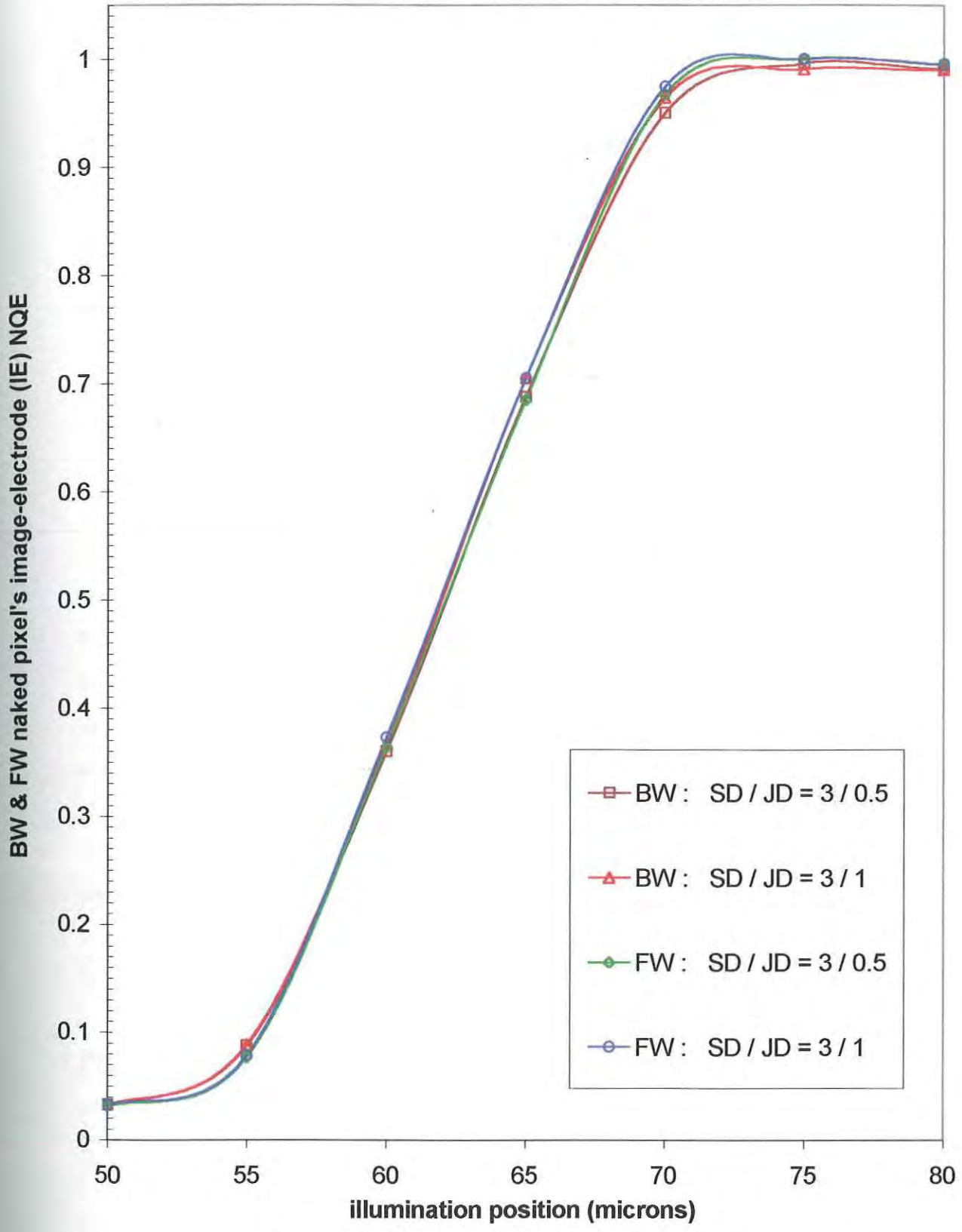

Figure 5.9 : BW & FW naked SJPD : single cathode (18um) on well: The pixel's normalized QE (NQE) for the left half of the central pixel; the BW & FW 3 um substrate naked pixels' responses are compared.

5.1.2 Effect of Boundary Trench Isolation (BTI) on Naked Pixels.

As stated in the method (Section 4.1.2, p 71) each BTI is 2 μm wide, and are centred 5 μm from the pixel boundary either side of the pixel's well. They are doped as p^+ 10^{19} cm^{-3}. Initially presented are the QE responses graphed against the illumination positions, for a representative selection of the total data set (Appendix III & IV). This small sample shows the general trend in the pixel response profile repeated in all pixel geometries, to a lesser or greater extent, as the BTI depth is varied.

Figure 5.10 shows the BW pixel QE response for different pixel configurations against the illumination position. The data is grouped by configuration, each consisting of the control pixel QE response (no BTI) and the QE response of the same pixel with the deepest BTI (test). Test and control Electron QEs are also demonstrated.

For BW pixels, the presence of the BTI suppresses the QE response from the boundary outwards, while enhancing the response inside the pixel. The exception is the 3/1 pixel with thickness 3 μm and a well depth 1 μm (3/1 pixel). The enhancement inside the well that is observed for the other pixels is reversed for this pixel configuration. Generally the electron QEs (nQE) are coincident with their associated total QEs from the well wall outwards. More noticeable in the deeper well pixels – e.g. the 6/4 pixel – inside the well, the nQE is greater than the total QE, implying a more significantly constant negative hole current. The presence of the BTI influences a suppression of both carrier QEs in the well.

Figure 5.11 shows the FW pixel QE response against the illumination position and data groups as in Figure 5.10. The general trend in QE profile is the same as for the BW pixel, including the exception for the shallowest pixel response in the well. The trend in nQE and inferred pQE is also the same, though for the FW pixel's well the pQE is suppressed more than the nQE, compared to their respective QE response for the non-BTI control. The FW pixel response profile becomes broader and steeper as thickness and well depth increases, compared to the BW pixel. The FW pixel profile is increasingly more resolved as pixel thickness and well depth increase.

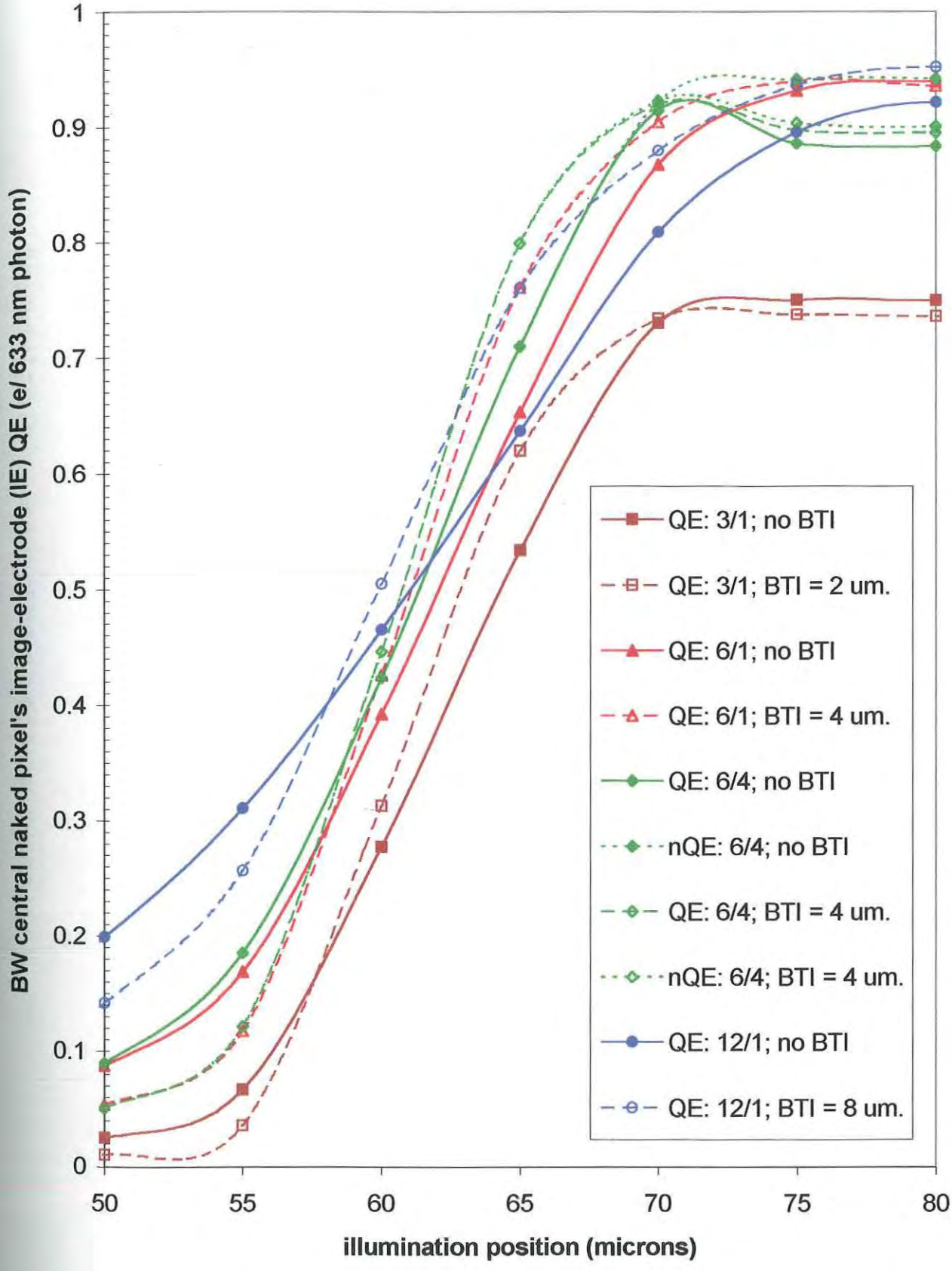

Figure 5.10: BW naked SJPD : single cathode (18 um) on well: The IE QE dependence on BTI depth for different pixel geometries for illuminations from the centre, to the well wall of the neighbouring pixel.

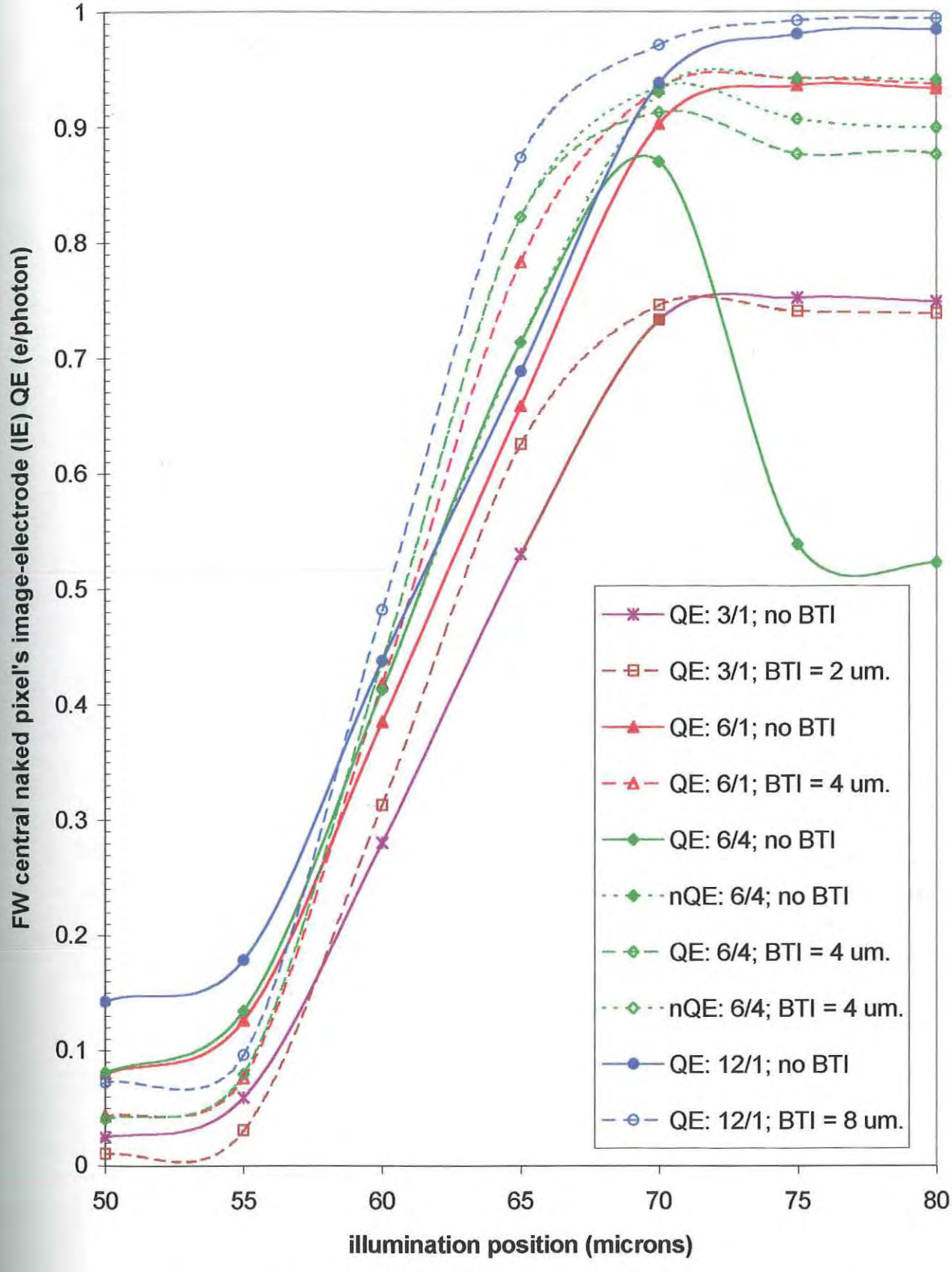

Figure 5.11: **FW naked SJPD : single cathode on well (18 um) : The IE QE dependence on BTI depth for different pixel geometries for illuminations from the centre, to the well wall of the neighbouring pixel.**

Figures 5.12 and 5.13 show the 6/2 central pixel QE response dependence on BTI well depth for illumination positions outside the central pixel up to the well wall (45 to 65 μm position), for BW and FW pixels, respectively. Note that "6/2" refers to a 6 μm substrate and a 2 μm well depth pixel. The trend in Figure 5.10 and Figure 5.11 is repeated here with the FW more suppressed than the BW pixel QE response. The exception being that the QE response's relationship to the BTI well depth can now be observed.

The Suppression tables (Appendices V & VI) indicate that for both BW and FW pixels, the presence of the BTI wells, which are equal to or greater than the pixel's well depth, suppress the pixels image QE response from the pixel boundary outwards (i.e. 45 to 55 μm illumination position QE response, given above).

The enhancement tables (Appendices V & VI) indicate a generally increasing enhancement of the QE response for illuminations between the pixel well wall and the nearest BTI well, with increasing BTI depth. This is for the 65 and 60 μm illumination position QE response in Figures 5.12 – 13, given above.

In both BW and FW pixels it can be seen that the suppressed QE response in the lower profiles (from the pixel boundary outwards), indicate a somewhat exponential trend in the QE suppression with arithmetically increasing BTI depth. This trend is generally apparent throughout all the pixel configurations simulated for this BTI investigation section. The full data set confirms this trend (Appendices III & IV).

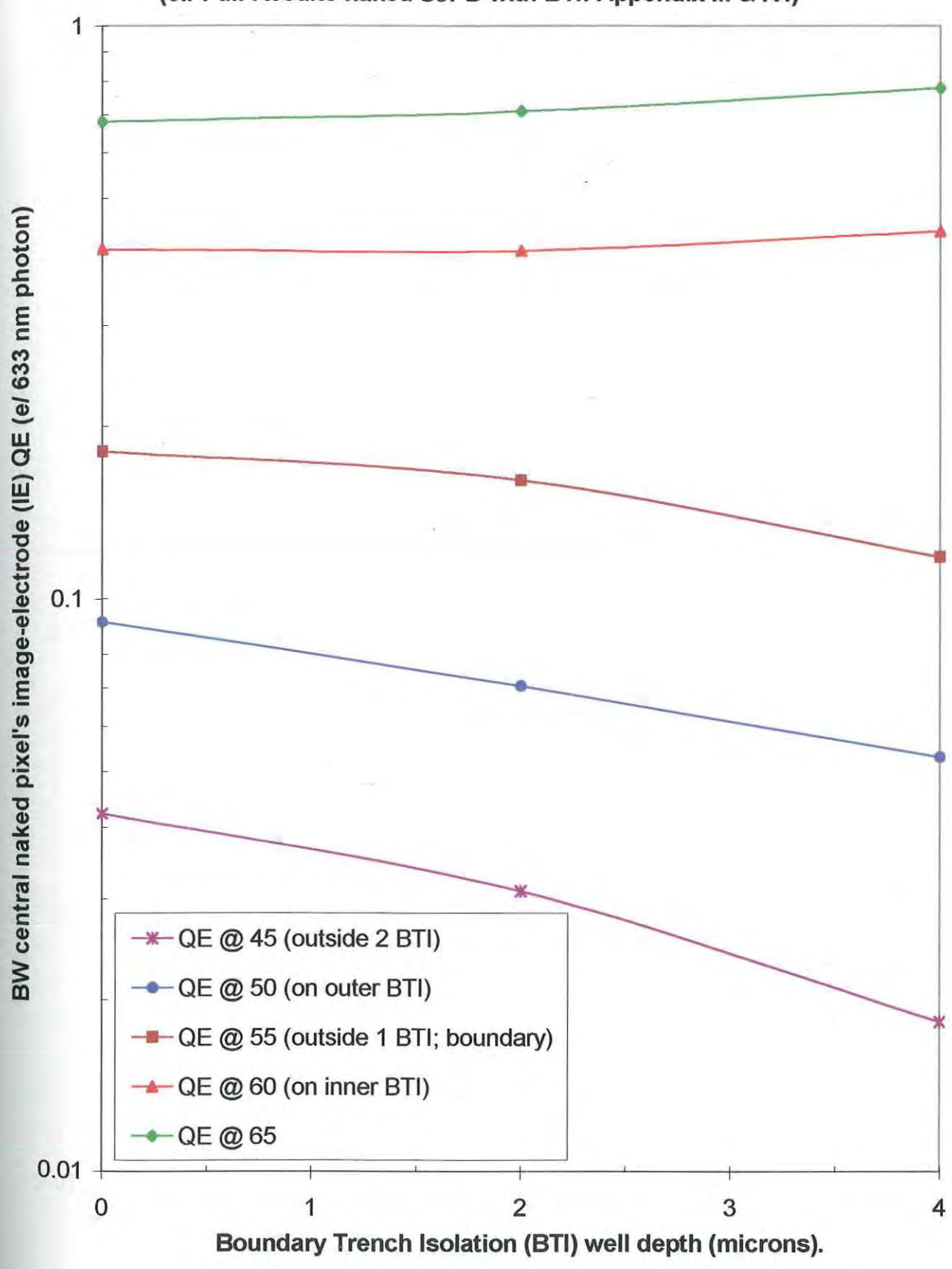

Figure 5.12: **BW SJPD : single electrode on well (18 um) : The IE QE dependence on BTI depth, for the 6/2 pixel geometry, for illuminations outside central well.**

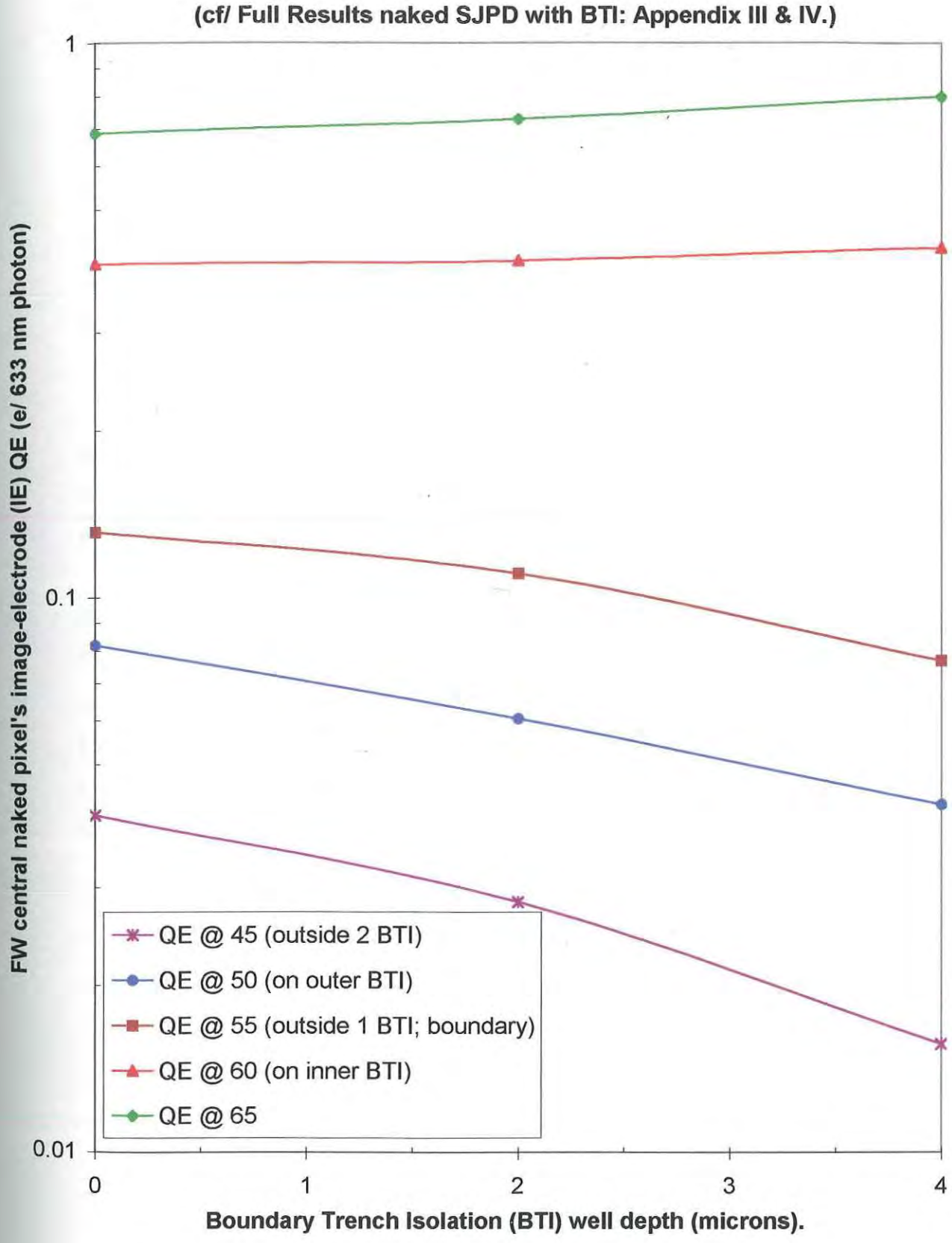

Fig 5.13: FW naked SJPD: single electrode (18 um) on well: The IE QE dependence on BTI depth, for the 6/2 pixel geometry, for illuminations outside central well.

Figure 5.14 shows the BW pixel QE response against a parameter that is related to the BTI well width: i.e. the number of BTI wells between the point of illumination and the central pixel image cathode. The QE response of the 6/2 and the 3/0.5 pixels are shown. The dashed profiles represent the non-BTI naked pixel control responses.

The slope increases with substrate thickness increase and with pixel well depth increase. Note the response is somewhat exponential, similar to the BTI well depth QE suppression response in Figure 5.12, though more so i.e. more linear on a log graph than the response in Figure 5.12.

Figure 5.15 shows the FW pixel QE response towards dependency on the number of BTI wells intervening between the illumination and the image cathode. The data is presented in the same way as Figure 5.14.

Note the semi-exponential trend again, which has a concave-down profile. This "bend" may be due to the FW pixel QE response for one BTI well intervening, being more suppressed than the BW pixel response. The two end points are similar for both BW and FW pixels; the FW is only bending down in the centre of the profile. Clearly there is more recombination occurring in the FW pixel response due to the closer proximity of the frontwall illumination to the BTI well.

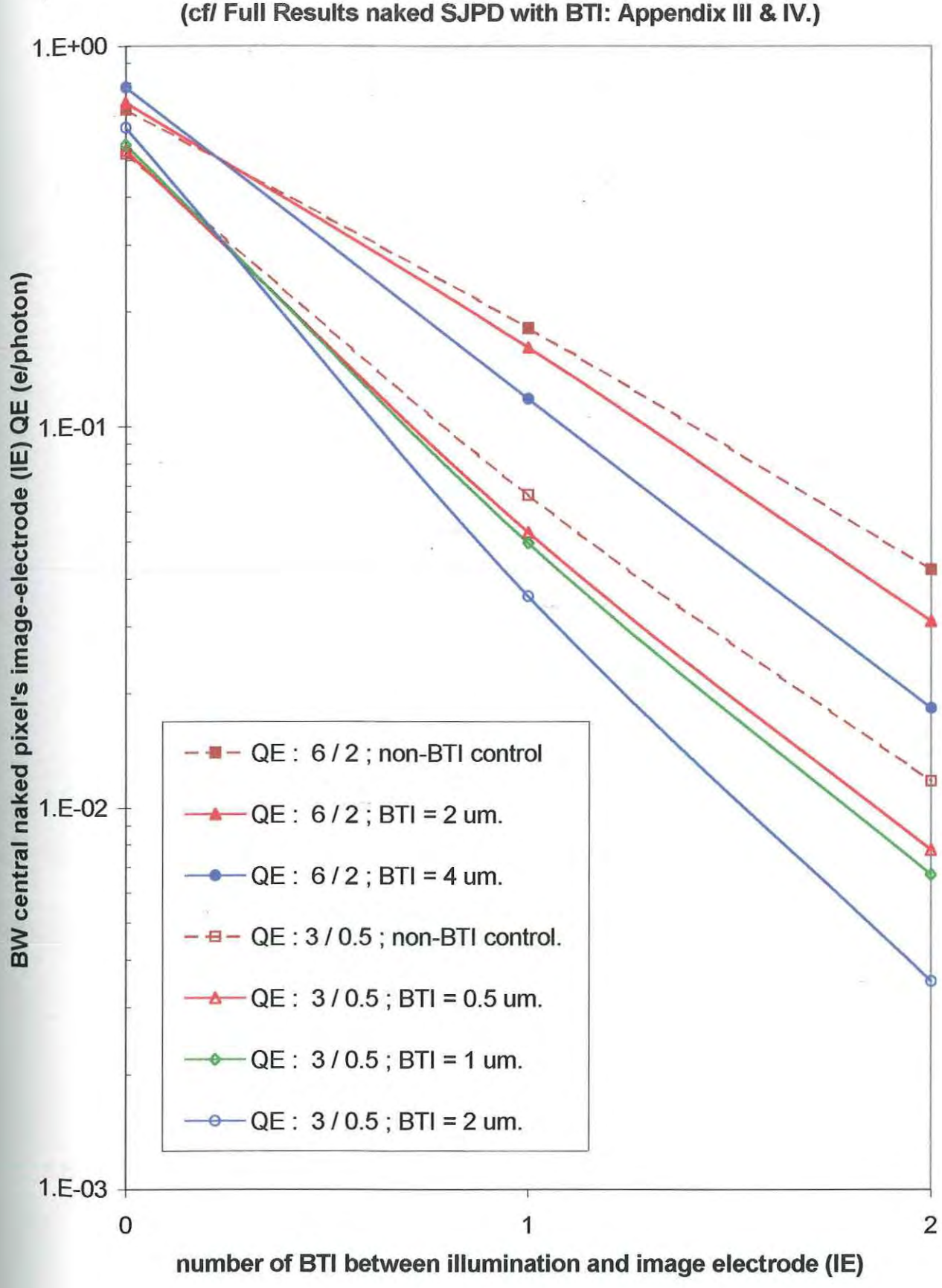

Figure 5.14: **BW naked SJPD: single electrode (18 um) on well: The IE QE dependence on the number of BTI wells between the illumination and IE, for different pixel geometry.**

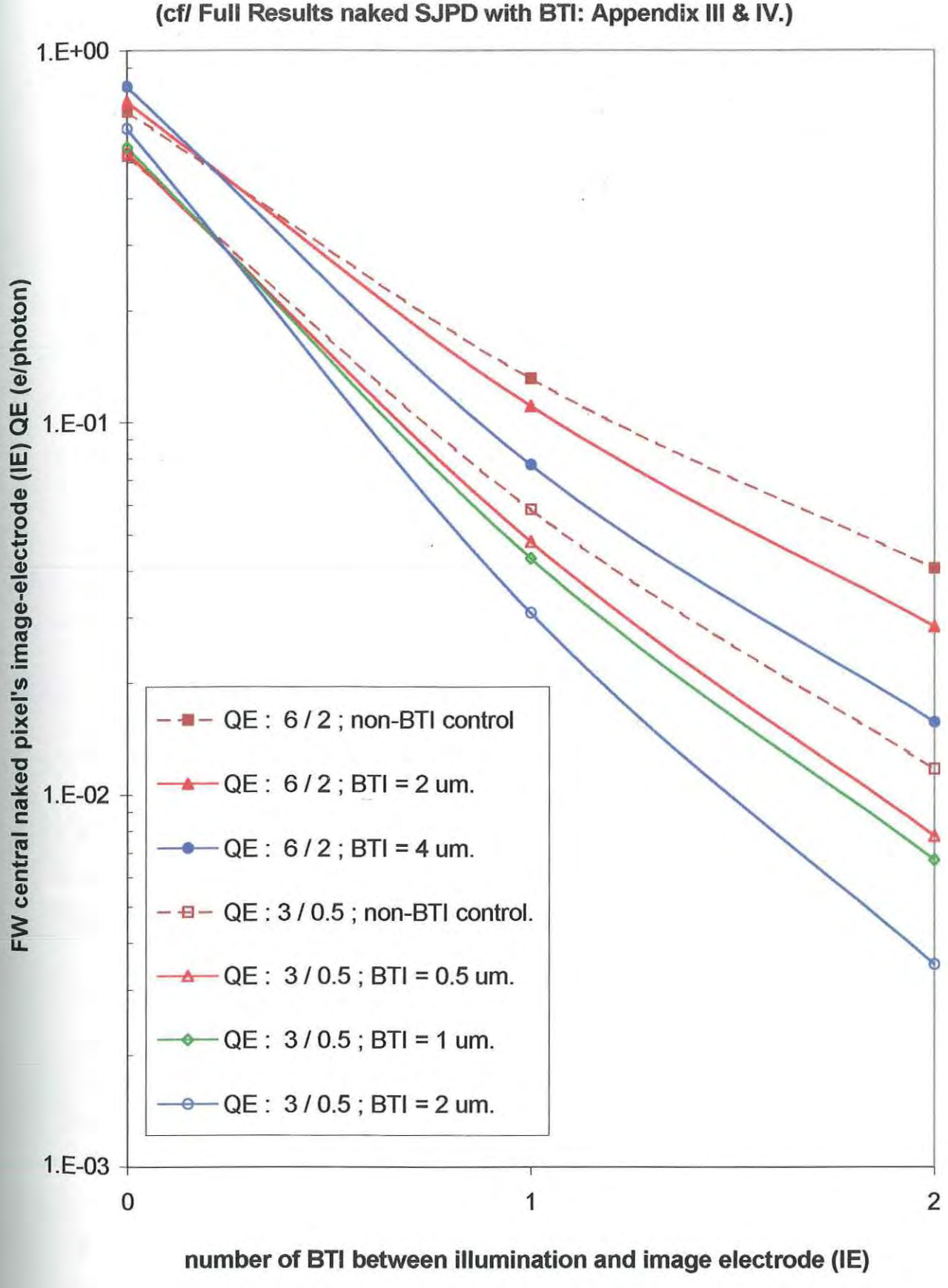

Figure 5.15: **FW naked SJPD: single electrode (18 um) on well: The IE QE dependence on the number of BTI wells between the illumination and IE, for different pixel geometry.**

Figure 5.16 show the response inside the well of the QE for 6/2 BW pixel; the response outside the pixel's well being considered previously (Figure 5.12). On the well wall (70 μm position), the hole QE (pQE) is immediately and totally suppressed while the the electron QE (nQE) is enhanced increasingly as BTI well depth increases. For illumination at the centre, both carrier QEs are immediately suppressed to levels that remain constant as BTI well depth increases. Also the maximum QE is more coincident with the response at the well centre than the response at the well walls.

Figure 5.17 show the response inside the well of the QE for 6/2 FW pixel. On the well wall (70 μm position), the pQE is suppressed immediately to a constant level, unlike the BW pixel's pQE which is totally suppressed and the nQE is enhanced increasingly as BTI well depth increases. For illumination at the centre, both carrier QEs are immediately suppressed to levels that remain constant as BTI well depth increases. Also the maximum QE is more coincident with the response at the well wall than the response at the well centre.

The nQE enhancements at the well wall and suppression at the well centre are similar for BW and FW pixels, though the well wall response is higher in the FW pixel as the non-BTI nQE value starts higher. The pQE suppression across the well is greater in the FW pixel. Also the maximum QE response is shifted more to the centre in the BW pixel, while shifted to the wall in the BW pixel.

With reference to the enhancement tables (Appendices V & VI), for thicker substrate, deeper junction pixels' QE response is similar to the enhancement outside the well. Shallower junction pixels' test and control QE response difference is insignificant (1%). For a given pixel configuration the enhancement of the QE response is immediate and constant as the depth of BTI wells increase.

For both BW and FW pixels, the electron current is enhanced at the well wall, while suppressed at the well's centre across all pixel configurations considered. But more noticeable is the immediate, nearly total suppression of hole current inside the well, for even the shallowest BTI wells, at pixel junction depth, across all pixel configurations considered.

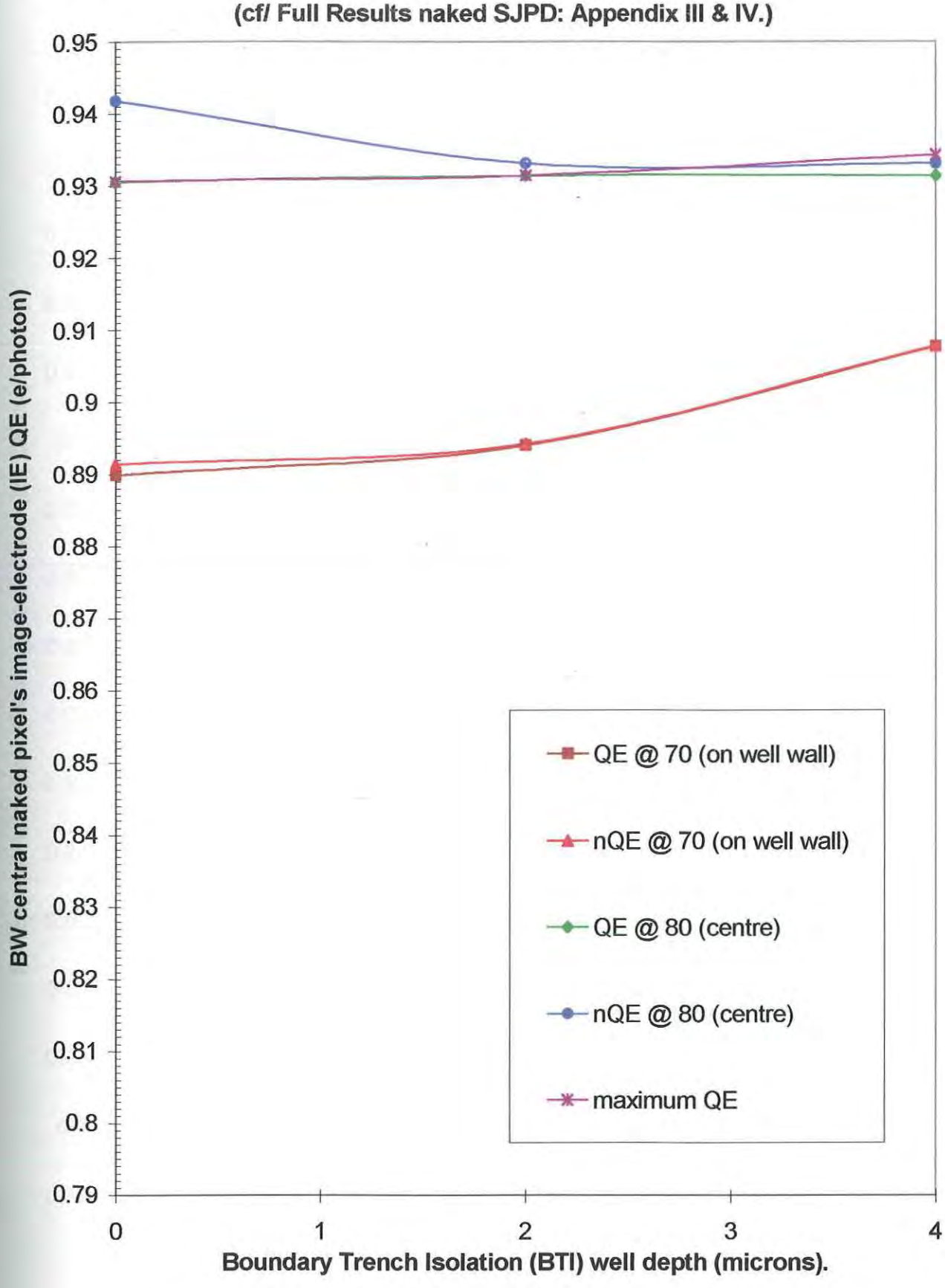

Figure 5.16: **BW naked SJPD : single electrode (18 um) on well: The IE QE dependence on BTI depth, for the 6/2 pixel geometry, for illuminations on the well wall and well centre.**

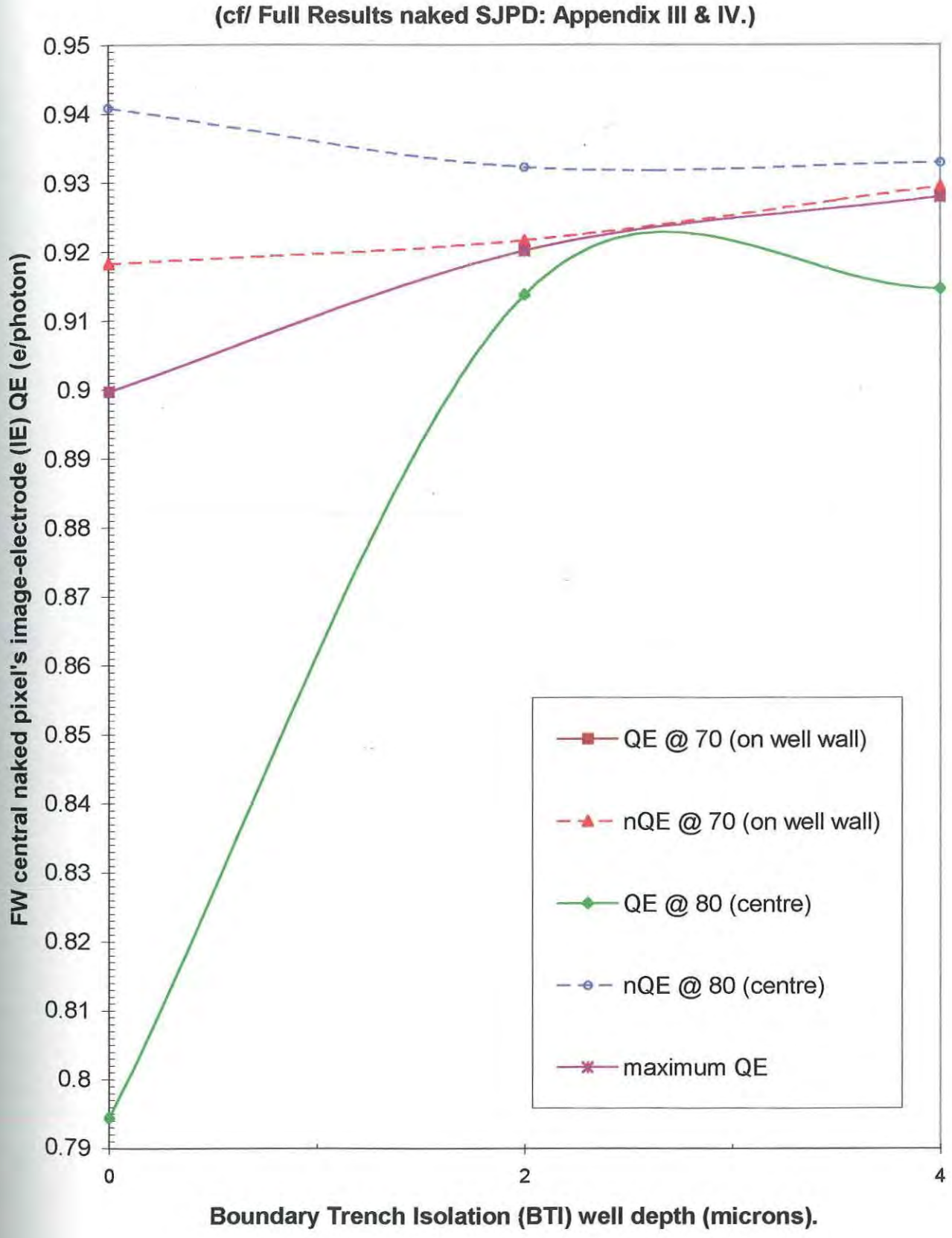

Figure 5.17: FW naked SJPD : single electrode (18 um) on well: The IE QE dependence on BTI depth, for the 6/2 pixel geometry, for illuminations on the well wall and well centre.

Figure 5.18 shows the pixel boundary NQE response (the relative crosstalk statistic) for the shallowest pixel configurations (3/0.5) with the minimum NQE response, which demonstrates that the FW profile is marginally lower. The gap between the two profiles, increasing with increasing substrate depth, results because of the increasing gap observed for the control pixel's response. This was observed in Section 5.1.1.

The NQE suppression profile on a log-linear graph demonstrates a semi-exponential trend, though the reason for the plateau that appears between 0.5 and 1 μm BTI depth is unclear, in both log and linear profiles. The minimum NQE value is 0.041, recorded for the shallowest well and substrate FW pixel with the deepest BTI well (2 μm). The same pixel BW, has an NQE value of 0.048, 17% more, and is also the minimum value for all the BW pixels considered.

The degree of suppression of NQE is slightly more (2%) in the BW pixel with the shallowest BTI well, while slightly more (2%) in the FW pixel with the deepest BTI well. Thus the substrate depth and junction depth are more responsible for the greater degree of suppression of the NQE in the FW pixel as its control NQE is already 12% below the BW pixel NQE. Thus the shallowest substrate pixel has the minimum relative crosstalk.

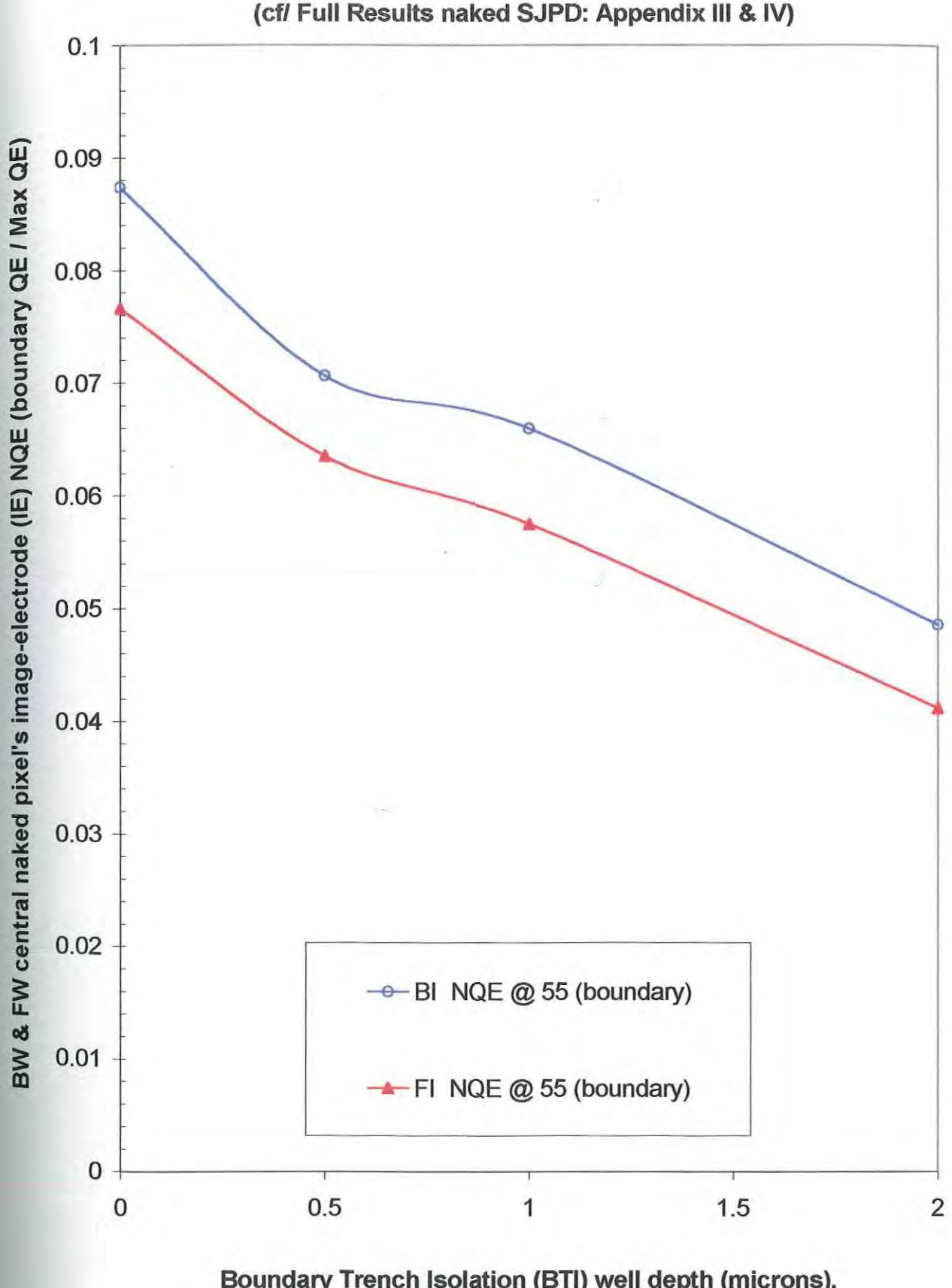

Figure 5.18: **BW & FW naked SJPD: single electrode (18 um) on well: The IE NQE (relative crosstalk) dependence on BTI depth, for the 3/0.5 pixel geometry, for illuminations on the pixel boundary.**

5.1.3 Effect of Guard-Ring Cathodes on Naked Pixels.

In this section the effect on the image-cathode's QE and NQE response of introducing a guard-ring cathode to the pixel's well surface is investigated. In 2D the guard-ring, biased equally with the image-cathode, appear as two cathodes symmetrically either side of the central image-cathode, contacting with the n-well front surface. For the BW and FW pixel QE and NQE results see Appendix VII.

Theoretically, the introduction of a guard-ring electrode reduces the capture envelope of the image electrode, by their electric fields competing for the image carrier population. Looking down on the pixel surface the guard ring takes the shape of a square annulus. The choice of size and position of the guard electrodes is retrospectively selected as a result of conclusions arrived at in experimental Section 5.1.4.

"Naked" pixel refers to the absence of a shielding-ring or guard-ring electrode around the central image electrode, forming an electrical "exhaust" for capturing crosstalk carriers. Like a protective piece of clothing, the guard if removed renders the image cathode "naked" or unprotected.

Figure 5.19 shows the BW pixel QE response across a selection of pixel geometry, comparing the naked and guarded pixel QE profiles against illumination position. SD and JD refer to substrate depth and junction depth (well depth) respectively. Only the left guard cathode QE profile is shown in Figure 5.19.

The guarded pixel profile is notably lower than for the best naked-pixel profile (Section 5.1.1). The shallowest pixel is still superior. The deeper well, 3/1 BW pixel (Thickness 3 μm and well depth 1 μm), with deeper SCR associated with the well wall (maximum SCR AVP), enhances guard capture efficiency, reducing the QE faster than the shallower well pixel response, as illumination approaches the well wall's SCR. This results in the 3/1 BW pixel reaching the most minimum QE of all the pixels sooner, as illumination moves outwards from the pixel's centre.

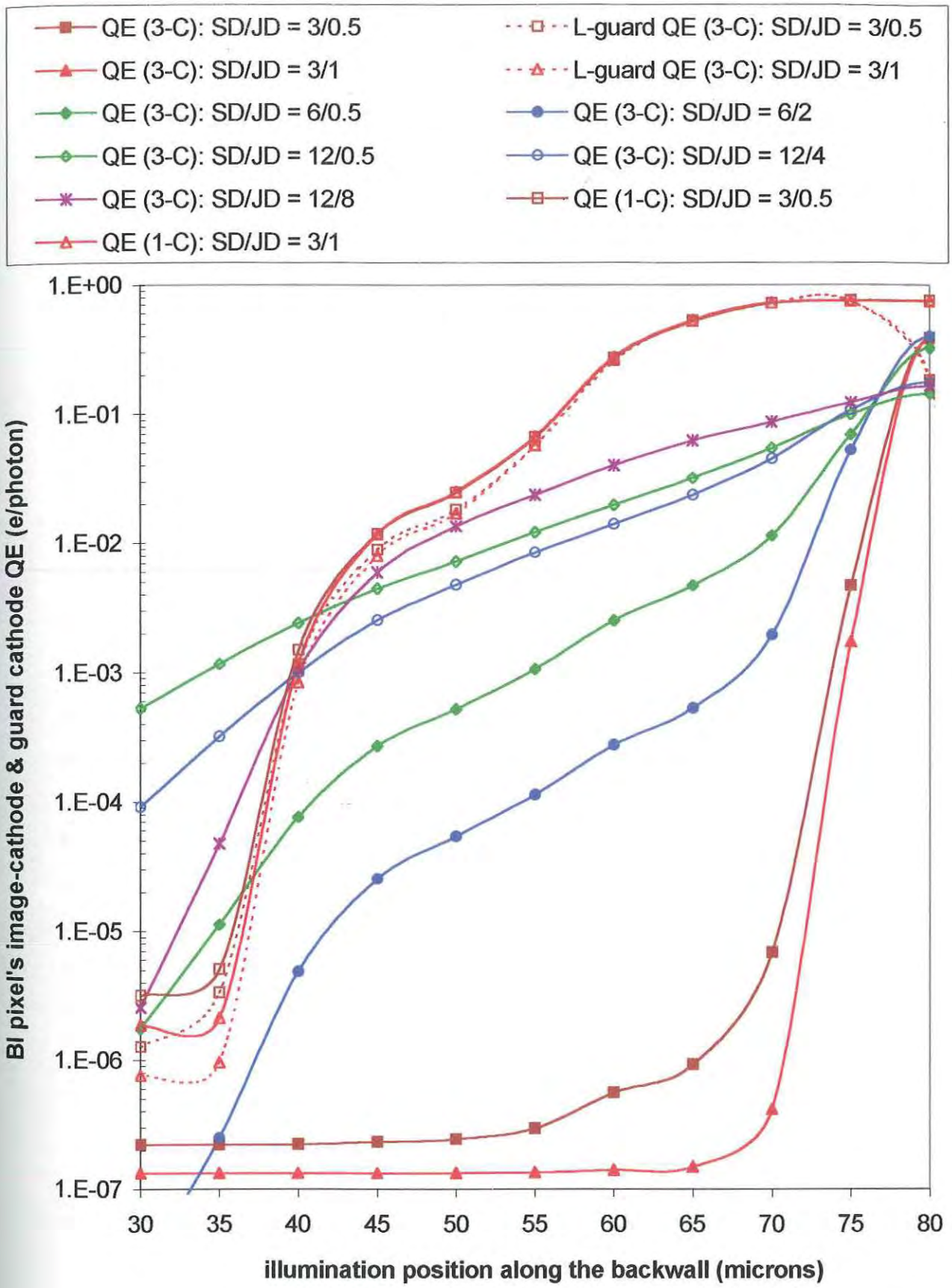

Figure 5.19: **BW SJPD pixels: comparing guarded pixel (3-C) QE profile with naked pixel (1-C) QE profile for various pixel geometries.**

Figure 5.20 shows the FW pixel QE profile against laser illumination position. This is for the same selection of pixel configurations compared in Figure 5.19.

Again the shallowest pixel is superior. Note the greater suppression of these shallowest pixel QEs, inside the well (70 – 80 μm position) compared to the same pixels backwall illuminated. Compared to the BW pixel's profile this suppression is increasingly more across the pixel as substrate thickness increases.

For the shallower FW pixels, an increased SCR volume at the well wall, for deeper wells, increases the wall's SCR surface in contact with the photogenerated carriers, for illuminations over the wall. This SCR surface contact is higher than the equivalent BW pixel wall's SCR surface contact, resulting in greater suppression in the FW pixel's QE response.

For Both BW and FW pixels, even the worst naked pixel, now protected with a guard-ring electrode, has a better, more suppressed, more resolved, QE response than the best naked pixel configuration from Section 5.1.1. Also the left guard QE profiles for the two shallowest pixel configurations (dotted profile in Figure 5.20) generally follow the naked pixels' response profiles. This indicates that the "lost" QE at the image cathode is captured by the guard ring cathode due to the cathodic electric fields competing in the well region for photogenerated carriers. All guarded pixel QEs, no matter the illumination position or mode of illumination, are below naked pixel values, implying reduced sensitivity. Note that the maximum QE is central where the result is dependent on the SCR AVP; the higher it is the higher the QE. Hence an increase in QE as SCR AVP increases with well depth in BW pixels while the reverse occurs in FW pixels.

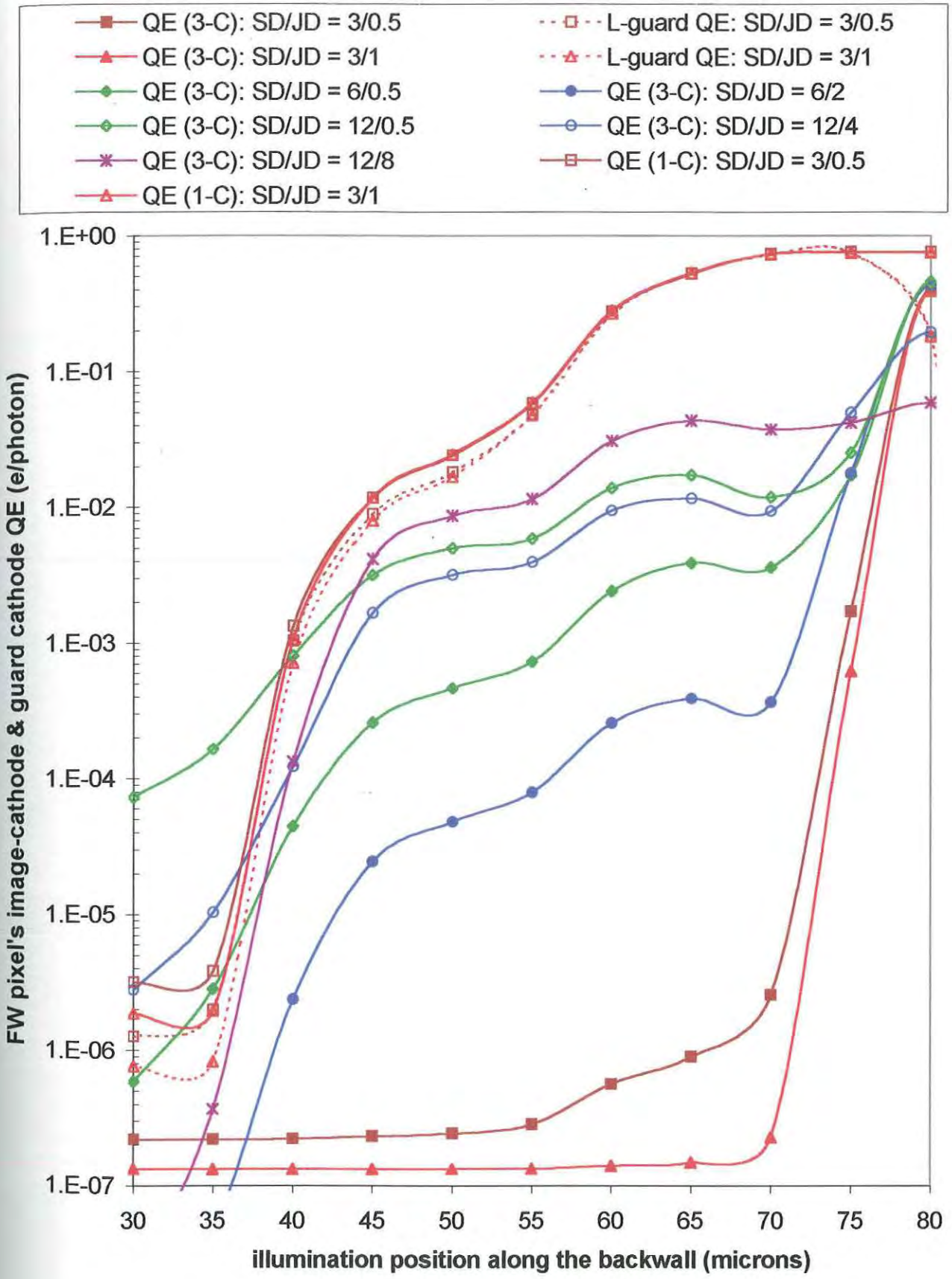

Figure 5.20: **FW SJPD pixels: comparing guarded pixel (3-C) QE profile with naked pixel (1-C) QE profile for various pixel geometries.**

Figure 5.21 shows a comparison of the electron QE (nQE) and hole QE (pQE) response between the naked (1-C) and guarded (3-C) BW pixels, using the shallowest pixel configurations. The black dashed pQE response represents negative hole current which is subtracting from the positive electron current, reducing the QE. Both pQE and nQE are reduced – by many orders of magnitude for nQE – below the naked pixel.

Figure 5.22 shows the electron and hole response for the shallowest substrate FW pixels, contrasting the naked and guarded configurations. The trends in the carrier profiles are more suppressed than the BW pixel carrier profile only for illuminations in the well.

Comparing the BW profile with the FW profile, the hole QE representing negative hole current, represented by the black dashed lines for well illuminations, is more pronounced in the FW response than for the BW response (Figure 5.21). This subtracting hole current, though reduced by the guard cathodes, is still noticeable for illuminations at the well centre. Notice the extent of the reduction in the FW pixel's maximum QE (Figure 5.20) as well depth increases, especially in the thicker substrate Pixels, compared to the BW response. The negative hole problem is more of a problem in the deeper substrate, deeper well, guarded-pixels, though not to the same extent as for the naked pixels.

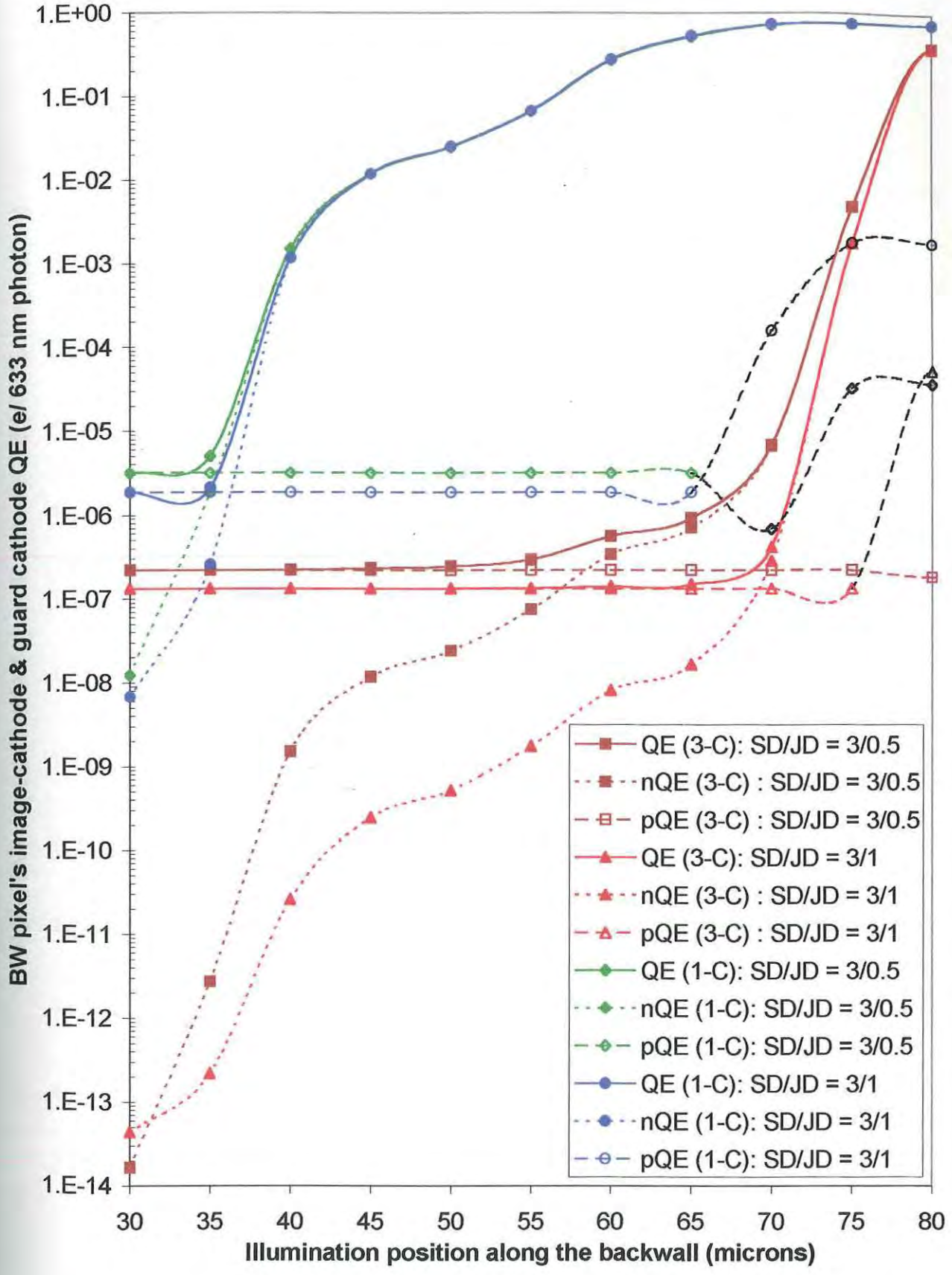

Figure 5.21: BW SJPD pixels : comparing guarded pixel (3-C) and naked pixel (1-C) electron (nQE) , hole (pQE) and total QE profiles for the two, 3 um substrate, SJPD pixel configurations.

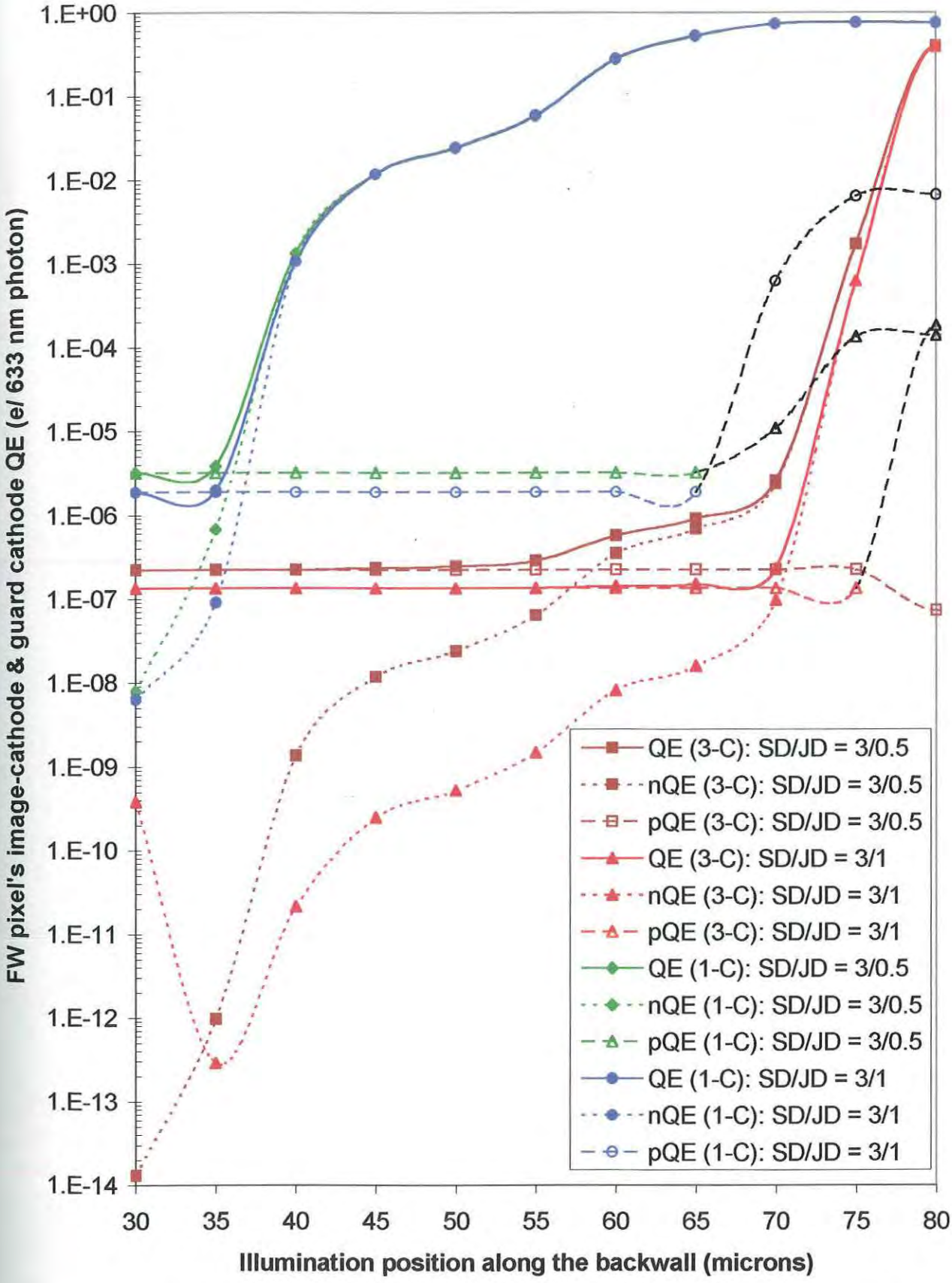

Figure 5.22: **FW SJPD pixels : comparing guarded pixel (3-C) and naked pixel (1-C) electron (nQE) , hole (pQE) and total QE profiles for the two, 3 um substrate, SJPD pixel configurations.**

The relationship between QE response of the guarded pixel and the ***well depth*** is important to compare with the naked pixel results in Section 5.1.1. Similar to the naked pixel, the thickest (12 μm) pixel's QE profile for increasing well depth will be graphed.

Figure 5.23 shows the BW guarded pixel QE response against well depth. This is for illumination positions from the centre of the central pixel outwards along the array.

Both naked (Figure 5.5) and guarded (Figure 5.23) pixels maximum QE is coincident with their associated central (80 μm) illumination QE response. The guard pixel response is suppressed from 5 to 50 times the naked response (Figures 5.3 & 5.5) as illumination moves from the pixel centre outwards. Note the initial suppression of the response across the guarded pixel, as the depth of the well increases to 1 μm, for illuminations outside (45 μm) to the centre (80 μm). From the well wall (70 μm) outwards, this is followed by a plateau to the next well depth (2 μm), followed by further suppression to the minimum QE for each illumination profile at the 4 μm well depth. The central response plateaus from the enhancement at the 2 μm well depth. This contrasts with the naked pixel QE response (Figures 5.3 and 5.5) that is enhanced throughout the profile across all illumination positions.

The nQE is coincident with the total QE for illuminations over the well, implying that the pQE has been suppressed down to insignificant values across the depth profile, inside the well. This contrasts marginally with the naked pixel, which suffers from an increased pQE for the deeper well pixels (Figure 5.5).

The central SCR AVP (80 μm position) responds exponentially to the increasing well depth, as the SCR approaches the back wall in both guarded and naked pixels (Figures 5.5 and 5.23). This is due to the increasing proximity of the SCR to the backwall illumination that is characteristically absorbed in an exponential manner into the substrate.

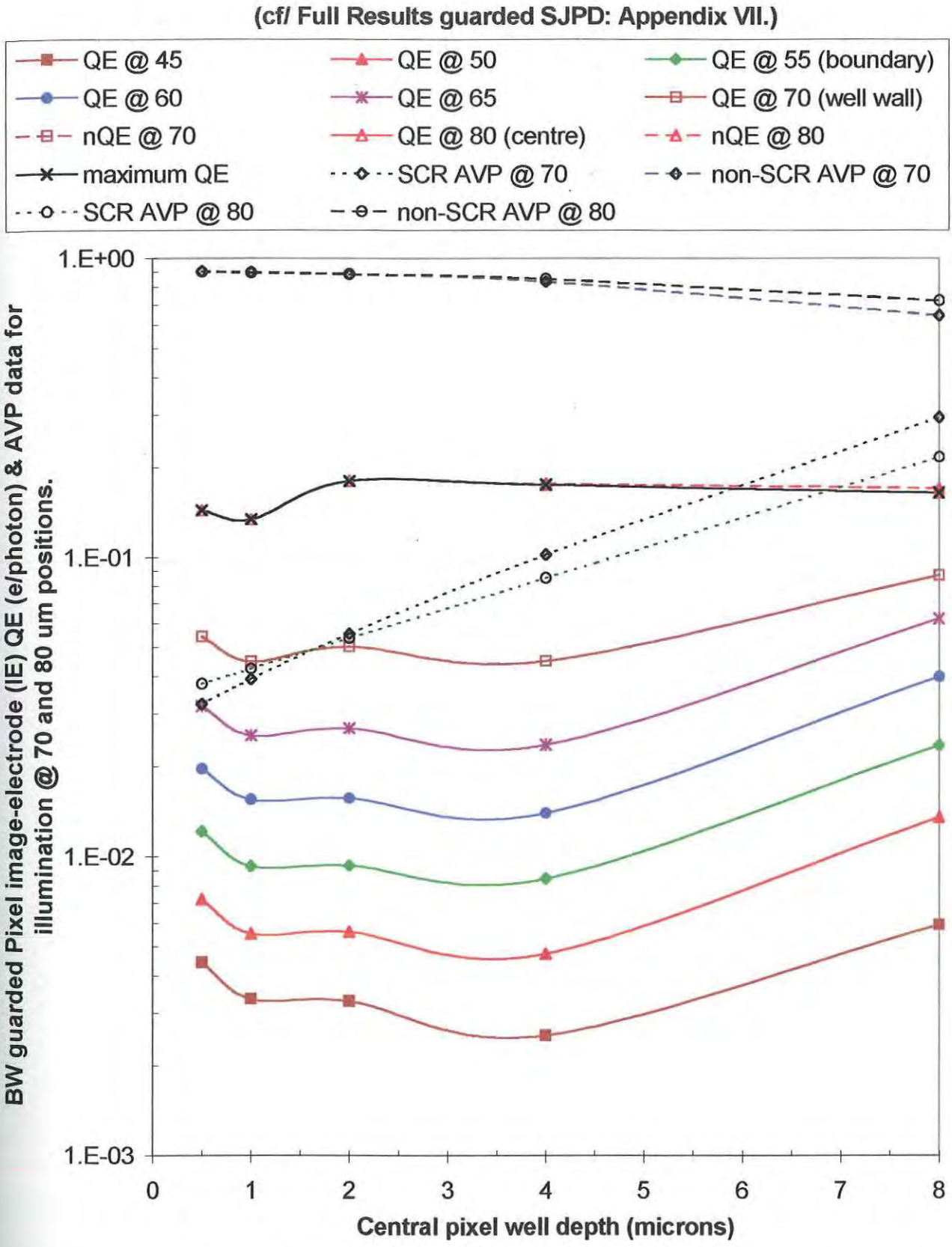

Figure 5.23: BW guarded SJPD : guard cathode (6.4 um): The IE (0.4 um) QE dependence on well depth, for 12 um substrate, for illuminations from the pixel centre outwards, compared to well wall & central AVP data.

Figure 5.24 shows the FW guarded pixel QE response against well depth. This is for the same illumination positions as for Figure 5.23.

Like the naked (Figure 5.5) and guarded BW pixel (Figure 5.23), the maximum QE profile for the FW guarded pixel is coincident with the central (80 μm position) illumination profile. This is in contrast to the FW naked pixel profile that is coincident with the well wall illumination (70 μm position) profile (Figure 5.6). This is due to the increased suppression for illumination towards the sides of the well for the guarded pixel, as the guard cathodes have greater capture efficiency at the well walls than at the centre, where the image cathode's electric field dominates more.

The maximum QE follows the decreasing SCR AVP as SCR depth increases. This is due mainly to the increasing pQE, though to a lesser extent than the naked FW pixel (Figure 5.6).

The suppression of QE over the well wall (70 μm position) is noticeable below the QE response for illuminations outside the well, in the pixel's substrate (60 and 65 μm positions). This is not due to increased pQE, as the nQE is coincident with the total QE. This is due to the photogenerated carrier envelope, being in much greater proximity to the guard cathode's electric field being captured more than for the BW pixel.

Outside the well, more carriers are captured by the Image cathode as they diffuse into it's electric field from underneath the well. This effect decreases as the well depth increases because the non-SCR AVP below the well decreases.

The nQE is coincident with the total QE for illuminations over the well wall, implying that the pQE has been suppressed down to insignificant values across the depth profile. This contrast marginally with the naked pixel which suffers from an increased pQE for the deeper well pixels (Figure 5.6).

(cf/ Full Results guarded SJPD: Appendix VII.)

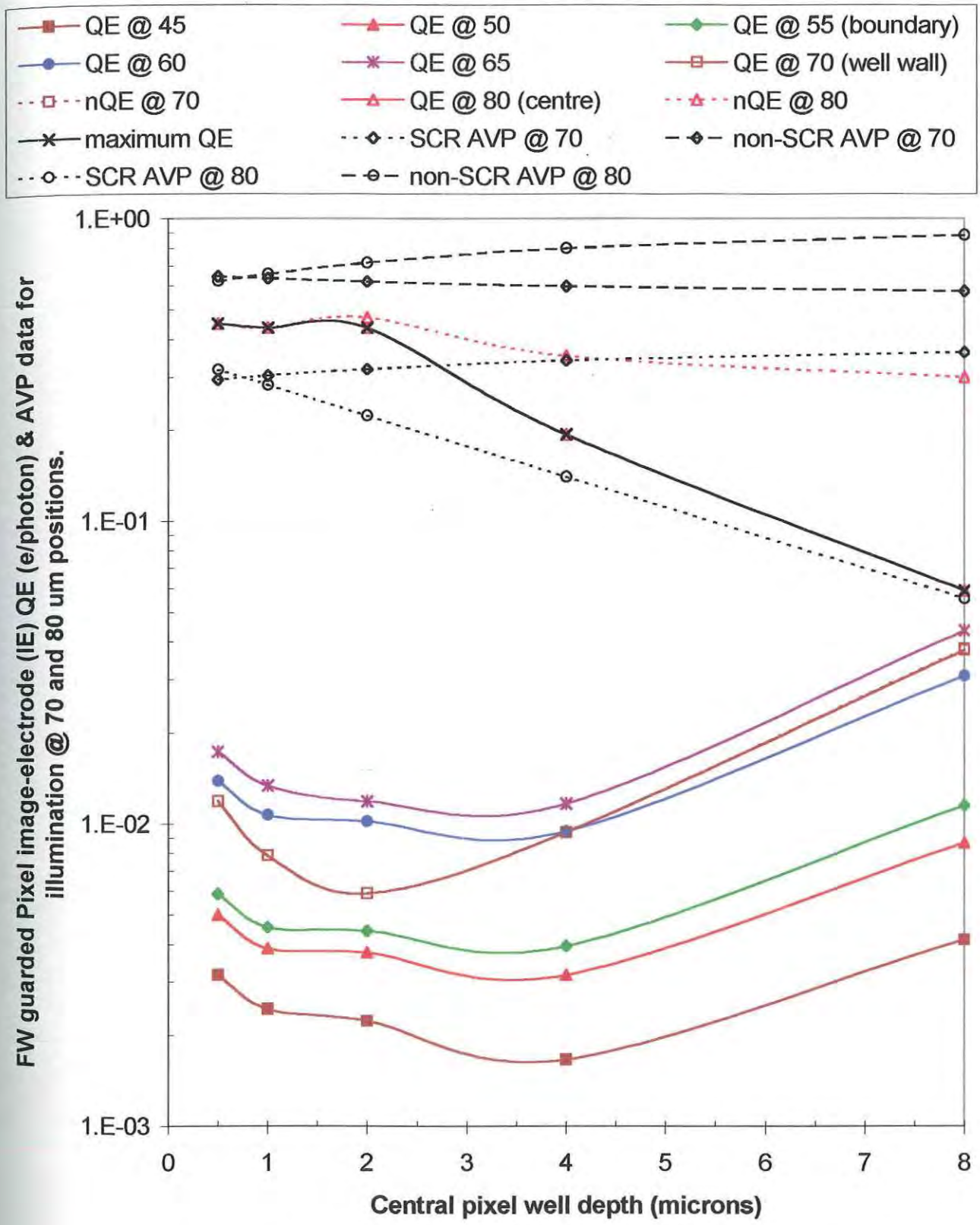

Figure 5.24: FW guarded SJPD : guard cathode (6.4 um): The IE (0.4 um) QE dependence on well depth, for 12 um substrate, for illuminations from the pixel centre outwards, compared to well wall & central AVP data.

Still considering Figure 5.24, the QE response at the centre shares some similarities with the FW naked SJPD pixel as the pQE increases with increasing well depth, though not as pronounced as for the naked pixel. Also, notice the central SCR AVP (80 μm position) responds exponentially to the increasing well depth, as the SCR approaches the back wall in both guarded and naked pixels (Figures 5.6 and 5.24) opposite to the BW pixels. This is due to the decreasing proximity of the SCR to the front wall illumination and a growing n-well region that increases the hole minority current that suppresses the total QE.

For both FW and BW guarded pixels, the left over QE not captured by the guard ring cathode is captured by the image cathode in the manner that is generally similar for all illumination outside the well, suppressed more in the FW case. Inside the well the FW and BW responses are characteristically different.

Overall the response is a changing response, which means it must be related to the configuration parameter that is changing in the pixel cross section: well depth. What really is changing, is the interaction between the SCR envelope (a changing depth profile causing increasing or decreasing AVP profiles depending on the position and mode of illumination) and the electrical flux density profile's of the guard and image cathodes (constant drift-initiating profile). Further investigation of the electrical flux profile for the cathodes in the array cross section, not available in this study, would reveal exactly how the field lines are deforming across the pixel as SCR depth increases and so lending weight to the explanation of the guarded pixel's response.

The relationship between QE response of the guarded pixel and the ***substrate depth*** is important to compare with the naked pixel results in Section 5.1.1. Here the 3/1, 6/1 and 12/1 guarded pixels will be considered (3/1 refers to a substrate and well depth of 3 μm and 1 μm, respectively).

Figure 5.25 shows the BW guarded pixel QE response against substrate thickness. This is for illuminations from the centre of the central pixel outwards towards the adjacent pixel.

Compared to the naked pixel QE response (Figure 5.7), the guarded pixel's maximum, central QE response is suppressed below the naked pixel's response by a half up to 6 times, as thickness increases. In contrast, as thickness decreases, the guarded pixel's QE response for illuminations over the well wall has been suppressed from 5 times to three million times, compared to the naked pixel. Opposite to the naked BW pixel response, the maximum QE decreases with increasing substrate depth due to an increasing volume of the substrate photocarriers underneath the well, being captured by the guard cathode electric fields, and narrowing of the image cathode capture window, sandwiched inside the guard ring. The central QE response follows the SCR AVP profile which is decreasing exponentially as the substrate thickness increases.

Figure 5.26 shows the FW guarded pixel QE response against substrate thickness.

Compared to the BW guarded pixel, this response is more suppressed, except at the centre where the response is more enhanced, following the constant SCR AVP profile. This is similar to the BW pixel response which also follows it's SCR AVP profile. Similar to the guarded pixel response in Figure 5.24, the response for illumination over the well wall (70 μm position) is suppressed below the responses for adjacent illumination (60 and 65 μm positions) for the same reason. That is because the guard-ring cathode has better capture efficiency for illumination at positions 60, 65 and 70 μm then at adjacent position in the substrate. Also like the BW guarded pixel response, the nQE and QE responses are coincident across all illumination positions. This is with the same exception that the pQE is increased for illuminations over the well, for the shallowest pixel, which represents a positive hole current; not a negative hole current as would be expected for illuminations over the pixel well. The reason for this is unclear.

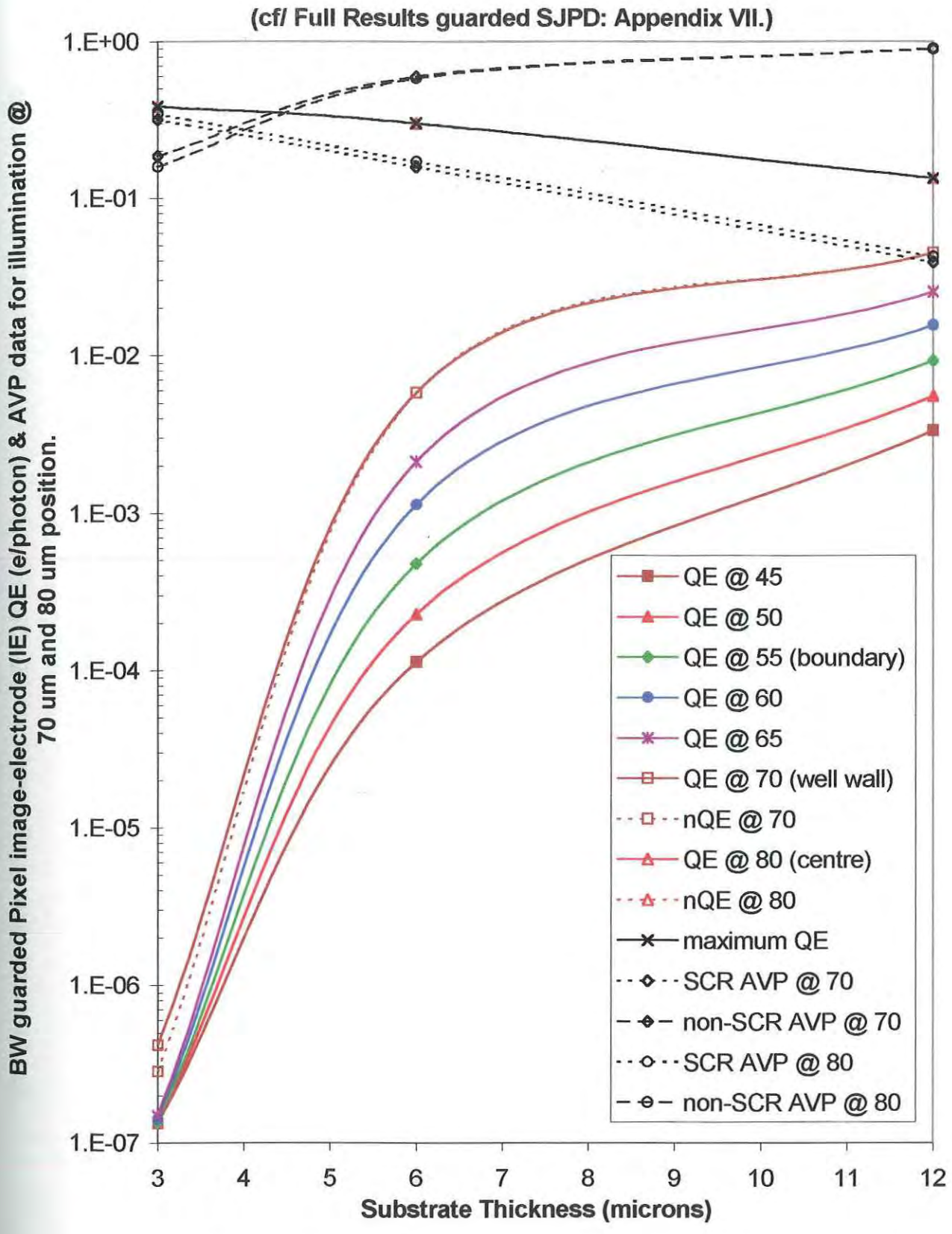

Figure 5.25: **BW SJPD : guard cathode (6.4 um): The IE (0.4 um) QE dependence on substrate thickness, with 1 um well depth, for illuminations from the pixel centre outwards, compared to well wall & central AVP data.**

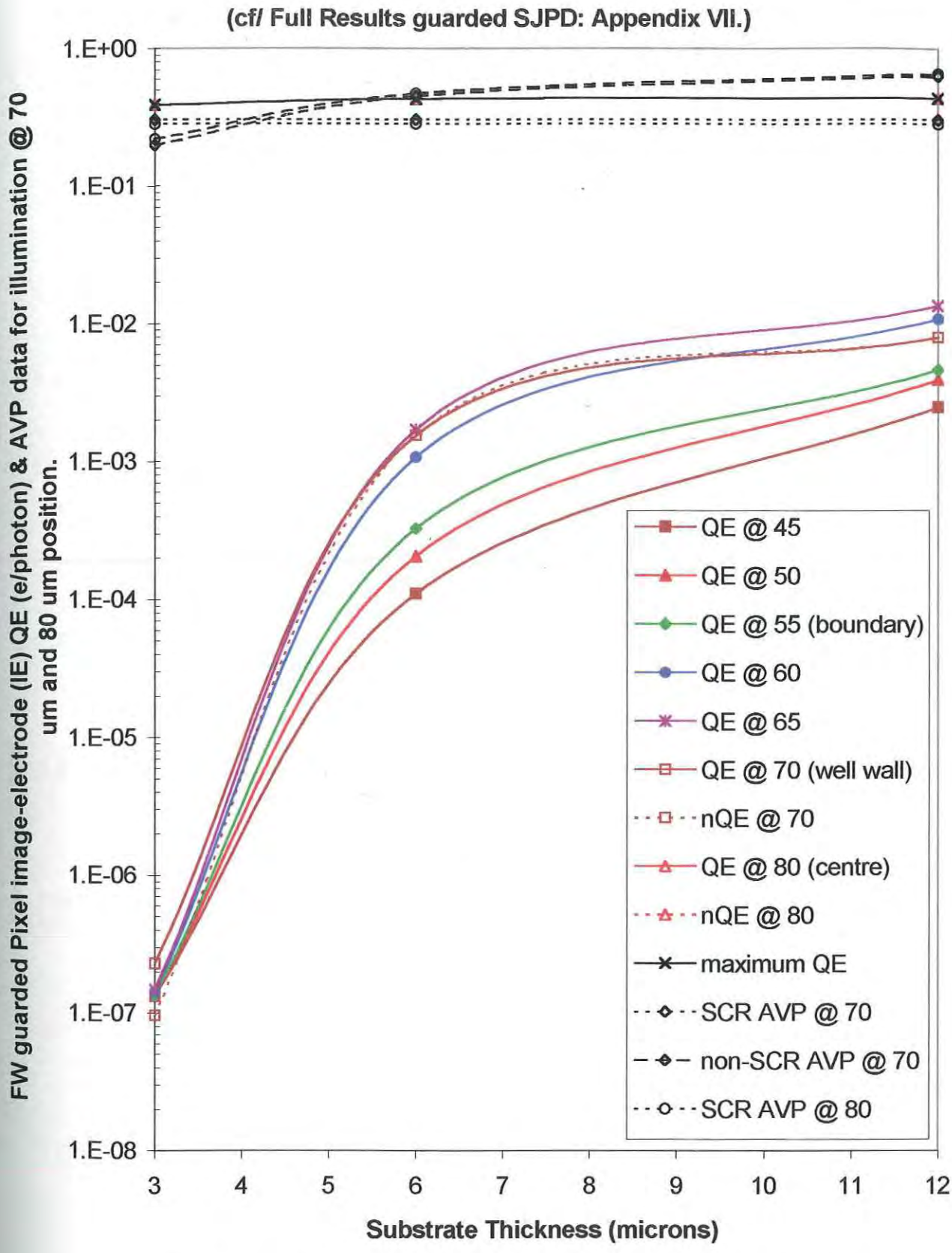

Figure 5.26: **FW SJPD: guard cathode (6.4 um): The IE (0.4 um) QE dependence on substrate thickness, with 1 um well depth, for illuminations from the pixel centre outwards, compared to well wall & central AVP data.**

Figure 5.27 shows the NQE response, comparing BW and FW guarded pixels. Note the FW response is more suppressed and the gap between the BW and FW responses is diminishing as the substrate thickness decreases until the shallowest pixels, where the difference between illumination responses is negligible. Also with the shallowest pixels the significantly reduced NQE is constant, from beside the central pixel well wall, right across to the centre of the neighbouring pixel !! The only conclusion: **negligible crosstalk !!**

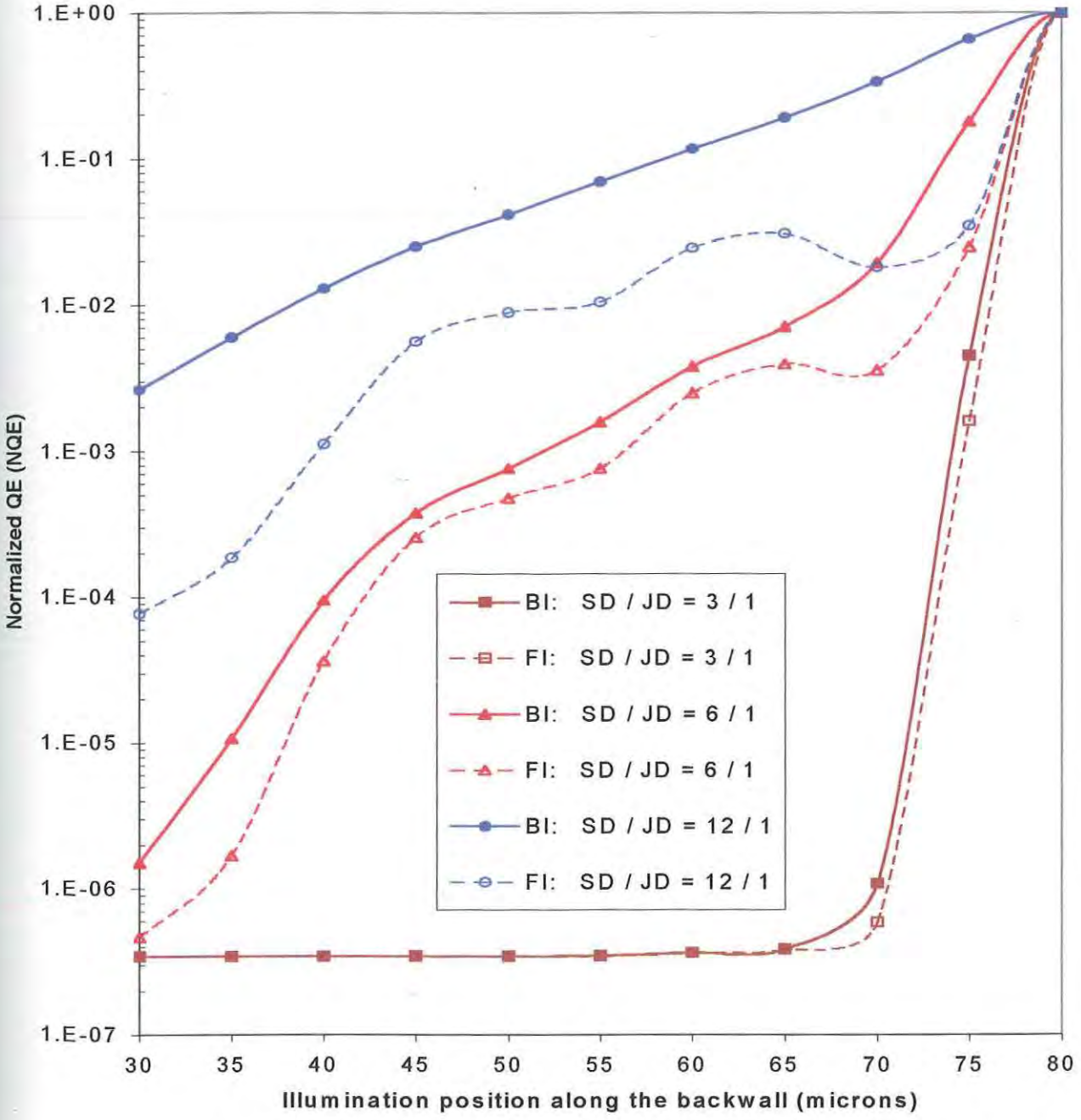

Figure 5.27: BW & FW SJPD guarded pixels : comparing NQE profiles for pixels of different substrate depth and illumination mode.

5.1.4 **Effect of Well-Electrode Position and Width on Guarded Pixels.**

The extent of suppression and shape of the QE and NQE response of a SJPD guarded pixel's image cathode, being dependent on the geometry of the pixel, may also be dependent on the juxtaposition of the two competing electric fields penetrating the well volume. Using a less than optimal pixel geometry, the effect of the geometry of the cathodes is investigated.

A range of electrode sizes and positions is simulated giving a total result set of 213 scans. The total BW pixel and FW pixel QE and NQE response for a selection of illumination positions from the total result set is presented as a table in Appendices VIII & IX, respectively. Each line in the table represents one "photodiode characteristic" (referred to as "PDC" in Appendices VIII & IX) that consists of the width of the central image cathode, the width of the guard cathode, followed by the "shift" distance all in microns. The shift distance is the distance between the edge of the guard cathode farthest from the pixel centre to the well edge. The table then consists of varying the image cathode width from 0.2 μm (the minimum electrode width for 0.18 μm CMOS technology) to 3.2 μm in a doubling geometric sequence. Then for each image cathode width, the guard width is varied similarly: 0.2 to 3.2 μm geometrically. Then for each guard width the shift distance is varied from 0 to 9 μm arithmetically. The shift distance may not always reach 9 μm for the "photodiode characteristics" with larger width electrodes. Hence there are 213 scans not 250 (5x5x10).

The QE or NQE results can be graphed in 2D against a composite number ("photodiode characteristic") that simultaneously represents the sizes of the guard cathode, the size of the image cathodes, and the distance the guard cathode is shifted from the well-substrate junction towards the image cathode (shift distance). The table contains the "photodiode characteristic" values and the formulae to interpret the "photodiode characteristic" at the bottom of each page of the data. However this graphical presentation is too complex to understand. Furthermore, having the "complex" graphical profile of the full data set available, summary trends in the data can now be presented as bivariate graphs.

The QE and NQE BW and FW guarded pixel responses, for illuminations positions inside the pixel, are graphed against the three configuration parameters ("photodiode characteristic") one at a time in the way outlined below. The non-varying pair is kept at constant optimum values. For guard, image and shift lengths they are 3.2, 0.4 and 1 μm, respectively.

1. Independent variable: Guard-cathode width against dependent variable
   (A) BW guarded pixel QE response.
   (B) FW guarded pixel QE response.
   (C) BW and FW guarded pixel NQE response at well wall and centre.

2. Independent variable: Image-cathode width against dependent variable
   (A) BW guarded pixel QE response.
   (B) FW guarded pixel QE response.
   (C) BW and FW guarded pixel NQE response at well wall and centre.

3. Independent variable: Shift distance against dependent variable
   (A) BW guarded pixel QE response.
   (B) FW guarded pixel QE response.
   (C) BW and FW guarded pixel NQE response at well wall and centre.

Figure 5.28 shows the BW guarded pixel QE profile against ***guard cathode*** width for illumination positions from pixel boundary to centre (55 to 80 μm, respectively). This is for constant optimal image-cathode width (0.4 μm) and optimal distance for the guard cathode to be shifted from the well edge (1 μm).

Note the somewhat exponentially decreasing trend in all the illumination position profiles. This may be due to the increasing guard-cathode field's capture-window, pressing in on the image-cathode's capture-window. The boundary QE profile is decreasing faster than the maximum QE which implies the boundary NQE will trend in the same manner as the boundary QE, minimizing the trend with the largest guard width. If so, then the limitation on the guard size will be the maximum QE being of sufficient value for practical amplification of the pixel image current.

(cf/ Result guarded SJPD: Appendix VIII.)

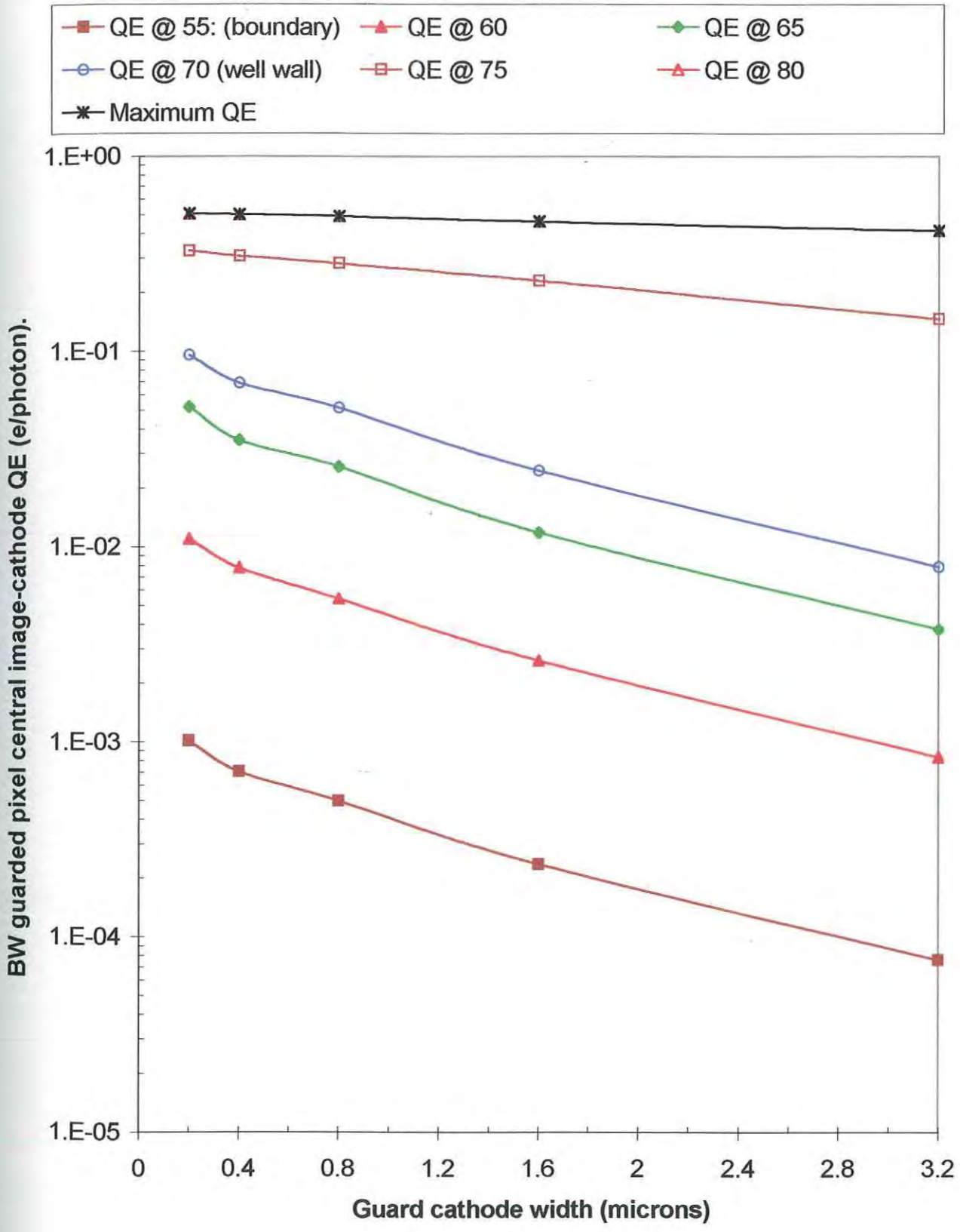

Figure 5.28: BW guarded SJPD pixel : Image cathode QE dependence on guard cathode width, optimally positioned 1 um from well edge and with the optimal image cathode width of 0.4 um.

Figure 5.29 shows the FW guarded pixel QE profile against ***guard cathode*** width for illumination positions from pixel boundary to the centre (55 to 80 μm, respectively). This is for the same optimal image cathode width (0.4 μm) and shift distance (1 μm), as in Figure 5.28. The latter is the distance the guard cathode is shifted away from the edge of the pixel's well.

Outside the well, the response is slightly more suppressed than the BW response (Figure 5.28) due to the closer proximity of the FW pixel's photocarrier population, outside the well, to the guard cathode capture window. The decreasing exponential trend towards minimum boundary QE at the largest guard width is equivalent to the BW response (Figure 5.28).

Figure 5.30 shows the BW and FW guarded pixel NQE profile against ***guard cathode*** width for illumination positions at the boundary. It shows the relative crosstalk statistic (55 μm illumination position) and the NQE statistic for illuminations over the well wall (70 μm illumination position). This is for the same optimal image cathode width (0.4 μm) and shift distance (1 μm) as in Figure 5.28 and Figure 5.29.

The well wall NQE statistic is a measure of the relative suppression of NQE into the pixel up to the well, providing valuable insight into pixel down scaling and resolution limits. As already predicted, the decreasing, somewhat exponential, NQE response at the boundary, indicates that the minimum relative crosstalk occurs for the largest guard width. Note that the BW and FW responses coincide at this maximum width guard cathode, at which the NQE is a minimum.

(cf/ Result guarded SJPD: Appendix IX.)

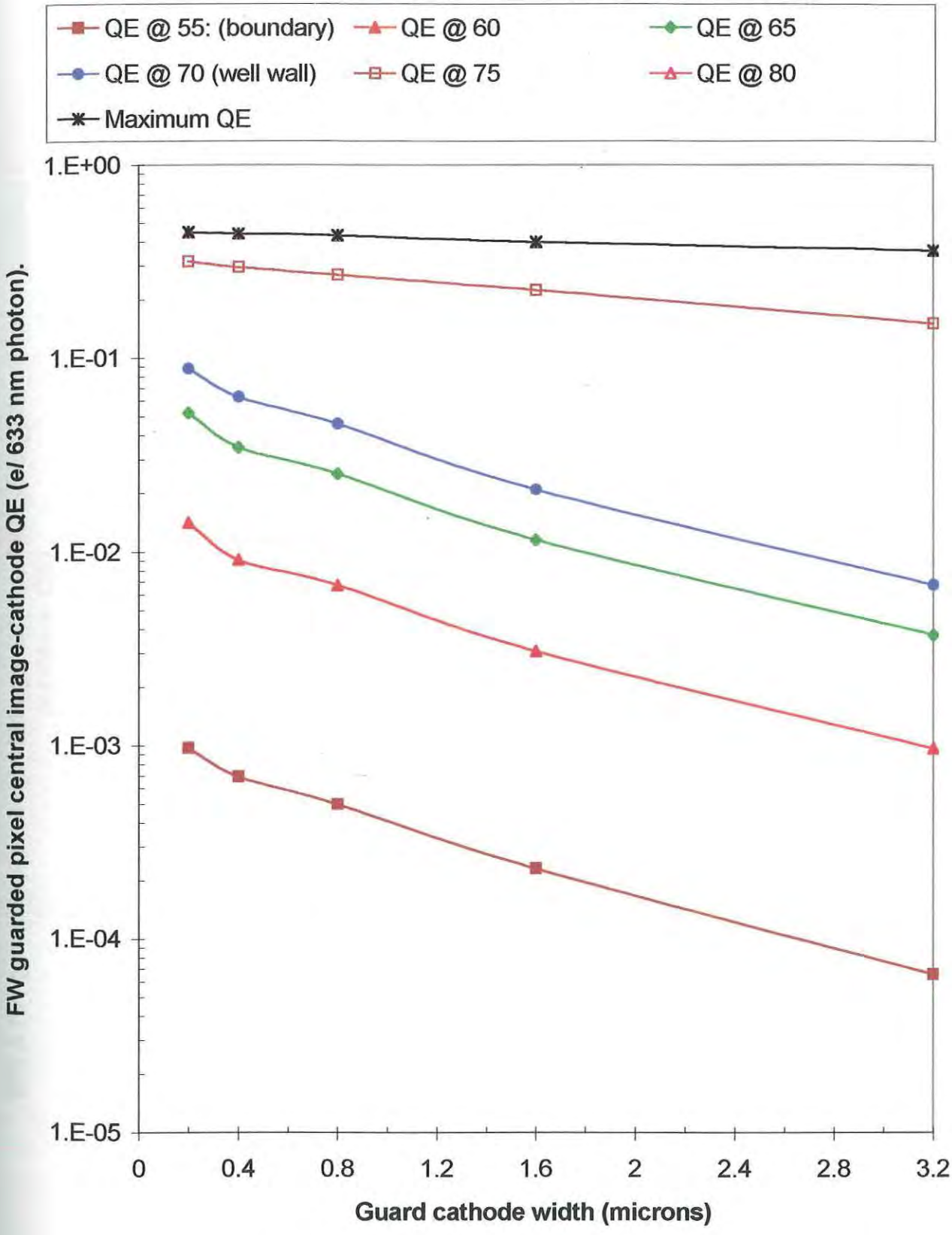

Figure 5.29: FW guarded SJPD pixel: Image cathode QE dependence on guard cathode width, optimally positioned 1 um from well edge and with the optimal image cathode width of 0.4 um.

(cf/ Result guarded SJPD: Appendix VIII & IX.)

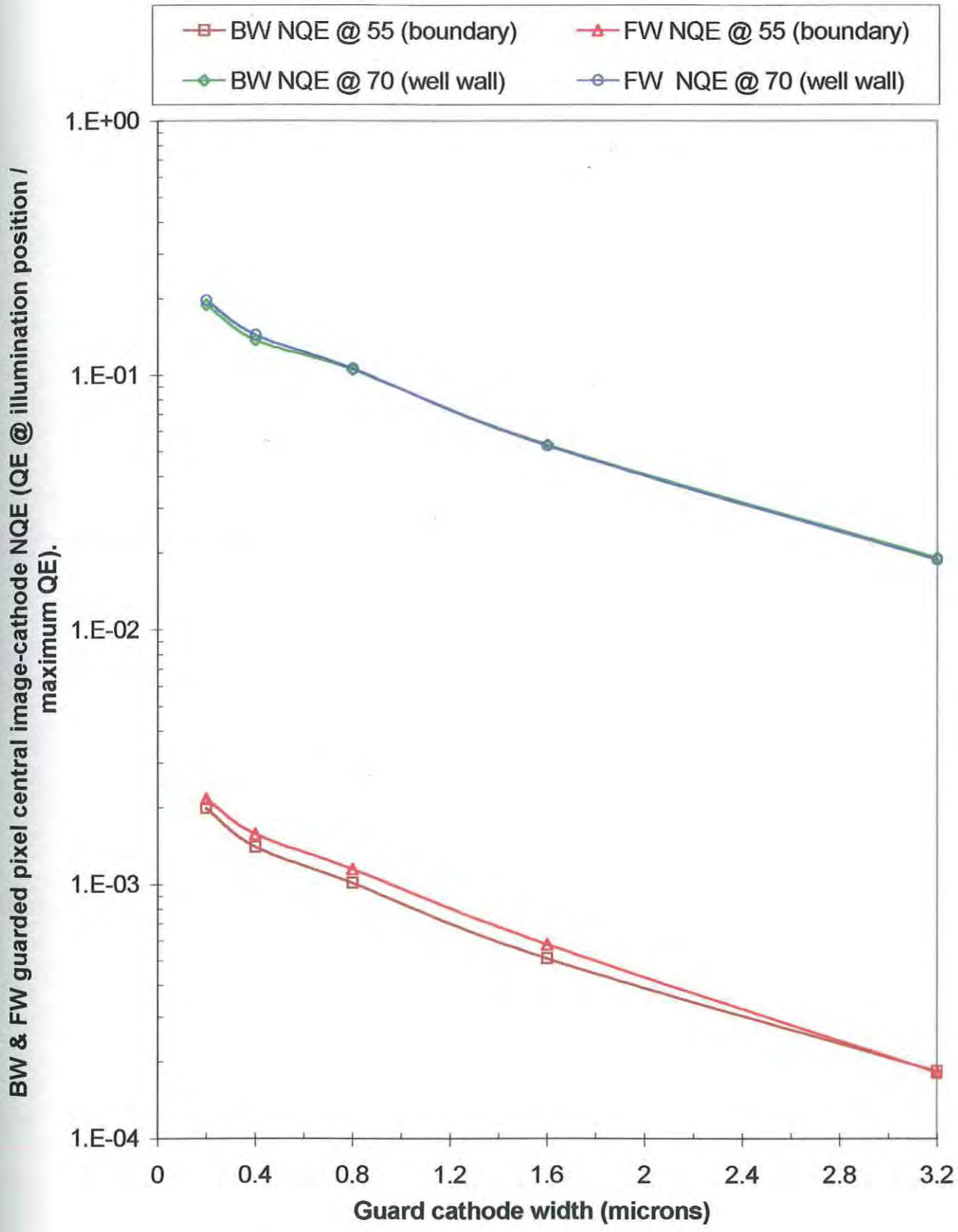

Figure 5.30: BW & FW guarded SJPD pixel : Image cathode NQE dependence on guard cathode width, optimally positioned 1 um from well edge and with the optimal image cathode width of 0.4 um.

Figure 5.31 shows the BW guarded pixel QE profile against ***image cathode*** width for illumination positions from pixel boundary to centre (55 to 80 μm, respectively). This is for constant optimal guard cathode width (3.2 μm) and optimal shift distance (1 μm).

All the QE profiles for illuminations outside the well minimize at 0.4 μm, slightly increasing exponentially either side of this width. The central response increases in QE by 0.15 e/photon over the extent of the guard widths, increasing faster for the shorter widths. The pixel's well wall QE response increases monotonically by only 0.05 e/photon over the same image cathode width domain. This increase may be due to an increasing image cathode capture window pressing in on the adjacent guard capture window, so acquiring a larger share of the available photocarrier population and a more suppressed guard capture efficiency.

Figure 5.32 shows the FW guarded pixel QE profile against ***image cathode*** width for illumination positions from pixel boundary to centre (55 to 80 μm, respectively). This is for the same optimal guard cathode width (3.2 μm) and shift distance (1 μm) as in Figure 5.31.

Generally the FW response is slightly lower in QE profile than the BW response (Figure 5.32), while the trend and minimum-QE-response image-cathode width (0.4 μm) are equivalent. Though the image cathode width increases geometrically, the unusually slight, somewhat exponential increase serves to show the extent this maximum width guard ring cathode controls the pixel capture volume. However the size of the guard makes no difference: the Full Results show the slight, nearly flat response is still the same (Appendix IX).

(cf/ Result guarded SJPD: Appendix VIII.)

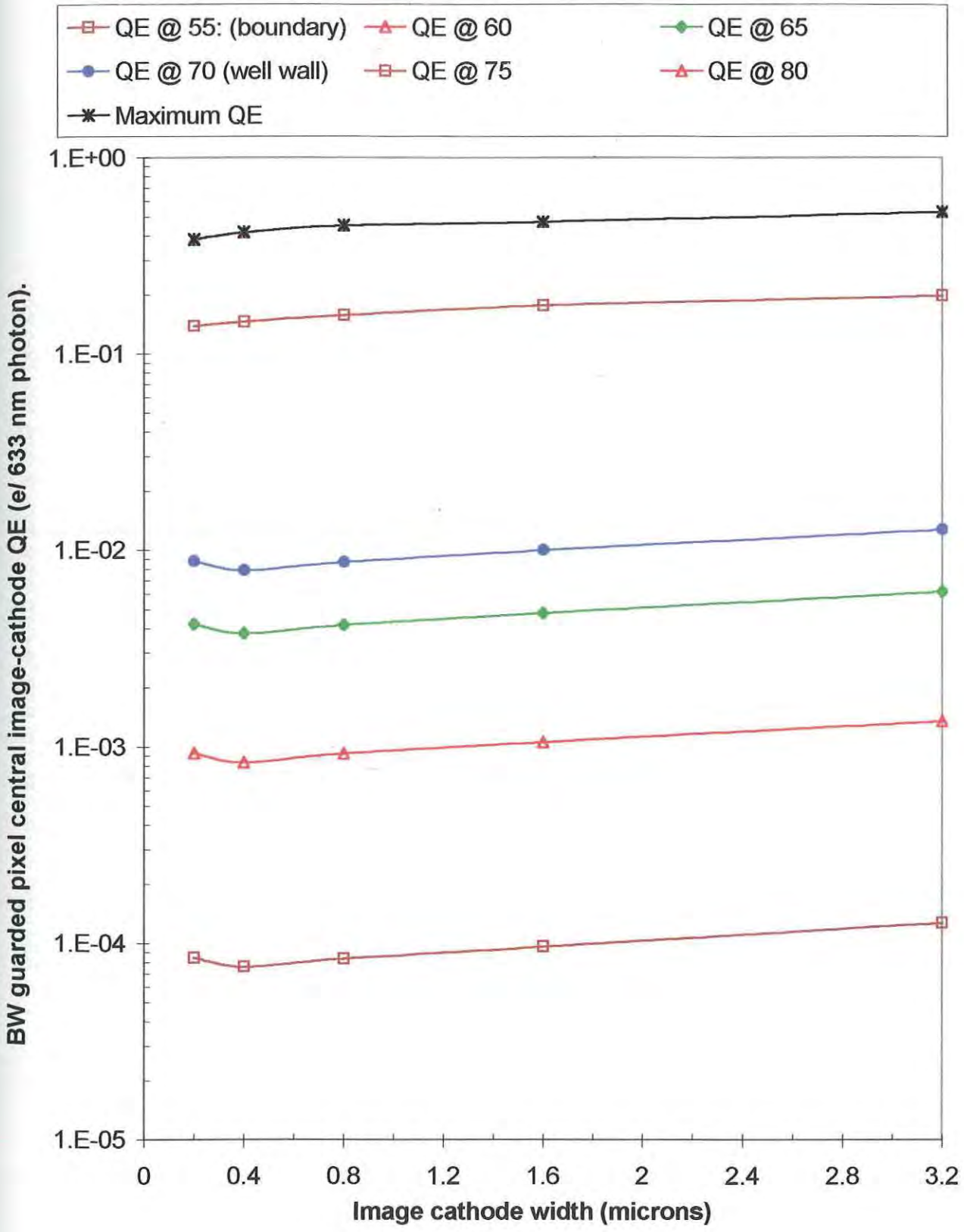

Figure 5.31: BW guarded SJPD pixel: Image cathode QE dependence on image cathode width, positioned optimally 1 um from well edge and with the optimal guard cathode width of 3.2 um.

(cf/ Result guarded SJPD: Appendix IX.)

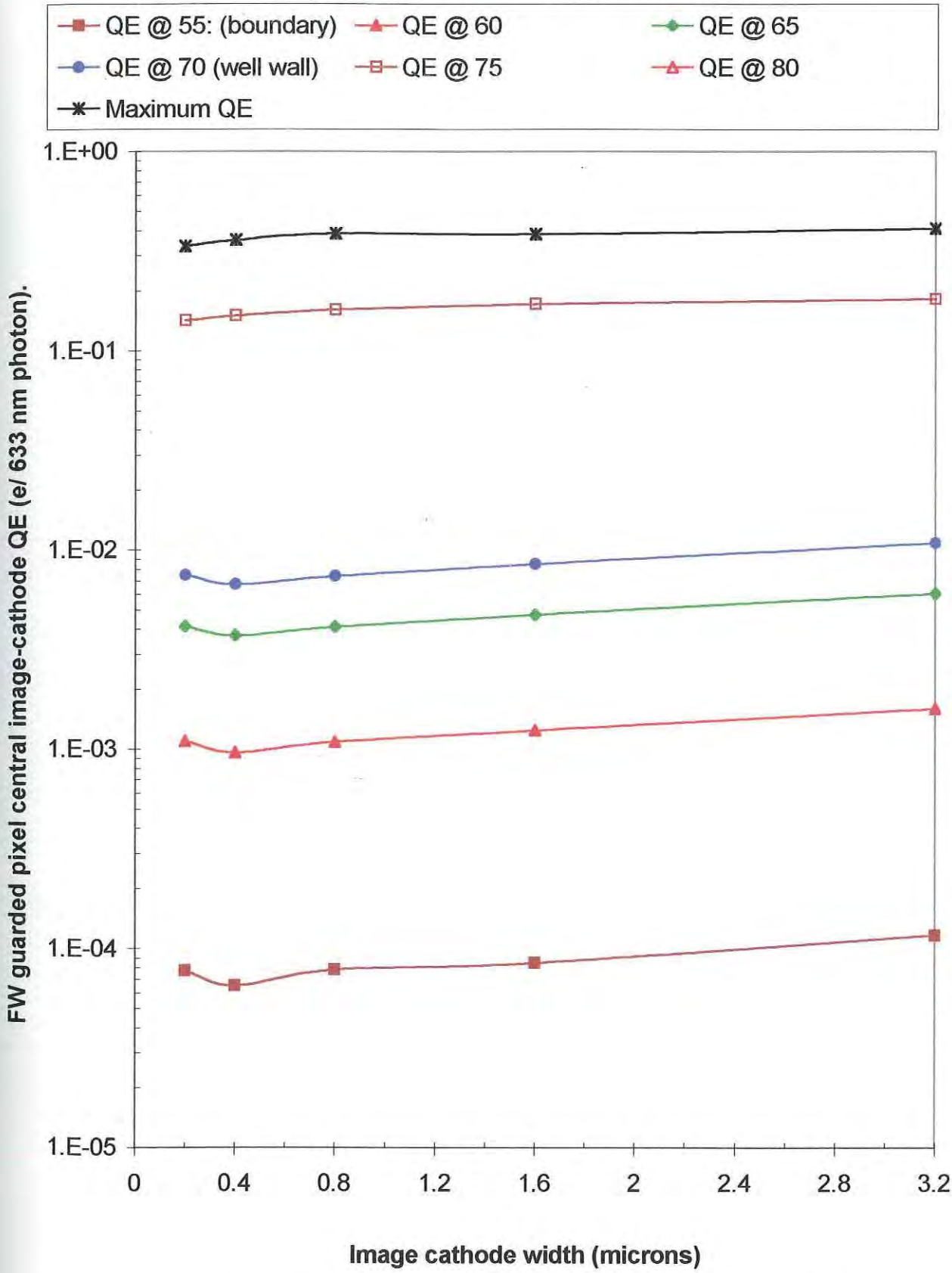

Figure 5.32: FW guarded SJPD pixel: Image cathode QE dependence on image cathode width, positioned optimally 1 um from well edge and with the optimal guard cathode width of 3.2 um.

Figure 5.33 shows the BW and FW guarded pixel NQE profile against ***image cathode*** width for illumination positions at the boundary. It shows the relative crosstalk statistic (at the 55 μm illumination position) and the NQE statistic for illuminations over the well wall (at the 70 μm position). This is for the same optimal guard cathode width (3.2 μm) and shift distance (1 μm) as in Figure 5.31 and Figure 5.32. Similar to Figure 5.30, the well wall NQE profile is also presented.

The NQE response parallels the QE response trend (Figure 5.31 and Figure 5.32). It results from the slight maximum QE response and minimizes at a image cathode width of 0.4 μm and 0.8 μm for the FW and BW response respectively, though both widths are equally minimal in the BW response. The BW response for the mirror side of the pixel (illumination @ 105 μm position) minimizes at 0.4 μm.

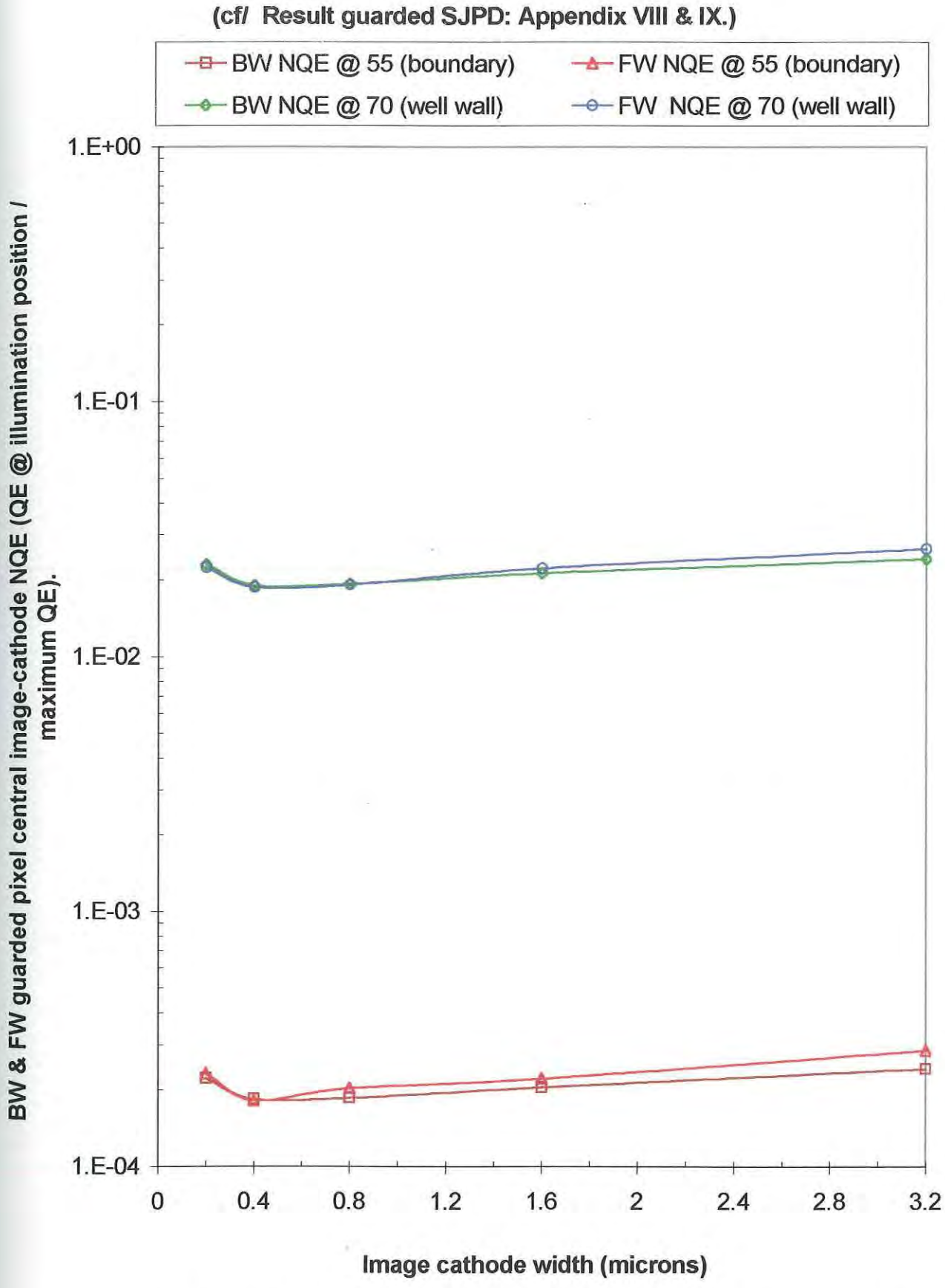

Figure 5.33: BW & FW guarded SJPD pixel: Image cathode QE dependence on image cathode width, positioned optimally 1 um from well edge and with the optimal guard cathode width of 3.2 um.

Figure 5.34 shows the BW guarded pixel QE profile against the ***shift distance***, for illumination positions from pixel boundary to centre (55 to 80 μm, respectively). This is for constant optimal image cathode width (0.4 μm) and optimal guard cathode width (3.2 μm).

The response outside the well mainly minimizes at a shift distance of 1 μm. It is unclear whether a shift distance of zero is better for illumination at the pixel boundary as the value is a minimum for illuminations on the pixel's left boundary (illumination position 55 μm) while not minimum for illuminations on the pixel's right boundary (illumination position 105 μm) as shown in the table of full results (Appendix VIII). The response for illuminations over the well is somewhat exponentially decreasing at the well wall. The response at the centre, viewed as a linear-linear graph, is bi-lineal; an initial linear response until a shift distance of 3 μm, followed by a steeper linear response, results in a total drop of 0.35 e/photon of QE.

Figure 5.35 shows the FW guarded pixel QE profile against ***shift distance***, for illumination positions from pixel boundary to centre (55 to 80 μm, respectively). This is for the same optimal image and guard cathode widths, which are 0.4 μm and 3.2 μm, respectively. This is similar to Figure 5.34.

The QE response is the same for the BW pixel (Figure 5.34), except that it is slightly lower for illuminations over the well and at the pixel boundary. Similar to the BW pixel response, after a shift distance of 2 μm, the response outside the well, especially at the pixel boundary, becomes relatively insensitive to further inward guard shifts, with the response increasing marginally elsewhere inside the pixel, outside the well.

(cf/ Result guarded SJPD: Appendix VIII.)

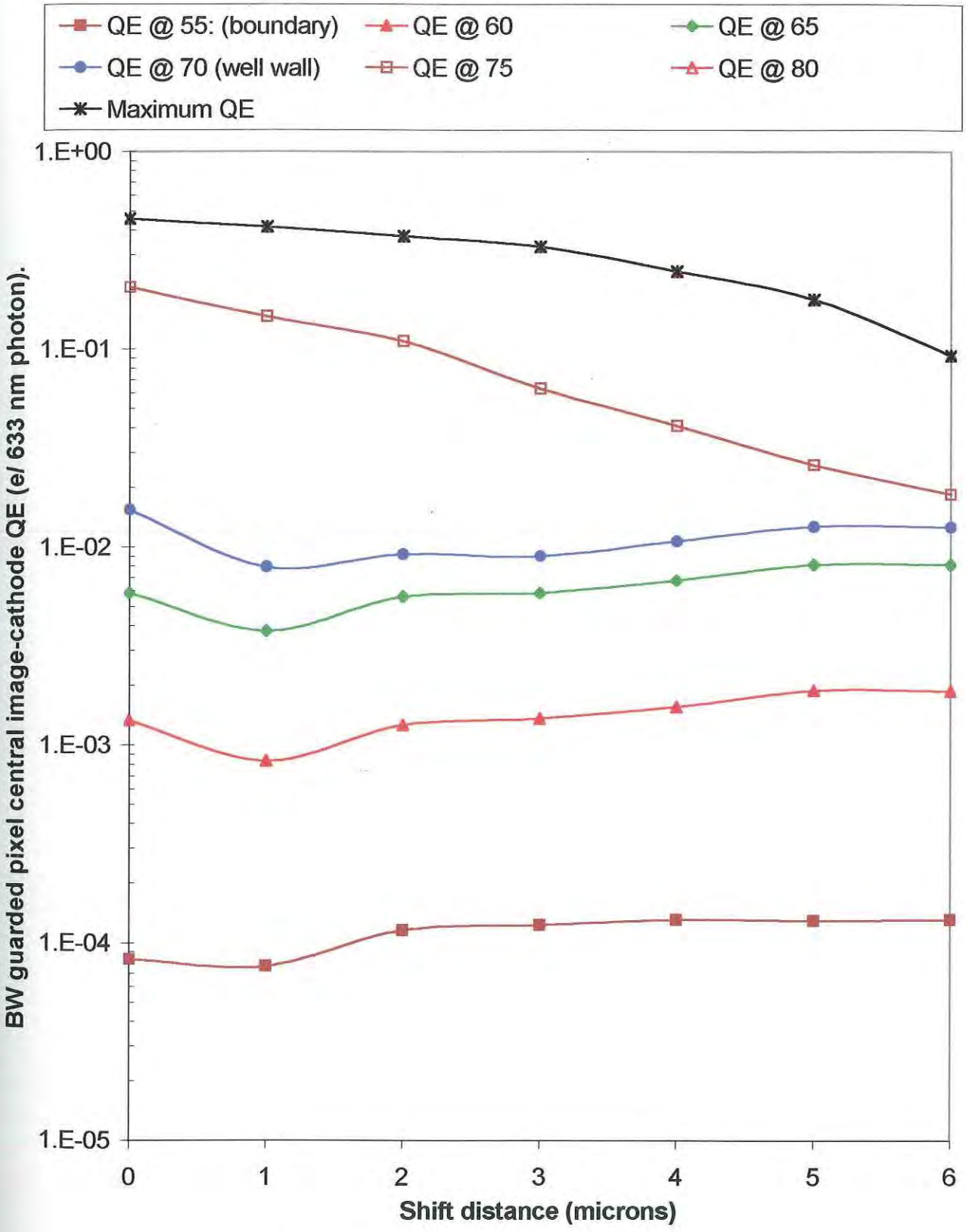

Figure 5.34: BW guarded SJPD pixel: Image cathode QE dependence on the distance the guard cathode is shifted from the well edge (shift distance), with optimal image & guard cathode widths of 0.4 & 3.2 um respectively.

(cf/ Result guarded SJPD: Appendix IX.)

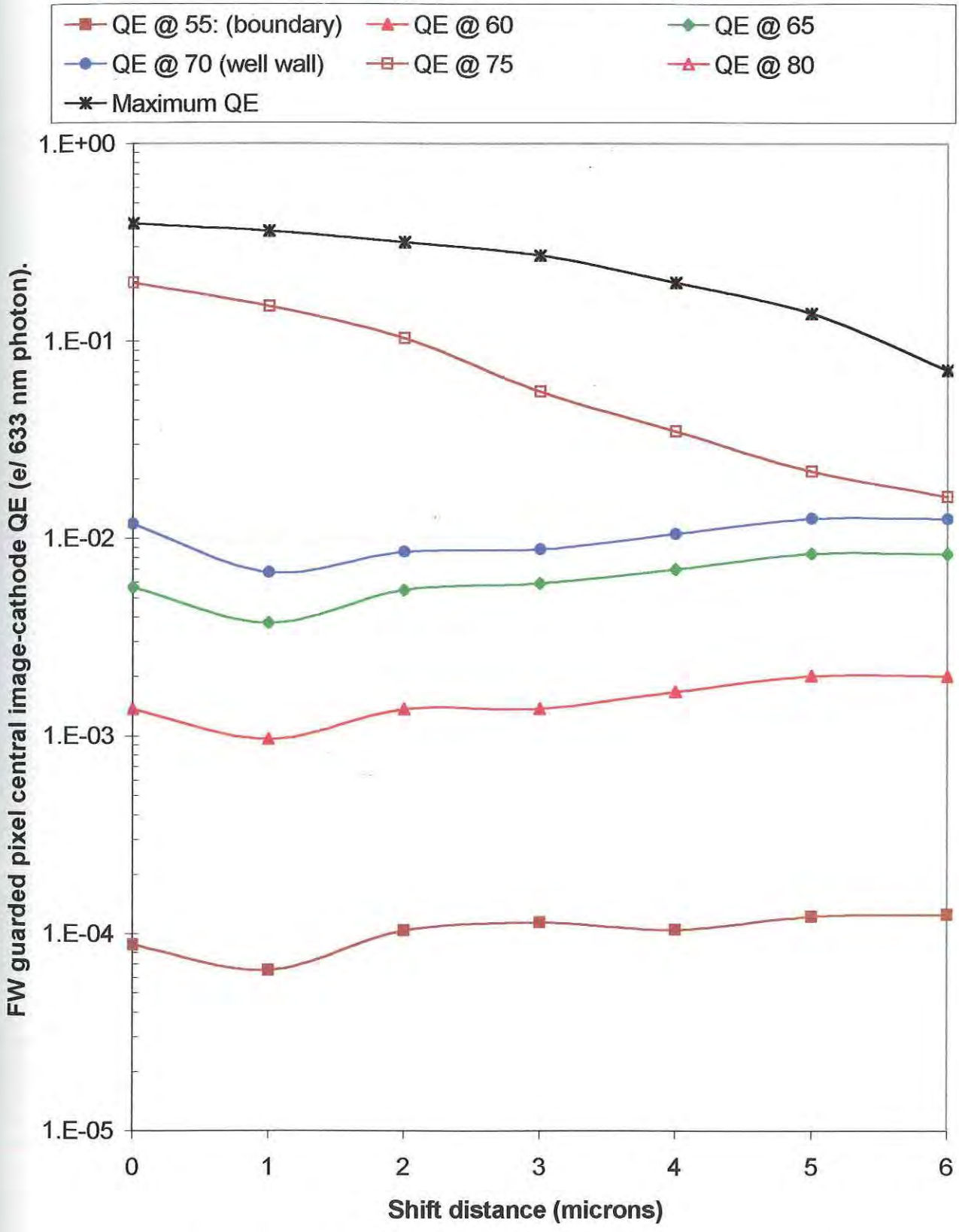

Figure 5.35: FW guarded SJPD pixel: Image cathode QE dependence on the distance the guard cathode is shifted from the well edge (shift distance), with optimal image & guard cathode widths of 0.4 & 3.2 um respectively.

Figure 5.36 shows the BW and FW guarded pixel NQE profile against ***shift distance*** for illumination positions at the boundary. It shows the relative crosstalk statistic (55 μm illumination position) and the NQE statistic for illuminations over the well wall (70 μm illumination position). This is for the same optimal image and guard cathode widths (0.4 μm, 3.2 μm, respectively) as in Figure 5.34 and Figure 5.35. Similar to Figure 5.30 and Figure 5.33, the well wall NQE profile is presented.

With a decreasing maximum QE response and a minimum boundary response at 1 μm, it is not surprising that the minimum NQE also occurs for a shift distance of 1 μm. The well wall NQE response minimizes similarly. It is noted that the guard cathode that reaches up to the edge of the pixel's well (shift = 0 μm), on top of the SCR, and the guard cathode significantly remove from the well edge, away from the SCR, have less capture efficiency than the guard just next to the SCR (shift = 1 μm). This seems to indicate that the guard field and the SCR interaction, play a major role in defining the image cathode's QE response. However further investigation is required as the boundary image NQE response for BW and FW pixel configurations with guard shift distances of 0 μm and 1 μm for illumination positions symmetrically opposite each other (55 and 105 μm) can differ significantly (Appendices VIII & IX).

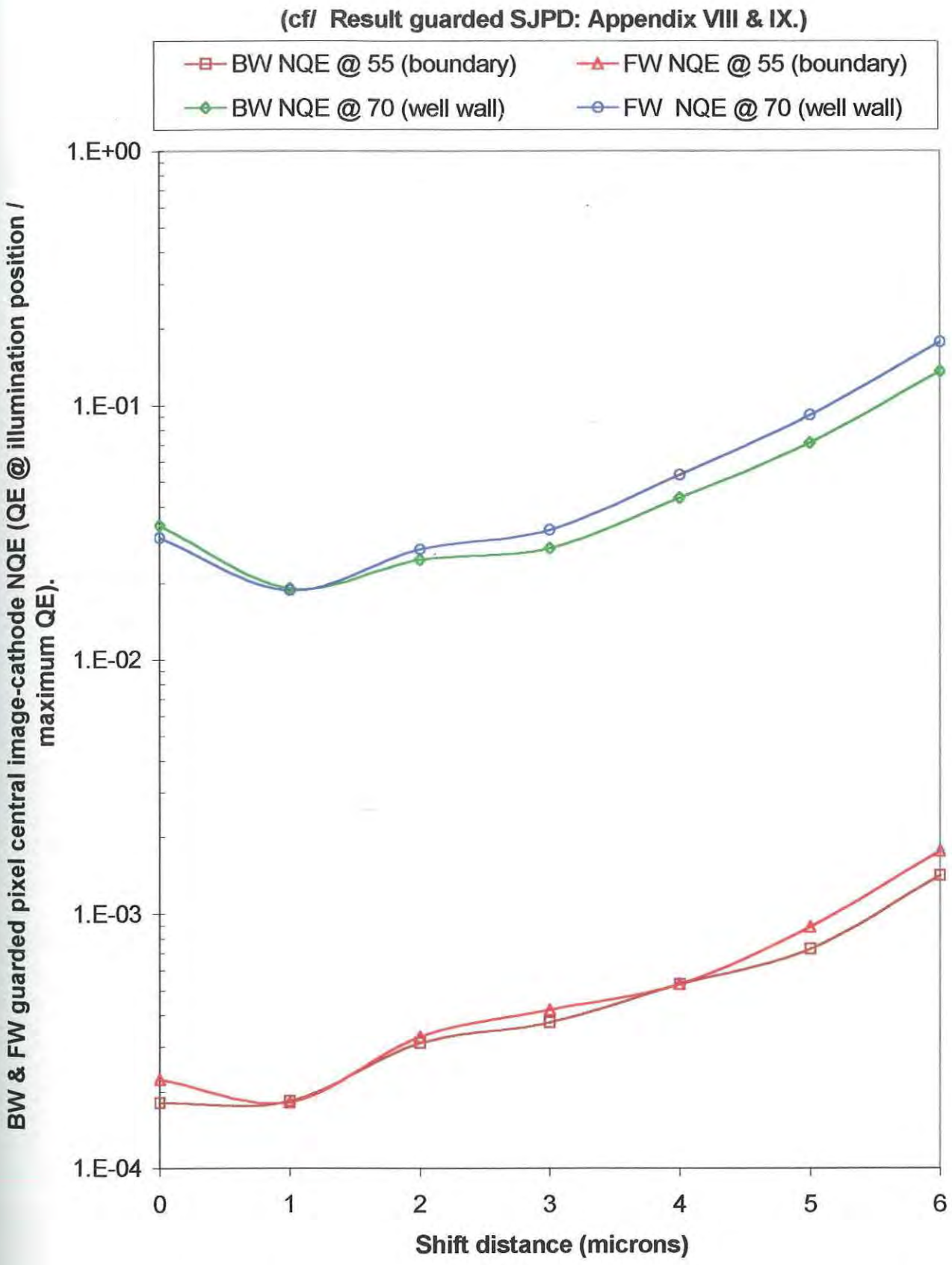

Figure 5.36: **BW & FW guarded SJPD pixel: Image cathode NQE dependence on the distance the guard cathode is shifted from the well edge (shift distance), with optimal image & guard cathode widths of 0.4 & 3.2 um respectively.**

Both Sections 5.1.4 and 5.1.3 have shown that maximizing the guard cathode width proved successful in contributing to the excellent reduction in NQE response, not just at the pixel boundary, but also into the pixel, outside the well without significantly reducing sensitivity compared to other guard-image electrode configurations, that reduce the sensitivity by approximately 50%. Its use produced a much more finely resolved response.

Certainly the use of a 3 μm thick substrate and a 2 μm deep well (3/2) pixel geometry, contributes to a less suppressed QE and NQE response in this study, compared to the response of the 3/1 guarded pixel in Section 5.1.3. The 3/2 pixel has a lower SCR AVP and a higher non-SCR AVP than the 3/1 pixel geometry, the later having the best response resolution profile in Section 5.1.3.

In summary, this study has demonstrated that the minimum relative crosstalk occurs with the maximum width guard cathode (3.2 μm) shifted 1 μm from the well edge towards a 0.4 μm wide image cathode, without significant loss in maximum QE or loss in sensitivity. Compared to the maximally sensitive configuration (QE = 0.5755), with maximum image width and minimum guard width and shift distance, there is a 28% and 20% loss in sensitivity for the minimum relative crosstalk configuration and the same configuration with a shift distance of zero, respectively.

Generally speaking, for a given dual cathode configuration, the BW guarded pixel's sensitivity is on average 10% better than the FW guarded pixel's sensitivity, where sensitivity is defined as the maximum pixel QE response. This was the reverse for the naked pixel results. For the same reason the SCR section associated with the FW naked pixel's well walls benefited its image-cathodes capture efficiency above that of the BW naked pixel, this same section of the FW guarded pixel's SCR benefits this pixel's guard capture efficiency, above that of the BW guarded pixel, with an associated reduction in the FW image-cathode's capture efficiency. This results in the sensitivity inversion between naked and guarded pixels for the two modes of illumination.

The results show that the image-cathode's relative crosstalk response is controlled more by the guard ring cathode's configuration, of size and position, than on its own configuration. The configurations of both cathodes are controlled by the physical constraints of well surface dimensions and minimum electrode size for a given CMOS technology: for 0.35 μm technology, 0.4 μm is the minimum electrode size.

However, optimization of the guarded pixel's dual-cathode configuration so that satisfactory sensitivity and crosstalk suppression is achieved, can only be obtained by a trade off between the two values being optimized. Further mathematical analysis is required to verify that the optimal configuration arrived at is the best optimal trade-off between sensitivity and crosstalk suppression the need for which an irregular result symmetry is partly responsible (Appendices VIII & IX).

Retrospectively, an extrapolation of this trend was applied in section 5.1.3, with the use of an even wider guard ring cathode of 6.4 μm. The use of this optimum dual-cathode configuration contributed to an excellent reduction in NQE response, not just at the pixel boundary (99.99% for BW & FW), but also into the pixel, outside the well. Additionally there is little loss in sensitivity (33% for BW, 20% for FW), compared to the maximally sensitive dual electrode configuration pixels (Appendices VII, VIII & IX). This demonstrates the benefit of obtaining trends in the electrode configurations, associated with the optimization of the dual cathode configuration.

5.1.5 **Effect of Doping Concentration on Guarded Pixels.**

Initially the width of the guard pixel's SCR is considered for various doping regimes of the substrate and well. This is best demonstrated as a table (Table 5.1). "(V = -1)" means that the PN junction is reverse biased by 1 volt.

Table 5.1: Width of SCR (μm) for Various Doping Concentrations.

p-substrate	n-well	V0	W (V=0)	W (V=-1)	W (V=-2)	W (V=-3)	W (V=-4)
1E+14	1E+14	0.456093	3.450715	6.165625	8.007649	9.498944	10.78598
1E+14	1E+15	0.515729	2.721291	4.665249	6.010297	7.105125	8.052448
1E+14	1E+16	0.575366	2.754232	4.557421	5.827038	6.86576	7.766785
1E+14	1E+17	0.635003	2.880532	4.62215	5.8678	6.89187	7.782331
1E+14	1E+18	0.69464	3.011406	4.703576	5.931162	6.945051	7.828716
1E+14	1E+19	0.754277	3.137873	4.785408	5.996166	7.000563	7.877929
1E+14	1E+20	0.813914	3.259547	4.866046	6.060707	7.055915	7.927149
1E+15	1E+14	0.515729	2.721291	4.665249	6.010297	7.105125	8.052448
1E+15	1E+15	0.575366	1.225617	2.028026	2.592998	3.055223	3.456174
1E+15	1E+16	0.635003	0.954887	1.532228	1.945157	2.284633	2.579818
1E+15	1E+17	0.69464	0.956992	1.494745	1.884858	2.207061	2.48788
1E+15	1E+18	0.754277	0.992774	1.514028	1.897093	2.214868	2.492453
1E+15	1E+19	0.813914	1.03081	1.538855	1.916659	2.231387	2.506909
1E+15	1E+20	0.873551	1.067859	1.563877	1.936776	2.248663	2.522276
1E+16	1E+14	0.575366	2.754232	4.557421	5.827038	6.86576	7.766785
1E+16	1E+15	0.635003	0.954887	1.532228	1.945157	2.284633	2.579818
1E+16	1E+16	0.69464	0.425856	0.665153	0.838751	0.982129	1.107092
1E+16	1E+17	0.754277	0.329101	0.501895	0.62888	0.734222	0.82624
1E+16	1E+18	0.813914	0.32758	0.489031	0.609093	0.70911	0.796668
1E+16	1E+19	0.873551	0.337854	0.494786	0.612765	0.711442	0.798008
1E+16	1E+20	0.933188	0.349039	0.502373	0.618813	0.716575	0.802515
1E+17	1E+14	0.635003	2.880532	4.62215	5.8678	6.89187	7.782331
1E+17	1E+15	0.69464	0.956992	1.494745	1.884858	2.207061	2.48788
1E+17	1E+16	0.754277	0.329101	0.501895	0.62888	0.734222	0.82624
1E+17	1E+17	0.813914	0.145771	0.217616	0.271043	0.31555	0.354513
1E+17	1E+18	0.873551	0.111997	0.16402	0.20313	0.235841	0.264537
1E+17	1E+19	0.933188	0.110921	0.159649	0.196652	0.22772	0.255031
1E+17	1E+20	0.992825	0.113899	0.161369	0.197754	0.228415	0.255422
1E+18	1E+14	0.69464	3.011406	4.703576	5.931162	6.945051	7.828716
1E+18	1E+15	0.754277	0.992774	1.514028	1.897093	2.214868	2.492453
1E+18	1E+16	0.813914	0.32758	0.489031	0.609093	0.70911	0.796668
1E+18	1E+17	0.873551	0.111997	0.16402	0.20313	0.235841	0.264537
1E+18	1E+18	0.933188	0.049359	0.071043	0.087509	0.101334	0.113487
1E+18	1E+19	0.992825	0.037757	0.053493	0.065555	0.075719	0.084671
1E+18	1E+20	1.052462	0.03725	0.052019	0.063439	0.073095	0.081617
1E+19	1E+14	0.754277	3.137873	4.785408	5.996166	7.000563	7.877929
1E+19	1E+15	0.813914	1.03081	1.538855	1.916659	2.231387	2.506909
1E+19	1E+16	0.873551	0.337854	0.494786	0.612765	0.711442	0.798008
1E+19	1E+17	0.933188	0.110921	0.159649	0.196652	0.22772	0.255031
1E+19	1E+18	0.992825	0.037757	0.053493	0.065555	0.075719	0.084671
1E+19	1E+19	1.052462	0.016576	0.023148	0.02823	0.032527	0.036319
1E+19	1E+20	1.112099	0.012637	0.017415	0.021139	0.024299	0.027093
1E+20	1E+14	0.813914	3.259547	4.866046	6.060707	7.055915	7.927149
1E+20	1E+15	0.873551	1.067859	1.563877	1.936776	2.248663	2.522276
1E+20	1E+16	0.933188	0.349039	0.502373	0.618813	0.716575	0.802515
1E+20	1E+17	0.992825	0.113899	0.161369	0.197754	0.228415	0.255422
1E+20	1E+18	1.052462	0.03725	0.052019	0.063439	0.073095	0.081617
1E+20	1E+19	1.112099	0.012637	0.017415	0.021139	0.024299	0.027093
1E+20	1E+20	1.171736	0.005531	0.00753	0.0091	0.010436	0.01162

The pixel configurations that are used in the simulations for this study have 4 μm thick substrates and 2 μm deep wells (4/2 pixel geometry). In the SCR-width part of the table, 6 clearly outlined groups are demonstrated, each containing 6 widths. These represent SCR widths for which the SCR does not contact the back wall or front wall of the simulated 4/2 pixel. While the pixel is not fully depleted in this way, the Shockley-Read-Hall model of drift and diffusion, as a result of which the electrode currents can be determined, applies to the reverse biased SJPD cross section. Other wise the simulation result may not be valid as the simulation parameters need to be reconfigured to include avalanche effects occurring in the device, and Auger recombination, due to the fully depleted substrate.

The boxes of data in table 5.1 are also colour coded. The *blue numbers* represent SCRs that penetrate into the well, more than into the substrate: inwardly depleted. The *red numbers* represent SCRs that penetrate into the substrate more than into the well: outwardly depleted. The *green numbers*, in between the red and blue numbers, represent SCRs that penetrate the same distance into well and substrate. From this selection of doping regimes a selection of valid simulation QE and NQE response data have been selected and are presented graphically in this section. Two doping profiles are compared in this study. They are the n-well / p-substrate pixel doping configuration, referred to as the n-well pixel, and the p-substrate / n-well pixel, referred to as the p-well pixel.

The QE and NQE BW and FW guarded n-well and p-well pixel responses, for illuminations positions inside the pixel, are graphed against the two doping concentration parameters, one at a time, beginning with the substrate doping dependency followed by the well doping dependency. Each treatment starts with the BW pixel QE response followed by the FW pixel QE response for illuminations across the pixel. Lastly, the BW and FW pixel NQE boundary and well wall response is presented. The well electrodes are each 4 μm wide and the guard shift distance is 1 μm.

For a full Result set of BW and FW pixel data see Appendices X and XI, respectively. They both contain QE and NQE data. For the pixels' AVP data see Appendix XII.

Figure 5.37 shows the BW n-well and p-well guarded pixel QE profiles against substrate doping concentration, for illumination positions from the pixel boundary to the centre (positions 55 to 80 μm, respectively). Graphs are shown for constant well doping (10^{17} cm^{-3}), reverse bias voltage (2 V = [2]) and electrode widths (4 μm), with possible optimal shift distance (1 μm).

The p-well and n-well responses are coincident, given a slight decline from the largest SCR pixel to a generally flat trend, for all pixel illumination positions. The minimum at a doping of 10^{16} cm^{-3} for the n-well pixel, is due to the crossover of decreasing SCR AVP, that contributes to the reduction of image capture efficiency, and an increasing non-SCR AVP that contributes to a greater diffusion in the substrate. This allows more image electron minority photocarriers to reach the image capture field. The reduction in the SCR AVP is greater than the increase in the non-SCR AVP and so the response is lower than the lower doping substrate pixels. The lower doped substrate pixels have greater SCR AVP, enhancing their capture efficiency, though not to the same extent as the higher doping substrate pixels which have greater "free" carrier diffusion in the substrate which increases their image-cathode capture efficiency even more.

Figure 5.38 shows the FW n-well and p-well guarded pixel QE profiles against substrate doping concentration, for illumination positions from the pixel boundary to the centre (positions 55 to 80 μm respectively). This is for the same constant configuration parameters as in Figure 5.37.

The FW n-well and p-well pixel QE profiles are again coincident, similar to the BW profile, though more suppressed. This again may be due to the photogenerated carrier envelope being closer to the guard capture field, resulting in increased guard capture volume and hence decreased image capture volume across the pixel. Similar to the BW response, the response is insensitive to doping regimes that cause the SCR to penetrate inwards, having substrate dopings of 10^{17} cm^{-3} to 10^{19} cm^{-3}. The very slight decrease, nearly flat, in maximum QE for increasing substrate doping, due to the much more rapid decreasing SCR AVP, in FW and BW pixels, demonstrates the degree to which the guard-cathode dominates the carrier capture volume.

(cf/ Result guarded SJPD: Appendix X & XII.)

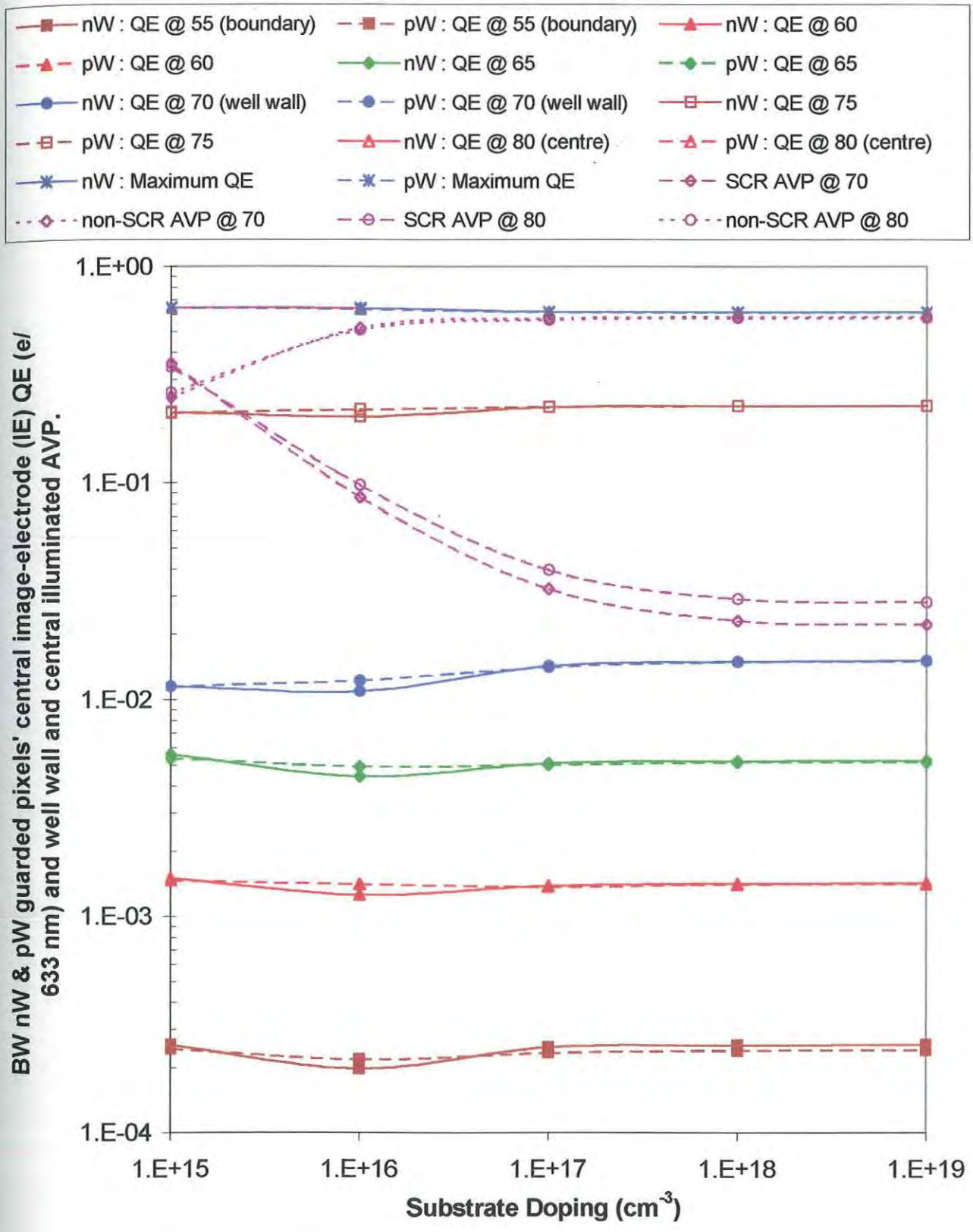

Figure 5.37: BW guarded SJPD n-well (nW) & p-well (pW) pixels: IE QE dependence on substrate doping compared to wall and central AVP, using 4 um well electrodes, guard shift distance of 1 um and a 10^{17} cm^{-3} doped well.

(cf/ Result guarded SJPD: Appendix XI & XII.)

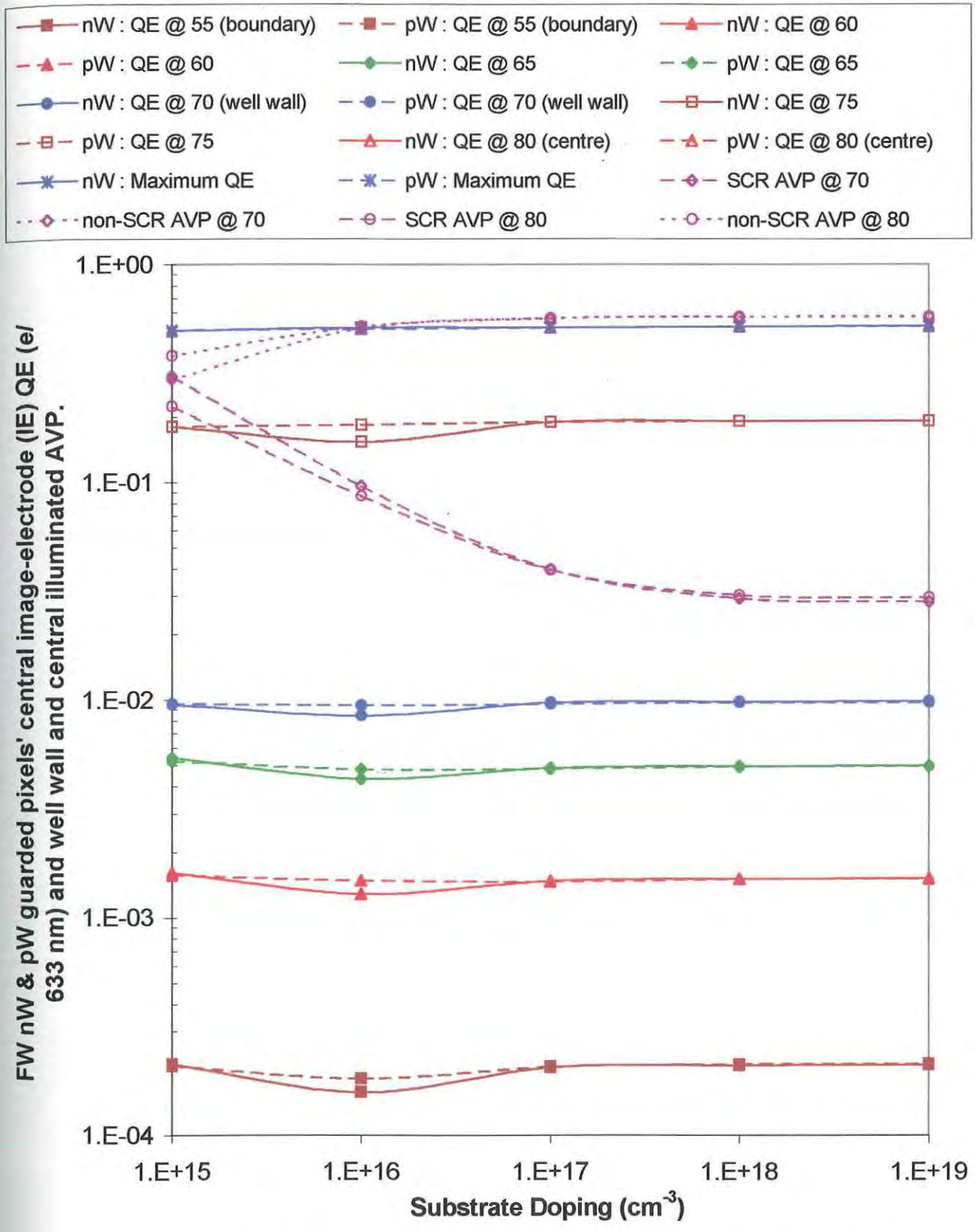

Figure 5.38: **FW guarded SJPD n-well (nW) & p-well (pW) pixels: IE QE dependence on substrate doping compared to wall and central AVP, using 4 um well electrodes, guard shift distance of 1 um and a 10^{17} cm^{-3} doped well.**

Figure 5.39 shows the BW and FW n-well and p-well guarded pixel NQE profiles against substrate doping concentration for illumination positions at the boundary. It shows the relative crosstalk (NQE at illumination position 55 μm) and the NQE for illumination over the well wall (at the 70 μm position). This is for the same constant configuration parameters as in Figures 5.37 and 5.38. The well wall NQE is a measure of the relative suppression of NQE into the pixel that allows comparison between the resolution profiles for different pixel substrate doping regimes.

Again the response initially mimics the decrease in drift component, which rises moderately to a plateau, demonstrating the diffusion dominance of the higher doped substrate pixels. Similar to the QE response in Figures 5.37 and 5.38, the p-well pixel's NQE is generally insensitive to substrate doping increase, for the range studied. This demonstrates that their guard anodes absorb more of the effects of the doping changes on the AVP profile than the guard cathodes in the n-well pixels. The BW and FW response for both n-well and p-well pixels are fairly coincident, thus for these doping regimes the guard pixels show only slightly suppressed internal pixel response and a minimum relative crosstalk at a substrate doping of 10^{16} cm^{-3}.

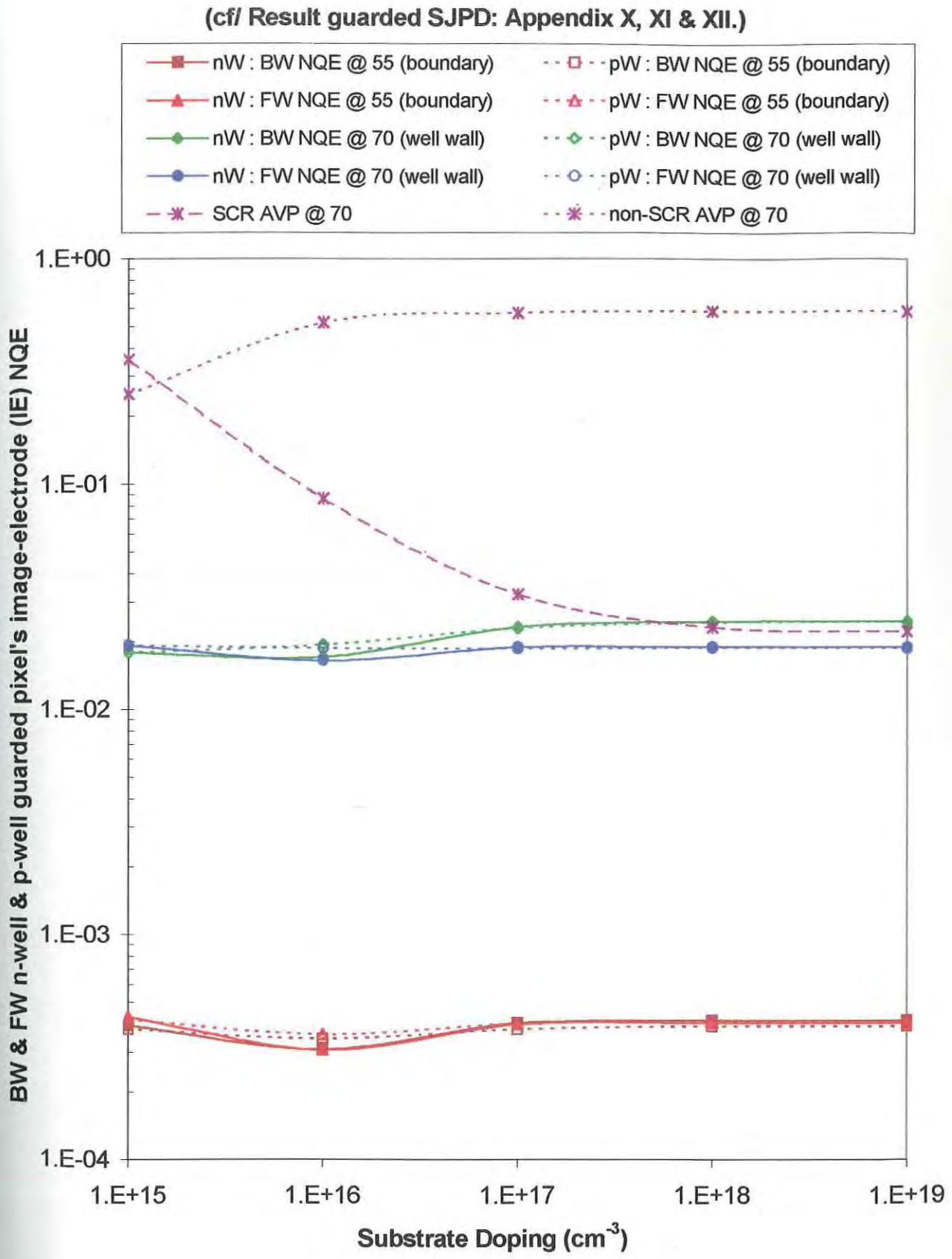

Figure 5.39: BW & FW guarded SJPD n-well (nW) & p-well (pW) pixels: IE NQE dependence on substrate doping compared to well wall AVP, for illuminations at the 55 & 70 micron positions; same parameters as for Figure 5.38.

Figure 5.40 shows the BW n-well and p-well guarded pixel QE profiles against well doping concentration across illumination positions from the boundary to the centre (positions 55 to 80 μm, respectively). This is for constant substrate doping (1e17 cm^{-3}), reverse bias voltage (2 V) and cathode widths (4 μm), with optimal shift distance (1 μm).

The SCR orientation is reversed to Figures 5.37 – 5.39. For the first well doping, the SCR is more internal to the well (0.57 μm), then it is split equally (0.14 μm out and in the well), after which it is more external to the well (0.18 to 0.195 μm). The QE response internal to the well is totally insensitive to the increasing doping of the well, except at the centre where the response parallels the SCR AVP profile, more noticeable on a linear-linear graph.

Figure 5.41 shows the FW n-well and p-well guarded pixel QE profiles against well doping concentration across illumination positions from the boundary to the centre (positions 55 to 80 μm, respectively). This is for the same constant configuration parameters as in Figure 5.40.

As for Figure 5.38, this FW response is also suppressed across all pixel illumination positions, compared to the BW pixels. The increasing trends from the well wall outwards are more pronounced. The decreasing trend for illumination at the centre of the pixel is also more pronounced. In contrast to the flat response at the 75 μm illumination position in the BW pixel (Figure 5.40), the FW pixel shows a very slight decreasing trend, following the FW SCR AVP profile because its photogenerated carrier guard:image capture ratio is more dominated by guard ring capture compared to the BW pixel, this ratio decreasing and then plateaus as the well doping increases. In contrast, for illuminations over the centre the image-electrodes capture efficiency decreases and then plateaus as the well doping increases. This leads to the conclusion that though there may be a slight benefit of inwardly depleted SCRs to increased response resolution, the main benefit of using a guard-ring configuration is that the guard-ring system robusts the pixel's response across 5 magnitudes of substrate and well doping variation.

(cf/ Result guarded SJPD: Appendix X & XII.)

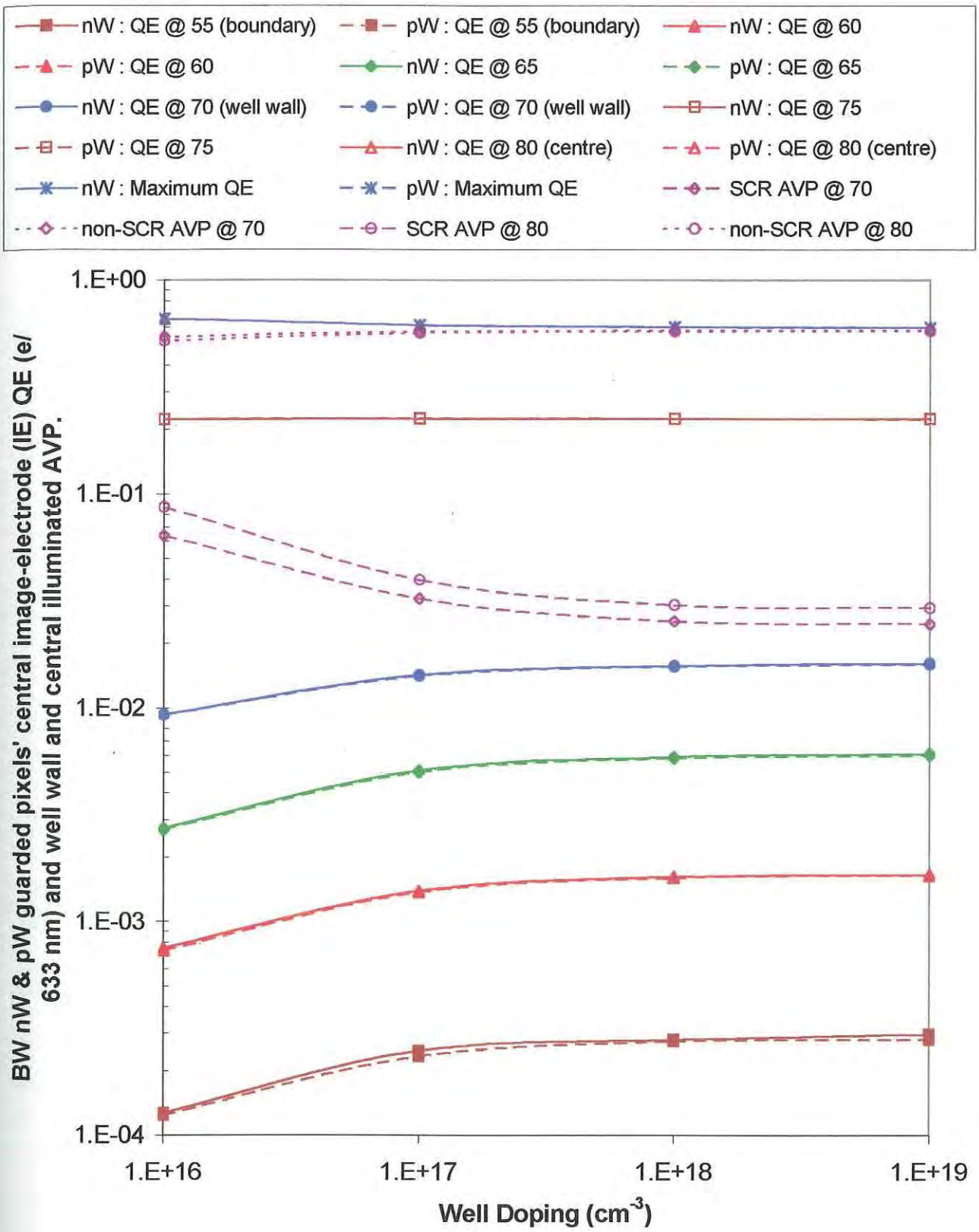

Figure 5.40: **BW guarded SJPD n-well (nW) & p-well (pW) pixels: IE QE dependence on well doping compared to wall and central AVP, using 4 um well electrodes, guard shift distance of 1 um and a 10^{17} cm^{-3} doped substrate.**

(cf/ Result guarded SJPD: Appendix XI & XII.)

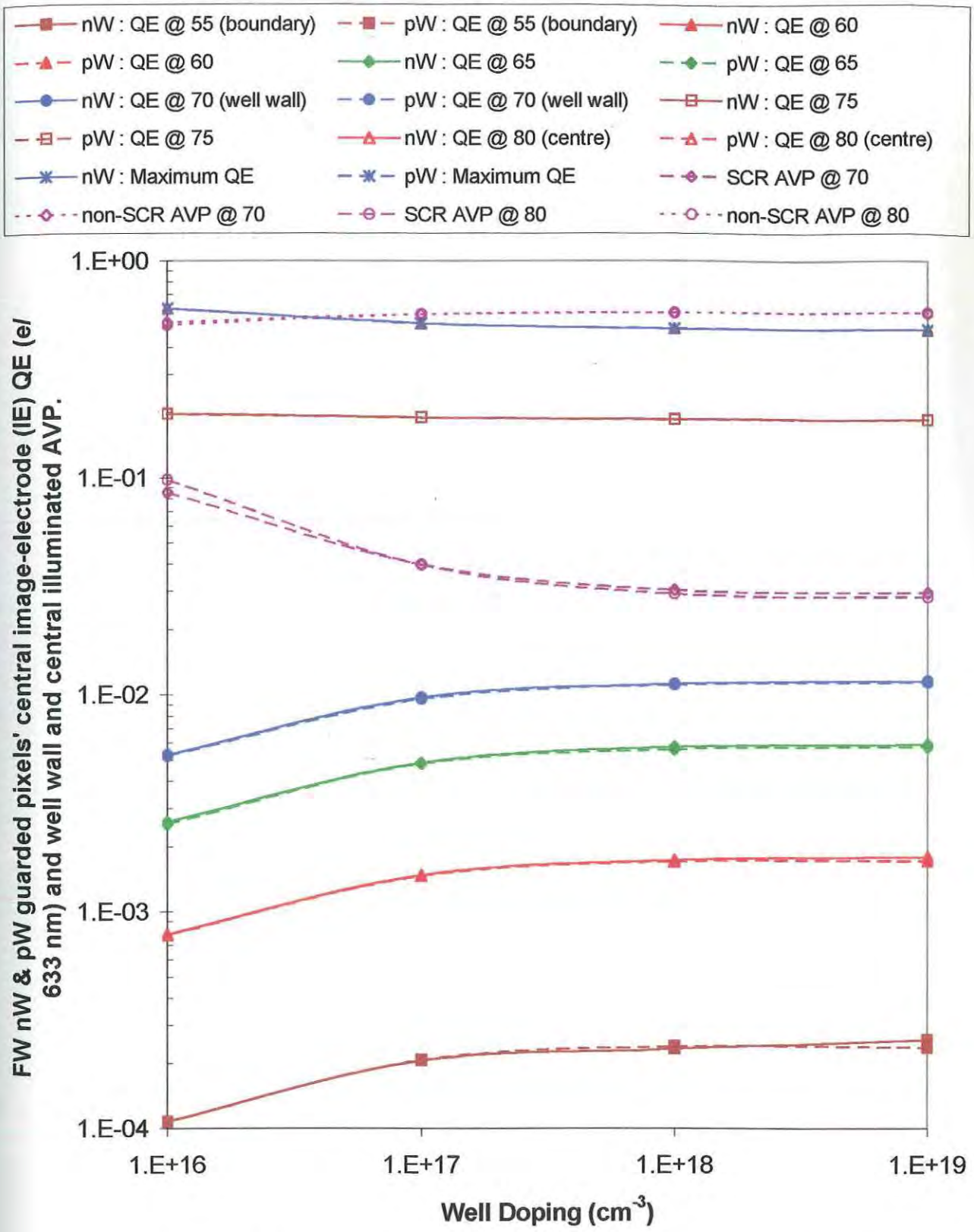

Figure 5.41: FW guarded SJPD n-well (nW) & p-well (pW) pixels: IE QE dependence on well doping compared to wall and central AVP, using 4 um well electrodes, guard shift distance of 1 um and a 10^{17} cm^{-3} doped substrate.

Figure 5.42 shows the BW and FW n-well and p-well guarded pixel NQE profile against well doping concentration for illumination positions at the boundary. It shows the relative crosstalk (NQE at illumination position 55 μm) and the NQE for illumination over the well wall (at the 70 μm position). This is for the same constant configuration parameters as in Figures 5.40 and 5.41.

The well wall NQE is a measure of the relative suppression of NQE into the pixel that allows comparison between the resolution profiles for different pixel well doping regimes. From the well wall NQE, the least doped, internal-SCR pixel has the greater internal pixel suppression and hence a better resolved response. It also presents the least relative crosstalk NQE of 1.921×10^{-4}, which is a local minimum.

In the substrate doping dependency study (Figures 5.37 to 5.39) the pixels with SCRs internal to the well showed enhanced image-electrode QE response, while in this well doping study (Figures 5.40 to 5.42) the reverse is true. Though this may appear contradictory, a possible reason is that in the well doping study the internal SCR pixel had the largest well wall illuminated SCR AVP (6.6 %, BW and 8.8% FW), which is 2 to 3 times greater than the well wall illuminated SCR AVP in the substrate doping study (3.8% – 2.2% BW and 4.55% – 2.83% FW) while their respective diffusion components are similar. In the substrate doping study the internal-SCR pixels have the smallest SCR AVPs with the largest diffusion component.

In diffusion dominated BW pixels more than FW pixels, where SCR AVP is minimized and the non-SCR AVP is maximized (especially the non-SCR AVP in the Substrate), for p-well pixels, the hole image carriers, being less mobile then electrons in n-well pixels, are less likely to reach the central image anode capture field. They rather diffuse into the increasing influence of the guard capture field, resulting in a very slight suppressed image anode QE response, increasingly more the closer the illumination to the pixel boundary (Figure 5.40). In the FW pixel both carriers are equally prone to guard capture, as the photogenerated minority carrier envelope is much closer to the SCR-associated with the well wall than in the BW pixel's photocarrier envelope orientation. Hence both n-well and p-well FW pixel QE responses are suppressed across the entire pixel, not just the already slightly retarded hole response.

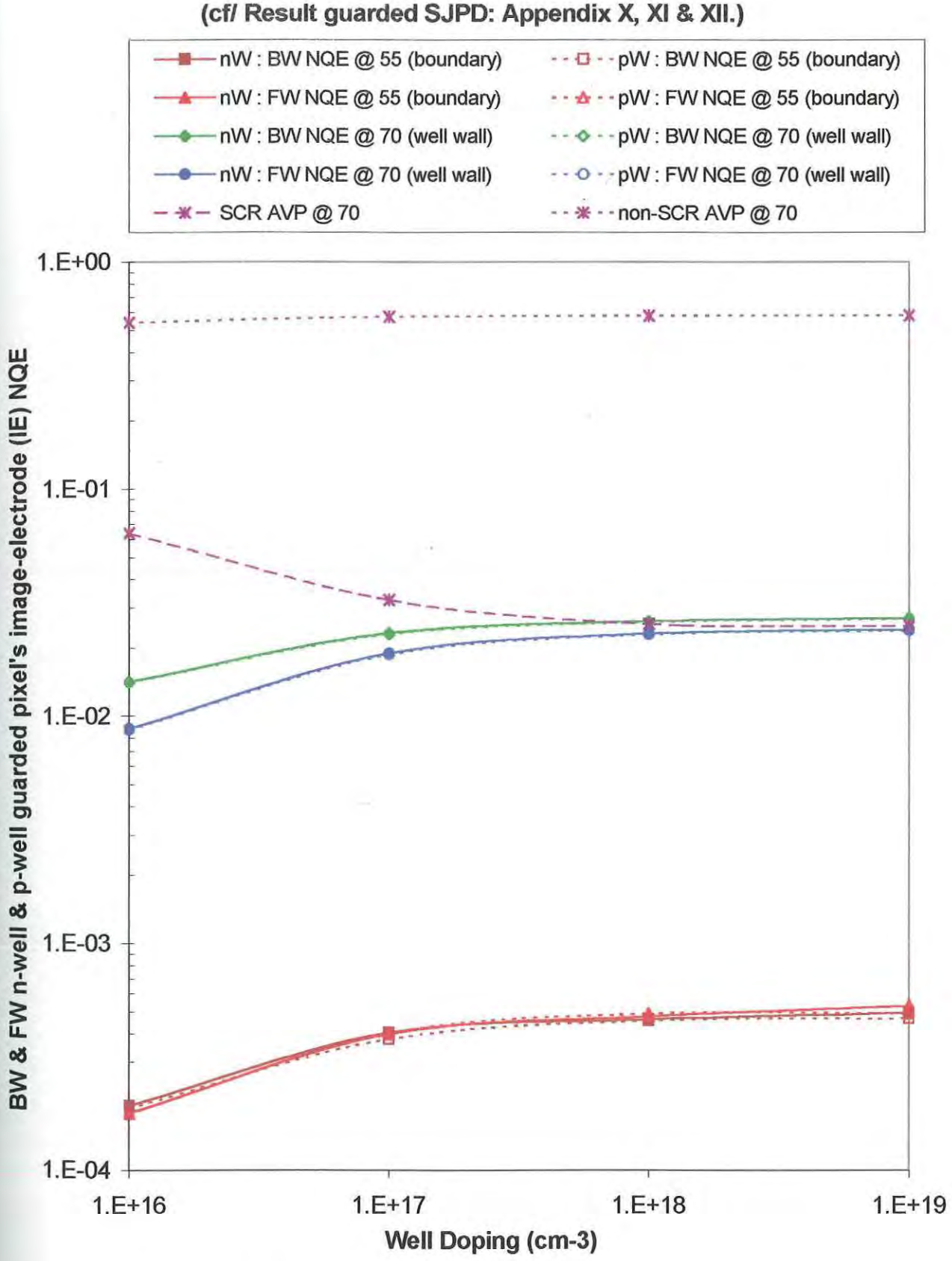

Figure 5.39: **BW & FW guarded SJPD n-well (nW) & p-well (pW) pixels: IE NQE dependence on well doping compared to well wall AVP, for illuminations at the 55 & 70 micron positions; same parameters as for Figure 5.38.**

If the local minima for relative crosstalk are allowed to intersect, then the global minimum for the 4 / 2 n-well and p-well pixel is a pixel with an equal substrate and well doping of 10^{16} cm^{-3} (substrate/well doping = 16/16). This agrees with the full table of doping concentration configurations in Appendices X and XI. The global minima for the 3/2, 4/2, 5/2 and 6/2 configuration geometry pixels is summarised in Table 5.2 and taken from the table of full results (Appendices X & XI).

Table 5.2 Pixel Geometries that Demonstrate Minimum NQE Response.

Pixel Geo-metry	Pixel Doping Geo-metry	Best Crosstalk Pixel						
		Doping concentration & SCR width (um)			NQE @ boundary (55)		Maximum QE Carriers / phtn	
		SCR	Subst	Well	BW	FW	BW	FW
3 / 2	nW	0.61276	1E+19	1E+16	3.02E-5	2.82E-5	0.5890	0.5262
	pW	0.61276	1E+19	1E+16	2.38E-5	2.38E-5	0.5875	0.5875
4 / 2	nW	0.83875	1E+16	1E+16	1.38E-4	1.35E-4	0.6906	0.6059
	pW	0.83875	1E+16	1E+16	1.58E-4	1.61E-4	0.6784	0.5847
5 / 2	nW	1.94516	1E+15	1E+16	4.82E-4	4.08E-4	0.7326	0.6552
	pW	1.94516	1E+15	1E+16	4.88E-4	4.71E-4	0.7308	0.5893
6 / 2	nW	1.94516	1E+15	1E+16	9.82E-4	8.06E-4	0.7362	0.6161
	pW	1.94516	1E+15	1E+16	9.96E-4	7.92E-4	0.7356	0.6204

These doping configuration minima also have the highest or nearly the highest maximum QE in each pixel geometry tested. The 5/2 FW p-well pixel doping geometry represented in the table is in fact the next best crosstalk configuration. The best is the pixel with equal substrate and well doping of 10^{16} cm^{-3}. It has a 0.2% lower pixel boundary NQE of 4.70×10^{-4} and an 8% better maximum QE of 0.6335 holes/photon than the next best pixel, outlined in Table 5.2.

5.1.6 **Effect of Voltage Bias on Guarded Pixels.**

Initially the QE data is presented graphically, BW pixel (Figures 5.43 to 5.44) response, followed by FW pixel (Figures 5.45 to 5.46) response. This is followed by the NQE response (Figures 5.47 to 5.48) where the BW and FW responses are presented together. Finally, the FW and BW pixel AVP data are compared to the QE and NQE profiles in the previous graphs (Figures 5.49 to 5.50). The latter trends are explained with reference to the former profiles. Note, pixel n-well and p-substrate doping is $10^{17}cm^{-3}$ and 10^{15} cm^{-3}, respectively.

Both QE and NQE data are presented graphically against the position of illumination of the 5 μm wide 633 nm laser. This allows simultaneous comparison of the effect of both bias change and thickness change. Though general changes due to QE or NQE response dependency on thickness and bias may be noted, the actual functional relationship (e.g. exponential or linear, etc) is not immediately clear.

The QE response data for both BW and FW pixels is grouped in order of increasing pixel thickness and then in order of increasing reverse bias. This generates four pixel-configuration data sets:

1. 3/2 zero reverse biased pixel, represented by brown squares.
2. 12/2 zero reverse biased pixel, represented by red triangles.
3. 12/2 1 volt reverse biased pixel, represented by green diamonds.
4. 12/2 2 volt reverse biased pixel, represented by blue circles.

NB: a 12/2 pixel is 12 μm thick and has a 2 μm deep well.

Within each bias type, the QE data is grouped in order of electrode configuration: naked image response, followed by guarded image response, followed by left guard response. The naked pixels data points are not filled in, appearing as the point geometry outlined and a solid line. The guarded pixel's two points are filled in. The guard image response is a solid line while the left guard response is a dashed line. For each pixel configuration group, the points are all the same colour and shape.

The NQE response data for both BW and FW pixels are grouped in the same way as the QE response data. The exception is that the guard response does not appear and the FW NQE response (dashed line in Figure 5.47 – 5.48) and BW NQE response (solid line in Figure 5.47 – 5.48) appear together. In a similar way to the QE data presentation, the naked pixels data points are not filled in, appearing as the point geometry outlined, while the guarded pixel points are completely coloured. Therefore each of the four pixel configurations contains four response profiles: the naked BW pixel NQE profile, the naked FW pixel NQE profile, the guarded BW pixel profile and finally the guarded FW pixel NQE profile. For each pixel configuration group, the points are all the same colour and shape.

Finally the SCR and non-SCR AVP data are presented graphically against the four different pixel configurations represented as an integer from –1 to 2 in Figure 5.49, Figure 5.50 and as defined in Table 5.2.

Note: A full appendix of results has not been prepared for this section as the graphs in this section demonstrate the relationships in the data sufficiently.

Figure 5.43 shows the naked and guarded BW pixel's ***linear*** QE response of the four pixel-configurations graphed against illumination position.

As bias increases for the thicker (12 μm) naked and guarded pixels, the image and guard QE responses increases across the whole pixel. The largest increase is for illuminations at the well wall, where there is more SCR illuminated, increasing the capture efficiency for both naked pixel image cathode and guarded pixel guard-ring cathode. The guarded pixel image-cathode QE also increases with increasing bias, but only near the centre of the well.

Figure 5.44 shows the naked and guarded BW pixel's ***logarithmic*** QE response of the four pixel-configurations graphed against illumination position.

Here the guarded pixel image cathode QE response is clearer. The thicker guarded pixel's image-cathode QE response decreases exponentially, from the centre outwards. Clarifying Figure 5.43, the increasing QE response trend is only similar to the naked pixel image cathode response at the well centre, where the image field has more capture efficiency. Elsewhere the increasing guard capture field actually inverts the trend, as the guarded pixel's image-cathode QE response decreases with increasing bias. This increasing response resolution for the guard-ring configuration, is magnified even more with the shallower pixel, for which the maximum QE is greater than the thicker guarded pixel's QE response, while the rest of the shallower guarded pixel's response is more suppressed. For this 3/2 guarded pixel, only the guard, not the image response is suppressed by the increased negative hole current inside the well.

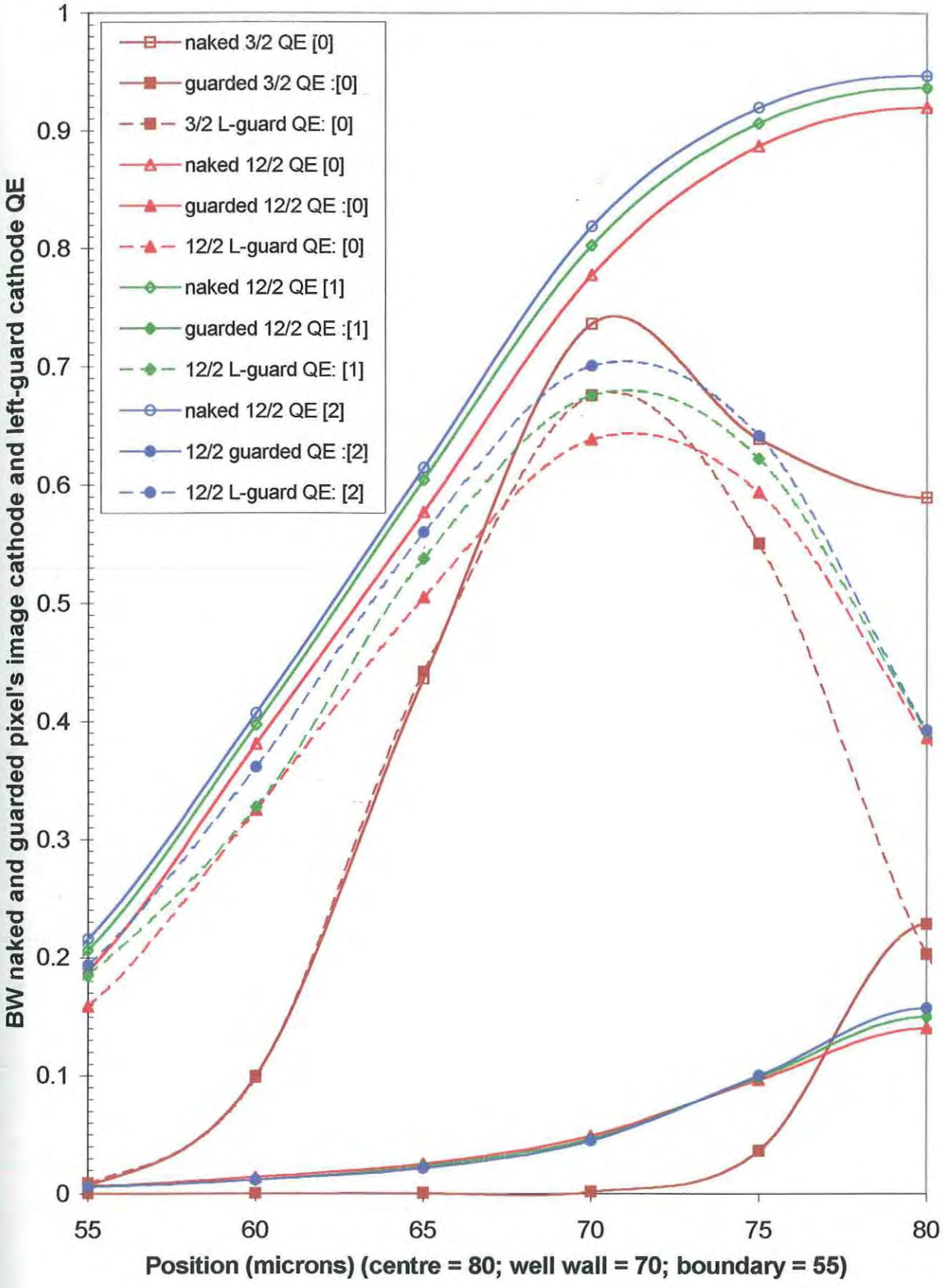

Figure 5.43: **BW naked and guarded SJPD pixels QE dependence on reverse bias and substrate thickness for illumination positions between adjacent pixel centres.**

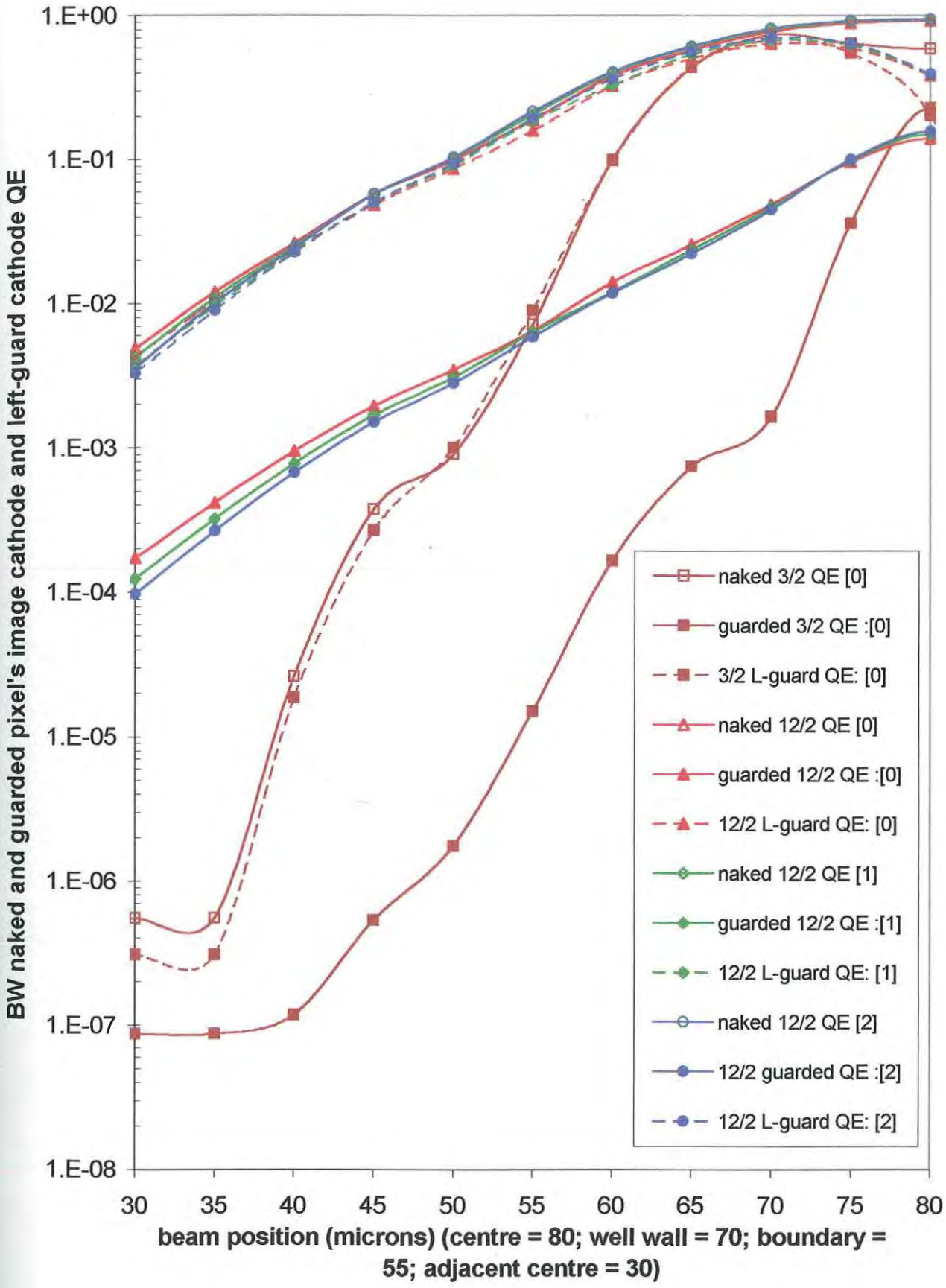

Figure 5.44: **BW naked and guarded SJPD pixels QE dependence on reverse bias and substrate thickness for illumination positions between adjacent pixel centres.**

Figure 5.45 shows the naked and guarded FW pixel's ***linear*** QE response of the four pixel-configurations graphed against illumination position.

The same trend as for the BW pixels is demonstrated, though here the response is more enhanced from the well wall outwards. The problem of increased hole current in the well is now also apparent for all pixel geometries: the naked pixel's image QE response and the guarded pixel's guard QE response are suppressed inside the well. The image response of the guarded pixel is protected in that the guard-ring's capture field removes this problem.

The resolution increase is similar to the BW guarded pixel. Though the central maximum QE for the shallower pixel is below the maximum QE for the other pixels, an inversion of the BW case, the QE response elsewhere is even more suppressed below the thicker pixel response.

Figure 5.46 shows the naked and guarded FW pixel's ***logarithmic*** QE response of the four pixel-configurations graphed against illumination position.

As in Figure 5.44, the guarded pixel image response is clearer. The QE response inversion observed here is similar to the BW case as bias increases for the thicker pixels. However the response does not decrease exponentially across the pixel, as the BW pixels do. Instead there is an even steeper, somewhat exponential, decrease from the centre to the well wall, followed by a plateau and a further less steep somewhat exponential decrease further away from the well wall. This response resolution is greater than the BW response, because the illumination is closer to both image and guard cathodes' capture field, and hence capture efficiency nearer each is enhanced.

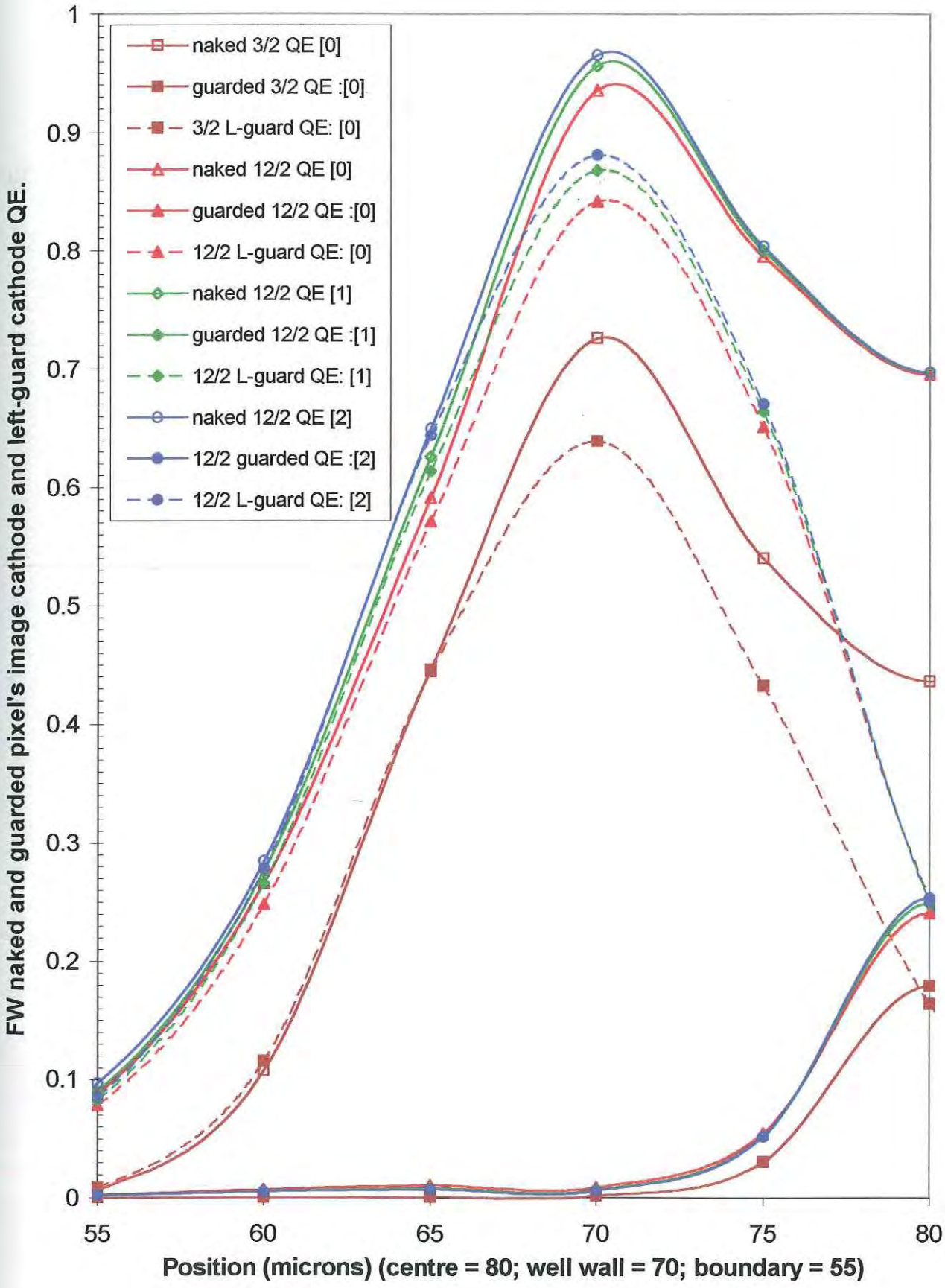

Figure 5.45: **FW naked and guarded SJPD pixels QE dependence on reverse bias and substrate thickness for illumination positions between adjacent pixel centres.**

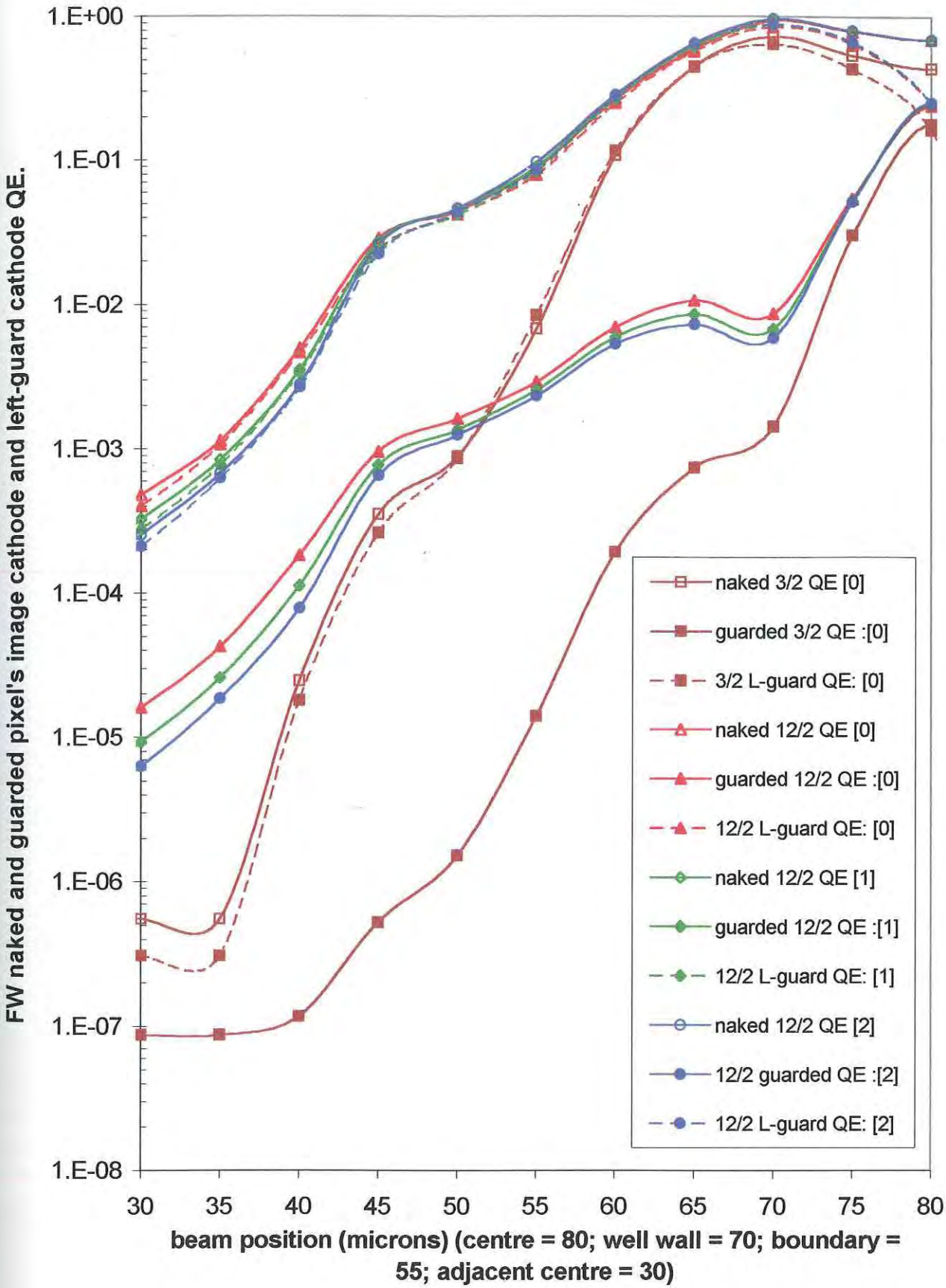

Figure 5.46: **FW naked and guarded SJPD pixels QE dependence on reverse bias and substrate thickness for illumination positions between adjacent pixel centres.**

Figure 5.47 shows the naked and guarded BW and FW pixels' ***linear*** image-cathode NQE response of the four pixel-configurations graphed against illumination position.

When the FW and BW responses are compared, the decreasing NQE response with increasing bias, for both FW and BW guarded pixels, compares inversely with the FW and BW naked pixel response. As noted for the QE profiles in Figures 5.43 to 5.46 this inversion is a reflection of both the increasing guard QE response and the increasing central image QE response. The guard QE response parallels the naked pixel response, absorbing an increasing proportion of the total pixel QE response. Thus the image QE and NQE response of the guarded pixels, compared to the naked pixels, is inverted, decreasing with increasing bias. This is for illumination at positions away from the image cathode's capture-field, where the guard field has more capture influence. The NQE response suppression is greater than the QE response suppression, as the maximum QE parallels the guard-ring and naked pixel QE increase as the reverse bias is increased.

Figure 5.48 shows the naked and guarded BW and FW pixels' ***logarithmic*** image-cathode NQE response of the four pixel-configurations graphed against illumination position.

Difficult to see on the linear graph, the FW guarded pixels NQE responses (dashed lines) are also inverted to the naked pixel NQE response trend. The BW and FW pixel image cathode's NQE response parallels their associated QE responses in Figure 5.44 and 5.46, respectively. The reasons for the trends in image NQE response across the BW and FW guarded pixel's are the same reasons for the tends in the BW (Figure 5.44) and FW (Figure 5.46) pixels' QE response already suggested. The guard-ring capture-field suppresses the image-cathode response away from the pixel centre where the image-cathode's capture-field has more influence. This suppression is less in the BW pixel because of the location of the photocarrier envelope further away from the SCR, encouraging more "free" carrier diffusion in the substrate that enhances the image response away from the pixel centre and thus raising the NQE response.

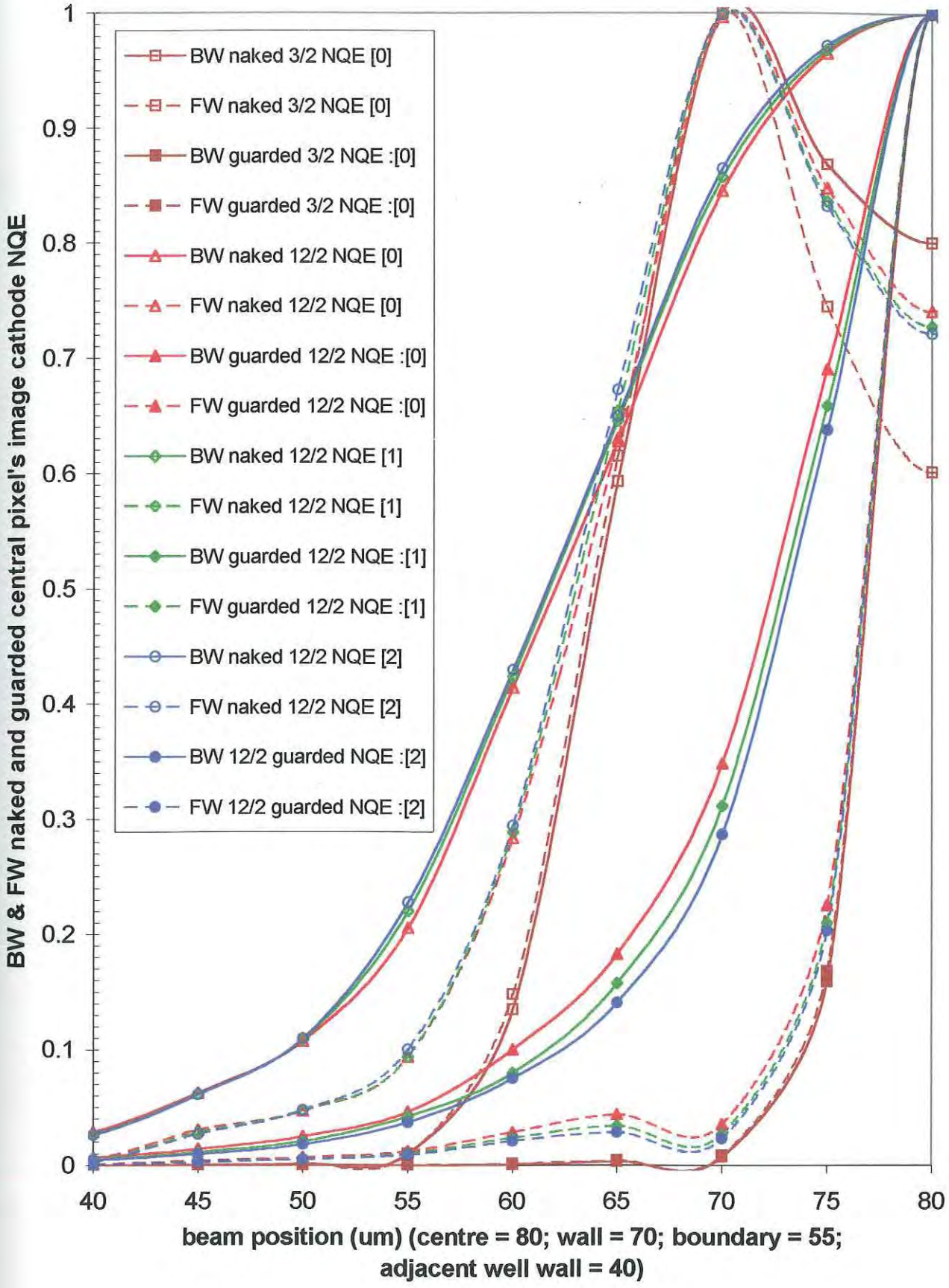

Figure 5.47: **BW & FW naked and guarded SJPD pixels NQE dependence on reverse bias and substrate thickness for illumination positions between adjacent pixel well walls.**

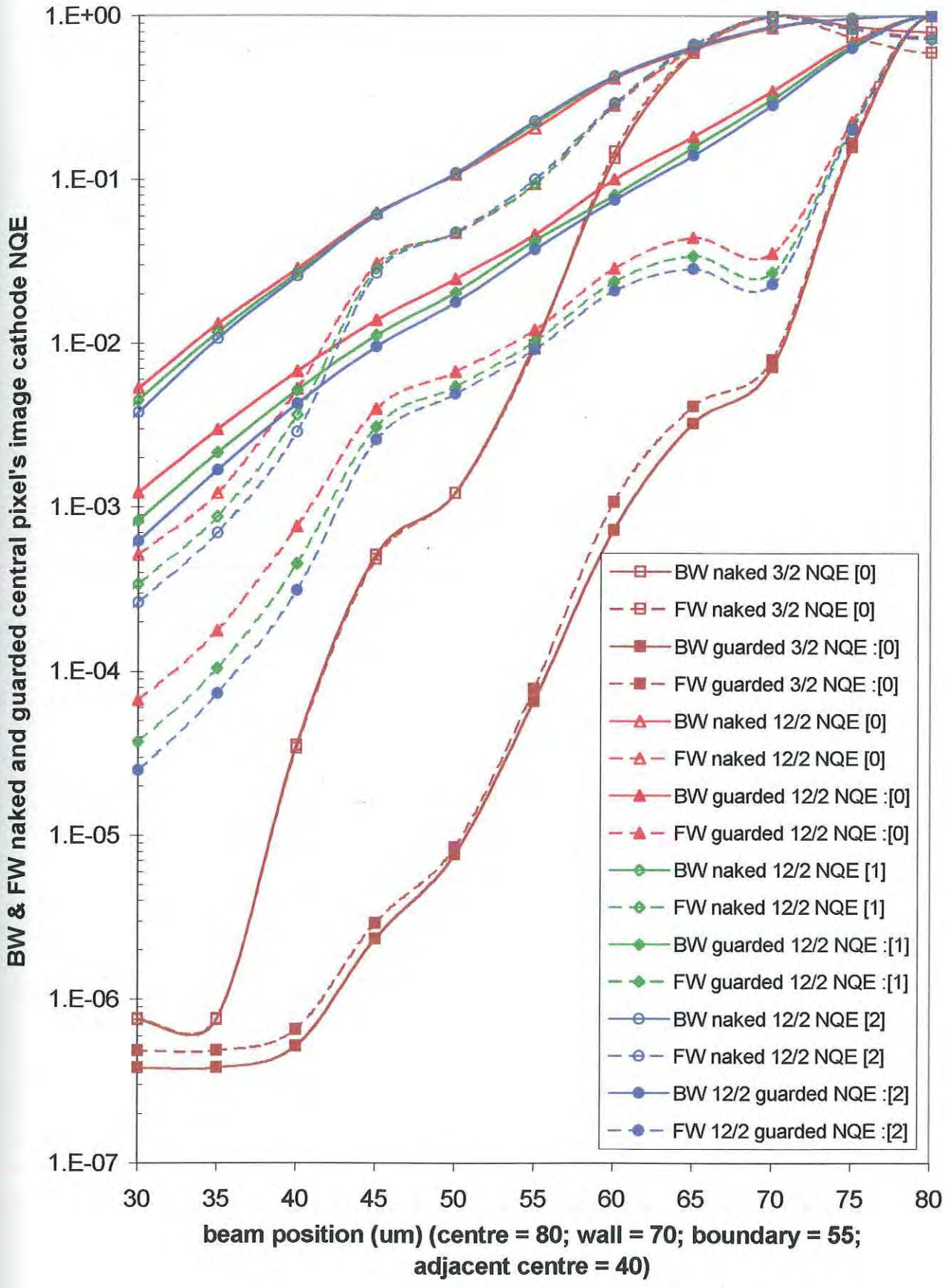

Figure 5.48: **BW & FW naked and guarded SJPD pixels NQE dependence on reverse bias and substrate thickness for illumination positions between adjacent pixel well walls.**

Finally the SCR and non-SCR AVP data is presented graphically against the four different pixel configurations (Figures 5.49 to 5.50) represented as an integer from −1 to 2 as defined in Table 5.2. The penetration depth of the SCR into the pixel's well and into the pixel's substrate, outside the well, are also included.

Figure 5.49 shows the BW pixel AVP response for the 2 μm well depth pixel configurations with substrate thickness of 3 μm and a reverse bias of 0 volts, as well as a substrate thickness of 12 μm and a reverse bias of 0, 1 and 2 volts.

Considering first the effect of increasing reverse bias on the BW pixel's QE response, the SCR AVP profiles, across both 2D and 3D results for the thicker 12 μm pixels are considered. Here, the increasing SCR AVP trend with increasing reverse bias parallels the naked BW pixel's image cathode QE (Figure 5.43) and NQE (Figure 5.47) response profiles as well as the guarded BW pixel's guard QE (Figure 5.43) response profile. Both AVP and QE profiles only slightly increase as the SCR is some distance from the illuminated back wall.

Table 5.3 shows that this increased SCR AVP is due to an increasing SCR penetration into the substrate, below the bottom of the well. This penetration of the SCR, brings the SCR closer to the photocarrier envelope. The wider, deeper SCR increases the capture efficiency of both the guard and image cathodes for both naked and guarded pixels, hence the increasing trend.

Table 5.3 : Configuration number definition and associated SCR width.

Configuration number	Description	SCR width In well (μm)	SCR width Outside well (μm)
-1	The 0 reverse bias 3/2 pixel	0.00956992	0.947422
0	The 0 reverse biased 12/2 pixel	0.00956992	0.947422
1	The 1 reverse biased 12/2 pixel	0.01494745	1.479798
2	The 2 reverse biased 12/2 pixel	0.01884858	1.866009

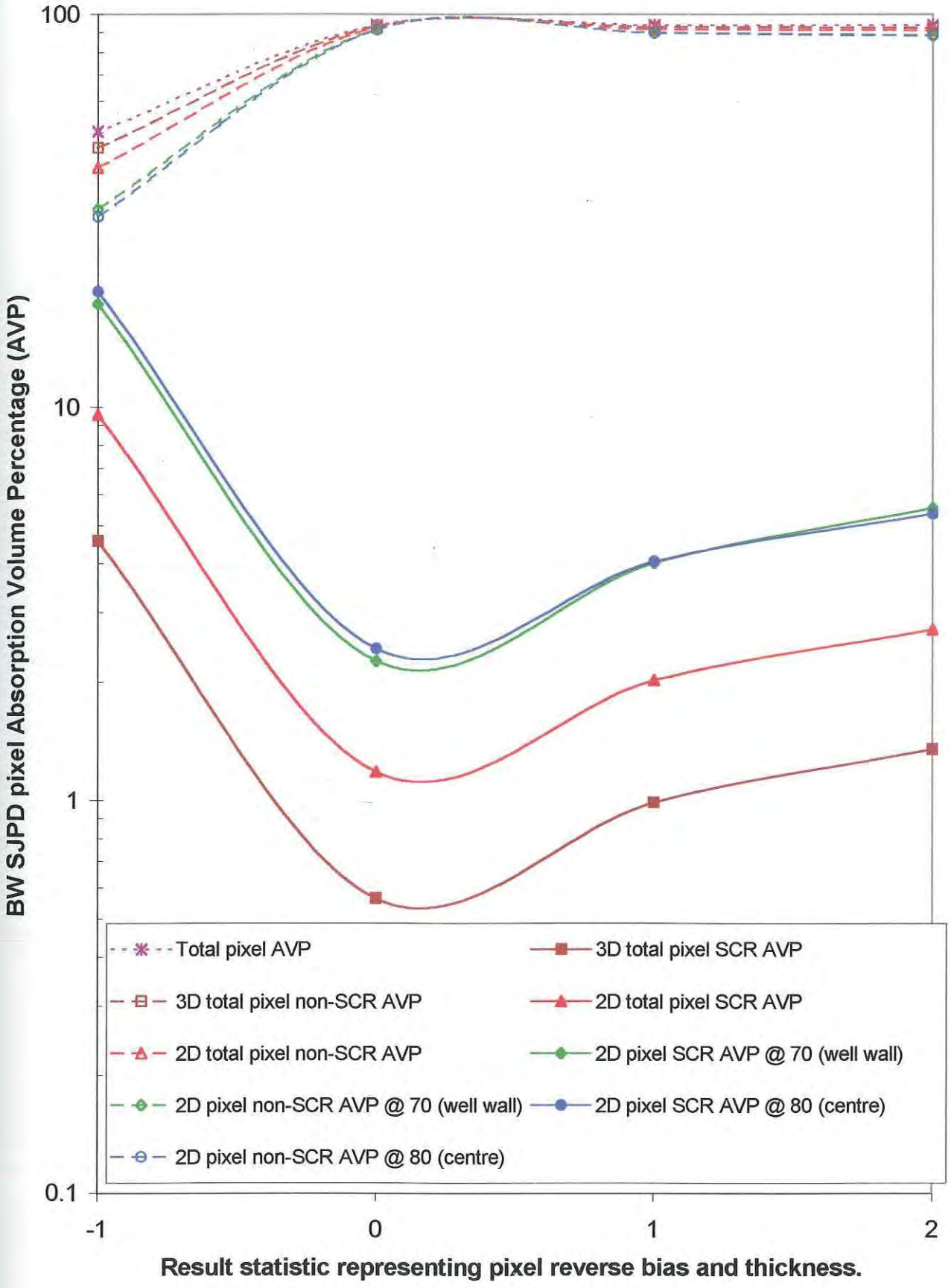

Figure 5.49: BW SJPD pixel AVP profile dependence on a composite result statistic: 0, 1 and 2 are the bias of the 12/2 pixel; -1 represents the 3/2 0 biased pixel.

The inversion of the guarded pixel's image-cathode QE response occurs because the guard-ring cathode has proportionately greater surface area than the image-cathode surface area and is closer to the SCR, for which the AVP is increasing (Table 5.3). The guard-ring capture field laterally surrounds the central image-cathode's capture field, like a cylinder. Thus the guard's capture efficiency increases faster (SCR AVP increasing) than the image-cathode's capture efficiency, causing an increasing deficit in the latter's QE, and hence the QE and NQE increasing trend inversion.

Still investigating Figure 5.49, the change in AVP from shallow to deep BW pixels is also reflected in the BW naked and guarded pixel QE profiles (Figures 5.43 to 5.44). This is for the same reason as occurred for increasing the reverse bias, except that the back wall, and hence the carrier envelope, is brought even closer to the SCR and cathode capture fields, without the SCR's width changing. This is in contrast to the reverse situation, as in the increasing bias case, where the SCR and cathode capture fields are brought slightly closer to the back wall, and hence slightly closer to the carrier envelope.

The non-SCR AVP, increasing considerably from shallow to deep pixels, and less for increasing bias, means there is more "free" diffusion in the substrate that increases the probability of photocarriers diffusing under the guard cathode's cylindrical capture field and drifting up into the image-cathode's capture field. This increases the image capture volume of photocarriers generated outside the guard-cathode capture field cylinder. This results in a reduction in QE response resolution, which includes an increase in crosstalk. Even the best resolved 3/2 zero biased pixel QE and NQE responses, presented in these results, is not reaching the minimum flat-line response until the 35 μm illumination position, which is well out of the central pixel's boundary (55 μm). With a non-optimally wide image-cathode (4 μm), the image-cathode's capture window is increased, suppressing the guard's capture efficiency. Additionally, the large non-SCR AVP results in "free" substrate diffusion of carriers under the guard-ring capture "curtain". Both image-cathode width and increased non-SCR AVP contribute to the lower response resolution as compared to the 3/1[2] guarded pixel.

Figure 5.50 shows the FW pixel AVP response for the same pixel configurations of thickness and reverse bias as in Figure 5.49.

Considering the effect of increasing reverse bias on the FW pixel's QE response, the SCR AVP profiles, across both 2D and 3D results for the thicker 12 μm pixels, are considered. Similar to the BW pixel trend (Figure 5.49), the increasing SCR AVP, with increasing bias, parallels the naked FW pixel's image-cathode QE (Figure 5.45) and NQE (Figure 5.47) response profiles as well as the guarded FW pixel's guard QE response (Figure 5.45). The slight increasing trend in the SCR AVP, with increasing bias, is also paralleled by the naked pixel and guard QE and NQE profiles.

As already stated under Figure 5.49, Table 5.3 shows that this increased SCR AVP is due to an increasing SCR penetration into the substrate, with minimal SCR penetration into the well. Although the wider SCR increases the capture efficiency of both the guard and image cathodes for both naked and guarded FW pixels, hence the increasing QE and NQE trend, the problem of negative hole current inside the well diffusion region, is not minimized. In contrast, for the BW pixel, its carrier envelope is photogenerated in the substrate. This trend inversion of the guarded pixel's image-cathode QE response occurs for the same reason as for the BW pixel, but proportionately more, as the guard capture efficiency is proportionately more enhanced by a much greater SCR AVP. Thus the guard's capture efficiency increases even faster than the image cathodes capture efficiency, compared to the BW pixel. This causes an even more increasing deficit in the image-cathode's QE and NQE, and hence the proportionately greater trend inversion, than for the BW pixel's response.

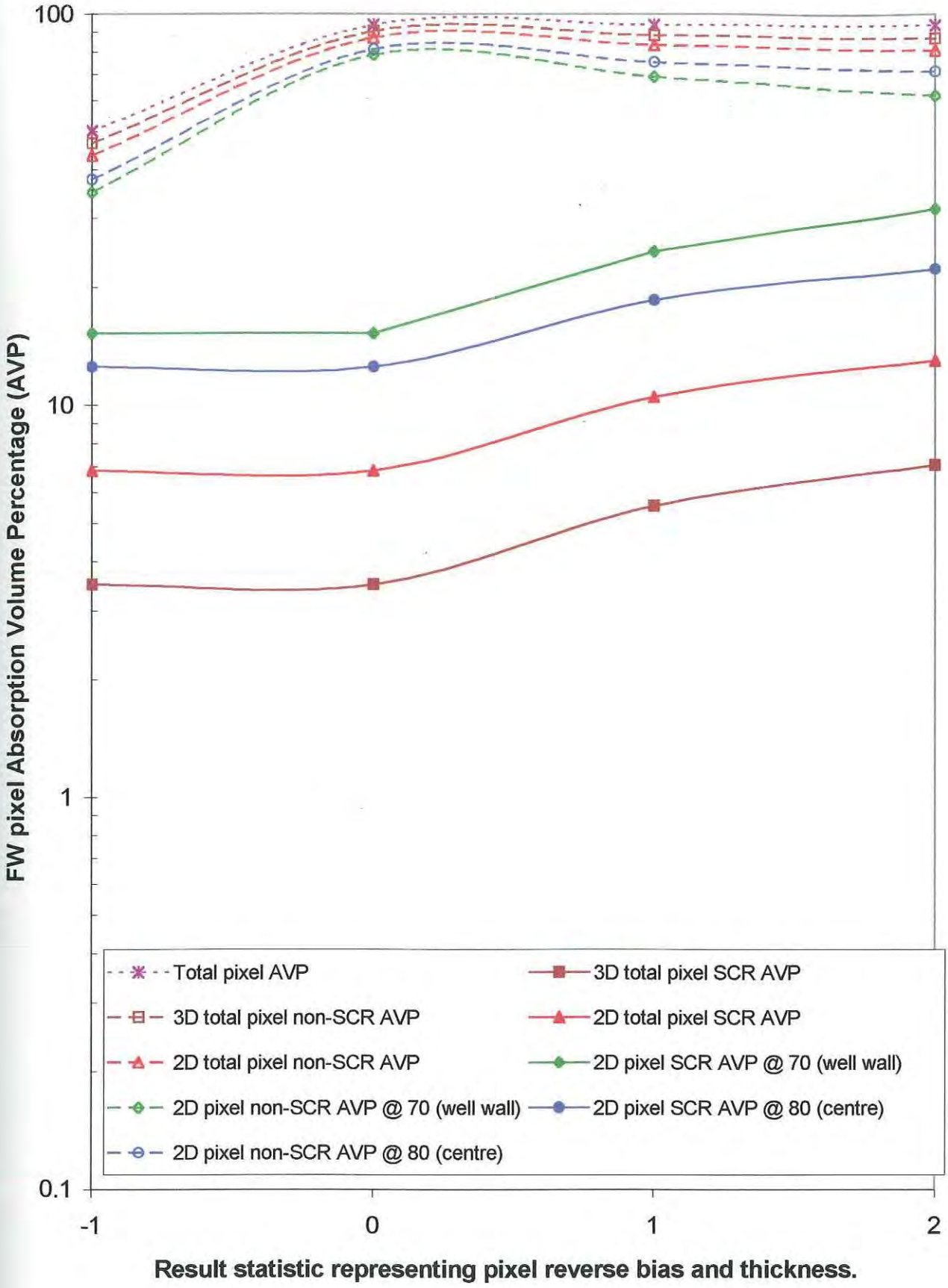

Figure 5.50 : **FW pixel AVP profile dependence on a composite result statistic: 0, 1 and 2 are the bias of the 12/2 pixel; -1 represents the 3/2 0 biased pixel.**

In contrast to any similarity with the BW pixel response, the FW pixel QE and NQE response profiles are more resolved from the well wall outwards. This is due to the FW pixel SCR AVP being approximately five times greater than for the BW pixel. This increase serves to enhance all cathode capture fields in both naked and guarded pixels, especially for illumination over the well wall (70 μm) where the SCR AVP is increased the most (Figures 5.49 to 5.50). This increased SCR AVP also results in a more resolved image-cathode QE and NQE profile. Firstly, due to the image capture efficiency enhancement, the central response is enhanced above the BW pixel response. Secondly, due to the guard capture efficiency enhancement, the image response for illuminations elsewhere in the FW pixel is suppressed below the BW pixel response.

In the well, mentioned above, the non-SCR AVP, a large portion of the pixel's non-SCR AVP, though not calculated, is much larger than the BW pixel, because of the much closer proximity of the illumination to the well, for the FW pixel. For increasing bias, this well AVP remains constant, though quite large compared to the BW pixel. The effect of this constant large AVP and diffusion volume inside the well is demonstrated by the equal extent of the problem of negative hole current across the three bias-type thicker pixels' QE profiles. This causes their profiles to coincide for illuminations at the centre, because the diffusion volume and AVP inside the well remains constant.

Lastly, the non-SCR AVP increases, as in the case of the BW pixel, but not to the same extent because the SCR AVP is enhanced and constant between pixel thicknesses, so suppressing the non-SCR AVP profile. The difference in non-SCR AVP for the different thickness pixels accounts for the greater "free" diffusion in the substrate. This enhances the image cathode response for illuminations outside the pixel well, lifting the NQE profile above that of the shallower, less substrate "free-diffusion" guarded pixel. Also the thicker pixel's total AVP is 94 % which is 87 % greater than the thinner pixel. This immediately imparts the benefit of an increased photocarrier population that enhances the image-cathode's QE and NQE responses.

5.2 The Vertical DJPD Pixel.

Results demonstrating the underlying trends in the total result set are presented graphically. A complete PNP DJPD pixel results table including QE, and NQE data can be viewed in Appendices XIII and XIV for BW and FW pixels, respectively. A complete NPN DJPD pixel results table including QE, nQE and NQE data can be viewed in Appendices XV and XVI for BW and FW pixels, respectively. The AVP data relevant to these Pixel's configurations may be viewed in Appendix XVII.

5.2.1 Effect of Inner (Image) Well Dimensions Against Illumination Position.

Similar to the treatment of the SJPD results, the two dimension variables of width and depth are studied together because they are related in terms of pixel response, though not in the same way as substrate thickness and well depth (Hinckley, Jansz, Gluszak, Eshraghian, 2002), (Hinckley, Gluszak, Eshraghian, 2000). All pixels considered in Section 5.2.1 to 5.2.3 have a 12 μm thickness and a 2 μm outer well depth (12/2). They have substrate and outer well doping concentrations of 10^{15} and 10^{17} cm^{-3} ("(15(17))"). All junctions are reverse biased by 2 volts. This includes the SJPD pixels ("[2]") and the DJPD pixels ("[2[2]]"). The DJPD pixels image well is doped at a concentration of 10^{18} cm^{-3}. Thus the doping shorthand for PNP is "(15(17(18p)))" and NPN is "(15(17(18n)))".

This section introduces the SCAN results of image-cathode QE and NQE graphed against the illumination position of the simulated 633nm, 5 μm wide laser beam ("beam"). Though trends in the profiles may be obvious in relation to the changing dimensional pixel parameters, the actual relationship of QE or NQE to the well width or depth will be clarified in the following Sections 5.2.2 and 5.2.3. Presenting the results in both these ways is helpful for understanding how the DJPD pixel compares qualitatively to the SJPD pixels investigated, as well as understanding how the pixel responds quantitatively to configuration parameter changes.

The QE data is presented in the first six graphs. Graphs of FW responses follow graphs of BW responses. Initially guarded and naked SJPD 12/2 [2] pixel responses for illumination positions across half the 3-pixel array (20 – 80 μm), are compared to the NPN and PNP DJPD responses of equal thickness, outer well depth and outer junction bias to the SJPD pixels (Figures 5.51 to 5.52). Then the NPN and PNP DJPD pixels' response are compared for illumination positions across half of the outer well (70 – 80 μm) and for pixels of shallowest and deepest image well depth, with four image well widths (Figures 5.53 to 5.54). Then, for the same illumination positions as Figure 5.54, the NPN pixel electron QE (nQE) and total QE responses are compared for pixels with the thinnest and widest image well and three image well depths (Figures 5.55 to 5.56). Both linear-linear and log-linear graphical representations are used for these six graphs.

The NQE response is presented in the last two graphs. Here the NQE response for the NPN pixels of same dimension as in Figure 5.56 is presented as log-linear and linear-linear graphs (Figures 5.57 to 5.58).

For the ***first four graphs***, the QE response data for both BW and FW DJPD pixels are grouped in order of increasing image well width and then in order of increasing image well depth and then NPN followed by PNP. This generates four pixel-configuration data sets. Note, a {2/0.2} DJPD pixel, has a 2 μm wide and 0.2 μm deep image well.

1. {2/0.2} and {2/1.25} pixel are represented by brown squares that are filled brown or are empty, respectively.
2. {4/0.2} and {4/1.25} pixel are represented by red triangles that are filled red or are empty, respectively.
3. {8/0.2} and {8/1.25} pixel are represented by green diamonds that are filled green or are empty, respectively.
4. {14/0.2} and {14/1.25} pixel are represented by blue circles that are filled blue or are empty, respectively.

The PNP responses are distinguished from the NPN responses by being dotted lines. Where applicable, the SJPD responses use asterisk point geometry.

The ***next four graphs*** are the QE and NQE response data for both BW and FW DJPD pixels are grouped in order of increasing image well depth (1, 2 and 4 above) and then in order of increasing image well width (2 μm points are filled in, and 14 μm points are empty). FW NQE and BW nQE and FW nQE are represented by dashed lines.

Figure 5.51 shows BW NPN and PNP DJPD and guarded and naked BW SJPD pixels' *logarithmic* image QE response dependence on the inner well's width and depth for illumination across half of their tri-pixel array. The PNP responses are represented by dotted lines.

The BW NPN and PNP DJPD pixels' maximum QE is about 100 times less than the maximum QE of the BW guarded SJPD pixel and about 500 times less than the maximum QE of the naked SJPD pixel. However both DJPD pixel responses are far more resolved, flat-lining after the central pixel's outer well wall (70 μm position); a reduction in QE of between about 99.9998% to 99.99998%. In contrast the SJPD guarded pixel finally flat-lines from the centre of the adjacent pixel (30 μm position), 2,000 times above the already flat-lined DJPD response. Outside the outer well, the flat-lined PNP response is noticeable above the NPN response, both QE responses increasing with increasing well width and depth.

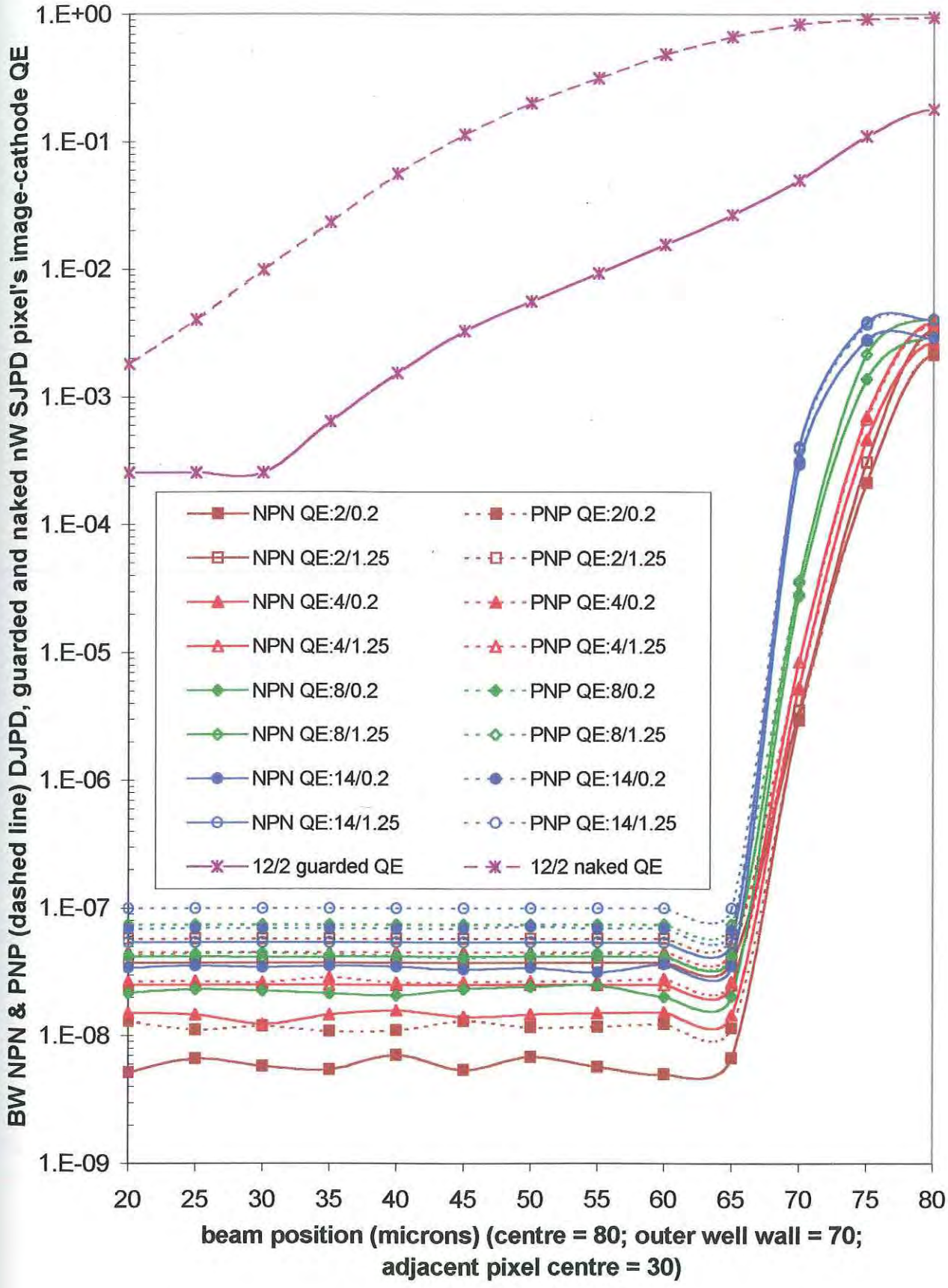

Figure 5.51: BW DJPD and SJPD pixel's image QE dependence on the image well's width and depth for illumination across half of a 3-pixel array.

Figure 5.52 shows FW NPN and PNP DJPD and guarded and naked FW SJPD pixels' *logarithmic* image QE response dependence on the inner well's width and depth for illumination across half of their tri-pixel array. The PNP responses are represented by dotted lines.

Here the maximum QE for all pixel types are equivalent, only doubled by the naked pixel, even though the guarded pixel response is enhanced above this pixel's BW response. Note that, for illuminations near the centre, the guarded response is suppressed below the lowest DJPD response, the guarded pixel's response being more resolved in this region. The flat-lining trend is the same, except the guarded response is here about 10 times less than its BW response (Figure 5.51) because it is more suppressed away from the pixel centre. This brings its flat line response closer to the DJPD flat-line responses which are not significantly different from their BW response. The trends between the NPN and PNP DJPD types and the DJPD pixel image well dimensions is similar to their BW response trends.

The DJPD responses for illuminations from the centre to the outer well wall are enhanced above the pixels' BW response by up to 200 times. This is due to the proximity of FW pixel illumination to the inner (image) SCR as reflected by the much larger FW pixels' inner SCR AVP (14.7%). This is ten times more than the BW image-pixel's SCR AVP (1.44 %).

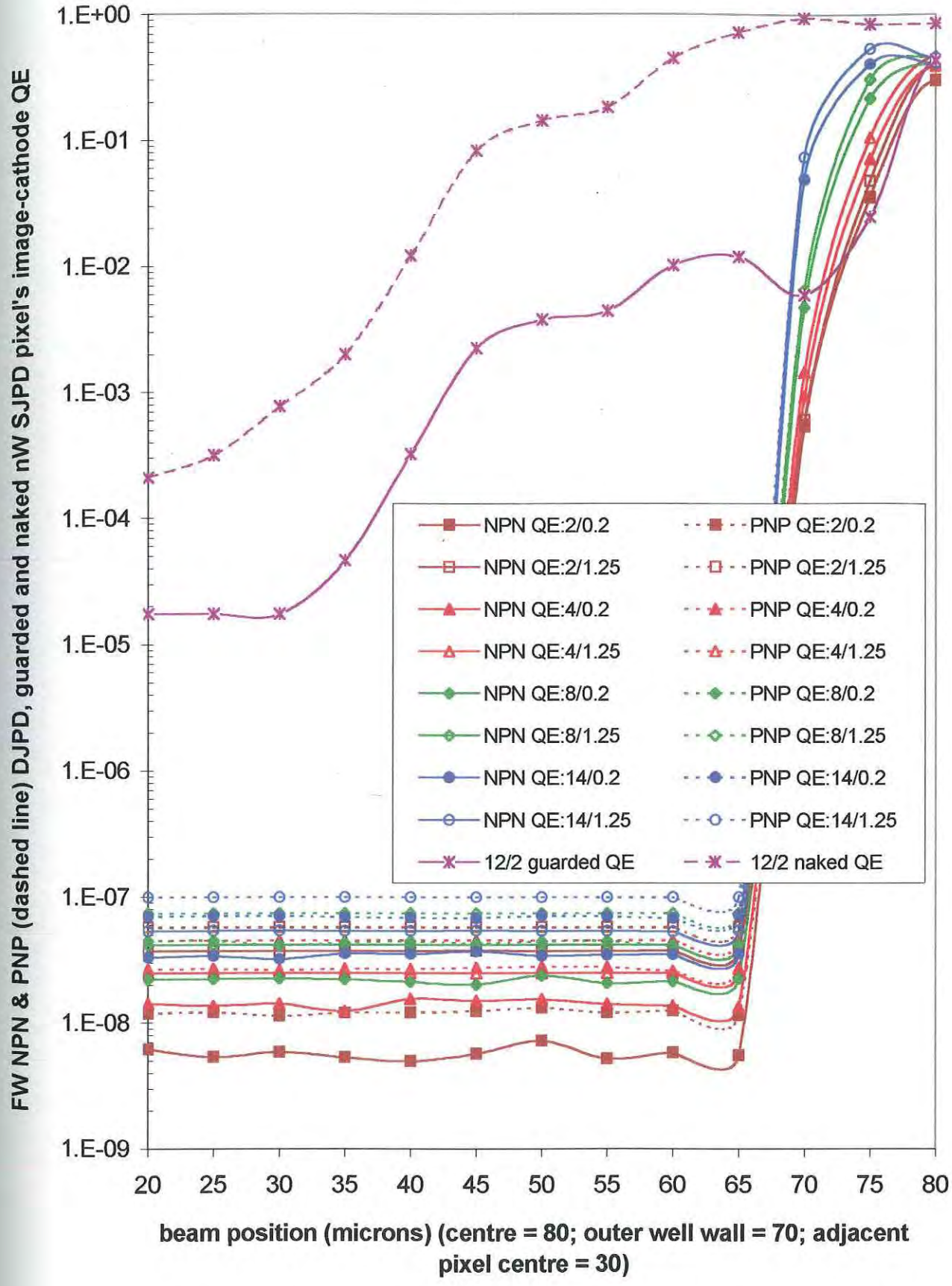

Figure 5.52: **FW DJPD and SJPD pixel's image QE dependence on the image well's width and depth for illumination across half of a 3-pixel array.**

Figure 5.53 shows BW NPN and PNP DJPD pixels' *linear* image QE response dependence on the inner well's width and depth for illumination across half of their outer well. The PNP responses are represented by dotted lines.

In the outer well, the PNP response is generally slightly below the NPN response. The pixels with the deeper image wells are more enhanced, especially for illuminations at the pixel centre. The response becomes increasingly more enhanced for increasing image well width at the 75 μm illumination position. The most resolved response occurring for the pixels with the thinner, deeper image wells.

Figure 5.54 shows FW NPN and PNP DJPD pixels' *linear* image QE response dependence on the inner well's width and depth for illumination across half of their outer well. The PNP responses are represented by dotted lines.

As already mentioned (Figure 5.52) this response is more than 100 times that of the BW response due to an order of magnitude difference in image-pixel AVP. The trends are the same. Note the more rapid increase in response with increase in width for an illumination that is 5 μm from the centre (75 μm position) compared to the BW pixel. For the widest and deepest image well, with the illumination 90 % inside the image well, the QE response is maximum, even higher than the central response. This has not occurred in the DJPD BW pixel response, where the central response is always maximal. This is one advantage of the BW pixel's illumination orientation.

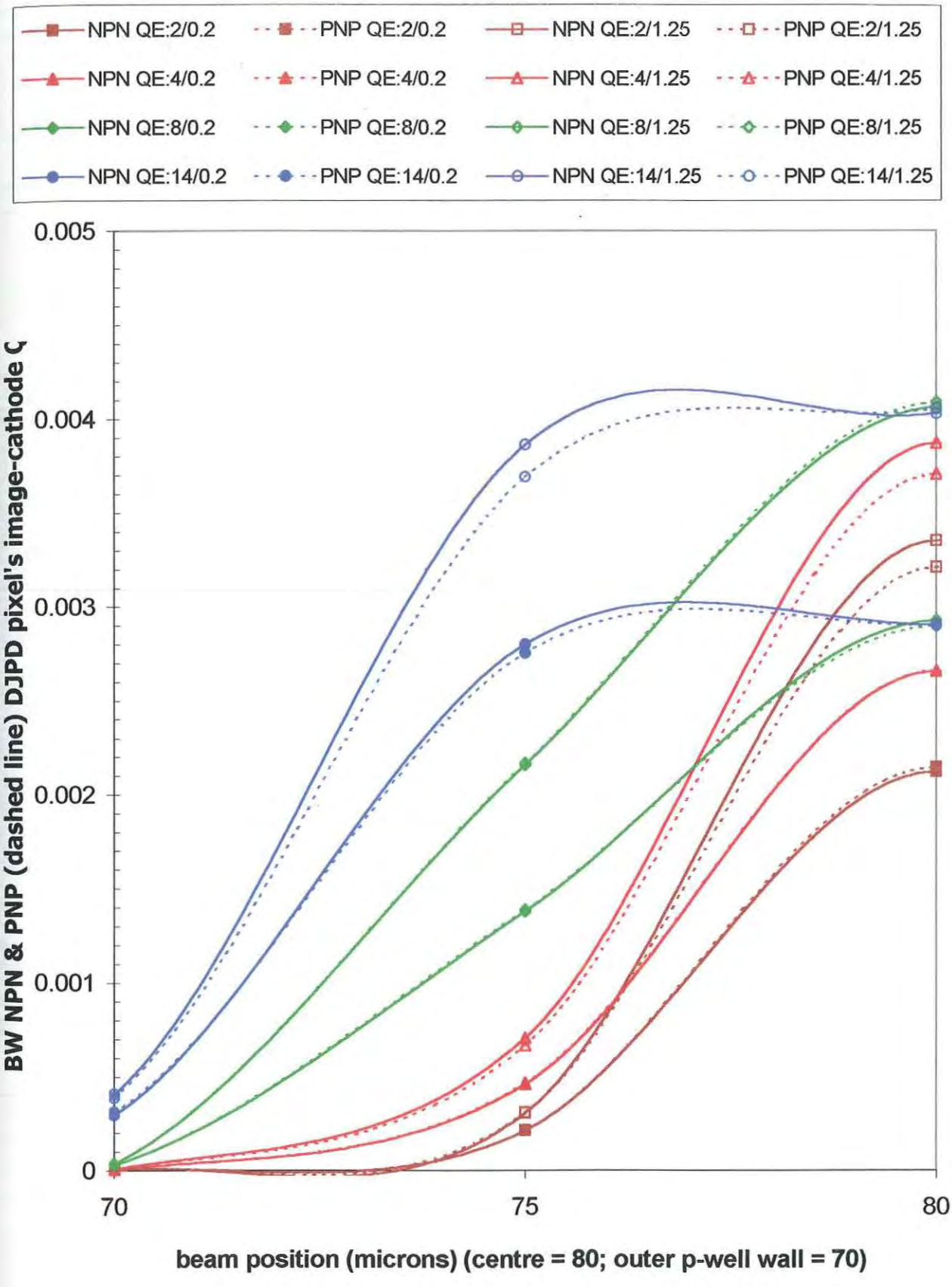

Figure 5.53: **BW NPN & PNP DJPD pixels' image QE dependence on the inner n^+ well's width and depth for illumination from centre to outer well wall. (2/0.2 um = width / depth ratio of n+ well)**

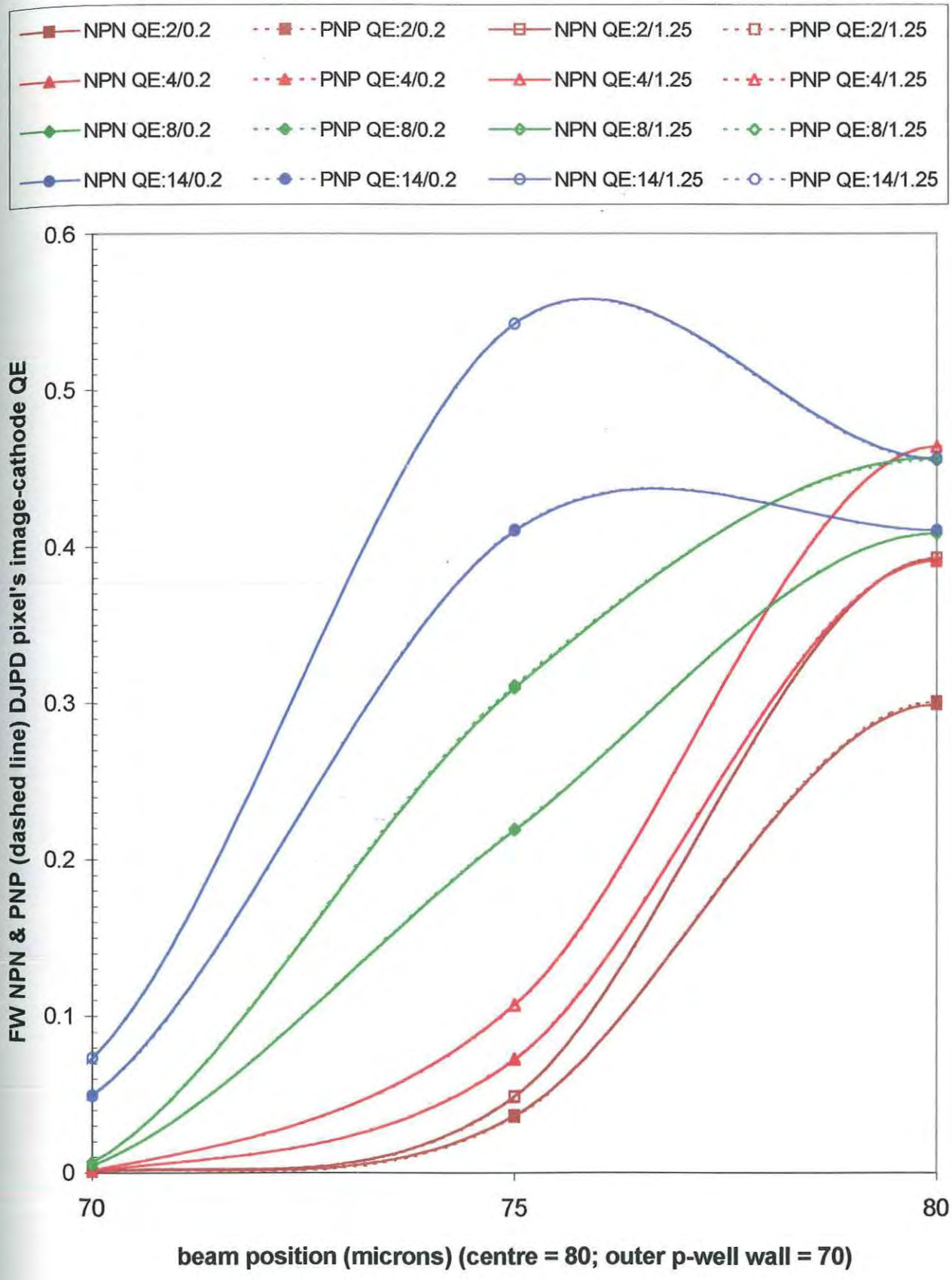

Figure 5.54: **FW NPN & PNP DJPD pixels' image QE dependence on the inner n+ well's width and depth for illumination from centre to outer well wall.**
(2/0.2 um = width / depth of n^+ well)

Figure 5.55 shows BW NPN DJPD pixels' *linear* image total (QE) and electron QE (nQE) responses' dependence on the inner well's width and depth for illumination across half of their outer well. The nQE responses are represented by dashed lines.

Both QE and nQE responses are not coincident only at the centre. This gap between the higher nQE and the QE increases with increasing depth and with increasing width. This gap is indicative of a growing subtracting hole current in the image well as more of the incident light is absorbed in this inner n-well, in which minority carrier holes are photogenerated increasingly with increasing width and especially with increasing depth. Again the best resolved response is for the deepest but thinnest pixel.

Figure 5.56 shows FW NPN DJPD pixel *linear* image total (QE) and electron QE (nQE) response dependence on the inner well's width and depth for illumination across half of their outer well. The nQE responses are represented by dashed lines.

Again this response profile is enhanced above the BW profile (Figure 5.55). Again the problem of increased hole current at the centre is present, explaining why the maximal response is at the 75 μm illumination position, away from the centre (Figure 5.54). As for the BW response, the wider image well pixels, with shallower depth, have a flat, broad response inside the outer well (75 to 80 μm positions) than the thinner, more finely resolved pixels with thinner image wells.

The FW pixel has much more of a hole problem as has already been discovered in the SJPD investigations. This is clear from the guarded FW pixel response at the 75 μm illumination position (Figure 5.52) as it does not suffer so, as its hole problem is captured by the guard ring electrode capture field. Hence its response at this position is below the DJPD FW pixel response.

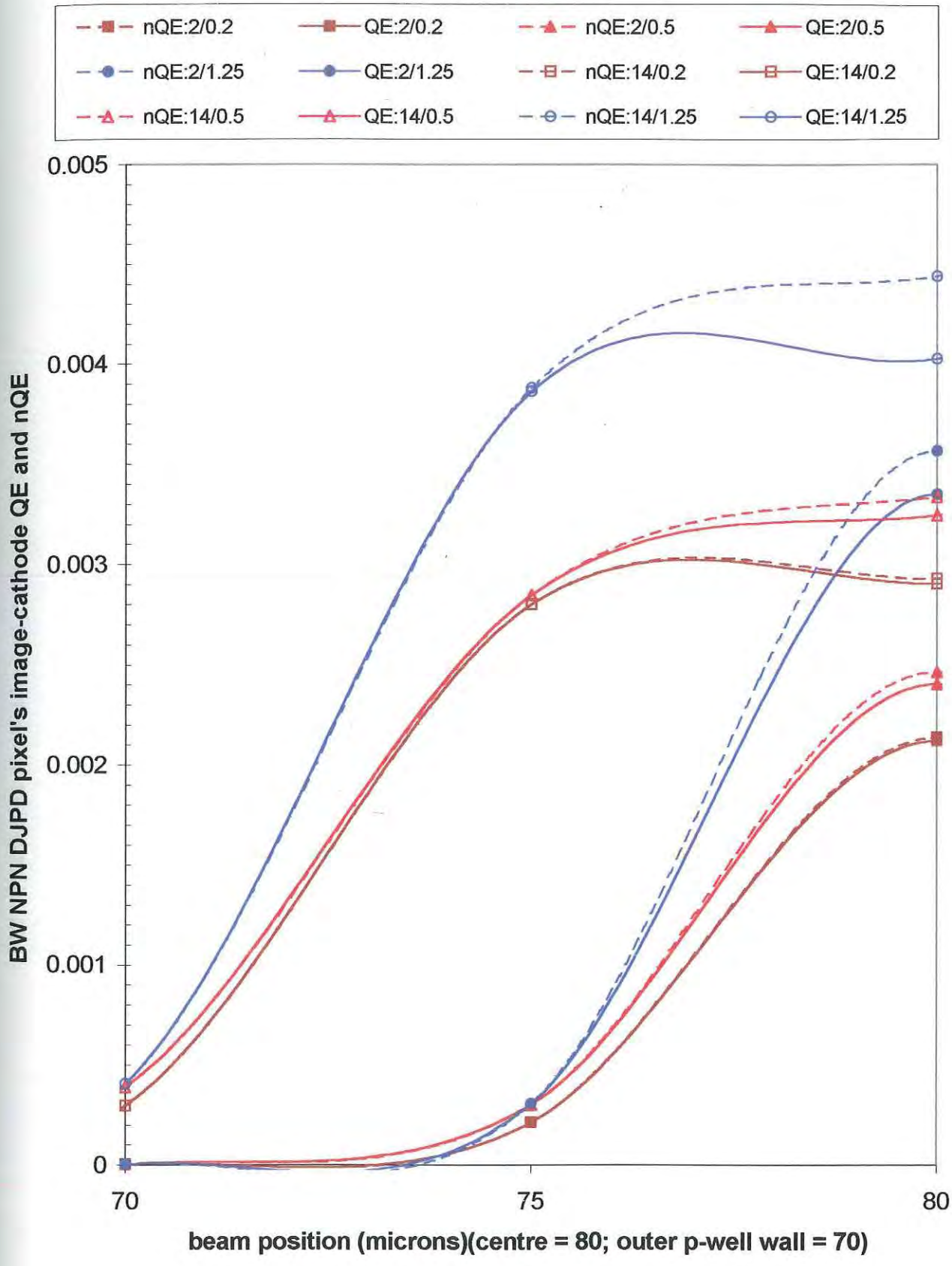

Figure 5.55: BW NPN DJPD pixel's image QE and nQE dependence on the n^+ well's width and depth for illumination from centre to outer well wall.
(2/0.2 um = well width / depth ratio of n^+ well)

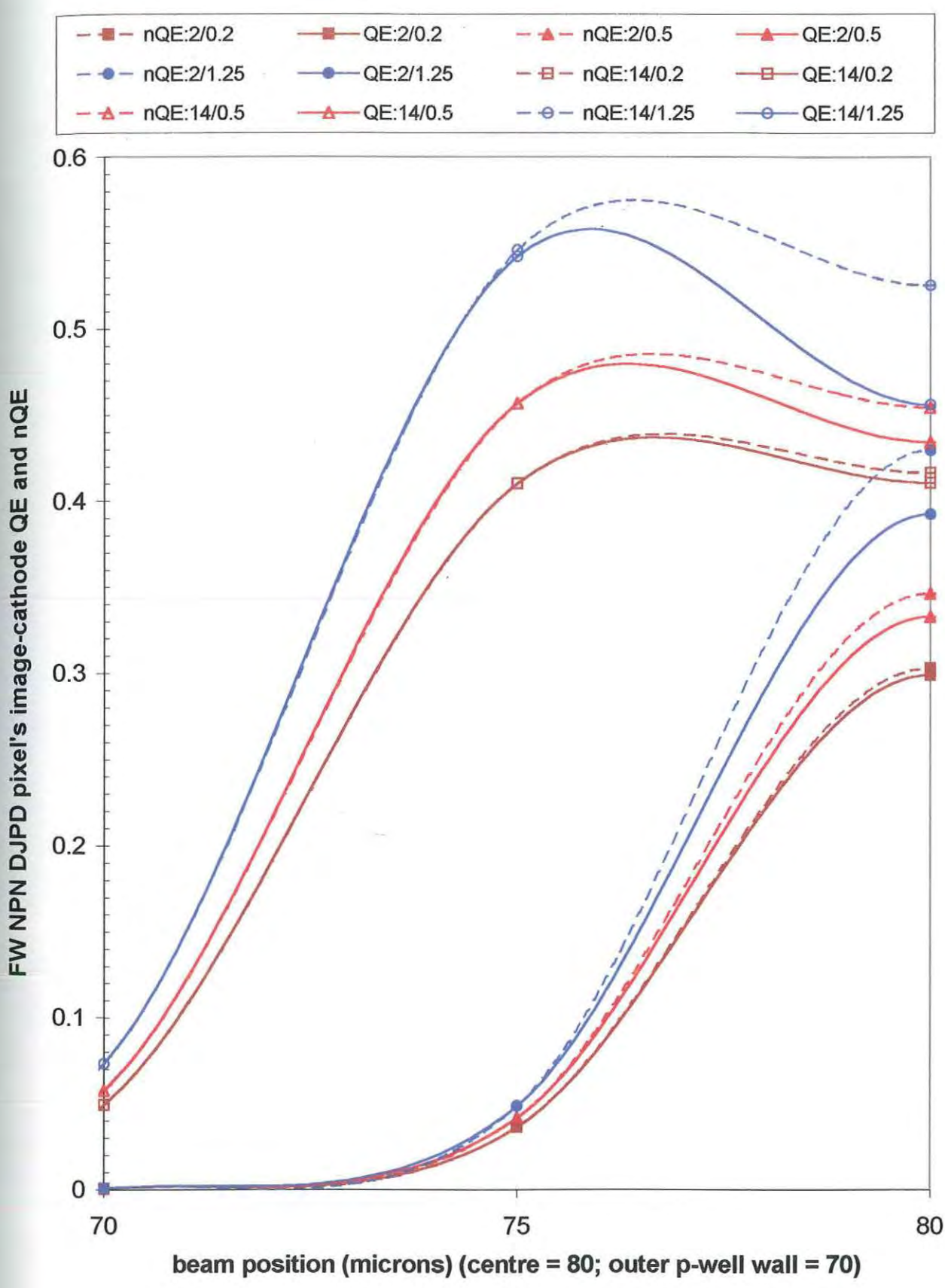

Figure 5.56: **FW DJPD pixel's image QE and nQE dependence on the inner n+ well's width and depth for illumination across one half of the outer well.**
(eg. 2/0.2 = width / depth of n^+ well)

Figure 5.57 shows BW & FW NPN DJPD, guarded and naked SJPD pixels' *logarithmic* image NQE responses' dependence on the inner well's width and depth for illumination outside the outer well, focusing on the flat line response.

All the FW pixels' responses are about 100 times less than the BW pixels' responses. The wider-image-well pixels' responses are much closer together and generally slightly above the thinner-well pixels' responses.

Figure 5.58 shows BW & FW NPN DJPD, guarded and naked SJPD pixels' *logarithmic* image NQE responses' dependence on the inner well's width and depth for illumination across half of their outer well.

The nQE responses are represented by dashed lines. In Figure 5.57 all the dashed / dotted lines (FW) were below the continuous lines (BW). Here the same occurs but now in two groups: all the empty points are above the filled in points. This indicates that all the thin-image-well BW and FW pixels have relatively less capture efficiency than the wider-image-well pixels. This is due to the wider image-well pixels having more SCR capture surface. For constant pixel image-well width the deeper the image-well the lower the response at the 70 and 75 μm illumination positions. This is indicative of their better response resolution, as the deeper pixels also have greater maximum QE (Figures 5.55 to 5.56).

Finally these results show that the DJPD is superior in response resolution and in response-shape control than the SJPD guarded pixel of equal bias, doping and geometry to that of the DJPD pixel's outer well and substrate, without the DJPD electrode size and placement being optimized. Comparing the PNP with NPN DJPD shows that the latter is superior owing to its image photocarriers being electrons which have higher mobility than holes. Significant reduction in maximum QE caused by the hole problem, is only apparent in the widest and deepest image-well pixels, but certainly not to the same degree as naked FW SJPD pixels.

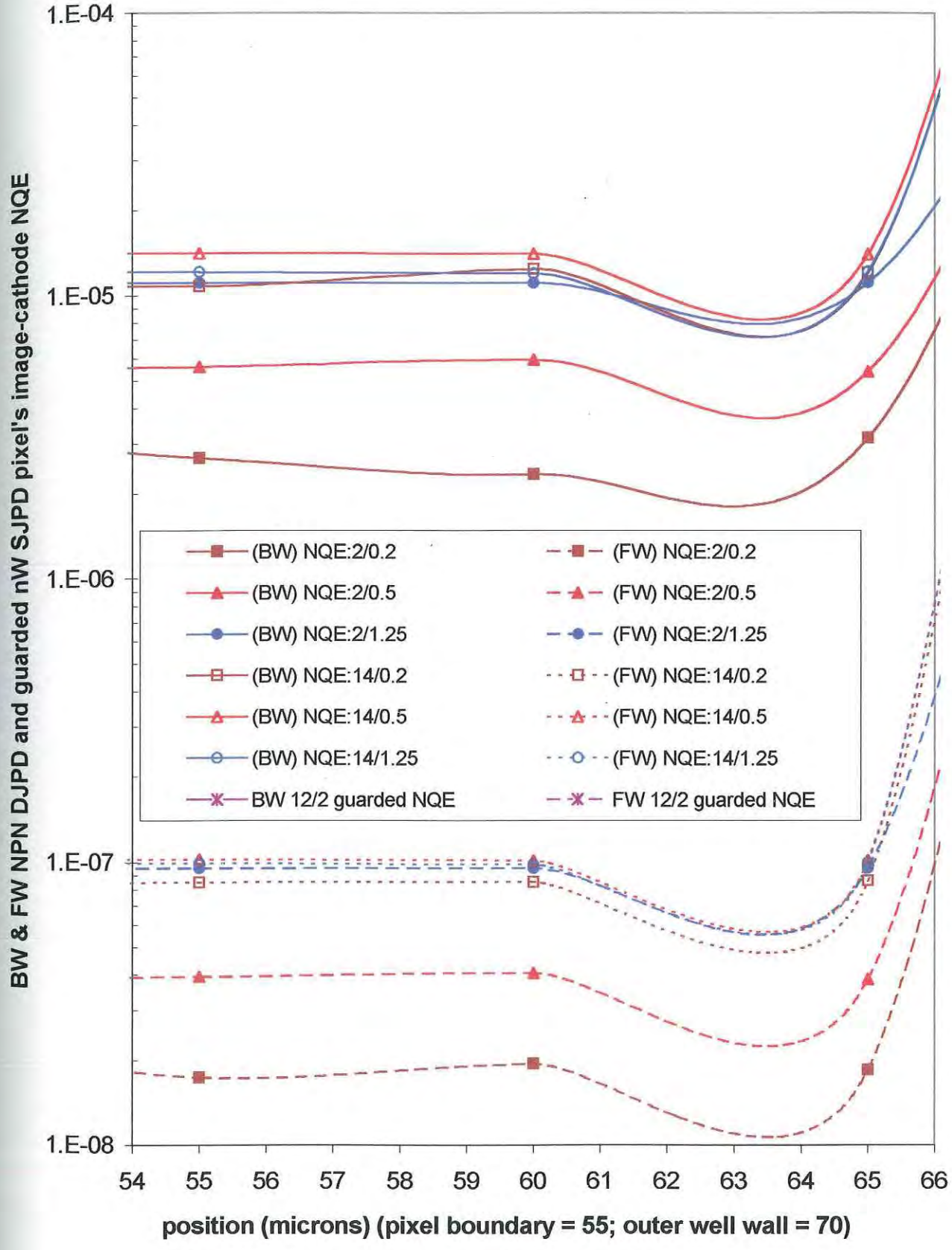

Figure 5.57: **BW & FW NPN DJPD pixels' image NQE dependence on the inner well width and depth for illumination outside the outer well**
(2/0.2 um = well width / depth ratio of n^+ well)

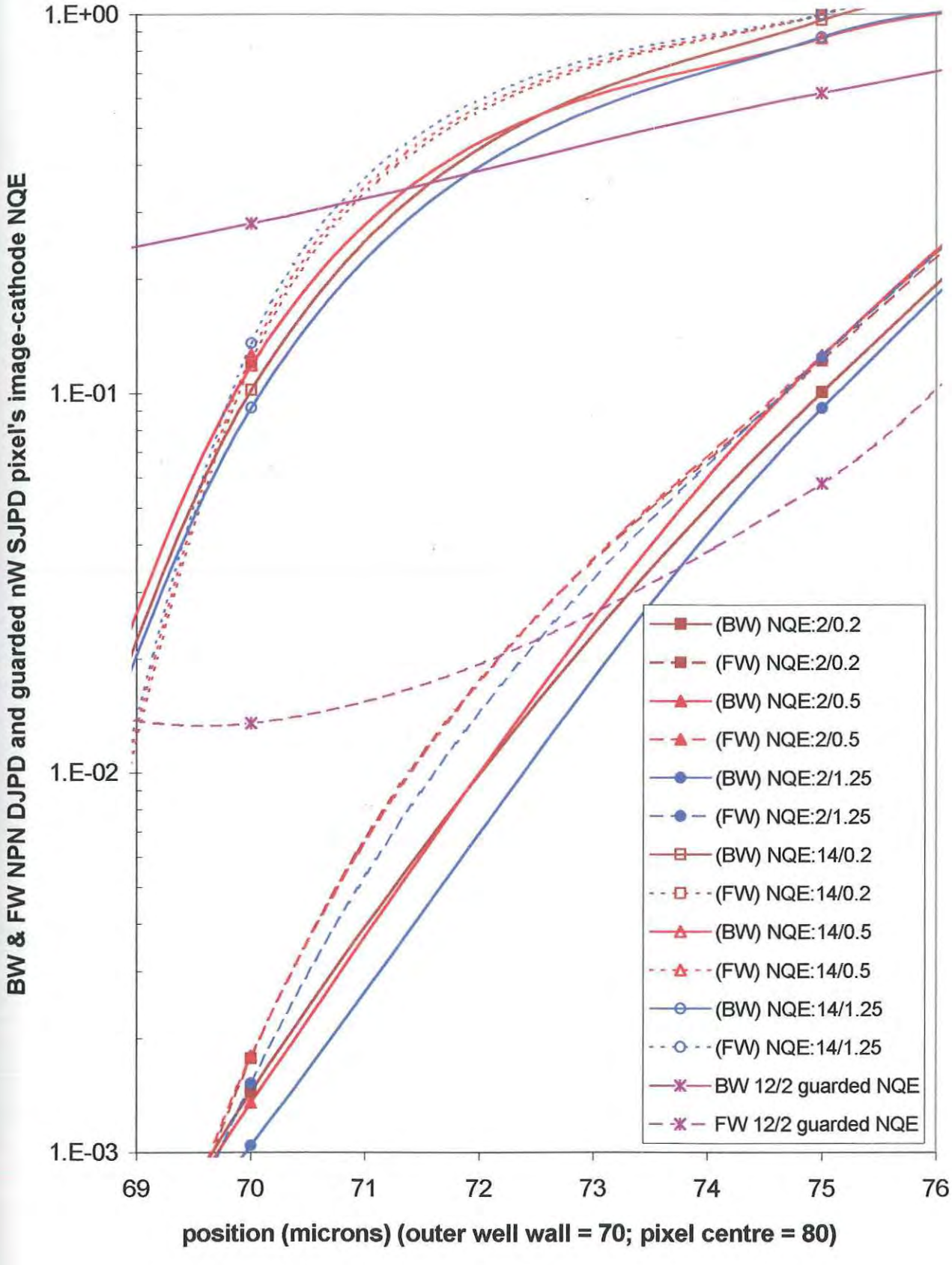

Figure 5.58: **BW & FW NPN DJPD pixels' image NQE dependence on the inner well width and depth for illumination inside the outer well**

(2/0.2 um = well width / depth ratio of n^+ well)

5.2.2 Effect of Inner (Image) Well Width on DJPD Pixels.

In this section the relationship of the NPN pixel's QE and NQE to the image-well width is investigated. The full set of result statistics generated from the simulation data for each parameter studied is tabulated in the results appendix, indicated above each graph where necessary. Results demonstrating the underlying trends in the total result set are presented as log-linear graphs. A complete NPN DJPD pixel results table including QE, nQE and NQE data can be viewed in Appendices XV and XVI for BW and FW pixels, respectively. The PNP DJPD pixel results are similar (Appendices XIII & XIV) so that only the NPN results need to be considered. The AVP data relevant to the Pixel configurations may be viewed in Appendix XVII.

The first four graphs present the effect of image well width on the image-cathodes QE and nQE responses, while only the NQE response follows in the last two graphs, where the BW and FW pixel responses are compared. In each mode of illumination the response for the deepest image-well follows the shallowest image-well response. In the QE graphs, only the responses for illuminations inside the outer well are considered (70, 75 and 80 μm illumination positions and maximum QE) as the flat-line response, beyond the outer well wall, has already been considered in Section 5.2.1. Only in the NQE graph is the boundary (55 μm position) NQE considered.

The point data representation used for the QE and nQE data is the square, triangle, diamond and circle which represent the 70, 75 and 80 μm illumination position responses and the maximum QE response respectively. The QE data are represented by solid lines and filled points, while the nQE data are represented by dash-dotted lines and filled points.

The point data representation used for the NQE data is the square, triangle and diamond. They represent the 55, 70 and 75 μm illumination position responses respectively. BW responses are represented by solid lines and filled points, while FW responses are represented by dash-dotted lines and empty points. All responses are compared to the total 2D pixel AVP data (squares) as well as AVP data for the 5 μm wide illuminations over the pixel centre (triangles). Both AVP data (empty points) include SCR (dashed lines) and non-SCR (dotted line) responses.

Figure 5.59 shows BW NPN DJPD pixels' *logarithmic* image QE and nQE response dependence on the *shallowest (0.2 μm) depth* inner well's width variation, for illumination across half of the central pixel's outer well. These responses are compared to the AVP data associated with the volume in the outer well (image pixel), including the inner-SCR AVP ("SCR AVP") and inner-non-SCR AVP ("non-SCR AVP") response profiles. Both total 2D pixel AVP data and AVP data for 5 μm wide illumination at the pixel centre are considered.

The response at the outer well wall (70 μm illumination position) is increasing exponentially with increasing image-well width due to the interaction of the linear increase of proximity of the image-well SCR and the absorption profile over the outer well SCR. The response at the 75 μm illumination position, between the outer well wall and centre is linear, paralleling the total image-pixel SCR AVP. The response at this position is linearly dependent on the linearly increasing image-well SCR proximity. Both maximum QE and central QE have the same profile as the central SCR AVP, increasing initially due to the illumination covering all of the image well SCR, which increases as the width increases until the image-well walls are beyond the beam width. This response profile across the outer well is dependant largely on the SCR AVP rather than absorption elsewhere in this well. The nQE is coincident with the QE implying there is no significant hole problem for these shallowest image pixels, confirming our findings in Figure 5.55.

Figure 5.60 shows BW NPN DJPD pixels' *logarithmic* image QE and nQE response dependence on the *deepest (1.25 μm) depth* inner well's width variation, for illumination across half of the central pixel's outer well. These responses are compared to the AVP data as for Figure 5.59.

The response profile across all illumination positions is above that of Figure 5.59, including the AVP profile. The response trends only differ at the centre where the higher nQE indicates a more significant and slightly linearly increasing hole current inside the image-well, as the image-well width increases. This is confirmed in Figure 5.55 again. The undulating central SCR-AVP profile is due to the same effect in the shallowest image-well being magnified due to the larger SCR volume.

(cf/ Results DJPD: Apppendix XV & XVII.)

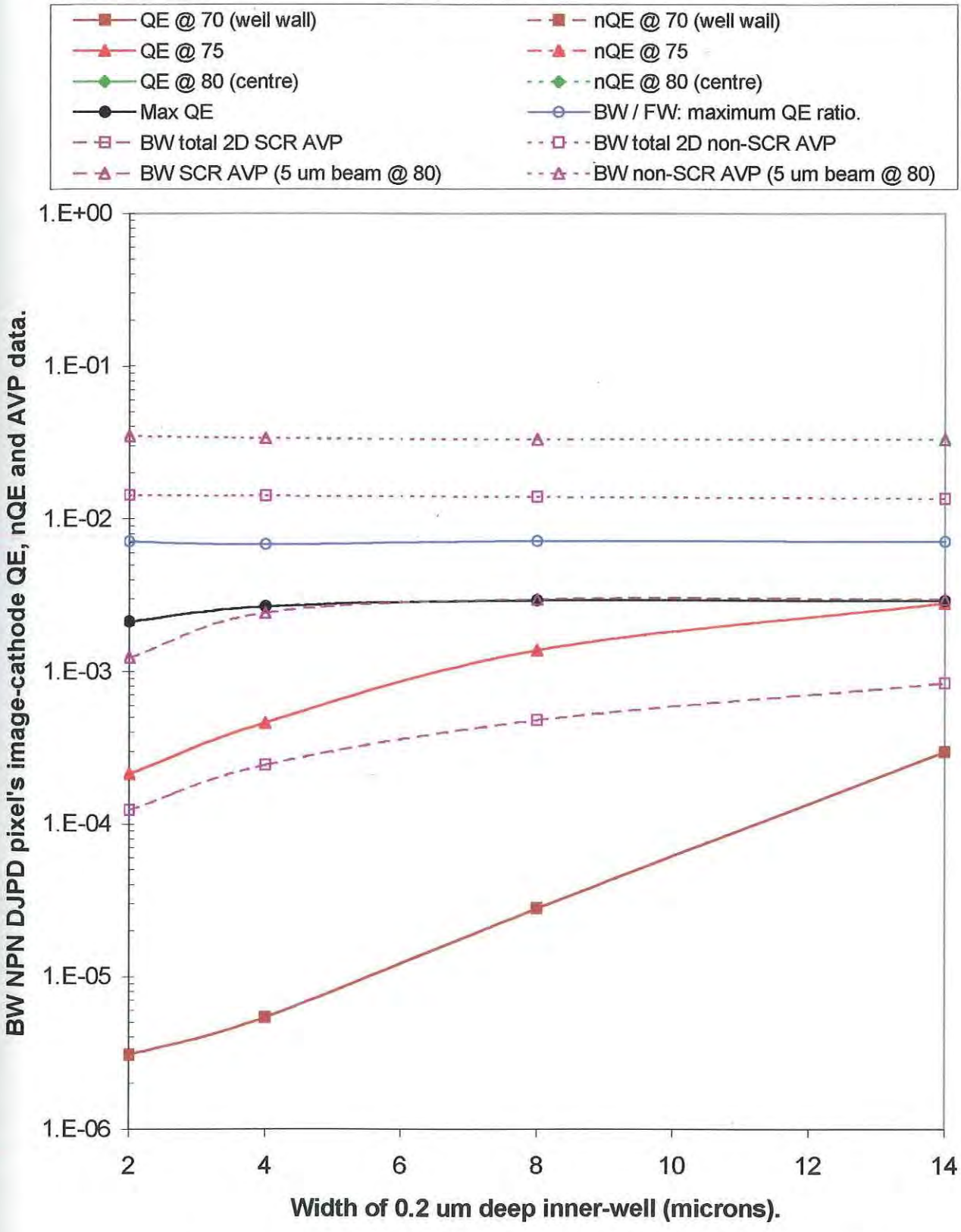

Figure 5.59: **BW NPN DJPD pixels: image-cathode's QE and nQE width dependence for pixels with the shallowest image-well, compared to AVP data for total 2D pixel and 5 um slice at 2D pixel centre.**

(cf/ Results DJPD: Apppendix XV & XVII.)

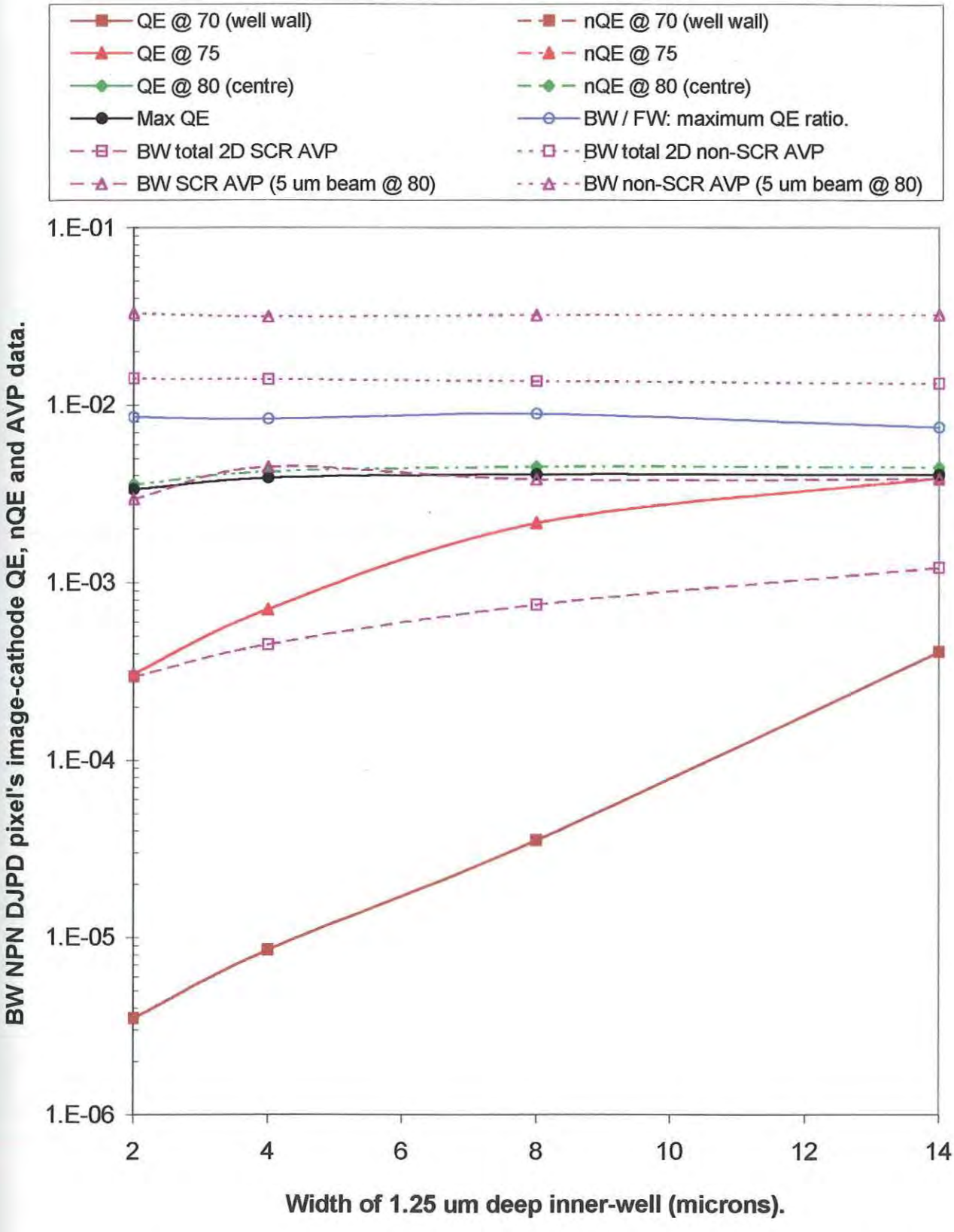

Figure 5.60: **BW NPN DJPD pixels: image-cathode's QE and nQE width dependence for pixels with the deepest image-well, compared to AVP data for total 2D pixel and 5 um slice at 2D pixel centre.**

Figure 5.61 shows FW NPN DJPD pixels' *logarithmic* image QE and nQE response dependence on the *shallowest (0.2 μm) depth* inner well's width variation, for illumination across half of the central pixel's outer well. These responses are compared to the AVP data as for Figure 5.59.

This response profile across all illumination positions parallels the BW profile in Figure 5.59 except the response is raised significantly as Figure 5.56 has already shown. The linear and exponential trends are the same and the AVP data response profile is also paralleled in the same way as in Figure 5.59. The central nQE is hardly noticeable above the QE response, though more than the BW profile.

Figure 5.62 shows FW NPN DJPD pixels' *logarithmic* image QE and nQE response dependence on the *deepest (1.25 μm) depth* inner well's width variation, for illumination across half of the central pixel's outer well. These responses are compared to the AVP data as for Figure 5.59.

The QE, nQE and AVP profiles are the same for the BW profile in Figure 5.60 except the response here is increased above the BW response as the image pixel AVP is significantly increased. This is important to note that BW and FW DJPD pixels respond in the same way in regards to their QE and nQE response trends for pixels of equal geometry. Unlike the SJPD, there is no substrate diffusion factoring into the response. Rather the DJPD response is totally dependent on the pixel configuration and AVP profile inside the outer-well.

(cf/ Results DJPD: Apppendix XVI & XVII.)

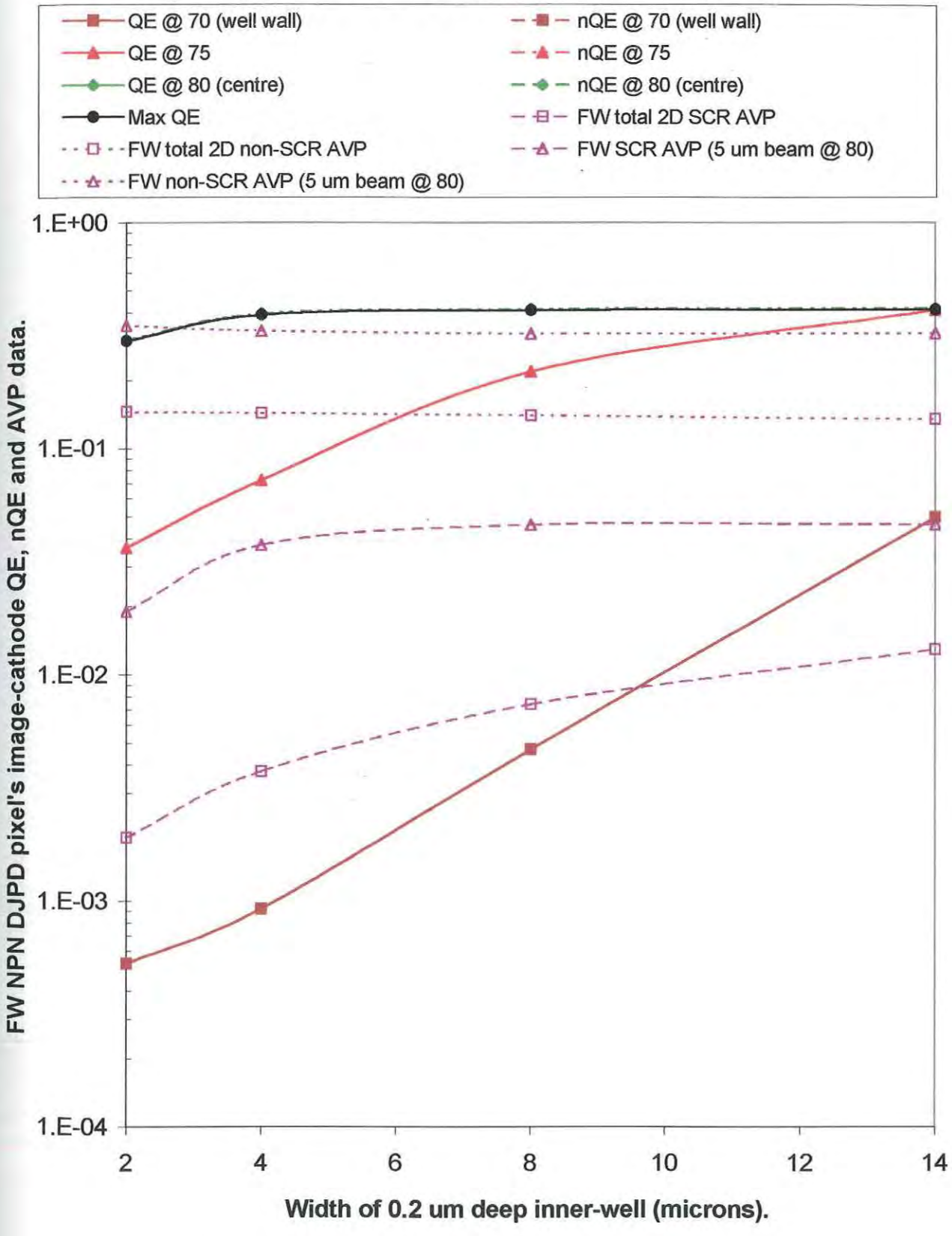

Figure 5.61: FW NPN DJPD pixels: image-cathode QE and nQE width dependence for pixels with the shallowest image-wells, compared to AVP data for total 2D pixel and 5 um slice at 2D pixel centre.

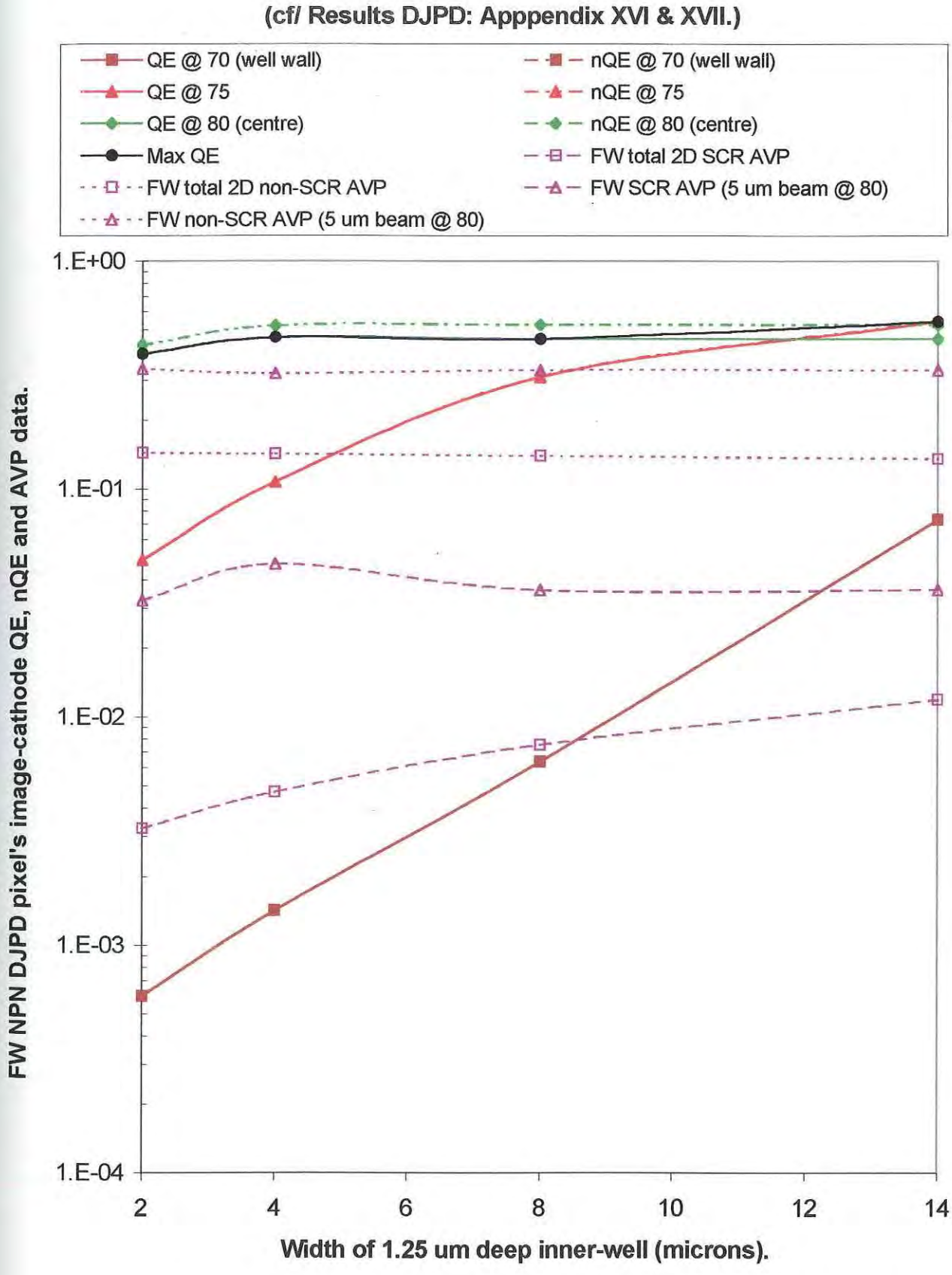

Figure 5.62: **FW NPN DJPD pixels: image-cathode's QE and nQE width dependence for pixels with the deepest image-wells, compared to AVP data for total 2D pixel and 5 um slice at 2D pixel centre.**

Figure 5.63 shows BW and FW NPN DJPD pixels' *logarithmic* image NQE response dependence on the *shallowest (0.2 μm) depth* inner well's width variation, for illumination across half of the central pixel. These responses are compared to the AVP data as for Figure 5.59 except only total 2D pixel AVP data is considered. Both BW and FW AVP responses are presented for comparison.

As expected, the BW pixel boundary NQE is 100 times greater than the FW pixel's NQE because the maximum QE is much lower in the former and both flat-line equivalently (Figures 5.51 to 5.52). In general, the BW responses parallel the FW responses. For illuminations inside the outer well (70 to 80 μm positions), the FW response is above the BW response, while the reverse is true outside the outer well. The FW response is therefore the more resolved response. The response inside the well trends as in the QE response cases (Figures 5.59 and 5.61) because the central QE response is quite flat and the image-well is very shallow. It is unclear why the pixel boundary response parallels the 2D image-pixel SCR AVP as in theory photocarriers produced in the substrate are captured by the outside SCR and thus don't impact on the image-cathode's capture volume. Maybe there is an indirect effect on electron diffusion in the outer well due to the increased hole population in the outer well that are being collected by the outer well anode.

Figure 5.64 shows BW and FW NPN DJPD pixels' *logarithmic* image NQE response dependence on the *deepest (1.25 μm) depth* inner well's width variation, for illumination across half of the central pixel. These responses are compared to the AVP data as for Figure 5.63.

This overall response profile is slightly increased above the previous profile owing to the enhanced QE profile due to the increased image-well SCR volume, with the deeper image-well. Otherwise the note about response trends and the response trends paralleling AVP data are identical to Figure 5.63.

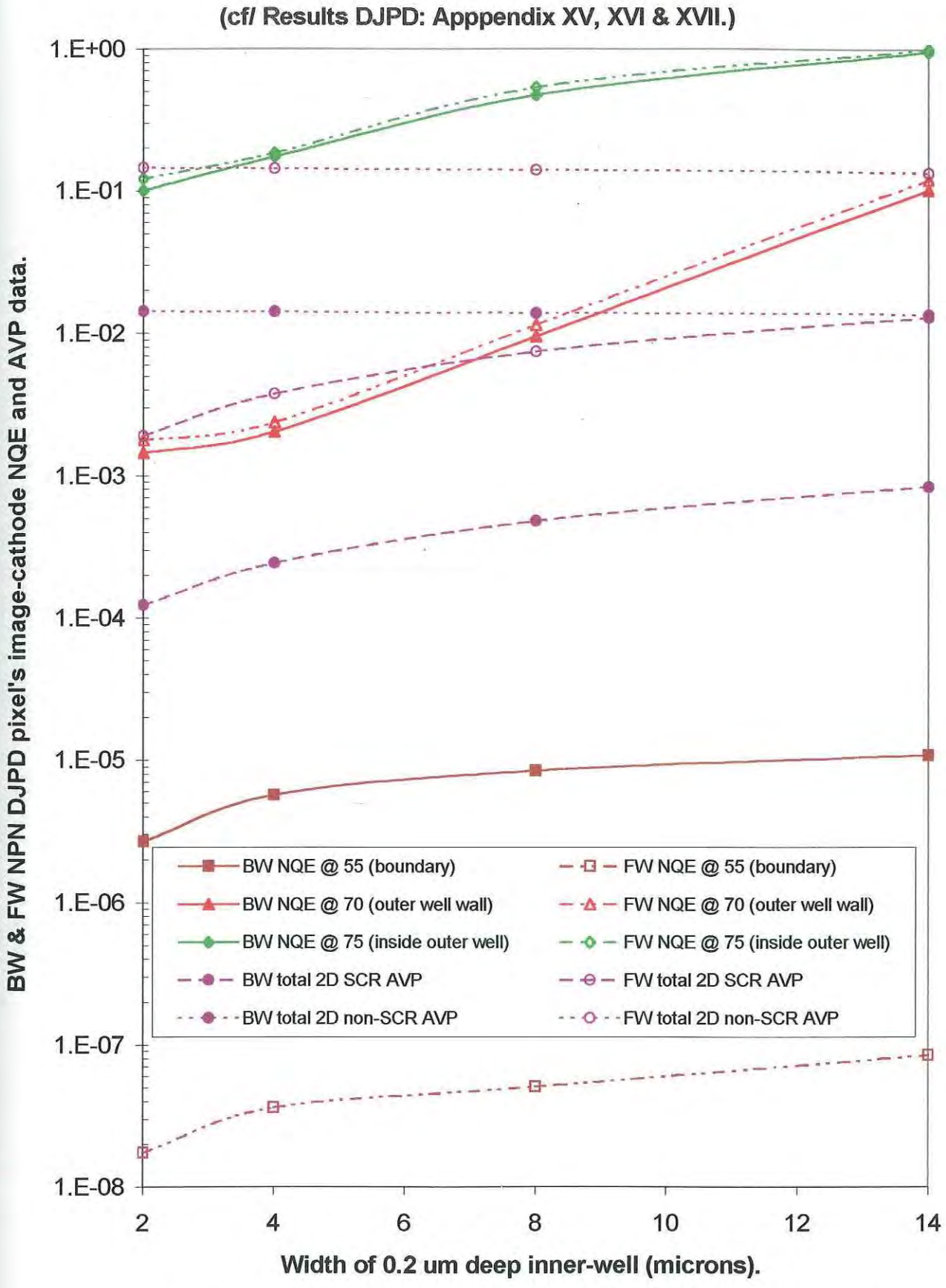

Figure 5.63: BW and FW NPN DJPD pixels: image-cathode's NQE width dependence for pixels with the shallowest image-wells, compared to AVP data for the total 2D pixel.

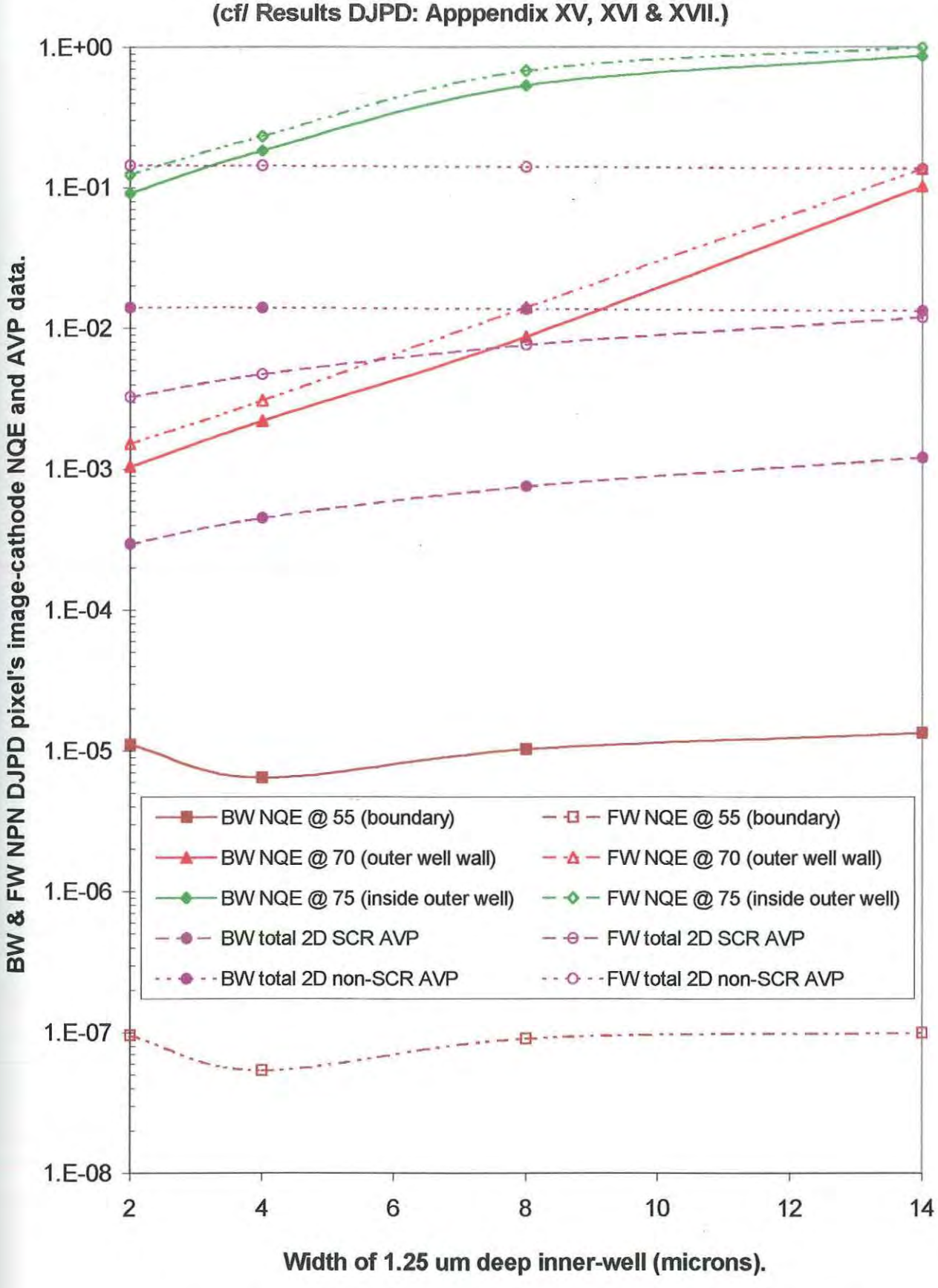

Figure 5.64: **BW and FW NPN DJPD pixels: image-cathode's NQE width dependence for pixels with the deepest image-wells, compared to AVP data for the total 2D pixel.**

5.2.3 **Effect of Image Well Depth on DJPD Pixels.**

In this section the relationship of QE and NQE to the image-well depth is investigated. Results demonstrating the underlying trends in the total result set are presented graphically. A complete NPN DJPD pixel results table including QE, nQE and NQE data can be viewed in Appendices XV and XVI for BW and FW pixels, respectively. The PNP DJPD pixel results (Appendices XIII & XIV) are similar so that only the NPN results need to be considered. The AVP data relevant to the Pixel configurations may be viewed in Appendix XVII.

The QE, nQE, NQE and AVP data responses and the graphical data representation configuration are presented in the same manner as for the previous section, except now the responses are graphed against the image-well's depth. The only change is the AVP data used in the NQE graphs. Here the AVP response for a 5 μm illumination at the centre is considered, not the total 2D pixel AVP data. The 5 μm central AVP data profiles relate more closely to the effect of inner well depth variation on the QE and NQE pixel responses.

Figure 5.65 shows the BW NPN DJPD pixels' *logarithmic* image QE and nQE response dependence on the *thinnest (2 μm) width* inner well's depth variation, for illumination across half of the central pixel's outer well. These responses are compared to the AVP data associated with the volume in the outer well (image pixel), including the inner-SCR AVP ("SCR AVP") and inner-non-SCR AVP ("non-SCR AVP") response profiles. Both total 2D pixel AVP data and AVP data for a 5 μm wide illumination at the pixel centre are considered.

The response at the outer well wall (70 μm illumination position) is increasing very slightly linearly for increasing image-well depth and constant thin width, indicating the constant distance between the image-well's SCR and the outer-well's SCR. It is increasing because the image-well SCR surface that is facing the outer-well SCR is increasing in surface area, increasing the capture efficiency of the image-cathode for electrons diffusing towards the image well, from their location of photogeneration.

The 75 μm illumination position response increases with increasing SCR AVP response, but increases only slightly after the middle depth. A possible reason for this is BW photocarrier diffusion to the bottom SCR surface is reduced, while the side SCR surface increases in the deepest image-well pixel, so that the total SCR surface area available to the diffusing photoelectrons remains similar for the two deeper image-well pixels.

As expected, the central response increases exponentially with both SCR AVP as the absorption profile always increases exponentially with decreasing penetration depth. The hole problem is seen to be increasing very slightly with increasing image-well depth, because the image-well volume is small already, being the thinnest well. Also the BW pixels already have a reduced hole problem, due to the distant proximity of the illumination to the image well.

(cf/ Results DJPD: Apppendix XV & XVII.)

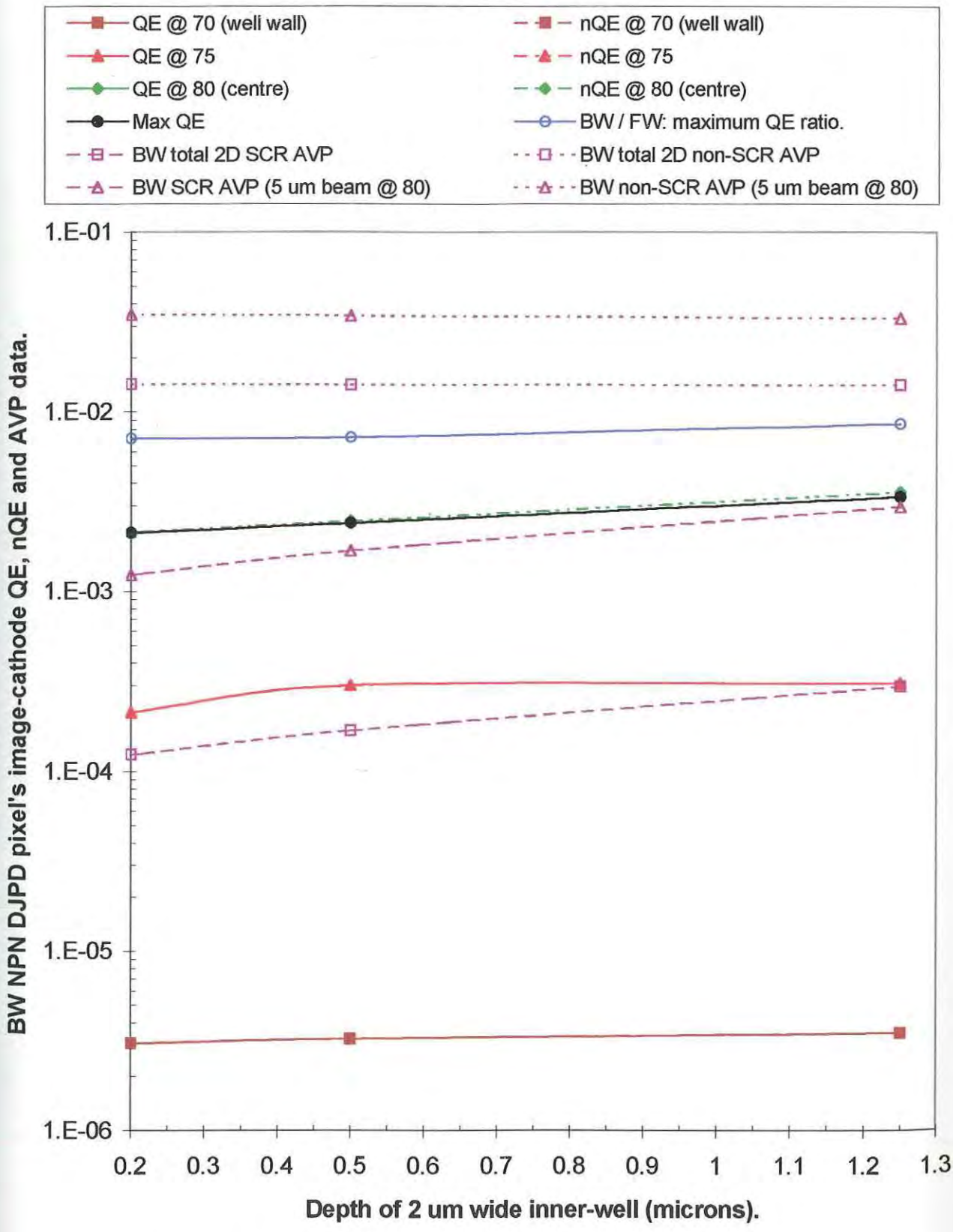

Figure 5.65: **BW NPN DJPD pixels: image-cathode QE and nQE depth dependence for pixels with the narrowest image-wells, compared to AVP data for total 2D pixel and 5 um slice at 2D pixel centre.**

Figure 5.66 shows the BW NPN DJPD pixels' *logarithmic* image QE and nQE response dependence on the *widest (1.25 μm) width* inner well's width variation, for illumination across half of the central pixel's outer well. These responses are compared to the AVP data as for Figure 5.65.

The response is broader and less resolved than the previous response, due to the very large increase in image-well SCR surface area and penetration into the outer well interior. Thus this 70 μm response looks like the 75 μm response in Figure 5.65 for the same reason.

The 75 μm response remains constant initially then increases because the illumination straddles the image-well wall SCR. The part of the SCR that is illuminated is "hockey-stick" shaped, with more SCR volume at the bottom edge of the image well wall. This means that the SCR volume illuminated doesn't just come closer to the illumination as image-well depth increases, its volume increases also. Note that the 75 μm response is nearly slightly under the central response indicating the degree of broadness of the whole QE profile.

The central response is exponential as expected. Now the hole problem increases with increasing well depth to a greater degree than the hole response in the thinner image-well pixels.

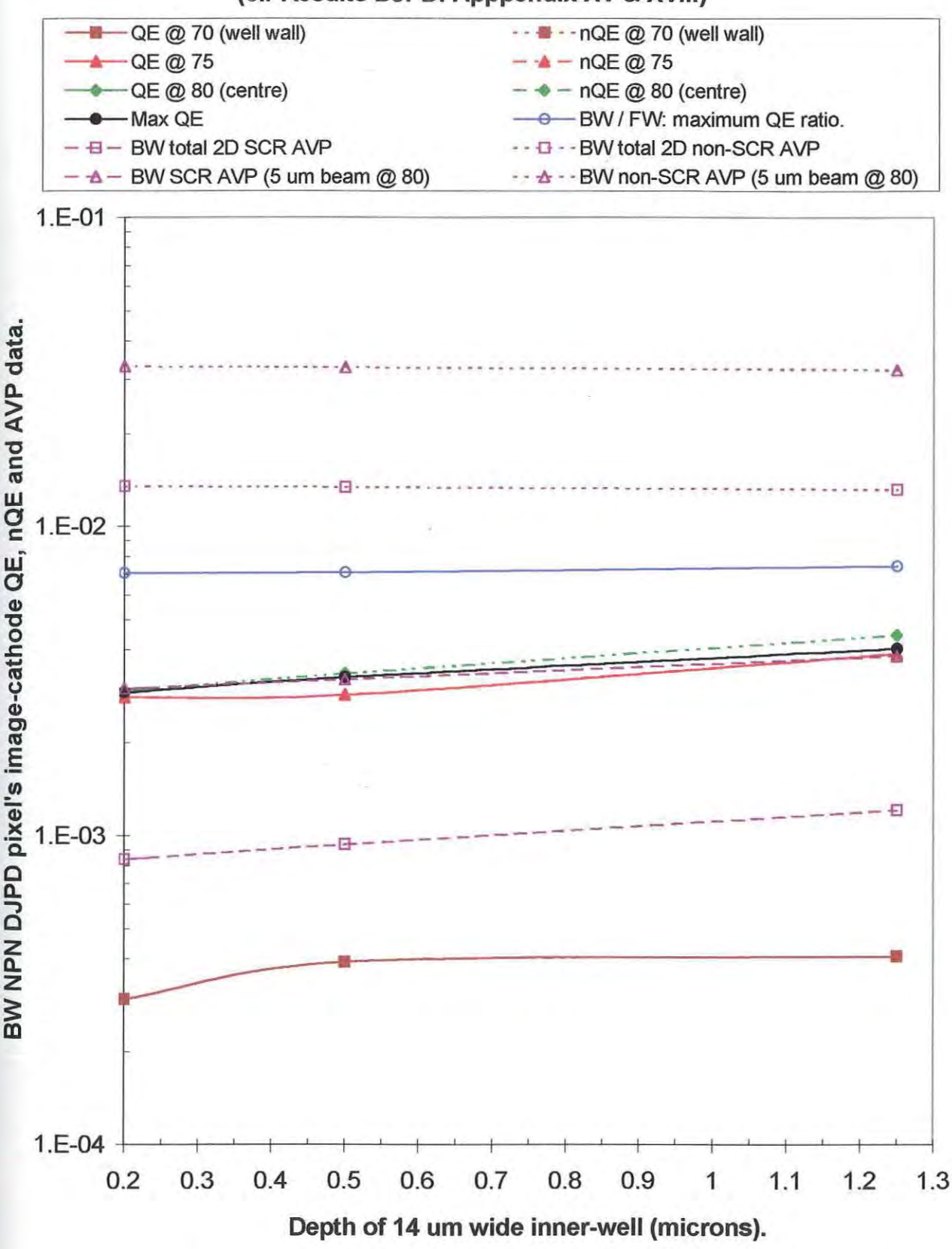

Figure 5.66: **BW NPN DJPD pixels: image-cathode QE and nQE depth dependence for pixels with the widest image-wells, compared to AVP data for total 2D pixel and 5 um slice at 2D pixel centre.**

Figure 5.67 shows FW NPN DJPD pixels' *logarithmic* image QE and nQE response dependence on the ***thinnest (2 μm) width*** inner well's depth variation, for illumination across half of the central pixel's outer well. These responses are compared to the AVP data as for Figure 5.65.

All responses, QE, nQE and AVP, are enhanced above the BW responses (Figure 5.65). Otherwise most of the response trends are generally similar to the BW responses for the same reasons. Again the FW response at the centre is affected, more than the BW responses by the increasing hole current with increasing image-well depth, due to its illumination proximity to the image-well. The central response parallels both SCR AVP profiles, increasing in a way that appears to be linear, because the whole image-well SCR is illuminated and the whole SCR volume increases proportionately to the well depth.

At the 75 μm illumination position the response trend is now less suppressed for the deepest image well, than the BW response (Figure 5.65). This is due to the photocarrier envelope being outside the image-well. The FW photocarrier diffusion is more associated with the image-well wall SCR surface than for BW photocarriers generated at the same illumination position. The latter photocarriers are more associated with the SCR surface at the bottom corner of the image-well and underneath the image-well. As the SCR surface, down the image-well wall, increases linearly, the capture volume increases with less suppression for the deepest well as there is less dependence of the response on diffusion to the SCR surface under the image-well. Hence its response continues to increase through to the deepest image-well depth, unlike the BW response (Figure 5.65).

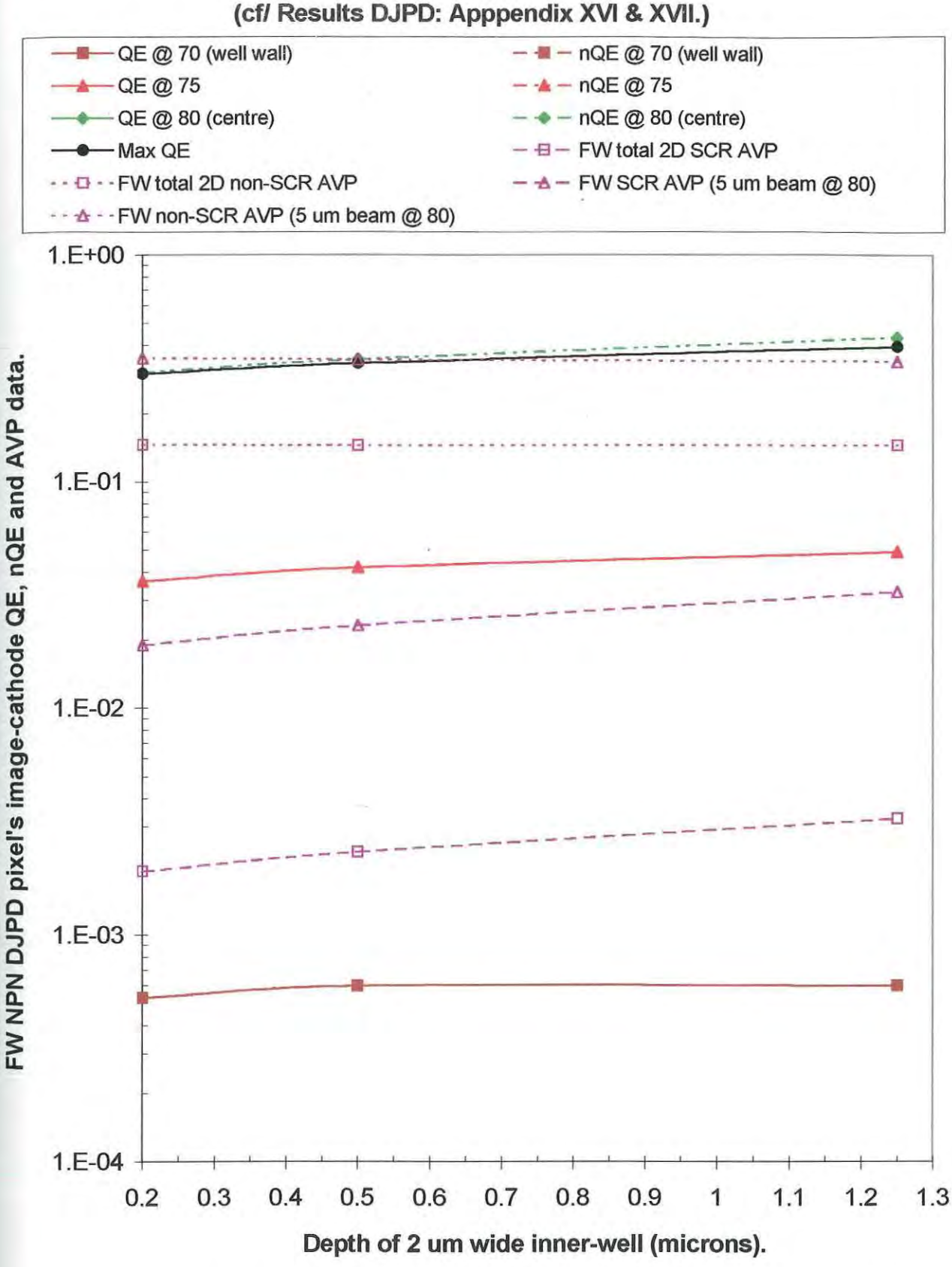

Figure 5.67: **FW NPN DJPD pixels: image-cathode QE and nQE depth dependence for pixels with the thinnest image-wells, compared to AVP data for total 2D pixel and 5 um slice at 2D pixel centre.**

Figure 5.68 shows BW NPN DJPD pixels' *logarithmic* image QE and nQE response dependence on the ***widest (1.25 μm) width*** inner well's width variation, for illumination across half of the central pixel's outer well. These responses are compared to the AVP data as for Figure 5.65.

At the 70 μm position, the QE response is increasing more than the thinnest pixel (Figure 5.67). Similar to the reason for this same enhancement for the BW response (Figure 5.66), the image-well's SCR outer boundary, that extends down the image-well's wall, is now much closer to the photogenerated carrier envelope diffusion, inside the outer well. Therefore its increase in surface area, with increasing image-well depth, impacts on the capture efficiency of the image-cathode, more than for the thinner image-well pixel where the SCR outer boundary is much farther away from the carrier envelope diffusion, photogenerated close to the outer-well wall.

At the 75 μm position, the QE response is coincident with the maximum QE profile, above the central (80 μm position) QE response, due to more inner SCR volume being FW, this SCR region down the image-well's wall increases in volume as the image-well deepens. The nQE also slightly increases with well depth at this position.

At the 80 μm position, the centre, the SCR AVP profile decreases, with a corresponding increase in non-SCR AVP. This means that any increasing central QE response is due to the increasing diffusion component. This has contributed to the increasing electron and hole current indicated by the increasing gap between the central QE and central nQE. Unlike the BW pixel response (Figure 5.66) this central response is no longer maximum. Though similar to the naked SJPD FW pixel's central responds, this response is less as the image-well AVP is less.

(cf/ Results DJPD: Apppendix XVI & XVII.)

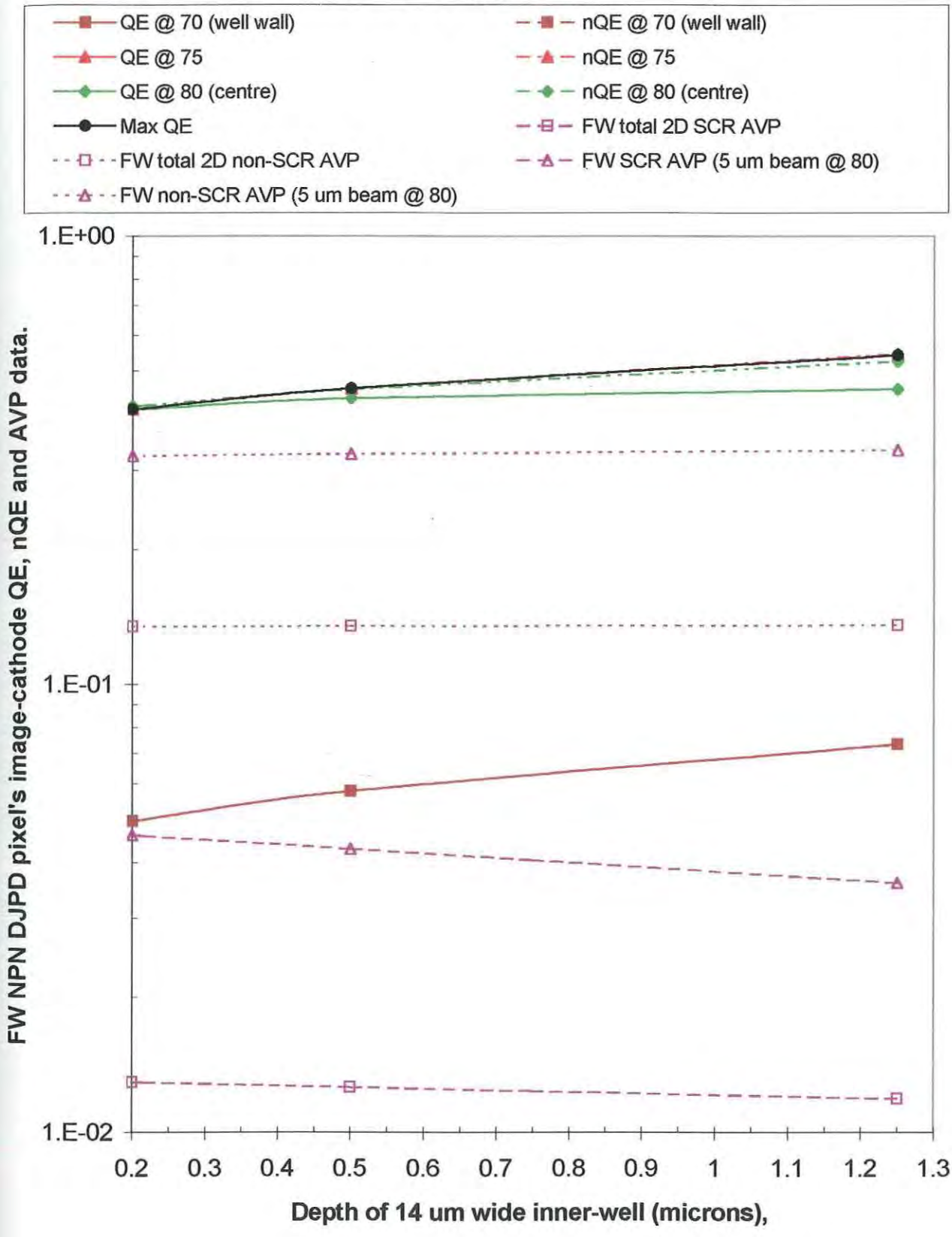

Figure 5.68: **FW NPN DJPD pixels: image-cathode QE and nQE depth dependence for pixels with the widest image-wells, compared to AVP data for total 2D pixel and 5 um slice at 2D pixel centre.**

Figure 5.69 shows BW and FW NPN DJPD pixels' *logarithmic* image NQE response dependence on the ***thinnest (2 μm) width*** inner well's depth variation, for illumination across half of the central pixel. These responses are compared to the AVP data as for Figure 5.59 except only the AVP data for a 5 μm wide illumination at the pixel centre is considered. Both BW and FW AVP responses are presented for comparison.

As was stated for the pixel boundary NQE response for the width investigation (Section 5.2.2, Figures 5.63 to 5.64), it is unclear as to why this NQE response at the image-cathode increases with increasing image-well depth, as the outer-well depth remains constant. As mentioned in Section 5.2.2 (Figure 5.63), it is unclear why the BW and FW pixel boundary responses parallels the image-pixel SCR AVP profiles. Also as suggested in Section 5.2.2 (Figure 5.63) there may be an indirect effect on electron diffusion in the outer well due to the increased hole population in the outer well that drift across the SCR to be collected by the outer well anode.

While the 70 μm position, the well wall, NQE response decreases, the 75 μm position NQE response bows upwards at the centre of its response, but then decreases to a minimum. This general decrease is due to the increasing central QE response, which parallels the SCR AVP profile. The minimum NQE responses occurring for the deepest image-well pixel, indicate that this pixel gave the most resolved response, but there is very little difference between these three different image-well-depth pixel responses.

Figure 5.70 shows BW and FW NPN DJPD pixels' *logarithmic* image NQE response dependence on the ***widest (1.25 μm) width*** inner well's width variation, for illumination across half of the central pixel. These responses are compared to the AVP data as for Figure 5.69.

Now the 70 μm and 75 μm position NQE response trends are reversed to Figure 5.69, with the 70 μm being bowed and the 75 μm decreasing. The deepest pixel still has the lowest NQE, and is therefore more resolved, but not by much. The thinner pixel response (Figure 5.69) is still the more finer, narrower and more resolved.

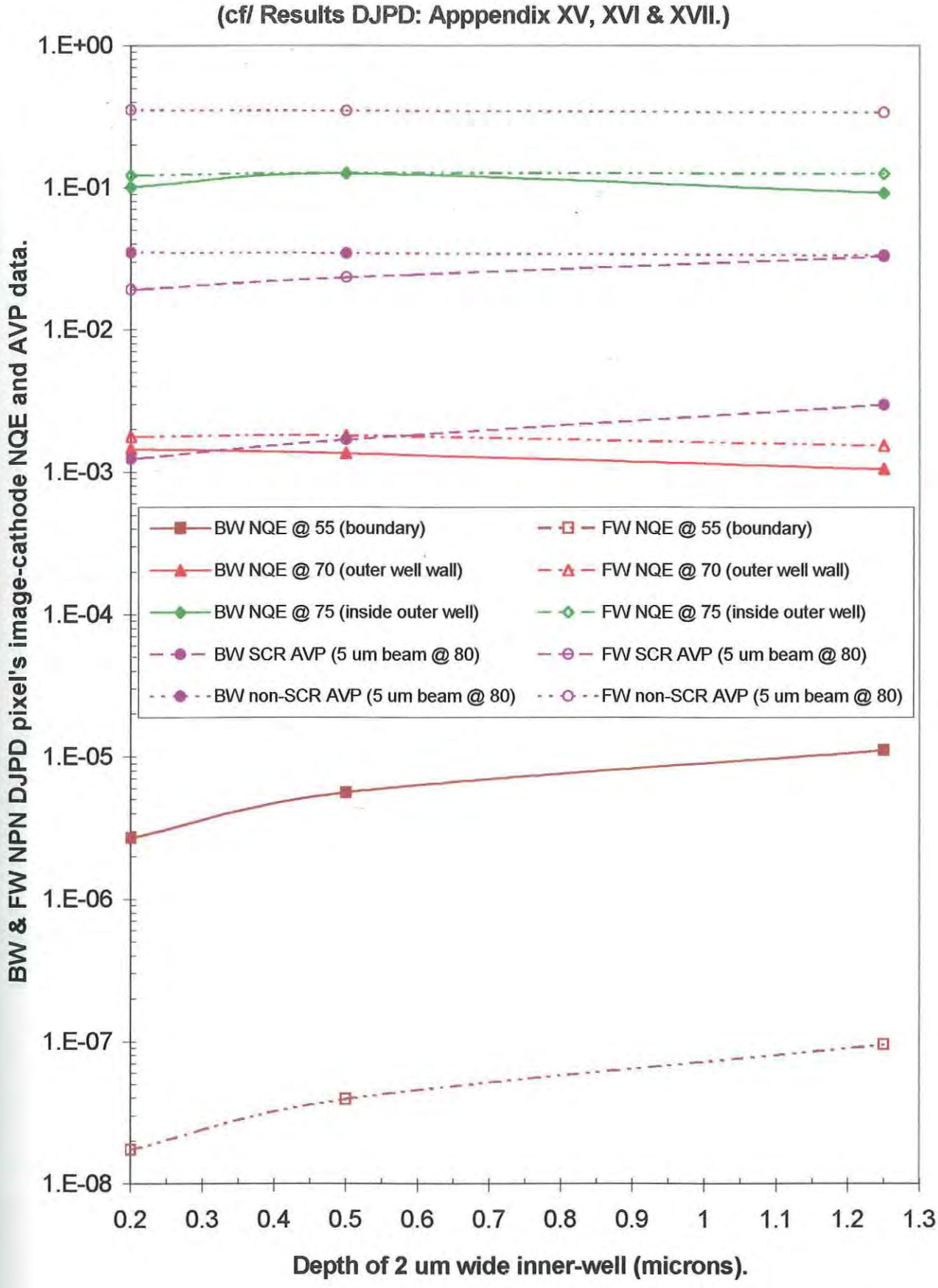

Figure 5.69: BW and FW NPN DJPD pixels: image-cathode NQE depth dependence for pixels with the thinnest image-wells, compared to AVP data for the total 2D pixel.

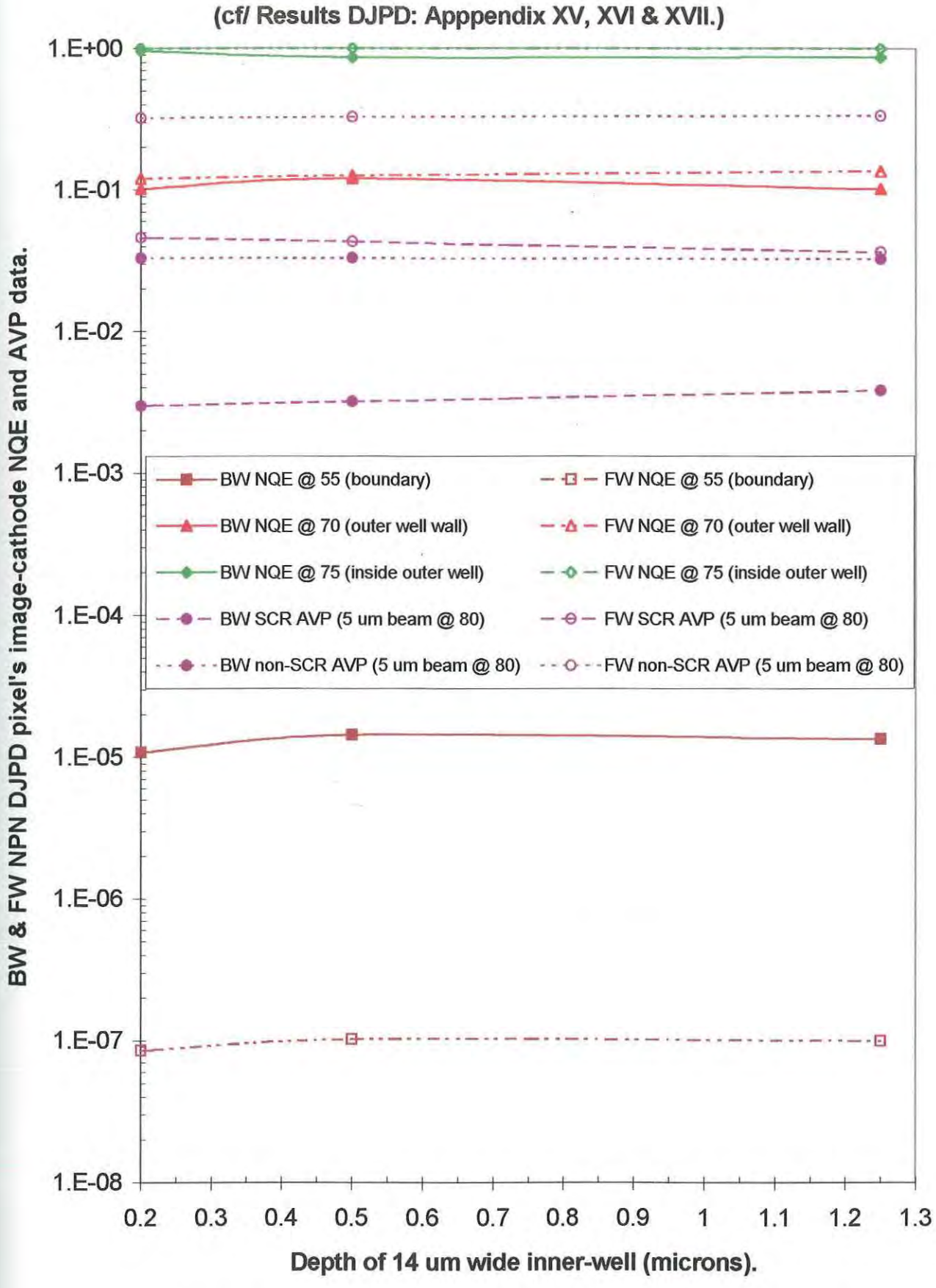

Figure 5.70: BW and FW NPN DJPD pixels: image-cathode NQE depth dependence for pixels with the widest image-wells, compared to AVP data for the total 2D pixel.

6. DISCUSSION

In this section the result findings are discussed, on a sectional basis. The most optimum pixel configuration of the sample space, will be recommended. "Optimum" implies the best combination of sufficiently suppressed crosstalk and sufficient maximum QE. Findings by other research groups will be compared and future direction of research recommended in each section, where applicable.

6.1 The Vertical SJPD Pixel.

Some of the principles for advantaging any Photodiode pixel have been revealed in the results section owing to the availability of carrier QEs and AVP data. For example, the electric field is the same for BW and FW pixels of equal configuration, what differs is the light absorption geometry across, ultimately, the 3D volume of the pixel array, which is precisely what the AVP data and resultant carrier QE demonstrate.

6.1.1 Effect of Substrate Thickness and Well Depth on Naked Pixels.

The results in Section 5.1.1 show that in the case of BW pixels, for illumination not close to the wall, the capture efficiency parallels the non-SCR AVP data which seems to indicate that contribution of the diffusion transport mechanism increases with Substrate depth, for constant well depth in BW Pixels. This is possibly due to the exponential decrease in Quantum budget of incident light that, for the BW pixel, generates the majority of photocarriers increasingly further away from the capture region of the Image cathode. This distancing problem can be overcome by bringing the SCR closer to the generated photocarrier population, increasing capture efficiency and hence QE. This is observed for illuminations close to the well wall, where the photocarriers are brought closer to the SCR, for increases in substrate depth and constant well depth. This is also observed for well depth increases, where

the SCR is brought closer to the photocarriers, for constant substrate depth. This indicates that the contribution of the drift transport mechanism increases with increasing proximity to the SCR i.e. with increasing well depth or SCR illumination proximity.

Thus for BW SJPD pixels, to keep boundary QE low, the back wall is brought closer to the SCR rather than the other way round. This maximizes the drift transport mechanism and radically cuts the diffusion component that is responsible for increased image cathode-capture-efficiency at the pixel boundary. Subtracting effects of increasing hole population with well depth is more apparent for deeper wells and only for illuminations cutting into the n-well region; over the well wall at the 70 μm position.

A depressed non-SCR AVP profile, in the FW case, translates to a reduction of the diffusion contribution to the total QE, which means less "free running" diffusion in the substrate, closer to the pixel edges and hence a reduced boundary QE. Especially in the deeper substrates, this "free running" diffusion causes an increasing crosstalk problem for both modes of illumination.

While the BW mode suffers from distancing from the SCR and surrounding capture region of the photogenerated faster electron minority carriers, the FW mode suffers from reduced QE at the well region due to increased photogeneration in the n-well, of the slower hole subtracting current. A depressed mobility outside the well, as would be expected in the n-substrate SJPD unbounded by a well enclosure, would serve to discourage free substrate diffusion, resulting in reduced crosstalk in SJPD, for both illumination modes. However sensitivity may be reduced as the hole is then the image carrier. Thus the general policy to have the SCR as close as possible to the point of incidence of the illumination as well as maximizing the SCR AVP, is concluded. This translates to a shallow substrate rather than a deep well as the above QE results indicate.

For the optimum shallow pixels the QE response is relatively high at 0.75, even though 50% of the illumination is transmitted and is therefore lost, i.e. a maximum of only half the quantum budget being available for photogeneration and resulting

image carrier capture. Due mainly to the SCR AVP dominating the available illumination quantum budget resulting in a drift dominated photo carrier response, the benefit of a reduced hole QE is also apparent. The deeper well is operationally better for the BW pixel as it is the more drift dominated and thus has a faster capture rate, translating ultimately to more frames/sec in real time visual application. That is not to say that this Pixel configuration is the one of choice. Rather, that the capture efficiency may be enhanced by maximizing the SCR AVP, which by itself may not increase sensitivity. The minimum well-AVP needs to be balanced with the maximum SCR AVP and the minimum non-SCR AVP. This is so that QE reducing well minority carriers and diffusion outside the well may be minimized and drift regions maximized. Reducing the AVP outside the SCR, outside the well, with a simultaneous increase in SCR AVP will minimize crosstalk in SJPD pixels.

This reiterates the conclusion in the study of the QE profile outside the well. That is that smaller well volumes and minimized diffusion outside the well, using shallower substrates, serve to maximize QE for illumination in and close to the well while minimizing QE for illumination further from the well and outside the pixel boundary. Suppression inside the pixel means that there is room for pixel pitch decrease, increasing physical resolution of the imaging array. It also means increasing well pitch which increases fill factor.

6.1.2 **Effect of Boundary Trench Isolation (BTI) on Naked Pixels.**

The results in Section 5.1.2 show that BTI wells effect the pixel response as follows:

1. Limited suppression of the QE and NQE for illuminations at the boundary and outwards from the pixel, due to suppression of minority current (electronic) transport towards the central pixel depletion region.

2. Enhancement inside the pixel, up to the well wall due to enhancement of minority current (electronic) in illuminated p-substrate.

3. Immediate suppression of minority photocurrent (holes) in illuminated wells.

Point (1) requires explanation. As carriers diffuse outwards from their photogeneration region in the substrate, in an SCR direction, they pass through the BTI "traps", where, due to the increased majority hole population, increased recombination results. This results in decreasing the minority carrier electron population and the suppression of the image cathode QE, which is mainly the electron QE. The direct relationship between the volume of BTI and the QE becomes more apparent (or more BTI weighted) as the BTI depth increases, due to more BTI taking up the "free diffusion" regions in the substrate, and exposing more of the photogenerated carrier envelope to the BTI surface. This also explains the case when the travel path of the minority carrier through the BTI wells increases, as is the case for two intervening BTI (or thicker BTI) wells.

This then explains the suppression from the inner BTI well, outwards from the central pixel being due to increased recombination in the more heavily P^+ doped BTI wells, intervening between the minority carrier envelope and the pixels depletion region. The semi-exponential suppression in QE and NQE with both BTI well width and depth needs further investigation across the full data set, however the proportional decrease in response with increase in BTI volume is clearly demonstrated. Maximum suppression of 46% for deepest BTI well in the shallowest substrate, with the shallowest well pixel, is due to the greater isolation imparted by the deepest BTI wells that penetrate to 1 μm from the back wall. This presents more of a barrier to "free run" diffusion in the substrate. BW pixel is less suppressed as the point of illumination incidence is closer to the 1 μm "non-isolated" opening at the bottom of the BTI wells.

For photogeneration between the inner BTI and the image cathode, the increasing depth serves to either enhance the generation of electron / hole pairs or enhance the mobility/life time of carriers or enhance the extent of the cathode's electric field thus enhancing minority carrier drift further away from the SCR, increasing capture efficiency, or all three. Though the actual mechanism is unclear, the benefits of introducing BTI to moderately suppress boundary QE while enhancing inner Pixel QE, up to the well wall, in BW VSJPD is of note.

What is obvious is that the presence of the BTI well enhances the QE response more, when more of the photogenerated minority carrier envelope is adjacent to the BTI surface and the SCR surface; the carrier envelope between the two structures. Similar responses for shallower substrate pixel configurations is due to the carrier envelopes being similarly adjacent to SCR and BTI well. The deeper the substrate and the deeper the BTI well the less similar the response. The 60 μm position is less enhanced than the 65 μm position, as the beam straddles the BTI well and so less of the beam is between the SCR and BTI well.

The recovery to the total QE for BW or FW BTI pixels for illuminations over the well, is fairly robust and immediate. The greater the negative hole current, demonstrated in deeper well non-BTI pixels, the greater the hole current suppression and hence the greater the total QE recovery, to approximately equal QE levels across pixel configurations of different well depth. This recovery effect, makes the image cathode QE less effected by the well depth variation, leaving only the increasing trend in QE due to increasing substrate depth unaffected by the presence of BTI wells. This indicates the benefit of BTI wells to deeper substrate SJPD pixels, especially in FW pixels. However this type of BTI well is of minor benefit to increasing QE for shallow BW single junction PD which always exhibited the better relative crosstalk.

For the shallowest pixels, for which the relative crosstalk is minimum, the BTI wells increasingly reduce the relative crosstalk by a maximum proportion of one half, for the deepest BTI well depth. However the relative crosstalk is still too high for practical use of the BW pixel, with pixel boundary QE of 0.036 e/photon equivalent to a NQE of 0.048.

There are mechanisms underlying the hole QE suppression in the well and electron QE enhancement outside the well that are unclear as yet. However, the more important mechanism of pixel boundary QE suppression due to the proximity, depth, width and number of the BTI wells has been explained on the basis of increased recombination of the photogenerated electronic minority carrier population. From this it can be concluded that a shallower substrate improves BW pixel boundary QE (crosstalk) suppression, bringing it down to similar FW pixel values.

Further investigation of wider and more doped BTI wells is called for. Also the use of single junction BTI with n-type centre surrounded by a p^+ sleeve and its own bias may also prove to be of more crosstalk reducing benefit to the SJPD pixel. This is because it introduces a depletion region (SCR) which is more effective at capturing "free" substrate minority carriers. Another approach that needs investigation is the introduction of insulating SiO_2 BTI. These should prevent all carrier transport between adjacent pixels to the depth of the BTI, resulting in a significant reduction in crosstalk. Thus the possible benefits of BTI type structures in the pixel cross section are not lost with the specific type of BTI well investigated in this honours project.

6.1.3 Effect of Guard-Ring Cathodes on Naked Pixels.

The results in Section 5.1.3 show that the 3-cathode-pixel (guard-ring SJPD pixel, referred to as the guarded pixel) profile has crosstalk reduction advantages over the unprotected single cathode SJPD pixel (naked pixel). The guarded pixel allows increased image-array resolution using smaller pitch pixels, indicated by the 5 orders of magnitude pixel boundary QE suppression, that becomes 6 orders of magnitude, up to the well wall is very clear. It is only inside the pixel wells that the image contribution QE is significant for the chosen cathode sizes: maximal guard ring and minimal image cathode dimensions. These dimensions have been inferred from the trends observed in electrode size and position studies (Section 5.1.4).

The image cathode size of 0.4 μm is the minimum width for 0.35 μm fabrication. Since this size, combined with the maximum size guard of 3.2 μm shifted 1 μm from each side of the well, gave the best suppressed relative crosstalk (boundary NQE) this configuration was used. One exception was that this study has used guard-ring cathodes double the maximum size of the guards use in Section 5.1.4. The trend of better crosstalk suppression resulting from an increase in guard size observed in Section 5.1.4 prompted the use in this section of a larger guard-ring cathode which is twice the optimal size obtained in Section 5.1.4.

A literature search has not revealed any research of late into guard ring CMOS SJPD technology, its advantages or disadvantages. This seems unusual as the process improves the crosstalk suppression profile of any SJPD pixel configuration compared to the same pixel naked, for the regime of pixel configurations simulated in this research. A more intense literature search and further investigation is warranted.

One disadvantage of the guard-ring configuration is that the voltage bias applied to each cathode on the well, the guard and image cathodes, must be perfectly equal. Any slight difference between the guard ring and the central image electrode will result in an appreciable current flowing between them as would happen if a potential difference was placed across any extrinsic or intrinsic semiconductor.

From the point of view of the BW pixel, the advantage that the guarded pixel engenders is equal crosstalk suppression to the FW pixel as Figure 5.21 in Section 5.1.3 shows. Their suppression is similar right up to the well, which means that the BW pixel can be scaled down in size similar to the FW pixel, for pixels of shallow substrate thickness. The optimum for this configuration of bias and doping regime is the 3/1 guarded pixel.

The production of the optimum BW guarded pixel does not directly depend on its geometry i.e. the shallowness of the substrate or the depth of the well. What does have direct effect on optimization is that the drift AVP component is maximized and the diffusion AVP component is minimized. For their associated AVPs this means that the SCR AVP is greater than the non-SCR AVP. This is the case for the shallowest 3/1 pixel, given the biasing and doping regimes of the pixel configurations simulated. Therefore it is highly probable that a thicker SJPD pixel, with a larger reverse bias and / or lower doped substrate with a well depth situated so that the SCR penetrates nearly to the back wall of the pixel, having a substrate nearly totally depleted, will improve on the AVP statistics associated with the current optimal pixel (3/1).

The AVP trend associated with optimality can and will be extrapolated to other photosensing crystalline Silicon pixels as well as pixels made with other direct or indirect extrinsic semiconductor materials. The latter can be used in concert with a

Silicon based signal Processing ASIC only when the photosensing arrays is backwall illuminated. Hence the advantage of the BW pixel. This requires further research to develop the AVP photonic probe statistic so that it can be applied to other Silicon, indirect and direct extrinsic photosensing pixels so that the response resolution of these devices can be optimized. In this way a range of optimized photosensing pixels may be developed for a range of wavelength regions, including infra-red, visible and ultra-violet.

6.1.4 **Effect of Well-Electrode Position and Width on Guarded Pixels.**

The results in Section 5.1.4 show that the extent of suppression and shape of the QE and NQE response of a SJPD guarded pixel depends mainly on the guard cathode configuration. This is due to this cathode's capture window dominating the SCR, enveloping the well wall, completely surrounding the central image cathode capture window, making access to the later only possible along the central pixel axis, normal to the surface. Hence there is more response resolution, while sensitivity is not significantly reduced. Compared to the naked pixel, this reduction in sensitivity is 50% in 3/2 pixels simulated in Section 5.1.4 and even less for the 3/1 pixel simulated in Section 5.1.3 having the local optimal cathode and pixel geometry. These promising findings must prompt further investigation that test the limits of resolution, with SJPD guarded pixels of reduced pitch and reduced well pitch. Correlation with AVP data could be employed so that guard pixels of optimal well and substrate geometry are used.

Possibly the down sizing will also down size the optimal cathode configuration of position and size, impacting on CMOS fabrication resolution. Already the size restraints apply if, for example, the reduced well pitch is 5 μm, the optimal 3.2 μm and 6.4 μm wide guard ring in Section 5.1.4 and Section 5.1.3, respectively are obviously too large. But, in what ever way the image and guard cathodes are configured and however large the pixel size reduction, the guarded pixel will always be more resolved and have less crosstalk than the over sensitive naked pixel configurations.

Lastly, a more effective BTI configuration may prove to be a worthy challenger of the guard ring configuration's local optimality, especially if the BTI consists of an insulator such a Silicon Dioxide. The BTI solution is external to the well and so internal well structures that reduce the degree of down sizing are eliminated. However with the use of BTI an inter-well structure is now introduced. This requires further investigation.

6.1.5 **Effect of Doping Concentration on Guarded Pixels.**

The results in Section 5.1.5 have shown that for the guarded pixel with 10^{17} cm^{-3} well doping, the 5 orders of magnitude change in ***doping of the substrate***, creates as much as a little dip at the substrate doping of 10^{16} cm^{-3}. This result is significant as the SCR penetration orientation changes from substrate penetrating to well penetrating, which is a significant SCR rearrangement. This image QE response is similarly robust for both p-well and n-well pixels in the presence of the guard-ring. This response seem to be totally insensitive to the significantly decreasing SCR AVP profile.

The result for the variation of well doping indicates that a larger SCR well penetration enhances the guard response, which suppresses the image response, though this is not an excessive image response suppression relative to the other responses. As the SCR width decreases while substrate penetration increases, the QE and NQE responses trend with the non-SCR AVP. This indicates the response is more diffusion dominated allowing more carriers access to the image-electrodes capture field and so raising the response. The presence of the guard field still robusts this increase, giving a very slight increase.

The suppressed p-well FW pixel NQE responses for illumination at the 70 μm position does not appear to be supported by the QE profile that coincides with the n-well FW pixel profile for both the 70 μm and central (maximum) illumination positions.

FW pixel QE and NQE response is always slightly more suppressed, especially closer to SCR due to the closer proximity of the FW photo-generated carrier envelope. However this is not significant when compared to the shocking naked pixel crosstalk and response resolution.

Results from Section 3.1.3 demonstrate far better response resolution for the 3/1 guarded pixel; even the well wall NQE is more suppressed than the lowest relative crosstalk of the most optimum guarded pixel in this study. When optimizing the SJPD guarded pixels, initially a substrate thickness is chosen for a given pixel and well pitch. Then for this thickness a regime of well depths is tested against a regime of doping concentrations and junction biases to optimize the well depth, doping and bias for the chosen thickness.

Certainly doping regimes that maximize the SCR AVP while minimizing the non-SCR AVP can result in good response resolution (3/1 pixel in Section 3.1.3) for both BW and FW guarded pixels. If the non-SCR AVP is increased by 65%, while maintaining the same SCR AVP (4/2 BW pixel with Section 5.1.1 doping and a well-external SCR), the response resolution is significantly reduced. Suppressing the "free" substrate photocarrier diffusion by increasing the guard capture field penetration depth, reduces the "free" diffusion "gap", between the back wall and the bottom of the guard capture-field envelope. This reduces the population of photocarriers, generated either side of the well, from diffusing under the guard-ring "curtain". Instead, they are absorbed in the image electrodes guarding "force-field". A maximized SCR AVP and minimized non-SCR AVP are symptoms of an optimum well-electrode capture field orientation and the proximity of the photogenerated minority carrier envelope to the guard ring.

Resolution decreases for decreasing well penetration in the 3/2 pixel but is reversed in the other pixel geometries that have thicker substrates. This maybe due to the 3/2 pixel being more drift dominated with the increased SCR penetration of the well in the optimum pixel with substrate / well doping of 10^{19} cm^{-3} / 10^{16} cm^{-3}. This doping regime may increases the SCR penetration into stronger electric field flux and thus increasing the guards capture efficiency about the well, while increasing the image electrode's capture efficiency at the centre. The thicker pixels have increasingly

more "free" diffusion in the substrate. Thus, larger SCR's that penetrate more into this region outside the well, see an increase in guard and image capture efficiency, resulting in an increase in the QE and NQE response resolution.

Finally, this section ends with an example that illustrates the use and possible abuse of AVP data. The following pixels are reverse biased by 2 volts.

(A) 3/1 Pixel AVP for a 5 μm wide illumination @ pixel centre, the 80 μm position (SCR / non-SCR):

BW = 34.38 % / 15.82 % ;

FW = 28.24% / 21.97%

(B) 4/2 Pixel AVP for a 5 μm wide illumination @ pixel centre, the 80 μm position (SCR / non-SCR):

BW = 34.38 % / 26.15 % ;

FW = 22.38% / 38.15%

In both n-well pixel examples,(A) and (B), the FW guarded pixel is slightly more resolved than the BW guarded pixel. However, the FW SCR and non-SCR AVPs are less maximized and less minimized, respectively, compared to the BW pixel. However, between different pixel geometries (A & B), with the same mode of illumination, the "maximize-minimize" criterion is vindicated, as the 4/2 pixel is much less resolved than the 3/1 pixel, for both illumination modes. This indicates, when utilizing AVP data as a guidepost in the pixel configuration optimization process, comparison between the same configured pixels illuminated differently, can be misleading without other resolution parameters being considered.

6.1.6 **Effect of Voltage Bias on Guarded Pixels.**

The results in Section 5.1.6 have shown that for increasing bias the naked pixel and guard cathode QE responses are increasing, while for the guarded image cathode the QE response is only increasing at the centre and decreasing elsewhere. The increasing capture efficiency of the guard-cathode possibly suppresses the image-

cathodes response away from the centre where the image has the least influence. This trend is apparent for both BW and FW guarded pixels.

The advantage of a better AVP profile of the 3/2 [0] guarded pixel, with higher SCR AVP and significantly reduced non-SCR AVP compared to the other pixel configurations, enhances the response profile of the 3/2 pixel significantly. Note that the BW and FW 3/2 [0] guarded pixel QE and NQE profiles are far less separated than the other pixel configurations. The reason the BW and FW 12/2 guarded pixels' QE and NQE responses differ so much is again the closer proximity of the FW photo-generated carrier envelope to the SCR and associated guard-ring cathode capture field.

The NQE results indicate that more biased is better for the pixel response resolution. However, similar to the doping investigation in Section 5.1.5, the change in the bias has less effect on changing the pixel response than changing the pixels regional geometry. This is clearly shown in the contrast between the 3/2[0] and the 12/2[0] guarded pixel responses. This is again reflected in the AV Percentage profiles in Figure 5.49 and Figure 5.50, indicating once again the usefulness of AVP data for initial prediction of a possible optimal pixel, in regards optimal response resolution that includes enhanced central sensitivity and crosstalk suppression.

Adding to this reverse biased investigation, an even more resolved NQE response is evident. The local-global optimal, 2 volt reverse biased ([2]), 3 μm thick and 1 μm deep well (3/1) guarded pixel (Figure 5.27) has higher SCR AVP and lower non-SCR AVP than the local optimal guarded pixel discussed in Section 5.1.6. This increased NQE response resolution is demonstrated by the response profile flat-lining from the pixel's well wall outwards. This means that the image-cathode's capture field is capturing no extra carriers than for illuminations at the far boundary of the adjacent pixels (5 μm and 155 μm positions). This indicates the central pixel's image response is dead beyond its well wall; a highly resolved response. Again its AVP profile is one signpost pointing towards its possible optimality.

Extrapolation of the reverse bias trend applied to a 3 μm thick (3/0.5) [3] guarded pixel has an even better AVP profile compared to the 3/1 [2] guarded pixel. This is demonstrated by the AVP profiles of the two pixel configurations compared in the Table 6.1.

Table 6.1 : AVP data for the 3/1[2] and 3/0.5[3] guarded pixels.

Total AVP = 50.206 %	Guarded pixel SCR AVP: (%)		Guarded pixel Non-SCR AVP: (%)	
Illumination Mode :	3 / 1; [2]	3 / 0.5; [3]	3 / 1; [2]	3 / 0.5; [3]
5 μm beam over well wall (@ 70 μm)	31.698 (BW) 30.314 (FW)	33.474 (BW) 35.331 (FW)	18.508 (BW) 19.892 (FW)	16.732 (BW) 14.875 (FW)
5 μm beam at well centre (@ 80 μm)	34.382 (BW) 28.236 (FW)	37.293 (BW) 35.905 (FW)	15.824 (BW) 21.970 (FW)	12.913 (BW) 14.300 (FW)
2D total pixel: 50 μm beam at well centre	16.654 (BW) 14.534 (FW)	17.883 (BW) 17.838 (FW)	33.552 (BW) 35.672 (FW)	32.323 (BW) 32.368 (FW)
3D total pixel: 50 μm^2 beam at well centre	7.9966 (BW) 7.2106 (FW)	8.5370 (BW) 8.5969 (FW)	42.209 (BW) 42.995 (FW)	41.669 (BW) 41.609 (FW)

Further investigation of the 3/0.5 [3] guarded pixel by simulation may confirm that for the more optimal guarded pixel, the higher BW SCR AVP for the 80 μm position illumination, will result in a higher central BW pixel QE response, because of the enhancement of the BW image capture efficiency. The higher FW SCR AVP for the 70 μm position illumination, will result in a more suppressed FW pixel QE response elsewhere in the pixel, because of the enhancement of the FW guard capture efficiency. Both of these effects cause a similar NQE response resolution for both modes of illumination, similar to the 3/1 [2] guarded pixel. Also it is expected that the proposed simulation investigation will confirm that the proposed optimal pixel has better QE and NQE response resolution than this latter pixel.

The use of AVP data has proven to be useful in providing an initial guide to find the most optimum SJPD pixel. It has been shown that the dramatic difference between the AVP profiles for the different thickness pixels is reflected in the QE and NQE responses. For the range of reverse biases studied, the thickness has had more of an effect on the increase in response resolution, than the changes in bias, because the thickness change is more extensive. This is due to the loss of substrate below the well, bringing the SCR closer to the back wall, as well as removing the large "free" region that encouraged crosstalk diffusion in the substrate for the thicker pixel.

In conclusion, for the range of pixel geometries investigated, the FW response resolution is better than the BW resolution with bias contributing little to this difference. However, as stated elsewhere, as BW and FW pixel AVP profiles coincide so does their response resolution. Furthermore these differences are not significant enough for the more optimal geometry FW guarded pixels to outweigh the TFA and omni-semiconductor-compatability advantages of the BW guarded pixels.

6.2 The Vertical DJPD Pixel.

In this investigation, as was true for the SJPD pixel research, carrier response QE and AVP data have helped to elucidate the operating mechanisms that advantage and disadvantage the DJPD pixel configuration over the previous SJPD pixel configurations.

The main advantage of the DJPD pixel is the presence of an outer junction, which acts as a junction-guard. Unlike the guard-ring electrode system, the guard-junction encapsulates the inner image-pixel so that image-electrode response for illuminations from the inner surface of the outer junction outwards into the substrate are nearly totally suppressed. Additionally the image-electrodes response profile can be maximized and varied to a much greater degree of flexibility than the guard-ring SJPD pixel. This is achieved by altering the image-well's geometry as the following sections demonstrate.

The main disadvantage of the DJPD pixel is the inability of the inner junction to be depleted to the backwall, as can be achieved with the guarded SJPD pixel. Deeper outer wells can overcome this problem, but this adds more complexity to image-array IC fabrication as already a double well diffusion process is needed. However having backwall-depletion may not be an advantage for the BW pixel because it may counteract the wavelength range selectivity that has been demonstrated as an advantage of BW pixels (Hinckley, Gluszak & Eshraghrian, 2000).

6.2.1 Effect of Inner (Image) Well Dimensions Against Illumination Position.

As has been noted, the results show that the DJPD is superior in response resolution and in response-shape control, than the SJPD guarded pixel of equal bias, doping and geometry to that of the DJPD pixel's outer well and substrate, even without the DJPD electrode size and placement being optimized. Also, significant reduction in maximum QE caused by the hole problem, is only apparent in the widest and deepest image-well pixels, but certainly not to the same degree as naked FW SJPD pixels.

The results also noted that the PNP DJPD is only slightly inferior to the NPN pixel due to its image carrier being holes, which have less mobility than electrons.

A reduction of substrate thickness will have the same benefit for BW DJPD as for all SJPD pixels, simply because the BW image pixel's AVP will then be similar to the FW value. The removed well-hole problem in guarded pixels is one advantage that may be used in the pitch reduced DJPD pixels for relatively deep image-wells, though the hole problem is not significant enough a problem for deep but thinner image-well pixels, as their intra-well NQE and degree of resolution are the best for this inner and outer SCR width of 0.2 μm and 1.88 μm, respectively.

What is relevant to the image response of the DJPD pixels is that there are two junctions formed by two wells. It is the response inside the outer well that is important, the response outside this well, in the substrate, always flat-lines. Exactly, this means there is never any problem of crosstalk; it's a non-issue.

It is therefore possible that the outer well may be fabricated as close as the width of a substrate electrode plus twice the outer well's SCR width in the substrate. For the doping regime in this investigation and the minimum electrode size of 0.4 μm for 0.35 μm CMOS technology, the wells could be separated by about 4 μm (1.86+1.86+0.4). Lets be generous, and grant it 5 μm. The pixel pitch has thus been reduced to 25 μm, increasing the image array's physical resolution by four times for the BW pixel with its ASIC indium bumped to the electrodes on the front surface.

Furthermore the present inter-well distance is 30 μm. 5 μm is a 6-fold reduction. Due to the predictable flat-line response profile for illuminations outside the outer well for DJPD pixels and the response-tailoring potential of the DJPD image well geometry it is conceivable that this 6-fold reduction could be applied to the whole pixel. This will result in a pitch of about 8 μm, with an image pixel pitch (outer well pitch) of about 3 μm, proportionately larger than the present pixel. Thus arriving at a 6.25-fold reduction in pixel pitch while increasing the resolution about 40 times. With a ten fold increase in substrate doping the outer well SCR width will

reduce to 0.566 μm, allowing even greater reduction in pitch and increase in resolution, if this reduction is applied across the whole pixel.

Certainly the guarded (3/1) [2] SJPD BW or FW pixels response is comparable to both the BW and FW DJPD response with the change to the latter's thickness so that the image-pixel AVP for BW and FW become equivalent. However it is less clear the effect that closer guard-ring capture fields would have on the SJPD pixel's image response if the gap between adjacent pixel wells was reduced. Needless to say both guarded and double junction pixels need further simulating for pixels of reduced pitch and well pitch to check the former effect and to verify the predicted advantages of the DJPD pixel configuration.

6.2.2 **Effect of Inner (Image) Well Width on DJPD Pixels.**

The results in this section have shown the linear response of the image-cathode to the linear change in width for illuminations inside the outer well. That is for most of the illumination area of the image-pixel, not the total pixel. Only at the outer-well edges does the image-cathode respond exponentially to changes in image-well width.

The results show that the image-cathode QE response of the NPN DJPD pixel response is largely dependent on the change in image-pixel SCR AVP that occur for increases in image-well SCR volume, resulting from the increase in image-well width. This paralleling of the image-pixel SCR AVP may allow the prediction of the response resolution of a DJPD for which this AVP and configuration of doping biasing and well geometry are known in comparison to another DJPD pixel AVP– configuration set.

Furthermore, the increasing hole problem is experienced by the deeper image-well FW pixels, rising slightly with increasing image-well width. However this increase does not significantly affect the FW pixels central response in the extreme way as for the naked SJPD FW pixel. If this is a problem, the use of the BW mode is recommended, though for thinner pixels this may become a problem for BW pixels if

deep and wide image-well pixels are used. Advocating a BW mode suits the purpose of this research significantly.

6.2.3 **Effect of Image (Inner) Well Depth on DJPD Pixels.**

The results in Section 5.2.3 have shown that a change in the image-well's depth has far less effect on the QE, nQE, pQE, NQE and AVP profiles than does a change in the image-well's width (Section 5.2.2). This is due to the greater change in the latter, effecting a greater change in AVP, which has a flow-on effect to cause a greater change in the other QE and NQE response profiles.

The results have also shown that the deeper well is more resolved and the thinner well has less of a hole problem. The reason for greater resolution is the increased SCR outer boundary area for the deeper image-wells. The reason that the thinner pixel is the better choice is that there is more p-outer-well volume in which more electronic minority carriers, more mobile than holes, can be photogenerated. This will enhance the image-cathodes capture volume, resulting in a better response resolution and less of an increased hole problem inside the image-well.

The results have also shown that the BW pixel is superior to the FW pixel with regard to the hole problem. This is mainly due to the thickness of the substrate of the pixels simulated in all the DJPD investigations. Bringing the incidence of illumination closer to the image-well, by reducing the pixel's thickness, will increase the hole problem in the BW pixel. However, as has been demonstrated in the naked SJPD simulations (Figures 5.1 and 5.2), the FW pixel hole response over the image-well is always more pronounced because its illumination is always closer to the image-well, resulting in a higher image-well AVP.

7. CONCLUSION

This research has made a comparative investigation of crosstalk in BW and FW vertical SJPD and DJPD CMOS compatible pixels using a commercial 2D device simulation package, SEMICAD DEVICE^{TM} (1994). Comparison of pixel total, electron and hole quantum efficiency (QE) response and Absorption Volume data was undertaken and qualitative understanding of the processes contributing to enhanced response resolution and reduced crosstalk was arrived at.

Thus this project has investigated the effect of varying the DJPD and SJPD pixel's geometry on response resolution and crosstalk. Only for the SJPD pixel, the effect of doping, biasing and introducing highly doped pixel boundary trenches (BTI) on response resolution was also undertaken. Additionally the effect on pixel resolution of introducing a guard-ring electrode to the SJPD pixel configuration was investigated.

For SJPD, the highly doped recombination boundary trench isolation (BTI), placed either side of the pixel's well, showed considerably less pixel response resolution and hence more crosstalk than using the guard-ring electrode configuration. However the BTI-pixel's response was an improvement on the unguarded (naked) single image-electrode SJPD pixel's response. The outer junction of the DJPD pixel acts in the same way as the guard-ring electrode for the SJPD, by suppressing the pixel response away from the pixel centre.

For thicker pixels with similar geometry of outer well and substrate to the SJPD guarded pixel, the outer junction guard improves the pixel response resolution more than the electrode guard does. The lower response resolution in the guarded pixel occurs because the photocarriers generated in the substrate are still able to gain access to the image capture field from underneath the guard-ring capture field "cylinder". The DJPD guard well that encapsulates the image well prevents axial access by "free"

substrate diffusing photocarriers, and hence there can not be any significant image response for illumination outside DJPD image-pixels.

For shallower guarded and DJPD pixels their response resolutions are not significantly different, in that now axial access to the image electrode, from underneath the guard field "cylinder", for guarded pixels is also prevented, resulting in insignificant response outside the "well" (outer well in DJPD). For DJPD pixels the response resolution is more flexibly varied inside the "well" than for the guarded SJPD pixel.

Generally the FW PD pixels have better response resolution and hence crosstalk suppression than the same pixel BI, due primarily to their greater SCR AVP, resulting from the closer proximity of their photogenerated carrier-envelope to the pixel's SCR. However as FW and BW pixel AVP profiles converge, due mainly to pixel thickness attenuation, their response resolution becomes less distinguishable.

The predictive advantage of pixel AVP data for optimal pixel response resolution is evident though simulation is still the necessary final arbiter without the more costly fabricated-device testing option available.

Finally the pixels in order of generally increasing response resolution:

For thicker pixels (12 μm):

Naked SJPD < naked SJPD + BTI < guard-ring SJPD < DJPD pixel.

For shallower pixels (3 μm):

Naked SJPD < naked SJPD + BTI < guard-ring SJPD = DJPD pixel.

REFERENCES

Briaire, J., & Krisch, K. S. (2000). Principles of substrate crosstalk generation in CMOS circuits. *IEEE Transactions on Computer-Aided Design Of Integrated Circuits And Systems*, 19(6), 645 – 653.

Brouk, I., Nemirovsky, Y., Lachowicz, S., Gluszak, E. A., Hinckley, S., & Eshraghian, K. (2002). Characterisation of crosstalk between CMOS photodiodes. *Solid State Electronics*, 46, 53-56.

Fujimori, I.L., Wang, C., & Sodini, C.G. (2000) A 256 x 256 CMOS differential passive pixel imager with FPN reduction techniques. *IEEE Journal of Solid-State circuits*, 35(12), 2031-2037.

Furumiya, M., Ohkubo, H., Muramatsu, Y., Kurosawa, S., Okamoto, F., Fujimoto, Y., & Nakashiba, Y. (2001). High-sensitivity and no-crosstalk pixel technology for embedded CMOS image sensor. *IEEE Trans. El. Devices*, 48, 2221-2226.

Hinckley, S., Gluszak,E. A., & Eshraghian,K. (2000). Modeling of device structure effects in backside illuminated CMOS compatible photodiodes. *Proceedings of COMMAD 2000*, Melbourne. IEEE Press.

Hinckley, S., Jansz, P.V., Gluszak, E.A., & Eshraghian, K. (2002). Modeling of device structure effects on electrical crosstalk in back illuminated CMOS compatible photodiodes. *Proceedings of COMMAD 2002*, Melb. IEEE Press. pp. 397 – 400.

Holland, S.E., Wang, N.W., Moses W.W. (n.d.) *Development of low noise, back-side illuminated silicon photodiode arrays*. Berkeley, California: University of California, Lawrence Berkeley National Laboratories.

IOFFE (2003). Auger-recombination Processes in Semiconductor Heterostructures. [on-line]. Available WWW:http://www.ioffe.rssi.ru/SVA/NSM/Auger/model.html [2003, July 21]

Kang,I.M. (2002). *The simulation of the crosstalk between photodiodes fabricated Using the 0.18 μ m CMOS Process*. Seoul, South Korea: Seoul National University, School of Electrical Engineering : SMDL Annual Report 2002.

Lulé, T., Benthien, S., Keller, H., Mütze, F., Rieve, P., Seibel, K., Sommer, M., & Böhm, M. (2000) Sensitivity of CMOS based imagers and scaling perspectives. *IEEE Transations on Electron Devices*, 47(11), 2110 – 22

Melchior H. (1972) "Demodulation and photodetector techniques," in Laser handbook Vol. 1, Arecchi F.T., Schulz-Dubios E.O. Eds. Amsterdam: North Holland, pp725 – 835.

Mutoh, H. (2003). 3-D optical and electrical simulation for CMOS image sensors. IEEE Transactions on Electron Devices, 50(1), 19 – 25.

Nextnano3 (2003). Auger-recombination. [on-line]. Available WWW:http://www.wsi.tu-muenchen.de/nextnano3/input_parser/database/Auger-recombination.htm [21-7-03]

Reynolds A. J. (2002) Growth dependent properties of undoped and insitu doped chemically deposited CdS thin films. B.Sc. (Physical Science) Honours Thesis. Edith Cowan University.

SEMICAD DEVICE manual (1994) version 1.2 Dawn Technologies Inc Sunnyvale, CA USA. pp 285 – 288

Singh J (1994) Semiconductor devices: An introduction. McGraw-hill, Inc. New York pp 460 – 480.

Van Zeghbroek B (2002). Principles of Semiconductor Devices. [on-line].Available WWW:http://www.colorado.edu/~bart/book [2003, July 20]

APPENDIX I : RESULTS - SJPD

BI-non-BTI-twin-control-1electrode-nwell-array2&3 -633; Normalized QE and scanned QE dependence on Well and Substrate depth.

SJPD PSE SIDE RESULTS

						Outside 2nd BTI		On 2nd BTI		On PSE boundary		On 1st BTI	
		Dp subst	Dp well	Dp bti	PDC	QE @ 45	QE @ 115	QE @ 50	QE @ 110	QE @ 55	QE @ 105	QE @ 60	QE @ 100
n well dope (e/ml)	1E+17	3	0.5	0	0	0.01176	0.01183	0.02458	0.02443	0.06614	0.06554	0.2722	0.2782
p substrate dope (h/ml)	1E+15	3	1	0	2	0.01175	0.01169	0.025	0.02521	0.06676	0.06918	0.277	0.2962
reverse bias (V)	2	6	0.5	0	10	0.04583	0.0457	0.08806	0.08918	0.1706	0.1705	0.3754	0.3831
width image elec (um)	18	6	1	0	12	0.04353	0.04413	0.08738	0.08809	0.1685	0.1842	0.3918	0.3919
width subst elec (um)	2	6	2	0	14	0.04219	0.04211	0.09102	0.08968	0.1807	0.1815	0.4071	0.4076
PSE width (um)	50	6	4	0	16	0.03762	0.03906	0.0899	0.09155	0.1852	0.1885	0.4233	0.4258
Well width (um)	20	12	0.5	0	20	0.1169	0.1179	0.1944	0.1944	0.303	0.3045	0.4548	0.4625
		12	1	0	22	0.1149	0.1248	0.1991	0.1983	0.3102	0.3067	0.4649	0.4694
		12	2	0	24	0.1136	0.1196	0.2006	0.1986	0.3159	0.3184	0.4857	0.4852
		12	4	0	26	0.1052	0.1103	0.201	0.2028	0.3303	0.3321	0.5104	0.5158
		12	8	0	28	0.09043	0.08976	0.2009	0.2025	0.3464	0.3483	0.5471	0.5493

PDC = <S><W> ; substrate depth = 3 x 2^(S); well depth = 0.5 x 2^(W/2)

BI-non-BTI-twin-control-1electrode-nwell-array2&3 -633; Normalized QE and scanned QE dependence on Well and Substrate depth.

SJPD PSE CENTRAL RESULTS

				No BTI:next to SCR		No BTI : On SCR				Expected Maximum QE			Max	Normalized PSE boundary QE	
Dp subst	Dp well	Dp bti	PDC	QE @ 65	QE @ 95	QE @ 70	nQE @ 70	pQE @ 80	QE @ 90	QE @ 80	nQE @ 80	pQE @ 80	QE	BI Nz QE @ 55	BI Nz QE @ 105
3	0.5	0	0	0.5204	0.5207	0.7194	0.7194	-6.83E-07	0.7002	0.7503	0.7503	-3.54E-05	0.7571	0.087359662	0.086567164
3	1	0	2	0.5334	0.5232	0.7299	0.7301	-1.57E-04	0.7174	0.7494	0.7511	-1.71E-03	0.7569	0.088201676	0.091399128
6	0.5	0	10	0.6348	0.6375	0.8522	0.8522	2.15E-06	0.8537	0.9367	0.9367	-6.29E-06	0.9367	0.18212875	0.182021992
6	1	0	12	0.6528	0.6557	0.8671	0.8672	-4.96E-05	0.8686	0.9394	0.9398	-3.99E-04	0.9394	0.179369811	0.196082606
6	2	0	14	0.6797	0.6858	0.8899	0.8914	-1.44E-03	0.8898	0.9305	0.9418	-1.13E-02	0.9306	0.194175801	0.195035461
6	4	0	16	0.7098	0.7168	0.9145	0.9214	-6.91E-03	0.9158	0.8835	0.9422	-5.87E-02	0.9158	0.202227561	0.205830967
12	0.5	0	20	0.6303	0.6418	0.7937	0.7937	3.11E-06	0.794	0.9097	0.9097	2.64E-06	0.9097	0.333076839	0.334725734
12	1	0	22	0.6366	0.6577	0.8086	0.8086	-1.44E-06	0.8109	0.9214	0.9214	-2.15E-05	0.9214	0.336661602	0.332663035
12	2	0	24	0.6659	0.68	0.8344	0.8345	-8.74E-05	0.8339	0.9412	0.9418	-6.60E-04	0.9412	0.335635359	0.338291543
12	4	0	26	0.7113	0.7232	0.8821	0.8825	-4.24E-04	0.8847	0.9718	0.9752	-3.38E-03	0.9718	0.33988475	0.341736983
12	8	0	28	0.7829	0.7809	0.9597	0.9607	-1.01E-03	0.9622	0.9807	0.9982	-1.75E-02	0.9837	0.35213988	0.354071363

PDC = <S><W> ; substrate depth = 3 x 2^(S); well depth = 0.5 x 2^(W/2)

FI-non-BTI-twin-control-1electrode-nwell-array2&3 -633; Normalized QE and scanned QE dependence on Well and Substrate depth.

SJPD PSE SIDE RESULTS

						Outside 2nd BTI		On 2nd BTI		On PSE boundary		On 1st BTI	
		Dp subst	Dp well	Dp bti	PDC	QE @ 45	QE @ 115	QE @ 50	QE @ 110	QE @ 55	QE @ 105	QE @ 60	QE @ 100
n well dope (e/ml)	1E+17	3	0.5	0	0	0.01173	0.01173	0.0241	0.02424	0.05824	0.05817	0.2766	0.272
p substrate dope (h/ml)	1E+15	3	1	0	2	0.01175	0.01162	0.0246	0.02509	0.059	0.06132	0.2801	0.29
reverse bias (V)	2	6	0.5	0	10	0.04372	0.04392	0.07994	0.08079	0.1255	0.1244	0.3644	0.3744
width image elec (um)	18	6	1	0	12	0.04188	0.04192	0.08036	0.07907	0.126	0.1255	0.3845	0.384
width subst elec (um)	2	6	2	0	14	0.04047	0.03992	0.08192	0.08109	0.131	0.1303	0.3988	0.3959
PSE width (um)	50	6	4	0	16	0.03606	0.03738	0.08094	0.08229	0.1345	0.1369	0.4124	0.4186
Well width (um)	20	12	0.5	0	20	0.09012	0.0904	0.1411	0.1414	0.1739	0.1735	0.4215	0.4214
		12	1	0	22	0.08822	0.08796	0.1426	0.1402	0.1785	0.1763	0.4376	0.4316
		12	2	0	24	0.08197	0.08125	0.143	0.1419	0.1826	0.1816	0.4475	0.4457
		12	4	0	26	0.07347	0.07473	0.1415	0.144	0.1893	0.1913	0.4711	0.4741
		12	8	0	28	0.06465	0.0653	0.1399	0.1415	0.1966	0.1993	0.4998	0.5008

PDC = <S><W> : substrate depth = 3 x 2^(S); well depth = 0.5 x 2^(W/2)

FI-non-BTI-twin-control-1electrode-nwell-array2&3 -633; Normalized QE and scanned QE dependence on Well and Substrate depth.

SJPD PSE CENTRAL RESULTS

				No BTI:next to SCR		No BTI : On SCR				Expected Maximum QE			Max	Normalized PSE boundary QE	
Dp subst	Dp well	Dp bti	PDC	QE @ 65	QE @ 95	QE @ 70	nQE @ 70	pQE @ 70	QE @ 90	QE @ 80	nQE @ 80	pQE @ 80	QE	FI Nz QE @ 55	FI Nz QE @ 105
3	0.5	0	0	0.5209	0.5213	0.7353	0.7353	-1.08E-05	0.7265	0.7561	0.7562	-1.37E-04	0.7603	0.076601342	0.076509273
3	1	0	2	0.5298	0.5239	0.7327	0.7334	-6.20E-04	0.7321	0.7483	0.7549	-6.63E-03	0.7518	0.078478319	0.081564246
6	0.5	0	10	0.6404	0.646	0.8927	0.8927	-1.26E-05	0.8893	0.9414	0.9416	-1.39E-04	0.9414	0.133312088	0.132143616
6	1	0	12	0.658	0.6613	0.9025	0.9033	-7.54E-04	0.9009	0.933	0.9393	-6.31E-03	0.9356	0.134672937	0.134138521
6	2	0	14	0.686	0.6873	0.8997	0.9182	-1.85E-02	0.8972	0.7944	0.9408	-1.47E-01	0.8997	0.14560409	0.144826053
6	4	0	16	0.7136	0.7221	0.8698	0.9301	-6.03E-02	0.8721	0.5222	0.9407	-4.19E-01	0.8721	0.154225433	0.156977411
12	0.5	0	20	0.6763	0.6777	0.9279	0.9279	-1.26E-05	0.9259	0.9868	0.9869	-1.42E-04	0.9868	0.176226186	0.175820835
12	1	0	22	0.6883	0.6935	0.9379	0.9387	-7.79E-04	0.9393	0.984	0.9903	-6.30E-03	0.984	0.181402439	0.179166667
12	2	0	24	0.7226	0.722	0.9421	0.9606	-1.85E-02	0.9417	0.8477	0.9941	-1.46E-01	0.9421	0.193822312	0.192760853
12	4	0	26	0.7604	0.7624	0.9217	0.9813	-5.96E-02	0.9262	0.5799	0.9976	-4.18E-01	0.9262	0.204383502	0.206542863
12	8	0	28	0.7976	0.7981	0.9108	0.9948	-8.41E-02	0.9231	0.3312	0.9986	-6.67E-01	0.9231	0.212978009	0.215902936

PDC = <S><W> ; substrate depth = 3 x 2^(S); well depth = 0.5 x 2^(W/2)

APPENDIX II : RESULTS - SJPD

BI & FI total 2D SJPD pixel : Depletion layer or Space Charge Region (SCR) & non-SCR Absorption Volume Proportion (AVP) data (%) for 5 um laser over well wall (@ position 70).

		Subst depth (um)	Well depth (um)	2D BI pixel SCR AVP (%) BI over well wall 5 um beam @ 70	2D BI pixel non-SCR AVP (%) BI over well wall 5 um beam @ 70	2D BI pixel SCR AVP (%) BI over well wall 5 um beam @ 70	2D BI pixel non-SCR AVP (%) BI over well wall 5 um beam @ 70
n dope (e/ml)	1E+17	3	0.5	26.1608019	24.04500863	29.40487626	20.80093426
p dope (h/ml)	1E+15	3	1	31.69763752	18.50817301	30.31413826	19.89167227
rev. bias (V)	2	6	0.5	13.02655927	62.17882768	29.40487626	45.80051069
pixel width (um)	50	6	1	15.78358168	59.42180527	30.31413826	44.89124869
well width (um)	20	6	2	22.35877263	52.84661432	31.84433209	43.36105486
laser width (um)	5	6	4	41.12059744	34.08478951	34.01849369	41.18689326
laser centre posn.	70 um	12	0.5	3.229884964	90.62238667	29.40487626	64.44739537
		12	1	3.913478004	89.93879363	30.31413826	63.53813337
		12	2	5.543771157	88.30850048	31.84433209	62.00793954
		12	4	10.19569302	83.65657862	34.01849369	59.83377795
		12	8	29.3872456	64.46502604	36.24245309	57.60981855

BI & FI total 2D SJPD pixel : SCR & non-SCR region AVP data (%) for 5 um laser centred on the pixel's well (@ position 80).

		Subst depth (um)	Well depth (um)	2D BI pixel SCR AVP (%) BI over well centre 5 um beam @ 80	2D BI pixel non-SCR AVP (%) BI over well centre 5 um beam @ 80	2D FI pixel SCR AVP (%) FI over well centre 5 um beam @ 80	2D FI pixel non-SCR AVP (%) FI over well centre 5 um beam @ 80
n dope (e/ml)	1E+17	3	0.5	30.60940336	19.59640717	31.71524004	18.49057049
p dope (h/ml)	1E+15	3	1	34.38152108	15.82428945	28.2356494	21.97016113
rev. bias (V)	2	6	0.5	15.2417043	59.96368265	31.71524004	43.49014691
pixel width (um)	50	6	1	17.11999975	58.0853872	28.2356494	46.96973755
well width (um)	20	6	2	21.59952488	53.60586207	22.37985851	52.82552844
laser width (um)	5	6	4	34.38152108	40.82386587	14.05971276	61.14567419
laser centre posn.	80 um	12	0.5	3.779121604	90.07315003	31.71524004	62.13703159
		12	1	4.244837692	89.60743394	28.2356494	65.61662223
		12	2	5.355518614	88.49675302	22.37985851	71.47241313
		12	4	8.524765112	85.32750652	14.05971276	79.79255887
		12	8	21.59952488	72.25274676	5.548999319	88.30327232

BI & FI total 2D SJPD pixel : SCR & non-SCR AVP data (%) for 50 um beam centred on the pixel (@ position 80).

		Subst depth (um)	Well depth (um)	Total 2D BI pixel SCR AVP (%) 50 um beam @ 80 across pixel	Total 2D BI pixel non-SCR AVP (%) 50 um beam @ 80 across pixel	Total 2D FI pixel SCR AVP (%) 50 um beam @ 80 across pixel	Total 2D FI pixel non-SCR AVP (%) 50 um beam @ 80 across pixel
n dope (e/ml)	1E+17	3	0.5	14.41498139	35.79082914	15.39554727	34.81026326
p dope (h/ml)	1E+15	3	1	16.65398383	33.5518267	14.53352247	35.67228806
rev. bias (V)	2	6	0.5	7.177823144	68.0275638	15.39554727	59.80983968
pixel width (um)	50	6	1	8.292716261	66.91267069	14.53352247	60.67186448
well width (um)	20	6	2	10.95161199	64.25377496	13.08282397	62.12256298
laser width (um)	50	6	4	18.53857581	56.66681114	11.02161257	64.18377438
laser centre posn.	80 um	12	0.5	1.779713474	92.07255816	15.39554727	78.45672437
		12	1	2.056146908	91.79612473	14.53352247	79.31874916
		12	2	2.715409816	91.13686182	13.08282397	80.76944766
		12	4	4.596568137	89.2557035	11.02161257	82.83065907
		12	8	12.35730658	81.49496505	8.913190414	84.93908122

BI & FI total 3D SJPD pixel : SCR & non-SCR AVP data for 50 x 50 um beam centred on the 50 um pitch pixel's well.

		Subst depth (um)	Well depth (um)	Total 3D BI pixel SCR AVP (%) 50 x 50 um beam across pixel	Total 3D BI pixel non-SCR AVP (%) 50 x 50 um beam across pixel	Total 3D FI pixel SCR AVP (%) 50 x 50 um beam across pixel	Total 3D FI pixel non-SCR AVP (%) 50 x 50 um beam across pixel
n dope (e/ml)	1E+17	3	0.5	6.765878458	43.43993207	7.30203492	42.90377561
p dope (h/ml)	1E+15	3	1	7.996579678	42.20923085	7.210560685	42.99524984
rev. bias (V)	2	6	0.5	3.369014339	71.83637261	7.30203492	67.90335203
pixel pitch (um x um)	50	6	1	3.981832036	71.22355491	7.210560685	67.99482626
well pitch (um x um)	20	6	2	5.44333389	69.76205306	7.056619014	68.14876793
laser pitch (um x um)	50	6	4	9.61362217	65.59176478	6.837892431	68.36749452
laser centre posn.	80 um	12	0.5	0.835334069	93.01693757	7.30203492	86.55023672
		12	1	0.987279846	92.86499179	7.210560685	86.64171095
		12	2	1.349653575	92.50261806	7.056619014	86.79565262
		12	4	2.383660417	91.46861122	6.837892431	87.01437921
		12	8	6.649466522	87.20280511	6.614156053	87.23811558

BI-BTI-twin-1electrode-nwell-array2&3 -633; Normalized QE and scanned QE dependence on BTI, Well and Substrate depth.

reverse bias	Doping		Elec. width (um)	
	p-substl	n-well	p-substl	n-well
2 volts	1E+15	1E+17	2	6.4

bti dope	Depth (um)				Outside 2nd BTI		On 2nd BTI		On PSE boundary		On 1st BTI		No BTI : next to SCR		No BTI : On SCR				Expect Max, plus e⁻ and h⁺ QEs.			Maximum	PSE Boundary		% Nz QE below FI PSE	
(h/ml)	subst.	well	bti	PDC	BI PSE QE @ 45	BI PSE QE @ 115	QE @ 50	QE @ 110	QE @ 55	QE @ 105	QE @ 60	QE @ 100	QE @ 65	QE @ 95	QE @ 70	nQE @70	pQE @ 70	QE @ 90	QE @ 80	nQE @ 80	pQE @ 80	PSE QE	Nz QE @ 55	Nz QE @ 105	% @ 55	% @ 105
1E+15	3	0.5	0	0	1.176E-02	1.183E-02	0.02458	0.02443	0.06614	0.06554	0.2722	0.2782	0.5204	0.5207	0.7194	0.7194	-6.83E-07	0.7002	0.7503	0.7503	-3.54E-05	0.7571	8.736E-02	8.657E-02	-14.045	-13.146
1E+19	3	0.5	0.5	0.1	7.752E-03	7.719E-03	0.01676	0.01674	0.05286	0.05273	0.2710	0.2680	0.5310	0.5306	0.7197	0.7197	3.34E-06	0.7135	0.7410	0.7410	3.34E-06	0.7490	7.057E-02	7.040E-02	-11.196	-13.517
1E+19	3	0.5	1	0.2	6.678E-03	6.733E-03	0.01540	0.01539	0.04955	0.04924	0.2791	0.2803	0.5494	0.5482	0.7215	0.7215	3.34E-06	0.7144	0.7428	0.7428	3.34E-06	0.7517	6.592E-02	6.550E-02	-14.705	-13.042
1E+19	3	0.5	2	0.3	3.515E-03	3.499E-03	0.01054	0.01048	0.03598	0.03569	0.3086	0.3095	0.6098	0.6104	0.7324	0.7324	3.34E-06	0.7162	0.7406	0.7406	3.34E-06	0.7421	4.848E-02	4.809E-02	-17.952	-16.433
1E+15	3	1	0	2	1.175E-02	1.169E-02	0.02500	0.02521	0.06676	0.06918	0.2770	0.2962	0.5334	0.5232	0.7299	0.7301	-1.57E-04	0.7174	0.7494	0.7511	-1.71E-03	0.7569	8.820E-02	9.140E-02	-12.390	-12.058
1E+19	3	1	1	2.2	6.134E-03	6.089E-03	0.01460	0.01455	0.04919	0.04799	0.2824	0.2814	0.5591	0.5564	0.7272	0.7272	2.20E-06	0.7205	0.7350	0.7350	1.87E-06	0.7433	6.618E-02	6.456E-02	-11.430	-9.4049
1E+19	3	1	2	2.3	3.334E-03	3.309E-03	0.01048	0.01040	0.03585	0.03641	0.3124	0.3156	0.6195	0.6155	0.7332	0.7332	2.20E-06	0.7243	0.7357	0.7357	1.87E-06	0.7396	4.847E-02	4.923E-02	-18.014	-15.447
1E+15	6	0.5	0	10	4.583E-02	4.570E-02	0.08806	0.08918	0.17060	0.17050	0.3754	0.3831	0.6348	0.6375	0.8522	0.8522	2.15E-06	0.8537	0.9367	0.9367	-6.29E-06	0.9367	1.821E-01	1.820E-01	-36.618	-37.746
1E+19	6	0.5	0.5	10.1	3.802E-02	3.782E-02	0.07445	0.07494	0.15270	0.15270	0.3727	0.3731	0.6402	0.6370	0.8536	0.8536	3.34E-06	0.8532	0.9327	0.9327	3.34E-06	0.9327	1.637E-01	1.637E-01	-41.152	-39.109
1E+19	6	0.5	1	10.2	3.730E-02	3.746E-02	0.07400	0.07456	0.15380	0.15280	0.3781	0.3819	0.6487	0.6504	0.8574	0.8574	3.37E-06	0.8669	0.9414	0.9414	3.37E-06	0.9414	1.634E-01	1.623E-01	-45.762	-42.933
1E+19	6	0.5	2	10.3	3.445E-02	3.400E-02	0.07048	0.07048	0.14750	0.14630	0.3918	0.3914	0.6745	0.6720	0.8636	0.8636	3.34E-06	0.8683	0.9403	0.9403	3.34E-06	0.9403	1.569E-01	1.556E-01	-50.916	-49.597
1E+19	6	0.5	4	10.4	2.005E-02	2.026E-02	0.05208	0.05246	0.11690	0.11680	0.4220	0.4209	0.7523	0.7509	0.8902	0.8902	3.36E-06	0.8931	0.9358	0.9358	3.36E-06	0.9376	1.247E-01	1.246E-01	-64.200	-62.500
1E+15	6	1	0	12	4.353E-02	4.413E-02	0.08738	0.08809	0.16850	0.18420	0.3918	0.3919	0.6528	0.6557	0.8671	0.8672	-4.96E-05	0.8686	0.9394	0.9398	-3.99E-04	0.9394	1.794E-01	1.961E-01	-33.189	-46.179
1E+19	6	1	1	12.2	3.558E-02	3.546E-02	0.07281	0.07307	0.15480	0.15220	0.3838	0.3838	0.6615	0.6599	0.8680	0.8680	2.21E-06	0.8671	0.9354	0.9354	2.13E-06	0.9354	1.655E-01	1.627E-01	-38.100	-37.245
1E+19	6	1	2	12.3	3.287E-02	3.307E-02	0.07007	0.07022	0.14890	0.14770	0.3961	0.3979	0.6852	0.6830	0.8856	0.8856	2.25E-06	0.8771	0.9410	0.9410	2.19E-06	0.9410	1.582E-01	1.570E-01	-46.364	-44.073
1E+19	6	1	4	12.4	1.989E-02	1.981E-02	0.05356	0.05334	0.11740	0.12030	0.4258	0.4225	0.7605	0.7581	0.9045	0.9045	2.21E-06	0.8980	0.9357	0.9357	2.13E-06	0.9400	1.249E-01	1.280E-01	-54.303	-56.312
1E+15	6	2	0	14	4.219E-02	4.211E-02	0.09102	0.08968	0.18070	0.18150	0.4071	0.4076	0.6797	0.6858	0.8899	0.8914	-1.44E-03	0.8898	0.9305	0.9418	-1.13E-02	0.9306	1.942E-01	1.950E-01	-33.359	-34.669
1E+19	6	2	2	14.3	3.091E-02	3.064E-02	0.07039	0.07012	0.16090	0.15140	0.4046	0.4107	0.7084	0.7115	0.8940	0.8942	-1.44E-04	0.8955	0.9314	0.9331	-1.77E-03	0.9314	1.728E-01	1.626E-01	-43.975	-38.999
1E+19	6	2	4	14.4	1.828E-02	1.750E-02	0.05296	0.05097	0.11820	0.11780	0.4382	0.4345	0.7780	0.7764	0.9077	0.9078	-1.46E-04	0.9111	0.9314	0.9331	-1.75E-03	0.9343	1.265E-01	1.261E-01	-53.011	-53.353
1E+15	6	4	0	16	3.762E-02	3.906E-02	0.08990	0.09155	0.18520	0.18850	0.4233	0.4258	0.7098	0.7168	0.9145	0.9214	-6.91E-03	0.9158	0.8835	0.9422	-5.87E-02	0.9158	2.022E-01	2.058E-01	-31.125	-31.121
1E+19	6	4	4	16.4	1.566E-02	1.581E-02	0.05097	0.05166	0.12130	0.12140	0.4462	0.4461	0.7993	0.7973	0.9195	0.9228	-3.24E-03	0.9232	0.8951	0.9005	-5.36E-03	0.9232	1.314E-01	1.315E-01	-50.808	-53.696
1E+15	12	0.5	0	20	1.169E-01	1.179E-01	0.19440	0.19440	0.30300	0.30450	0.4548	0.4625	0.6303	0.6418	0.7937	0.7937	3.11E-06	0.7940	0.9097	0.9097	2.64E-06	0.9097	3.331E-01	3.347E-01	-89.005	-90.379
1E+19	12	0.5	0.5	20.1	1.088E-01	1.100E-01	0.18370	0.18330	0.29030	0.29250	0.4521	0.4516	0.6351	0.6379	0.7909	0.7909	3.34E-06	0.7929	0.9084	0.9084	3.34E-06	0.9084	3.196E-01	3.220E-01	-99.405	-99.904
1E+19	12	0.5	1	20.2	1.109E-01	1.120E-01	0.18360	0.18420	0.28860	0.29790	0.4578	0.4561	0.6447	0.6459	0.7961	0.7961	3.37E-06	0.7990	0.9140	0.9140	3.37E-06	0.9140	3.158E-01	3.259E-01	-96.380	-103.74
1E+19	12	0.5	2	20.3	1.081E-01	1.131E-01	0.18410	0.18630	0.29190	0.29640	0.4606	0.4629	0.6493	0.6480	0.8058	0.8058	3.34E-06	0.8024	0.9136	0.9136	3.34E-06	0.9136	3.195E-01	3.244E-01	-111.73	-114.85
1E+19	12	0.5	4	20.4	1.056E-01	1.059E-01	0.18040	0.17910	0.30010	0.29360	0.4803	0.4763	0.6719	0.6749	0.8214	0.8214	3.34E-06	0.8202	0.9257	0.9257	3.34E-06	0.9257	3.242E-01	3.172E-01	-143.39	-139.57
1E+19	12	0.5	8	20.5	7.231E-02	7.187E-02	0.14410	0.14460	0.25720	0.25630	0.5023	0.5039	0.7546	0.7532	0.8733	0.8733	3.36E-06	0.8730	0.9466	0.9466	3.36E-06	0.9466	2.717E-01	2.708E-01	-188.91	-187.41
1E+15	12	1	0	22	1.149E-01	1.248E-01	0.19910	0.19830	0.31020	0.30670	0.4649	0.4694	0.6366	0.6577	0.8086	0.8086	-1.44E-06	0.8109	0.9214	0.9214	-2.15E-05	0.9214	3.367E-01	3.329E-01	-85.588	-85.784
1E+19	12	1	1	22.2	1.083E-01	1.086E-01	0.18310	0.18780	0.29290	0.29720	0.4495	0.4608	0.6509	0.6498	0.8048	0.8048	2.21E-06	0.8076	0.9200	0.9200	2.20E-06	0.9200	3.184E-01	3.230E-01	-90.790	-94.771
1E+19	12	1	2	22.3	1.101E-01	1.109E-01	0.18540	0.18180	0.30370	0.29550	0.4748	0.4681	0.6527	0.6580	0.8013	0.8013	2.25E-06	0.8155	0.9225	0.9225	2.25E-06	0.9225	3.292E-01	3.203E-01	-104.82	-100.17
1E+19	12	1	4	22.4	1.034E-01	1.054E-01	0.17880	0.17980	0.30030	0.29520	0.4832	0.4832	0.6791	0.6827	0.8261	0.8261	2.21E-06	0.8330	0.9313	0.9313	2.21E-06	0.9313	3.225E-01	3.170E-01	-132.84	-128.05
1E+19	12	1	8	22.5	6.982E-02	7.065E-02	0.14200	0.14430	0.25650	0.25940	0.5045	0.5050	0.7601	0.7595	0.8794	0.8794	2.28E-06	0.8794	0.9522	0.9522	2.27E-06	0.9522	2.694E-01	2.724E-01	-179.33	-180.58
1E+15	12	2	0	24	1.136E-01	1.196E-01	0.20060	0.19880	0.31590	0.31840	0.4857	0.4852	0.6659	0.6800	0.8344	0.8345	-8.74E-05	0.8339	0.9412	0.9418	-6.60E-04	0.9412	3.356E-01	3.383E-01	-73.167	-75.498
1E+19	12	2	2	24.3	1.068E-01	1.092E-01	0.18570	0.18970	0.30380	0.30710	0.4803	0.4856	0.6793	0.6829	0.8399	0.8399	-7.91E-06	0.8409	0.9427	0.9428	-1.05E-04	0.9427	3.223E-01	3.258E-01	-91.688	-96.407
1E+19	12	2	4	24.4	9.983E-02	9.962E-02	0.18060	0.18030	0.30280	0.30100	0.4953	0.4973	0.7054	0.7043	0.8525	0.8525	-8.38E-06	0.8537	0.9486	0.9487	-9.13E-05	0.9486	3.192E-01	3.173E-01	-121.88	-119.15
1E+15	12	4	0	26	1.052E-01	1.103E-01	0.20100	0.20280	0.33030	0.33210	0.5104	0.5158	0.7113	0.7232	0.8821	0.8825	-4.24E-04	0.8847	0.9718	0.9752	-3.38E-03	0.9718	3.399E-01	3.417E-01	-66.30	-65.46
1E+19	12	4	4	26.4	9.357E-02	9.219E-02	0.18080	0.17990	0.31400	0.31100	0.5207	0.5211	0.7424	0.7401	0.8946	0.8948	-2.20E-04	0.8949	0.9747	0.9750	-3.06E-04	0.9747	3.222E-01	3.191E-01	-108.46	-105.38

PDC = <S><W>.<B>; Substrate depth = 3 x 2^(S); Well depth = 0.5 x 2^(W/2); BTI depth = 0.25 x 2^(B); if B = 0 then BTI depth = 0.

BI-BTI-twin-1electrode-nwell-array2&3 -633; Normalized QE and scanned QE dependence on BTI, Well and Substrate depth.

For illumination positions in the neighbouring PSE to just before the central PSE well wall.

reverse bias	Doping		Elec. width (um)	
	p-substr	n-well	p-substr	n-well
2 volts	1E+15	1E+17	2	6.4

bti dope	Depth (um)				Outside 2nd BTI				On 2nd BTI				On PSE boundary				On 1st BTI				No BTI ; next to SCR			
(h/ml)	subst.	well	bti	PDC	QE @ 45	nQE @ 45	pQE @ 45	QE @ 115	QE @ 50	nQE @ 50	pQE @ 50	QE @ 110	QE @ 55	nQE @ 55	pQE @ 55	QE @ 105	QE @ 60	nQE @ 60	pQE @ 60	QE @ 100	QE @ 65	nQE @ 65	pQE @ 65	QE @ 95
1E+15	3	0.5	0	0	1.176E-02	1.176E-02	3.161E-06	1.183E-02	0.02458	0.02457	3.161E-06	0.02443	0.06614	0.06613	3.161E-06	0.06554	0.2722	0.2722	3.161E-06	0.2782	0.5204	0.5204	3.161E-06	0.5207
1E+19	3	0.5	0.5	0.1	7.752E-03	7.748E-03	3.344E-06	7.719E-03	0.01676	0.01676	3.344E-06	0.01674	0.05286	0.05286	3.344E-06	0.05273	0.2710	0.2710	3.344E-06	0.2680	0.5310	0.5310	3.344E-06	0.5306
1E+19	3	0.5	1	0.2	6.678E-03	6.674E-03	3.343E-06	6.733E-03	0.01540	0.01540	3.343E-06	0.01539	0.04955	0.04955	3.343E-06	0.04924	0.2791	0.2791	3.343E-06	0.2803	0.5494	0.5494	3.343E-06	0.5482
1E+19	3	0.5	2	0.3	3.515E-03	3.512E-03	3.338E-06	3.499E-03	0.01054	0.01053	3.338E-06	0.01048	0.03598	0.03597	3.338E-06	0.03569	0.3086	0.3086	3.338E-06	0.3095	0.6098	0.6098	3.338E-06	0.6104
1E+15	3	1	0	2	1.175E-02	1.175E-02	1.860E-06	1.169E-02	0.02500	0.02499	1.860E-06	0.02521	0.06676	0.06676	1.860E-06	0.06918	0.2770	0.2769	1.859E-06	0.2962	0.5334	0.5334	1.859E-06	0.5232
1E+19	3	1	1	2.2	6.134E-03	6.132E-03	2.212E-06	6.089E-03	0.01460	0.01459	2.212E-06	0.01455	0.04919	0.04919	2.212E-06	0.04799	0.2824	0.2824	2.211E-06	0.2814	0.5591	0.5591	2.211E-06	0.5564
1E+19	3	1	2	2.3	3.334E-03	3.331E-03	2.207E-06	3.309E-03	0.01048	0.01048	2.207E-06	0.01040	0.03585	0.03585	2.207E-06	0.03641	0.3124	0.3124	2.207E-06	0.3156	0.6195	0.6195	2.207E-06	0.6155
1E+15	6	0.5	0	10	4.583E-02	4.582E-02	3.171E-06	4.570E-02	0.08806	0.08806	3.171E-06	0.08918	0.17060	0.17060	3.171E-06	0.17050	0.3754	0.3754	3.171E-06	0.3831	0.6348	0.6348	3.171E-06	0.6375
1E+19	6	0.5	0.5	10.1	3.802E-02	3.802E-02	3.338E-06	3.782E-02	0.07445	0.07445	3.338E-06	0.07494	0.15270	0.15270	3.338E-06	0.15270	0.3727	0.3727	3.338E-06	0.3731	0.6402	0.6402	3.338E-06	0.6370
1E+19	6	0.5	1	10.2	3.730E-02	3.729E-02	3.365E-06	3.746E-02	0.07400	0.07400	3.365E-06	0.07456	0.15380	0.15380	3.365E-06	0.15280	0.3781	0.3781	3.365E-06	0.3819	0.6487	0.6487	3.365E-06	0.6504
1E+19	6	0.5	2	10.3	3.445E-02	3.445E-02	3.340E-06	3.400E-02	0.07048	0.07048	3.340E-06	0.07048	0.14750	0.14750	3.340E-06	0.14630	0.3918	0.3918	3.340E-06	0.3914	0.6745	0.6745	3.339E-06	0.6720
1E+19	6	0.5	4	10.4	2.005E-02	2.004E-02	3.356E-06	2.026E-02	0.05208	0.05208	3.356E-06	0.05246	0.11690	0.11690	3.356E-06	0.11680	0.4220	0.4220	3.356E-06	0.4209	0.7523	0.7523	3.356E-06	0.7509
1E+15	6	1	0	12	4.353E-02	4.353E-02	1.866E-06	4.413E-02	0.08738	0.08738	1.866E-06	0.08809	0.16850	0.16850	1.866E-06	0.18420	0.3918	0.3918	1.866E-06	0.3919	0.6528	0.6528	1.866E-06	0.6557
1E+19	6	1	1	12.2	3.558E-02	3.557E-02	2.208E-06	3.546E-02	0.07281	0.07280	2.208E-06	0.07307	0.15480	0.15480	2.208E-06	0.15220	0.3838	0.3838	2.208E-06	0.3838	0.6615	0.6615	2.208E-06	0.6599
1E+19	6	1	2	12.3	3.287E-02	3.287E-02	2.248E-06	3.307E-02	0.07007	0.07007	2.248E-06	0.07022	0.14890	0.14890	2.248E-06	0.14770	0.3961	0.3961	2.248E-06	0.3979	0.6852	0.6852	2.247E-06	0.6830
1E+19	6	1	4	12.4	1.989E-02	1.988E-02	2.209E-06	1.981E-02	0.05356	0.05356	2.209E-06	0.05334	0.11740	0.11740	2.209E-06	0.12030	0.4258	0.4258	2.209E-06	0.4225	0.7605	0.7605	2.209E-06	0.7581
1E+15	6	2	0	14	4.219E-02	4.219E-02	2.961E-07	4.211E-02	0.09102	0.09102	2.961E-07	0.08968	0.18070	0.18070	2.960E-07	0.18150	0.4071	0.4071	2.960E-07	0.4076	0.6797	0.6797	2.960E-07	0.6858
1E+19	6	2	2	14.3	3.091E-02	3.091E-02	3.724E-07	3.064E-02	0.07039	0.07039	3.724E-07	0.07012	0.16090	0.16090	3.724E-07	0.15140	0.4046	0.4046	3.724E-07	0.4107	0.7084	0.7084	3.724E-07	0.7115
1E+19	6	2	4	14.4	1.828E-02	1.828E-02	3.745E-07	1.750E-02	0.05296	0.05296	3.745E-07	0.05097	0.11820	0.11820	3.745E-07	0.11780	0.4382	0.4382	3.744E-07	0.4345	0.7780	0.7780	3.744E-07	0.7764
1E+15	6	4	0	16	3.762E-02	3.762E-02	1.076E-07	3.906E-02	0.08990	0.08990	1.076E-07	0.09155	0.18520	0.18520	1.076E-07	0.18850	0.4233	0.4233	1.076E-07	0.4258	0.7098	0.7098	1.076E-07	0.7168
1E+19	6	4	4	16.4	1.566E-02	1.566E-02	1.574E-07	1.581E-02	0.05097	0.05097	1.574E-07	0.05166	0.12130	0.12130	1.574E-07	0.12140	0.4462	0.4462	1.574E-07	0.4461	0.7993	0.7993	1.574E-07	0.7973
1E+15	12	0.5	0	20	1.169E-01	1.169E-01	3.171E-06	1.179E-01	0.19440	0.19440	3.171E-06	0.19440	0.30300	0.30300	3.171E-06	0.30450	0.4548	0.4548	3.171E-06	0.4625	0.6303	0.6303	3.171E-06	0.6418
1E+19	12	0.5	0.5	20.1	1.088E-01	1.088E-01	3.337E-06	1.100E-01	0.18370	0.18370	3.337E-06	0.18330	0.29030	0.29030	3.337E-06	0.29250	0.4521	0.4521	3.337E-06	0.4516	0.6351	0.6351	3.337E-06	0.6379
1E+19	12	0.5	1	20.2	1.109E-01	1.109E-01	3.372E-06	1.120E-01	0.18360	0.18360	3.372E-06	0.18420	0.28860	0.28860	3.372E-06	0.29790	0.4578	0.4578	3.372E-06	0.4561	0.6447	0.6447	3.372E-06	0.6459
1E+19	12	0.5	2	20.3	1.081E-01	1.081E-01	3.338E-06	1.131E-01	0.18410	0.18410	3.338E-06	0.18630	0.29190	0.29190	3.338E-06	0.29640	0.4606	0.4606	3.338E-06	0.4629	0.6493	0.6493	3.337E-06	0.6480
1E+19	12	0.5	4	20.4	1.056E-01	1.056E-01	3.344E-06	1.059E-01	0.18040	0.18040	3.344E-06	0.17910	0.30010	0.30010	3.344E-06	0.29360	0.4803	0.4803	3.344E-06	0.4763	0.6719	0.6719	3.343E-06	0.6749
1E+19	12	0.5	8	20.5	7.231E-02	7.230E-02	3.356E-06	7.187E-02	0.14410	0.14410	3.356E-06	0.14460	0.25720	0.25720	3.356E-06	0.25630	0.5023	0.5023	3.356E-06	0.5039	0.7546	0.7546	3.356E-06	0.7532
1E+15	12	1	0	22	1.149E-01	1.149E-01	1.866E-06	1.248E-01	0.19910	0.19910	1.866E-06	0.19830	0.31020	0.31020	1.866E-06	0.30670	0.4649	0.4649	1.866E-06	0.4694	0.6366	0.6366	1.866E-06	0.6577
1E+19	12	1	1	22.2	1.083E-01	1.083E-01	2.208E-06	1.086E-01	0.18310	0.18310	2.208E-06	0.18780	0.29290	0.29290	2.208E-06	0.29720	0.4495	0.4495	2.208E-06	0.4608	0.6509	0.6509	2.208E-06	0.6498
1E+19	12	1	2	22.3	1.101E-01	1.101E-01	2.252E-06	1.109E-01	0.18540	0.18540	2.252E-06	0.18180	0.30370	0.30370	2.252E-06	0.29550	0.4748	0.4748	2.252E-06	0.4681	0.6527	0.6527	2.252E-06	0.6580
1E+19	12	1	4	22.4	1.034E-01	1.034E-01	2.210E-06	1.054E-01	0.17880	0.17880	2.210E-06	0.17980	0.30030	0.30030	2.210E-06	0.29520	0.4832	0.4832	2.210E-06	0.4832	0.6791	0.6791	2.210E-06	0.6827
1E+19	12	1	8	22.5	6.982E-02	6.982E-02	2.276E-06	7.065E-02	0.14200	0.14200	2.276E-06	0.14430	0.25650	0.25650	2.276E-06	0.25940	0.5045	0.5045	2.276E-06	0.5050	0.7601	0.7601	2.276E-06	0.7595
1E+15	12	2	0	24	1.136E-01	1.136E-01	2.960E-07	1.196E-01	0.20060	0.20060	2.960E-07	0.19880	0.31590	0.31590	2.960E-07	0.31840	0.4857	0.4857	2.960E-07	0.4852	0.6659	0.6659	2.960E-07	0.6800
1E+19	12	2	2	24.3	1.068E-01	1.068E-01	3.752E-07	1.092E-01	0.18570	0.18570	3.752E-07	0.18970	0.30380	0.30380	3.752E-07	0.30710	0.4803	0.4803	3.752E-07	0.4856	0.6793	0.6793	3.752E-07	0.6829
1E+19	12	2	4	24.4	9.983E-02	9.983E-02	3.767E-07	9.962E-02	0.18060	0.18060	3.767E-07	0.18030	0.30280	0.30280	3.767E-07	0.30100	0.4953	0.4953	3.767E-07	0.4973	0.7054	0.7054	3.767E-07	0.7043
1E+15	12	4	0	26	1.052E-01	1.052E-01	1.089E-07	1.103E-01	0.20100	0.20100	1.089E-07	0.20280	0.33030	0.33030	1.089E-07	0.33210	0.5104	0.5104	1.089E-07	0.5158	0.7113	0.7113	1.089E-07	0.7232
1E+19	12	4	4	26.4	9.357E-02	9.357E-02	1.451E-07	9.219E-02	0.18080	0.18080	1.451E-07	0.17990	0.31400	0.31400	1.451E-07	0.31100	0.5207	0.5207	1.451E-07	0.5211	0.7424	0.7424	1.451E-07	0.7401

PDC = <S><W>.<B>; Substrate depth = 3 x 2^(S); Well depth = 0.5 x 2^(W/2); BTI depth = 0.25 x 2^(B); if B = 0 then BTI depth = 0.

FI-BTI-twin-1electrode-nwell-array2&3 -633; Normalized QE and scanned QE dependence on BTI, Well and Substrate depth.

reverse	Doping		Elec. width (um)	
bias	p-subst	n-well	p-subst	n-well
2 volts	1E+15	1E+17	2	6.4

bti dope	Depth (um)				Outside 2nd BTI		On 2nd BTI		On PSE boundary		On 1st BTI		No BTI : next to SCR		No BTI : On SCR				Expect Maximum, plus e⁻ and h⁺ QEs.			Maximum	PSE Boundary		% Nz QE below Bti PSE	
(h/ml)	subst.	well	bti	PDC	QE @ 45	QE @ 115	QE @ 50	QE @ 110	QE @ 55	QE @ 105	QE @ 60	QE @ 100	QE @ 65	QE @ 95	QE @ 70	nQE @70	pQE @ 70	QE @ 90	QE @ 80	nQE @ 80	pQE @ 80	PSE QE	Nz QE @ 55	Nz QE @105	% @ 55	% @ 105
1E+15	3	0.5	0	0	1.17E-02	1.17E-02	0.02410	0.02424	0.05824	0.05817	0.2766	0.2720	0.5209	0.5213	0.7353	0.7353	-1.08E-05	0.7265	0.7561	0.7562	-1.37E-04	0.7603	7.66E-02	7.65E-02	89.791	89.803
1E+19	3	0.5	0.5	0.1	7.75E-03	7.70E-03	0.01641	0.01639	0.04769	0.04660	0.2695	0.2708	0.5313	0.5304	0.7370	0.7370	3.34E-06	0.7216	0.7453	0.7453	3.34E-06	0.7514	6.35E-02	6.20E-02	91.435	91.631
1E+19	3	0.5	1	0.2	6.70E-03	6.65E-03	0.01501	0.01503	0.04306	0.04342	0.2784	0.2775	0.5493	0.5511	0.7385	0.7385	3.34E-06	0.7252	0.7443	0.7443	3.34E-06	0.7493	5.75E-02	5.79E-02	92.263	92.199
1E+19	3	0.5	2	0.3	3.50E-03	3.46E-03	0.01023	0.01014	0.03073	0.03088	0.3101	0.3079	0.6170	0.6124	0.7476	0.7475	3.34E-06	0.7322	0.7450	0.7450	3.34E-06	0.7476	4.11E-02	4.13E-02	94.45	94.423
1E+15	3	1	0	2	1.18E-02	1.16E-02	0.02460	0.02509	0.05900	0.06132	0.2801	0.2900	0.5298	0.5239	0.7327	0.7334	-6.20E-04	0.7321	0.7483	0.7549	-6.63E-03	0.7518	7.85E-02	8.16E-02	89.528	89.141
1E+19	3	1	1	2.2	6.13E-03	6.07E-03	0.01419	0.01418	0.04418	0.04390	0.2816	0.2815	0.5602	0.5597	0.7410	0.7410	2.19E-06	0.7288	0.7387	0.7387	1.14E-06	0.7439	5.94E-02	5.90E-02	91.92	91.971
1E+19	3	1	2	2.3	3.31E-03	3.26E-03	0.01018	0.01001	0.03062	0.03179	0.3126	0.3122	0.6251	0.6217	0.7455	0.7455	2.18E-06	0.7330	0.7378	0.7378	1.14E-06	0.7455	4.11E-02	4.26E-02	94.417	94.204
1E+15	6	0.5	0	10	4.37E-02	4.39E-02	0.07994	0.08079	0.12550	0.12440	0.3644	0.3744	0.6404	0.6460	0.8927	0.8927	-1.26E-05	0.8893	0.9414	0.9416	-1.39E-04	0.9414	1.33E-01	1.32E-01	85.768	85.893
1E+19	6	0.5	0.5	10.1	3.64E-02	3.62E-02	0.06612	0.06600	0.10890	0.11050	0.3640	0.3659	0.6481	0.6465	0.8977	0.8977	3.34E-06	0.8882	0.9389	0.9389	3.34E-06	0.9389	1.16E-01	1.18E-01	87.564	87.382
1E+19	6	0.5	1	10.2	3.55E-02	3.55E-02	0.06517	0.06577	0.10640	0.10780	0.3697	0.3764	0.6604	0.6608	0.9005	0.9005	3.37E-06	0.8991	0.9386	0.9386	3.36E-06	0.9493	1.12E-01	1.14E-01	88.094	87.937
1E+19	6	0.5	2	10.3	3.19E-02	3.17E-02	0.06084	0.06064	0.09836	0.09842	0.3816	0.3819	0.6885	0.6913	0.9043	0.9043	3.34E-06	0.9000	0.9393	0.9393	3.34E-06	0.9463	1.04E-01	1.04E-01	88.946	88.939
1E+19	6	0.5	4	10.4	1.77E-02	1.77E-02	0.04269	0.04277	0.07190	0.07259	0.4131	0.4137	0.7788	0.7741	0.9194	0.9194	3.36E-06	0.9119	0.9395	0.9395	3.35E-06	0.9469	7.59E-02	7.67E-02	91.886	91.808
1E+15	6	1	0	12	4.19E-02	4.19E-02	0.08036	0.07907	0.12600	0.12550	0.3845	0.3840	0.6580	0.6613	0.9025	0.9033	-7.54E-04	0.9009	0.9330	0.9393	-6.31E-03	0.9356	1.35E-01	1.34E-01	85.664	85.727
1E+19	6	1	1	12.2	3.37E-02	3.34E-02	0.06439	0.06400	0.11250	0.11130	0.3747	0.3762	0.6736	0.6725	0.9073	0.9073	2.18E-06	0.8997	0.9361	0.9361	1.22E-06	0.9388	1.20E-01	1.19E-01	87.189	87.326
1E+19	6	1	2	12.3	3.04E-02	3.02E-02	0.06046	0.06005	0.10370	0.10450	0.3870	0.3866	0.7060	0.7033	0.9114	0.9114	2.23E-06	0.9041	0.9387	0.9387	1.51E-06	0.9592	1.08E-01	1.09E-01	88.511	88.422
1E+19	6	1	4	12.4	1.75E-02	1.72E-02	0.04318	0.04323	0.07627	0.07715	0.4174	0.4145	0.7831	0.7818	0.9329	0.9329	2.18E-06	0.9150	0.9372	0.9372	1.23E-06	0.9423	8.09E-02	8.19E-02	91.35	91.25
1E+15	6	2	0	14	4.05E-02	3.99E-02	0.08192	0.08109	0.13100	0.13030	0.3988	0.3959	0.6860	0.6873	0.8997	0.9182	-1.85E-02	0.8972	0.7944	0.9408	-1.47E-01	0.8997	1.46E-01	1.45E-01	84.352	84.622
1E+19	6	2	2	14.3	2.83E-02	2.80E-02	0.06039	0.05992	0.11040	0.10760	0.4042	0.4027	0.7277	0.7310	0.9201	0.9216	-1.56E-03	0.9154	0.9137	0.9322	-1.84E-02	0.9201	1.20E-01	1.17E-01	87.118	87.467
1E+19	6	2	4	14.4	1.57E-02	1.50E-02	0.04229	0.04118	0.07672	0.07629	0.4267	0.4259	0.7998	0.8005	0.9279	0.9294	-1.53E-03	0.9215	0.9146	0.9329	-1.82E-02	0.9279	8.27E-02	8.22E-02	91.123	91.189
1E+15	6	4	0	16	3.61E-02	3.74E-02	0.08094	0.08229	0.13450	0.13690	0.4124	0.4186	0.7136	0.7221	0.8698	0.9301	-6.03E-02	0.8721	0.5222	0.9407	-4.19E-01	0.8721	1.54E-01	1.57E-01	82.544	83.339
1E+19	6	4	4	16.4	1.33E-02	1.33E-02	0.04064	0.04150	0.07951	0.07808	0.4370	0.4404	0.8221	0.8199	0.9126	0.9342	-2.16E-02	0.8896	0.8759	0.8993	-2.34E-02	0.9126	8.71E-02	8.56E-02	90.266	90.499
1E+15	12	0.5	0	20	9.01E-02	9.04E-02	0.14110	0.14140	0.17390	0.17350	0.4216	0.4214	0.6763	0.6777	0.9279	0.9279	-1.26E-05	0.9259	0.9868	0.9869	-1.42E-04	0.9868	1.76E-01	1.76E-01	80.628	80.673
1E+19	12	0.5	0.5	20.1	8.30E-02	8.27E-02	0.12700	0.12720	0.15810	0.15890	0.4096	0.4110	0.6786	0.6777	0.9289	0.9289	3.34E-06	0.9242	0.9865	0.9864	3.34E-06	0.9865	1.60E-01	1.61E-01	82.358	82.268
1E+19	12	0.5	1	20.2	8.25E-02	8.26E-02	0.12690	0.12750	0.15740	0.15820	0.4155	0.4157	0.6891	0.6901	0.9320	0.9320	3.37E-06	0.9297	0.9889	0.9889	3.37E-06	0.9889	1.59E-01	1.60E-01	82.586	82.497
1E+19	12	0.5	2	20.3	8.10E-02	8.08E-02	0.12380	0.12370	0.14900	0.14910	0.4216	0.4219	0.7124	0.7110	0.9358	0.9358	3.34E-06	0.9299	0.9874	0.9874	3.34E-06	0.9874	1.51E-01	1.51E-01	83.483	83.472
1E+19	12	0.5	4	20.4	7.19E-02	6.97E-02	0.11200	0.11020	0.13200	0.13120	0.4444	0.4407	0.7736	0.7667	0.9444	0.9444	3.34E-06	0.9396	0.9910	0.9910	3.34E-06	0.9910	1.33E-01	1.32E-01	85.611	85.698
1E+19	12	0.5	8	20.5	3.94E-02	3.83E-02	0.07556	0.07479	0.09333	0.09349	0.4743	0.4744	0.8683	0.8641	0.9684	0.9684	3.36E-06	0.9624	0.9924	0.9924	3.35E-06	0.9924	9.40E-02	9.42E-02	90.065	90.048
1E+15	12	1	0	22	8.82E-02	8.80E-02	0.14260	0.14020	0.17850	0.17630	0.4376	0.4316	0.6883	0.6935	0.9379	0.9387	-7.79E-04	0.9393	0.9840	0.9903	-6.30E-03	0.9840	1.81E-01	1.79E-01	80.312	80.555
1E+19	12	1	1	22.2	7.88E-02	7.83E-02	0.12460	0.12460	0.16510	0.16410	0.4202	0.4203	0.7024	0.7018	0.9420	0.9420	2.18E-06	0.9389	0.9894	0.9894	1.22E-06	0.9894	1.67E-01	1.66E-01	81.862	81.972
1E+19	12	1	2	22.3	7.76E-02	7.72E-02	0.12370	0.12140	0.15900	0.15830	0.4314	0.4287	0.7301	0.7270	0.9464	0.9464	2.23E-06	0.9428	0.9892	0.9892	1.56E-06	0.9892	1.61E-01	1.60E-01	82.576	82.653
1E+19	12	1	4	22.4	6.81E-02	6.83E-02	0.10890	0.10920	0.13720	0.13770	0.4468	0.4461	0.7811	0.7797	0.9546	0.9546	2.19E-06	0.9506	0.9907	0.9907	1.23E-06	0.9907	1.38E-01	1.39E-01	85.13	85.075
1E+19	12	1	8	22.5	3.65E-02	3.68E-02	0.07233	0.07173	0.09583	0.09648	0.4813	0.4765	0.8733	0.8729	0.9709	0.9709	2.26E-06	0.9687	0.9937	0.9937	1.67E-06	0.9937	9.64E-02	9.71E-02	89.872	89.803
1E+15	12	2	0	24	8.20E-02	8.13E-02	0.14300	0.14190	0.18260	0.18160	0.4475	0.4457	0.7226	0.7220	0.9421	0.9606	-1.85E-02	0.9417	0.8477	0.9941	-1.46E-01	0.9421	1.94E-01	1.93E-01	79.407	79.533
1E+19	12	2	2	24.3	7.20E-02	6.99E-02	0.12190	0.12090	0.16390	0.16170	0.4462	0.4439	0.7595	0.7550	0.9634	0.9649	-1.51E-03	0.9596	0.9749	0.9933	-1.84E-02	0.9749	1.68E-01	1.66E-01	82.166	82.407
1E+19	12	2	4	24.4	6.25E-02	6.11E-02	0.10820	0.10790	0.14030	0.14120	0.4604	0.4600	0.8078	0.8052	0.9681	0.9696	-1.54E-03	0.9650	0.9752	0.9936	-1.84E-02	0.9752	1.44E-01	1.45E-01	84.834	84.738
1E+15	12	4	0	26	7.35E-02	7.47E-02	0.14150	0.14400	0.18930	0.19130	0.4711	0.4741	0.7604	0.7624	0.9217	0.9813	-5.96E-02	0.9262	0.5799	0.9976	-4.18E-01	0.9262	2.04E-01	2.07E-01	78.969	78.82
1E+19	12	4	4	26.4	5.22E-02	5.10E-02	0.10510	0.10420	0.15010	0.15090	0.4824	0.4833	0.8467	0.8425	0.9567	0.9864	-2.97E-02	0.9445	0.9713	0.9947	-2.34E-02	0.9713	1.55E-01	1.55E-01	84.145	84.066

PDC = <S><W>.<B>; Substrate depth = 3 x 2^(S); Well depth = 0.5 x 2^(W/2); BTI depth = 0.25 x 2^(B); if B = 0 then BTI depth = 0.

FI-BTI-twin-1electrode-nwell-array2&3 -633; Normalized QE and scanned QE dependence on BTI, Well and Substrate depth.

For illumination positions in the neighbouring PSE to just before the central PSE well wall.

reverse	Doping		Elec. width (um)	
bias	p-substr	n-well	p-substr	n-well
2 volts	1E+15	1E+17	2	6.4

bti dope	Depth (um)				Outside 2nd BTI				On 2nd BTI				On PSE boundary				On 1st BTI				No BTI : next to SCR			
(h/ml)	substr.	well	bti	PDC	QE @ 45	nQE @ 45	pQE @ 45	QE @ 115	QE @ 50	nQE @ 50	pQE @ 50	QE @ 110	QE @ 55	nQE @ 55	pQE @ 55	QE @ 105	QE @ 60	nQE @ 60	pQE @ 60	QE @ 100	QE @ 65	nQE @ 65	pQE @ 65	QE @ 95
1E+15	3	0.5	0	0	1.173E-02	1.173E-02	3.161E-06	1.173E-02	0.02410	0.02410	3.161E-06	0.02424	0.05824	0.05824	3.161E-06	0.05817	0.2766	0.2765	3.161E-06	0.2720	0.5209	0.5209	3.161E-06	0.5213
1E+19	3	0.5	0.5	0.1	7.748E-03	7.745E-03	3.344E-06	7.698E-03	0.01641	0.01641	3.344E-06	0.01639	0.04769	0.04768	3.344E-06	0.04660	0.2695	0.2695	3.344E-06	0.2708	0.5313	0.5313	3.344E-06	0.5304
1E+19	3	0.5	1	0.2	6.695E-03	6.692E-03	3.343E-06	6.649E-03	0.01501	0.01501	3.343E-06	0.01503	0.04306	0.04306	3.343E-06	0.04342	0.2784	0.2784	3.343E-06	0.2775	0.5493	0.5493	3.343E-06	0.5511
1E+19	3	0.5	2	0.3	3.497E-03	3.493E-03	3.338E-06	3.463E-03	0.01023	0.01022	3.338E-06	0.01014	0.03073	0.03073	3.338E-06	0.03088	0.3101	0.3101	3.338E-06	0.3079	0.6170	0.6170	3.338E-06	0.6124
1E+15	3	1	0	2	1.175E-02	1.174E-02	1.860E-06	1.162E-02	0.02460	0.02460	1.860E-06	0.02509	0.05900	0.05900	1.860E-06	0.06132	0.2801	0.2801	1.859E-06	0.2900	0.5298	0.5297	1.859E-06	0.5239
1E+19	3	1	1	2.2	6.125E-03	6.123E-03	2.212E-06	6.071E-03	0.01419	0.01419	2.212E-06	0.01418	0.04418	0.04418	2.212E-06	0.04390	0.2816	0.2815	2.211E-06	0.2815	0.5602	0.5602	2.211E-06	0.5597
1E+19	3	1	2	2.3	3.312E-03	3.310E-03	2.207E-06	3.261E-03	0.01018	0.01018	2.207E-06	0.01001	0.03062	0.03062	2.207E-06	0.03179	0.3126	0.3126	2.207E-06	0.3122	0.6251	0.6251	2.207E-06	0.6217
1E+15	6	0.5	0	10	4.372E-02	4.371E-02	3.171E-06	4.392E-02	0.07994	0.07993	3.171E-06	0.08079	0.12550	0.12550	3.171E-06	0.12440	0.3644	0.3644	3.171E-06	0.3744	0.6404	0.6404	3.171E-06	0.6460
1E+19	6	0.5	0.5	10.1	3.637E-02	3.637E-02	3.338E-06	3.616E-02	0.06612	0.06612	3.338E-06	0.06600	0.10890	0.10890	3.338E-06	0.11050	0.3640	0.3640	3.338E-06	0.3659	0.6481	0.6481	3.338E-06	0.6465
1E+19	6	0.5	1	10.2	3.554E-02	3.553E-02	3.365E-06	3.549E-02	0.06517	0.06517	3.365E-06	0.06577	0.10640	0.10640	3.365E-06	0.10780	0.3697	0.3697	3.365E-06	0.3764	0.6604	0.6604	3.365E-06	0.6608
1E+19	6	0.5	2	10.3	3.186E-02	3.186E-02	3.340E-06	3.168E-02	0.06084	0.06084	3.340E-06	0.06064	0.09836	0.09835	3.340E-06	0.09842	0.3816	0.3816	3.340E-06	0.3819	0.6885	0.6885	3.339E-06	0.6913
1E+19	6	0.5	4	10.4	1.773E-02	1.773E-02	3.356E-06	1.774E-02	0.04269	0.04268	3.356E-06	0.04277	0.07190	0.07189	3.356E-06	0.07259	0.4131	0.4131	3.356E-06	0.4137	0.7788	0.7788	3.356E-06	0.7741
1E+15	6	1	0	12	4.188E-02	4.188E-02	1.866E-06	4.192E-02	0.08036	0.08035	1.866E-06	0.07907	0.12600	0.12600	1.866E-06	0.12550	0.3845	0.3845	1.866E-06	0.3840	0.6580	0.6580	1.866E-06	0.6613
1E+19	6	1	1	12.2	3.367E-02	3.367E-02	2.208E-06	3.339E-02	0.06439	0.06439	2.208E-06	0.06400	0.11250	0.11250	2.208E-06	0.11130	0.3747	0.3747	2.208E-06	0.3762	0.6738	0.6738	2.208E-06	0.6725
1E+19	6	1	2	12.3	3.042E-02	3.042E-02	2.248E-06	3.016E-02	0.06046	0.06046	2.248E-06	0.06005	0.10370	0.10370	2.248E-06	0.10450	0.3870	0.3870	2.248E-06	0.3866	0.7060	0.7060	2.247E-06	0.7033
1E+19	6	1	4	12.4	1.746E-02	1.746E-02	2.209E-06	1.720E-02	0.04318	0.04318	2.209E-06	0.04323	0.07627	0.07626	2.209E-06	0.07715	0.4174	0.4174	2.209E-06	0.4145	0.7831	0.7831	2.209E-06	0.7818
1E+15	6	2	0	14	4.047E-02	4.047E-02	2.961E-07	3.992E-02	0.08192	0.08192	2.961E-07	0.08109	0.13100	0.13100	2.961E-07	0.13030	0.3988	0.3988	2.960E-07	0.3959	0.6860	0.6860	2.960E-07	0.6873
1E+19	6	2	2	14.3	2.827E-02	2.827E-02	3.724E-07	2.804E-02	0.06039	0.06039	3.724E-07	0.05992	0.11040	0.11040	3.724E-07	0.10760	0.4042	0.4042	3.724E-07	0.4027	0.7277	0.7277	3.724E-07	0.7310
1E+19	6	2	4	14.4	1.567E-02	1.567E-02	3.745E-07	1.502E-02	0.04229	0.04229	3.745E-07	0.04118	0.07672	0.07672	3.745E-07	0.07629	0.4267	0.4267	3.744E-07	0.4259	0.7998	0.7998	3.744E-07	0.8005
1E+15	6	4	0	16	3.606E-02	3.606E-02	1.076E-07	3.738E-02	0.08094	0.08094	1.076E-07	0.08229	0.13450	0.13450	1.076E-07	0.13690	0.4124	0.4124	1.076E-07	0.4186	0.7136	0.7136	1.076E-07	0.7221
1E+19	6	4	4	16.4	1.327E-02	1.327E-02	1.574E-07	1.329E-02	0.04064	0.04064	1.574E-07	0.04150	0.07951	0.07951	1.574E-07	0.07808	0.4370	0.4370	1.574E-07	0.4404	0.8221	0.8221	1.574E-07	0.8199
1E+15	12	0.5	0	20	9.012E-02	9.012E-02	3.171E-06	9.040E-02	0.14110	0.14110	3.171E-06	0.14140	0.17390	0.17390	3.171E-06	0.17350	0.4216	0.4216	3.171E-06	0.4214	0.6763	0.6763	3.171E-06	0.6777
1E+19	12	0.5	0.5	20.1	8.295E-02	8.294E-02	3.337E-06	8.272E-02	0.12700	0.12700	3.337E-06	0.12720	0.15810	0.15810	3.337E-06	0.15890	0.4096	0.4096	3.337E-06	0.4110	0.6786	0.6786	3.337E-06	0.6777
1E+19	12	0.5	1	20.2	8.247E-02	8.247E-02	3.372E-06	8.255E-02	0.12690	0.12690	3.372E-06	0.12750	0.15740	0.15740	3.372E-06	0.15820	0.4155	0.4155	3.372E-06	0.4157	0.6891	0.6891	3.372E-06	0.6901
1E+19	12	0.5	2	20.3	8.102E-02	8.102E-02	3.338E-06	8.078E-02	0.12380	0.12380	3.338E-06	0.12370	0.14900	0.14900	3.338E-06	0.14910	0.4216	0.4216	3.338E-06	0.4219	0.7124	0.7124	3.337E-06	0.7110
1E+19	12	0.5	4	20.4	7.194E-02	7.194E-02	3.344E-06	6.972E-02	0.11200	0.11200	3.344E-06	0.11020	0.13200	0.13200	3.344E-06	0.13120	0.4444	0.4444	3.344E-06	0.4407	0.7736	0.7735	3.343E-06	0.7667
1E+19	12	0.5	8	20.5	3.935E-02	3.934E-02	3.356E-06	3.830E-02	0.07556	0.07556	3.356E-06	0.07479	0.09333	0.09333	3.356E-06	0.09349	0.4743	0.4743	3.356E-06	0.4744	0.8683	0.8682	3.356E-06	0.8641
1E+15	12	1	0	22	8.822E-02	8.822E-02	1.866E-06	8.796E-02	0.14260	0.14260	1.866E-06	0.14020	0.17850	0.17850	1.866E-06	0.17630	0.4376	0.4376	1.866E-06	0.4316	0.6883	0.6883	1.866E-06	0.6935
1E+19	12	1	1	22.2	7.882E-02	7.882E-02	2.208E-06	7.832E-02	0.12460	0.12460	2.208E-06	0.12460	0.16510	0.16510	2.208E-06	0.16410	0.4202	0.4202	2.208E-06	0.4203	0.7024	0.7024	2.208E-06	0.7018
1E+19	12	1	2	22.3	7.764E-02	7.764E-02	2.252E-06	7.717E-02	0.12370	0.12370	2.252E-06	0.12140	0.15900	0.15900	2.252E-06	0.15830	0.4314	0.4314	2.252E-06	0.4287	0.7301	0.7301	2.252E-06	0.7270
1E+19	12	1	4	22.4	6.812E-02	6.812E-02	2.210E-06	6.829E-02	0.10890	0.10880	2.210E-06	0.10920	0.13720	0.13720	2.210E-06	0.13770	0.4468	0.4468	2.210E-06	0.4461	0.7811	0.7811	2.210E-06	0.7797
1E+19	12	1	8	22.5	3.648E-02	3.648E-02	2.276E-06	3.683E-02	0.07233	0.07233	2.276E-06	0.07173	0.09583	0.09583	2.276E-06	0.09648	0.4813	0.4813	2.276E-06	0.4765	0.8733	0.8733	2.276E-06	0.8729
1E+15	12	2	0	24	8.197E-02	8.197E-02	2.960E-07	8.125E-02	0.14300	0.14300	2.960E-07	0.14190	0.18260	0.18260	2.960E-07	0.18160	0.4475	0.4475	2.960E-07	0.4457	0.7226	0.7226	2.960E-07	0.7220
1E+19	12	2	2	24.3	7.200E-02	7.200E-02	3.752E-07	6.993E-02	0.12190	0.12190	3.752E-07	0.12090	0.16390	0.16390	3.752E-07	0.16170	0.4462	0.4462	3.752E-07	0.4439	0.7595	0.7595	3.752E-07	0.7550
1E+19	12	2	4	24.4	6.245E-02	6.245E-02	3.767E-07	6.113E-02	0.10820	0.10820	3.767E-07	0.10790	0.14030	0.14030	3.767E-07	0.14120	0.4604	0.4604	3.767E-07	0.4600	0.8078	0.8078	3.767E-07	0.8052
1E+15	12	4	0	26	7.347E-02	7.347E-02	1.089E-07	7.473E-02	0.14150	0.14150	1.089E-07	0.14400	0.18930	0.18930	1.089E-07	0.19130	0.4711	0.4711	1.089E-07	0.4741	0.7604	0.7604	1.089E-07	0.7624
1E+19	12	4	4	26.4	5.216E-02	5.216E-02	1.451E-07	5.100E-02	0.10510	0.10510	1.451E-07	0.10420	0.15010	0.15010	1.451E-07	0.15090	0.4824	0.4824	1.451E-07	0.4833	0.8467	0.8467	1.451E-07	0.8425

PDC = <S><W>.<B>; Substrate depth = 3 x 2^(S); Well depth = 0.5 x 2^(W/2); BTI depth = 0.25 x 2^(B); if B = 0 then BTI depth = 0.

BI-BTI-twin-1electrode-nwell-array2&3 -633; Suppression and enhancement ratio dependence on BTI, Well and Substrate depth.

reverse	Doping		Elec. width (um)		Suppression Ratio (SR) = control / statistic; SR ratio (SRR) = ratio given.												Enhancement Ratio (ER) = statistic / control; ER ratio (ERR) = ratio given.														
bias	p-subst	n-well	p-subst	n-well																											
2 volts	1E+15	1E+17	2	6.4																											
bti dope	Depth (um)				SR	SRR	SR	SRR	SR	SRR	SR	SRR	SR	SRR	SR	SRR	ER	ERR	ER	ERR	ER	ERR	ER	ERR	ER	ERR	ER	ERR	ER	ERR	ERR
(h/ml)	subst.	well	bti	PDC	at 45	45 / 45	at 115	45 / 115	at 50	45/50	at 110	115/110	at 55	45/55	at 105	115/105	at 60	60/60	at 100	60/100	at 65	65/60	at 95	95/100	at 70	70/60	at 90	90/100	at 80	80/60	at Max	max/60	max/100
1E+15	3	0.5	0	0	1	1	1	1	1	1	1	1	1	1	1	1	1	1	1	1	1	1	1	1	1	1	1	1	1	1	1	1
1E+19	3	0.5	0.5	0.1	1.517	1	1.533	0.99	1.467	1.034	1.459	1.05	1.251	1.212	1.243	1.233	0.996	1	0.963	1.033	1.02	1.025	1.019	1.058	1	1.005	1.019	1.058	0.988	0.992	0.989	0.994	1.027
1E+19	3	0.5	1	0.2	1.761	1	1.757	1.002	1.596	1.103	1.587	1.107	1.335	1.319	1.331	1.32	1.025	1	1.008	1.018	1.056	1.03	1.053	1.045	1.003	0.978	1.02	1.013	0.99	0.966	0.993	0.968	0.9854
1E+19	3	0.5	2	0.3	3.346	1	3.381	0.99	2.332	1.435	2.331	1.45	1.838	1.82	1.836	1.841	1.134	1	1.113	1.019	1.172	1.034	1.172	1.054	1.018	0.898	1.023	0.919	0.987	0.871	0.98	0.865	0.8811
1E+15	3	1	0	2	1	1	1	1	1	1	1	1	1	1	1	1	1	1	1	1	1	1	1	1	1	1	1	1	1	1	1	1	1
1E+19	3	1	1	2.2	1.916	1	1.92	0.998	1.712	1.119	1.733	1.108	1.357	1.411	1.442	1.332	1.019	1	0.95	1.073	1.048	1.028	1.063	1.119	0.996	0.977	1.004	1.057	0.981	0.962	0.982	0.963	1.0337
1E+19	3	1	2	2.3	3.524	1	3.533	0.998	2.385	1.477	2.424	1.457	1.862	1.893	1.9	1.859	1.128	1	1.065	1.058	1.161	1.03	1.176	1.104	1.005	0.891	1.01	0.948	0.982	0.87	0.977	0.866	0.9171
1E+15	6	0.5	0	10	1	1	1	1	1	1	1	1	1	1	1	1	1	1	1	1	1	1	1	1	1	1	1	1	1	1	1	1	1
1E+19	6	0.5	0.5	10.1	1.205	1	1.208	0.998	1.183	1.019	1.19	1.015	1.117	1.079	1.117	1.082	0.993	1	0.974	1.019	1.009	1.016	0.999	1.026	1.002	1.009	0.999	1.026	0.996	1.003	0.996	1.003	1.0224
1E+19	6	0.5	1	10.2	1.229	1	1.22	1.007	1.19	1.033	1.196	1.02	1.109	1.108	1.116	1.093	1.007	1	0.997	1.01	1.022	1.015	1.02	1.023	1.006	0.999	1.015	1.019	1.005	0.998	1.005	0.998	1.0082
1E+19	6	0.5	2	10.3	1.33	1	1.344	0.99	1.249	1.065	1.265	1.062	1.157	1.15	1.165	1.153	1.044	1	1.022	1.022	1.063	1.018	1.054	1.032	1.013	0.971	1.017	0.996	1.004	0.962	1.004	0.962	0.9826
1E+19	6	0.5	4	10.4	2.286	1	2.256	1.013	1.691	1.352	1.7	1.327	1.459	1.566	1.46	1.545	1.124	1	1.099	1.023	1.185	1.054	1.178	1.072	1.045	0.929	1.046	0.952	0.999	0.889	1.001	0.89	0.9111
1E+15	6	1	0	12	1	1	1	1	1	1	1	1	1	1	1	1	1	1	1	1	1	1	1	1	1	1	1	1	1	1	1	1	1
1E+19	6	1	1	12.2	1.223	1	1.245	0.983	1.2	1.019	1.206	1.032	1.089	1.124	1.21	1.028	0.98	1	0.979	1	1.013	1.034	1.006	1.028	1.001	1.022	0.998	1.019	0.996	1.016	0.996	1.016	1.0168
1E+19	6	1	2	12.3	1.324	1	1.334	0.992	1.247	1.062	1.254	1.064	1.132	1.17	1.247	1.07	1.011	1	1.015	0.996	1.05	1.038	1.042	1.026	1.021	1.01	1.01	0.995	1.002	0.991	1.002	0.991	0.9866
1E+19	6	1	4	12.4	2.189	1	2.228	0.982	1.631	1.341	1.651	1.349	1.435	1.525	1.531	1.455	1.087	1	1.078	1.008	1.165	1.072	1.156	1.072	1.043	0.96	1.034	0.959	0.996	0.917	1.001	0.921	0.9282
1E+15	6	2	0	14	1	1	1	1	1	1	1	1	1	1	1	1	1	1	1	1	1	1	1	1	1	1	1	1	1	1	1	1	1
1E+19	6	2	2	14.3	1.365	1	1.374	0.993	1.293	1.056	1.279	1.075	1.123	1.215	1.199	1.146	0.994	1	1.008	0.986	1.042	1.049	1.037	1.03	1.005	1.011	1.006	0.999	1.001	1.007	1.001	1.007	0.9933
1E+19	6	2	4	14.4	2.308	1	2.406	0.959	1.719	1.343	1.759	1.368	1.529	1.51	1.541	1.562	1.076	1	1.066	1.01	1.145	1.063	1.132	1.062	1.02	0.948	1.024	0.961	1.001	0.93	1.004	0.933	0.9418
1E+15	6	4	0	16	1	1	1	1	1	1	1	1	1	1	1	1	1	1	1	1	1	1	1	1	1	1	1	1	1	1	1	1	1
1E+19	6	4	4	16.4	2.402	1	2.471	0.972	1.764	1.362	1.772	1.394	1.527	1.573	1.553	1.591	1.054	1	1.048	1.006	1.126	1.068	1.112	1.062	1.005	0.954	1.008	0.962	1.013	0.961	1.008	0.956	0.9622
1E+15	12	0.5	0	20	1	1	1	1	1	1	1	1	1	1	1	1	1	1	1	1	1	1	1	1	1	1	1	1	1	1	1	1	1
1E+19	12	0.5	0.5	20.1	1.074	1	1.072	1.002	1.058	1.015	1.061	1.011	1.044	1.029	1.041	1.03	0.994	1	0.976	1.018	1.008	1.014	0.994	1.018	0.996	1.002	0.999	1.023	0.999	1.005	0.999	1.005	1.0227
1E+19	12	0.5	1	20.2	1.054	1	1.053	1.001	1.059	0.996	1.055	0.997	1.05	1.004	1.022	1.03	1.007	1	0.986	1.021	1.023	1.016	1.006	1.021	1.003	0.996	1.006	1.02	1.005	0.998	1.005	0.998	1.0188
1E+19	12	0.5	2	20.3	1.081	1	1.042	1.037	1.056	1.024	1.043	0.999	1.038	1.042	1.027	1.015	1.013	1	1.001	1.012	1.03	1.017	1.01	1.009	1.015	1.002	1.011	1.01	1.004	0.992	1.004	0.992	1.0034
1E+19	12	0.5	4	20.4	1.107	1	1.113	0.994	1.078	1.027	1.085	1.026	1.01	1.096	1.037	1.073	1.056	1	1.03	1.025	1.066	1.009	1.052	1.021	1.035	0.98	1.033	1.003	1.018	0.964	1.018	0.964	0.9881
1E+19	12	0.5	8	20.5	1.617	1	1.64	0.985	1.349	1.198	1.344	1.22	1.178	1.372	1.188	1.381	1.104	1	1.09	1.014	1.197	1.084	1.174	1.077	1.1	0.996	1.099	1.009	1.041	0.942	1.041	0.942	0.9551
1E+15	12	1	0	22	1	1	1	1	1	1	1	1	1	1	1	1	1	1	1	1	1	1	1	1	1	1	1	1	1	1	1	1	1
1E+19	12	1	1	22.2	1.061	1	1.149	0.923	1.087	0.976	1.056	1.088	1.059	1.002	1.032	1.114	0.967	1	0.982	0.985	1.022	1.057	0.988	1.006	0.995	1.029	0.996	1.015	0.998	1.033	0.998	1.033	1.0171
1E+19	12	1	2	22.3	1.044	1	1.125	0.927	1.074	0.972	1.091	1.032	1.021	1.022	1.038	1.084	1.021	1	0.997	1.024	1.025	1.004	1	1.003	0.991	0.97	1.006	1.008	1.001	0.98	1.001	0.98	1.004
1E+19	12	1	4	22.4	1.111	1	1.184	0.938	1.114	0.998	1.103	1.074	1.033	1.076	1.039	1.14	1.039	1	1.029	1.01	1.067	1.026	1.038	1.008	1.022	0.983	1.027	0.998	1.011	0.972	1.011	0.972	0.9819
1E+19	12	1	8	22.5	1.646	1	1.766	0.932	1.402	1.174	1.374	1.285	1.209	1.361	1.182	1.494	1.085	1	1.076	1.009	1.194	1.1	1.155	1.073	1.088	1.002	1.084	1.008	1.033	0.952	1.033	0.952	0.9606
1E+15	12	2	0	24	1	1	1	1	1	1	1	1	1	1	1	1	1	1	1	1	1	1	1	1	1	1	1	1	1	1	1	1	1
1E+19	12	2	2	24.3	1.064	1	1.095	0.971	1.08	0.985	1.048	1.045	1.04	1.023	1.037	1.056	0.989	1	1.001	0.988	1.02	1.032	1.004	1.003	1.007	1.018	1.008	1.008	1.002	1.013	1.002	1.013	1.0008
1E+19	12	2	4	24.4	1.138	1	1.201	0.948	1.111	1.024	1.103	1.089	1.043	1.091	1.058	1.135	1.02	1	1.025	0.995	1.059	1.039	1.036	1.011	1.022	1.002	1.024	0.999	1.008	0.988	1.008	0.988	0.9833
1E+15	12	4	0	26	1	1	1	1	1	1	1	1	1	1	1	1	1	1	1	1	1	1	1	1	1	1	1	1	1	1	1	1	1
1E+19	12	4	4	26.4	1.124	1	1.196	0.94	1.112	1.011	1.127	1.061	1.052	1.069	1.068	1.12	1.02	1	1.01	1.01	1.044	1.023	1.023	1.013	1.014	0.994	1.012	1.001	1.003	0.983	1.003	0.983	0.9928

PDC = <S><W>.<B>; Substrate depth = 3 x 2^(S); Well depth = 0.5 x 2^(W/2); BTI depth = 0.25 x 2^(B); if B = 0 then BTI depth = 0.

FI-BTI-twin-1electrode-nwell-array2&3 -633; Suppression and enhancement ratio dependence on BTI, Well and Substrate depth.

reverse	Doping		Elec. width (um)		Suppression Ratio (SR) = control / statistic; SR ratio (SRR) = ratio given.												Enhancement Ratio (ER) = statistic / control; ER ratio (ERR) = ratio given																
bias	p-subst	n-well	p-subst	n-well																														
2 volts	1E+15	1E+17	2	6.4																														
bti dope	Depth (um)				SR	SRR	SR	SRR	SR	SRR	SR	SRR	SR	SRR	SR	SRR	ER	ERR	ER	ERR	ER	ERR	ER	ERR	ER	ERR	ER	ERR	ER	ERR	ER	ERR	ER	ERR
(h/ml)	subst.	well	bti	PDC	at 45	45 / 45	at 115	45 / 115	at 50	45/50	at 110	115/110	at 55	45/55	at 105	115/105	at 60	60/60	at 100	60/100	at 65	65/60	at 95	95/100	at 70	70/60	at 90	90/100	at 80	80/60	at Max	max/60	max/100
1E+15	3	0.5	0	0	1	1	1	1	1	1	1	1	1	1	1	1	1	1	1	1	1	1	1	1	1	1	1	1	1	1	1	1	1	1
1E+19	3	0.5	0.5	0.1	1.514	1	1.524	0.9935	1.469	1.031	1.479	1.0303	1.221	1.24	1.246	1.2207	0.974	1	0.996	0.979	1.02	1.047	1.017	1.022	1.002	1.029	0.993	0.998	0.986	1.012	0.988	1.014	0.9927
1E+19	3	0.5	1	0.2	1.752	1	1.764	0.9931	1.606	1.091	1.613	1.0939	1.353	1.295	1.34	1.3168	1.007	1	1.02	0.987	1.055	1.048	1.057	1.036	1.004	0.998	0.998	0.978	0.984	0.978	0.986	0.979	0.966
1E+19	3	0.5	2	0.3	3.354	1	3.387	0.9903	2.356	1.424	2.391	1.4169	1.895	1.77	1.884	1.7981	1.121	1	1.132	0.99	1.184	1.057	1.175	1.038	1.017	0.907	1.008	0.89	0.985	0.879	0.983	0.877	0.8686
1E+15	3	1	0	2	1	1	1	1	1	1	1	1	1	1	1	1	1	1	1	1	1	1	1	1	1	1	1	1	1	1	1	1	1	1
1E+19	3	1	1	2.2	1.918	1	1.914	1.0023	1.734	1.107	1.769	1.0817	1.335	1.436	1.397	1.3703	1.005	1	0.971	1.036	1.057	1.052	1.068	1.101	1.011	1.006	0.995	1.026	0.987	0.982	0.989	0.984	1.0194
1E+19	3	1	2	2.3	3.548	1	3.563	0.9956	2.417	1.468	2.506	1.4216	1.927	1.841	1.929	1.8473	1.116	1	1.077	1.037	1.18	1.057	1.187	1.102	1.017	0.912	1.001	0.93	0.986	0.883	0.992	0.889	0.9211
1E+15	6	0.5	0	10	1	1	1	1	1	1	1	1	1	1	1	1	1	1	1	1	1	1	1	1	1	1	1	1	1	1	1	1	1	1
1E+19	6	0.5	0.5	10.1	1.202	1	1.215	0.9897	1.209	0.994	1.224	0.9922	1.152	1.043	1.126	1.0789	0.999	1	0.977	1.022	1.012	1.013	1.001	1.024	1.006	1.007	0.999	1.022	0.997	0.998	0.997	0.998	1.0205
1E+19	6	0.5	1	10.2	1.23	1	1.238	0.994	1.227	1.003	1.228	1.0075	1.18	1.043	1.154	1.0724	1.015	1	1.005	1.009	1.031	1.016	1.023	1.017	1.009	0.994	1.011	1.006	0.997	0.983	1.008	0.994	1.003
1E+19	6	0.5	2	10.3	1.372	1	1.386	0.9898	1.314	1.044	1.332	1.0406	1.276	1.075	1.264	1.0968	1.047	1	1.02	1.027	1.075	1.027	1.07	1.049	1.013	0.967	1.012	0.992	0.998	0.953	1.005	0.96	0.9855
1E+19	6	0.5	4	10.4	2.466	1	2.476	0.996	1.873	1.317	1.889	1.3107	1.745	1.413	1.714	1.4447	1.134	1	1.105	1.026	1.216	1.073	1.198	1.084	1.03	0.908	1.025	0.928	0.998	0.88	1.006	0.887	0.9103
1E+15	6	1	0	12	1	1	1	1	1	1	1	1	1	1	1	1	1	1	1	1	1	1	1	1	1	1	1	1	1	1	1	1	1	1
1E+19	6	1	1	12.2	1.244	1	1.255	0.9907	1.248	0.997	1.235	1.0162	1.12	1.111	1.128	1.1134	0.975	1	0.98	0.995	1.024	1.051	1.017	1.038	1.005	1.032	0.999	1.019	1.003	1.03	1.003	1.03	1.0242
1E+19	6	1	2	12.3	1.377	1	1.39	0.9905	1.329	1.036	1.317	1.0556	1.215	1.133	1.201	1.1573	1.007	1	1.007	1	1.073	1.066	1.064	1.056	1.01	1.003	1.004	0.997	1.006	1	1.025	1.019	1.0183
1E+19	6	1	4	12.4	2.399	1	2.437	0.9842	1.861	1.289	1.829	1.3325	1.652	1.452	1.627	1.4983	1.086	1	1.079	1.006	1.19	1.096	1.182	1.095	1.034	0.952	1.016	0.941	1.005	0.925	1.007	0.928	0.9331
1E+15	6	2	0	14	1	1	1	1	1	1	1	1	1	1	1	1	1	1	1	1	1	1	1	1	1	1	1	1	1	1	1	1	1	1
1E+19	6	2	2	14.3	1.432	1	1.424	1.0055	1.357	1.055	1.353	1.052	1.187	1.206	1.211	1.1757	1.014	1	1.017	0.996	1.061	1.047	1.064	1.046	1.023	1.009	1.02	1.003	1.15	1.135	1.023	1.009	1.0054
1E+19	6	2	4	14.4	2.583	1	2.658	0.9717	1.937	1.333	1.969	1.3497	1.708	1.513	1.708	1.5561	1.07	1	1.076	0.995	1.166	1.09	1.165	1.083	1.031	0.964	1.027	0.955	1.151	1.076	1.031	0.964	0.9587
1E+15	6	4	0	16	1	1	1	1	1	1	1	1	1	1	1	1	1	1	1	1	1	1	1	1	1	1	1	1	1	1	1	1	1	1
1E+19	6	4	4	16.4	2.717	1	2.813	0.9661	1.992	1.364	1.983	1.4185	1.692	1.606	1.753	1.6042	1.06	1	1.052	1.007	1.152	1.087	1.135	1.079	1.049	0.99	1.02	0.97	1.677	1.583	1.046	0.988	0.9946
1E+15	12	0.5	0	20	1	1	1	1	1	1	1	1	1	1	1	1	1	1	1	1	1	1	1	1	1	1	1	1	1	1	1	1	1	1
1E+19	12	0.5	0.5	20.1	1.086	1	1.093	0.9941	1.111	0.978	1.112	0.9831	1.1	0.988	1.092	1.0009	0.972	1	0.975	0.996	1.003	1.033	1	1.025	1.001	1.03	0.998	1.023	1	1.029	1	1.029	1.025
1E+19	12	0.5	1	20.2	1.093	1	1.095	0.9979	1.112	0.983	1.109	0.9874	1.105	0.989	1.097	0.9985	0.986	1	0.986	0.999	1.019	1.034	1.018	1.032	1.004	1.019	1.004	1.018	1.002	1.017	1.002	1.017	1.0159
1E+19	12	0.5	2	20.3	1.112	1	1.119	0.9939	1.14	0.976	1.143	0.979	1.167	0.953	1.164	0.9617	1	1	1.001	0.999	1.053	1.053	1.049	1.048	1.009	1.009	1.004	1.003	1.001	1.001	1.001	1.001	0.9994
1E+19	12	0.5	4	20.4	1.253	1	1.297	0.9661	1.26	0.994	1.283	1.0105	1.317	0.951	1.322	0.9805	1.054	1	1.046	1.008	1.144	1.085	1.131	1.082	1.018	0.966	1.015	0.97	1.004	0.953	1.004	0.953	0.9603
1E+19	12	0.5	8	20.5	2.29	1	2.36	0.9703	1.867	1.226	1.891	1.2484	1.863	1.229	1.856	1.2718	1.125	1	1.126	0.999	1.284	1.141	1.275	1.133	1.044	0.928	1.039	0.923	1.006	0.894	1.006	0.894	0.8933
1E+15	12	1	0	22	1	1	1	1	1	1	1	1	1	1	1	1	1	1	1	1	1	1	1	1	1	1	1	1	1	1	1	,1	1
1E+19	12	1	1	22.2	1.119	1	1.123	0.9966	1.144	0.978	1.125	0.9981	1.081	1.035	1.074	1.0454	0.96	1	0.974	0.986	1.02	1.063	1.012	1.039	1.004	1.046	1	1.026	1.005	1.047	1.005	1.047	1.0325
1E+19	12	1	2	22.3	1.136	1	1.14	0.9969	1.153	0.986	1.155	0.987	1.123	1.012	1.114	1.0234	0.986	1	0.993	0.993	1.061	1.076	1.048	1.055	1.009	1.024	1.004	1.011	1.005	1.02	1.005	1.02	1.0121
1E+19	12	1	4	22.4	1.295	1	1.288	1.0055	1.309	0.989	1.284	1.0032	1.301	0.995	1.28	1.006	1.021	1	1.034	0.988	1.135	1.111	1.124	1.088	1.018	0.997	1.012	0.979	1.007	0.986	1.007	0.986	0.9741
1E+19	12	1	8	22.5	2.418	1	2.388	1.0126	1.972	1.227	1.955	1.2219	1.863	1.298	1.827	1.307	1.1	1	1.104	0.996	1.269	1.154	1.259	1.14	1.035	0.941	1.031	0.934	1.01	0.918	1.01	0.918	0.9147
1E+15	12	2	0	24	1	1	1	1	1	1	1	1	1	1	1	1	1	1	1	1	1	1	1	1	1	1	1	1	1	1	1	1	1	1
1E+19	12	2	2	24.3	1.138	1	1.162	0.9799	1.173	0.97	1.174	0.9899	1.114	1.022	1.123	1.0346	0.997	1	0.996	1.001	1.051	1.054	1.046	1.05	1.023	1.026	1.019	1.023	1.15	1.153	1.035	1.038	1.039
1E+19	12	2	4	24.4	1.313	1	1.329	0.9875	1.322	0.993	1.315	1.0107	1.301	1.009	1.286	1.0334	1.029	1	1.032	0.997	1.118	1.087	1.115	1.081	1.028	0.999	1.025	0.993	1.15	1.118	1.035	1.006	1.003
1E+15	12	4	0	26	1	1	1	1	1	1	1	1	1	1	1	1	1	1	1	1	1	1	1	1	1	1	1	1	1	1	1	1	1
1E+19	12	4	4	26.4	1.409	1	1.465	0.9613	1.346	1.046	1.382	1.0603	1.261	1.117	1.268	1.1558	1.024	1	1.019	1.004	1.113	1.087	1.105	1.084	1.038	1.014	1.02	1	1.675	1.636	1.049	1.024	1.0287

PDC = <S><W>.<B>; Substrate depth = 3 x 2^(S); Well depth = 0.5 x 2^(W/2); BTI depth = 0.25 x 2^(B); if B = 0 then BTI depth = 0.

APPENDIX VII : RESULTS - SJPD

BI-non-BTI-twin-control-3electrode-nwell-array2&3 -633; Normalized QE and scanned QE dependence on Well and Substrate depth.

SJPD PSE SIDE RESULTS

						Outside 2nd BTI		On 2nd BTI		On PSE boundary		On 1st BTI	
		Dp subst	Dp well	Dp bti	PDC	QE @ 45	QE @ 115	QE @ 50	QE @ 110	QE @ 55	QE @ 105	QE @ 60	QE @ 100
n well dope (e/ml)	1E+17	3	0.5	0	0	2.321E-07	2.413E-07	2.442E-07	2.631E-07	2.952E-07	3.54E-07	5.594E-07	8.298E-07
p substrate dope (h/ml)	1E+15	3	1	0	2	1.33E-07	1.331E-07	1.333E-07	1.334E-07	1.345E-07	1.348E-07	1.409E-07	1.423E-07
reverse bias (V)	2	6	0.5	0	10	0.000269	0.0002716	0.0005193	0.0005268	0.00106	0.001067	0.002517	0.002547
width image elec (um)	0.4	6	1	0	12	0.0001132	0.0001158	0.0002282	0.0002328	0.0004772	0.0004786	0.001135	0.001169
width guard elec (um)	6.4	6	2	0	14	2.545E-05	3.298E-05	5.414E-05	7.104E-05	0.0001137	0.0001478	0.0002738	0.0003528
width subst elec (um)	2	6	4	0	16	0.0002773	0.0002991	0.0006627	0.000715	0.001475	0.001564	0.003603	0.003836
PSE width (um)	50	12	0.5	0	20	0.004434	0.004456	0.007199	0.007422	0.01217	0.01196	0.01966	0.02056
Well width (um)	20	12	1	0	22	0.003343	0.00331	0.005531	0.005617	0.009288	0.009213	0.01553	0.01533
		12	2	0	24	0.003287	0.003219	0.00561	0.005735	0.009337	0.009569	0.01566	0.01602
		12	4	0	26	0.002523	0.002623	0.004744	0.004998	0.008447	0.008443	0.01397	0.01466
		12	8	0	28	0.005921	0.005904	0.01353	0.01352	0.02355	0.02474	0.03988	0.03979

PDC = <S><W> ; substrate depth = 3 x 2^(S); well depth = 0.5 x 2^(W/2)

BI-non-BTI-twin-control-3electrode-nwell-array2&3 -633; Normalized QE and scanned QE dependence on Well and Substrate depth.

SJPD PSE CENTRAL RESULTS

						No BTI:next to SCR		No BTI : On SCR		Exp Max	Maximum	Normalized PSE boundary QE	
		Dp subst	Dp well	Dp bti	PDC	QE @ 65	QE @ 95	QE @ 70	QE @ 90	QE @ 80	Max QE	Normz@ 55	Normz@105
n dope (e/ml)	1E+17	3	0.5	0	0	9.215E-07	1.441E-06	0.0000068	9.29E-06	0.3879	0.3879	7.61021E-07	9.12606E-07
p dope (h/ml)	1E+15	3	1	0	2	1.492E-07	1.524E-07	4.165E-07	4.839E-07	0.3852	0.3852	3.49169E-07	3.49948E-07
rev. bias (V)	2	6	0.5	0	10	0.00469	0.004704	0.01137	0.01146	0.3241	0.3241	0.003270595	0.003292194
W image elec (um)	0.4	6	1	0	12	0.002125	0.002152	0.005801	0.005945	0.3005	0.3005	0.00158802	0.001592679
W guard elec (um)	6.4	6	2	0	14	0.0005302	0.0006816	0.001943	0.002417	0.3986	0.3986	0.000285248	0.000370798
W subst elec (um)	2	6	4	0	16	0.006632	0.007072	0.01175	0.01278	0.2724	0.2724	0.005414831	0.005741557
Width PSE (um)	50	12	0.5	0	20	0.03186	0.03182	0.05432	0.0539	0.1438	0.1438	0.084631433	0.083171071
Width well (um)	20	12	1	0	22	0.02541	0.02466	0.04482	0.04314	0.1339	0.1339	0.069365198	0.068805078
		12	2	0	24	0.02681	0.0264	0.05021	0.05025	0.1798	0.1798	0.051929922	0.053220245
		12	4	0	26	0.0236	0.02427	0.045	0.04494	0.1748	0.1748	0.048323799	0.048300915
		12	8	0	28	0.06229	0.06199	0.08693	0.08646	0.1644	0.1644	0.143248175	0.150486618

PDC = <S><W> : substrate depth = 3 x 2^(S); well depth = 0.5 x 2^(W/2)

FI-non-BTI-twin-control-3electrode-nwell-array2&3 -633; Normalized QE and scanned QE dependence on Well and Substrate depth.

SJPD PSE SIDE RESULTS

						Outside 2nd BTI		On 2nd BTI		On PSE boundary		On 1st BTI	
		Dp subst	Dp well	Dp bti	PDC	QE @ 45	QE @ 115	QE @ 50	QE @ 110	QE @ 55	QE @ 105	QE @ 60	QE @ 100
n well dope (e/ml)	1E+17	3	0.5	0	0	2.321E-07	2.414E-07	2.441E-07	2.629E-07	2.836E-07	3.354E-07	5.642E-07	8.382E-07
p substrate dope (h/ml)	1E+15	3	1	0	2	1.33E-07	1.331E-07	1.333E-07	1.334E-07	1.342E-07	1.345E-07	1.409E-07	1.425E-07
reverse bias (V)	2	6	0.5	0	10	0.000258	0.000258	0.0004642	0.000467	0.0007287	0.0007358	0.002406	0.002412
width image elec (um)	0.4	6	1	0	12	0.0001101	0.0001111	0.0002048	0.0002077	0.0003263	0.0003351	0.001069	0.001087
width guard elec (um)	6.4	6	2	0	14	2.439E-05	3.125E-05	0.0000481	6.267E-05	7.927E-05	0.0001014	0.0002563	0.0003305
width subst elec (um)	2	6	4	0	16	0.0002619	0.0002903	0.0005798	0.0006291	0.0009908	0.001059	0.003451	0.003673
PSE width (um)	50	12	0.5	0	20	0.003166	0.003158	0.005011	0.00501	0.005873	0.005918	0.01386	0.01391
Well width (um)	20	12	1	0	22	0.002442	0.0024	0.003871	0.003791	0.004557	0.004425	0.01068	0.01031
		12	2	0	24	0.002232	0.00223	0.003756	0.003779	0.004431	0.004501	0.01018	0.01038
		12	4	0	26	0.001665	0.001722	0.003169	0.003262	0.00395	0.004072	0.009442	0.009751
		12	8	0	28	0.00414	0.004099	0.008653	0.008571	0.01149	0.01141	0.0308	0.03059

PDC = <S><W> : substrate depth = 3 x 2^(S); well depth = 0.5 x 2^(W/2)

FI-non-BTI-twin-control-3electrode-nwell-array2&3 -633; Normalized QE and scanned QE dependence on Well and Substrate depth.

SJPD PSE CENTRAL RESULTS

						No BTI:next to SCR		No BTI : On SCR		Exp Max	Maximum	Normalized PSE boundary QE	
		Dp subst	Dp well	Dp bti	PDC	QE @ 65	QE @ 95	QE @ 70	QE @ 90	QE @ 80	Max QE	Normz@ 55	Normz@105
n dope (e/ml)	1E+17	3	0.5	0	0	8.987E-07	1.413E-06	2.558E-06	3.658E-06	0.3991	0.3991	7.10599E-07	8.40391E-07
p dope (h/ml)	1E+15	3	1	0	2	1.485E-07	1.516E-07	2.284E-07	2.544E-07	0.3888	0.3888	3.45165E-07	3.45936E-07
rev. bias (V)	2	6	0.5	0	10	0.003894	0.003901	0.003617	0.003646	0.4585	0.4585	0.001589313	0.001604798
W image elec (um)	0.4	6	1	0	12	0.001692	0.001737	0.001537	0.001595	0.4296	0.4296	0.000759544	0.000780028
W guard elec (um)	6.4	6	2	0	14	0.0003886	0.0005095	0.0003658	0.000481	0.4295	0.4295	0.000184563	0.000236088
W subst elec (um)	2	6	4	0	16	0.005808	0.006132	0.006948	0.007462	0.1832	0.1832	0.005408297	0.005780568
Width PSE (um)	50	12	0.5	0	20	0.01732	0.01737	0.01187	0.01195	0.4509	0.4509	0.013025061	0.013124861
Width well (um)	20	12	1	0	22	0.01336	0.01293	0.007845	0.007422	0.4361	0.4361	0.010449438	0.010146755
		12	2	0	24	0.01186	0.01211	0.005892	0.005948	0.4363	0.4363	0.010155856	0.010316296
		12	4	0	26	0.01165	0.01205	0.009366	0.009855	0.1936	0.1936	0.020402893	0.021033058
		12	8	0	28	0.04344	0.04332	0.03742	0.03708	0.05891	0.05891	0.195043286	0.193685283

PDC = <S><W> ; substrate depth = 3 x 2^(S); well depth = 0.5 x 2^(W/2)

APPENDIX VIII.1 : RESULTS - SJPD

BI SJPD PSE 3 electrodes shifted on n-well: Image electrode (IE) QE dependence on IE width, outer electrode width and distance from the well edge (shift).

central el. wth (um)	outer elec(OE) wth(um)	OE shift (um)	well/subst. depth = 2/3 um; well/subst. dope = 1E17(e/ml) / 1E15 (h/ml); reverse bias = 2 volts; 5 um beam (633 nm). cw/ow/sh PDC	PSE Boundary QE @ 55	PSE Boundary QE @ 105	On SCR QE@70	On SCR QE@90	In well QE@75	In well QE@95	Exp Max QE@ 80	Max Max QE	PSE Boundary Nz QE -Nz @ 55	PSE Boundary Nz QE Nz @ 105	Nz QE On SCR Nz@70	Nz QE On SCR Nz@90
0.2	0.2	0	0	1.609E-03	1.780E-03	0.1570	0.1562	0.3782	0.3739	0.5172	0.5172	3.112E-03	3.441E-03	0.3036	0.3019
0.2	0.2	1	0.1	8.112E-04	8.064E-04	0.0813	0.0814	0.3132	0.3077	0.4869	0.4869	**1.666E-03**	**1.660E-03**	0.1669	0.1672
0.2	0.2	2	0.2	8.960E-04	8.893E-04	0.0709	0.0699	0.2707	0.2656	0.4655	0.4655	1.925E-03	1.910E-03	0.1523	0.1502
0.2	0.2	3	0.3	1.195E-03	1.145E-03	0.0829	0.0814	0.2281	0.2237	0.4338	0.4338	2.756E-03	2.639E-03	0.1910	0.1876
0.2	0.2	4	0.4	8.137E-04	7.974E-04	0.0807	0.0792	0.1825	0.1824	0.4139	0.4139	1.966E-03	1.927E-03	0.1949	0.1912
0.2	0.2	5	0.5	8.881E-04	8.985E-04	0.0890	0.0874	0.1490	0.1488	0.3768	0.3768	2.357E-03	2.384E-03	0.2361	0.2319
0.2	0.2	6	0.6	1.051E-03	1.051E-03	0.1024	0.1006	0.1287	0.1325	0.3303	0.3303	3.181E-03	3.181E-03	0.3099	0.3046
0.2	0.2	7	0.7	1.455E-03	1.189E-03	0.1197	0.1173	0.1283	0.1282	0.2685	0.2685	5.420E-03	4.427E-03	0.4457	0.4371
0.2	0.2	8	0.8	1.350E-03	1.438E-03	0.1398	0.1373	0.1415	0.1417	0.2075	0.2075	6.509E-03	6.934E-03	0.6737	0.6616
0.2	0.2	9	0.9	1.580E-03	1.506E-03	0.1467	0.1450	0.1466	0.1482	0.1590	0.1590	9.935E-03	9.472E-03	0.9226	0.9121
0.2	0.4	0	1	8.498E-04	1.064E-03	0.1208	0.1203	0.3549	0.3490	0.5046	0.5046	1.684E-03	2.109E-03	0.2395	0.2385
0.2	0.4	1	1.1	6.757E-04	6.708E-04	0.0659	0.0698	0.2964	0.2973	0.4785	0.4785	**1.412E-03**	**1.402E-03**	0.1377	0.1459
0.2	0.4	2	1.2	7.095E-04	7.478E-04	0.0563	0.0557	0.2445	0.2445	0.4485	0.4485	1.582E-03	1.667E-03	0.1255	0.1241
0.2	0.4	3	1.3	8.155E-04	7.774E-04	0.0598	0.0585	0.2049	0.2051	0.4341	0.4341	1.878E-03	1.791E-03	0.1377	0.1348
0.2	0.4	4	1.4	8.624E-04	6.981E-04	0.0691	0.0678	0.1626	0.1635	0.3908	0.3908	2.207E-03	1.787E-03	0.1768	0.1734
0.2	0.4	5	1.5	7.221E-04	7.647E-04	0.0731	0.0716	0.1291	0.1324	0.3619	0.3619	1.995E-03	2.113E-03	0.2020	0.1979
0.2	0.4	6	1.6	8.555E-04	8.239E-04	0.0843	0.0835	0.1064	0.1091	0.3142	0.3142	2.723E-03	2.622E-03	0.2681	0.2657
0.2	0.4	7	1.7	1.007E-03	1.074E-03	0.0989	0.1013	0.1067	0.1108	0.2453	0.2453	4.106E-03	4.377E-03	0.4030	0.4130
0.2	0.4	8	1.8	1.167E-03	1.156E-03	0.1150	0.1127	0.1165	0.1164	0.1774	0.1774	6.574E-03	6.514E-03	0.6479	0.6351
0.2	0.4	9	1.9	1.107E-03	1.126E-03	0.1098	0.1076	0.1103	0.1097	0.1184	0.1184	9.353E-03	9.511E-03	0.9272	0.9086
0.2	0.8	0	2	5.195E-04	1.111E-03	0.0834	0.0878	0.3282	0.3252	0.4913	0.4913	1.058E-03	2.262E-03	0.1698	0.1788
0.2	0.8	1	2.1	4.897E-04	4.502E-04	0.0494	0.0479	0.2777	0.2720	0.4683	0.4683	**1.046E-03**	**9.614E-04**	0.1055	0.1023
0.2	0.8	2	2.2	5.085E-04	5.331E-04	0.0405	0.0402	0.2249	0.2251	0.4463	0.4463	1.139E-03	1.194E-03	0.0909	0.0900
0.2	0.8	3	2.3	5.340E-04	5.519E-04	0.0391	0.0384	0.1759	0.1766	0.4169	0.4169	1.281E-03	1.324E-03	0.0938	0.0922
0.2	0.8	4	2.4	4.373E-04	4.540E-04	0.0431	0.0424	0.1319	0.1330	0.3798	0.3798	1.151E-03	1.195E-03	0.1134	0.1115
0.2	0.8	5	2.5	6.192E-04	7.144E-04	0.0499	0.0508	0.0949	0.1017	0.3378	0.3378	1.833E-03	2.115E-03	0.1478	0.1505
0.2	0.8	6	2.6	5.770E-04	5.768E-04	0.0573	0.0561	0.0774	0.0774	0.2761	0.2761	2.090E-03	2.089E-03	0.2073	0.2030
0.2	0.8	7	2.7	6.985E-04	6.728E-04	0.0666	0.0674	0.0727	0.0750	0.2000	0.2000	3.493E-03	3.364E-03	0.3328	0.3370
0.2	0.8	8	2.8	8.392E-04	8.302E-04	0.0775	0.0785	0.0785	0.0823	0.1330	0.1330	6.311E-03	6.244E-03	0.5829	0.5906
0.2	1.6	0	3	2.375E-04	3.853E-04	0.0484	0.0471	0.2803	0.2789	0.4750	0.4750	5.000E-04	8.112E-04	0.1019	0.0992
0.2	1.6	1	3.1	2.204E-04	2.137E-04	0.0229	0.0228	0.2153	0.2200	0.4308	0.4308	**5.116E-04**	**4.961E-04**	0.0531	0.0530
0.2	1.6	2	3.2	2.428E-04	2.404E-04	0.0186	0.0186	0.1692	0.1654	0.3967	0.3967	6.121E-04	6.061E-04	0.0470	0.0468
0.2	1.6	3	3.3	2.583E-04	2.712E-04	0.0190	0.0188	0.1201	0.1192	0.3629	0.3629	7.117E-04	7.474E-04	0.0525	0.0519
0.2	1.6	4	3.4	2.230E-04	2.253E-04	0.0220	0.0220	0.0863	0.0857	0.3382	0.3382	6.593E-04	6.663E-04	0.0651	0.0651
0.2	1.6	5	3.5	3.317E-04	2.905E-04	0.0269	0.0270	0.0538	0.0572	0.2950	0.2950	1.124E-03	9.847E-04	0.0913	0.0915
0.2	1.6	6	3.6	3.021E-04	4.096E-04	0.0309	0.0289	0.0456	0.0433	0.2082	0.2082	1.451E-03	1.967E-03	0.1482	0.1389
0.2	1.6	7	3.7	3.374E-04	3.590E-04	0.0352	0.0344	0.0394	0.0394	0.1327	0.1327	2.543E-03	2.705E-03	0.2652	0.2596
0.2	1.6	8	3.8	2.720E-04	2.769E-04	0.0259	0.0257	0.0270	0.0270	0.0504	0.0504	5.395E-03	5.492E-03	0.5146	0.5095
0.2	3.2	0	4	7.444E-05	1.180E-04	0.0139	0.0140	0.1884	0.1878	0.4153	0.4153	1.793E-04	2.842E-04	0.0334	0.0338
0.2	3.2	1	4.1	8.469E-05	8.471E-05	0.0088	0.0092	0.1386	0.1394	0.3823	0.3823	**2.215E-04**	**2.216E-04**	0.0230	0.0240
0.2	3.2	2	4.2	8.451E-05	1.045E-04	0.0067	0.0079	0.0897	0.0969	0.3335	0.3335	2.534E-04	3.133E-04	0.0201	0.0238
0.2	3.2	3	4.3	1.163E-04	1.175E-04	0.0081	0.0082	0.0590	0.0586	0.2834	0.2834	4.105E-04	4.145E-04	0.0286	0.0289
0.2	3.2	4	4.4	1.028E-04	9.837E-05	0.0095	0.0093	0.0364	0.0373	0.2194	0.2194	4.684E-04	4.483E-04	0.0432	0.0425
0.2	3.2	5	4.5	1.166E-04	1.135E-04	0.0112	0.0111	0.0230	0.0239	0.1549	0.1549	7.530E-04	7.330E-04	0.0723	0.0720
0.2	3.2	6	4.6	1.153E-04	1.189E-04	0.0110	0.0108	0.0160	0.0159	0.0813	0.0813	1.418E-03	1.462E-03	0.1348	0.1323
0.4	0.2	0	10	1.650E-03	1.764E-03	0.1620	0.1613	0.3843	0.3855	0.5321	0.5321	3.101E-03	3.316E-03	0.3044	0.3032
0.4	0.2	1	10.1	1.011E-03	1.008E-03	0.0956	0.0954	0.3268	0.3301	0.5066	0.5066	1.995E-03	1.990E-03	0.1888	0.1883
0.4	0.2	2	10.2	9.301E-04	9.336E-04	0.0738	0.0730	0.2760	0.2826	0.4858	0.4858	**1.915E-03**	**1.922E-03**	0.1520	0.1503
0.4	0.2	3	10.3	1.211E-03	1.194E-03	0.0882	0.0869	0.2381	0.2449	0.4616	0.4616	2.622E-03	2.588E-03	0.1910	0.1882
0.4	0.2	4	10.4	8.973E-04	8.738E-04	0.0849	0.0830	0.1893	0.1900	0.4383	0.4383	2.047E-03	1.994E-03	0.1937	0.1895
0.4	0.2	5	10.5	9.786E-04	9.696E-04	0.0946	0.0929	0.1565	0.1633	0.3949	0.3949	2.478E-03	2.455E-03	0.2395	0.2352
0.4	0.2	6	10.6	1.142E-03	1.117E-03	0.1094	0.1076	0.1372	0.1418	0.3488	0.3488	3.273E-03	3.203E-03	0.3136	0.3085
0.4	0.2	7	10.7	1.366E-03	1.551E-03	0.1289	0.1289	0.1379	0.1408	0.2867	0.2867	4.764E-03	5.407E-03	0.4494	0.4497
0.4	0.2	8	10.8	1.580E-03	1.557E-03	0.1544	0.1518	0.1563	0.1565	0.2261	0.2261	6.988E-03	6.886E-03	0.6829	0.6715
0.4	0.2	9	10.9	1.660E-03	1.774E-03	0.1667	0.1662	0.1665	0.1699	0.1809	0.1809	9.179E-03	9.810E-03	0.9215	0.9189
0.4	0.4	0	11	1.085E-03	8.722E-04	0.1248	0.1242	0.3584	0.3584	0.5242	0.5242	2.069E-03	1.664E-03	0.2382	0.2369
0.4	0.4	1	11.1	7.042E-04	7.215E-04	0.0687	0.0714	0.3074	0.3044	0.5017	0.5017	**1.404E-03**	**1.438E-03**	0.1370	0.1424
0.4	0.4	2	11.2	7.605E-04	8.061E-04	0.0607	0.0599	0.2610	0.2601	0.4801	0.4801	1.584E-03	1.679E-03	0.1264	0.1249
0.4	0.4	3	11.3	8.555E-04	8.565E-04	0.0625	0.0613	0.2122	0.2110	0.4579	0.4579	1.868E-03	1.871E-03	0.1366	0.1339
0.4	0.4	4	11.4	7.511E-04	7.340E-04	0.0743	0.0729	0.1735	0.1717	0.4216	0.4216	1.782E-03	1.741E-03	0.1763	0.1730
0.4	0.4	5	11.5	7.821E-04	8.157E-04	0.0776	0.0763	0.1369	0.1435	0.3812	0.3812	2.052E-03	2.140E-03	0.2037	0.2001
0.4	0.4	6	11.6	9.350E-04	9.203E-04	0.0905	0.0893	0.1144	0.1178	0.3370	0.3370	2.775E-03	2.731E-03	0.2687	0.2650
0.4	0.4	7	11.7	1.122E-03	1.095E-03	0.1078	0.1095	0.1162	0.1197	0.2636	0.2636	4.257E-03	4.154E-03	0.4089	0.4153
0.4	0.4	8	11.8	1.304E-03	1.700E-03	0.1286	0.1379	0.1303	0.1418	0.2008	0.2008	6.493E-03	8.467E-03	0.6405	0.6866
0.4	0.4	9	11.9	1.339E-03	1.261E-03	0.1266	0.1242	0.1271	0.1265	0.1370	0.1370	9.771E-03	9.208E-03	0.9239	0.9066
0.4	0.8	0	12	6.616E-04	7.101E-04	0.0865	0.0910	0.3350	0.3348	0.5123	0.5123	1.292E-03	1.386E-03	0.1688	0.1776
0.4	0.8	1	12.1	4.960E-04	4.661E-04	0.0513	0.0499	0.2811	0.2797	0.4905	0.4905	**1.011E-03**	**9.504E-04**	0.1047	0.1017
0.4	0.8	2	12.2	5.311E-04	5.480E-04	0.0424	0.0420	0.2340	0.2322	0.4691	0.4691	1.132E-03	1.168E-03	0.0904	0.0896
0.4	0.8	3	12.3	5.617E-04	5.923E-04	0.0408	0.0413	0.1829	0.1888	0.4343	0.4343	1.293E-03	1.364E-03	0.0939	0.0950
0.4	0.8	4	12.4	4.795E-04	4.508E-04	0.0455	0.0458	0.1397	0.1417	0.3963	0.3963	1.210E-03	1.138E-03	0.1149	0.1156
0.4	0.8	5	12.5	6.620E-04	5.431E-04	0.0535	0.0533	0.1037	0.1050	0.3629	0.3629	1.824E-03	1.496E-03	0.1474	0.1469
0.4	0.8	6	12.6	5.980E-04	6.251E-04	0.0616	0.0605	0.0834	0.0832	0.2930	0.2930	2.041E-03	2.133E-03	0.2104	0.2063
0.4	0.8	7	12.7	7.727E-04	8.072E-04	0.0733	0.0758	0.0800	0.0844	0.2186	0.2186	3.534E-03	3.692E-03	0.3351	0.3468
0.4	0.8	8	12.8	9.089E-04	1.531E-03	0.0884	0.0867	0.0896	0.0907	0.1494	0.1494	6.082E-03	1.024E-02	0.5917	0.5801

PDC = <n><m>.<shrink distance (um)> : central ew = 0.2*2^n: shielding ew = 0.2*2^m (um).

APPENDIX VIII.2 : RESULTS - SJPD

BI-SJPD-PSE-3electrodes-shifted continued: page 2 of 3.

central el. wth (um)	outer elec(OE) wth(um)	OE shift (um)	Highlighted Normalized (Nz) QE is lowest crosstalk value for total parameter permutation set.												
			cw/ow/sh	PSE Boundary		On SCR		In well		Exp Max	Max	PSE Boundary Nz QE		Nz QE On SCR	
			PDC	QE @ 55	QE @ 105	QE@70	QE@90	QE@75	QE@95	QE@ 80	Max QE	Nz @ 55	Nz @ 105	Nz@70	Nz@90
0.4	1.6	0	13	2.475E-04	3.986E-04	0.0504	0.0490	0.2899	0.2924	0.4909	0.4909	5.042E-04	8.121E-04	0.1027	0.0998
0.4	1.6	1	13.1	2.353E-04	2.290E-04	0.0245	0.0245	0.2298	0.2285	0.4614	0.4614	**5.100E-04**	**4.964E-04**	0.0531	0.0530
0.4	1.6	2	13.2	2.579E-04	2.654E-04	0.0208	0.0206	0.1823	0.1799	0.4432	0.4432	5.819E-04	5.988E-04	0.0469	0.0465
0.4	1.6	3	13.3	2.946E-04	3.060E-04	0.0216	0.0213	0.1330	0.1337	0.4090	0.4090	7.202E-04	7.481E-04	0.0527	0.0520
0.4	1.6	4	13.4	2.410E-04	2.459E-04	0.0234	0.0240	0.0917	0.0928	0.3531	0.3531	6.826E-04	6.965E-04	0.0663	0.0679
0.4	1.6	5	13.5	2.816E-04	2.950E-04	0.0292	0.0299	0.0586	0.0639	0.3107	0.3107	9.065E-04	9.495E-04	0.0939	0.0961
0.4	1.6	6	13.6	3.130E-04	3.676E-04	0.0312	0.0340	0.0461	0.0509	0.2245	0.2245	1.394E-03	1.637E-03	0.1391	0.1514
0.4	1.6	7	13.7	3.910E-04	4.023E-04	0.0386	0.0377	0.0432	0.0432	0.1464	0.1464	2.670E-03	2.748E-03	0.2634	0.2577
0.4	1.6	8	13.8	3.342E-04	3.244E-04	0.0315	0.0310	0.0327	0.0327	0.0610	0.0610	5.481E-03	5.320E-03	0.5169	0.5089
0.4	3.2	0	14	8.257E-05	1.333E-04	0.0154	0.0158	0.2053	0.2051	0.4559	0.4559	1.811E-04	2.924E-04	0.0337	0.0347
0.4	3.2	1	14.1	7.607E-05	7.990E-05	0.0079	0.0086	0.1458	0.1478	0.4149	0.4149	**1.833E-04**	**1.926E-04**	0.0190	0.0206
0.4	3.2	2	14.2	1.156E-04	1.039E-04	0.0092	0.0078	0.1094	0.1047	0.3721	0.3721	3.105E-04	2.792E-04	0.0247	0.0210
0.4	3.2	3	14.3	1.229E-04	1.231E-04	0.0090	0.0088	0.0632	0.0624	0.3284	0.3284	3.744E-04	3.748E-04	0.0274	0.0269
0.4	3.2	4	14.4	1.306E-04	1.112E-04	0.0107	0.0105	0.0409	0.0419	0.2475	0.2475	5.275E-04	4.495E-04	0.0432	0.0423
0.4	3.2	5	14.5	1.294E-04	1.266E-04	0.0127	0.0122	0.0259	0.0263	0.1782	0.1782	7.263E-04	7.116E-04	0.0711	0.0686
0.4	3.2	6	14.6	1.310E-04	1.364E-04	0.0126	0.0125	0.0184	0.0184	0.0929	0.0929	1.410E-03	1.468E-03	0.1356	0.1343
0.8	0.2	0	20	1.763E-03	1.856E-03	0.1700	0.1690	0.3984	0.4014	0.5696	0.5696	3.095E-03	3.259E-03	0.2985	0.2968
0.8	0.2	1	20.1	8.795E-04	9.144E-04	0.0895	0.0897	0.3313	0.3358	0.5488	0.5488	**1.603E-03**	**1.666E-03**	0.1630	0.1635
0.8	0.2	2	20.2	9.888E-04	9.607E-04	0.0787	0.0776	0.2858	0.2901	0.5340	0.5340	1.852E-03	1.799E-03	0.1474	0.1454
0.8	0.2	3	20.3	1.323E-03	1.292E-03	0.0961	0.0945	0.2520	0.2506	0.5162	0.5162	2.562E-03	2.504E-03	0.1862	0.1830
0.8	0.2	4	20.4	9.700E-04	9.517E-04	0.0924	0.0900	0.2029	0.2139	0.4634	0.4634	2.093E-03	2.054E-03	0.1993	0.1942
0.8	0.2	5	20.5	1.010E-03	1.809E-03	0.1033	0.1017	0.1735	0.1741	0.4200	0.4200	2.406E-03	4.307E-03	0.2460	0.2421
0.8	0.2	6	20.6	1.242E-03	1.205E-03	0.1213	0.1193	0.1518	0.1532	0.3780	0.3780	3.286E-03	3.188E-03	0.3210	0.3155
0.8	0.2	7	20.7	1.549E-03	1.513E-03	0.1479	0.1452	0.1581	0.1579	0.3180	0.3180	4.871E-03	4.760E-03	0.4652	0.4568
0.8	0.2	8	20.8	1.721E-03	1.856E-03	0.1764	0.1743	0.1784	0.1794	0.2553	0.2553	6.742E-03	7.269E-03	0.6908	0.6825
0.8	0.2	9	20.9	2.173E-03	2.143E-03	0.2043	0.2020	0.2041	0.2063	0.2184	0.2184	9.946E-03	9.811E-03	0.9353	0.9245
0.8	0.4	0	21	9.594E-04	9.949E-04	0.1328	0.1320	0.3729	0.3762	0.5627	0.5627	1.705E-03	1.768E-03	0.2360	0.2346
0.8	0.4	1	21.1	7.448E-04	7.242E-04	0.0728	0.0758	0.3183	0.3223	0.5431	0.5431	**1.372E-03**	**1.334E-03**	0.1340	0.1395
0.8	0.4	2	21.2	8.141E-04	8.410E-04	0.0648	0.0640	0.2732	0.2742	0.5299	0.5299	1.536E-03	1.587E-03	0.1223	0.1209
0.8	0.4	3	21.3	9.207E-04	1.076E-03	0.0672	0.0723	0.2271	0.2347	0.4730	0.4730	1.946E-03	2.274E-03	0.1421	0.1528
0.8	0.4	4	21.4	8.524E-04	1.205E-03	0.0820	0.0816	0.1821	0.1928	0.4716	0.4716	1.807E-03	2.554E-03	0.1738	0.1730
0.8	0.4	5	21.5	8.608E-04	1.030E-03	0.0855	0.0848	0.1503	0.1520	0.4063	0.4063	2.119E-03	2.535E-03	0.2103	0.2086
0.8	0.4	6	21.6	1.025E-03	1.041E-03	0.1022	0.1008	0.1321	0.1314	0.3586	0.3586	2.857E-03	2.904E-03	0.2851	0.2812
0.8	0.4	7	21.7	1.260E-03	1.297E-03	0.1231	0.1258	0.1324	0.1370	0.2946	0.2946	4.278E-03	4.403E-03	0.4178	0.4270
0.8	0.4	8	21.8	1.511E-03	2.948E-03	0.1483	0.1634	0.1502	0.1679	0.2298	0.2298	6.576E-03	1.283E-02	0.6454	0.7109
0.8	0.4	9	21.9	1.677E-03	1.658E-03	0.1622	0.1591	0.1629	0.1620	0.1728	0.1728	9.702E-03	9.596E-03	0.9385	0.9207
0.8	0.8	0	22	7.362E-04	8.522E-04	0.0914	0.0961	0.3470	0.3503	0.5350	0.5350	1.376E-03	1.593E-03	0.1708	0.1796
0.8	0.8	1	22.1	5.421E-04	5.213E-04	0.0546	0.0534	0.2989	0.3015	0.5017	0.5017	**1.081E-03**	**1.039E-03**	0.1088	0.1065
0.8	0.8	2	22.2	5.670E-04	5.841E-04	0.0455	0.0450	0.2430	0.2467	0.5178	0.5178	1.095E-03	1.128E-03	0.0879	0.0869
0.8	0.8	3	22.3	6.039E-04	6.255E-04	0.0443	0.0438	0.1930	0.2051	0.4655	0.4655	1.297E-03	1.344E-03	0.0952	0.0941
0.8	0.8	4	22.4	5.052E-04	5.921E-04	0.0501	0.0491	0.1525	0.1525	0.4235	0.4235	1.193E-03	1.398E-03	0.1182	0.1160
0.8	0.8	5	22.5	6.220E-04	6.053E-04	0.0592	0.0590	0.1113	0.1173	0.3906	0.3906	1.592E-03	1.550E-03	0.1515	0.1510
0.8	0.8	6	22.6	6.710E-04	7.625E-04	0.0699	0.0696	0.0941	0.0958	0.3238	0.3238	2.072E-03	2.355E-03	0.2159	0.2150
0.8	0.8	7	22.7	9.036E-04	9.338E-04	0.0865	0.0866	0.0943	0.0962	0.2489	0.2489	3.631E-03	3.752E-03	0.3475	0.3479
0.8	0.8	8	22.8	1.055E-03	1.058E-03	0.1021	0.1002	0.1035	0.1042	0.1758	0.1758	6.001E-03	6.016E-03	0.5807	0.5701
0.8	1.6	0	23	2.587E-04	4.259E-04	0.0528	0.0521	0.2997	0.3036	0.5374	0.5374	4.814E-04	7.925E-04	0.0982	0.0969
0.8	1.6	1	23.1	2.599E-04	2.514E-04	0.0269	0.0268	0.2457	0.2606	0.4932	0.4932	**5.269E-04**	**5.097E-04**	0.0546	0.0544
0.8	1.6	2	23.2	2.932E-04	2.952E-04	0.0226	0.0223	0.1969	0.1998	0.4581	0.4581	6.401E-04	6.444E-04	0.0492	0.0488
0.8	1.6	3	23.3	3.213E-04	3.068E-04	0.0236	0.0233	0.1387	0.1510	0.4398	0.4398	7.305E-04	6.975E-04	0.0536	0.0529
0.8	1.6	4	23.4	2.646E-04	3.231E-04	0.0260	0.0281	0.1012	0.1056	0.3847	0.3847	6.878E-04	8.398E-04	0.0677	0.0732
0.8	1.6	5	23.5	3.421E-04	3.953E-04	0.0331	0.0369	0.0676	0.0787	0.3354	0.3354	1.020E-03	1.178E-03	0.0988	0.1099
0.8	1.6	6	23.6	3.967E-04	3.878E-04	0.0373	0.0367	0.0549	0.0549	0.2557	0.2557	1.551E-03	1.517E-03	0.1458	0.1435
0.8	1.6	7	23.7	4.495E-04	5.562E-04	0.0446	0.0438	0.0501	0.0502	0.1735	0.1735	2.591E-03	3.207E-03	0.2571	0.2527
0.8	3.2	0	24	9.115E-05	1.482E-04	0.0168	0.0173	0.2112	0.2208	0.4793	0.4793	1.902E-04	3.093E-04	0.0351	0.0361
0.8	3.2	1	24.1	8.353E-05	9.435E-05	0.0087	0.0098	0.1574	0.1556	0.4498	0.4498	**1.857E-04**	**2.097E-04**	0.0193	0.0218
0.8	3.2	2	24.2	1.138E-04	1.259E-04	0.0086	0.0104	0.1148	0.1211	0.3990	0.3990	2.851E-04	3.156E-04	0.0216	0.0260
0.8	3.2	3	24.3	1.267E-04	1.301E-04	0.0093	0.0091	0.0559	0.0592	0.3918	0.3918	3.234E-04	3.320E-04	0.0237	0.0232
0.8	3.2	4	24.4	1.219E-04	1.283E-04	0.0122	0.0118	0.0461	0.0464	0.2836	0.2836	4.299E-04	4.523E-04	0.0429	0.0416
0.8	3.2	5	24.5	1.642E-04	1.655E-04	0.0156	0.0151	0.0319	0.0323	0.2071	0.2071	7.931E-04	7.994E-04	0.0754	0.0727
0.8	3.2	6	24.6	1.571E-04	1.517E-04	0.0156	0.0152	0.0226	0.0224	0.1131	0.1131	1.389E-03	1.341E-03	0.1381	0.1346
1.6	0.2	0	30	1.896E-03	2.035E-03	0.1818	0.1812	0.4279	0.4253	0.5484	0.5484	3.458E-03	3.712E-03	0.3315	0.3304
1.6	0.2	1	30.1	1.003E-03	9.737E-04	0.0972	0.0989	0.3633	0.3619	0.5270	0.5270	**1.904E-03**	**1.848E-03**	0.1845	0.1876
1.6	0.2	2	30.2	1.089E-03	1.081E-03	0.0862	0.0850	0.3182	0.3160	0.5144	0.5144	2.117E-03	2.102E-03	0.1675	0.1652
1.6	0.2	3	30.3	1.460E-03	1.517E-03	0.1065	0.1045	0.2824	0.2809	0.5022	0.5022	2.907E-03	3.020E-03	0.2121	0.2081
1.6	0.2	4	30.4	1.059E-03	1.024E-03	0.1038	0.1007	0.2296	0.2269	0.4767	0.4767	2.222E-03	2.147E-03	0.2177	0.2112
1.6	0.2	5	30.5	1.210E-03	1.515E-03	0.1182	0.1167	0.1969	0.1930	0.4487	0.4487	2.696E-03	3.377E-03	0.2635	0.2601
1.6	0.2	6	30.6	1.421E-03	1.427E-03	0.1406	0.1387	0.1753	0.1761	0.4128	0.4128	3.443E-03	3.458E-03	0.3406	0.3361
1.6	0.2	7	30.7	1.743E-03	1.830E-03	0.1727	0.1696	0.1838	0.1836	0.3550	0.3550	4.910E-03	5.154E-03	0.4865	0.4777
1.6	0.2	8	30.8	2.226E-03	3.778E-03	0.2181	0.2135	0.2192	0.2194	0.2991	0.2991	7.441E-03	1.263E-02	0.7290	0.7139

PDC = <n><m>.<shrink distance (um)> ; central ew = 0.2*2^n; shielding ew = 0.2*2^m (um).

APPENDIX VIII.3 : RESULTS - SJPD

central	outer	OE	Bolded values represent lowest relative crosstalk for each shift permutation set.												
el. wth	elec(OE)	shift	cw/ow/sh	PSE Boundary		On SCR		In well		Exp Max	Max	PSE Boundary Nz QE		Nz QE On SCR	
(um)	wth(um)	(um)	PDC	QE @ 55	QE @ 105	QE@70	QE@90	QE@75	QE@95	QE@ 80	Max QE	Nz @ 55	Nz @ 105	Nz@70	Nz@90
1.6	0.4	0	31	1.203E-03	9.845E-04	0.1412	0.1419	0.4043	0.4027	0.5384	0.5384	2.235E-03	1.829E-03	0.2623	0.2635
1.6	0.4	1	31.1	7.904E-04	7.935E-04	0.0792	0.0812	0.3509	0.3497	0.5227	0.5227	**1.512E-03**	**1.518E-03**	0.1516	0.1554
1.6	0.4	2	31.2	8.977E-04	9.711E-04	0.0712	0.0703	0.3021	0.2999	0.5107	0.5107	1.758E-03	1.902E-03	0.1394	0.1377
1.6	0.4	3	31.3	1.024E-03	9.988E-04	0.0749	0.0736	0.2534	0.2506	0.4922	0.4922	2.079E-03	2.029E-03	0.1522	0.1495
1.6	0.4	4	31.4	1.019E-03	1.635E-03	0.0934	0.0917	0.2149	0.2133	0.4720	0.4720	2.159E-03	3.464E-03	0.1978	0.1942
1.6	0.4	5	31.5	9.961E-04	1.366E-03	0.0982	0.0979	0.1697	0.1719	0.4351	0.4351	2.289E-03	3.139E-03	0.2256	0.2250
1.6	0.4	6	31.6	1.160E-03	1.181E-03	0.1171	0.1168	0.1477	0.1505	0.4027	0.4027	2.880E-03	2.933E-03	0.2907	0.2899
1.6	0.4	7	31.7	1.569E-03	1.507E-03	0.1451	0.1466	0.1550	0.1595	0.3284	0.3284	4.778E-03	4.589E-03	0.4420	0.4470
1.6	0.4	8	31.8	1.916E-03	2.130E-03	0.1875	0.2006	0.1895	0.2055	0.2738	0.2738	6.997E-03	7.778E-03	0.6849	0.7326
1.6	0.8	0	32	6.593E-04	7.888E-04	0.0988	0.1048	0.3782	0.3753	0.5321	0.5321	1.239E-03	1.482E-03	0.1857	0.1969
1.6	0.8	1	32.1	5.788E-04	5.910E-04	0.0597	0.0597	0.3256	0.3231	0.5164	0.5164	**1.121E-03**	**1.144E-03**	0.1156	0.1157
1.6	0.8	2	32.2	6.332E-04	6.679E-04	0.0505	0.0500	0.2748	0.2722	0.5003	0.5003	1.266E-03	1.335E-03	0.1010	0.0999
1.6	0.8	3	32.3	6.781E-04	7.011E-04	0.0496	0.0490	0.2190	0.2175	0.4807	0.4807	1.411E-03	1.459E-03	0.1031	0.1020
1.6	0.8	4	32.4	5.760E-04	6.752E-04	0.0568	0.0562	0.1700	0.1699	0.4510	0.4510	1.277E-03	1.497E-03	0.1259	0.1246
1.6	0.8	5	32.5	6.765E-04	6.913E-04	0.0673	0.0682	0.1288	0.1318	0.4182	0.4182	1.618E-03	1.653E-03	0.1610	0.1630
1.6	0.8	6	32.6	8.901E-04	9.229E-04	0.0826	0.0854	0.1101	0.1161	0.3627	0.3627	2.454E-03	2.544E-03	0.2277	0.2354
1.6	0.8	7	32.7	1.092E-03	1.055E-03	0.1066	0.1067	0.1158	0.1181	0.2860	0.2860	3.819E-03	3.688E-03	0.3726	0.3732
1.6	0.8	8	32.8	1.431E-03	1.452E-03	0.1373	0.1347	0.1388	0.1396	0.2188	0.2188	6.538E-03	6.634E-03	0.6273	0.6157
1.6	1.6	0	33	2.895E-04	4.640E-04	0.0585	0.0568	0.3337	0.3303	0.5170	0.5170	5.600E-04	8.975E-04	0.1131	0.1099
1.6	1.6	1	33.1	2.858E-04	2.866E-04	0.0297	0.0297	0.2750	0.2720	0.5015	0.5015	**5.699E-04**	**5.714E-04**	0.0592	0.0592
1.6	1.6	2	33.2	3.130E-04	3.329E-04	0.0251	0.0258	0.2224	0.2182	0.4803	0.4803	6.518E-04	6.931E-04	0.0523	0.0538
1.6	1.6	3	33.3	3.578E-04	4.230E-04	0.0263	0.0288	0.1603	0.1701	0.4565	0.4565	7.837E-04	9.265E-04	0.0576	0.0630
1.6	1.6	4	33.4	3.066E-04	3.227E-04	0.0312	0.0312	0.1211	0.1166	0.4177	0.4177	7.340E-04	7.726E-04	0.0748	0.0747
1.6	1.6	5	33.5	4.069E-04	4.265E-04	0.0407	0.0400	0.0845	0.0842	0.3721	0.3721	1.093E-03	1.151E-03	0.1093	0.1075
1.6	1.6	6	33.6	4.271E-04	4.198E-04	0.0417	0.0411	0.0612	0.0611	0.2966	0.2966	1.440E-03	1.416E-03	0.1408	0.1385
1.6	1.6	7	33.7	5.674E-04	6.245E-04	0.0566	0.0576	0.0657	0.0658	0.2088	0.2088	2.717E-03	2.991E-03	0.2808	0.2759
1.6	3.2	0	34	9.880E-05	1.551E-04	0.0185	0.0184	0.2398	0.2389	0.4885	0.4885	2.022E-04	3.176E-04	0.0379	0.0377
1.6	3.2	1	34.1	9.617E-05	9.480E-05	0.0100	0.0099	0.1769	0.1735	0.4708	0.4708	**2.043E-04**	**2.013E-04**	0.0212	0.0210
1.6	3.2	2	34.2	1.301E-04	1.217E-04	0.0103	0.0101	0.1301	0.1276	0.4338	0.4338	2.999E-04	2.805E-04	0.0238	0.0232
1.6	3.2	3	34.3	1.705E-04	1.800E-04	0.0125	0.0122	0.0857	0.0857	0.3880	0.3880	4.394E-04	4.639E-04	0.0321	0.0315
1.6	3.2	4	34.4	1.418E-04	1.351E-04	0.0134	0.0132	0.0517	0.0507	0.3289	0.3289	4.304E-04	4.108E-04	0.0407	0.0401
1.6	3.2	5	34.5	1.990E-04	1.933E-04	0.0190	0.0183	0.0386	0.0391	0.2485	0.2485	8.009E-04	7.780E-04	0.0764	0.0737
3.2	0.2	0	40	2.057E-03	2.253E-03	0.2000	0.1992	0.4406	0.4334	0.5755	0.5755	3.574E-03	3.915E-03	0.3475	0.3462
3.2	0.2	1	40.1	1.124E-03	1.100E-03	0.1088	0.1081	0.3766	0.3982	0.5572	0.5572	**2.017E-03**	**1.975E-03**	0.1952	0.1939
3.2	0.2	2	40.2	1.268E-03	1.293E-03	0.0963	0.0950	0.3444	0.3554	0.5368	0.5368	2.363E-03	2.409E-03	0.1795	0.1770
3.2	0.2	3	40.3	1.657E-03	1.759E-03	0.1200	0.1178	0.3093	0.3117	0.5244	0.5244	3.159E-03	3.353E-03	0.2289	0.2247
3.2	0.2	4	40.4	1.227E-03	2.310E-03	0.1198	0.1182	0.2502	0.2518	0.5199	0.5199	2.361E-03	4.443E-03	0.2305	0.2274
3.2	0.2	5	40.5	1.798E-03	1.475E-03	0.1713	0.1376	0.2493	0.2247	0.4865	0.4865	3.696E-03	3.031E-03	0.3520	0.2827
3.2	0.2	6	40.6	1.873E-03	1.873E-03	0.1754	0.1725	0.2130	0.2159	0.4571	0.4571	4.098E-03	4.098E-03	0.3837	0.3774
3.2	0.2	7	40.7	2.279E-03	2.332E-03	0.2255	0.2206	0.2363	0.2363	0.4080	0.4080	5.584E-03	5.714E-03	0.5527	0.5411
3.2	0.2	8	40.8	3.254E-03	3.246E-03	0.3160	0.3107	0.3170	0.3172	0.3874	0.3874	8.399E-03	8.379E-03	0.8156	0.8019
3.2	0.4	0	41	1.114E-03	1.150E-03	0.1561	0.1538	0.4308	0.4308	0.5727	0.5727	1.944E-03	2.008E-03	0.2725	0.2686
3.2	0.4	1	41.1	9.619E-04	9.415E-04	0.0889	0.0928	0.3680	0.3619	0.5633	0.5633	**1.708E-03**	**1.671E-03**	0.1576	0.1648
3.2	0.4	2	41.2	1.068E-03	1.055E-03	0.0810	0.0802	0.3221	0.3183	0.5543	0.5543	1.926E-03	1.903E-03	0.1462	0.1447
3.2	0.4	3	41.3	1.182E-03	1.357E-03	0.0866	0.0967	0.2734	0.2814	0.5439	0.5439	2.174E-03	2.495E-03	0.1593	0.1777
3.2	0.4	4	41.4	1.095E-03	1.150E-03	0.1096	0.1076	0.2334	0.2347	0.5311	0.5311	2.062E-03	2.164E-03	0.2064	0.2026
3.2	0.4	5	41.5	1.232E-03	2.031E-03	0.1178	0.1154	0.1982	0.2000	0.4759	0.4759	2.588E-03	4.268E-03	0.2474	0.2424
3.2	0.4	6	41.6	1.550E-03	1.521E-03	0.1492	0.1471	0.1877	0.1869	0.4357	0.4357	3.558E-03	3.491E-03	0.3424	0.3377
3.2	0.4	7	41.7	2.004E-03	2.016E-03	0.1935	0.1961	0.2055	0.2110	0.3882	0.3882	5.162E-03	5.192E-03	0.4984	0.5051
3.2	0.8	0	42	9.490E-04	7.340E-04	0.1189	0.1149	0.3945	0.4049	0.5576	0.5576	1.702E-03	1.316E-03	0.2132	0.2061
3.2	0.8	1	42.1	6.569E-04	6.237E-04	0.0680	0.0658	0.3454	0.3374	0.5572	0.5572	**1.179E-03**	**1.119E-03**	0.1221	0.1181
3.2	0.8	2	42.2	7.187E-04	7.704E-04	0.0575	0.0573	0.2944	0.2907	0.5511	0.5511	1.304E-03	1.398E-03	0.1043	0.1040
3.2	0.8	3	42.3	7.859E-04	8.432E-04	0.0575	0.0573	0.2387	0.2457	0.5203	0.5203	1.510E-03	1.621E-03	0.1105	0.1102
3.2	0.8	4	42.4	6.877E-04	6.918E-04	0.0674	0.0662	0.1947	0.1984	0.4885	0.4885	1.408E-03	1.416E-03	0.1360	0.1354
3.2	0.8	5	42.5	8.255E-04	9.044E-04	0.0841	0.0843	0.1534	0.1632	0.4695	0.4695	1.756E-03	1.926E-03	0.1791	0.1796
3.2	0.8	6	42.6	1.111E-03	1.183E-03	0.1103	0.1081	0.1446	0.1449	0.4082	0.4082	2.721E-03	2.899E-03	0.2701	0.2649
3.2	0.8	7	42.7	1.526E-03	1.944E-03	0.1500	0.1501	0.1615	0.1646	0.3523	0.3523	4.331E-03	5.518E-03	0.4257	0.4261
3.2	1.6	0	43	3.191E-04	5.690E-04	0.0644	0.0659	0.3537	0.3653	0.5537	0.5537	5.764E-04	1.028E-03	0.1163	0.1191
3.2	1.6	1	43.1	3.409E-04	3.978E-04	0.0349	0.0426	0.2846	0.3195	0.5443	0.5443	**6.264E-04**	**7.310E-04**	0.0641	0.0782
3.2	1.6	2	43.2	3.690E-04	4.406E-04	0.0295	0.0332	0.2324	0.2424	0.5352	0.5352	6.894E-04	8.232E-04	0.0552	0.0621
3.2	1.6	3	43.3	4.426E-04	4.442E-04	0.0325	0.0321	0.1816	0.1839	0.5215	0.5215	8.487E-04	8.517E-04	0.0623	0.0615
3.2	1.6	4	43.4	4.279E-04	4.836E-04	0.0407	0.0407	0.1399	0.1436	0.4655	0.4655	9.191E-04	1.039E-03	0.0875	0.0874
3.2	1.6	5	43.5	5.107E-04	5.089E-04	0.0495	0.0486	0.0902	0.0878	0.4555	0.4555	1.121E-03	1.117E-03	0.1086	0.1066
3.2	1.6	6	43.6	6.752E-04	6.705E-04	0.0644	0.0634	0.0927	0.0926	0.3496	0.3496	1.931E-03	1.918E-03	0.1842	0.1813
3.2	3.2	0	44	1.211E-04	1.947E-04	0.0226	0.0227	0.2630	0.2622	0.5358	0.5358	2.260E-04	3.633E-04	0.0421	0.0423
3.2	3.2	1	44.1	1.273E-04	1.267E-04	0.0127	0.0133	0.1976	0.1996	0.5276	0.5276	**2.413E-04**	**2.402E-04**	0.0241	0.0253
3.2	3.2	2	44.2	1.346E-04	1.379E-04	0.0107	0.0104	0.1270	0.1232	0.5138	0.5138	2.619E-04	2.684E-04	0.0208	0.0202
3.2	3.2	3	44.3	1.974E-04	1.992E-04	0.0145	0.0142	0.0874	0.0901	0.4801	0.4801	4.113E-04	4.150E-04	0.0301	0.0296
3.2	3.2	4	44.4	2.133E-04	2.045E-04	0.0200	0.0197	0.0748	0.0756	0.3782	0.3782	5.641E-04	5.407E-04	0.0526	0.0522
3.2	3.2	5	44.5	2.787E-04	2.789E-04	0.0281	0.0272	0.0602	0.0595	0.3024	0.3024	9.215E-04	9.221E-04	0.0929	0.0899

PDC = <n><m>.<shrink distance (um)> ; central ew = 0.2*2^n; shielding ew = 0.2*2^m (um).

APPENDIX IX.1 : RESULTS - SJPD

FI SJPD PSE 3 electrodes shifted on n-well: Image electrode (IE) QE dependence on IE width, outer electrode width and placement from the well edge (shift).

central el. wth (um)	outer elec(OE) wth(um)	OE shift (um)	well/subst. depth = 2/3 um; well/subst. dope = 1E17(e/ml) / 1E15 (h/ml); reverse bias = 2 volts; 5 um beam (633 nm) cw/ow/sh PDC	PSE Boundary QE @ 55	PSE Boundary QE @ 105	On SCR QE@70	On SCR QE@90	In well QE@75	In well QE@95	Exp Max QE@ 80	Max Max QE	PSE Boundary Nz QE Nz @ 55	PSE Boundary Nz QE Nz @ 105	Nz QE On SCR Nz@70	Nz QE On SCR Nz@90
0.2	0.2	0	0	1.400E-03	1.734E-03	0.1407	0.1413	0.3660	0.3698	0.4601	0.4601	3.042E-03	3.768E-03	0.3058	0.3072
0.2	0.2	1	0.1	7.234E-04	8.247E-04	0.0743	0.0733	0.2999	0.3034	0.4336	0.4336	**1.669E-03**	**1.902E-03**	0.1713	0.1690
0.2	0.2	2	0.2	7.886E-04	8.769E-04	0.0662	0.0666	0.2567	0.2597	0.4114	0.4114	1.917E-03	2.132E-03	0.1610	0.1618
0.2	0.2	3	0.3	1.067E-03	1.112E-03	0.0815	0.0810	0.2149	0.2181	0.3815	0.3815	2.795E-03	2.914E-03	0.2137	0.2122
0.2	0.2	4	0.4	7.898E-04	8.096E-04	0.0797	0.0799	0.1711	0.1740	0.3580	0.3580	2.206E-03	2.262E-03	0.2227	0.2232
0.2	0.2	5	0.5	9.554E-04	8.934E-04	0.0887	0.0888	0.1390	0.1378	0.3213	0.3213	2.974E-03	2.781E-03	0.2761	0.2762
0.2	0.2	6	0.6	1.010E-03	9.878E-04	0.1023	0.1022	0.1206	0.1181	0.2777	0.2777	3.636E-03	3.557E-03	0.3683	0.3681
0.2	0.2	7	0.7	1.238E-03	1.174E-03	0.1190	0.1193	0.1200	0.1199	0.2169	0.2169	5.710E-03	5.413E-03	0.5487	0.5500
0.2	0.2	8	0.8	1.679E-03	1.342E-03	0.1391	0.1395	0.1374	0.1373	0.1614	0.1614	1.040E-02	8.313E-03	0.8618	0.8638
0.2	0.2	9	0.9	1.459E-03	1.474E-03	0.1457	0.1472	0.1448	0.1457	0.1288	0.1472	9.912E-03	1.001E-02	0.9897	1.0000
0.2	0.4	0	1	6.589E-04	1.419E-03	0.1064	0.1062	0.3425	0.3452	0.4489	0.4489	1.913E-03	3.160E-03	0.2370	0.2366
0.2	0.4	1	1.1	6.177E-04	7.201E-04	0.0606	0.0603	0.2915	0.2934	0.4239	0.4239	**1.457E-03**	**1.699E-03**	0.1429	0.1422
0.2	0.4	2	1.2	6.810E-04	7.403E-04	0.0527	0.0529	0.2363	0.2367	0.3949	0.3949	1.725E-03	1.875E-03	0.1335	0.1338
0.2	0.4	3	1.3	7.513E-04	7.598E-04	0.0583	0.0579	0.2037	0.2010	0.3794	0.3794	1.980E-03	2.003E-03	0.1536	0.1526
0.2	0.4	4	1.4	7.058E-04	6.950E-04	0.0682	0.0683	0.1530	0.1531	0.3401	0.3401	2.075E-03	2.043E-03	0.2006	0.2009
0.2	0.4	5	1.5	7.252E-04	7.464E-04	0.0726	0.0728	0.1221	0.1198	0.3087	0.3087	2.349E-03	2.416E-03	0.2353	0.2357
0.2	0.4	6	1.6	8.171E-04	8.208E-04	0.0839	0.0841	0.0996	0.0994	0.2632	0.2632	3.104E-03	3.119E-03	0.3188	0.3197
0.2	0.4	7	1.7	9.760E-04	1.024E-03	0.0993	0.1029	0.0999	0.1039	0.1971	0.1971	4.953E-03	5.194E-03	0.5041	0.5221
0.2	0.4	8	1.8	1.169E-03	1.140E-03	0.1144	0.1147	0.1125	0.1127	0.1397	0.1397	8.364E-03	8.156E-03	0.8185	0.8205
0.2	0.4	9	1.9	1.106E-03	1.098E-03	0.1094	0.1094	0.1082	0.1089	0.0979	0.1094	1.011E-02	1.004E-02	1.0000	1.0000
0.2	0.8	0	2	5.403E-04	5.607E-04	0.0727	0.0760	0.3160	0.3223	0.4351	0.4351	1.242E-03	1.289E-03	0.1670	0.1746
0.2	0.8	1	2.1	4.563E-04	4.593E-04	0.0436	0.0428	0.2650	0.2671	0.4133	0.4133	**1.104E-03**	**1.111E-03**	0.1056	0.1035
0.2	0.8	2	2.2	4.724E-04	5.419E-04	0.0378	0.0380	0.2206	0.2216	0.3894	0.3894	1.213E-03	1.392E-03	0.0971	0.0975
0.2	0.8	3	2.3	5.342E-04	5.393E-04	0.0383	0.0377	0.1754	0.1715	0.3651	0.3651	1.463E-03	1.477E-03	0.1050	0.1033
0.2	0.8	4	2.4	4.165E-04	4.371E-04	0.0427	0.0426	0.1259	0.1272	0.3274	0.3274	1.272E-03	1.335E-03	0.1305	0.1300
0.2	0.8	5	2.5	5.011E-04	5.187E-04	0.0501	0.0507	0.0925	0.0931	0.2852	0.2852	1.757E-03	1.819E-03	0.1756	0.1776
0.2	0.8	6	2.6	5.906E-04	6.461E-04	0.0570	0.0569	0.0695	0.0701	0.2251	0.2251	2.623E-03	2.870E-03	0.2531	0.2527
0.2	0.8	7	2.7	6.597E-04	6.987E-04	0.0664	0.0686	0.0679	0.0694	0.1595	0.1595	4.136E-03	4.380E-03	0.4161	0.4299
0.2	0.8	8	2.8	7.862E-04	7.957E-04	0.0770	0.0797	0.0767	0.0787	0.1036	0.1036	7.587E-03	7.678E-03	0.7432	0.7689
0.2	1.6	0	3	2.553E-04	3.937E-04	0.0410	0.0406	0.2718	0.2738	0.4155	0.4155	6.145E-04	9.476E-04	0.0986	0.0978
0.2	1.6	1	3.1	2.275E-04	2.171E-04	0.0196	0.0197	0.2163	0.2135	0.3792	0.3792	**5.999E-04**	**5.725E-04**	0.0516	0.0520
0.2	1.6	2	3.2	2.206E-04	2.420E-04	0.0173	0.0174	0.1642	0.1671	0.3484	0.3484	6.332E-04	6.946E-04	0.0497	0.0500
0.2	1.6	3	3.3	2.283E-04	2.648E-04	0.0185	0.0185	0.1170	0.1182	0.3146	0.3146	7.255E-04	8.415E-04	0.0589	0.0589
0.2	1.6	4	3.4	2.277E-04	3.729E-04	0.0219	0.0217	0.0822	0.0802	0.2854	0.2854	7.978E-04	1.307E-03	0.0768	0.0761
0.2	1.6	5	3.5	2.636E-04	2.756E-04	0.0268	0.0273	0.0469	0.0493	0.2400	0.2400	1.098E-03	1.148E-03	0.1118	0.1137
0.2	1.6	6	3.6	2.985E-04	3.009E-04	0.0308	0.0294	0.0398	0.0383	0.1656	0.1656	1.803E-03	1.817E-03	0.1859	0.1773
0.2	1.6	7	3.7	3.631E-04	3.335E-04	0.0351	0.0350	0.0364	0.0364	0.1021	0.1021	3.556E-03	3.265E-03	0.3436	0.3429
0.2	1.6	8	3.8	2.683E-04	2.640E-04	0.0260	0.0261	0.0259	0.0260	0.0395	0.0395	6.794E-03	6.685E-03	0.6590	0.6600
0.2	3.2	0	4	8.255E-05	1.246E-04	0.0107	0.0109	0.1820	0.1837	0.3641	0.3641	2.267E-04	3.422E-04	0.0294	0.0300
0.2	3.2	1	4.1	7.749E-05	8.667E-05	0.0075	0.0079	0.1419	0.1369	0.3348	0.3348	**2.314E-04**	**2.589E-04**	0.0224	0.0235
0.2	3.2	2	4.2	8.131E-05	1.041E-04	0.0063	0.0075	0.0894	0.0902	0.2883	0.2883	2.820E-04	3.610E-04	0.0218	0.0259
0.2	3.2	3	4.3	9.866E-05	1.214E-04	0.0079	0.0081	0.0542	0.0553	0.2379	0.2379	4.148E-04	5.103E-04	0.0334	0.0340
0.2	3.2	4	4.4	9.688E-05	9.480E-05	0.0094	0.0094	0.0310	0.0281	0.1774	0.1774	5.461E-04	5.344E-04	0.0527	0.0529
0.2	3.2	5	4.5	1.145E-04	1.146E-04	0.0111	0.0113	0.0193	0.0197	0.1197	0.1197	9.569E-04	9.579E-04	0.0929	0.0944
0.2	3.2	6	4.6	1.109E-04	1.089E-04	0.0110	0.0109	0.0141	0.0134	0.0622	0.0622	1.785E-03	1.751E-03	0.1764	0.1753
0.4	0.2	0	10	1.460E-03	1.805E-03	0.1451	0.1458	0.3733	0.3782	0.4732	0.4732	3.086E-03	3.814E-03	0.3067	0.3082
0.4	0.2	1	10.1	9.713E-04	1.103E-03	0.0882	0.0870	0.3166	0.3225	0.4481	0.4481	2.168E-03	2.462E-03	0.1968	0.1942
0.4	0.2	2	10.2	9.052E-04	9.287E-04	0.0690	0.0695	0.2654	0.2681	0.4198	0.4198	**2.156E-03**	**2.212E-03**	0.1643	0.1656
0.4	0.2	3	10.3	1.095E-03	1.256E-03	0.0868	0.0864	0.2237	0.2275	0.3982	0.3982	2.749E-03	3.158E-03	0.2178	0.2171
0.4	0.2	4	10.4	8.828E-04	8.636E-04	0.0839	0.0839	0.1779	0.1781	0.3757	0.3757	2.350E-03	2.299E-03	0.2233	0.2232
0.4	0.2	5	10.5	9.764E-04	9.968E-04	0.0943	0.0943	0.1491	0.1448	0.3356	0.3356	2.909E-03	2.970E-03	0.2809	0.2811
0.4	0.2	6	10.6	1.138E-03	1.106E-03	0.1091	0.1093	0.1277	0.1257	0.2911	0.2911	3.911E-03	3.600E-03	0.3750	0.3755
0.4	0.2	7	10.7	1.294E-03	1.260E-03	0.1280	0.1310	0.1288	0.1316	0.2310	0.2310	5.602E-03	5.455E-03	0.5542	0.5673
0.4	0.2	8	10.8	1.513E-03	1.642E-03	0.1540	0.1542	0.1517	0.1516	0.1762	0.1762	8.588E-03	9.322E-03	0.8741	0.8751
0.4	0.2	9	10.9	1.731E-03	1.737E-03	0.1656	0.1687	0.1645	0.1670	0.1472	0.1687	1.026E-02	1.030E-02	0.9813	1.0000
0.4	0.4	0	11	8.661E-04	8.626E-04	0.1103	0.1099	0.3480	0.3531	0.4657	0.4657	1.860E-03	1.852E-03	0.2369	0.2359
0.4	0.4	1	11.1	6.920E-04	7.407E-04	0.0631	0.0614	0.2956	0.2995	0.4398	0.4398	**1.573E-03**	**1.684E-03**	0.1434	0.1396
0.4	0.4	2	11.2	6.812E-04	7.994E-04	0.0568	0.0569	0.2502	0.2532	0.4186	0.4186	1.627E-03	1.910E-03	0.1358	0.1360
0.4	0.4	3	11.3	7.576E-04	8.243E-04	0.0611	0.0607	0.2008	0.2059	0.3998	0.3998	1.895E-03	2.062E-03	0.1528	0.1518
0.4	0.4	4	11.4	7.562E-04	7.270E-04	0.0734	0.0735	0.1606	0.1617	0.3613	0.3613	2.093E-03	2.012E-03	0.2032	0.2034
0.4	0.4	5	11.5	7.945E-04	7.705E-04	0.0771	0.0774	0.1280	0.1253	0.3227	0.3227	2.462E-03	2.388E-03	0.2389	0.2399
0.4	0.4	6	11.6	9.386E-04	8.885E-04	0.0904	0.0900	0.1054	0.1037	0.2777	0.2777	3.380E-03	3.199E-03	0.3254	0.3241
0.4	0.4	7	11.7	1.127E-03	1.098E-03	0.1077	0.1112	0.1087	0.1123	0.2106	0.2106	5.350E-03	5.213E-03	0.5115	0.5281
0.4	0.4	8	11.8	1.306E-03	1.394E-03	0.1282	0.1401	0.1259	0.1375	0.1573	0.1573	8.299E-03	8.861E-03	0.8147	0.8908
0.4	0.4	9	11.9	1.289E-03	1.283E-03	0.1261	0.1262	0.1248	0.1254	0.1147	0.1262	1.021E-02	1.016E-02	0.9992	1.0000
0.4	0.8	0	12	5.566E-04	5.537E-04	0.0753	0.0787	0.3238	0.3297	0.4491	0.4491	1.240E-03	1.233E-03	0.1677	0.1752
0.4	0.8	1	12.1	4.960E-04	4.826E-04	0.0456	0.0445	0.2697	0.2736	0.4320	0.4320	**1.148E-03**	**1.117E-03**	0.1056	0.1030
0.4	0.8	2	12.2	4.975E-04	5.507E-04	0.0395	0.0397	0.2265	0.2283	0.4065	0.4065	1.224E-03	1.355E-03	0.0972	0.0976
0.4	0.8	3	12.3	4.934E-04	5.878E-04	0.0400	0.0405	0.1825	0.1799	0.3741	0.3741	1.319E-03	1.571E-03	0.1069	0.1083
0.4	0.8	4	12.4	4.620E-04	4.838E-04	0.0451	0.0460	0.1344	0.1348	0.3397	0.3397	1.360E-03	1.424E-03	0.1326	0.1354
0.4	0.8	5	12.5	5.423E-04	5.537E-04	0.0536	0.0531	0.0952	0.0958	0.3017	0.3017	1.798E-03	1.835E-03	0.1776	0.1761
0.4	0.8	6	12.6	6.188E-04	6.230E-04	0.0615	0.0613	0.0747	0.0753	0.2385	0.2385	2.595E-03	2.612E-03	0.2576	0.2571
0.4	0.8	7	12.7	7.637E-04	6.039E-04	0.0734	0.0771	0.0746	0.0781	0.1735	0.1735	4.403E-03	4.635E-03	0.4229	0.4446
0.4	0.8	8	12.8	8.873E-04	8.720E-04	0.0879	0.0880	0.0873	0.0868	0.1173	0.1173	7.565E-03	7.435E-03	0.7492	0.7500

PDC = <n><m>.<shrink distance (um)> : central ew = 0.2*2^n; shielding ew = 0.2*2^m (um).

APPENDIX IX.2 : RESULTS - SJPD

FI-SJPD-PSE-3electrodes-shifted continued page 2 of 3.

Highlighted Normalized (Nz) QE is lowest crosstalk value for total parameter permutation set.

central el. wth (um)	outer elec(OE) wth(um)	OE shift (um)	cw/ow/sh PDC	PSE Boundary QE @ 55	PSE Boundary QE @ 105	On SCR QE@70	On SCR QE@90	In well QE@75	In well QE@95	Exp Max QE@ 80	Max Max QE	PSE Boundary Nz QE Nz @ 55	PSE Boundary Nz QE Nz @ 105	Nz QE On SCR Nz@70	Nz QE On SCR Nz@90
0.4	1.6	0	13	2.626E-04	4.073E-04	0.0428	0.0423	0.2809	0.2832	0.4247	0.4247	6.183E-04	9.589E-04	0.1007	0.0995
0.4	1.6	1	13.1	2.308E-04	2.310E-04	0.0209	0.0211	0.2247	0.2267	0.3978	0.3978	**5.802E-04**	**5.807E-04**	0.0526	0.0530
0.4	1.6	2	13.2	2.320E-04	2.632E-04	0.0193	0.0194	0.1767	0.1799	0.3833	0.3833	6.052E-04	6.866E-04	0.0505	0.0506
0.4	1.6	3	13.3	2.591E-04	3.011E-04	0.0210	0.0209	0.1295	0.1301	0.3472	0.3472	7.462E-04	8.672E-04	0.0605	0.0603
0.4	1.6	4	13.4	2.373E-04	2.593E-04	0.0233	0.0237	0.0871	0.0873	0.2989	0.2989	7.938E-04	8.674E-04	0.0780	0.0791
0.4	1.6	5	13.5	2.938E-04	2.995E-04	0.0290	0.0302	0.0510	0.0558	0.2508	0.2508	1.171E-03	1.194E-03	0.1156	0.1204
0.4	1.6	6	13.6	2.948E-04	3.405E-04	0.0310	0.0345	0.0403	0.0448	0.1777	0.1777	1.659E-03	1.916E-03	0.1747	0.1940
0.4	1.6	7	13.7	4.010E-04	3.868E-04	0.0384	0.0384	0.0399	0.0399	0.1134	0.1134	3.535E-03	3.411E-03	0.3388	0.3388
0.4	1.6	8	13.8	2.997E-04	3.125E-04	0.0314	0.0315	0.0313	0.0315	0.0482	0.0482	6.217E-03	6.482E-03	0.6511	0.6527
0.4	3.2	0	14	8.785E-05	1.379E-04	0.0118	0.0124	0.1974	0.1986	0.3925	0.3925	2.238E-04	3.513E-04	0.0302	0.0317
0.4	3.2	1	14.1	6.524E-05	8.748E-05	0.0067	0.0074	0.1497	0.1461	0.3592	0.3592	**1.816E-04**	**2.436E-04**	0.0187	0.0205
0.4	3.2	2	14.2	1.038E-04	1.019E-04	0.0086	0.0073	0.1034	0.1000	0.3156	0.3156	3.289E-04	3.229E-04	0.0272	0.0232
0.4	3.2	3	14.3	1.139E-04	1.262E-04	0.0088	0.0087	0.0554	0.0571	0.2712	0.2712	4.200E-04	4.653E-04	0.0324	0.0321
0.4	3.2	4	14.4	1.049E-04	1.164E-04	0.0105	0.0105	0.0348	0.0330	0.1978	0.1978	5.302E-04	5.883E-04	0.0533	0.0533
0.4	3.2	5	14.5	1.223E-04	1.269E-04	0.0126	0.0124	0.0218	0.0207	0.1379	0.1379	8.871E-04	9.206E-04	0.0913	0.0899
0.4	3.2	6	14.6	1.249E-04	2.175E-04	0.0126	0.0126	0.0162	0.0155	0.0710	0.0710	1.758E-03	3.062E-03	0.1768	0.1779
0.8	0.2	0	20	1.477E-03	1.926E-03	0.1525	0.1530	0.3902	0.3908	0.4871	0.4871	3.031E-03	3.954E-03	0.3131	0.3140
0.8	0.2	1	20.1	8.716E-04	8.954E-04	0.0814	0.0805	0.3221	0.3240	0.4659	0.4659	**1.871E-03**	**1.922E-03**	0.1746	0.1727
0.8	0.2	2	20.2	9.599E-04	9.745E-04	0.0735	0.0739	0.2756	0.2775	0.4502	0.4502	2.132E-03	2.164E-03	0.1633	0.1642
0.8	0.2	3	20.3	1.256E-03	1.291E-03	0.0946	0.0939	0.2412	0.2361	0.4259	0.4259	2.949E-03	3.030E-03	0.2220	0.2206
0.8	0.2	4	20.4	8.932E-04	8.936E-04	0.0913	0.0906	0.1945	0.1854	0.3929	0.3929	2.273E-03	2.274E-03	0.2323	0.2312
0.8	0.2	5	20.5	1.029E-03	1.068E-03	0.1030	0.1033	0.1579	0.1563	0.3533	0.3533	2.912E-03	3.022E-03	0.2915	0.2923
0.8	0.2	6	20.6	1.265E-03	2.069E-03	0.1213	0.1212	0.1397	0.1381	0.3117	0.3117	4.058E-03	6.637E-03	0.3893	0.3887
0.8	0.2	7	20.7	1.464E-03	1.494E-03	0.1474	0.1475	0.1475	0.1474	0.2532	0.2532	5.784E-03	5.902E-03	0.5821	0.5826
0.8	0.2	8	20.8	1.789E-03	1.851E-03	0.1765	0.1770	0.1730	0.1737	0.1982	0.1982	9.027E-03	9.339E-03	0.8902	0.8927
0.8	0.2	9	20.9	2.082E-03	2.336E-03	0.2043	0.2049	0.2016	0.2027	0.1790	0.2049	1.016E-02	1.140E-02	0.9971	1.0000
0.8	0.4	0	21	9.437E-04	9.240E-04	0.1182	0.1161	0.3649	0.3656	0.4811	0.4811	1.962E-03	1.921E-03	0.2457	0.2413
0.8	0.4	1	21.1	7.466E-04	7.425E-04	0.0669	0.0651	0.3093	0.3109	0.4614	0.4614	**1.618E-03**	**1.609E-03**	0.1449	0.1410
0.8	0.4	2	21.2	7.297E-04	9.058E-04	0.0607	0.0608	0.2636	0.2626	0.4440	0.4440	1.644E-03	2.040E-03	0.1367	0.1370
0.8	0.4	3	21.3	9.009E-04	1.108E-03	0.0656	0.0720	0.2226	0.2249	0.4057	0.4057	2.221E-03	2.730E-03	0.1617	0.1776
0.8	0.4	4	21.4	8.249E-04	9.315E-04	0.0812	0.0823	0.1706	0.1802	0.3778	0.3778	2.183E-03	2.465E-03	0.2150	0.2178
0.8	0.4	5	21.5	8.744E-04	8.785E-04	0.0849	0.0861	0.1383	0.1396	0.3401	0.3401	2.571E-03	2.583E-03	0.2497	0.2530
0.8	0.4	6	21.6	1.037E-03	1.030E-03	0.1018	0.1016	0.1191	0.1196	0.2934	0.2934	3.534E-03	3.510E-03	0.3469	0.3464
0.8	0.4	7	21.7	1.245E-03	1.296E-03	0.1237	0.1277	0.1238	0.1283	0.2326	0.2326	5.353E-03	5.570E-03	0.5318	0.5491
0.8	0.4	8	21.8	1.533E-03	1.706E-03	0.1479	0.1661	0.1452	0.1626	0.1798	0.1798	8.524E-03	9.487E-03	0.8227	0.9237
0.8	0.4	9	21.9	2.002E-03	1.643E-03	0.1613	0.1617	0.1598	0.1607	0.1449	0.1617	1.238E-02	1.016E-02	0.9973	1.0000
0.8	0.8	0	22	6.724E-04	6.086E-04	0.0812	0.0838	0.3507	0.3401	0.4705	0.4705	1.429E-03	1.294E-03	0.1725	0.1781
0.8	0.8	1	22.1	5.085E-04	5.154E-04	0.0483	0.0476	0.2944	0.2915	0.4324	0.4324	**1.176E-03**	**1.192E-03**	0.1116	0.1100
0.8	0.8	2	22.2	5.040E-04	5.933E-04	0.0424	0.0425	0.2363	0.2377	0.4347	0.4347	1.159E-03	1.365E-03	0.0976	0.0977
0.8	0.8	3	22.3	5.344E-04	6.206E-04	0.0433	0.0430	0.1969	0.1871	0.3957	0.3957	1.351E-03	1.568E-03	0.1095	0.1088
0.8	0.8	4	22.4	5.042E-04	5.030E-04	0.0497	0.0494	0.1440	0.1438	0.3574	0.3574	1.411E-03	1.407E-03	0.1389	0.1381
0.8	0.8	5	22.5	5.921E-04	6.131E-04	0.0594	0.0588	0.1049	0.1012	0.3233	0.3233	1.832E-03	1.897E-03	0.1839	0.1818
0.8	0.8	6	22.6	6.867E-04	6.911E-04	0.0696	0.0707	0.0841	0.0864	0.2595	0.2595	2.647E-03	2.663E-03	0.2681	0.2723
0.8	0.8	7	22.7	8.873E-04	8.803E-04	0.0863	0.0880	0.0878	0.0888	0.1958	0.1958	4.533E-03	4.497E-03	0.4406	0.4495
0.8	0.8	8	22.8	1.049E-03	1.031E-03	0.1015	0.1016	0.1008	0.1002	0.1391	0.1391	7.545E-03	7.411E-03	0.7295	0.7305
0.8	1.6	0	23	2.871E-04	4.359E-04	0.0446	0.0449	0.2905	0.2909	0.4553	0.4553	6.306E-04	9.573E-04	0.0979	0.0986
0.8	1.6	1	23.1	2.534E-04	2.550E-04	0.0230	0.0231	0.2518	0.2414	0.4220	0.4220	**6.005E-04**	**6.042E-04**	0.0546	0.0548
0.8	1.6	2	23.2	2.663E-04	3.348E-04	0.0209	0.0209	0.1958	0.1936	0.3906	0.3906	6.819E-04	8.573E-04	0.0536	0.0536
0.8	1.6	3	23.3	3.093E-04	3.138E-04	0.0229	0.0228	0.1443	0.1347	0.3702	0.3702	8.356E-04	8.478E-04	0.0620	0.0616
0.8	1.6	4	23.4	2.705E-04	2.775E-04	0.0260	0.0279	0.0938	0.0956	0.3209	0.3209	8.428E-04	8.648E-04	0.0811	0.0868
0.8	1.6	5	23.5	3.337E-04	3.774E-04	0.0331	0.0373	0.0586	0.0685	0.2691	0.2691	1.240E-03	1.403E-03	0.1229	0.1364
0.8	1.6	6	23.6	3.743E-04	3.823E-04	0.0372	0.0372	0.0479	0.0482	0.2010	0.2010	1.862E-03	1.902E-03	0.1851	0.1853
0.8	1.6	7	23.7	4.379E-04	4.565E-04	0.0447	0.0447	0.0463	0.0463	0.1359	0.1359	3.222E-03	3.359E-03	0.3286	0.3286
0.8	3.2	0	24	9.095E-05	1.551E-04	0.0133	0.0139	0.2112	0.2167	0.4025	0.4025	2.259E-04	3.852E-04	0.0332	0.0345
0.8	3.2	1	24.1	7.847E-05	9.291E-05	0.0074	0.0084	0.1605	0.1492	0.3872	0.3872	**2.026E-04**	**2.399E-04**	0.0191	0.0218
0.8	3.2	2	24.2	9.707E-05	1.299E-04	0.0081	0.0097	0.1075	0.1156	0.3350	0.3350	2.897E-04	3.876E-04	0.0241	0.0289
0.8	3.2	3	24.3	1.158E-04	1.504E-04	0.0091	0.0090	0.0491	0.0510	0.3154	0.3154	3.671E-04	4.769E-04	0.0287	0.0285
0.8	3.2	4	24.4	1.249E-04	1.205E-04	0.0120	0.0119	0.0386	0.0367	0.2257	0.2257	5.534E-04	5.341E-04	0.0532	0.0526
0.8	3.2	5	24.5	1.614E-04	2.593E-04	0.0155	0.0153	0.0258	0.0254	0.1585	0.1585	1.018E-03	1.636E-03	0.0980	0.0963
0.8	3.2	6	24.6	1.592E-04	1.566E-04	0.0156	0.0154	0.0200	0.0190	0.0877	0.0877	1.814E-03	1.785E-03	0.1775	0.1760
1.6	0.2	0	30	1.747E-03	2.055E-03	0.1629	0.1647	0.4096	0.4108	0.4642	0.4642	3.764E-03	4.427E-03	0.3509	0.3549
1.6	0.2	1	30.1	1.011E-03	1.016E-03	0.0885	0.0874	0.3456	0.3492	0.4426	0.4426	**2.285E-03**	**2.295E-03**	0.2000	0.1974
1.6	0.2	2	30.2	1.021E-03	1.068E-03	0.0805	0.0809	0.2989	0.3003	0.4314	0.4314	2.366E-03	2.475E-03	0.1865	0.1874
1.6	0.2	3	30.3	1.338E-03	1.502E-03	0.1048	0.1043	0.2624	0.2634	0.3947	0.3947	3.391E-03	3.807E-03	0.2654	0.2642
1.6	0.2	4	30.4	1.007E-03	1.028E-03	0.1024	0.1016	0.2094	0.2098	0.3916	0.3916	2.572E-03	2.626E-03	0.2616	0.2595
1.6	0.2	5	30.5	1.180E-03	1.177E-03	0.1178	0.1183	0.1736	0.1745	0.3647	0.3647	3.236E-03	3.229E-03	0.3230	0.3243
1.6	0.2	6	30.6	1.403E-03	1.448E-03	0.1403	0.1408	0.1583	0.1590	0.3295	0.3295	4.257E-03	4.395E-03	0.4258	0.4273
1.6	0.2	7	30.7	1.723E-03	1.734E-03	0.1726	0.1722	0.1708	0.1707	0.2773	0.2773	6.214E-03	6.254E-03	0.6224	0.6210
1.6	0.2	8	30.8	2.104E-03	2.253E-03	0.2167	0.2169	0.2124	0.2118	0.2310	0.2310	9.108E-03	9.754E-03	0.9380	0.9388

PDC = <n><m>.<shrink distance (um)> : central ew = 0.2*2^n; shielding ew = 0.2*2^m (um).

APPENDIX IX.3 : RESULTS - SJPD

FI-SJPD-PSE-3electrodes-shifted continued: page 3 of 3

Bolded values represent lowest relative crosstalk for each shift permutation set.

central el. wth (um)	outer elec(OE) wth(um)	OE shift (um)	cw/ow/sh PDC	PSE Boundary QE @ 55	PSE Boundary QE @ 105	On SCR QE@70	On SCR QE@90	In well QE@75	In well QE@95	Exp Max QE@ 80	Max Max QE	PSE Boundary Nz QE Nz @ 55	PSE Boundary Nz QE Nz @ 105	Nz QE On SCR Nz@70	Nz QE On SCR Nz@90
1.6	0.4	0	31	9.876E-04	9.937E-04	0.1252	0.1239	0.3670	0.3898	0.4546	0.4546	2.173E-03	2.186E-03	0.2753	0.2727
1.6	0.4	1	31.1	7.024E-04	8.039E-04	0.0727	0.0708	0.3337	0.3372	0.4369	0.4369	**1.608E-03**	**1.840E-03**	0.1664	0.1621
1.6	0.4	2	31.2	8.002E-04	9.411E-04	0.0666	0.0667	0.2832	0.2848	0.4283	0.4283	1.868E-03	2.198E-03	0.1556	0.1557
1.6	0.4	3	31.3	1.022E-03	1.135E-03	0.0731	0.0727	0.2367	0.2379	0.4062	0.4062	2.504E-03	2.780E-03	0.1791	0.1781
1.6	0.4	4	31.4	9.340E-04	9.570E-04	0.0925	0.0924	0.1945	0.1960	0.3664	0.3664	2.549E-03	2.612E-03	0.2525	0.2521
1.6	0.4	5	31.5	9.619E-04	1.111E-03	0.0976	0.0993	0.1536	0.1561	0.3552	0.3552	2.708E-03	3.129E-03	0.2747	0.2795
1.6	0.4	6	31.6	1.215E-03	1.188E-03	0.1169	0.1177	0.1327	0.1354	0.3170	0.3170	3.633E-03	3.748E-03	0.3689	0.3713
1.6	0.4	7	31.7	1.478E-03	1.427E-03	0.1451	0.1490	0.1445	0.1492	0.2551	0.2551	5.794E-03	5.592E-03	0.5688	0.5842
1.6	0.4	8	31.8	1.871E-03	2.037E-03	0.1869	0.2039	0.1829	0.1990	0.2143	0.2143	8.730E-03	9.505E-03	0.8720	0.9515
1.6	0.8	0	32	6.487E-04	6.665E-04	0.0870	0.0920	0.3590	0.3611	0.4495	0.4495	1.443E-03	1.483E-03	0.1935	0.2048
1.6	0.8	1	32.1	5.605E-04	5.692E-04	0.0529	0.0532	0.3079	0.3089	0.4326	0.4326	**1.296E-03**	**1.362E-03**	0.1222	0.1231
1.6	0.8	2	32.2	5.855E-04	6.634E-04	0.0471	0.0472	0.2601	0.2616	0.4157	0.4157	1.408E-03	1.596E-03	0.1133	0.1135
1.6	0.8	3	32.3	6.402E-04	7.662E-04	0.0486	0.0482	0.2067	0.2071	0.3978	0.3978	1.609E-03	1.926E-03	0.1221	0.1211
1.6	0.8	4	32.4	5.825E-04	5.745E-04	0.0563	0.0564	0.1560	0.1577	0.3694	0.3694	1.577E-03	1.555E-03	0.1523	0.1527
1.6	0.8	5	32.5	6.518E-04	6.911E-04	0.0675	0.0679	0.1156	0.1195	0.3340	0.3340	1.951E-03	2.069E-03	0.2022	0.2032
1.6	0.8	6	32.6	9.965E-04	9.158E-04	0.0822	0.0866	0.0976	0.1037	0.2840	0.2840	3.509E-03	3.225E-03	0.2893	0.3049
1.6	0.8	7	32.7	1.062E-03	1.069E-03	0.1063	0.1085	0.1078	0.1090	0.2222	0.2222	4.780E-03	4.812E-03	0.4786	0.4882
1.6	0.8	8	32.8	1.426E-03	1.340E-03	0.1366	0.1366	0.1352	0.1342	0.1737	0.1737	8.208E-03	7.711E-03	0.7864	0.7862
1.6	1.6	0	33	2.995E-04	4.881E-04	0.0495	0.0490	0.3156	0.3170	0.4328	0.4328	6.921E-04	1.128E-03	0.1145	0.1132
1.6	1.6	1	33.1	2.400E-04	2.811E-04	0.0254	0.0256	0.2614	0.2632	0.4182	0.4182	**5.739E-04**	**6.720E-04**	0.0607	0.0611
1.6	1.6	2	33.2	2.958E-04	3.429E-04	0.0234	0.0242	0.2084	0.2098	0.3969	0.3969	7.453E-04	8.640E-04	0.0589	0.0611
1.6	1.6	3	33.3	3.494E-04	4.118E-04	0.0256	0.0283	0.1515	0.1584	0.3753	0.3753	9.310E-04	1.097E-03	0.0681	0.0755
1.6	1.6	4	33.4	3.026E-04	5.238E-04	0.0311	0.0309	0.1042	0.1066	0.3372	0.3372	8.976E-04	1.554E-03	0.0923	0.0915
1.6	1.6	5	33.5	3.890E-04	4.202E-04	0.0405	0.0405	0.0716	0.0726	0.2930	0.2930	1.328E-03	1.434E-03	0.1380	0.1380
1.6	1.6	6	33.6	4.389E-04	4.259E-04	0.0415	0.0416	0.0530	0.0534	0.2324	0.2324	1.889E-03	1.833E-03	0.1787	0.1792
1.6	1.6	7	33.7	5.939E-04	5.935E-04	0.0586	0.0587	0.0606	0.0606	0.1635	0.1635	3.632E-03	3.629E-03	0.3586	0.3590
1.6	3.2	0	34	1.293E-04	1.638E-04	0.0144	0.0145	0.2251	0.2285	0.4080	0.4080	3.166E-04	4.015E-04	0.0353	0.0355
1.6	3.2	1	34.1	8.475E-05	9.998E-05	0.0085	0.0084	0.1713	0.1689	0.3839	0.3839	**2.208E-04**	**2.604E-04**	0.0222	0.0220
1.6	3.2	2	34.2	1.294E-04	1.247E-04	0.0096	0.0094	0.1190	0.1194	0.3503	0.3503	3.695E-04	3.561E-04	0.0275	0.0268
1.6	3.2	3	34.3	1.593E-04	1.726E-04	0.0121	0.0120	0.0747	0.0776	0.3087	0.3087	5.161E-04	5.590E-04	0.0393	0.0390
1.6	3.2	4	34.4	1.277E-04	1.317E-04	0.0132	0.0133	0.0418	0.0419	0.2579	0.2579	4.952E-04	5.108E-04	0.0512	0.0514
1.6	3.2	5	34.5	1.939E-04	1.901E-04	0.0188	0.0185	0.0323	0.0307	0.1922	0.1922	1.008E-03	9.891E-04	0.0980	0.0965
3.2	0.2	0	40	1.750E-03	2.232E-03	0.1785	0.1793	0.3965	0.3965	0.4502	0.4502	3.887E-03	4.956E-03	0.3964	0.3982
3.2	0.2	1	40.1	9.919E-04	1.097E-03	0.0992	0.0965	0.3403	0.3664	0.4402	0.4402	**2.253E-03**	**2.491E-03**	0.2253	0.2192
3.2	0.2	2	40.2	1.110E-03	1.259E-03	0.0899	0.0906	0.3248	0.3197	0.4326	0.4326	2.567E-03	2.910E-03	0.2079	0.2095
3.2	0.2	3	40.3	1.561E-03	1.705E-03	0.1179	0.1175	0.2846	0.2826	0.3978	0.3978	3.925E-03	4.286E-03	0.2964	0.2955
3.2	0.2	4	40.4	1.231E-03	1.201E-03	0.1183	0.1192	0.2349	0.2212	0.4173	0.4173	2.950E-03	2.879E-03	0.2836	0.2857
3.2	0.2	5	40.5	1.749E-03	1.447E-03	0.1706	0.1394	0.2210	0.1961	0.3868	0.3868	4.522E-03	3.741E-03	0.4410	0.3605
3.2	0.2	6	40.6	1.776E-03	1.763E-03	0.1753	0.1751	0.1898	0.1882	0.3611	0.3611	4.917E-03	4.881E-03	0.4854	0.4848
3.2	0.2	7	40.7	2.253E-03	2.214E-03	0.2243	0.2239	0.2186	0.2184	0.3156	0.3156	7.139E-03	7.015E-03	0.7108	0.7096
3.2	0.2	8	40.8	3.140E-03	3.134E-03	0.3144	0.3154	0.3060	0.3058	0.3074	0.3154	9.956E-03	9.938E-03	0.9969	1.0000
3.2	0.4	0	41	1.100E-03	1.120E-03	0.1380	0.1353	0.4080	0.4049	0.4481	0.4481	2.455E-03	2.500E-03	0.3080	0.3021
3.2	0.4	1	41.1	8.628E-04	9.126E-04	0.0816	0.0794	0.3313	0.3287	0.4408	0.4408	**1.957E-03**	**2.070E-03**	0.1852	0.1802
3.2	0.4	2	41.2	9.890E-04	1.034E-03	0.0758	0.0760	0.2901	0.2877	0.4349	0.4349	2.274E-03	2.378E-03	0.1743	0.1748
3.2	0.4	3	41.3	1.143E-03	1.590E-03	0.0845	0.0964	0.2485	0.2493	0.4271	0.4271	2.677E-03	3.722E-03	0.1979	0.2257
3.2	0.4	4	41.4	1.315E-03	1.076E-03	0.1083	0.1083	0.2041	0.2033	0.3849	0.3849	3.416E-03	2.794E-03	0.2814	0.2815
3.2	0.4	5	41.5	1.183E-03	1.186E-03	0.1169	0.1172	0.1745	0.1734	0.3792	0.3792	3.121E-03	3.128E-03	0.3082	0.3090
3.2	0.4	6	41.6	1.510E-03	1.554E-03	0.1487	0.1483	0.1649	0.1657	0.3421	0.3421	4.415E-03	4.544E-03	0.4347	0.4336
3.2	0.4	7	41.7	1.947E-03	1.960E-03	0.1941	0.1990	0.1907	0.1960	0.2899	0.2899	6.718E-03	6.760E-03	0.6697	0.6865
3.2	0.8	0	42	9.166E-04	7.368E-04	0.1022	0.1010	0.3586	0.3810	0.4230	0.4230	2.167E-03	1.742E-03	0.2417	0.2388
3.2	0.8	1	42.1	6.171E-04	6.685E-04	0.0603	0.0584	0.3136	0.3054	0.4383	0.4383	**1.408E-03**	**1.525E-03**	0.1375	0.1332
3.2	0.8	2	42.2	6.339E-04	7.680E-04	0.0535	0.0540	0.2707	0.2638	0.4300	0.4300	1.474E-03	1.786E-03	0.1245	0.1257
3.2	0.8	3	42.3	6.669E-04	8.192E-04	0.0562	0.0564	0.2292	0.2275	0.4108	0.4108	1.624E-03	1.994E-03	0.1369	0.1373
3.2	0.8	4	42.4	6.883E-04	6.646E-04	0.0668	0.0664	0.1760	0.1735	0.3900	0.3900	1.765E-03	1.704E-03	0.1712	0.1704
3.2	0.8	5	42.5	8.408E-04	1.390E-03	0.0846	0.0840	0.1373	0.1330	0.3698	0.3698	2.274E-03	3.759E-03	0.2287	0.2271
3.2	0.8	6	42.6	1.122E-03	1.122E-03	0.1100	0.1097	0.1270	0.1279	0.3172	0.3172	3.537E-03	3.539E-03	0.3470	0.3457
3.2	0.8	7	42.7	1.493E-03	1.508E-03	0.1492	0.1525	0.1499	0.1515	0.2777	0.2777	5.375E-03	5.428E-03	0.5372	0.5493
3.2	1.6	0	43	4.112E-04	5.584E-04	0.0538	0.0548	0.3264	0.3393	0.4359	0.4359	9.433E-04	1.281E-03	0.1233	0.1258
3.2	1.6	1	43.1	3.256E-04	4.080E-04	0.0298	0.0368	0.2442	0.2689	0.4294	0.4294	**7.582E-04**	**9.502E-04**	0.0694	0.0858
3.2	1.6	2	43.2	3.372E-04	4.542E-04	0.0274	0.0312	0.2077	0.2190	0.4228	0.4228	7.976E-04	1.074E-03	0.0649	0.0738
3.2	1.6	3	43.3	4.051E-04	4.310E-04	0.0316	0.0314	0.1655	0.1658	0.4039	0.4039	1.003E-03	1.067E-03	0.0782	0.0778
3.2	1.6	4	43.4	3.886E-04	4.029E-04	0.0406	0.0403	0.1249	0.1212	0.3682	0.3682	1.055E-03	1.094E-03	0.1104	0.1093
3.2	1.6	5	43.5	4.750E-04	4.983E-04	0.0492	0.0491	0.0779	0.0755	0.3539	0.3539	1.342E-03	1.408E-03	0.1391	0.1389
3.2	1.6	6	43.6	6.602E-04	6.337E-04	0.0639	0.0642	0.0801	0.0806	0.2738	0.2738	2.411E-03	2.315E-03	0.2335	0.2346
3.2	3.2	0	44	1.272E-04	2.024E-04	0.0174	0.0180	0.2345	0.2341	0.4245	0.4245	2.996E-04	4.767E-04	0.0411	0.0424
3.2	3.2	1	44.1	1.168E-04	1.253E-04	0.0108	0.0114	0.1818	0.1804	0.4104	0.4104	**2.846E-04**	**3.053E-04**	0.0264	0.0278
3.2	3.2	2	44.2	1.172E-04	1.468E-04	0.0100	0.0097	0.0991	0.1019	0.4014	0.4014	2.920E-04	3.657E-04	0.0248	0.0243
3.2	3.2	3	44.3	1.914E-04	2.043E-04	0.0141	0.0140	0.0720	0.0725	0.3704	0.3704	5.167E-04	5.517E-04	0.0381	0.0378
3.2	3.2	4	44.4	2.031E-04	2.126E-04	0.0197	0.0198	0.0613	0.0606	0.2966	0.2966	6.850E-04	7.167E-04	0.0666	0.0667
3.2	3.2	5	44.5	2.871E-04	2.789E-04	0.0280	0.0275	0.0494	0.0475	0.2369	0.2369	1.212E-03	1.177E-03	0.1183	0.1162

PDC = <n><m>.<shrink distance (um)> : central ew = 0.2*2^n; shielding ew = 0.2*2^m (um).

APPENDIX X.1 : RESULTS - SJPD

BI SJPD PSE 3 electrodes on n-well: Image electrode (IE) QE dependence on substrate depth, n-well and p-substrate doping.

Subst	P-subst	n-well	well depth = 2 um; reverse bias = 2 volts; n-well electrode width = 4 um; outer electrodes end 1 um from well wall; 5 um beam (633 nm)													
depth	doping	doping	sd/pd/nd	PSE Boundary		On SCR		near PSE centre		Exp Max	PSE	Boundary Nz QE		well wall Nz QE	
(um)	(h/ml)	(e/ml)	PDC	QE @ 55	QE @ 105	QE @ 70	QE @ 90	QE@75	QE@95	QE@80	Max QE	at 55	at 105	at 70	at 90
3	1.E+14	1.E+16	34.6	1.669E-04	1.648E-04	8.360E-03	8.464E-03	0.1340	0.1362	0.4655	0.4655	3.585E-04	3.541E-04	0.017962	0.018184
3	1.E+14	1.E+17	34.7	1.737E-04	1.688E-04	8.963E-03	9.014E-03	0.1526	0.1549	0.5061	0.5061	3.431E-04	3.335E-04	0.017708	0.017809
3	1.E+14	1.E+18	34.8	1.829E-04	1.807E-04	9.374E-03	9.418E-03	0.1557	0.1582	0.5109	0.5109	3.579E-04	3.537E-04	0.018347	0.018433
3	1.E+14	1.E+19	34.9	1.881E-04	1.770E-04	9.682E-03	9.765E-03	0.1562	0.1587	0.5098	0.5098	3.689E-04	3.472E-04	0.018993	0.019157
3	1.E+15	1.E+16	35.6	8.506E-05	6.687E-05	9.362E-03	7.493E-03	0.1745	0.1542	0.5284	0.5284	1.610E-04	1.265E-04	0.017715	0.014179
3	1.E+15	1.E+17	35.7	1.067E-04	8.523E-05	1.099E-02	8.779E-03	0.1744	0.1539	0.5138	0.5138	2.077E-04	1.659E-04	0.021398	0.017066
3	1.E+15	1.E+18	35.8	1.128E-04	8.813E-05	1.150E-02	9.230E-03	0.1751	0.1544	0.5124	0.5124	2.202E-04	1.720E-04	0.022446	0.018015
3	1.E+15	1.E+19	35.9	1.156E-04	9.256E-05	1.190E-02	9.364E-03	0.1753	0.1547	0.5108	0.5108	2.263E-04	1.812E-04	0.023306	0.018331
3	1.E+16	1.E+16	36.6	3.126E-05	2.917E-05	3.673E-03	3.789E-03	0.1590	0.1507	0.5929	0.5929	5.273E-05	4.919E-05	0.006194	0.006391
3	1.E+16	1.E+17	36.7	7.175E-05	6.955E-05	7.541E-03	7.716E-03	0.1579	0.1502	0.5292	0.5292	1.356E-04	1.314E-04	0.014251	0.014579
3	1.E+16	1.E+18	36.8	8.032E-05	7.571E-05	8.425E-03	8.554E-03	0.1576	0.1499	0.5195	0.5195	1.546E-04	1.457E-04	0.016218	0.016467
3	1.E+16	1.E+19	36.9	8.700E-05	8.061E-05	8.666E-03	8.797E-03	0.1576	0.1504	0.5176	0.5176	1.681E-04	1.558E-04	0.016744	0.016996
3	1.E+17	1.E+16	37.6	1.968E-05	2.378E-05	3.394E-03	3.336E-03	0.1771	0.1767	0.5867	0.5867	3.354E-05	4.054E-05	0.005786	0.005686
3	1.E+17	1.E+17	37.7	4.255E-05	6.306E-05	7.766E-03	7.640E-03	0.1779	0.1772	0.5276	0.5276	8.064E-05	1.195E-04	0.014757	0.014480
3	1.E+17	1.E+18	37.8	5.355E-05	7.782E-05	9.503E-03	9.334E-03	0.1764	0.1757	0.5062	0.5062	1.058E-04	1.537E-04	0.018773	0.018439
3	1.E+17	1.E+19	37.9	5.552E-05	8.528E-05	9.888E-03	9.742E-03	0.1763	0.1756	0.5020	0.5020	1.106E-04	1.699E-04	0.019695	0.019405
3	1.E+18	1.E+16	38.6	1.820E-05	2.196E-05	3.245E-03	3.187E-03	0.1773	0.1770	0.5884	0.5884	3.093E-05	3.731E-05	0.005514	0.005417
3	1.E+18	1.E+17	38.7	3.942E-05	5.840E-05	7.450E-03	7.313E-03	0.1790	0.1783	0.5311	0.5311	7.424E-05	1.100E-04	0.014028	0.013771
3	1.E+18	1.E+18	38.8	5.092E-05	7.390E-05	9.331E-03	9.124E-03	0.1781	0.1774	0.5090	0.5090	1.000E-04	1.452E-04	0.018331	0.017923
3	1.E+18	1.E+19	38.9	5.445E-05	8.344E-05	9.890E-03	9.708E-03	0.1777	0.1770	0.5020	0.5020	1.085E-04	1.662E-04	0.019701	0.019338
3	1.E+19	1.E+16	39.6	1.779E-05	2.147E-05	3.203E-03	3.147E-03	0.1774	0.1770	0.5890	0.5890	3.021E-05	3.646E-05	0.005438	0.005343
3	1.E+19	1.E+17	39.7	3.884E-05	5.755E-05	7.388E-03	7.256E-03	0.1791	0.1784	0.5316	0.5316	7.307E-05	1.083E-04	0.013899	0.013650
3	1.E+19	1.E+18	39.8	4.976E-05	7.220E-05	9.204E-03	9.001E-03	0.1785	0.1778	0.5101	0.5101	9.754E-05	1.415E-04	0.018042	0.017644
3	1.E+19	1.E+19	39.9	5.351E-05	8.199E-05	9.822E-03	9.647E-03	0.1781	0.1774	0.5025	0.5025	1.065E-04	1.632E-04	0.019547	0.019198
4	1.E+14	1.E+16	44.6	4.093E-04	2.661E-04	1.270E-02	1.158E-02	0.2041	0.1922	0.6474	0.6474	6.322E-04	4.110E-04	0.019616	0.017887
4	1.E+14	1.E+17	44.7	4.321E-04	2.905E-04	1.278E-02	1.173E-02	0.2042	0.1922	0.6461	0.6461	6.688E-04	4.497E-04	0.019781	0.018155
4	1.E+14	1.E+18	44.8	4.524E-04	3.124E-04	1.311E-02	1.203E-02	0.2044	0.1928	0.6444	0.6444	7.020E-04	4.848E-04	0.020349	0.018667
4	1.E+14	1.E+19	44.9	4.674E-04	3.234E-04	1.350E-02	1.242E-02	0.2060	0.1933	0.6431	0.6431	7.268E-04	5.029E-04	0.020987	0.019314
4	1.E+15	1.E+16	45.6	1.705E-04	1.500E-04	8.688E-03	7.610E-03	0.2107	0.1911	0.6666	0.6666	2.558E-04	2.250E-04	0.013033	0.011416
4	1.E+15	1.E+17	45.7	2.538E-04	2.114E-04	1.151E-02	9.998E-03	0.2123	0.1928	0.6443	0.6443	3.938E-04	3.282E-04	0.017863	0.015517
4	1.E+15	1.E+18	45.8	2.670E-04	2.255E-04	1.223E-02	1.062E-02	0.2132	0.1935	0.6418	0.6418	4.161E-04	3.514E-04	0.019052	0.016550
4	1.E+15	1.E+19	45.9	2.778E-04	2.346E-04	1.263E-02	1.104E-02	0.2136	0.1942	0.6399	0.6399	4.341E-04	3.666E-04	0.019739	0.017248
4	1.E+16	1.E+16	46.6	9.519E-05	9.532E-05	6.414E-03	6.809E-03	0.2005	0.2004	0.6906	0.6906	1.378E-04	1.380E-04	0.009288	0.009860
4	1.E+16	1.E+17	46.7	1.980E-04	1.845E-04	1.092E-02	1.140E-02	0.2021	0.2027	0.6419	0.6419	3.084E-04	2.874E-04	0.017007	0.017755
4	1.E+16	1.E+18	46.8	2.184E-04	2.023E-04	1.178E-02	1.191E-02	0.2024	0.2029	0.6349	0.6349	3.441E-04	3.187E-04	0.018554	0.018759
4	1.E+16	1.E+19	46.9	2.216E-04	2.050E-04	1.219E-02	1.242E-02	0.2028	0.2033	0.6326	0.6326	3.504E-04	3.240E-04	0.019274	0.019634
4	1.E+17	1.E+16	47.6	1.266E-04	8.669E-05	9.321E-03	9.247E-03	0.2223	0.2212	0.6590	0.6590	1.921E-04	1.315E-04	0.014143	0.014031
4	1.E+17	1.E+17	47.7	2.481E-04	1.599E-04	1.426E-02	1.392E-02	0.2241	0.2235	0.6160	0.6160	4.028E-04	2.596E-04	0.023152	0.022598
4	1.E+17	1.E+18	47.8	2.787E-04	2.017E-04	1.572E-02	1.529E-02	0.2238	0.2226	0.6024	0.6024	4.626E-04	3.347E-04	0.026098	0.025377
4	1.E+17	1.E+19	47.9	2.959E-04	1.851E-04	1.615E-02	1.567E-02	0.2238	0.2227	0.5993	0.5993	4.936E-04	3.088E-04	0.026950	0.026144
4	1.E+18	1.E+16	48.6	1.275E-04	8.732E-05	9.552E-03	9.480E-03	0.2230	0.2219	0.6583	0.6583	1.937E-04	1.326E-04	0.014510	0.014401
4	1.E+18	1.E+17	48.7	2.533E-04	1.637E-04	1.497E-02	1.464E-02	0.2260	0.2255	0.6137	0.6137	4.128E-04	2.667E-04	0.024385	0.023862
4	1.E+18	1.E+18	48.8	2.936E-04	2.127E-04	1.710E-02	1.666E-02	0.2268	0.2257	0.5974	0.5974	4.915E-04	3.561E-04	0.028621	0.027890
4	1.E+18	1.E+19	48.9	3.153E-04	1.977E-04	1.763E-02	1.715E-02	0.2266	0.2254	0.5927	0.5927	5.319E-04	3.336E-04	0.029749	0.028930
4	1.E+19	1.E+16	49.6	1.276E-04	8.741E-05	9.597E-03	9.527E-03	0.2231	0.2220	0.6583	0.6583	1.938E-04	1.328E-04	0.014580	0.014473
4	1.E+19	1.E+17	49.7	2.544E-04	1.645E-04	1.509E-02	1.477E-02	0.2264	0.2258	0.6133	0.6133	4.148E-04	2.682E-04	0.024605	0.024089
4	1.E+19	1.E+18	49.8	2.950E-04	2.139E-04	1.729E-02	1.686E-02	0.2274	0.2262	0.5968	0.5968	4.943E-04	3.583E-04	0.028976	0.028248
4	1.E+19	1.E+19	49.9	3.203E-04	2.010E-04	1.804E-02	1.755E-02	0.2273	0.2262	0.5911	0.5911	5.419E-04	3.401E-04	0.030517	0.029695

PDC = <subst depth (um)><p>.<n> ; $N_A = 1E(10+p)$ (h/ml); $N_D = 1E(10+n)$ (e/ml).

APPENDIX X.2 : RESULTS - SJPD

BI SJPD PSE 3 electrodes on n-well: Image electrode (IE) QE dependence on substrate depth, n-well and p-substrate doping cont. page 2 / 2.

Subst	P-subst	n-well	well depth = 2 um; reverse bias = 2 volts; n-well electrode width = 4 um; outer electrodes end 1 um from well wall; 5 um beam (633 nm).													
depth	doping	doping	sd/pd/nd	PSE Boundary		On SCR			near PSE centre		Exp Max	PSE	Boundary Nz QE		well wall Nz QE	
(um)	(h/ml)	(e/ml)	PDC	QE @ 55	QE @ 105	QE @ 70	QE @ 90		QE@75	QE@95	QE@80	Max QE	at 55	at 105	at 70	at 90
5	1.E+14	1.E+16	54.6	7.487E-04	5.207E-04	1.767E-02	1.660E-02		0.2329	0.2306	0.7324	0.7324	1.022E-03	7.110E-04	0.024124	0.022670
5	1.E+14	1.E+17	54.7	8.157E-04	5.839E-04	1.780E-02	1.676E-02		0.2323	0.2304	0.7287	0.7287	1.119E-03	8.012E-04	0.024420	0.022993
5	1.E+14	1.E+18	54.8	8.458E-04	5.826E-04	1.819E-02	1.731E-02		0.2340	0.2304	0.7264	0.7264	1.164E-03	8.021E-04	0.025043	0.023827
5	1.E+14	1.E+19	54.9	8.823E-04	6.025E-04	1.864E-02	1.769E-02		0.2328	0.2315	0.7243	0.7243	1.218E-03	8.318E-04	0.025730	0.024423
5	1.E+15	1.E+16	55.6	3.531E-04	2.129E-04	1.121E-02	9.969E-03		0.2365	0.2125	0.7326	0.7326	4.820E-04	2.906E-04	0.015303	0.013609
5	1.E+15	1.E+17	55.7	4.611E-04	3.064E-04	1.400E-02	1.231E-02		0.2382	0.2149	0.7152	0.7152	6.447E-04	4.284E-04	0.019571	0.017208
5	1.E+15	1.E+18	55.8	5.032E-04	3.151E-04	1.470E-02	1.316E-02		0.2406	0.2156	0.7123	0.7123	7.064E-04	4.423E-04	0.020632	0.018477
5	1.E+15	1.E+19	55.9	5.154E-04	3.450E-04	1.515E-02	1.364E-02		0.2408	0.2161	0.7108	0.7108	7.251E-04	4.853E-04	0.021320	0.019187
5	1.E+16	1.E+16	56.6	3.615E-04	2.790E-04	1.593E-02	1.657E-02		0.2376	0.2282	0.7158	0.7158	5.050E-04	3.898E-04	0.022251	0.023147
5	1.E+16	1.E+17	56.7	5.196E-04	4.144E-04	2.003E-02	2.103E-02		0.2412	0.2314	0.6821	0.6821	7.618E-04	6.075E-04	0.029370	0.030829
5	1.E+16	1.E+18	56.8	5.702E-04	4.175E-04	2.080E-02	2.162E-02		0.2409	0.2318	0.6771	0.6771	8.422E-04	6.167E-04	0.030726	0.031934
5	1.E+16	1.E+19	56.9	5.890E-04	4.164E-04	2.120E-02	2.197E-02		0.2412	0.2322	0.6755	0.6755	8.720E-04	6.165E-04	0.031380	0.032528
5	1.E+17	1.E+16	57.6	4.659E-04	4.479E-04	2.494E-02	2.501E-02		0.2597	0.2596	0.6628	0.6628	7.029E-04	6.758E-04	0.037624	0.037736
5	1.E+17	1.E+17	57.7	6.288E-04	8.062E-04	2.960E-02	2.963E-02		0.2620	0.2621	0.6320	0.6320	9.949E-04	1.276E-03	0.046828	0.046874
5	1.E+17	1.E+18	57.8	6.133E-04	6.438E-04	3.033E-02	3.027E-02		0.2601	0.2616	0.6244	0.6244	9.823E-04	1.031E-03	0.048571	0.048486
5	1.E+17	1.E+19	57.9	6.946E-04	6.833E-04	3.070E-02	3.072E-02		0.2608	0.2616	0.6222	0.6222	1.116E-03	1.098E-03	0.049348	0.049373
5	1.E+18	1.E+16	58.6	4.807E-04	4.622E-04	2.566E-02	2.573E-02		0.2604	0.2602	0.6605	0.6605	7.277E-04	6.998E-04	0.038847	0.038961
5	1.E+18	1.E+17	58.7	6.775E-04	8.706E-04	3.165E-02	3.171E-02		0.2637	0.2638	0.6262	0.6262	1.082E-03	1.390E-03	0.050543	0.050648
5	1.E+18	1.E+18	58.8	6.894E-04	7.252E-04	3.370E-02	3.368E-02		0.2629	0.2643	0.6143	0.6143	1.122E-03	1.180E-03	0.054856	0.054820
5	1.E+18	1.E+19	58.9	7.823E-04	7.714E-04	3.409E-02	3.415E-02		0.2634	0.2642	0.6114	0.6114	1.279E-03	1.262E-03	0.055761	0.055852
5	1.E+19	1.E+16	59.6	4.841E-04	4.656E-04	2.582E-02	2.589E-02		0.2605	0.2604	0.6601	0.6601	7.334E-04	7.053E-04	0.039112	0.039227
5	1.E+19	1.E+17	59.7	6.862E-04	8.823E-04	3.200E-02	3.207E-02		0.2640	0.2641	0.6252	0.6252	1.098E-03	1.411E-03	0.051182	0.051300
5	1.E+19	1.E+18	59.8	7.036E-04	7.403E-04	3.430E-02	3.428E-02		0.2633	0.2648	0.6128	0.6128	1.148E-03	1.208E-03	0.055965	0.055940
5	1.E+19	1.E+19	59.9	8.087E-04	7.978E-04	3.507E-02	3.513E-02		0.2641	0.2649	0.6086	0.6086	1.329E-03	1.311E-03	0.057616	0.057723
6	1.E+14	1.E+16	64.6	1.037E-03	9.637E-04	2.262E-02	2.090E-02		0.2650	0.2534	0.7891	0.7891	1.314E-03	1.221E-03	0.028669	0.026492
6	1.E+14	1.E+17	64.7	1.130E-03	1.082E-03	2.298E-02	2.132E-02		0.2642	0.2528	0.7843	0.7843	1.440E-03	1.380E-03	0.029297	0.027183
6	1.E+14	1.E+18	64.8	1.182E-03	1.125E-03	2.344E-02	2.205E-02		0.2652	0.2534	0.7822	0.7822	1.512E-03	1.438E-03	0.029964	0.028194
6	1.E+14	1.E+19	64.9	1.229E-03	1.187E-03	2.416E-02	2.260E-02		0.2651	0.2537	0.7800	0.7800	1.576E-03	1.522E-03	0.030976	0.028980
6	1.E+15	1.E+16	65.6	7.230E-04	4.809E-04	2.013E-02	1.752E-02		0.2558	0.2456	0.7362	0.7362	9.822E-04	6.533E-04	0.027343	0.023796
6	1.E+15	1.E+17	65.7	8.724E-04	8.632E-04	2.220E-02	1.947E-02		0.2674	0.2482	0.7248	0.7248	1.204E-03	1.191E-03	0.030633	0.026867
6	1.E+15	1.E+18	65.8	9.310E-04	6.220E-04	2.272E-02	2.031E-02		0.2658	0.2488	0.7228	0.7228	1.288E-03	8.606E-04	0.031439	0.028096
6	1.E+15	1.E+19	65.9	9.569E-04	6.831E-04	2.315E-02	2.059E-02		0.2687	0.2492	0.7214	0.7214	1.326E-03	9.469E-04	0.032092	0.028538
6	1.E+16	1.E+16	66.6	1.331E-03	1.158E-03	3.552E-02	3.593E-02		0.2687	0.2619	0.6843	0.6843	1.946E-03	1.692E-03	0.051911	0.052505
6	1.E+16	1.E+17	66.7	1.518E-03	1.320E-03	3.866E-02	3.922E-02		0.2714	0.2646	0.6613	0.6613	2.295E-03	1.995E-03	0.058454	0.059307
6	1.E+16	1.E+18	66.8	1.552E-03	1.378E-03	3.917E-02	3.974E-02		0.2712	0.2649	0.6581	0.6581	2.358E-03	2.093E-03	0.059511	0.060381
6	1.E+16	1.E+19	66.9	1.577E-03	1.383E-03	3.955E-02	4.011E-02		0.2727	0.2652	0.6568	0.6568	2.401E-03	2.106E-03	0.060220	0.061065
6	1.E+17	1.E+16	67.6	1.480E-03	1.590E-03	4.785E-02	5.012E-02		0.2829	0.2669	0.6310	0.6310	2.346E-03	2.519E-03	0.075841	0.079436
6	1.E+17	1.E+17	67.7	1.667E-03	1.747E-03	5.182E-02	5.400E-02		0.2851	0.2683	0.6102	0.6102	2.732E-03	2.864E-03	0.084928	0.088494
6	1.E+17	1.E+18	67.8	1.701E-03	1.748E-03	5.201E-02	5.448E-02		0.2850	0.2686	0.6064	0.6064	2.805E-03	2.882E-03	0.085767	0.089835
6	1.E+17	1.E+19	67.9	1.680E-03	1.954E-03	5.232E-02	5.467E-02		0.2850	0.2686	0.6047	0.6047	2.778E-03	3.232E-03	0.086522	0.090416
6	1.E+18	1.E+16	68.6	1.522E-03	1.631E-03	4.885E-02	5.111E-02		0.2833	0.2872	0.6280	0.6280	2.424E-03	2.597E-03	0.077788	0.081374
6	1.E+18	1.E+17	68.7	1.801E-03	1.876E-03	5.472E-02	5.684E-02		0.2861	0.2892	0.6027	0.6027	2.988E-03	3.112E-03	0.090788	0.094298
6	1.E+18	1.E+18	68.8	1.907E-03	1.950E-03	5.659E-02	5.905E-02		0.2857	0.2901	0.5944	0.5944	3.209E-03	3.281E-03	0.095220	0.099350
6	1.E+18	1.E+19	68.9	1.882E-03	2.181E-03	5.685E-02	5.922E-02		0.2866	0.2900	0.5924	0.5924	3.177E-03	3.681E-03	0.095971	0.099958
6	1.E+19	1.E+16	69.6	1.532E-03	1.641E-03	4.908E-02	5.133E-02		0.2834	0.2872	0.6275	0.6275	2.442E-03	2.615E-03	0.078217	0.081801
6	1.E+19	1.E+17	69.7	1.825E-03	1.898E-03	5.521E-02	5.732E-02		0.2863	0.2893	0.6015	0.6015	3.033E-03	3.155E-03	0.091779	0.095286
6	1.E+19	1.E+18	69.8	1.949E-03	1.989E-03	5.744E-02	5.988E-02		0.2870	0.2903	0.5924	0.5924	3.290E-03	3.358E-03	0.096959	0.101081
6	1.E+19	1.E+19	69.9	1.946E-03	2.248E-03	5.817E-02	6.051E-02		0.2871	0.2904	0.5891	0.5891	3.303E-03	3.816E-03	0.098736	0.102706

PDC = <subst depth (um)><p>.<n> : N_a = 1E(10+p) (h/ml); N_n = 1E(10+n) (e/ml).

APPENDIX XI.1 : RESULTS - SJPD

FI SJPD PSE 3 electrodes on n-well: Image electrode (IE) QE dependence on substrate depth, n-well and p-substrate doping.

Subst	P-subst	n-well	well depth = 2 um; reverse bias = 2 volts; n-well electrode width = 4 um; outer electrodes end 1 um from well wall, 5 um beam (633 nm).													
depth	doping	doping	sd/pd/nd	PSE Boundary		On SCR		near PSE centre		Exp Max	PSE	Boundary Nz QE		well wall Nz QE	
(um)	(h/ml)	(e/ml)	PDC	QE @ 55	QE @ 105	QE @ 70	QE @ 90	QE@75	QE@95	QE@80	Max QE	at 55	at 105	at 70	at 90
3	1.E+14	1.E+16	34.6	1.597E-04	1.597E-04	6.999E-03	6.802E-03	0.1104	0.1056	0.3649	0.3649	4.377E-04	4.377E-04	0.019180	0.018639
3	1.E+14	1.E+17	34.7	1.599E-04	1.886E-04	7.582E-03	7.375E-03	0.1251	0.1190	0.3948	0.3948	4.050E-04	4.778E-04	0.019205	0.018681
3	1.E+14	1.E+18	34.8	1.604E-04	1.737E-04	7.929E-03	7.714E-03	0.1277	0.1218	0.3991	0.3991	4.018E-04	4.351E-04	0.019866	0.019327
3	1.E+14	1.E+19	34.9	1.588E-04	1.818E-04	8.253E-03	7.991E-03	0.1282	0.1215	0.3980	0.3980	3.990E-04	4.567E-04	0.020735	0.020077
3	1.E+15	1.E+16	35.6	8.448E-05	6.771E-05	7.368E-03	6.196E-03	0.1533	0.1287	0.4173	0.4173	2.024E-04	1.622E-04	0.017654	0.014846
3	1.E+15	1.E+17	35.7	9.504E-05	8.505E-05	8.717E-03	7.293E-03	0.1513	0.1272	0.4006	0.4006	2.372E-04	2.123E-04	0.021758	0.018204
3	1.E+15	1.E+18	35.8	9.720E-05	8.989E-05	9.161E-03	7.703E-03	0.1518	0.1275	0.3992	0.3992	2.434E-04	2.251E-04	0.022945	0.019293
3	1.E+15	1.E+19	35.9	1.035E-04	9.206E-05	9.440E-03	7.885E-03	0.1519	0.1281	0.3979	0.3979	2.602E-04	2.314E-04	0.023727	0.019818
3	1.E+16	1.E+16	36.6	2.710E-05	3.000E-05	3.254E-03	3.186E-03	0.1332	0.1393	0.5135	0.5135	5.277E-05	5.842E-05	0.006337	0.006204
3	1.E+16	1.E+17	36.7	6.263E-05	6.552E-05	6.680E-03	6.584E-03	0.1243	0.1295	0.4246	0.4246	1.475E-04	1.543E-04	0.015735	0.015507
3	1.E+16	1.E+18	36.8	7.144E-05	7.733E-05	7.328E-03	7.260E-03	0.1234	0.1277	0.4137	0.4137	1.727E-04	1.870E-04	0.017714	0.017550
3	1.E+16	1.E+19	36.9	7.446E-05	7.701E-05	7.674E-03	7.591E-03	0.1234	0.1285	0.4111	0.4111	1.811E-04	1.873E-04	0.018668	0.018466
3	1.E+17	1.E+16	37.6	1.643E-05	2.706E-05	2.778E-03	2.743E-03	0.1667	0.1667	0.5207	0.5207	3.155E-05	5.198E-05	0.005335	0.005267
3	1.E+17	1.E+17	37.7	4.338E-05	6.317E-05	6.669E-03	6.540E-03	0.1579	0.1580	0.4332	0.4332	1.001E-04	1.458E-04	0.015394	0.015097
3	1.E+17	1.E+18	37.8	6.914E-05	9.116E-05	8.233E-03	8.057E-03	0.1539	0.1532	0.4054	0.4054	1.706E-04	2.249E-04	0.020309	0.019877
3	1.E+17	1.E+19	37.9	5.848E-05	8.399E-05	8.516E-03	8.411E-03	0.1536	0.1535	0.4005	0.4005	1.460E-04	2.097E-04	0.021265	0.021002
3	1.E+18	1.E+16	38.6	1.520E-05	2.498E-05	2.611E-03	2.576E-03	0.1671	0.1672	0.5250	0.5250	2.894E-05	4.759E-05	0.004974	0.004908
3	1.E+18	1.E+17	38.7	4.020E-05	5.850E-05	6.282E-03	6.162E-03	0.1592	0.1593	0.4401	0.4401	9.133E-05	1.329E-04	0.014274	0.014002
3	1.E+18	1.E+18	38.8	6.575E-05	8.656E-05	7.961E-03	7.773E-03	0.1557	0.1550	0.4116	0.4116	1.597E-04	2.103E-04	0.019342	0.018885
3	1.E+18	1.E+19	38.9	5.732E-05	8.218E-05	8.411E-03	8.293E-03	0.1546	0.1545	0.4028	0.4028	1.423E-04	2.040E-04	0.020883	0.020589
3	1.E+19	1.E+16	39.6	1.466E-05	2.443E-05	2.565E-03	2.532E-03	0.1672	0.1673	0.5262	0.5262	2.823E-05	4.643E-05	0.004875	0.004812
3	1.E+19	1.E+17	39.7	3.960E-05	5.766E-05	6.209E-03	6.093E-03	0.1594	0.1595	0.4412	0.4412	8.975E-05	1.307E-04	0.014072	0.013809
3	1.E+19	1.E+18	39.8	6.425E-05	8.457E-05	7.818E-03	7.634E-03	0.1560	0.1554	0.4136	0.4136	1.553E-04	2.045E-04	0.018904	0.018458
3	1.E+19	1.E+19	39.9	5.634E-05	8.076E-05	8.308E-03	8.193E-03	0.1550	0.1549	0.4042	0.4042	1.394E-04	1.998E-04	0.020555	0.020271
4	1.E+14	1.E+16	44.6	3.750E-04	2.307E-04	9.262E-03	8.001E-03	0.1565	0.1549	0.5049	0.5049	7.427E-04	4.569E-04	0.018343	0.015846
4	1.E+14	1.E+17	44.7	3.850E-04	3.413E-04	9.565E-03	8.309E-03	0.1566	0.1550	0.5032	0.5032	7.652E-04	6.782E-04	0.019007	0.016512
4	1.E+14	1.E+18	44.8	3.809E-04	2.597E-04	9.862E-03	8.638E-03	0.1572	0.1558	0.5031	0.5031	7.570E-04	5.161E-04	0.019601	0.017168
4	1.E+14	1.E+19	44.9	3.848E-04	2.715E-04	1.014E-02	8.975E-03	0.1577	0.1561	0.5015	0.5015	7.674E-04	5.415E-04	0.020224	0.017896
4	1.E+15	1.E+16	45.6	1.567E-04	1.449E-04	7.073E-03	6.089E-03	0.1831	0.1542	0.5280	0.5280	2.969E-04	2.745E-04	0.013396	0.011532
4	1.E+15	1.E+17	45.7	2.123E-04	2.059E-04	9.486E-03	8.173E-03	0.1802	0.1531	0.4945	0.4945	4.293E-04	4.163E-04	0.019184	0.016527
4	1.E+15	1.E+18	45.8	2.295E-04	2.074E-04	1.005E-02	8.634E-03	0.1804	0.1526	0.4909	0.4909	4.674E-04	4.224E-04	0.020464	0.017587
4	1.E+15	1.E+19	45.9	2.185E-04	2.159E-04	1.040E-02	8.948E-03	0.1806	0.1522	0.4890	0.4890	4.469E-04	4.414E-04	0.021265	0.018297
4	1.E+16	1.E+16	46.6	8.155E-05	8.633E-05	4.439E-03	4.503E-03	0.1611	0.1687	0.6059	0.6059	1.346E-04	1.425E-04	0.007326	0.007432
4	1.E+16	1.E+17	46.7	1.575E-04	1.725E-04	8.448E-03	8.344E-03	0.1530	0.1588	0.5145	0.5145	3.060E-04	3.352E-04	0.016419	0.016215
4	1.E+16	1.E+18	46.8	1.752E-04	1.857E-04	9.244E-03	9.106E-03	0.1521	0.1584	0.5033	0.5033	3.482E-04	3.690E-04	0.018368	0.018095
4	1.E+16	1.E+19	46.9	1.877E-04	1.933E-04	9.613E-03	9.497E-03	0.1523	0.1574	0.5005	0.5005	3.751E-04	3.863E-04	0.019207	0.018975
4	1.E+17	1.E+16	47.6	1.076E-04	1.032E-04	5.298E-03	5.237E-03	0.1974	0.1987	0.6038	0.6038	1.781E-04	1.709E-04	0.008773	0.008673
4	1.E+17	1.E+17	47.7	2.051E-04	1.351E-04	9.699E-03	9.460E-03	0.1893	0.1903	0.5149	0.5149	3.983E-04	2.623E-04	0.018836	0.018371
4	1.E+17	1.E+18	47.8	2.323E-04	1.574E-04	1.122E-02	1.096E-02	0.1852	0.1859	0.4873	0.4873	4.766E-04	3.230E-04	0.023024	0.022488
4	1.E+17	1.E+19	47.9	2.556E-04	1.612E-04	1.160E-02	1.132E-02	0.1842	0.1854	0.4823	0.4823	5.299E-04	3.342E-04	0.024051	0.023461
4	1.E+18	1.E+16	48.6	1.083E-04	1.039E-04	5.302E-03	5.245E-03	0.1981	0.1994	0.6073	0.6073	1.783E-04	1.711E-04	0.008729	0.008636
4	1.E+18	1.E+17	48.7	2.094E-04	1.383E-04	9.788E-03	9.558E-03	0.1911	0.1921	0.5200	0.5200	4.027E-04	2.659E-04	0.018824	0.018400
4	1.E+18	1.E+18	48.8	2.447E-04	1.660E-04	1.166E-02	1.141E-02	0.1877	0.1884	0.4909	0.4909	4.985E-04	3.382E-04	0.023750	0.023244
4	1.E+18	1.E+19	48.9	2.724E-04	1.723E-04	1.218E-02	1.191E-02	0.1859	0.1871	0.4821	0.4821	5.651E-04	3.574E-04	0.025262	0.024699
4	1.E+19	1.E+16	49.6	1.084E-04	1.040E-04	5.296E-03	5.241E-03	0.1982	0.1996	0.6084	0.6084	1.781E-04	1.710E-04	0.008705	0.008615
4	1.E+19	1.E+17	49.7	2.103E-04	1.389E-04	9.805E-03	9.589E-03	0.1914	0.1924	0.5208	0.5208	4.037E-04	2.668E-04	0.018827	0.018413
4	1.E+19	1.E+18	49.8	2.459E-04	1.669E-04	1.167E-02	1.143E-02	0.1882	0.1889	0.4923	0.4923	4.995E-04	3.390E-04	0.023708	0.023212
4	1.E+19	1.E+19	49.9	2.768E-04	1.752E-04	1.231E-02	1.204E-02	0.1865	0.1877	0.4827	0.4827	5.733E-04	3.628E-04	0.025497	0.024947

PDC = <subst depth (um)><p>.<n> ; N_a = 1E(10+p) (h/ml); N_d = 1E(10+n) (e/ml).

APPENDIX XI.2 : RESULTS - SJPD

FI SJPD PSE 3 electrodes on n-well: Image electrode (IE) QE dependence on substrate depth, n-well and p-substrate doping cont. page 2 / 2.

Subst	P-subst	n-well	well depth = 2 um; reverse bias = 2 volts; n-well electrode width = 4 um; outer electrodes end 1 um from well wall; 5 um beam (633 nm).													
depth	doping	doping	sd/pd/nd	PSE Boundary		On SCR		near PSE centre		Exp Max	PSE	Boundary Nz QE		well wall Nz QE	
(um)	(h/ml)	(e/ml)	PDC	QE @ 55	QE @ 105	QE @ 70	QE @ 90	QE@75	QE@95	QE@80	Max QE	at 55	at 105	at 70	at 90
5	1.E+14	1.E+16	54.6	5.695E-04	3.893E-04	1.049E-02	9.120E-03	0.1744	0.1644	0.5547	0.5547	1.027E-03	7.019E-04	0.018913	0.016442
5	1.E+14	1.E+17	54.7	6.328E-04	4.206E-04	1.101E-02	9.612E-03	0.1743	0.1642	0.5503	0.5503	1.150E-03	7.643E-04	0.020009	0.017466
5	1.E+14	1.E+18	54.8	6.678E-04	4.471E-04	1.142E-02	1.000E-02	0.1751	0.1649	0.5498	0.5498	1.215E-03	8.132E-04	0.020764	0.018194
5	1.E+14	1.E+19	54.9	6.758E-04	4.620E-04	1.174E-02	1.039E-02	0.1754	0.1652	0.5480	0.5480	1.233E-03	8.431E-04	0.021423	0.018950
5	1.E+15	1.E+16	55.6	2.579E-04	2.169E-04	8.030E-03	6.938E-03	0.2020	0.1735	0.5851	0.5851	4.407E-04	3.707E-04	0.013724	0.011858
5	1.E+15	1.E+17	55.7	3.633E-04	3.204E-04	1.069E-02	9.151E-03	0.1996	0.1719	0.5511	0.5511	6.593E-04	5.815E-04	0.019403	0.016606
5	1.E+15	1.E+18	55.8	3.859E-04	3.238E-04	1.128E-02	9.742E-03	0.1994	0.1727	0.5473	0.5473	7.051E-04	5.915E-04	0.020607	0.017799
5	1.E+15	1.E+19	55.9	4.040E-04	3.312E-04	1.162E-02	1.002E-02	0.1993	0.1712	0.5453	0.5453	7.409E-04	6.073E-04	0.021316	0.018376
5	1.E+16	1.E+16	56.6	2.673E-04	2.669E-04	7.120E-03	7.505E-03	0.1814	0.1875	0.6552	0.6552	4.079E-04	4.073E-04	0.010866	0.011454
5	1.E+16	1.E+17	56.7	4.126E-04	4.080E-04	1.115E-02	1.148E-02	0.1739	0.1790	0.5636	0.5636	7.320E-04	7.239E-04	0.019789	0.020360
5	1.E+16	1.E+18	56.8	4.119E-04	4.076E-04	1.187E-02	1.220E-02	0.1731	0.1771	0.5523	0.5523	7.457E-04	7.380E-04	0.021492	0.022094
5	1.E+16	1.E+19	56.9	4.118E-04	4.107E-04	1.217E-02	1.261E-02	0.1731	0.1772	0.5495	0.5495	7.493E-04	7.474E-04	0.022153	0.022940
5	1.E+17	1.E+16	57.6	4.509E-04	3.473E-04	1.062E-02	1.069E-02	0.2215	0.2192	0.6447	0.6447	6.994E-04	5.386E-04	0.016777	0.016588
5	1.E+17	1.E+17	57.7	5.919E-04	4.499E-04	1.533E-02	1.489E-02	0.2131	0.2122	0.5559	0.5559	1.065E-03	8.093E-04	0.027586	0.026790
5	1.E+17	1.E+18	57.8	6.222E-04	4.637E-04	1.643E-02	1.611E-02	0.2089	0.2074	0.5289	0.5289	1.176E-03	8.768E-04	0.031056	0.030449
5	1.E+17	1.E+19	57.9	6.201E-04	4.692E-04	1.688E-02	1.642E-02	0.2083	0.2062	0.5239	0.5239	1.183E-03	8.955E-04	0.032222	0.031331
5	1.E+18	1.E+16	58.6	4.652E-04	3.584E-04	1.108E-02	1.095E-02	0.2223	0.2200	0.6476	0.6476	7.184E-04	5.534E-04	0.017105	0.016917
5	1.E+18	1.E+17	58.7	6.378E-04	4.859E-04	1.615E-02	1.572E-02	0.2150	0.2142	0.5595	0.5595	1.140E-03	8.684E-04	0.028868	0.028089
5	1.E+18	1.E+18	58.8	6.994E-04	5.223E-04	1.791E-02	1.760E-02	0.2115	0.2102	0.5304	0.5304	1.319E-03	9.848E-04	0.033766	0.033184
5	1.E+18	1.E+19	58.9	6.984E-04	5.298E-04	1.846E-02	1.800E-02	0.2102	0.2082	0.5217	0.5217	1.339E-03	1.016E-03	0.035384	0.034498
5	1.E+19	1.E+16	59.6	4.685E-04	3.610E-04	1.113E-02	1.101E-02	0.2224	0.2202	0.6485	0.6485	7.225E-04	5.567E-04	0.017167	0.016981
5	1.E+19	1.E+17	59.7	6.460E-04	4.924E-04	1.630E-02	1.587E-02	0.2153	0.2145	0.5601	0.5601	1.153E-03	8.791E-04	0.029101	0.028327
5	1.E+19	1.E+18	59.8	7.137E-04	5.332E-04	1.815E-02	1.784E-02	0.2121	0.2107	0.5314	0.5314	1.343E-03	1.003E-03	0.034149	0.033576
5	1.E+19	1.E+19	59.9	7.219E-04	5.480E-04	1.891E-02	1.845E-02	0.2108	0.2089	0.5217	0.5217	1.384E-03	1.050E-03	0.036246	0.035363
6	1.E+14	1.E+16	64.6	7.110E-04	5.081E-04	1.115E-02	9.681E-03	0.1869	0.1774	0.5958	0.5958	1.193E-03	8.527E-04	0.018718	0.016198
6	1.E+14	1.E+17	64.7	7.833E-04	6.547E-04	1.189E-02	1.028E-02	0.1866	0.1770	0.5890	0.5890	1.330E-03	1.112E-03	0.020190	0.017461
6	1.E+14	1.E+18	64.8	7.996E-04	5.802E-04	1.226E-02	1.080E-02	0.1871	0.1777	0.5881	0.5881	1.360E-03	9.868E-04	0.020845	0.018356
6	1.E+14	1.E+19	64.9	8.552E-04	7.120E-04	1.276E-02	1.118E-02	0.1872	0.1777	0.5862	0.5862	1.459E-03	1.215E-03	0.021765	0.019077
6	1.E+15	1.E+16	65.6	4.965E-04	3.305E-04	9.732E-03	8.400E-03	0.2151	0.1896	0.6161	0.6161	8.058E-04	5.364E-04	0.015796	0.013634
6	1.E+15	1.E+17	65.7	5.961E-04	4.052E-04	1.236E-02	1.057E-02	0.2121	0.1856	0.5822	0.5822	1.024E-03	6.960E-04	0.021234	0.018149
6	1.E+15	1.E+18	65.8	6.394E-04	4.264E-04	1.290E-02	1.111E-02	0.2117	0.1850	0.5785	0.5785	1.105E-03	7.370E-04	0.022295	0.019206
6	1.E+15	1.E+19	65.9	6.565E-04	4.361E-04	1.324E-02	1.147E-02	0.2124	0.1870	0.5765	0.5765	1.139E-03	7.564E-04	0.022974	0.019888
6	1.E+16	1.E+16	66.6	8.890E-04	8.858E-04	1.256E-02	1.237E-02	0.1970	0.2042	0.6766	0.6766	1.314E-03	1.309E-03	0.018568	0.018287
6	1.E+16	1.E+17	66.7	1.062E-03	1.001E-03	1.604E-02	1.583E-02	0.1889	0.1923	0.5854	0.5854	1.815E-03	1.710E-03	0.027405	0.027041
6	1.E+16	1.E+18	66.8	1.055E-03	1.017E-03	1.669E-02	1.653E-02	0.1878	0.1904	0.5742	0.5742	1.837E-03	1.771E-03	0.029064	0.028786
6	1.E+16	1.E+19	66.9	1.107E-03	1.028E-03	1.705E-02	1.683E-02	0.1883	0.1914	0.5714	0.5714	1.938E-03	1.799E-03	0.029838	0.029450
6	1.E+17	1.E+16	67.6	9.995E-04	1.067E-03	1.672E-02	1.815E-02	0.2359	0.2325	0.6636	0.6636	1.506E-03	1.607E-03	0.025202	0.027354
6	1.E+17	1.E+17	67.7	1.135E-03	1.359E-03	2.065E-02	2.209E-02	0.2277	0.2256	0.5752	0.5752	1.974E-03	2.362E-03	0.035892	0.038403
6	1.E+17	1.E+18	67.8	1.177E-03	1.215E-03	2.169E-02	2.298E-02	0.2235	0.2210	0.5488	0.5488	2.145E-03	2.215E-03	0.039527	0.041867
6	1.E+17	1.E+19	67.9	1.231E-03	1.207E-03	2.197E-02	2.340E-02	0.2229	0.2201	0.5438	0.5438	2.263E-03	2.219E-03	0.040395	0.043021
6	1.E+18	1.E+16	68.6	1.028E-03	1.094E-03	1.716E-02	1.860E-02	0.2366	0.2334	0.6661	0.6661	1.543E-03	1.643E-03	0.025760	0.027925
6	1.E+18	1.E+17	68.7	1.227E-03	1.459E-03	2.201E-02	2.347E-02	0.2295	0.2275	0.5780	0.5780	2.123E-03	2.525E-03	0.038088	0.040509
6	1.E+18	1.E+18	68.8	1.320E-03	1.357E-03	2.389E-02	2.528E-02	0.2261	0.2236	0.5489	0.5489	2.405E-03	2.471E-03	0.043525	0.046062
6	1.E+18	1.E+19	68.9	1.379E-03	1.347E-03	2.420E-02	2.577E-02	0.2247	0.2220	0.5403	0.5403	2.553E-03	2.494E-03	0.044781	0.047688
6	1.E+19	1.E+16	69.6	1.035E-03	1.101E-03	1.726E-02	1.870E-02	0.2368	0.2335	0.6669	0.6669	1.551E-03	1.651E-03	0.025876	0.028045
6	1.E+19	1.E+17	69.7	1.243E-03	1.477E-03	2.225E-02	2.372E-02	0.2298	0.2278	0.5784	0.5784	2.149E-03	2.553E-03	0.038477	0.041006
6	1.E+19	1.E+18	69.8	1.349E-03	1.384E-03	2.430E-02	2.570E-02	0.2266	0.2241	0.5497	0.5497	2.455E-03	2.518E-03	0.044215	0.046756
6	1.E+19	1.E+19	69.9	1.426E-03	1.389E-03	2.489E-02	2.647E-02	0.2252	0.2226	0.5400	0.5400	2.641E-03	2.573E-03	0.046082	0.049009

PDC = <subst depth (um)><p>.<n> ; N_a = 1E(10+p) (h/ml); N_n = 1E(10+n) (e/ml).

SJPD PSE Doping expt: % of light (633 nm) absorbed in SCR and non-SCR for the PDC range use for the SJPD doping simulation.

(pixel)

Laser width(um)		5	Temp	In
			300	100
Well	Substr	Bias	Substr	Well
(e/ml)	(h/ml)	(V)	Dp (um)	Dp (um)

PDC	PSE width 50 nm PSE %Abs	Drift component 3D PSE Bl % abs SCR	3D PSE Fl % abs SCR	Diffusion component 3D PSE Bl % abs non-SCR	3D PSE Fl % abs non-SCR	2D PSE Bl % abs SCR	2D PSE Fl % abs SCR	Diffusion component 2D PSE Bl % abs non-SCR	2D PSE Fl % abs non-SCR	SCR (Drift) % Abs 70 2D Bl PSE 5 um beam on well wall	2D Fl PSE 5 um beam on well wall	non-SCR (diffusion) %Abs 2D Bl PSE 5 um beam on well wall	2D Fl PSE 5 um beam on well wall	SCR (Drift) % Abs 80 2D Bl PSE 5 um beam centre of well	2D Fl PSE 5 um beam centre of well	non-SCR (diffusion) %Abs 2D Bl PSE 5 um beam centre of well	2D Fl PSE 5 um beam centre of well	CONDITIONS MUST NOT BE NEGATIVE !!!! Outer SCR & PSE condition	Outer SCR & Substr depth condition	Inner SCR & Inner well condition	LASER Width condition
34.6	50.206	1.000	1.000	1.00	1.00	1.000	1.000	1.00	1.00	1.000	1.000	1.00	1.00	1.000	1.000	1.00	1.00	16.46	-4.769	19.88	-3.269
34.7	50.206	1.000	1.000	1.00	1.00	1.000	1.000	1.00	1.00	1.000	1.000	1.00	1.00	1.000	1.000	1.00	1.00	16.28	-4.861	19.99	-3.361
34.8	50.206	1.000	1.000	1.00	1.00	1.000	1.000	1.00	1.00	1.000	1.000	1.00	1.00	1.000	1.000	1.00	1.00	16.14	-4.930	20.00	-3.430
34.9	50.206	1.000	1.000	1.00	1.00	1.000	1.000	1.00	1.00	1.000	1.000	1.00	1.00	1.000	1.000	1.00	1.00	16.01	-4.995	20.00	-3.495
35.6	50.206	1.000	1.000	1.00	1.00	1.000	1.000	1.00	1.00	1.000	1.000	1.00	1.00	1.000	1.000	1.00	1.00	26.46	-0.768	19.65	0.732
35.7	50.206	1.000	1.000	1.00	1.00	1.000	1.000	1.00	1.00	1.000	1.000	1.00	1.00	1.000	1.000	1.00	1.00	26.27	-0.866	19.96	0.634
35.8	50.206	1.000	1.000	1.00	1.00	1.000	1.000	1.00	1.00	1.000	1.000	1.00	1.00	1.000	1.000	1.00	1.00	26.21	-0.895	20.00	0.605
35.9	50.206	1.000	1.000	1.00	1.00	1.000	1.000	1.00	1.00	1.000	1.000	1.00	1.00	1.000	1.000	1.00	1.00	26.17	-0.916	20.00	0.584
36.6	50.206	3.257	2.937	46.95	47.27	7.499	6.368	42.71	43.84	14.283	13.444	35.92	36.76	15.474	12.265	34.73	37.94	29.16	0.581	19.16	2.081
36.7	50.206	2.739	2.263	47.47	47.94	6.232	4.798	43.97	45.41	12.699	11.004	37.51	39.20	12.308	8.656	37.90	41.55	28.86	0.428	19.89	1.928
36.8	50.206	2.700	2.199	47.51	48.01	6.126	4.643	44.08	45.56	12.575	10.759	37.63	39.45	12.035	8.303	38.17	41.90	28.79	0.397	19.99	1.897
36.9	50.206	2.725	2.213	47.48	47.99	6.174	4.667	44.03	45.54	12.677	10.824	37.53	39.38	12.128	8.339	38.08	41.87	28.78	0.388	20.00	1.888
37.6	50.206	2.151	2.132	48.05	48.07	4.953	4.687	45.25	45.52	8.381	8.801	41.82	41.40	10.921	9.756	39.26	40.45	29.89	0.943	18.86	2.443
37.7	50.206	1.053	0.954	49.15	49.25	2.462	2.097	47.74	48.11	4.819	4.550	45.39	45.66	4.993	3.958	45.21	46.25	29.73	0.864	19.73	2.364
37.8	50.206	0.820	0.721	49.39	49.48	1.978	1.628	48.23	48.58	4.165	3.774	46.04	46.43	3.815	2.909	46.39	47.30	29.63	0.815	19.96	2.315
37.9	50.206	0.798	0.699	49.41	49.51	1.937	1.585	48.27	48.62	4.127	3.716	46.08	46.49	3.705	2.808	46.50	47.40	29.61	0.805	20.00	2.305
38.6	50.206	2.039	2.052	48.17	48.15	4.666	4.499	45.54	45.71	7.614	8.187	42.59	42.02	10.476	9.539	39.73	40.67	29.99	0.994	18.79	2.494
38.7	50.206	0.758	0.707	49.45	49.50	1.705	1.509	48.50	48.70	3.021	3.009	47.18	47.20	3.670	3.024	46.54	47.18	29.96	0.982	19.63	2.482
38.8	50.206	0.340	0.308	49.87	49.90	0.799	0.681	49.41	49.52	1.578	1.490	48.63	48.72	1.612	1.278	48.59	48.93	29.91	0.956	19.91	2.456
38.9	50.206	0.258	0.232	49.95	49.97	0.635	0.534	49.57	49.67	1.350	1.242	48.86	48.96	1.215	0.951	48.99	49.25	29.88	0.940	19.99	2.440
39.6	50.206	2.044	2.062	48.16	48.14	4.674	4.522	45.53	45.68	7.589	8.189	42.62	42.02	10.522	9.613	39.68	40.59	30.00	0.999	18.78	2.499
39.7	50.206	0.729	0.684	49.48	49.52	1.624	1.446	48.58	48.76	2.805	2.826	47.40	47.38	3.542	2.936	46.66	47.27	30.00	0.998	19.61	2.498
39.8	50.206	0.252	0.230	49.95	49.98	0.562	0.486	49.64	49.72	1.010	0.987	49.20	49.22	1.200	0.963	49.01	49.24	29.99	0.994	19.88	2.494
39.9	50.206	0.110	0.099	50.10	50.11	0.258	0.220	49.95	49.99	0.511	0.483	49.69	49.72	0.520	0.412	49.69	49.79	29.97	0.986	19.97	2.486
44.6	60.533	1.000	1.000	1.00	1.00	1.000	1.000	1.00	1.00	1.000	1.000	1.00	1.00	1.000	1.000	1.00	1.00	16.46	-3.769	19.88	-3.269
44.7	60.533	1.000	1.000	1.00	1.00	1.000	1.000	1.00	1.00	1.000	1.000	1.00	1.00	1.000	1.000	1.00	1.00	16.28	-3.861	19.99	-3.361
44.8	60.533	1.000	1.000	1.00	1.00	1.000	1.000	1.00	1.00	1.000	1.000	1.00	1.00	1.000	1.000	1.00	1.00	16.14	-3.930	20.00	-3.430
44.9	60.533	1.000	1.000	1.00	1.00	1.000	1.000	1.00	1.00	1.000	1.000	1.00	1.00	1.000	1.000	1.00	1.00	16.01	-3.995	20.00	-3.495
45.6	60.533	8.510	7.224	52.02	53.31	16.19	12.82	44.35	47.72	29.241	28.369	31.29	32.16	34.460	23.806	26.07	36.73	26.46	0.232	19.65	0.732
45.7	60.533	8.665	7.057	51.87	53.48	16.07	12.13	44.46	48.40	28.780	27.102	31.75	33.43	34.382	22.380	26.15	38.15	26.27	0.134	19.96	0.634
45.8	60.533	8.801	7.111	51.73	53.42	16.23	12.15	44.30	48.38	28.966	27.144	31.57	33.39	34.792	22.408	25.74	38.12	26.21	0.105	20.00	0.605
45.9	60.533	8.934	7.188	51.60	53.34	16.42	12.24	44.11	48.29	29.227	27.329	31.31	33.20	35.251	22.582	25.28	37.95	26.17	0.084	20.00	0.584
46.6	60.533	2.581	2.937	57.95	57.60	5.944	6.368	54.59	54.16	11.321	13.444	49.21	47.09	12.265	12.265	48.27	48.27	29.16	1.581	19.16	2.081
46.7	60.533	2.171	2.263	58.36	58.27	4.940	4.798	55.59	55.73	10.066	11.004	50.47	49.53	9.756	8.656	50.78	51.88	28.86	1.428	19.89	1.928
46.8	60.533	2.140	2.199	58.39	58.33	4.855	4.643	55.68	55.89	9.967	10.759	50.57	49.77	9.539	8.303	50.99	52.23	28.79	1.397	19.99	1.897
46.9	60.533	2.160	2.213	58.37	58.32	4.893	4.667	55.64	55.87	10.048	10.824	50.49	49.71	9.613	8.339	50.92	52.19	28.78	1.388	20.00	1.888
47.6	60.533	1.705	2.132	58.83	58.40	3.926	4.687	56.61	55.85	6.643	8.801	53.89	51.73	8.656	9.756	51.88	50.78	29.89	1.943	18.86	2.443
47.7	60.533	0.834	0.954	59.70	59.58	1.951	2.097	58.58	58.44	3.820	4.550	56.71	55.98	3.958	3.958	56.57	56.57	29.73	1.864	19.73	2.364
47.8	60.533	0.650	0.721	59.88	59.81	1.567	1.628	58.97	58.91	3.301	3.774	57.23	56.76	3.024	2.909	57.51	57.62	29.63	1.815	19.96	2.315
47.9	60.533	0.633	0.699	59.90	59.83	1.535	1.585	59.00	58.95	3.271	3.716	57.26	56.82	2.936	2.808	57.60	57.72	29.61	1.805	20.00	2.305
48.6	60.533	1.616	2.052	58.92	58.48	3.698	4.499	56.83	56.03	6.035	8.187	54.50	52.35	8.303	9.539	52.23	50.99	29.99	1.994	18.79	2.494
48.7	60.533	0.601	0.707	59.93	59.83	1.352	1.509	59.18	59.02	2.395	3.009	58.14	57.52	2.909	3.024	57.62	57.51	29.96	1.982	19.63	2.482
48.8	60.533	0.270	0.308	60.26	60.22	0.633	0.681	59.90	59.85	1.251	1.490	59.28	59.04	1.278	1.278	59.26	59.26	29.91	1.956	19.91	2.456
48.9	60.533	0.205	0.232	60.33	60.30	0.503	0.534	60.03	60.00	1.070	1.242	59.46	59.29	0.963	0.951	59.57	59.58	29.88	1.940	19.99	2.440
49.6	60.533	1.620	2.062	58.91	58.47	3.705	4.522	56.83	56.01	6.015	8.189	54.52	52.34	8.339	9.613	52.19	50.92	30.00	1.999	18.78	2.499
49.7	60.533	0.578	0.684	59.96	59.85	1.287	1.446	59.25	59.09	2.223	2.826	58.31	57.71	2.808	2.936	57.72	57.60	30.00	1.998	19.61	2.498
49.8	60.533	0.199	0.230	60.33	60.30	0.445	0.486	60.09	60.05	0.800	0.987	59.73	59.55	0.951	0.963	59.58	59.57	29.99	1.994	19.88	2.494
49.9	60.533	0.087	0.099	60.45	60.43	0.205	0.220	60.33	60.31	0.405	0.483	60.13	60.05	0.412	0.412	60.12	60.12	29.97	1.986	19.97	2.486

PDC = <subst depth (um)><p>.<n> ; N_A = 1E(10+p) (h/ml); N_D = 1E(10+n) (e/ml).

SJPD PSE (pixel) Doping expt: % light (633 nm) absorbed in SCR and non-SCR for the PDC range use for the SJPD doping simulation cont page 2 of 2.

Laser width(um)		S	temp	Ia			Drift component		diffusion component		Drift component		diffusion component		SCR (Drift) % Abs.		non-SCR (diffusion) %Abs.		SCR (Drift) % Abs.		non-SCR (diffusion) %Abs.		CONDITIONS MUST NOT BE NEGATIVE !!!!			
Well	Substr	Bias	Substr	Well		PSE width	3D PSE	3D PSE	3D PSE	3D PSE	2D PSE	2D PSE	2D PSE	2D PSE	2D BI PSE	2D FI PSE	2D BI PSE	2D FI PSE	2D BI PSE	2D FI PSE	2D BI PSE	2D FI PSE	2D BI PSE	2D FI PSE				
(a/ml)	(h/ml)	(V)	Dp (um)	Dp (um)	PDC	50 nm PSE %Abs	BI % abs SCR	FI % abs SCR	BI % abs non-SCR	FI % abs non-SCR	BI % abs SCR	FI % abs SCR	BI % abs non-SCR	FI % abs non-SCR	5 um beam on well wall	5 um beam on well wall	5 um beam on well wall	5 um beam on well wall	5 um beam centre of well	5 um beam centre of well	5 um beam centre of well	5 um beam centre of well	Outer SCR & PSE condition	Centre SCR & Substr depth condition	Inner SCR & ionic well condition	LASER Width condition
1.E+16	1.E+14	-2	5	2	54.6	68.718	1.000	1.000	1.00	1.00	1.000	1.000	1.00	1.00	1.000	1.000	1.00	1.00	1.000	1.000	1.00	1.00	18.46	-2.769	19.88	-3.269
1.E+17	1.E+14	-2	5	2	54.7	68.718	1.000	1.000	1.00	1.00	1.000	1.000	1.00	1.00	1.000	1.000	1.00	1.00	1.000	1.000	1.00	1.00	18.28	-2.861	19.99	-3.361
1.E+18	1.E+14	-2	5	2	54.8	68.718	1.000	1.000	1.00	1.00	1.000	1.000	1.00	1.00	1.000	1.000	1.00	1.00	1.000	1.000	1.00	1.00	18.14	-2.930	20.00	-3.430
1.E+19	1.E+14	-2	5	2	54.9	68.718	1.000	1.000	1.00	1.00	1.000	1.000	1.00	1.00	1.000	1.000	1.00	1.00	1.000	1.000	1.00	1.00	18.01	-2.995	20.00	-3.495
1.E+16	1.E+15	-2	5	2	55.6	68.718	6.745	7.224	61.97	61.49	12.83	12.82	55.89	55.90	23.177	28.369	45.54	40.35	27.313	23.806	41.40	44.91	26.46	1.232	19.65	0.732
1.E+17	1.E+15	-2	5	2	55.7	68.718	6.868	7.057	61.85	61.66	12.74	12.13	55.98	56.58	22.811	27.102	45.91	41.62	27.251	22.380	41.47	46.34	26.27	1.134	19.96	0.634
1.E+18	1.E+15	-2	5	2	55.8	68.718	6.976	7.111	61.74	61.61	12.86	12.15	55.85	56.57	22.959	27.144	45.76	41.57	27.577	22.408	41.14	46.31	26.21	1.105	20.00	0.605
1.E+19	1.E+15	-2	5	2	55.9	68.718	7.081	7.188	61.64	61.53	13.02	12.24	55.70	56.48	23.166	27.329	45.55	41.39	27.940	22.582	40.78	46.14	26.17	1.084	20.00	0.584
1.E+16	1.E+16	-2	5	2	56.6	68.718	2.046	2.937	66.67	65.78	4.711	6.368	64.01	62.35	8.973	13.444	59.74	55.27	9.721	12.265	59.00	56.45	29.16	2.581	19.16	2.081
1.E+17	1.E+16	-2	5	2	56.7	68.718	1.721	2.263	67.00	66.46	3.915	4.798	64.80	63.92	7.978	11.004	60.74	57.71	7.733	8.656	60.99	60.06	28.86	2.428	19.89	1.928
1.E+18	1.E+16	-2	5	2	56.8	68.718	1.696	2.199	67.02	66.52	3.848	4.643	64.87	64.07	7.900	10.759	60.82	57.96	7.561	8.303	61.16	60.41	28.79	2.397	19.99	1.897
1.E+19	1.E+16	-2	5	2	56.9	68.718	1.712	2.213	67.01	66.50	3.879	4.667	64.84	64.05	7.964	10.824	60.75	57.89	7.619	8.339	61.10	60.38	28.78	2.388	20.00	1.888
1.E+16	1.E+17	-2	5	2	57.6	68.718	1.352	2.132	67.37	66.59	3.111	4.687	65.61	64.03	5.265	8.801	63.45	59.92	6.861	9.756	61.86	58.96	29.89	2.943	18.86	2.443
1.E+17	1.E+17	-2	5	2	57.7	68.718	0.861	0.954	68.06	67.76	1.547	2.097	67.17	66.62	3.028	4.550	65.69	64.17	3.137	3.958	65.58	64.76	29.73	2.864	19.73	2.364
1.E+18	1.E+17	-2	5	2	57.8	68.718	0.515	0.721	68.20	68.00	1.242	1.628	67.48	67.09	2.617	3.774	66.10	64.94	2.397	2.909	66.32	65.81	29.63	2.815	19.96	2.315
1.E+19	1.E+17	-2	5	2	57.9	68.718	0.501	0.699	68.22	68.02	1.217	1.585	67.50	67.13	2.593	3.716	66.12	65.00	2.327	2.808	66.39	65.91	29.61	2.805	20.00	2.305
1.E+16	1.E+18	-2	5	2	58.6	68.718	1.281	2.052	67.44	66.67	2.931	4.499	65.79	64.22	4.783	8.187	63.93	60.53	6.581	9.539	62.14	59.18	29.99	2.994	18.79	2.494
1.E+17	1.E+18	-2	5	2	58.7	68.718	0.476	0.707	68.24	68.01	1.071	1.509	67.65	67.21	1.898	3.009	66.82	65.71	2.306	3.024	66.41	65.69	29.96	2.982	19.63	2.482
1.E+18	1.E+18	-2	5	2	58.8	68.718	0.214	0.308	68.50	68.41	0.502	0.681	68.22	68.04	0.991	1.490	67.73	67.23	1.013	1.278	67.71	67.44	29.91	2.956	19.91	2.456
1.E+19	1.E+18	-2	5	2	58.9	68.718	0.162	0.232	68.56	68.49	0.399	0.534	68.32	68.18	0.846	1.242	67.87	67.46	0.763	0.951	67.95	67.77	29.88	2.940	19.99	2.440
1.E+16	1.E+19	-2	5	2	59.6	68.718	1.284	2.062	67.43	66.66	2.936	4.522	65.78	64.20	4.767	8.189	63.95	60.53	6.610	9.613	62.11	59.10	30.00	2.999	18.78	2.499
1.E+17	1.E+19	-2	5	2	59.7	68.718	0.458	0.684	68.26	68.03	1.020	1.446	67.70	67.27	1.762	2.826	66.96	65.89	2.225	2.936	66.49	65.76	30.00	2.998	19.61	2.498
1.E+18	1.E+19	-2	5	2	59.8	68.718	0.158	0.230	68.56	68.49	0.353	0.486	68.36	68.23	0.634	0.987	68.08	67.73	0.754	0.963	67.96	67.75	29.99	2.994	19.88	2.494
1.E+19	1.E+19	-2	5	2	59.9	68.718	0.069	0.099	68.65	68.62	0.162	0.220	68.56	68.50	0.321	0.483	68.40	68.23	0.327	0.412	68.39	68.31	29.97	2.986	19.97	2.486
1.E+16	1.E+14	-2	6	2	64.6	75.205	1.000	1.000	1.00	1.00	1.000	1.000	1.00	1.00	1.000	1.000	1.00	1.00	1.000	1.000	1.00	1.00	18.46	-1.769	19.88	-3.269
1.E+17	1.E+14	-2	6	2	64.7	75.205	1.000	1.000	1.00	1.00	1.000	1.000	1.00	1.00	1.000	1.000	1.00	1.00	1.000	1.000	1.00	1.00	18.28	-1.861	19.99	-3.361
1.E+18	1.E+14	-2	6	2	64.8	75.205	1.000	1.000	1.00	1.00	1.000	1.000	1.00	1.00	1.000	1.000	1.00	1.00	1.000	1.000	1.00	1.00	18.14	-1.930	20.00	-3.430
1.E+19	1.E+14	-2	6	2	64.9	75.205	1.000	1.000	1.00	1.00	1.000	1.000	1.00	1.00	1.000	1.000	1.00	1.00	1.000	1.000	1.00	1.00	18.01	-1.995	20.00	-3.495
1.E+16	1.E+15	-2	6	2	65.6	75.205	5.346	7.224	69.86	67.98	10.17	12.82	65.04	62.39	18.370	28.369	56.84	46.84	21.649	23.806	53.56	51.40	26.46	2.232	19.65	0.732
1.E+17	1.E+15	-2	6	2	65.7	75.205	5.443	7.057	69.76	68.15	10.10	12.13	65.11	63.07	18.081	27.102	57.12	48.10	21.600	22.380	53.61	52.83	26.27	2.134	19.96	0.634
1.E+18	1.E+15	-2	6	2	65.8	75.205	5.529	7.111	69.68	68.09	10.20	12.15	65.01	63.05	18.197	27.144	57.01	48.06	21.858	22.408	53.35	52.80	26.21	2.105	20.00	0.605
1.E+19	1.E+15	-2	6	2	65.9	75.205	5.613	7.188	69.59	68.02	10.32	12.24	64.89	62.97	18.361	27.329	56.84	47.88	22.146	22.582	53.06	52.62	26.17	2.084	20.00	0.584
1.E+16	1.E+16	-2	6	2	66.6	75.205	1.622	2.937	73.58	72.27	3.734	6.368	71.47	68.84	7.112	13.444	68.09	61.76	7.705	12.265	67.50	62.94	29.16	3.581	19.16	2.081
1.E+17	1.E+16	-2	6	2	66.7	75.205	1.364	2.263	73.84	72.94	3.103	4.798	72.10	70.41	6.324	11.004	68.88	64.20	6.129	8.656	69.08	66.55	28.86	3.428	19.89	1.928
1.E+18	1.E+16	-2	6	2	66.8	75.205	1.344	2.199	73.86	73.01	3.050	4.643	72.16	70.56	6.262	10.759	68.94	64.45	5.993	8.303	69.21	66.90	28.79	3.397	19.99	1.897
1.E+19	1.E+16	-2	6	2	66.9	75.205	1.357	2.213	73.85	72.99	3.074	4.667	72.13	70.54	6.312	10.824	68.89	64.38	6.039	8.339	69.17	66.87	28.78	3.388	20.00	1.888
1.E+16	1.E+17	-2	6	2	67.6	75.205	1.071	2.132	74.13	73.07	2.466	4.687	72.74	70.52	4.173	8.801	71.03	66.40	5.438	9.756	69.77	65.45	29.89	3.943	18.86	2.443
1.E+17	1.E+17	-2	6	2	67.7	75.205	0.524	0.954	74.68	74.25	1.226	2.097	73.98	73.11	2.400	4.550	72.81	70.66	2.486	3.958	72.72	71.25	29.73	3.864	19.73	2.364
1.E+18	1.E+17	-2	6	2	67.8	75.205	0.408	0.721	74.80	74.48	0.985	1.628	74.22	73.58	2.074	3.774	73.13	71.43	1.900	2.909	73.31	72.30	29.63	3.815	19.96	2.315
1.E+19	1.E+17	-2	6	2	67.9	75.205	0.397	0.699	74.81	74.51	0.964	1.585	74.24	73.62	2.055	3.716	73.15	71.49	1.845	2.808	73.36	72.40	29.61	3.805	20.00	2.305
1.E+16	1.E+18	-2	6	2	68.6	75.205	1.015	2.052	74.19	73.15	2.323	4.499	72.88	70.71	3.791	8.187	71.41	67.02	5.216	9.539	69.99	65.67	29.99	3.994	18.79	2.494
1.E+17	1.E+18	-2	6	2	68.7	75.205	0.377	0.707	74.83	74.50	0.849	1.509	74.36	73.70	1.504	3.009	73.70	72.20	1.828	3.024	73.38	72.18	29.96	3.982	19.63	2.482
1.E+18	1.E+18	-2	6	2	68.8	75.205	0.169	0.308	75.04	74.90	0.398	0.681	74.81	74.52	0.786	1.490	74.42	73.71	0.803	1.278	74.40	73.93	29.91	3.956	19.91	2.456
1.E+19	1.E+18	-2	6	2	68.9	75.205	0.128	0.232	75.08	74.97	0.316	0.534	74.89	74.67	0.672	1.242	74.53	73.96	0.605	0.951	74.60	74.25	29.88	3.940	19.99	2.440
1.E+16	1.E+19	-2	6	2	69.6	75.205	1.018	2.062	74.19	73.14	2.327	4.522	72.88	70.68	3.779	8.189	71.43	67.02	5.239	9.613	69.97	65.59	30.00	3.999	18.78	2.499
1.E+17	1.E+19	-2	6	2	69.7	75.205	0.363	0.684	74.84	74.52	0.809	1.446	74.40	73.76	1.397	2.826	73.81	72.38	1.764	2.936	73.44	72.27	30.00	3.998	19.61	2.498
1.E+18	1.E+19	-2	6	2	69.8	75.205	0.125	0.230	75.08	74.96	0.280	0.486	74.93	74.72	0.503	0.987	74.70	74.22	0.598	0.963	74.61	74.24	29.99	3.994	19.88	2.494
1.E+19	1.E+19	-2	6	2	69.9	75.205	0.055	0.099	75.15	75.11	0.129	0.220	75.08	74.99	0.255	0.483	74.95	74.72	0.259	0.412	74.95	74.79	29.97	3.986	19.97	2.486

PDC = <subst depth (um)><p>.<n> ; N_A = 1E(10+p) (h/ml); N_D = 1E(10+n) (e/ml).

BI PNP-DJPD : Image electrode (IE) QE & normalized QE dependence on P+ doping, well width, depth and outer n-well electrode (0.8 um) placement (0 or 2 um from the outer well edge ("shrink")).

well n-dope	substrate p-dope	rev. bias both junct	subst / well depth (um)																					
1.E+17	1.E+15	2 V	(12)/(2)	pd/w/d/sh	PSE Boundary		next to outer well		on outer well wall		Max	Max	PSE Boundary		next to outer well		on outer well wall		% below FI		% below FI		% below FI	
P+ dope	P+ width	P+ depth	shrink	PDC	QE @ 55	QE @ 105	QE @ 65	QE @ 95	QE @ 70	QE @ 90	QE@80	QE BI/FI	Nz @ 55	Nz @ 105	Nz @ 65	Nz @ 95	Nz @ 70	Nz @ 90	Nz@55	Nz@105	Nz@65	Nz@95	Nz@70	Nz@90
1.E+18	2	0.2	0	100	1.167E-08	1.185E-08	1.142E-08	1.159E-08	2.958E-06	2.687E-06	2.143E-03	7.128E-03	5.443E-06	5.528E-06	5.331E-06	5.406E-06	1.380E-03	1.254E-03	-13508	-12746	-13917	-13987	24.55	9.15
1.E+18	2	0.2	2	100.4	1.104E-08	1.178E-08	1.205E-08	1.242E-08	9.774E-07	8.027E-07	2.118E-03	7.043E-03	5.215E-06	5.563E-06	5.690E-06	5.864E-06	4.615E-04	3.791E-04	-14016	-13384	-13372	-15699	-21.60	7.81
1.E+18	2	0.5	0	102	2.296E-08	2.298E-08	2.341E-08	2.343E-08	3.342E-06	3.136E-06	2.449E-03	7.337E-03	9.375E-06	9.383E-06	9.559E-06	9.567E-06	1.365E-03	1.280E-03	-13600	-13612	-13692	-13703	23.24	14.75
1.E+18	2	0.5	2	102.4	2.318E-08	2.318E-08	2.343E-08	2.343E-08	1.140E-06	9.721E-07	2.504E-03	7.501E-03	9.255E-06	9.255E-06	9.357E-06	9.357E-06	4.550E-04	3.882E-04	-13276	-13276	-13321	-13321	-7.44	-3.83
1.E+18	2	1.25	0	104	5.711E-08	5.713E-08	5.717E-08	5.719E-08	3.535E-06	3.397E-06	3.209E-03	8.171E-03	1.780E-05	1.780E-05	1.782E-05	1.782E-05	1.102E-03	1.059E-03	-12139	-12143	-12147	-12147	27.52	31.24
1.E+18	2	1.25	2	104.4	5.707E-08	5.707E-08	5.709E-08	5.711E-08	1.334E-06	1.273E-06	3.244E-03	8.257E-03	1.759E-05	1.759E-05	1.760E-05	1.760E-05	4.111E-04	3.923E-04	-12015	-12015	-12015	-12020	-9.38	-7.40
1.E+18	4	0.2	0	120	2.665E-08	2.683E-08	2.636E-08	2.648E-08	5.189E-06	4.404E-06	2.657E-03	6.787E-03	1.003E-05	1.010E-05	9.919E-06	9.963E-06	1.953E-03	1.657E-03	-14071	-15113	-14260	-14493	16.79	17.94
1.E+18	4	0.2	2	120.4	2.300E-08	2.204E-08	2.408E-08	2.302E-08	2.247E-06	1.810E-06	2.567E-03	6.533E-03	8.960E-06	8.586E-06	9.381E-06	8.968E-06	8.754E-04	7.050E-04	-14849	-14912	-15576	-16133	-35.64	1.36
1.E+18	4	0.5	0	122	3.680E-08	3.678E-08	3.729E-08	3.729E-08	6.648E-06	4.708E-06	2.975E-03	7.045E-03	1.237E-05	1.236E-05	1.253E-05	1.253E-05	2.234E-03	1.582E-03	-14148	-14141	-14216	-14216	20.07	27.51
1.E+18	4	0.5	2	122.4	3.637E-08	3.637E-08	3.605E-08	3.666E-08	2.387E-06	2.495E-06	2.807E-03	6.602E-03	1.296E-05	1.296E-05	1.285E-05	1.306E-05	8.503E-04	8.888E-04	-15080	-15080	-14868	-15120	-21.74	-16.39
1.E+18	4	1.25	0	124	4.500E-08	4.526E-08	4.500E-08	4.500E-08	8.512E-06	7.713E-06	3.706E-03	7.997E-03	1.215E-05	1.221E-05	1.215E-05	1.215E-05	2.297E-03	2.082E-03	-12405	-12476	-12335	-12405	26.51	34.28
1.E+18	4	1.25	2	124.4	4.553E-08	4.553E-08	4.553E-08	4.553E-08	3.052E-06	2.966E-06	3.564E-03	7.669E-03	1.278E-05	1.278E-05	1.278E-05	1.278E-05	8.563E-04	8.320E-04	-12940	-12940	-12940	-12940	-14.88	-11.82
1.E+18	8	0.2	0	140	4.396E-08	4.198E-08	4.273E-08	4.198E-08	2.895E-05	2.610E-05	2.897E-03	7.096E-03	1.518E-05	1.449E-05	1.475E-05	1.449E-05	9.993E-03	9.011E-03	-13830	-13695	-14242	-13564	12.48	14.92
1.E+18	8	0.2	2	140.4	4.357E-08	4.398E-08	4.316E-08	4.438E-08	1.086E-05	8.973E-06	2.891E-03	7.085E-03	1.507E-05	1.521E-05	1.493E-05	1.535E-05	3.755E-03	3.104E-03	-14234	-13688	-13925	-14314	-21.73	-1.49
1.E+18	8	0.5	0	142	5.596E-08	5.598E-08	5.568E-08	5.576E-08	3.146E-05	3.282E-05	3.191E-03	7.394E-03	1.753E-05	1.754E-05	1.745E-05	1.747E-05	9.859E-03	1.028E-02	-13223	-13476	-13287	-13297	23.56	15.02
1.E+18	8	0.5	2	142.4	5.174E-08	5.166E-08	5.113E-08	5.111E-08	1.199E-05	1.128E-05	3.248E-03	7.506E-03	1.593E-05	1.590E-05	1.574E-05	1.573E-05	3.692E-03	3.473E-03	-13118	-13103	-13032	-13032	-6.96	-3.70
1.E+18	8	1.25	0	144	7.370E-08	7.380E-08	7.370E-08	7.370E-08	3.651E-05	3.550E-05	4.088E-03	8.982E-03	1.803E-05	1.805E-05	1.803E-05	1.803E-05	8.929E-03	8.685E-03	-11033	-11048	-11018	-11033	36.69	38.56
1.E+18	8	1.25	2	144.4	7.380E-08	7.380E-08	7.380E-08	7.370E-08	1.357E-05	1.356E-05	4.057E-03	8.887E-03	1.819E-05	1.819E-05	1.819E-05	1.817E-05	3.344E-03	3.342E-03	-11153	-11153	-11168	-11138	0.25	2.64
1.E+18	14	0.2	0	160	6.916E-08	6.834E-08	6.699E-08	6.981E-08	3.125E-04	2.920E-04	2.901E-03	7.068E-03	2.384E-05	2.356E-05	2.309E-05	2.407E-05	1.077E-01	1.007E-01	-13897	-13595	-13216	-13778	9.62	13.05
1.E+18	14	0.2	2	160.4	7.543E-08	7.692E-08	7.503E-08	7.704E-08	1.769E-04	1.333E-04	2.512E-03	5.976E-03	3.002E-05	3.062E-05	2.987E-05	3.066E-05	7.041E-02	5.305E-02	-16531	-16440	-16117	-16991	-39.12	-5.99
1.E+18	14	0.5	0	162	8.510E-08	8.514E-08	8.498E-08	8.502E-08	3.456E-04	3.629E-04	3.248E-03	7.482E-03	2.620E-05	2.621E-05	2.616E-05	2.618E-05	1.064E-01	1.117E-01	-13303	-13315	-13189	-13213	20.64	12.86
1.E+18	14	0.5	2	162.4	1.014E-07	1.014E-07	1.016E-07	1.015E-07	2.167E-04	1.980E-04	2.771E-03	6.123E-03	3.659E-05	3.658E-05	3.666E-05	3.664E-05	7.819E-02	7.146E-02	-16263	-16257	-16209	-16197	-23.07	-19.32
1.E+18	14	1.25	0	164	9.945E-08	9.921E-08	9.945E-08	9.933E-08	3.892E-04	4.277E-04	4.057E-03	8.909E-03	2.451E-05	2.446E-05	2.451E-05	2.448E-05	9.594E-02	1.054E-01	-11151	-11111	-11137	-11137	40.63	32.49
1.E+18	14	1.25	2	164.4	1.464E-07	1.463E-07	1.464E-07	1.463E-07	3.523E-04	3.382E-04	3.425E-03	7.079E-03	4.274E-05	4.271E-05	4.274E-05	4.271E-05	1.029E-01	9.874E-02	-14037	-14026	-14037	-14026	-20.86	-16.57

PDC = <pdope><w><d>.<shrink distance/2> ; P+ = 10^(17+pdope) (h/ml); P+ width (um) = 2 x 2^(w/2); P+ depth (um) = 0.2 x 2.5^(d/2).

BI PNP-DJPD : IE QE & normalized QE dependence on P+ doping, well width, depth and outer n-well electrode (0.8 um) placement (0 or 2 um from the outer well edge ("shrink")); cont page 2 / 2.

well n-dope	substrate p-dope	rev. bias both junct	subst / well depth (um)																					
1.E+17	1.E+15	2 V	(12)/(2)	pd/w/d/sh	PSE Boundary		next to outer well		on outer well wall		Max	Max	PSE Boundary		next to outer well		on outer well wall		% below FI		% below FI		% below FI	
P+ dope	P+ width	P+ depth	shrink	PDC	QE @ 55	QE @ 105	QE @ 65	QE @ 95	QE @ 70	QE @ 90	QE@80	QE BI/FI	Nz @ 55	Nz @ 105	Nz @ 65	Nz @ 95	Nz @ 70	Nz @ 90	Nz@55	Nz@105	Nz@65	Nz@95	Nz@70	Nz@90
1.E+19	2	0.2	0	200	1.212E-07	1.217E-07	1.218E-07	1.218E-07	3.193E-06	2.846E-06	2.082E-03	6.881E-03	5.821E-05	5.845E-05	5.849E-05	5.850E-05	1.533E-03	1.367E-03	-14459	-14462	-14476	-14480	14.17	2.21
1.E+19	2	0.2	2	200.4	1.163E-07	1.163E-07	1.162E-07	1.162E-07	1.135E-06	9.205E-07	2.151E-03	7.098E-03	5.408E-05	5.407E-05	5.401E-05	5.401E-05	5.276E-04	4.279E-04	-14064	-14062	-14016	-14011	-36.65	-2.83
1.E+19	2	0.5	0	202	1.625E-07	1.625E-07	1.625E-07	1.625E-07	3.547E-06	3.327E-06	2.502E-03	7.452E-03	6.493E-05	6.493E-05	6.493E-05	6.493E-05	1.417E-03	1.329E-03	-13320	-13320	-13320	-13320	21.29	12.35
1.E+19	2	0.5	2	202.4	1.625E-07	1.625E-07	1.625E-07	1.625E-07	1.301E-06	1.131E-06	2.473E-03	7.351E-03	6.571E-05	6.571E-05	6.571E-05	6.571E-05	5.261E-04	4.574E-04	-13503	-13503	-13503	-13503	-22.79	-21.24
1.E+19	2	1.25	0	204	2.840E-07	2.840E-07	2.840E-07	2.840E-07	3.790E-06	3.702E-06	3.419E-03	8.688E-03	8.307E-05	8.307E-05	8.307E-05	8.307E-05	1.108E-03	1.083E-03	-11410	-11410	-11410	-11410	27.77	30.31
1.E+19	2	1.25	2	204.4	2.840E-07	2.840E-07	2.840E-07	2.840E-07	1.579E-06	1.511E-06	3.287E-03	8.346E-03	8.639E-05	8.639E-05	8.639E-05	8.639E-05	4.802E-04	4.596E-04	-11882	-11882	-11882	-11882	-26.47	-24.63
1.E+19	4	0.2	0	220	2.294E-07	2.294E-07	2.302E-07	2.306E-07	5.362E-06	4.752E-06	2.671E-03	6.805E-03	8.589E-05	8.589E-05	8.619E-05	8.633E-05	2.007E-03	1.779E-03	-14608	-14608	-14608	-14645	16.27	13.42
1.E+19	4	0.2	2	220.4	2.181E-07	2.182E-07	2.188E-07	2.184E-07	2.485E-06	2.049E-06	2.581E-03	6.552E-03	8.449E-05	8.456E-05	8.479E-05	8.464E-05	9.627E-04	7.939E-04	-15162	-15176	-15190	-15162	-46.16	-8.91
1.E+19	4	0.5	0	222	2.705E-07	2.710E-07	2.705E-07	2.705E-07	6.785E-06	5.013E-06	2.985E-03	7.065E-03	9.060E-05	9.080E-05	9.060E-05	9.060E-05	2.273E-03	1.679E-03	-14055	-14086	-14024	-14055	23.70	24.22
1.E+19	4	0.5	2	222.4	2.685E-07	2.679E-07	2.710E-07	2.705E-07	2.656E-06	2.765E-06	2.816E-03	6.622E-03	9.533E-05	9.512E-05	9.624E-05	9.603E-05	9.429E-04	9.819E-04	-14891	-14859	-15178	-14968	-32.67	-26.50
1.E+19	4	1.25	0	224	3.452E-07	3.452E-07	3.452E-07	3.452E-07	8.877E-06	8.076E-06	3.745E-03	8.095E-03	9.219E-05	9.219E-05	9.219E-05	9.219E-05	2.371E-03	2.157E-03	-12253	-12253	-12253	-12253	24.90	32.57
1.E+19	4	1.25	2	224.4	3.452E-07	3.452E-07	3.452E-07	3.452E-07	3.452E-06	3.291E-06	3.570E-03	7.695E-03	9.670E-05	9.670E-05	9.670E-05	9.670E-05	9.670E-04	9.219E-04	-12896	-12896	-12896	-12896	-28.28	-22.58
1.E+19	8	0.2	0	240	4.245E-07	4.245E-07	4.255E-07	4.257E-07	2.970E-05	2.689E-05	2.897E-03	7.113E-03	1.465E-04	1.465E-04	1.469E-04	1.470E-04	1.025E-02	9.282E-03	-13978	-13971	-13971	-13984	11.85	13.94
1.E+19	8	0.2	2	240.4	4.324E-07	4.322E-07	4.330E-07	4.330E-07	1.126E-05	9.495E-06	2.891E-03	7.102E-03	1.496E-04	1.495E-04	1.498E-04	1.498E-04	3.895E-03	3.284E-03	-13993	-13980	-13993	-13993	-23.89	-5.45
1.E+19	8	0.5	0	242	4.654E-07	4.654E-07	4.652E-07	4.654E-07	3.180E-05	3.346E-05	3.189E-03	7.417E-03	1.459E-04	1.459E-04	1.458E-04	1.459E-04	9.969E-03	1.049E-02	-13389	-13383	-13377	-13377	20.60	15.08
1.E+19	8	0.5	2	242.4	4.347E-07	4.349E-07	4.347E-07	4.347E-07	1.261E-05	1.186E-05	3.374E-03	7.657E-03	1.289E-04	1.289E-04	1.289E-04	1.289E-04	3.736E-03	3.515E-03	-12954	-12960	-12948	-12960	-8.34	-4.97
1.E+19	8	1.25	0	244	5.619E-07	5.619E-07	5.615E-07	5.619E-07	3.755E-05	3.594E-05	4.084E-03	9.009E-03	1.376E-04	1.376E-04	1.375E-04	1.376E-04	9.193E-03	8.799E-03	-11008	-11000	-10993	-11000	35.81	36.71
1.E+19	8	1.25	2	244.4	5.649E-07	5.615E-07	5.615E-07	5.615E-07	1.408E-05	1.411E-05	4.053E-03	8.909E-03	1.394E-04	1.385E-04	1.385E-04	1.385E-04	3.475E-03	3.482E-03	-11156	-11137	-11125	-11059	-2.35	0.03
1.E+19	14	0.2	0	260	7.107E-07	7.103E-07	7.117E-07	7.117E-07	3.213E-04	2.975E-04	2.901E-03	7.085E-03	2.450E-04	2.449E-04	2.453E-04	2.453E-04	1.108E-01	1.026E-01	-14029	-14021	-14025	-14029	9.68	13.09
1.E+19	14	0.2	2	260.4	7.238E-07	7.242E-07	7.246E-07	7.246E-07	1.840E-04	1.386E-04	2.528E-03	6.016E-03	2.863E-04	2.865E-04	2.866E-04	2.866E-04	7.278E-02	5.482E-02	-16527	-16541	-16532	-16541	-37.17	-5.74
1.E+19	14	0.5	0	262	7.584E-07	7.584E-07	7.582E-07	7.580E-07	3.527E-04	3.698E-04	3.246E-03	7.505E-03	2.336E-04	2.336E-04	2.336E-04	2.335E-04	1.086E-01	1.139E-01	-13225	-13229	-13218	-13222	20.84	13.04
1.E+19	14	0.5	2	262.4	7.955E-07	7.959E-07	7.957E-07	7.959E-07	2.232E-04	2.045E-04	2.756E-03	6.110E-03	2.887E-04	2.888E-04	2.887E-04	2.888E-04	8.098E-02	7.422E-02	-16255	-16251	-16251	-16268	-22.03	-20.53
1.E+19	14	1.25	0	264	8.575E-07	8.575E-07	8.575E-07	8.579E-07	3.937E-04	4.345E-04	4.053E-03	8.932E-03	2.116E-04	2.116E-04	2.116E-04	2.117E-04	9.714E-02	1.072E-01	-11091	-11096	-11096	-11096	40.60	32.44
1.E+19	14	1.25	2	264.4	9.384E-07	9.340E-07	9.384E-07	9.387E-07	3.684E-04	3.450E-04	3.425E-03	7.108E-03	2.740E-04	2.727E-04	2.740E-04	2.741E-04	1.076E-01	1.007E-01	-14025	-13904	-13998	-13975	-26.11	-16.72

PDC = <pdope><w><d>.<shrink distance/2> ; P+ = 10^(17+pdope) (h/ml); P+ width (um) = 2 x 2^(w/2); P+ depth (um) = 0.2 x 2.5^(d/2).

FI PNP-DJPD : Image electrode (IE) QE & normalized QE dependence on P+ doping, well width, depth and outer n-well electrode (0.8 um) placement (0 or 2 um from the outer well edge ("shrink")).

well n-dope	substrate p-dope	rev. bias both junct	subst / well depth (um)		PSE Boundary		next to outer well		on outer well wall		Max	Max	PSE Boundary		next to outer well		on outer well wall		% below BI		% below BI		% below BI	
1.E+17	1.E+15	2 V	(12)/(2)	pd/w/d/sh	QE @ 55	QE @ 105	QE @ 65	QE @ 95	QE @ 70	QE @ 90	QE@80	QE Bi/Fl	Nz @ 55	Nz @ 105	Nz @ 65	Nz @ 95	Nz @ 70	Nz @ 90	Nz@55	Nz@105	Nz@65	Nz@95	Nz@70	Nz@90
P+ dope	P+ width	P+ depth	shrink	PDC																				
1.E+18	2	0.2	0	100	1.203E-08	1.294E-08	1.143E-08	1.154E-08	5.499E-04	4.149E-04	3.007E-01	7.128E-03	4.000E-08	4.304E-08	3.803E-08	3.837E-08	1.829E-03	1.380E-03	99.27	99.22	99.29	99.29	-32.53	-10.07
1.E+18	2	0.2	2	100.4	1.111E-08	1.241E-08	1.270E-08	1.116E-08	1.141E-04	1.236E-04	3.007E-01	7.043E-03	3.695E-08	4.126E-08	4.223E-08	3.711E-08	3.796E-04	4.112E-04	99.29	99.26	99.26	99.37	17.76	-8.47
1.E+18	2	0.5	0	102	2.285E-08	2.285E-08	2.314E-08	2.314E-08	5.935E-04	5.015E-04	3.339E-01	7.337E-03	6.843E-08	6.843E-08	6.931E-08	6.931E-08	1.778E-03	1.502E-03	99.27	99.27	99.27	99.28	-30.28	-17.31
1.E+18	2	0.5	2	102.4	2.310E-08	2.310E-08	2.328E-08	2.328E-08	1.414E-04	1.248E-04	3.339E-01	7.501E-03	6.919E-08	6.919E-08	6.972E-08	6.972E-08	4.235E-04	3.738E-04	99.25	99.25	99.25	99.25	6.92	3.69
1.E+18	2	1.25	0	104	5.711E-08	5.711E-08	5.713E-08	5.715E-08	5.969E-04	6.047E-04	3.927E-01	8.171E-03	1.454E-07	1.454E-07	1.455E-07	1.455E-07	1.520E-03	1.540E-03	99.18	99.18	99.18	99.18	-37.97	-45.43
1.E+18	2	1.25	2	104.4	5.706E-08	5.706E-08	5.707E-08	5.707E-08	1.477E-04	1.435E-04	3.929E-01	8.257E-03	1.452E-07	1.452E-07	1.453E-07	1.453E-07	3.758E-04	3.653E-04	99.17	99.17	99.17	99.17	8.57	6.89
1.E+18	4	0.2	0	120	2.771E-08	2.599E-08	2.705E-08	2.673E-08	9.189E-04	7.908E-04	3.916E-01	6.787E-03	7.078E-08	6.637E-08	6.907E-08	6.827E-08	2.347E-03	2.020E-03	99.29	99.34	99.30	99.31	-20.18	-21.86
1.E+18	4	0.2	2	120.4	2.355E-08	2.247E-08	2.351E-08	2.171E-08	2.536E-04	2.809E-04	3.929E-01	6.533E-03	5.994E-08	5.719E-08	5.984E-08	5.524E-08	6.454E-04	7.148E-04	99.33	99.33	99.36	99.38	26.28	-1.38
1.E+18	4	0.5	0	122	3.666E-08	3.666E-08	3.698E-08	3.698E-08	1.181E-03	9.221E-04	4.224E-01	7.045E-03	8.680E-08	8.680E-08	8.755E-08	8.755E-08	2.795E-03	2.183E-03	99.30	99.30	99.30	99.30	-25.11	-37.96
1.E+18	4	0.5	2	122.4	3.629E-08	3.629E-08	3.649E-08	3.649E-08	2.970E-04	3.246E-04	4.251E-01	6.602E-03	8.536E-08	8.536E-08	8.583E-08	8.583E-08	6.985E-04	7.636E-04	99.34	99.34	99.33	99.34	17.85	14.09
1.E+18	4	1.25	0	124	4.500E-08	4.500E-08	4.526E-08	4.500E-08	1.448E-03	1.468E-03	4.634E-01	7.997E-03	9.712E-08	9.712E-08	9.767E-08	9.712E-08	3.126E-03	3.167E-03	99.20	99.20	99.20	99.20	-36.07	-52.16
1.E+18	4	1.25	2	124.4	4.553E-08	4.553E-08	4.553E-08	4.553E-08	3.464E-04	3.458E-04	4.648E-01	7.669E-03	9.797E-08	9.797E-08	9.797E-08	9.797E-08	7.454E-04	7.441E-04	99.23	99.23	99.23	99.23	12.95	10.57
1.E+18	8	0.2	0	140	4.447E-08	4.288E-08	4.198E-08	4.330E-08	4.661E-03	4.324E-03	4.082E-01	7.096E-03	1.089E-07	1.050E-07	1.028E-07	1.061E-07	1.142E-02	1.059E-02	99.28	99.28	99.30	99.27	-14.26	-17.54
1.E+18	8	0.2	2	140.4	4.290E-08	4.502E-08	4.343E-08	4.345E-08	1.259E-03	1.248E-03	4.080E-01	7.085E-03	1.051E-07	1.103E-07	1.064E-07	1.065E-07	3.085E-03	3.058E-03	99.30	99.27	99.29	99.31	17.85	1.47
1.E+18	8	0.5	0	142	5.680E-08	5.576E-08	5.625E-08	5.629E-08	5.566E-03	5.223E-03	4.316E-01	7.394E-03	1.316E-07	1.292E-07	1.303E-07	1.304E-07	1.290E-02	1.210E-02	99.25	99.26	99.25	99.25	-30.82	-17.68
1.E+18	8	0.5	2	142.4	5.215E-08	5.213E-08	5.187E-08	5.185E-08	1.494E-03	1.449E-03	4.328E-01	7.506E-03	1.205E-07	1.205E-07	1.199E-07	1.198E-07	3.452E-03	3.349E-03	99.24	99.24	99.24	99.24	6.51	3.56
1.E+18	8	1.25	0	144	7.370E-08	7.370E-08	7.380E-08	7.370E-08	6.420E-03	6.434E-03	4.551E-01	8.982E-03	1.619E-07	1.619E-07	1.621E-07	1.619E-07	1.411E-02	1.414E-02	99.10	99.10	99.10	99.10	-57.96	-62.76
1.E+18	8	1.25	2	144.4	7.380E-08	7.380E-08	7.370E-08	7.380E-08	1.531E-03	1.567E-03	4.565E-01	8.887E-03	1.617E-07	1.617E-07	1.614E-07	1.617E-07	3.353E-03	3.432E-03	99.11	99.11	99.11	99.11	-0.25	-2.71
1.E+18	14	0.2	0	160	6.991E-08	7.060E-08	7.117E-08	7.117E-08	4.891E-02	4.752E-02	4.104E-01	7.068E-03	1.703E-07	1.720E-07	1.734E-07	1.734E-07	1.192E-01	1.158E-01	99.29	99.27	99.25	99.28	-10.64	-15.00
1.E+18	14	0.2	2	160.4	7.590E-08	7.782E-08	7.743E-08	7.543E-08	2.128E-02	2.104E-02	4.204E-01	5.976E-03	1.805E-07	1.851E-07	1.842E-07	1.794E-07	5.061E-02	5.005E-02	99.40	99.40	99.38	99.41	28.12	5.66
1.E+18	14	0.5	0	162	8.487E-08	8.483E-08	8.547E-08	8.536E-08	5.821E-02	5.566E-02	4.341E-01	7.482E-03	1.955E-07	1.954E-07	1.969E-07	1.966E-07	1.341E-01	1.282E-01	99.25	99.25	99.25	99.25	-26.02	-14.76
1.E+18	14	0.5	2	162.4	1.012E-07	1.012E-07	1.017E-07	1.017E-07	2.875E-02	2.710E-02	4.526E-01	6.123E-03	2.236E-07	2.236E-07	2.248E-07	2.248E-07	6.353E-02	5.989E-02	99.39	99.39	99.39	99.39	18.75	16.19
1.E+18	14	1.25	0	164	9.921E-08	9.933E-08	9.933E-08	9.921E-08	7.358E-02	7.111E-02	4.553E-01	8.909E-03	2.179E-07	2.181E-07	2.181E-07	2.179E-07	1.616E-01	1.562E-01	99.11	99.11	99.11	99.11	-68.44	-48.14
1.E+18	14	1.25	2	164.4	1.463E-07	1.463E-07	1.463E-07	1.463E-07	4.118E-02	4.098E-02	4.838E-01	7.079E-03	3.024E-07	3.024E-07	3.024E-07	3.024E-07	8.511E-02	8.471E-02	99.29	99.29	99.29	99.29	17.26	14.21

PDC = <pdope><w><d>.<shrink distance/2> ; P+ = 10^(17+pdope) (h/ml); P+ width (um) = 2 x 2^(w/2); P+ depth (um) = 0.2 x 2.5^(d/2).

FI PNP-DJPD : IE QE & normalized QE dependence on P+ doping, well width, depth and outer n-well electrode (0.8 um) placement (0 or 2 um from the outer well edge ("shrink")); cont page 2 / 2.

well n-dope	substrate p-dope	rev. bias both junct	subst / well depth (um)																					
1.E+17	1.E+15	2 V	(12)/(2)	pd/w/d/sh	PSE Boundary		next to outer well		on outer well wall		Max	Max	PSE Boundary		next to outer well		on outer well wall		% below BI		% below BI		% below BI	
P+ dope	P+ width	P+ depth	shrink	PDC	QE @ 55	QE @ 105	QE @ 65	QE @ 95	QE @ 70	QE @ 90	QE@80	QE BI/FI	Nz @ 55	Nz @ 105	Nz @ 65	Nz @ 95	Nz @ 70	Nz @ 90	Nz@55	Nz@105	Nz@65	Nz@95	Nz@70	Nz@90
1.E+19	2	0.2	0	200	1.210E-07	1.215E-07	1.215E-07	1.214E-07	5.407E-04	4.230E-04	3.026E-01	6.881E-03	3.998E-07	4.014E-07	4.013E-07	4.012E-07	1.787E-03	1.398E-03	99.31	99.31	99.31	99.31	-16.51	-2.26
1.E+19	2	0.2	2	200.4	1.157E-07	1.157E-07	1.160E-07	1.160E-07	1.170E-04	1.261E-04	3.030E-01	7.098E-03	3.818E-07	3.818E-07	3.826E-07	3.828E-07	3.861E-04	4.161E-04	99.29	99.29	99.29	99.29	26.82	2.76
1.E+19	2	0.5	0	202	1.625E-07	1.625E-07	1.625E-07	1.625E-07	6.047E-04	5.093E-04	3.358E-01	7.452E-03	4.839E-07	4.839E-07	4.839E-07	4.839E-07	1.801E-03	1.517E-03	99.25	99.25	99.25	99.25	-27.06	-14.08
1.E+19	2	0.5	2	202.4	1.625E-07	1.625E-07	1.625E-07	1.625E-07	1.441E-04	1.269E-04	3.364E-01	7.351E-03	4.831E-07	4.831E-07	4.831E-07	4.831E-07	4.285E-04	3.772E-04	99.26	99.26	99.26	99.26	18.56	17.52
1.E+19	2	1.25	0	204	2.840E-07	2.840E-07	2.840E-07	2.840E-07	6.039E-04	6.114E-04	3.935E-01	8.688E-03	7.217E-07	7.217E-07	7.217E-07	7.217E-07	1.535E-03	1.554E-03	99.13	99.13	99.13	99.13	-38.45	-43.50
1.E+19	2	1.25	2	204.4	2.840E-07	2.840E-07	2.840E-07	2.840E-07	1.496E-04	1.453E-04	3.939E-01	8.346E-03	7.210E-07	7.210E-07	7.210E-07	7.210E-07	3.797E-04	3.688E-04	99.17	99.17	99.17	99.17	20.93	19.76
1.E+19	4	0.2	0	220	2.292E-07	2.292E-07	2.300E-07	2.298E-07	9.411E-04	8.065E-04	3.925E-01	6.805E-03	5.840E-07	5.840E-07	5.860E-07	5.855E-07	2.398E-03	2.055E-03	99.32	99.32	99.32	99.32	-19.44	-15.50
1.E+19	4	0.2	2	220.4	2.181E-07	2.181E-07	2.184E-07	2.184E-07	2.595E-04	2.871E-04	3.939E-01	6.552E-03	5.536E-07	5.536E-07	5.546E-07	5.546E-07	6.587E-04	7.289E-04	99.34	99.35	99.35	99.34	31.58	8.18
1.E+19	4	0.5	0	222	2.705E-07	2.705E-07	2.710E-07	2.705E-07	1.259E-03	9.364E-04	4.226E-01	7.065E-03	6.400E-07	6.400E-07	6.414E-07	6.400E-07	2.979E-03	2.216E-03	99.29	99.30	99.29	99.29	-31.05	-31.97
1.E+19	4	0.5	2	222.4	2.705E-07	2.705E-07	2.679E-07	2.710E-07	3.023E-04	3.301E-04	4.253E-01	6.622E-03	6.359E-07	6.359E-07	6.299E-07	6.373E-07	7.107E-04	7.762E-04	99.33	99.33	99.35	99.34	24.63	20.95
1.E+19	4	1.25	0	224	3.452E-07	3.452E-07	3.452E-07	3.452E-07	1.460E-03	1.480E-03	4.626E-01	8.095E-03	7.463E-07	7.463E-07	7.463E-07	7.463E-07	3.157E-03	3.199E-03	99.19	99.19	99.19	99.19	-33.16	-48.31
1.E+19	4	1.25	2	224.4	3.452E-07	3.452E-07	3.452E-07	3.452E-07	3.497E-04	3.490E-04	4.640E-01	7.695E-03	7.441E-07	7.441E-07	7.441E-07	7.441E-07	7.538E-04	7.521E-04	99.23	99.23	99.23	99.23	22.05	18.42
1.E+19	8	0.2	0	240	4.239E-07	4.241E-07	4.251E-07	4.249E-07	4.736E-03	4.392E-03	4.073E-01	7.113E-03	1.041E-06	1.041E-06	1.044E-06	1.043E-06	1.163E-02	1.079E-02	99.29	99.29	99.29	99.29	-13.45	-16.20
1.E+19	8	0.2	2	240.4	4.320E-07	4.322E-07	4.326E-07	4.326E-07	1.280E-03	1.268E-03	4.071E-01	7.102E-03	1.061E-06	1.062E-06	1.063E-06	1.063E-06	3.144E-03	3.115E-03	99.29	99.29	99.29	99.29	19.28	5.17
1.E+19	8	0.5	0	242	4.652E-07	4.654E-07	4.654E-07	4.655E-07	5.399E-03	5.313E-03	4.300E-01	7.417E-03	1.082E-06	1.082E-06	1.082E-06	1.083E-06	1.256E-02	1.236E-02	99.26	99.26	99.26	99.26	-25.95	-17.75
1.E+19	8	0.5	2	242.4	4.349E-07	4.349E-07	4.351E-07	4.347E-07	1.520E-03	1.475E-03	4.406E-01	7.657E-03	9.871E-07	9.871E-07	9.875E-07	9.866E-07	3.449E-03	3.348E-03	99.23	99.23	99.23	99.23	7.69	4.74
1.E+19	8	1.25	0	244	5.615E-07	5.619E-07	5.619E-07	5.619E-07	6.493E-03	6.508E-03	4.534E-01	9.009E-03	1.239E-06	1.239E-06	1.239E-06	1.239E-06	1.432E-02	1.435E-02	99.10	99.10	99.10	99.10	-55.78	-63.15
1.E+19	8	1.25	2	244.4	5.633E-07	5.609E-07	5.615E-07	5.649E-07	1.545E-03	1.584E-03	4.549E-01	8.909E-03	1.238E-06	1.233E-06	1.234E-06	1.242E-06	3.395E-03	3.483E-03	99.11	99.11	99.11	99.10	2.30	-0.03
1.E+19	14	0.2	0	260	7.099E-07	7.099E-07	7.111E-07	7.109E-07	5.021E-02	4.832E-02	4.094E-01	7.085E-03	1.734E-06	1.734E-06	1.737E-06	1.736E-06	1.226E-01	1.180E-01	99.29	99.29	99.29	99.29	-10.72	-15.07
1.E+19	14	0.2	2	260.4	7.236E-07	7.234E-07	7.242E-07	7.238E-07	2.230E-02	2.179E-02	4.202E-01	6.016E-03	1.722E-06	1.722E-06	1.723E-06	1.723E-06	5.306E-02	5.184E-02	99.40	99.40	99.40	99.40	27.10	5.43
1.E+19	14	0.5	0	262	7.584E-07	7.582E-07	7.586E-07	7.582E-07	5.937E-02	5.666E-02	4.326E-01	7.505E-03	1.753E-06	1.753E-06	1.754E-06	1.753E-06	1.373E-01	1.310E-01	99.25	99.25	99.25	99.25	-26.33	-15.00
1.E+19	14	0.5	2	262.4	7.961E-07	7.967E-07	7.965E-07	7.959E-07	2.993E-02	2.777E-02	4.510E-01	6.110E-03	1.765E-06	1.766E-06	1.766E-06	1.765E-06	6.636E-02	6.158E-02	99.39	99.39	99.39	99.39	18.05	17.03
1.E+19	14	1.25	0	264	8.579E-07	8.575E-07	8.575E-07	8.579E-07	7.421E-02	7.201E-02	4.538E-01	8.932E-03	1.891E-06	1.890E-06	1.890E-06	1.891E-06	1.635E-01	1.587E-01	99.11	99.11	99.11	99.11	-68.35	-48.01
1.E+19	14	1.25	2	264.4	9.346E-07	9.384E-07	9.364E-07	9.384E-07	4.110E-02	4.159E-02	4.818E-01	7.108E-03	1.940E-06	1.947E-06	1.943E-06	1.947E-06	8.530E-02	8.631E-02	99.29	99.29	99.29	99.29	20.70	14.32

PDC = <pdope><w><d>.<shrink distance/2> ; P+ = 10^(17+pdope) (h/ml); P+ width (um) = 2 x 2^(w/2); P+ depth (um) = 0.2 x 2.5^(d/2).

BI NPN DJPD ; Image cathode QE & NQE dependence on N+ doping, N+ well width, N+ well depth and outer p-well anode (0.8 um) placement (0 um from the outer well edge).

Maximum and minimum values for each of the 3 doping regimes are shaded and outlined respectively.

outer well p-dope	substrate n-dope	rev. bias both junct	subst / outer well depth: (12)/(2) um																							
1.E+17	1.E+15	2 V		pixel boundary		next to outer well		on outer well wall		next to well centre		Max	Max QE	Pixel Boundary		on outer well wall		inside outer well		% BI NQE below FI		% BI NQE below FI		% BI NQE below FI	
N+ dope	N+ width	N+ depth	PDC	QE 55	QE 105	QE 65	QE 95	QE 70	QE 90	QE 75	QE 85	QE 80	BI/FI	NQE 55	NQE 105	NQE 70	NQE 90	NQE 75	NQE 85	at 55	at 105	at 70	at 90	at 75	at 85
1.E+18	2	0.2	100	5.67E-09	5.46E-09	6.66E-09	7.16E-09	3.06E-06	2.48E-06	2.13E-04	2.38E-04	2.12E-03		2.67E-06	2.58E-06	1.44E-03	1.17E-03	1.00E-01	1.12E-01	-15301	-12014	18.33	16.33	17.59	-2.26
1.E+18	2	0.5	102	1.35E-08	1.36E-08	1.30E-08	1.33E-08	3.25E-06	3.24E-06	3.01E-04	2.70E-04	2.40E-03		5.60E-06	5.68E-06	1.35E-03	1.35E-03	1.25E-01	1.13E-01	-14139	-13609	24.66	11.43	0.41	1.34
1.E+18	2	1.25	104	3.71E-08	3.70E-08	3.73E-08	3.72E-08	3.50E-06	3.62E-06	3.06E-04	3.57E-04	3.35E-03		1.11E-05	1.10E-05	1.04E-03	1.08E-03	9.13E-02	1.06E-01	-11559	-11541	31.39	31.34	26.53	12.54
1.E+18	4	0.2	120	1.50E-08	1.46E-08	1.45E-08	1.26E-08	5.38E-06	4.12E-06	4.61E-04	4.83E-04	2.66E-03		5.67E-06	5.48E-06	2.03E-03	1.55E-03	1.74E-01	1.82E-01	-15611	-16351	14.02	23.86	6.14	-1.19
1.E+18	4	0.5	122	2.13E-08	2.12E-08	2.06E-08	2.13E-08	6.80E-06	4.91E-06	6.19E-04	5.34E-04	2.95E-03		7.22E-06	7.17E-06	2.30E-03	1.66E-03	2.10E-01	1.81E-01	-14723	-14620	21.73	24.44	12.91	8.18
1.E+18	4	1.25	124	2.49E-08	2.49E-08	2.49E-08	2.49E-08	8.49E-06	8.04E-06	7.07E-04	7.73E-04	3.87E-03		6.43E-06	6.43E-06	2.19E-03	2.08E-03	1.83E-01	2.00E-01	-11883	-11883	28.14	38.99	21.09	18.16
1.E+18	8	0.2	140	2.47E-08	2.19E-08	2.02E-08	2.07E-08	2.78E-05	2.55E-05	1.38E-03	1.51E-03	2.93E-03		8.43E-06	7.50E-06	9.49E-03	8.71E-03	4.71E-01	5.15E-01	-16502	-14233	17.05	17.72	12.04	3.98
1.E+18	8	0.5	142	3.05E-08	2.98E-08	3.06E-08	3.06E-08	3.80E-05	3.34E-05	1.66E-03	1.74E-03	3.22E-03		9.45E-06	9.25E-06	1.18E-02	1.04E-02	5.16E-01	5.41E-01	-13237	-12737	5.17	14.34	12.31	7.19
1.E+18	8	1.25	144	4.15E-08	4.14E-08	4.15E-08	4.17E-08	3.52E-05	3.78E-05	2.16E-03	2.39E-03	4.06E-03		1.02E-05	1.02E-05	8.67E-03	9.30E-03	5.31E-01	5.89E-01	-11175	-11136	37.90	33.15	21.73	12.44
1.E+18	14	0.2	160	3.13E-08	3.42E-08	3.50E-08	3.30E-08	2.96E-04	2.55E-04	2.80E-03	2.82E-03	2.90E-03		1.08E-05	1.18E-05	1.02E-01	8.77E-02	9.64E-01	9.72E-01	-12619	-13918	15.41	24.33	3.51	2.73
1.E+18	14	0.5	162	4.65E-08	4.71E-08	4.61E-08	4.60E-08	3.90E-04	3.62E-04	2.85E-03	3.30E-03	3.25E-03		1.43E-05	1.45E-05	1.20E-01	1.11E-01	8.64E-01	1	-13229	-13833	9.46	13.09	13.65	-0.08
1.E+18	14	1.25	164	5.37E-08	5.37E-08	5.40E-08	5.32E-08	4.07E-04	4.36E-04	3.86E-03	4.44E-03	4.03E-03		1.33E-05	1.33E-05	1.01E-01	1.08E-01	8.70E-01	1	-11220	-11251	37.25	30.13	13.05	-0.10
1.E+19	2	0.2	200	2.34E-07	2.33E-07	2.33E-07	2.33E-07	2.91E-06	2.29E-06	2.18E-04	2.43E-04	2.15E-03		1.09E-04	1.09E-04	1.35E-03	1.07E-03	1.02E-01	1.13E-01	-13881	-13810	24.72	24.30	17.89	-1.90
1.E+19	2	0.5	202	3.69E-07	3.69E-07	3.69E-07	3.69E-07	2.93E-06	2.91E-06	3.06E-04	2.75E-04	2.43E-03		1.52E-04	1.52E-04	1.21E-03	1.20E-03	1.26E-01	1.13E-01	-13699	-13699	33.53	21.92	0.84	1.78
1.E+19	2	1.25	204	7.57E-07	7.57E-07	7.57E-07	7.57E-07	2.75E-06	2.87E-06	3.09E-04	3.60E-04	3.37E-03		2.24E-04	2.24E-04	8.14E-04	8.51E-04	9.16E-02	1.07E-01	-11559	-11563	46.88	46.33	26.95	13.01
1.E+19	4	0.2	220	4.63E-07	4.63E-07	4.63E-07	4.64E-07	5.05E-06	3.74E-06	4.72E-04	4.93E-04	2.67E-03		1.73E-04	1.73E-04	1.89E-03	1.40E-03	1.77E-01	1.85E-01	-14546	-14547	21.54	32.56	6.48	-0.84
1.E+19	4	0.5	222	5.90E-07	5.90E-07	5.90E-07	5.90E-07	6.32E-06	4.38E-06	6.31E-04	5.42E-04	2.96E-03		1.99E-04	1.99E-04	2.13E-03	1.48E-03	2.13E-01	1.83E-01	-14155	-14155	28.82	33.83	13.20	8.50
1.E+19	4	1.25	224	7.25E-07	7.25E-07	7.25E-07	7.25E-07	7.82E-06	7.38E-06	7.13E-04	7.82E-04	3.88E-03		1.87E-04	1.87E-04	2.02E-03	1.90E-03	1.84E-01	2.02E-01	-11848	-11848	34.58	44.75	21.33	18.39
1.E+19	8	0.2	240	8.09E-07	8.07E-07	8.08E-07	8.11E-07	2.74E-05	2.51E-05	1.39E-03	1.52E-03	2.93E-03		2.76E-04	2.76E-04	9.37E-03	8.58E-03	4.76E-01	5.20E-01	-13695	-13641	19.68	20.54	12.24	4.21
1.E+19	8	0.5	242	9.52E-07	9.52E-07	9.52E-07	9.52E-07	3.75E-05	3.31E-05	1.68E-03	1.76E-03	3.22E-03		2.96E-04	2.96E-04	1.16E-02	1.03E-02	5.21E-01	5.47E-01	-13262	-13260	7.80	17.00	12.42	7.37
1.E+19	8	1.25	244	1.20E-06	1.20E-06	1.20E-06	1.20E-06	3.45E-05	3.71E-05	2.18E-03	2.41E-03	4.06E-03		2.95E-04	2.95E-04	8.49E-03	9.13E-03	5.36E-01	5.94E-01	-11104	-11104	40.19	35.46	21.77	12.51
1.E+19	14	0.2	260	1.34E-06	1.34E-06	1.34E-06	1.35E-06	3.04E-04	2.58E-04	2.82E-03	2.83E-03	2.90E-03		4.61E-04	4.63E-04	1.05E-01	8.88E-02	9.69E-01	9.76E-01	-13947	-14026	16.04	24.93	3.05	2.27
1.E+19	14	0.5	262	1.52E-06	1.52E-06	1.52E-06	1.52E-06	3.98E-04	3.66E-04	2.86E-03	3.31E-03	3.24E-03		4.70E-04	4.70E-04	1.23E-01	1.13E-01	8.64E-01	1	-13249	-13247	9.96	13.64	13.59	-0.13
1.E+19	14	1.25	264	1.73E-06	1.73E-06	1.73E-06	1.73E-06	4.09E-04	4.41E-04	3.88E-03	4.46E-03	4.03E-03		4.31E-04	4.31E-04	1.02E-01	1.10E-01	8.69E-01	1	-11201	-11198	37.58	30.42	13.08	-0.06
1.E+20	2	0.2	300	6.71E-07	6.71E-07	6.70E-07	6.70E-07	2.48E-06	1.86E-06	2.19E-04	2.43E-04	2.15E-03		3.12E-04	3.12E-04	1.15E-03	8.67E-04	1.02E-01	1.13E-01	-13936	-13936	36.22	38.83	18.17	-1.56
1.E+20	2	0.5	302	9.53E-07	9.55E-07	9.53E-07	9.55E-07	2.36E-06	2.33E-06	3.07E-04	2.75E-04	2.43E-03		3.92E-04	3.93E-04	9.71E-04	9.60E-04	1.26E-01	1.13E-01	-13656	-13680	46.73	37.63	1.16	2.12
1.E+20	2	1.25	304	1.75E-06	1.75E-06	1.75E-06	1.75E-06	1.76E-06	1.89E-06	3.09E-04	3.60E-04	3.37E-03		5.19E-04	5.19E-04	5.23E-04	5.59E-04	9.16E-02	1.07E-01	-11550	-11550	65.95	64.83	27.26	13.34
1.E+20	4	0.2	320	1.26E-06	1.26E-06	1.26E-06	1.26E-06	4.27E-06	2.96E-06	4.74E-04	4.95E-04	2.67E-03		4.73E-04	4.73E-04	1.60E-03	1.11E-03	1.78E-01	1.85E-01	-14566	-14570	34.07	46.97	6.75	-0.56
1.E+20	4	0.5	322	1.54E-06	1.54E-06	1.54E-06	1.54E-06	5.39E-06	3.44E-06	6.33E-04	5.43E-04	2.96E-03		5.20E-04	5.20E-04	1.82E-03	1.16E-03	2.14E-01	1.84E-01	-14037	-14136	39.55	48.23	13.43	8.77
1.E+20	4	1.25	324	1.91E-06	1.91E-06	1.91E-06	1.91E-06	6.64E-06	6.21E-06	7.13E-04	7.83E-04	3.87E-03		4.94E-04	4.94E-04	1.72E-03	1.61E-03	1.84E-01	2.02E-01	-11838	-11838	44.49	53.59	21.51	18.57
1.E+20	8	0.2	340	2.27E-06	2.27E-06	2.26E-06	2.26E-06	2.61E-05	2.37E-05	1.39E-03	1.52E-03	2.92E-03		7.76E-04	7.76E-04	8.94E-03	8.13E-03	4.78E-01	5.22E-01	-13805	-13811	24.00	25.23	12.43	4.42
1.E+20	8	0.5	342	2.58E-06	2.57E-06	2.58E-06	2.57E-06	3.59E-05	3.16E-05	1.68E-03	1.76E-03	3.21E-03		8.03E-04	8.00E-04	1.12E-02	9.84E-03	5.23E-01	5.49E-01	-13295	-13200	11.85	21.10	12.58	7.54
1.E+20	8	1.25	344	3.12E-06	3.12E-06	3.12E-06	3.12E-06	3.26E-05	3.52E-05	2.18E-03	2.41E-03	4.05E-03		7.71E-04	7.70E-04	8.06E-03	8.71E-03	5.38E-01	5.96E-01	-11099	-11118	43.53	38.82	21.84	12.60
1.E+20	14	0.2	360	3.86E-06	3.86E-06	3.85E-06	3.85E-06	3.03E-04	2.56E-04	2.82E-03	2.83E-03	2.90E-03		1.33E-03	1.33E-03	1.05E-01	8.85E-02	9.72E-01	9.79E-01	-14113	-13984	16.81	25.73	2.77	1.98
1.E+20	14	0.5	362	4.20E-06	4.19E-06	4.20E-06	4.20E-06	3.97E-04	3.65E-04	2.86E-03	3.31E-03	3.23E-03		1.30E-03	1.30E-03	1.23E-01	1.13E-01	8.64E-01	1	-13268	-13234	10.61	14.33	13.59	-0.14
1.E+20	14	1.25	364	4.63E-06	4.63E-06	4.64E-06	4.63E-06	4.07E-04	4.40E-04	3.88E-03	4.46E-03	4.01E-03		1.16E-03	1.15E-03	1.02E-01	1.10E-01	8.69E-01	1	-11176	-11167	38.03	30.87	13.09	-0.06

PDC = <pdope><w><d>.<shrink distance/2> ; P+ = 10^(17+pdope) (h/ml); P+ width (um) = 2 x 2^(w/2); P+ depth (um) = 0.2 x 2.5^(d/2).

BI NPN DJPD : Image cathode QE & nQE (electron current QE) dependence on N+ doping, N+ well width, N+ well depth and outer p-well anode (0.8 um) placement (0 um from the outer well edge).

(NB/ QE can only be positive : negative nQE & QE serve to indicate the nQE & QE were calculated from negative electron and total currents).

Maximum and minimum values for each of the 3 doping regimes are shaded and outlined respectively.

outer well	substrate	rev. bias	subst / outer well depth:																	
p-dope	n-dope	both junct	(12)/(2) um																	
1.E+17	1.E+15	2 V		pixel boundary			next to outer well			on outer well wall			next to well centre			Expected Max QE		Maximum QE	
N+ dope	N+ width	N+ depth	PDC	QE @ 55	nQE @ 55	QE @ 105	QE @ 65	nQE @ 65	QE @ 95	QE @ 70	nQE @ 70	QE @ 90	QE @ 75	nQE @ 75	QE @ 85	QE @ 80	nQE @ 80	Max QE	BI / FI
1.E+18	2	0.2	100	5.671E-09	5.649E-09	5.463E-09	6.663E-09	6.641E-09	7.161E-09	3.063E-06	3.063E-06	2.478E-06	2.127E-04	2.127E-04	2.381E-04	2.120E-03	2.136E-03	2.120E-03	7.094E-03
1.E+18	2	0.5	102	1.347E-08	1.346E-08	1.365E-08	1.296E-08	1.295E-08	1.325E-08	3.247E-06	3.247E-06	3.236E-06	3.007E-04	3.007E-04	2.705E-04	2.403E-03	2.463E-03	2.403E-03	7.224E-03
1.E+18	2	1.25	104	3.710E-08	3.710E-08	3.704E-08	3.727E-08	3.726E-08	3.725E-08	3.498E-06	3.498E-06	3.623E-06	3.059E-04	3.059E-04	3.567E-04	3.352E-03	3.566E-03	3.352E-03	8.544E-03
1.E+18	4	0.2	120	1.505E-08	1.502E-08	1.455E-08	1.447E-08	1.444E-08	1.256E-08	5.385E-06	5.385E-06	4.124E-06	4.607E-04	4.607E-04	4.834E-04	2.655E-03	2.671E-03	2.655E-03	6.792E-03
1.E+18	4	0.5	122	2.132E-08	2.131E-08	2.117E-08	2.059E-08	2.058E-08	2.125E-08	6.796E-06	6.796E-06	4.911E-06	6.194E-04	6.194E-04	5.337E-04	2.951E-03	3.023E-03	2.951E-03	6.995E-03
1.E+18	4	1.25	124	2.489E-08	2.488E-08	2.489E-08	2.489E-08	2.488E-08	2.489E-08	8.492E-06	8.492E-06	8.040E-06	7.068E-04	7.068E-04	7.734E-04	3.870E-03	4.200E-03	3.870E-03	8.345E-03
1.E+18	8	0.2	140	2.466E-08	2.463E-08	2.195E-08	2.020E-08	2.016E-08	2.069E-08	2.777E-05	2.777E-05	2.549E-05	1.379E-03	1.379E-03	1.508E-03	2.925E-03	2.949E-03	2.925E-03	7.163E-03
1.E+18	8	0.5	142	3.047E-08	3.045E-08	2.980E-08	3.062E-08	3.061E-08	3.060E-08	3.798E-05	3.798E-05	3.341E-05	1.664E-03	1.664E-03	1.743E-03	3.223E-03	3.315E-03	3.223E-03	7.465E-03
1.E+18	8	1.25	144	4.154E-08	4.153E-08	4.139E-08	4.154E-08	4.153E-08	4.168E-08	3.523E-05	3.523E-05	3.780E-05	2.159E-03	2.169E-03	2.393E-03	4.063E-03	4.478E-03	4.063E-03	8.901E-03
1.E+18	14	0.2	160	3.131E-08	3.128E-08	3.419E-08	3.500E-08	3.496E-08	3.305E-08	2.959E-04	2.959E-04	2.546E-04	2.801E-03	2.801E-03	2.823E-03	2.904E-03	2.927E-03	2.904E-03	7.076E-03
1.E+18	14	0.5	162	4.649E-08	4.647E-08	4.713E-08	4.614E-08	4.613E-08	4.603E-08	3.899E-04	3.899E-04	3.615E-04	2.847E-03	2.847E-03	3.297E-03	3.246E-03	3.337E-03	3.246E-03	7.474E-03
1.E+18	14	1.25	164	5.372E-08	5.372E-08	5.372E-08	5.402E-08	5.401E-08	5.321E-08	4.067E-04	4.067E-04	4.361E-04	3.864E-03	3.881E-03	4.443E-03	4.028E-03	4.441E-03	4.028E-03	8.834E-03
1.E+19	2	0.2	200	-2.342E-07	-2.342E-07	-2.330E-07	-2.327E-07	-2.327E-07	-2.325E-07	2.906E-06	2.906E-06	2.292E-06	2.183E-04	2.183E-04	2.427E-04	2.147E-03	2.168E-03	2.147E-03	7.112E-03
1.E+19	2	0.5	202	-3.691E-07	-3.691E-07	-3.691E-07	-3.691E-07	-3.691E-07	-3.691E-07	2.929E-06	2.929E-06	2.909E-06	3.064E-04	3.064E-04	2.747E-04	2.430E-03	2.496E-03	2.430E-03	7.247E-03
1.E+19	2	1.25	204	-7.566E-07	-7.566E-07	-7.566E-07	-7.566E-07	-7.566E-07	-7.566E-07	2.748E-06	2.748E-06	2.871E-06	3.092E-04	3.092E-04	3.602E-04	3.375E-03	3.600E-03	3.375E-03	8.574E-03
1.E+19	4	0.2	220	-4.628E-07	-4.628E-07	-4.627E-07	-4.627E-07	-4.627E-07	-4.639E-07	5.054E-06	5.054E-06	3.739E-06	4.723E-04	4.723E-04	4.934E-04	2.671E-03	2.692E-03	2.671E-03	6.808E-03
1.E+19	4	0.5	222	-5.905E-07	-5.905E-07	-5.905E-07	-5.905E-07	-5.905E-07	-5.905E-07	6.319E-06	6.319E-06	4.380E-06	6.313E-04	6.313E-04	5.420E-04	2.963E-03	3.043E-03	2.963E-03	7.015E-03
1.E+19	4	1.25	224	-7.254E-07	-7.254E-07	-7.254E-07	-7.254E-07	-7.254E-07	-7.254E-07	7.816E-06	7.816E-06	7.378E-06	7.129E-04	7.129E-04	7.820E-04	3.878E-03	4.221E-03	3.878E-03	8.369E-03
1.E+19	8	0.2	240	-8.089E-07	-8.089E-07	-8.073E-07	-8.076E-07	-8.076E-07	-8.113E-07	2.743E-05	2.743E-05	2.511E-05	1.393E-03	1.393E-03	1.522E-03	2.926E-03	2.958E-03	2.926E-03	7.180E-03
1.E+19	8	0.5	242	-9.522E-07	-9.522E-07	-9.520E-07	-9.523E-07	-9.523E-07	-9.524E-07	3.747E-05	3.747E-05	3.309E-05	1.680E-03	1.680E-03	1.762E-03	3.221E-03	3.323E-03	3.221E-03	7.483E-03
1.E+19	8	1.25	244	-1.200E-06	-1.200E-06	-1.200E-06	-1.200E-06	-1.200E-06	-1.200E-06	3.446E-05	3.446E-05	3.707E-05	2.177E-03	2.188E-03	2.412E-03	4.061E-03	4.493E-03	4.061E-03	8.923E-03
1.E+19	14	0.2	260	-1.338E-06	-1.338E-06	-1.344E-06	-1.344E-06	-1.344E-06	-1.347E-06	3.037E-04	3.037E-04	2.577E-04	2.815E-03	2.815E-03	2.834E-03	2.904E-03	2.935E-03	2.904E-03	7.092E-03
1.E+19	14	0.5	262	-1.525E-06	-1.525E-06	-1.524E-06	-1.525E-06	-1.525E-06	-1.525E-06	3.980E-04	3.980E-04	3.665E-04	2.859E-03	2.860E-03	3.309E-03	3.243E-03	3.344E-03	3.243E-03	7.491E-03
1.E+19	14	1.25	264	-1.733E-06	-1.733E-06	-1.734E-06	-1.733E-06	-1.733E-06	-1.733E-06	4.092E-04	4.092E-04	4.413E-04	3.877E-03	3.895E-03	4.460E-03	4.026E-03	4.455E-03	4.026E-03	8.854E-03
1.E+20	2	0.2	300	-6.710E-07	-6.710E-07	-6.710E-07	-6.704E-07	-6.704E-07	-6.704E-07	2.478E-06	2.478E-06	1.862E-06	2.191E-04	2.191E-04	2.435E-04	2.149E-03	2.174E-03	2.149E-03	7.122E-03
1.E+20	2	0.5	302	-9.529E-07	-9.529E-07	-9.546E-07	-9.529E-07	-9.529E-07	-9.546E-07	2.359E-06	2.359E-06	2.333E-06	3.071E-04	3.071E-04	2.752E-04	2.430E-03	2.502E-03	2.430E-03	7.257E-03
1.E+20	2	1.25	304	-1.750E-06	-1.750E-06	-1.750E-06	-1.750E-06	-1.750E-06	-1.750E-06	1.765E-06	1.765E-06	1.885E-06	3.089E-04	3.089E-04	3.601E-04	3.371E-03	3.606E-03	3.371E-03	8.584E-03
1.E+20	4	0.2	320	-1.262E-06	-1.262E-06	-1.263E-06	-1.262E-06	-1.262E-06	-1.262E-06	4.271E-06	4.271E-06	2.956E-06	4.741E-04	4.741E-04	4.951E-04	2.669E-03	2.696E-03	2.669E-03	6.816E-03
1.E+20	4	0.5	322	-1.540E-06	-1.540E-06	-1.540E-06	-1.539E-06	-1.539E-06	-1.541E-06	5.392E-06	5.392E-06	3.442E-06	6.331E-04	6.331E-04	5.432E-04	2.959E-03	3.046E-03	2.959E-03	7.024E-03
1.E+20	4	1.25	324	-1.912E-06	-1.912E-06	-1.912E-06	-1.912E-06	-1.912E-06	-1.912E-06	6.643E-06	6.643E-06	6.211E-06	7.131E-04	7.131E-04	7.826E-04	3.869E-03	4.225E-03	3.869E-03	8.377E-03
1.E+20	8	0.2	340	-2.265E-06	-2.265E-06	-2.266E-06	-2.263E-06	-2.263E-06	-2.264E-06	2.609E-05	2.609E-05	2.374E-05	1.395E-03	1.395E-03	1.524E-03	2.920E-03	2.958E-03	2.920E-03	7.190E-03
1.E+20	8	0.5	342	-2.579E-06	-2.579E-06	-2.570E-06	-2.579E-06	-2.579E-06	-2.570E-06	3.595E-05	3.595E-05	3.161E-05	1.681E-03	1.681E-03	1.764E-03	3.212E-03	3.323E-03	3.212E-03	7.491E-03
1.E+20	8	1.25	344	-3.119E-06	-3.119E-06	-3.118E-06	-3.123E-06	-3.123E-06	-3.115E-06	3.263E-05	3.263E-05	3.525E-05	2.178E-03	2.190E-03	2.414E-03	4.047E-03	4.494E-03	4.047E-03	8.930E-03
1.E+20	14	0.2	360	-3.856E-06	-3.856E-06	-3.855E-06	-3.854E-06	-3.854E-06	-3.854E-06	3.032E-04	3.032E-04	2.564E-04	2.816E-03	2.816E-03	2.835E-03	2.896E-03	2.934E-03	2.896E-03	7.099E-03
1.E+20	14	0.5	362	-4.199E-06	-4.199E-06	-4.189E-06	-4.203E-06	-4.203E-06	-4.205E-06	3.972E-04	3.972E-04	3.654E-04	2.859E-03	2.860E-03	3.309E-03	3.233E-03	3.343E-03	3.233E-03	7.497E-03
1.E+20	14	1.25	364	-4.634E-06	-4.634E-06	-4.631E-06	-4.640E-06	-4.640E-06	-4.631E-06	4.072E-04	4.072E-04	4.398E-04	3.876E-03	3.895E-03	4.460E-03	4.010E-03	4.455E-03	4.010E-03	8.859E-03

PDC = <pdope><w><d>.<shrink distance/2> ; P+ = 10^(17+pdope) (h/ml); P+ width (um) = 2 x 2^(w/2); P+ depth (um) = 0.2 x 2.5^(d/2).

FI_NPN_DJPD : Image cathode QE & nQE (electron current QE) dependence on N+ doping, N+ well width, N+ well depth and outer p-well anode (0.8 um) placement (0 um from the outer well edge).

(NB/ QE can only be positive : negative nQE & QE serve to indicate the nQE & QE were calculated from negative electron and total currents).

Maximum and minimum values for each of the 3 doping regimes are shaded and outlined respectively.

outer well p-dope	substrate n-dope	rev. bias both junct	subst / outer well depth: (12)/(2) um																	
1.E+17	1.E+15	2 V		pixel boundary			next to outer well			on outer well wall			next to well centre			Expected Max QE		Maximum QE	
N+ dope	N+ width	N+ depth	PDC	QE @ 55	nQE @ 55	QE @ 105	QE @ 65	nQE @ 65	QE @ 95	QE @ 70	nQE @ 70	QE @ 90	QE @ 75	nQE @ 75	QE @ 85	QE @ 80	nQE @ 80	Max QE	FI / BI
1.E+18	2	0.2	100	5.191E-09	5.169E-09	6.357E-09	5.509E-09	5.487E-09	6.569E-09	5.286E-04	5.286E-04	4.174E-04	0.036391	0.036391	0.032822	0.298892	0.302794	0.29889	141.0
1.E+18	2	0.5	102	1.309E-08	1.308E-08	1.378E-08	1.282E-08	1.281E-08	1.313E-08	5.966E-04	5.966E-04	5.058E-04	0.041800	0.041800	0.037948	0.332697	0.346132	0.33270	156.9
1.E+18	2	1.25	104	3.725E-08	3.724E-08	3.724E-08	3.733E-08	3.733E-08	3.720E-08	5.967E-04	5.967E-04	6.176E-04	0.048741	0.048741	0.047734	0.392320	0.429583	0.39232	132.9
1.E+18	4	0.2	120	1.410E-08	1.408E-08	1.303E-08	1.341E-08	1.338E-08	1.360E-08	9.221E-04	9.221E-04	7.975E-04	0.072271	0.072271	0.070338	0.390916	0.395107	0.39092	132.5
1.E+18	4	0.5	122	2.056E-08	2.055E-08	2.056E-08	2.098E-08	2.097E-08	2.120E-08	1.241E-03	1.241E-03	9.292E-04	0.101664	0.101664	0.083096	0.421864	0.438876	0.42186	143.0
1.E+18	4	1.25	124	2.489E-08	2.488E-08	2.489E-08	2.489E-08	2.488E-08	2.489E-08	1.416E-03	1.416E-03	1.579E-03	0.107335	0.107335	0.113240	0.463793	0.522612	0.46379	157.2
1.E+18	8	0.2	140	2.074E-08	2.070E-08	2.138E-08	2.242E-08	2.239E-08	2.034E-08	4.673E-03	4.673E-03	4.325E-03	0.218813	0.218813	0.219237	0.408392	0.414272	0.40839	138.4
1.E+18	8	0.5	142	3.060E-08	3.059E-08	3.110E-08	3.015E-08	3.014E-08	3.027E-08	5.366E-03	5.366E-03	5.226E-03	0.254226	0.254255	0.251641	0.431787	0.452026	0.43179	146.3
1.E+18	8	1.25	144	4.139E-08	4.138E-08	4.139E-08	4.154E-08	4.153E-08	4.154E-08	6.373E-03	6.373E-03	6.352E-03	0.309891	0.312019	0.307045	0.456468	0.526058	0.45647	154.7
1.E+18	14	0.2	160	3.479E-08	3.476E-08	3.447E-08	3.521E-08	3.518E-08	3.389E-08	4.944E-02	4.944E-02	4.755E-02	0.410172	0.410172	0.410094	0.410423	0.416302	0.41042	139.1
1.E+18	14	0.5	162	4.666E-08	4.665E-08	4.525E-08	4.631E-08	4.629E-08	4.606E-08	5.763E-02	5.763E-02	5.566E-02	0.456803	0.456868	0.456427	0.434240	0.454458	0.43424	147.1
1.E+18	14	1.25	164	5.372E-08	5.372E-08	5.358E-08	5.402E-08	5.401E-08	5.358E-08	7.337E-02	7.337E-02	7.066E-02	0.542374	0.545909	0.541854	0.455995	0.525578	0.45599	154.5
1.E+19	2	0.2	200	-2.355E-07	-2.355E-07	-2.355E-07	-2.348E-07	-2.348E-07	-2.331E-07	5.429E-04	5.429E-04	4.257E-04	0.037390	0.037390	0.033492	0.301848	0.306996	0.30185	102.3
1.E+19	2	0.5	202	-3.691E-07	-3.691E-07	-3.691E-07	-3.691E-07	-3.691E-07	-3.691E-07	6.081E-04	6.081E-04	5.141E-04	0.042632	0.042632	0.038597	0.335274	0.350116	0.33527	113.6
1.E+19	2	1.25	204	-7.568E-07	-7.568E-07	-7.566E-07	-7.566E-07	-7.566E-07	-7.568E-07	6.035E-04	6.035E-04	6.240E-04	0.049360	0.049360	0.048289	0.393617	0.432498	0.39362	133.4
1.E+19	4	0.2	220	-4.641E-07	-4.641E-07	-4.640E-07	-4.613E-07	-4.613E-07	-4.621E-07	9.461E-04	9.461E-04	8.144E-04	0.074183	0.074183	0.071864	0.392284	0.397825	0.39228	132.9
1.E+19	4	0.5	222	-5.905E-07	-5.905E-07	-5.905E-07	-5.905E-07	-5.905E-07	-5.905E-07	1.265E-03	1.265E-03	9.436E-04	0.103680	0.103680	0.084437	0.422321	0.441114	0.42232	143.1
1.E+19	4	1.25	224	-7.254E-07	-7.254E-07	-7.254E-07	-7.254E-07	-7.254E-07	-7.254E-07	1.428E-03	1.428E-03	1.596E-03	0.108272	0.108272	0.114504	0.463418	0.524202	0.46342	157.0
1.E+19	8	0.2	240	-8.166E-07	-8.166E-07	-8.182E-07	-8.135E-07	-8.135E-07	-8.091E-07	4.757E-03	4.757E-03	4.400E-03	0.221056	0.221056	0.221319	0.407550	0.415301	0.40755	138.1
1.E+19	8	0.5	242	-9.523E-07	-9.523E-07	-9.523E-07	-9.521E-07	-9.521E-07	-9.523E-07	5.432E-03	5.432E-03	5.329E-03	0.256300	0.256336	0.254163	0.430517	0.452868	0.43052	145.9
1.E+19	8	1.25	244	-1.200E-06	-1.200E-06	-1.200E-06	-1.200E-06	-1.200E-06	-1.200E-06	6.457E-03	6.457E-03	6.436E-03	0.311883	0.314162	0.308990	0.455141	0.527022	0.45514	154.2
1.E+19	14	0.2	260	-1.343E-06	-1.343E-06	-1.342E-06	-1.342E-06	-1.342E-06	-1.346E-06	5.102E-02	5.102E-02	4.841E-02	0.412176	0.412178	0.411642	0.409462	0.417210	0.40946	138.7
1.E+19	14	0.5	262	-1.525E-06	-1.525E-06	-1.525E-06	-1.525E-06	-1.525E-06	-1.525E-06	5.900E-02	5.900E-02	5.665E-02	0.458429	0.458509	0.457816	0.432910	0.455251	0.43291	146.7
1.E+19	14	1.25	264	-1.732E-06	-1.732E-06	-1.733E-06	-1.733E-06	-1.733E-06	-1.733E-06	7.404E-02	7.404E-02	7.164E-02	0.543320	0.547083	0.542969	0.454666	0.526545	0.45467	154.1
1.E+20	2	0.2	300	-6.712E-07	-6.712E-07	-6.712E-07	-6.707E-07	-6.708E-07	-6.708E-07	5.455E-04	5.455E-04	4.274E-04	0.037599	0.037599	0.033660	0.301658	0.307915	0.30166	102.2
1.E+20	2	0.5	302	-9.546E-07	-9.546E-07	-9.546E-07	-9.546E-07	-9.546E-07	-9.546E-07	6.101E-04	6.101E-04	5.155E-04	0.042814	0.042814	0.038746	0.334872	0.350948	0.33487	113.5
1.E+20	2	1.25	304	-1.750E-06	-1.750E-06	-1.750E-06	-1.750E-06	-1.750E-06	-1.748E-06	6.038E-04	6.038E-04	6.245E-04	0.049466	0.049466	0.048406	0.392765	0.433071	0.39277	133.1
1.E+20	4	0.2	320	-1.262E-06	-1.262E-06	-1.263E-06	-1.262E-06	-1.262E-06	-1.263E-06	9.505E-04	9.505E-04	8.177E-04	0.074590	0.074590	0.072229	0.391637	0.398382	0.39164	132.7
1.E+20	4	0.5	322	-1.551E-06	-1.551E-06	-1.540E-06	-1.539E-06	-1.539E-06	-1.550E-06	1.270E-03	1.270E-03	9.463E-04	0.104115	0.104115	0.084768	0.421222	0.441585	0.42122	142.7
1.E+20	4	1.25	324	-1.912E-06	-1.912E-06	-1.912E-06	-1.912E-06	-1.912E-06	-1.912E-06	1.429E-03	1.429E-03	1.598E-03	0.108454	0.108454	0.114734	0.461934	0.524516	0.46193	156.5
1.E+20	8	0.2	340	-2.266E-06	-2.266E-06	-2.265E-06	-2.265E-06	-2.265E-06	-2.264E-06	4.775E-03	4.775E-03	4.417E-03	0.221553	0.221555	0.221788	0.406074	0.415475	0.40607	137.6
1.E+20	8	0.5	342	-2.570E-06	-2.570E-06	-2.580E-06	-2.580E-06	-2.580E-06	-2.570E-06	5.444E-03	5.444E-03	5.348E-03	0.256648	0.256693	0.254652	0.428796	0.453010	0.42880	145.3
1.E+20	8	1.25	344	-3.119E-06	-3.119E-06	-3.113E-06	-3.118E-06	-3.118E-06	-3.119E-06	6.471E-03	6.471E-03	6.452E-03	0.312142	0.314566	0.309279	0.453186	0.527205	0.45319	153.6
1.E+20	14	0.2	360	-3.821E-06	-3.821E-06	-3.856E-06	-3.857E-06	-3.857E-06	-3.855E-06	5.133E-02	5.133E-02	4.863E-02	0.412551	0.412551	0.411958	0.407954	0.417354	0.40795	138.2
1.E+20	14	0.5	362	-4.189E-06	-4.189E-06	-4.190E-06	-4.205E-06	-4.205E-06	-4.205E-06	5.927E-02	5.927E-02	5.689E-02	0.458711	0.458807	0.458091	0.431169	0.455375	0.43117	146.1
1.E+20	14	1.25	364	-4.639E-06	-4.639E-06	-4.639E-06	-4.628E-06	-4.628E-06	-4.640E-06	7.417E-02	7.417E-02	7.183E-02	0.543324	0.547308	0.543010	0.452705	0.526728	0.45271	153.4

PDC = <pdope><w><d>.<shrink distance/2> ; P+ = 10^(17+pdope) (h/ml); P+ width (um) = 2 x 2^(w/2); P+ depth (um) = 0.2 x 2.5^(d/2).

FI NPN DJPD : Image cathode QE & NQE dependence on N+ doping, N+ well width, N+ well depth and outer p-well anode (0.8 um) placement (0 um from the outer well edge).

Maximum and minimum values for each of the 3 doping regimes are shaded and outlined respectively.

outer well	substrate	rev. bias	subst / outer well depth: (12)/(2) um																							
p-dope	n-dope	both junct		pixel boundary		next to outer well		on outer well wall		next to well centre		Max	Max QE	Pixel Boundary		on outer well wall		inside outer well		% FI NQE below BI		% FI NQE below BI		% FI NQE below BI	
1.E+17	1.E+15	2 V																							
N+ dope	N+ width	N+ depth	PDC	QE 55	QE 105	QE 65	QE 95	QE 70	QE 90	QE 75	QE 85	QE 80	FI / BI	NQE 55	NQE 105	NQE 70	NQE 90	NQE 75	NQE 85	at 55	at 105	at 70	at 90	at 75	at 85
1.E+18	2	0.2	100	5.19E-09	6.36E-09	5.51E-09	6.57E-09	5.29E-04	4.17E-04	0.03639	0.03282	0.2989		1.74E-08	2.13E-08	1.77E-03	1.40E-03	0.1218	0.1098	99.35	99.17	-22.44	-19.52	-21.34	2.21
1.E+18	2	0.5	102	1.31E-08	1.38E-08	1.28E-08	1.31E-08	5.97E-04	5.06E-04	0.04180	0.03795	0.3327		3.93E-08	4.14E-08	1.79E-03	1.52E-03	0.1256	0.1141	99.30	99.27	-32.74	-12.91	-0.41	-1.36
1.E+18	2	1.25	104	3.73E-08	3.72E-08	3.73E-08	3.72E-08	5.97E-04	6.18E-04	0.04874	0.04773	0.3923		9.49E-08	9.49E-08	1.52E-03	1.57E-03	0.1242	0.1217	99.14	99.14	-45.75	-45.64	-36.12	-14.34
1.E+18	4	0.2	120	1.41E-08	1.30E-08	1.34E-08	1.36E-08	9.22E-04	7.98E-04	0.07227	0.07034	0.3909		3.61E-08	3.33E-08	2.36E-03	2.04E-03	0.1849	0.1799	99.36	99.39	-16.31	-31.33	-6.54	1.18
1.E+18	4	0.5	122	2.06E-08	2.06E-08	2.10E-08	2.12E-08	1.24E-03	9.29E-04	0.10166	0.08310	0.4219		4.87E-08	4.87E-08	2.94E-03	2.20E-03	0.2410	0.1970	99.33	99.32	-27.77	-32.35	-14.83	-8.91
1.E+18	4	1.25	124	2.49E-08	2.49E-08	2.49E-08	2.49E-08	1.42E-03	1.58E-03	0.10733	0.11324	0.4638		5.37E-08	5.37E-08	3.05E-03	3.40E-03	0.2314	0.2442	99.17	99.17	-39.16	-63.90	-26.73	-22.18
1.E+18	8	0.2	140	2.07E-08	2.14E-08	2.24E-08	2.03E-08	4.67E-03	4.33E-03	0.21881	0.21924	0.4084		5.08E-08	5.23E-08	1.14E-02	1.06E-02	0.5358	0.5368	99.40	99.30	-20.55	-21.54	-13.68	-4.15
1.E+18	8	0.5	142	3.06E-08	3.11E-08	3.01E-08	3.03E-08	5.37E-03	5.23E-03	0.25423	0.25164	0.4318		7.09E-08	7.20E-08	1.24E-02	1.21E-02	0.5888	0.5828	99.25	99.22	-5.46	-16.75	-14.04	-7.75
1.E+18	8	1.25	144	4.14E-08	4.14E-08	4.15E-08	4.15E-08	6.37E-03	6.35E-03	0.30989	0.30705	0.4565		9.07E-08	9.07E-08	1.40E-02	1.39E-02	0.6789	0.6727	99.11	99.11	-61.02	-49.59	-27.76	-14.20
1.E+18	14	0.2	160	3.48E-08	3.45E-08	3.52E-08	3.39E-08	4.94E-02	4.75E-02	0.41017	0.41009	0.4104		8.48E-08	8.40E-08	1.20E-01	1.16E-01	0.9994	0.9992	99.21	99.29	-18.21	-32.16	-3.64	-2.81
1.E+18	14	0.5	162	4.67E-08	4.53E-08	4.63E-08	4.61E-08	5.76E-02	5.57E-02	0.45680	0.45643	0.4342		1.07E-07	1.04E-07	1.33E-01	1.28E-01	1.0000	0.9992	99.25	99.28	-10.45	-15.07	-15.80	0.08
1.E+18	14	1.25	164	5.37E-08	5.36E-08	5.40E-08	5.36E-08	7.34E-02	7.07E-02	0.54237	0.54185	0.4560		1.18E-07	1.17E-07	1.61E-01	1.55E-01	1.0000	0.9990	99.12	99.12	-59.37	-43.13	-15.01	0.10
1.E+19	2	0.2	200	2.36E-07	2.36E-07	2.35E-07	2.33E-07	5.43E-04	4.26E-04	0.03739	0.03349	0.3018		7.80E-07	7.80E-07	1.80E-03	1.41E-03	0.1239	0.1110	99.28	99.28	-32.85	-32.10	-21.79	1.86
1.E+19	2	0.5	202	3.69E-07	3.69E-07	3.69E-07	3.69E-07	6.08E-04	5.14E-04	0.04263	0.03860	0.3353		1.10E-06	1.10E-06	1.81E-03	1.53E-03	0.1272	0.1151	99.28	99.28	-50.45	-28.07	-0.84	-1.81
1.E+19	2	1.25	204	7.57E-07	7.57E-07	7.57E-07	7.57E-07	6.03E-04	6.24E-04	0.04936	0.04829	0.3936		1.92E-06	1.92E-06	1.53E-03	1.59E-03	0.1254	0.1227	99.14	99.14	-88.27	-86.33	-36.89	-14.95
1.E+19	4	0.2	220	4.64E-07	4.64E-07	4.61E-07	4.62E-07	9.46E-04	8.14E-04	0.07418	0.07186	0.3923		1.18E-06	1.18E-06	2.41E-03	2.08E-03	0.1891	0.1832	99.32	99.32	-27.45	-48.28	-6.93	0.84
1.E+19	4	0.5	222	5.90E-07	5.90E-07	5.90E-07	5.90E-07	1.27E-03	9.44E-04	0.10368	0.08444	0.4223		1.40E-06	1.40E-06	3.00E-03	2.23E-03	0.2455	0.1999	99.30	99.30	-40.49	-51.12	-15.21	-9.29
1.E+19	4	1.25	224	7.25E-07	7.25E-07	7.25E-07	7.25E-07	1.43E-03	1.60E-03	0.10827	0.11450	0.4634		1.57E-06	1.57E-06	3.08E-03	3.44E-03	0.2336	0.2471	99.16	99.16	-52.86	-81.00	-27.11	-22.54
1.E+19	8	0.2	240	8.17E-07	8.18E-07	8.13E-07	8.09E-07	4.76E-03	4.40E-03	0.22106	0.22132	0.4076		2.00E-06	2.01E-06	1.17E-02	1.08E-02	0.5424	0.5430	99.28	99.27	-24.51	-25.85	-13.94	-4.39
1.E+19	8	0.5	242	9.52E-07	9.52E-07	9.52E-07	9.52E-07	5.43E-03	5.33E-03	0.25630	0.25416	0.4305		2.21E-06	2.21E-06	1.26E-02	1.24E-02	0.5953	0.5904	99.25	99.25	-8.46	-20.48	-14.18	-7.95
1.E+19	8	1.25	244	1.20E-06	1.20E-06	1.20E-06	1.20E-06	6.46E-03	6.44E-03	0.31188	0.30899	0.4551		2.64E-06	2.64E-06	1.42E-02	1.41E-02	0.6852	0.6789	99.11	99.11	-67.19	-54.95	-27.82	-14.30
1.E+19	14	0.2	260	1.34E-06	1.34E-06	1.34E-06	1.35E-06	5.10E-02	4.84E-02	0.41218	0.41164	0.4095		3.28E-06	3.28E-06	1.25E-01	1.18E-01	1.0000	0.9987	99.29	99.29	-19.11	-33.21	-3.15	-2.32
1.E+19	14	0.5	262	1.52E-06	1.52E-06	1.52E-06	1.52E-06	5.90E-02	5.66E-02	0.45843	0.45782	0.4329		3.52E-06	3.52E-06	1.36E-01	1.31E-01	1.0000	0.9987	99.25	99.25	-11.06	-15.80	-15.73	0.13
1.E+19	14	1.25	264	1.73E-06	1.73E-06	1.73E-06	1.73E-06	7.40E-02	7.16E-02	0.54332	0.54297	0.4547		3.81E-06	3.81E-06	1.63E-01	1.58E-01	1.0000	0.9994	99.12	99.11	-60.21	-43.73	-15.05	0.06
1.E+20	2	0.2	300	6.71E-07	6.71E-07	6.71E-07	6.71E-07	5.46E-04	4.27E-04	0.03760	0.03366	0.3017		2.23E-06	2.23E-06	1.81E-03	1.42E-03	0.1246	0.1116	99.29	99.29	-56.78	-63.47	-22.21	1.54
1.E+20	2	0.5	302	9.55E-07	9.55E-07	9.55E-07	9.55E-07	6.10E-04	5.15E-04	0.04281	0.03875	0.3349		2.85E-06	2.85E-06	1.82E-03	1.54E-03	0.1279	0.1157	99.27	99.27	-87.72	-60.34	-1.17	-2.16
1.E+20	2	1.25	304	1.75E-06	1.75E-06	1.75E-06	1.75E-06	6.04E-04	6.25E-04	0.04947	0.04841	0.3928		4.45E-06	4.45E-06	1.54E-03	1.59E-03	0.1259	0.1232	99.14	99.14	-193.65	-184.31	-37.47	-15.39
1.E+20	4	0.2	320	1.26E-06	1.26E-06	1.26E-06	1.26E-06	9.51E-04	8.18E-04	0.07459	0.07223	0.3916		3.22E-06	3.22E-06	2.43E-03	2.09E-03	0.1905	0.1844	99.32	99.32	-51.67	-88.57	-7.24	0.56
1.E+20	4	0.5	322	1.55E-06	1.54E-06	1.54E-06	1.55E-06	1.27E-03	9.46E-04	0.10411	0.08477	0.4212		3.68E-06	3.66E-06	3.01E-03	2.25E-03	0.2472	0.2012	99.29	99.30	-65.43	-93.15	-15.51	-9.61
1.E+20	4	1.25	324	1.91E-06	1.91E-06	1.91E-06	1.91E-06	1.43E-03	1.60E-03	0.10845	0.11473	0.4619		4.14E-06	4.14E-06	3.09E-03	3.46E-03	0.2348	0.2484	99.16	99.16	-80.16	-115.46	-27.40	-22.80
1.E+20	8	0.2	340	2.27E-06	2.27E-06	2.27E-06	2.26E-06	4.77E-03	4.42E-03	0.22155	0.22179	0.4061		5.58E-06	5.58E-06	1.18E-02	1.09E-02	0.5456	0.5462	99.28	99.28	-31.58	-33.74	-14.20	-4.62
1.E+20	8	0.5	342	2.57E-06	2.58E-06	2.58E-06	2.57E-06	5.44E-03	5.35E-03	0.25665	0.25465	0.4288		5.99E-06	6.02E-06	1.27E-02	1.25E-02	0.5985	0.5939	99.25	99.25	-13.45	-26.74	-14.39	-8.16
1.E+20	8	1.25	344	3.12E-06	3.11E-06	3.12E-06	3.12E-06	6.47E-03	6.45E-03	0.31214	0.30928	0.4532		6.88E-06	6.87E-06	1.43E-02	1.42E-02	0.6888	0.6825	99.11	99.11	-77.09	-63.46	-27.95	-14.42
1.E+20	14	0.2	360	3.82E-06	3.86E-06	3.86E-06	3.86E-06	5.13E-02	4.86E-02	0.41255	0.41196	0.4080		9.37E-06	9.45E-06	1.26E-01	1.19E-01	1.0000	0.9986	99.30	99.29	-20.21	-34.64	-2.85	-2.02
1.E+20	14	0.5	362	4.19E-06	4.19E-06	4.20E-06	4.20E-06	5.93E-02	5.69E-02	0.45871	0.45809	0.4312		9.72E-06	9.72E-06	1.37E-01	1.32E-01	1.0000	0.9986	99.25	99.25	-11.67	-16.73	-15.73	0.14
1.E+20	14	1.25	364	4.64E-06	4.64E-06	4.63E-06	4.64E-06	7.42E-02	7.18E-02	0.54332	0.54301	0.4527		1.02E-05	1.02E-05	1.64E-01	1.59E-01	1.0000	0.9994	99.11	99.11	-61.37	-44.66	-15.07	0.06

PDC = <pdope><w><d>.<shrink distance/2> ; P+ = 10^(17+pdope) (h/ml); P+ width (um) = 2 x 2^(w/2); P+ depth (um) = 0.2 x 2.5^(d/2).

BI & FI DJPD : % absorbance in the P+/N+ well's SCR (drift component) and non-SCR (diffusion component) dependence on P+/N+ well, N/P well and P/N substrate doping, bias, well width and depth.

well n-dope	substrate p-dope	rev. bias both junct	subst/well depth (um)		2D PSE total abs drift component	2D Pse total abs drift component	2D PSE total abs diffusion component	2D Pse total abs diffusion component	2D PSE: 5 um wide laser 80 um pos'n : PSE centre	2D PSE: 5 um wide laser 80 um pos'n : PSE centre	2D PSE: 5 um wide laser 80 um pos'n : PSE centre	2D PSE: 5 um wide laser 80 um pos'n : PSE centre
1.E+17	1.E+15	2 V	(3)/(2)	pd/w/d/sh	2D %abs SCR (BI)	2D %abs SCR (FI)	%abs. non-SCR (BI)	%abs non-SCR (FI)	BI SCR %abs: DRIFT	FI SCR %abs: DRIFT	BI non-SCR %abs: DIFFUSION	FI non-SCR %abs: DIFFUSION
P+ dope	P+ width	P+ depth	shrink	PDC								
1.E+18	2	0.2	NA	100	0.099815473	0.189999043	11.52796916	14.54401014	0.998154732	1.899990433	28.12565084	35.00389385
1.E+18	2	0.5	"	102	0.099815473	0.189999043	11.52796916	14.54401014	0.998154732	1.899990433	28.12565084	35.00389385
1.E+18	2	1.25	"	104	0.099815473	0.189999043	11.52796916	14.54401014	0.998154732	1.899990433	28.12565084	35.00389385
1.E+18	4	0.2	NA	120	0.19643634	0.373775396	11.4313483	14.36023379	1.964363404	3.737753957	27.15944217	33.16613033
1.E+18	4	0.5	"	122	0.19643634	0.373775396	11.4313483	14.36023379	1.964363404	3.737753957	27.15944217	33.16613033
1.E+18	4	1.25	"	124	0.19643634	0.373775396	11.4313483	14.36023379	1.964363404	3.737753957	27.15944217	33.16613033
1.E+18	8	0.2	NA	140	0.389678075	0.7413281	11.23810656	13.99268108	2.415521679	4.594408809	26.70828389	32.30947548
1.E+18	8	0.5	"	142	0.389678075	0.7413281	11.23810656	13.99268108	2.415521679	4.594408809	26.70828389	32.30947548
1.E+18	8	1.25	"	144	0.389678075	0.7413281	11.23810656	13.99268108	2.415521679	4.594408809	26.70828389	32.30947548
1.E+18	14	0.2	"	160	0.979179345	1.188658474	10.64860529	13.54535071	3.083176634	3.599499931	26.04062894	33.30438435
1.E+18	14	0.5	"	162	0.979179345	1.188658474	10.64860529	13.54535071	3.083176634	3.599499931	26.04062894	33.30438435
1.E+18	14	1.25	"	164	0.979179345	1.188658474	10.64860529	13.54535071	3.083176634	3.599499931	26.04062894	33.30438435
1.E+19	2	0.2	NA	200	0.093916376	0.179782909	11.53386826	14.55422627	0.939163755	1.797829091	28.18464181	35.10605519
1.E+19	2	0.5	"	202	0.093916376	0.179782909	11.53386826	14.55422627	0.939163755	1.797829091	28.18464181	35.10605519
1.E+19	2	1.25	"	204	0.093916376	0.179782909	11.53386826	14.55422627	0.939163755	1.797829091	28.18464181	35.10605519
1.E+19	4	0.2	NA	220	0.187166625	0.358246338	11.44061801	14.37576284	1.871666246	3.582463378	27.25213932	33.32142091
1.E+19	4	0.5	"	222	0.187166625	0.358246338	11.44061801	14.37576284	1.871666246	3.582463378	27.25213932	33.32142091
1.E+19	4	1.25	"	224	0.187166625	0.358246338	11.44061801	14.37576284	1.871666246	3.582463378	27.25213932	33.32142091
1.E+19	8	0.2	NA	240	0.373667123	0.715173195	11.25411751	14.01883599	2.331256227	4.461585717	26.79254934	32.44229857
1.E+19	8	0.5	"	242	0.373667123	0.715173195	11.25411751	14.01883599	2.331256227	4.461585717	26.79254934	32.44229857
1.E+19	8	1.25	"	244	0.373667123	0.715173195	11.25411751	14.01883599	2.331256227	4.461585717	26.79254934	32.44229857
1.E+19	14	0.2	NA	260	0.942269743	1.150068782	10.68551489	13.5839404	2.975620045	3.495439381	26.14818552	33.4084449
1.E+19	14	0.5	"	262	0.942269743	1.150068782	10.68551489	13.5839404	2.975620045	3.495439381	26.14818552	33.4084449
1.E+19	14	1.25	"	264	0.942269743	1.150068782	10.68551489	13.5839404	2.975620045	3.495439381	26.14818552	33.4084449
1.E+20	2	0.2	NA	300	0.09396734	0.180048822	11.5338173	14.55396036	0.939673405	1.800488216	28.18413217	35.10339607
1.E+20	2	0.5	"	302	0.09396734	0.180048822	11.5338173	14.55396036	0.939673405	1.800488216	28.18413217	35.10339607
1.E+20	2	1.25	"	304	0.09396734	0.180048822	11.5338173	14.55396036	0.939673405	1.800488216	28.18413217	35.10339607
1.E+20	4	0.2	NA	320	0.229683412	0.388654948	11.39810122	14.34535423	2.296834123	3.886549477	26.82697145	33.01733481
1.E+20	4	0.5	"	322	0.229683412	0.388654948	11.39810122	14.34535423	2.296834123	3.886549477	26.82697145	33.01733481
1.E+20	4	1.25	"	324	0.229683412	0.388654948	11.39810122	14.34535423	2.296834123	3.886549477	26.82697145	33.01733481
1.E+20	8	0.2	NA	340	0.430664249	0.723584791	11.19712039	14.01042439	2.512260458	4.186623035	26.61154511	32.71726125
1.E+20	8	0.5	"	342	0.430664249	0.723584791	11.19712039	14.01042439	2.512260458	4.186623035	26.61154511	32.71726125
1.E+20	8	1.25	"	344	0.430664249	0.723584791	11.19712039	14.01042439	2.512260458	4.186623035	26.61154511	32.71726125
1.E+20	14	0.2	NA	360	0.946555178	1.156378088	10.68122946	13.57763109	2.990680341	3.5168879	26.13312523	33.38699638
1.E+20	14	0.5	"	362	0.946555178	1.156378088	10.68122946	13.57763109	2.990680341	3.5168879	26.13312523	33.38699638
1.E+20	14	1.25	"	364	0.946555178	1.156378088	10.68122946	13.57763109	2.990680341	3.5168879	26.13312523	33.38699638

PDC = <pdope><w><d>.<shrink distance/2> ; P+ = 10^(17+pdope) (h/ml); P+ width (um) = 2 x 2^(w/2); P+ depth (um) = 0.2 x 2.5^(d/2).

APPENDIX XX : RESEARCH JOURNAL – AVP EQUATION DEVELOPMENT

NEW IMPROVED SOLUTION 9/6/03

-32-

START HERE

LASER SLICE SCAN - X1

DRIFT COMPENSATION

2D CASE (FI)

@ 70. (FI). I_{abs} (A) $= I_o(1 - \exp(-\alpha(d_w - w_{in})))$ — (32)

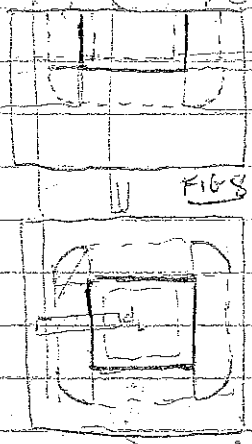

FIG 8

$prop$ (A) $= (w \times d_w \times d_H)/(w_L \times d_L \times d_H) = w/w_L$ — (33)

I_{ABS} (B) $= I_o(\exp(-\alpha(d_w - w_{in})) - \exp(-\alpha d_w))$ — (34)

$prop$ (B) $= (w_L/2 + w_{out}) \times d_H \times d_B / w_L \times d_L \times d_H$

$= (w_L/2 + w_{out})/w_L$ — (35)

I_{ABS} (C) $= I_o(\exp(-\alpha d_w) - \exp(-\alpha(d_w + w_{out}))$ — (36)

$prop$ (C) $= [(w_L/2) \times d_C \times d_L + \cdots] / w_L \times d_L \times d_L$

$= [w_L/2 + w_{out}) \times d_C + \cdots] / w_L \times d_L \times d_L$

$= w_L \times d_L [w_L/2 + \cdots] / w_L \times w_L \times d_L$

$= (w_L/2 + \cdots)/w_L$ — (37)

FIG 9

FIG 10

I_{abs} in total strip $= I_o(1 - \exp(-\alpha(d_s))) \times Prop.$

$= I_o(1 - \exp(-\alpha d_s)) \times 1$ — (38)

$I_{ABS\,(2D)}$ (FI) @ 70 $= \left(\frac{I_o}{w_L}\right)\Big(\Big([1 - \exp(-\alpha(d_w - w_{in}))][w]\Big) + \Big([\exp(-\alpha(d_w - w_{in})) - \exp(-\alpha d_s)][w_L/2 + w_{out}]\Big)$

ST $w_L/2 - w_{out} \geq 0$ $+ \Big([-\exp(-\alpha d_w) - \exp(-\alpha(d_w + w_{out}))][w_L/2 + \cdots]\Big)\Big)$ — (39)

2D CASE (BI) @ 70.

Refer to Fig 8 + 9. all prop are same as for FI & keep (32) (33) (35) (37).

only I_A, I_B & I_C change due to BI configuration.

here I_{ABS} (BI) (A) $= I_o(\exp(-\alpha(d_s - d_w + w_{in})) - \exp(-\alpha d_s))$ — (40)

I_{ABS} (BI) (B) $= I_o(\exp(-\alpha(d_s - d_w)) - \exp(-\alpha(d_s - d_w + w_{in})))$ — (41)

I_{ABS} (BI) (C) $= I_o(\exp(-\alpha(d_s - d_w - w_{out})) - \exp(-\alpha(d_s - d_w)))$ — (42)

$I_{ABS\,(2D)}$ (BI) @ 70 $= \left(\frac{I_o}{w_L}\right)\Big(\Big([\exp(-\alpha(d_s - d_w + w_{in})) - \exp(-\alpha(d_s))][w]\Big) + \Big([\exp(-\alpha(d_s - d_w)) - \exp(-\alpha(d_s - d_w + w_{in}))]$

$\times [w_L/2 + w_{out}]\Big) + \Big([\exp(-\alpha(d_s - d_w - w_{out})) - \exp(-\alpha(d_s - d_w))][w_L/2 + \cdots]\Big)\Big)$

$\forall$ variable ST. $w_L/2 - w_{out} \geq 0$ — (43)

2D CASE (FI) @ 80 cf (21) ; 2D CASE (BI) @ 80 cf (25)

cf (39) p38

If $I_o = 100$ from (39), (43), (21), & (25) give % Abs by SCR

of laser of width w_L ST. $[w_{well} - w_{in} - (w_L/2) \geq 0]$.

we used 5 mm $\Rightarrow$ +ve condition.

TOTAL-XT

1D TOTAL PSE I_{ABS} by SCR

DRIFT COMPONENT

Total PSE Abs by SCR : (FI).

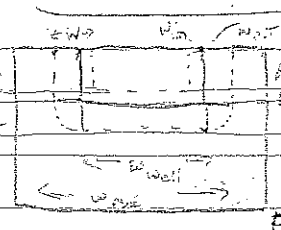

Fig 11

$I_{Abs}^{(A)} = I_o(1-\exp(-\alpha(d_w - W_{in}))$ — (44)

prop (A) Abs by light = $2w / W_{PSE}$ — (45).

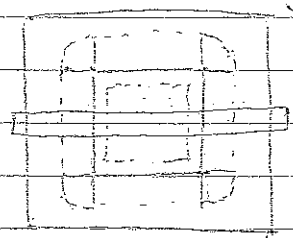

Fig 12

$I_{Abs}^{(FI)}{}_{(A)} = (32)$.

prop (A) abs light = $2w / w_{PSE}$ — (44)

$I_{Abs}^{(FI)}{}_{(B)} = (34)$

prop (B) abs light = $(W_{well} + 2W_{out}) \times d_1 \times \alpha(d_3) / W_{PSE} \times d_1 \times \alpha(d_3)$

$= (W_{well} + 2W_{out}) / W_{PSE}$ — (45).

$I_{Abs}^{(FI)}{}_{(C)} = (36)$; prop (C) abs light = $W_{well} \times \alpha(d_3) \times d_1 + 2(\pi (W_{out})^{\frac{1}{2}} \times \alpha(d_3)) / W_{PSE} \cdot d_1 \times \alpha(d_3)$

$d_1 = W_{out}$; $= (W_{well} + \pi W_{out}) / W_{PSE}$ — (46)

cf p40

$\therefore I_{Abs}^{(FI)}{}_{PSE} = (32) \times (44) + (34) \times (45) + (36) \times (46)$

$I_{Abs}^{(FI)}{}_{PSE} = \left(\frac{I_o}{W_{PSE}}\right) \cdot \{ [1-\exp(-\alpha(d_3 - W_{in}))] \cdot [2w] + [\exp(-\alpha(d_w - W_{in})) - \exp(-\alpha d_w)] \cdot [W_{well} + 2W_{out}] + [\exp(-\alpha(d_w)) - \exp(-\alpha(d_w + W_{out}))] \cdot [W_{well} + \pi W_{out}] \}$

(47) cf p36

Total PSE Abs by SCR : (BI).

ref Fig 11 + 12. $I_{Abs}^{(BI)}{}_{(A)} = (40)$; prop Abs in (A) = (33)

$I_{Abs}^{(BI)}{}_{(B)} = (41)$; " " " (B) = (35)

$I_{Abs}^{(BI)}{}_{(C)} = (42)$; " " " (C) = (37)

} Same as for (FI)

$\therefore I_{Abs}^{(BI)}{}_{PSE} = (40) \times (44) + (41) \times (45) + (42) \times (46)$.

$I_{Abs}^{(BI)}{}_{PSE} = \left(\frac{I_o}{W_{PSE}}\right) \cdot \{ [\exp(-\alpha(d_3 - d_w + W_{in})) - \exp(-\alpha d_3)] \cdot [2W] + [\exp(-\alpha(d_3 - d_w)) - \exp(-\alpha(d_3 - d_w + W_{in}))] \cdot [W_{well} + 2W_{out}] + [\exp(-\alpha(d_3 - d_w - W_{out})) - \exp(-\alpha(d_3 - d_w))] \cdot [W_{well} + \pi W_{out}] \}$

(48) cf p42

PSE CONDITION : $W_w + 2W_{out} \leq W_{PSE}$ or $W_{PSE} - (W_w + 2W_{out}) \geq 0$ need to be +ve.

WELL CONDITION. $W_w \geq 2 \times W_{in}$ or $W_w - 2W_{in} \geq 0$ needs to be +ve.

SUBST DEPTH CONDITION: $d_3 \geq d_w + W_{out}$ or $d_3 - (d_w + W_{out}) \geq 0$ needs to be +ve.

- 3rd Proposition — SCAN-XT

DIFFUSION COMPONENT

2D CASE (FI)

@ 70

I_{Abs}^{FI} @ (70) = Total Substrate Abs in ... w/ slice − Drift component (FI) @ 70

(Diffusion) = (38) − (56) − ε_{drift}

$= I_0[1 - \exp(-\alpha d_s)]$ − (39). — (49)

I_{Abs}^{BI} @ (70) = Total Substrate Abs − Drift component (BI) @ 70

(Diffusion) = (38) − (56) − ε_{drift} — (50)

@ 80

I_{Abs}^{FI} @ (80) = total substrate Abs − Drift component (FI) @ 80.

(Diffusion) = (38) − (21) − ε_{drift} — (51)

I_{Abs}^{BI} @ (80) = (38) − (25) − ε_{drift} — (52)

(Diffusion)

Total PSE

I_{Abs}^{FI} @ (80) across PSE total = (38) − (57) − ε_{drift} — (53)

I_{Abs}^{BI} @ (80) across total PSE = (38) − (58) − ε_{drift} — (54)

Total PSE

CONT. for 3D CASE

NBp Need to consider layer D in 2D case.

$I_{Abs}^{FI} = \int_0^{(W_{pit})}$

$x^2 + y^2 = r^2$

– 35 –

3 D case Absorbate !

The $\overleftarrow{I_{ABS}}$ per layer A, B, C are same as 2D CASE.

(FI) $\left\{ \begin{array}{l} I_{ABS}^{(FI)}(A) = (32) \\ I_{ABS}^{(FI)}(B) = (34) \\ I_{ABS}^{(FI)}(C) = (36) \end{array} \right.$

(BI) $\left\{ \begin{array}{l} I_{ABS}^{(BI)}(A) = (40) \\ I_{ABS}^{(BI)}(B) = (41) \\ I_{ABS}^{(BI)}(C) = (42) \end{array} \right.$

Proportion ~~for~~ Both FI and BI are same.

§ LAYER A.

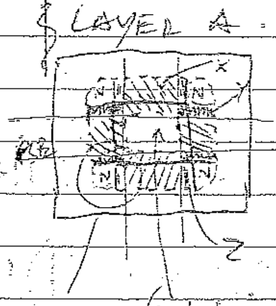

(Include in Prop(B).)

Prop(A) = ~~4(X) + 4(Y) + 4(Z) + 4(N)~~

$$= (W_w + 2W_{out})^2 - (W_w - 2W_{in})^2 - 4Q \Big/ (W_{PSB})^2$$

$$= (W_w + 2W_{out})^2 - (W_w - 2W_{in})^2 - 4\left((W_{out})^2 - \tfrac{\pi}{4}(W_{out})^2\right) \Big/ (W_{PSB})^2$$

$$= (W_w + 2W_{out})^2 + \pi(W_{out})^2 - (W_w - 2W_{in})^2 - 4(W_{out})^2 \Big/ (W_{PSB})^2$$

$$= (W_w + 2W_o)^2 + (\pi - 4)(W_o)^2 - (W_w - 2W_{in})^2 \Big/ (W_{PSB})^2 \quad (59)$$

$$Q = \square - \square = W_{out}^2 - \tfrac{\pi}{4}(W_{out})^2$$

$$\text{Prop}(B) = \text{Prop}(A) + (W_w - 2W_{in})^2 \Big/ (W_{PSB})^2$$

$$= (W_w + 2W_{out})^2 + \pi(W_{out})^2 - 4(W_{out})^2 \Big/ (W_{PSB})^2 \quad (60)$$

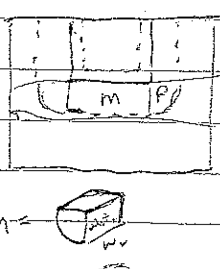

$$\text{Prop}(C) = 4V_m + 4V_p \;(+\text{ [illegible]}) = 4\left(\tfrac{\pi}{4}(W_{out})^2 \cdot W_{well}\right) + 4\left(\tfrac{4}{3}\pi (W_{out})^3 \cdot \tfrac{1}{8}\right) \;(+ (W_{well})^2 \ldots)$$

$$= \pi (W_{out})^2 \cdot W_{well} + \tfrac{2}{3}\pi (W_{out})^2 \Big/ (W_{PSB})^2 \neq W_{out} \qquad \Big/ W_B \cdot W_0$$

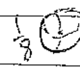

m =

P = $\frac{1}{8}$ (sphere) sphere. r = W_{out}.

$$= \pi(W_{out}) \cdot W_{well} + \tfrac{2}{3}\pi W_{out} \;(+W_o) \Big/ (W_{PSB})^2$$

$$= (W_o +) W_{out} \left(\pi \cdot W_{well} + \tfrac{2}{3}\pi\right) \Big/ (W_{PSB})^2$$

$$= (W_{well})^2 + W_{out}\left(\pi W_{well} + \tfrac{2}{3}\pi\right) \Big/ (W_{PSB})^2 . \quad (61)$$

-36-

Bop (C) should be broken into 2 PARTS:

PART 1 = M – straight forward – Spherical PART.

PART 2 = $\frac{1}{8}$ spheres on each ~~corner~~ bottom corner (X4)

need to integrate the I_{ABS} to be integrated over the volume and 4XPART 2 would be added to the rest of the calculation.

3D CASE: FI

$$I^{(FI)}_{ABS,\ 3D\ PSE} = \frac{I_o}{(W_{PSE})^2}\left\{\left(\left[1-\exp(-\alpha(d_w-w_{in}))\right]\cdot\left[(w_{out}+2w_{out})^2+\pi(w_{out})^2(\pi-4)-(w_w-2w_{in})^2\right]\right)+\right.$$

$$\left(\left[\exp(-\alpha(d_w-w_{in}))-\exp(-\alpha d_w)\right]\cdot\left[(w_w+2w_{out})^2+(\pi-4)(w_{out})^2\right]\right)+$$

$$\left.\left(\left[\exp(-\alpha d_w)-\exp(-\alpha(d_w+w_{out}))\right]\cdot\left[(w_w)^2+w_{out}\left(\pi w_w+\tfrac{2}{3}\pi\right)\right]\right)\right\}$$

(62)

Similarly in (BI). – 3D CASE

$$I^{(BI)}_{ABS,\ 3D\ PSE,\ total} = \frac{I_o}{(W_{PSE})^2}\left\{\left(\left[\exp(-\alpha(d_s-d_w+w_{in}))-\exp(-\alpha d_s)\right]\cdot\left[(w_w+2w_{out})^2+(w_{out})^2(\pi-4)-(w_w-2w_{in})^2\right]\right)+\right.$$

$$\left(\left[\exp(-\alpha(d_s-d_w))-\exp(-\alpha(d_s-d_w+w_{in}))\right]\cdot\left[(w_w+2w_{out})^2+(\pi-4)(w_{out})^2\right]\right)+$$

$$\left.\left(\left[\exp(-\alpha(d_s-d_w-w_{out}))-\exp(-\alpha(d_s-d_w))\right]\cdot\left[(w_w)^2+w_{out}\left(\pi w_w+\tfrac{2}{3}\pi\right)\right]\right)\right\}$$

(63)

NB: These are only approximations for the volumes that are curved. (eg 4 x spherical well edges).

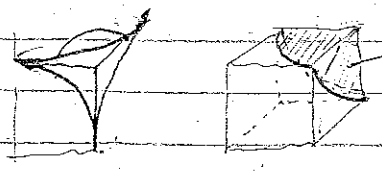

I is integrated over this area for FI + BI

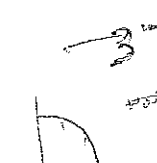

Need to consider Front-wall illuminated.

(FI) 2D of Layer 1

or (FW)

$$\int_0^{90^\circ} I_0 \exp(-\alpha(d_w)) - I_0 \exp(-\alpha(d_w + \text{NewDist})) \cdot d\theta$$

$$= \int_0^{90^\circ} I_0 \left(\exp(-\alpha(d_w)) - \exp(-\alpha(d_w + W_{wt}\sin\theta))\right) d\theta$$

$$= I_0 \int_0^{\frac{\pi}{2}} \exp(-\alpha d_w) - \exp(-\alpha(d_w + W_{wt}\sin\theta))\, d\theta$$

$d_w + W_{wt}$ becomes the problem in the problem

$$= I_0 \left[\int_0^{\frac{\pi}{2}} \exp(-\alpha d_w)\, d\theta + \int_0^{\frac{\pi}{2}} \exp(-\alpha(d_w + W_{wt}\sin\theta))\, d\theta \right]$$

$$= I_0 \left[\left[\theta \cdot \exp(-\alpha d_w) \right]_0^{\frac{\pi}{2}} - \right.$$

Time to approximate

$x = W_{wt}$

$$\int_0^{\alpha} \exp^{-\alpha a} \cdot \exp^{-\alpha B \sin\theta}\, d\theta$$

$$\int_0^{\alpha} \exp^{-\alpha a} \cdot \exp^{-\alpha \sqrt{B^2 - x^2}}\, d\theta = \int_0^{W_{wt}} \sum_{n=1}^{n_0} \exp\left(-\alpha\left(d_w + \sqrt{W_{wt}^2 - x^2}\right)\right)$$

CRC STANDARD MATHEMATICAL TABLES & FORMULAE

Zwillinger D. (1996) – CRC Press LLC New York. p391 – 3.X.

$$\sum_{i=1}^{n} \exp\left(-\alpha\left(d_w + \sqrt{(W_{wt})^2 - \left(i\frac{W_{wt}}{n}\right)^2}\right)\right) \cdot (\text{prop})$$

$\frac{W_{wt}}{n}$ / d_x W_{PSE}.

$$\text{prop} = \frac{W_{wt}}{n} \times \sqrt{W_{wt}^2 - \left(\frac{iW_{wt}}{n}\right)^2} \times dx \Big/ W_L \times dx$$

$$= \frac{W_{wt}}{n} \times \frac{\sqrt{n^2 W_{wt}^2 - i^2 W_{wt}^2}}{n^2} \Big/ W_L = \frac{W_0\sqrt{n^2 - i^2}}{n^2 W_L}$$

$W_0\sqrt{n^2 - i^2}$

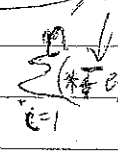

$$\approx \sum_{i=1}^{n} I_0 \left(\exp(-\alpha d_w) - \exp\left(-\alpha\left(d_w + \sqrt{(W_{wt})^2 - \left(i\frac{W_{wt}}{n}\right)^2}\right)\right)\right) \cdot \frac{\sqrt{n^2 W_0^2 - i^2 W_0^2}}{n^2 \cdot W_{PSE}}$$

-38

$$\sum_{i=1}^{n} I_0\left[\exp(-\alpha d_w) - \exp\left(-\alpha\left(d_w + \frac{w_{out}\sqrt{n^2-i^2}}{n}\right)\right)\right]\left(\frac{w_{out}}{n^2 w_L}\sqrt{n^2-i^2}\right) \quad (B)$$

$$\frac{P_0 \cdot w_{out}}{n^2 \cdot w_L}\sum_{i=1}^{n}\sqrt{n^2-i^2}\left[\exp(-\alpha d_w) - \exp\left(-\alpha\left(d_w + \frac{w_{out}\sqrt{n^2-i^2}}{n}\right)\right)\right]$$

(FI) (layer D)

(BI) CASE, $I_0\left(\exp(-\alpha(d_s - d_w - NWO)) - \exp(-\alpha(d_s - d_w))\right) \times$ prop as before.

$$NWO = \sqrt{w_{out}^2 - \left(\frac{i w_{out}}{n}\right)^2} = \sqrt{w_0^2\left(n^2 - i^2\right)/n^2} = \frac{w_0}{n}\sqrt{n^2 - i^2}$$

prop as before $= \frac{w_{out}\sqrt{n^2-i^2}}{n^2 w_L}$ — (γ)

(BI) layer D $\quad I_{BSE} = \frac{I_0 \cdot w_{out}}{n^2 w_L}\sum_{i=1}^{n}\sqrt{n^2-i^2}\left[\exp\left(-\alpha\left(d_s - d_w - \frac{w_{out}}{n}\sqrt{n^2-i^2}\right)\right) - \exp(-\alpha(d_s - d_w))\right]$ (γ)

(BI)

This is for the @ 2o position 2D

also for total 2D use

2 × (β) For (FI) @ 80 Total PSE cam 2D

2 × (γ) For (BI) @ 80

multiply cam ten by $\frac{n}{\sqrt{n^2-i^2}}$ = 1.0

1.1790295122566971080142366421790084 = 1.179029512256697

1.1790295122566971080142366421790084504447585615172232...

∴ Corrected 2D CASES

(FI) @ (70) including (B) p 38 (Drift component)

$$I_{ABS/SCR}^{(FI)(70)} = \left(\frac{I_o}{w_{i,n}}\right)\left\{\left(\left[1-\exp(-\alpha(d_\omega^{dj}-w_{in}))\right].[w_b]\right)+\left(\left[\exp(-\alpha(d_\omega^{dj}-w_{in}))-\exp(-\alpha d_\omega^{dj})\right].\left[w_{i,n}/2+w_{out}\right]\right)\right.$$

$$\left.+\left(\left[\exp(-\alpha(d_\omega^{dj}))-\exp(-\alpha(d_\omega^{dj}+w_{out}))\right].[w_{i,n}/2]\right)\right.$$

(39)+(B)

$$\left.+\left(\frac{w_{out}}{n^2}\sum_{i=1}^{n}\sqrt{n^2-i^2}\cdot\left[\exp(-\alpha d_\omega^{dj})-\exp\left(-\alpha\left(d_\omega^{dj}+\frac{w_{out}}{n}\sqrt{n^2-i^2}\right)\right)\right]\right)\right\}$$

(55)

(BI) @ (70) including (B) p 38 (Drift component)

$$I_{ABS/SCR}^{(BI)(70)} = \left(\frac{I_o}{w_{i,n}}\right)\left\{\left(\left[\exp(-\alpha(d_s^T-d_\omega^{dj}+w_{in}))-\exp(-\alpha d_s^T)\right].[w_b]\right)+\right.$$

(43)+(8)

$$+\left(\left[\exp(-\alpha(d_s^T-d_\omega^{dj}))-\exp(-\alpha(d_s^T-d_\omega^{dj}+w_{in}))\right].\left[w_{i,n}/2+w_{out}\right]\right)+$$

$$+\left(\left[\exp(-\alpha(d_s^T-d_\omega^{dj}-w_{out}))-\exp(-\alpha(d_s^T-d_\omega^{dj}))\right].[w_{i,n}/2]\right)+$$

$$\left.\left(\frac{w_{out}}{n^2}\sum_{i=1}^{n}\sqrt{n^2-i^2}\left[\exp\left(-\alpha\left(d_s^T-d_\omega^{dj}-\frac{w_{out}}{n}\sqrt{n^2-i^2}\right)\right)-\exp(-\alpha(d_s^T-d_\omega^{dj}))\right]\right)\right\}$$

(56)

(FI) @ (80) $w_{i,n}$ slice ($w_{i,n}=5\mu m$) = (21)

$$I_{ABS/SCR}^{(FI)(80)} = I_o\left(\exp(-\alpha(d_\omega-w_{in}))-\exp(-\alpha(d_\omega+w_{out}))\right) \quad (21)$$

(BI) @ (80) $w_{i,n}$ slice ($w_{i,n}=5\mu m$) = (25)

$$I_{ABS/SCR}^{(BI)(80)} = I_o\left(\exp(-\alpha(d_s^T-d_\omega^{dj}-w_{out}))-\exp(-\alpha(d_s^T-d_\omega^{dj}+w_{in}))\right) \quad (25)$$

– 40 –

Correct 2-D case TOTAL PSE SLICE

(FI) @ 80 with $w_i = w_{PSE}$ = (47) + 2×(b) p38.

$$I_{ABS/SCR\ Total\ PSE\ slice}^{(FI)} = \left(\frac{I_o}{w_{PSE}}\right)\left\{\left([1-\exp(-\alpha(d_{ip}-w_{in}))]\cdot[2w]\right)+\right.$$

$$\left([\exp(-\alpha(d_{ip}-w_{in}))-\exp(-\alpha d_{ip})]\cdot[w_{well}+(2w_{oot})]\right)+$$

$$\left([\exp(-\alpha d_w^{(i)})-\exp(-\alpha(d_w^{(i)}+w_{oot}))]\cdot[w_{well}]\right)+$$

$$\left.\left(\frac{2w_{oot}}{n^2}\sum_{i=1}^{n}[\quad]\cdot[\exp(-\alpha d_w)-\exp(-\alpha(d_w+\tfrac{w_{oot}}{n}\sqrt{n^2-i^2}))]\right)\right\}$$

(57)

(BI) @ 80 with $w_i = w_{PSE}$ = (48) + 2×(a) p38.

$$I_{ABS/SCR\ PSE\ slice}^{(BI)\ Total} = \left(\frac{I_o}{w_{PSE}}\right)\left\{\left([\exp(-\alpha(d_s^{(1)}-d_w^{(d_s)}+w_{in}))-\exp(-\alpha d_s^{(1)})]\cdot[2w]\right)+\right.$$

$$\left([\exp(-\alpha(d_s^{(1)}-d_w^{(d_s)}))-\exp(-\alpha(d_s^{(1)}-d_w^{(d_s)}+w_{in}))]\cdot[w_{well}+(2w_{oot})]\right)+$$

$$\left([\exp(-\alpha(d_s^{(1)}-d_w^{(d_s)}-dw_{oot}))-\exp(-\alpha(d_s^{(1)}-d_w^{(d_s)}))]\cdot[w_{well}]\right)+$$

$$\left.\left(\frac{2w_{oot}}{n^2}\sum_{i=1}^{n}[\quad]\cdot[\exp(-\alpha(d_s^{(1)}-d_w^{(d_s)}-\tfrac{w_{oot}}{n}\sqrt{n^2-i^2}))-\exp(-\alpha(d_s^{(1)}-d_w^{(d_s)}))]\right)\right\}$$

(58)

BI C1 = 55 65 70 ×4% BI only. (×2)

C2 = 75 – 80 + 同時×4% BI only. (×3)

C3 = 55 + 70 N2. 兩次 BI + PI only 2D 的 BI + FI. (×3)

PI C1 = 55, 65, 70 ×4% PI only. (×3)

C2 = 75, 80 + 同時×4% PI only. (×3)

– 41 –

Completed 3D case

2/6/03 21:22

For PHD

DJ PD

%Abs in Image SCR is SSPD Result!

FI

IS

@ 70 μm: 20μm, 50μm

2+4 case @ 80. (i.e. image well width = 2 + 4 μm pitch).

5μm, PEPI, PW, PSUB, SCR, FI

$= I_0(1-\exp(-\alpha(d_{PEPI} - W_{inv,PW}))$ – Abs PT SCR with well = 6 $W_{inv,PW}$ and

8+14 case I₀ th vs SSPD case, for SCR.

for NON SCR FI $\%Abs = I_0(1-\exp(-\alpha(d_N - W_{inv,PW}) -$ Abs PT SCR

in SSPD.

FI 2D in SSPD %Abs by visual PD. → in sheet 2!

Diffusion

$I_0(1-\exp(-\alpha(d_N - W_{inv}))\times(W_{well}-2W_{inv})/W_{PSE}$ – SCR Abs in sheet 1!

NON SCR.

FI 3D %Abs by visual PD.

$I_0(1-\exp(-\alpha(d_W - W_{inv}))\times(W_{well}-2W_{inv})^2/W_{PSE}^2$

PSE PD %Abs by visual PD.

$I_0(\exp(-\alpha(d_S - d_W + W_{inv})) - \exp(-\alpha d_S)) \times W_{well} - 2W_{inv} / W_{PSE}$

PSE. PD PSE total Abs in Real well

FI

%

I_0

"You've got to try a little kindness
And overlook the blindness
Of a narrow minded people
In a narrow minded world!"